IAEA-190

NUCLEAR THEORY IN NEUTRON NUCLEAR DATA EVALUATION

VOL.II

PROCEEDINGS OF A CONSULTANTS MEETING
ON THE USE OF NUCLEAR THEORY
IN NEUTRON NUCLEAR DATA EVALUATION
ORGANIZED BY
THE IAEA NUCLEAR DATA SECTION
IN CO-OPERATION WITH
THE INTERNATIONAL CENTRE FOR THEORETICAL PHYSICS, TRIESTE,
AND HELD AT TRIESTE, 8–11 DECEMBER 1975

A TECHNICAL DOCUMENT ISSUED BY THE
INTERNATIONAL ATOMIC ENERGY AGENCY, VIENNA, 1976

Foreword

This Consultants Meeting, recommended by the International Nuclear Data Committee (INDC) and convened by the IAEA Nuclear Data Section in cooperation with the International Centre for Theoretical Physics (ICTP) in Trieste, had the objectives to review the status and the use of nuclear theories, models and computer codes in the evaluation of neutron nuclear data needed for fission and fusion reactor design and other nuclear applications and to work out recommendations for future developments, with particular consideration of the requirements and possible cooperation of nuclear scientists from developing countries.

The meeting clearly demonstrated the importance of current research in basic nuclear theory for an improved understanding and determination of nuclear model parameters, a more adequate and detailed description of nuclear properties and reactions and thus for improvements in the prediction of neutron nuclear reaction data needed in nuclear energy applications. Eight review and twenty contributed papers presented in plenary followed by working group discussions formed the basis for a detailed review of the current and required developments in the following areas of nuclear theory:

- resonance and statistical theory;
- capture mechanism;
- nuclear level densities;
- optical model;
- pre-compound decay; and
- fission theory;

including a survey of available and required nuclear model computer codes. The meeting was thus in keeping with the traditional nuclear theory activities of the ICTP.

The most important result of the meeting is therefore the recommendation of an extended seminar of several weeks duration on nuclear theory and nuclear model computer codes for applications to be held in 1977. As appropriate places the meeting suggested the ICTP in Trieste for the nuclear theory part, and the Centro di Calcolo of CNEN in Bologna or the NEA Computer Program Library at Ispra for the computer code part of the seminar.

The proceedings of this meeting are published in two volumes. Volume I contains the summary report of the meeting and the review papers presented at the meeting, Volume II the contributed papers presented at the meeting.

The meeting was attended by 39 representatives from 16 countries and three international organizations. The excellent assistance by staff from the ICTP and the Institute of Theoretical Physics of the Trieste University contributed greatly to the success of the meeting and is most gratefully acknowledged.

Table of Contents

VOLUME I

VOLUME II

Contributed papers

Contributed Paper No. 1

*R-MATRIX METHODS FOR LIGHT SYSTEMS.**

by

G.M. HALE
Los Alamos Scientific Laboratory

and

Service de Physique Nucléaire
Centre d'Etudes de Bruyères-le-Châtel

ABSTRACT.

The R-matrix formulation of nuclear reaction theory is briefly reviewed, using the Green's function operator approach. General features of comprehensive R-matrix analyses of reactions in light systems are discussed, illustrated by a description of an analysis of reactions in the ^{7}Li system. Some characteristics of dispersion expansions for the R-and S-matrices are compared.

* Work performed under the auspices of the United States Energy research and development administration.

1. INTRODUCTION.

Since the development of R-matrix theory almost 30 years ago by WIGNER and EISENBUD [1], it has been used extensively to describe nuclear reactions in which resonance phenomena are important. Applications of the theory as a phenomenological tool to describe experimental data have ranged in complexity from using the celebrated BREIT-WIGNER line shape to represent isolated resonances to implementing the full multichannel, multilevel treatment to account simultaneously for data in several reactions over an energy interval which includes many (possibly interfering) resonances. Extensions of the "conventional" R-matrix approach have also provided the framework for calculations which use microscopic model Hamiltonians and wavefunctions that give the proper bound-state spectrum to generate resonances in the continuum states. The general concern of this paper, however, will be with essentially model-independent applications of R-matrix theory to represent data from nuclear reactions, with particular attention to detailed analyses that have been performed in recent years for reactions in light systems.

Some of the R-matrix formalism is briefly developed in the next section. Although the dispersion form of the R-matrix is most rigorously established by the conventional approach of WIGNER and EISENBUD [1] and LANE and THOMAS [2], we shall use the Green's function method introduced by BLOCH [3] which appears in many modern descriptions of the theory. The dispersion form of the R-matrix comes naturally and directly out of this representation, and extensions or generalizations of the conventional theory are easily seen. Applications of the conventional theory to phenomenological analyses of data from reactions among light elements are discussed in section 3. Systematic features that have occured in comprehensive R-matrix studies made at Los Alamos are noted, and some results from the analysis of reactions in the ^{7}Li system are shown to illustrate the technique. In the last section, some features of R-matrix and S-matrix parameterizations are compared. Alternative expansions which have characteristics of both theories are suggested.

2. *FORMAL CONSIDERATIONS.*

R-matrix theory takes advantage of the short range of nuclear forces to divide configuration space into two regions : an "interior" region in which little is known about the forces or wavefunction, and an "exterior" region in which both the forces and the form of the wavefunction are presumed to be known. The boundary separating these two regions is called the "channel surface", since the form taken for the wavefunction in the exterior region is that for a superposition of separated two-body pairs (channels) between which (at most) Coulomb forces act. Information is transferred between the interior and exterior regions by continuity conditions on the wavefunction at the channel surface.

In order to make this matching process explicit, BLOCH [3] introduced a method in which an operator $\mathcal{L}_B$ which projects onto the channel surface is artificially added to both sides of Schroedinger's equation in the interior region,

$$(H - \varepsilon + \mathcal{L}_B)\ \psi = \mathcal{L}_B\ \psi. \qquad (1)$$

The projection can be accomplished by defining channel surface "functions" :

$$|c) = \left(\frac{\hbar^2}{2\ M_c\ a_c} \right)^{1/2} \quad \frac{\delta\ (r_c - a_c)}{a_c}\ Y_c^J\ (\hat{r}_c) \qquad (2)$$

in terms of the channel reduced mass M_c, radius $r_c = a_c$, and spin-angle eigenfunction of total angular momentum and parity, $Y_c^J\ (\hat{r}_c)$.

Solving equation (1) formally for the wavefunction gives :

$$\psi = (H - \varepsilon + \mathcal{L}_B)^{-1}\ \mathcal{L}_B\ \psi. \qquad (3)$$

If $\mathcal{L}_B$ is taken to have the form :

$$\mathcal{L}_B = \sum_c |c)\ (a_c \frac{d}{dr_c} - B_c)\ (c|, \tag{4}$$

then :

$$\mathcal{L}_B \psi = \sum_c |c)\ (a_c \frac{d}{dr_c} - B_c)\ (c|\ \psi) \tag{5}$$

and the projection of ψ at the surface is given by :

$$(c'|\ \psi) = \sum_c (c'|\ (H - \varepsilon + \mathcal{L}_B)^{-1}\ |c)\ (a_c \frac{d}{dr_c} - B_c)\ (c|\ \psi).$$

With the associations $(c|\psi) = V_c$, $a_c \frac{d}{dr_c} (c|\psi) = D_c$, and $(c'|\ (H - \varepsilon + \mathcal{L}_B)^{-1}|c) = R_{c'c}$, because of the particular form (4) taken for $\mathcal{L}_B$, equation (5) reduces to the customary definition of the R-matrix [2],

$$V_{c'} = \sum_c R_{c'c}\ (D_c - B_c\ V_c) \tag{6}$$

Thus, the R-matrix can be considered as the channel surface matrix elements of a Green's function operator $G_B = (H - \varepsilon + \mathcal{L}_B)^{-1}$ which depends on the parameters B_c through $\mathcal{L}_B$, although the wavefunction in (1) or (3) is clearly independent of $\mathcal{L}_B$.

A generalized form of the R-matrix results from expanding the Green's function operator in any complete set of functions $|\mu)$,

$$G_B = \sum_{\mu,\nu} |\mu)\ (\mu|\ (H - \varepsilon + \mathcal{L}_B)^{-1}\ |\nu)\ (\nu| \tag{7}$$

$$= \sum_{\mu,\nu} |\mu)\ A^{-1}_{\mu,\nu}\ (\nu|,$$

where $A_{\mu\nu} = (\mu|H - \varepsilon + \mathcal{L}_B|\nu)$ is a generalization of the level matrix.

This type of expansion has been used in several calculations [4 - 7] that predict the resonances of compound systems based on shell-model Hamiltonians and wavefunctions which have successfully reproduced the bound states.

For phenomenological applications, however, it is more advantageous to expand the Green's function in terms of the eigenfunctions $|\lambda)$ of $H - \varepsilon + \mathcal{L}_B$ which satisfy :

$$(H - \varepsilon_\lambda + \mathcal{L}_B)\ |\lambda) = 0.$$

If these form a complete set, the expression (7) simplifies to :

$$G_B = \sum_\lambda |\lambda)\ (\varepsilon_\lambda - \varepsilon)^{-1}\ (\lambda|,$$

giving the R-matrix :

$$R_{c'c} = (c'|G_B|c) = \sum_\lambda (c'|\lambda)\ (\varepsilon_\lambda - \varepsilon)^{-1}\ (\lambda|c)$$

$$= \sum_\lambda \gamma_{c'\lambda}\ (\varepsilon_\lambda - \varepsilon)^{-1}\ \gamma^T_{c\lambda}\ , \text{with } \gamma_{c\lambda} = (c|\lambda), \qquad (8)$$

in its familiar dispersion form.

Since the completeness property for the eigenfunctions $|\lambda)$ cannot be established for Hamiltonians and boundary conditions in the general case, the conventional approach [1,2] restricts the boundary conditions (and Hamiltonian) to be energy independent so that R satisfies the first-order, non-linear differential equation of RICATTI. The dispersion form then follows from the fact that solutions of the RICCATTI equation can be expanded in an absolutely convergent MITTAG-LEFFLER series [2]. It is this expansion in the eigenfunctions of $(H-\varepsilon+\mathcal{L}_B)$ with B independent of energy that has been implied by the term "conventional" R-matrix theory in the preceeding discussions.

The R-matrix for the boundary condition B' that is equivalent to

the R-matrix for boundary condition B (in the sense that it gives the same wavefunction) is given by :

$$R_{B'} = \left[(1 - R_B (B' - B) \right]^{-1} R_B \qquad (9)$$

The transformation of resonance parameters between equivalent R-matrices for energy-independent boundary conditions ($B \longrightarrow B'$) can be accomplished analytically, as was pointed out by BARKER[8], by diagonalizing the level matrix,

$$A_{\lambda'\lambda} = \varepsilon_\lambda \delta_{\lambda'\lambda} - \sum_c \gamma_{c\lambda'} (B'_c - B_c) \gamma_{c\lambda}.$$

The eigenvalues of this matrix are the new pole positions ε'_λ, and the new widths are given in terms of V, the matrix of A's eigenvectors by :

$$\gamma'_{c\lambda} = \sum_{\lambda'} \gamma_{c\lambda'} V_{\lambda'\lambda} .$$

In order to calculate the results of experimental measurements, the information contained in the R-matrix about the projections of the interior wavefunction on the channel surface must be propogated to similar projections of the exterior wavefunction. Since the exterior wave function is a superposition of channel states, $\psi = \sum_c \psi_c$, these projections can be thought to form the elements $U_{c'c} \sim (c' | \psi_c)$ of a matrix which has known radial dependence in the external region. In general,

$$U = U_1 A_1 + U_2 A_2, \qquad (10)$$

where A_1 and A_2 are radius-independent matrices in the exterior region, and U_1 and U_2 are diagonal matrices containing, for each channel, two independent radial solutions of Schroedinger's equation for Coulomb scattering. Measurements generally detect only the relative amplitudes of the U_1 and U_2 functions, and thus depend on quantities of the form $X = A_2 A_1^{-1}$. If U_1 and U_2 are chosen such that their elements have essentially unit Wronskians with each other, then matching surface projections (6) of the internal wavefunction to those of the external

wavefunction in the form $U_1 + U_2 X$ gives a simple relation for X,

$$X = U_2^{-1} R_2 U_2^{-1} - U_1 U_2^{-1}, \qquad (11)$$

in terms of the R-matrix, R_2, having boundary conditions $B_{2c} = a_c U'_{2c} / U_{2c}$. Of course R_2, having energy-dependent boundary conditions, is not "conventional", but it is easily related to an R-matrix having energy-independent boundary conditions using equation (9).

Depending on the choices of U_1 and U_2, X in equation (11) becomes the S - (or collision) matrix, T - (or transition) matrix, K - (or reactance) matrix, etc. For instance, if $U_{1c} = (K_c a_c)^{-1/2} F_c$ and $U_{2c} = (K_c a_c)^{-1/2} (G_c + iF_c)$, where F_c and G_c are, respectively, the regular and irregular Coulomb functions evaluated at $r_c = a_c$ for channel c in which the wave number is K_c, X represents the amplitudes of outgoing spherical waves for incident plane waves of unit flux, which is sometimes called the nuclear T-matrix. In this case,

$$\begin{aligned} B_2 = L &= a\,(G' + iF') \,/\, (G + iF) \\ &= S + iP, \end{aligned}$$

and from (11) we have :

$$\begin{aligned} T_N &= (Ka)^{1/2} (G + iF)^{-1} R_L (G + iF)^{-1} (Ka)^{1/2} - F (G + iF)^{-1} \\ &= e^{-i\phi} P^{1/2} R_L P^{1/2} e^{-i\phi} - e^{-i\phi} \sin \phi, \qquad (12) \end{aligned}$$

where S and P are the Coulomb shift and penetrability functions and $\phi = \arg (G + iF)$ is the negative of the so-called "hard sphere" phase shift. The quantity T_N is important for calculating the observables of nuclear reactions, because it contains the matrix elements of Wolfenstein's M-matrix [9] in the basis of channel eigenfunctions (Y_c^J) of total angular momentum and parity. A simple change of basis to the channel spin functions allows one to calculate arbitrary observables for each reaction from the T-matrix and the initial-and final-state spin operators, using Wolfenstein's trace prescription.

We mention finally in this section an interesting property of R-matrices of the type R_2 that occurs in equation 11. If the dispersion form were justified for this function (either by completeness arguments, or by the Mittag-Leffer expansion) the pole positions and residues of the associated matrix X of relative amplitudes are independent of the matching radius in the exterior region. This can be seen by considering linear combinations of the columns of the U-matrix of equation (10) to give elements of the value vector $V_c = (c|\psi)$ appearing in equation (6) :

$$v = U \quad \alpha = U_1 \, \alpha_1 + U_2 \, \alpha_2 .$$

The vectors $\alpha_1 = A_1 \, \alpha$ and $\alpha_2 = A_2 \, \alpha$ are independent of matching radius in the exterior region since A_1 and A_2 have the same property. The vector α is determined to within an overall constant by a subsequent condition on α which is also radius independent. This condition is that at the ε_λ of X (and of R_2), $\alpha_1 = 0$ (or det $(A_1) = 0$). Thus the vector γ_λ of elements $(c|\lambda)$ is given by :

$$\gamma_\lambda = U_{2\lambda} \, \alpha_{2\lambda},$$

and R_2 has the expansion :

$$R_2 = \sum_\lambda (U_{2\lambda} \, \alpha_{2\lambda}) \, (\varepsilon_\lambda - \varepsilon)^{-1} \, (U_{2\lambda} \, \alpha_{2\lambda})^T . \qquad (13)$$

Inserting this expression into (11) gives :

$$X = \sum_\lambda (U_{2\lambda} \, U_2^{-1}) \, \frac{\alpha_{2\lambda} \, \alpha_{2\lambda}^T}{\varepsilon_\lambda - \varepsilon} \, (U_{2\lambda} \, U_2^{-1}) - U_1 \, U_2^{-1} . \qquad (14)$$

Thus, the poles ε_λ and residues $\alpha_{2\lambda} \, \alpha_{2\lambda}^T$ of X have the stated property due to the radial independence of α_1 and α_2 in the external region.

3. APPLICATIONS TO LIGHT NUCLEI.

In this section, we discuss the phenomenological application of conventional R-matrix theory to analyse data from reactions among light nuclei. The restriction to light nuclei is not essential in principle, but in practice, the large number of open channels and resonances encountered in heavier compound systems does not allow R-matrix theory to be applied without severe approximations. Limited computing resources often force approximations in R-matrix calculations even for light systems.

The most common approximation technique is to perform single-level fits, either to experimental data, or to individual-energy phase-shifts determined from data, to find the R-matrix parameters. In either case, the T-matrix of equation (12) is used, which for a single level reduces to :

$$T_{c'c} = e^{-i\phi_{c'}} \frac{\Gamma_{c'}\Gamma_{c}}{\Gamma} e^{i\beta} \sin\beta \, e^{-i\phi_{c}} - \delta_{c'c} e^{-i\phi_{c}} \sin\phi_{c} \quad ,$$

where $\beta = \tan^{-1}\left(\frac{1/2\,\Gamma}{\varepsilon_\lambda + \Delta - \varepsilon}\right)$,

and $\Gamma = \sum_c \Gamma_c$ with $\Gamma_c = 2\, P_c\, \gamma_{c\lambda}^2$,

$\Delta = \sum_c \Delta_c$ with $\Delta_c = -\, S_c\, \gamma_{c\lambda}^2$.

The BREIT-WIGNER form, which is actually a special case of these expressions in which Δ_c and Γ_c are taken to be energy independent, holds for resonances that are relatively narrow and have no appreciable width in channels that are close to threshold. The single level approximation has been widely used to represent qualitatively isolated resonant features in experimental data, and has been, for the most part, successful in identifying their spins and parities.

Since resonances are rarely truly isolated, however, multilevel and distant-level (or background) effects must be taken into account in order to obtain resonable fits to experimental data over appreciable intervals of energy. This is the situation that usually confronts evaluators of neutron cross sections, for instance. Multilevel R-matrix codes have been used at several institutions (Ohio U., Yale, Argonne, Oak Ridge, Cal. Tech., Duke, Karlsruhe, Geel, and Lasl, to name a few) to fit data from reactions among light nuclei. These fits have accounted for distant-level contributions in various ways, and in some cases have allowed for multichannel affects. We will summarize in the remainder of this section some of our experiences in using perhaps the most general of these codes to analyze light systems.

3.1 General Features.

The energy dependent analysis (EDA) code [10], developed at Los Alamos under the direction of D. DODDER, is a general R-matrix fitting code which accepts two-body channels having particles of arbitrary spins, masses, charges, parities, and relative angular momentum. Starting from a parameterization of the multichannel R-matrix,

$$R_{c'c} = \sum_{\lambda} \frac{\gamma_{\lambda c'} \gamma_{\lambda c}}{\varepsilon_{\lambda} - \varepsilon} ,$$

at channel radii a_c for boundary conditions B_c, the code essentially transforms R to R_L using equation (9), and then calculates elements of the T-matrix from equation (12). By implementing the Wolfenstein M-matrix formalism [9] in its general form, EDA is able to calculate arbitrary experimental observables for any of the two-body reactions possible in the system. Given a set of experimental measurements for these reactions, an automated search routine adjusts the R-matrix parameters to achieve a "best fit" in the usual least-squares sense to all the data included.

In the last few years, analyses using this code have been perfor-

med for reactions in several light compound systems, including ^{4}Li, ^{5}Li, ^{5}He, ^{7}Li, ^{11}B, ^{13}C, ^{15}N and ^{17}O. Typically, these analyses have spanned something like 10 MeV excitation energy in the compound systems, and have obtained good fits to almost all available data for reactions among the open two-body channels. Many of these analyses have been discussed elsewhere [11-14], so that only certain general features they have in common will be considered here.

3.1.1. Parameters.

The parameterization of the R-matrix involves specifying the following different types of quantities :

Boundary conditions :

As was pointed out in the previous section, the choice of boundary conditions has no effect on the wavefunction, and thus upon the calculation of measured quantities, so that one chooses these numbers only to simplify the interpretation, or perhaps the relations of the resonance parameters. For energy-independent boundary conditions, it is difficult to choose a single number for each state which simplifies interpretation of the parameters at all energies. For instance, the common choice $B_c = S_c(\varepsilon_o)$ forces a maximum of the T-matrix to correspond with a pole of the R-matrix (no level shift) only at $\varepsilon = \varepsilon_o$. For simple potential scattering in each channel from a square well of radius a_c, the choice $B_c = -l_c$ (l_c being the relative orbital momentum quantum number in channel c) results in reduced widths :

$$\gamma_{c\lambda}^2 = \frac{\hbar^2}{M_c a_c^2}$$

that are independent of λ and l_c. Although we have found this relation to hold approximately in simple cases like the scattering of nucleons from ^{4}He [11], it has not proved useful for accurate representations of experimental data. Our approach for data fitting, therefore, has been to specify R-matrix parameters for some convenient choice of boundary conditions (usually B = 0),knowing that this set can be transformed

analytically to any other set corresponding to energy independent boundary conditions more appropriate for interpreting the resonance parameters.

Channel radii.

The extensive use of the single-level approximation has left the impression that R-matrix fits in general are artificially sensitive to the choice of channel radii. We have found that this apparent sensitively comes indeed from the neglect of "background", or distant-level contributions, and that one can use radii roughly equal to the sum of the radii of the interacting particles in all channels, provided the background contribution is taken into account. In particular, this approach appears to better represent (with the same number of parameters) "hard sphere" s-wave phase shifts over large energy regions than does the usual technique of choosing separate "hard sphere radii" in the s-wave states.

Distant levels :

We represent the distant-level contribution in these analyses with a few-pole terms in the R-matrix, located both above and below the energy region of interest. Since these poles do not necessarily correspond to known resonances outside the region of interest, their positions are generally quite uncertain, and often have to be fixed at large numbers in the analyses. The reduced widths found in these distant pole terms are also generally large, giving rise to a slowly varying, non diagonal background that is significant at all energies. These non diagonal distant-level contributions are interpreted as indications that direct reaction mechanisms are present [2].

Resonance parameters :

The parameters $(\varepsilon_\lambda, \gamma_{c\lambda})$ of pole terms in the R-matrix corresponding to actual resonances in the energy region of interest are determined by fitting resonant features in the data. For light nuclei, these features range from relatively narrow and distinct peaks to broad and

overlapping structures. In the latter case, especially (as for the ^{5}Li and ^{5}He systems), it has been necessary to include measurements of several different types in order to establish resonance parameters for the anomalies.

3.1.2. Data.

Our general approach has been to include all available experimental data for reaction among the open channels. For neutron cross section evaluation, this has often meant including data (ie, charged particle cross sections, polarizations, etc.) for which smoothed representations are not required in the file. However, a comprehensive approach has proved to be valuable, particularly in cases where the neutron cross sections of interest are uncertain due to the difficulty in measuring them [12]. In all cases, the use of data from several different reactions and from many different observable types is designed to limit the multiplicity of possible solutions for the resonance parameters that might exist if, for instance, only total cross sections were included in the fit. At the same time, the analyses have checked the consistency of all the experimental information included, making allowances automatically for possible differences in normalization and energy scale among different data sets.

3.2. Analysis of reactions in the ^{7}Li system.

An analysis which illustrates many of the points just discussed is that performed for the reactions in the ^{7}Li system. At excitation energies below 9.4 MeV, the open two-body channels are t + ^{4}He and n + ^{6}Li (photon channels are neglected). The analysis takes into account most of the known data for the reactions ^{4}He(t,t)^{4}He, ^{6}Li(n,t)^{4}He, and ^{6}Li(n,n)^{6}Li (see Table 1), and most of the known levels in this energy region (see Fig. 1). For reasonable values of the channel radii ($\sim$ 4.2.f. for n + ^{6}Li and 4.0.f. for t + ^{4}He), non-diagonal distant-level contributions were required in all states.

The calculations shown in Figs. 2-4 are representative of the generally excellent fits obtained to ^{4}He(t,t)^{4}He scattering data at

triton energies between 2 and 11 MeV. The energy region shown (7,5 - 10 MeV) is of particular interest in this analysis since it contains two $^{5}/2$ - resonances, one of which lies below the n + ^{6}Li threshold, and the second of which shows up prominantly in the n + ^{6}Li reactions at low neutron energies. Measurements of neutron cross sections [15-17] in the vacinity of the second resonance show substantial disagreements, and appear to be inconsistent with unitary conditions relating them. The data shown in figs.2-4 are accurate new measurements of the ^{4}He(t,t)^{4}He differential cross section which were made recently by JARMIE, et al [18] to introduce independent experimental information into the determination of parameters for these levels. Including these new measurements in the analysis indeed imposed stringent additional constraints on the values of the neutron cross sections. The resulting curves for the neutron total cross section and the (n,α) integrated cross section are shown over the resonance in fig. 5. The total cross section agrees reasonably well with recent measurements [15,19,20], while the (n,α) cross section lies between the values of recent measurements [16,21], which differ by more than 25 % in the peak of the resonance. Curves for the ^{6}Li(n,t)^{4}He differential cross section are shown in Fig.6. The calculations reproduce the large asymmetry seen by SCHRODER, et al [22] in the angular distribution at 25 KeV, and agree fairly well with the measurements of OVERLEY, et al [23] at higher energies. Good fits (not shown) were also obtained to LANE's measurements [17] of n + ^{6}Li elastic angular distributions and polarizations.

The predictive capability of the R-matrix parameters obtained from this analysis is illustrated in the last figure. Shown in Fig. 7 are predictions of ^{4}He(t,t)^{4}He and ^{6}Li(n,t)^{4}He polarizations compared with recent measurements [24,25]. One sees that the measurements were anticipated by the calculations in considerable detail, even to the threshold effect (insert, top part of figure) evident in the ^{4}He(t,t) polarization excitation functions.

Thus, we feel that the ^{7}Li system is phenomenologically well understood at excitation energies below $\sim$ 10 MeV in terms of a single set of R-matrix parameters that can reproduce (or predict) the results

of any experiment performed for the reactions of tritons with alpha particles, or for those of neutrons with ^{6}Li. These parameters obviously have direct value in obtaining evaluated nuclear data for these reactions, and with the proper interpretation, could be used to guide microscopic structure calculations for ^{7}Li.

4. DISCUSSION AND CONCLUSIONS.

A question often asked proponents of R-matrix theory is, "why aren't you using S-matrix theory, instead ?". S-matrix expansions were developed in a series of papers by HUMBLET [26-28] to answer what he felt was a serious defect in R-matrix theory, namely : that individual terms of the collision matrix ($S = 1 + 2iT$) derived from the theory were not explicitly independent of the matching radius in the exterior region. HUMBLET's direct expansions indeed have this property, but they rely on the background contribution to give the S-matrix a number of other important features, such as unitarity, threshold effects, and truncation of the partial-wave series, that come automatically from R-matrix theory. Our feeling is that it is preferable to use background terms in the R-matrix to supply the radial independence of the S-matrix, than to depend on similar terms in the S-matrix to give important properties of nuclear reactions.

However, the considerations at the end of section 2 show that radial independence of asymptotic quantities derived from the R-matrix could be made more explicit if the boundary conditions were chosen to be logarithmic derivatives of solutions of the wave equation in the external region. In fact, choosing $B = a(G' + iF')\ (G + iF)^{-1} = L$ generates the S-matrix expansion given (but not recommended) by HUMBLET in eq. A1.8 of ref. [28]. Equating the boundary condition to the logarithmic derivative of a real solution in the external region would result in an expansion for the real asymptotic quantity X having similar properties of radial independence, but avoiding the complications of having complex poles and residues. A dispersion form is not immediately justified for this type of R-matrix, of course, since it has energy-dependent boundary conditions.

The analyses we have performed in the light systems indicate that conventional R-matrix theory can be used to give a detailed accounting of data for several reactions simultaneously, and is therefore a useful tool for evaluators with access to large computers. Methods of representing the distant-level, or background contributions in these calculations is an area that deserves more study. It is interesting to note, however, that the background contributions which JOHNSON [29] calculated from an optical potential for his analysis of n + ^{16}O resembled distant pole terms, which indicates that even this simple representation may suffice for purposes of data fitting.

Most of the analyses mentioned above were done in collaboration with one or more of the following people : D. DODDER, K. WITTE, R. NISLEY, J. DEVANEY, E. ARTHUR, and G. AUCHAMPAUGH. Valuabe assistance in obtaining and interpreting experimental data was given by P. YOUNG, N. JARMIE, L. STEWART, and G. OHLSEN. The author gratefully acknowledges the help of the staff of the Service de Physique Nucléaire de Bruyères-le-Châtel in preparing this paper.

REFERENCES.

[1] WIGNER, E.P., EISENBUD, J.T., Phys. Rev. 72 (1947) 29.

[2] LANE, A.M., THOMAS, R.G., Rev. Mod. Phys. 30 (1958) 257.

[3] BLOCH, C., Nucl. Phys. 4 (1957) 503.

[4] PURCELL, J.E., Phys. Rev. 185 (1969) 1279.

[5] ROBSON, B.A., VAN MEGEN, W.J., Nucl. Phys. A184 (1972) 50.

[6] AYAD, A.A., ROWE, D.J., Nucl. Phys. A218 (1974) 307.

[7] GEORGE, J., PHILPOTT, R.J., Phys. Rev. Lett. 32 (1974) 901.

[8] BARKER, F.C., Aust. J. Phys. 25 (1972) 341.

[9] WOLFENSTEIN, L., Ann. Rev. Nucl. Sci. 6 (1956) 43.

[10] DODDER, D.C., WITTE, K., HALE, G.M., The energy-dependent analysis code EDA, unpublished.

[11] DODDER, D.C., HALE, G.M., NISLEY, R.A., WITTE, R., YOUNG, P.G., EANDC Topical Discussion on "Critique of Nuclear Models and their Validity in the Evaluation of Nuclear Data" (Proc. Tokyo, 1974) NEANDC (J) 38 L/INDC (JAP) 25 L, JAERI, Tokai (1975) 1.

[12] HALE, G.M., Bull. Am. Phys. Soc. 20 (1975) 148, and Conference on Nuclear Cross Sections and Technology (Proc. Conf. Washington, D.C., 1975) to be published.

[13] HALE, G.M., DEVANEY, J.J., DODDER, D.C., WITTE, K., Bull. Am. Phys. Soc. 19 (1974) 506.

[14] HALE, G.M., YOUNG, P.G., FOSTER, D.G., Jr., Bull. Am. Phys. Soc. 17 (1972) 915.

[15] DIMENT, K.M., UTTLEY, C.A., Harwell Reps. AERE-PR/NP 14 (1968) 20, and AERE-PR/NP 15 (1969) 12.

[16] COATES, M.S., HUNT, G.J., UTTLEY, C.A., Neutron Reference Standard Data, IAEA, Vienna (1974) 113.

[17] LANE, R.O., ELWYN, A.J., LANGSDORF, A., Jr., Phys. Rev. B136 (1964) 1710.

[18] JARMIE, N., et al, Bull. Am. Phys. Soc. 20 (1975) 596.

[19] HARVEY, J.A., HILL, N.W., Bull. Am. Phys. Soc. 20 (1975) 145, and private communication (1975).

[20] KNITTER, H.-H., private communication (1975).

[21] FRIESENHAHN, S.J., ORPHAN, V.J., CARLSON, A.D., FRICKE, M.P., LOPEZ, W.M., Bull. Am. Phys. Soc. 20 (1975) 144.

[22] SCHRÖDER, I.G., McGARRY, E.D., DE LEEUW, S., DE LEEUW-GIERTS, G., Bull. Am. Phys. Soc. 20 (1975) 145.

[23] OVERLEY, J.C., SEALOCK, R.M., EHLERS, D.H., Nucl. Phys. A221 (1974) 573.

[24] HARDEKOPF, R.A., JARMIE, N., OHLSEN, G.G., POORE, R.V., Fourth International Symposium on Polarization Phenomena in Nuclear Reactions (Proc. Conf. Zurich, 1975) to be published.

[25] KARIM, M., OVERLEY, J.C., Bull. Am. Phys. Soc. 20 (1975) 167, and private communication (1975).

[26] HUMBLET, J., ROSENFELD, L., Nucl. Phys. 26 (1961) 529.

[27] HUMBLET, J., Nucl. Phys. 31 (1962) 544.

[28] HUMBLET, J., Nucl. Phys. 50 (1964) 1.

[29] JOHNSON, C.H., Phys. Rev. C7 (1973) 561.

^{7}Li SYSTEM

OBSERVABLE TYPES ANALYZED :

Reaction	Total neutron Cross Section	Integrated Cross Section	Differential Cross Section	Polarization
^{6}Li	X			
^{6}Li(n,n)^{6}Li		X	X	X
^{6}Li(n,α)T		X	X	
^{4}He(t,t)^{4}He			X	X

TABLE 1.

Types of data included in ^{7}Li analysis.

FIGURE CAPTIONS.

Fig. 1. Level diagram for ^{7}Li. The dotted lines indicate the range over which data were included. Checked levels correspond approximately to those in our analysis. Additional levels found in the analysis are indicated in parentheses.

Fig. 2. ^{4}He(t,t)^{4}He excitation functions at center-of-mass angles of 26.3, 49.6, 69.0, and 123.0 degrees. The solid curve in this, and all subsequent figures, gives the R-matrix calculation. Data points are from Ref.[18].

Fig. 3. ^{4}He(t,t)^{4}He excitation function at 150 degrees center-of-mass angle, showing the effects of both 5/2 - resonances.

Fig. 4. ^{4}He(t,t)^{4}He angular distributions at E_t = 8.229, 8.580, 8.980, and 9.844 MeV. The measurements are from Ref.[18].

Fig. 5. Predicted values of the neutron total cross section (upper curve) and of the ^{6}Li(n,α) reaction cross section (lower curve).

Fig. 6. ^{6}Li(n,t)^{4}He angular distributions at E_n = .025, .100, .240, and .400 MeV. Data at the upper three energies are those of OVERLEY et al. Ref.[23].

Fig. 7. Polarization predictions for reactions in ^{7}Li :

a) Excitation functions for the ^{4}He(t,t)^{4}He analyzing power.

b) Angular distributions for the ^{4}He(t,t) analyzing power. Data are from Ref [24].

c) Excitation curve for ^{6}Li(n,t)^{4}He analyzing power. Data are from Ref. [25].

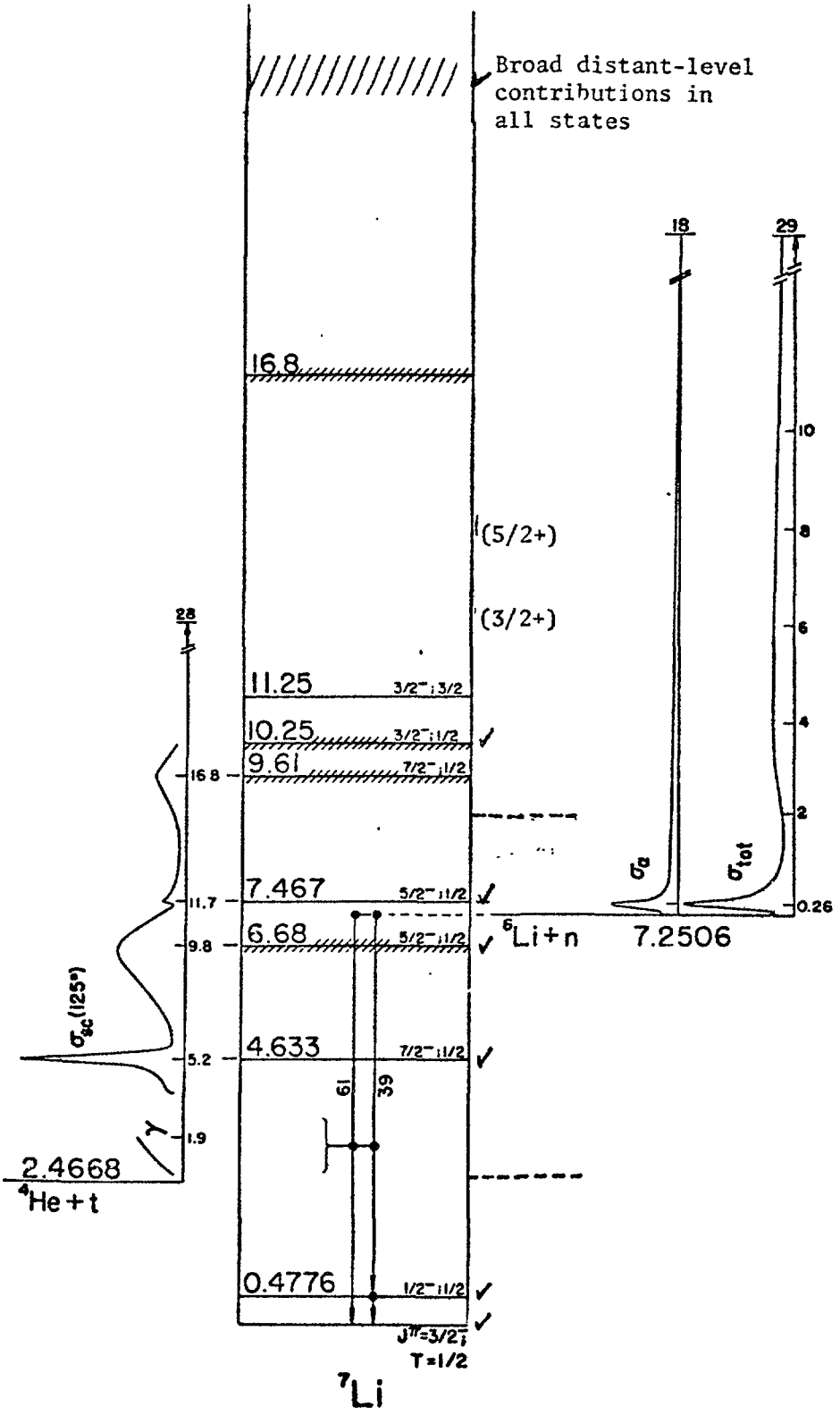

Fig. 1. Level diagram for ^{7}Li. The dotted lines indicate the range over which data were included. Checked levels correspond approximately to those in our analysis. Additional levels found in the analysis are indicated in parentheses or brackets.

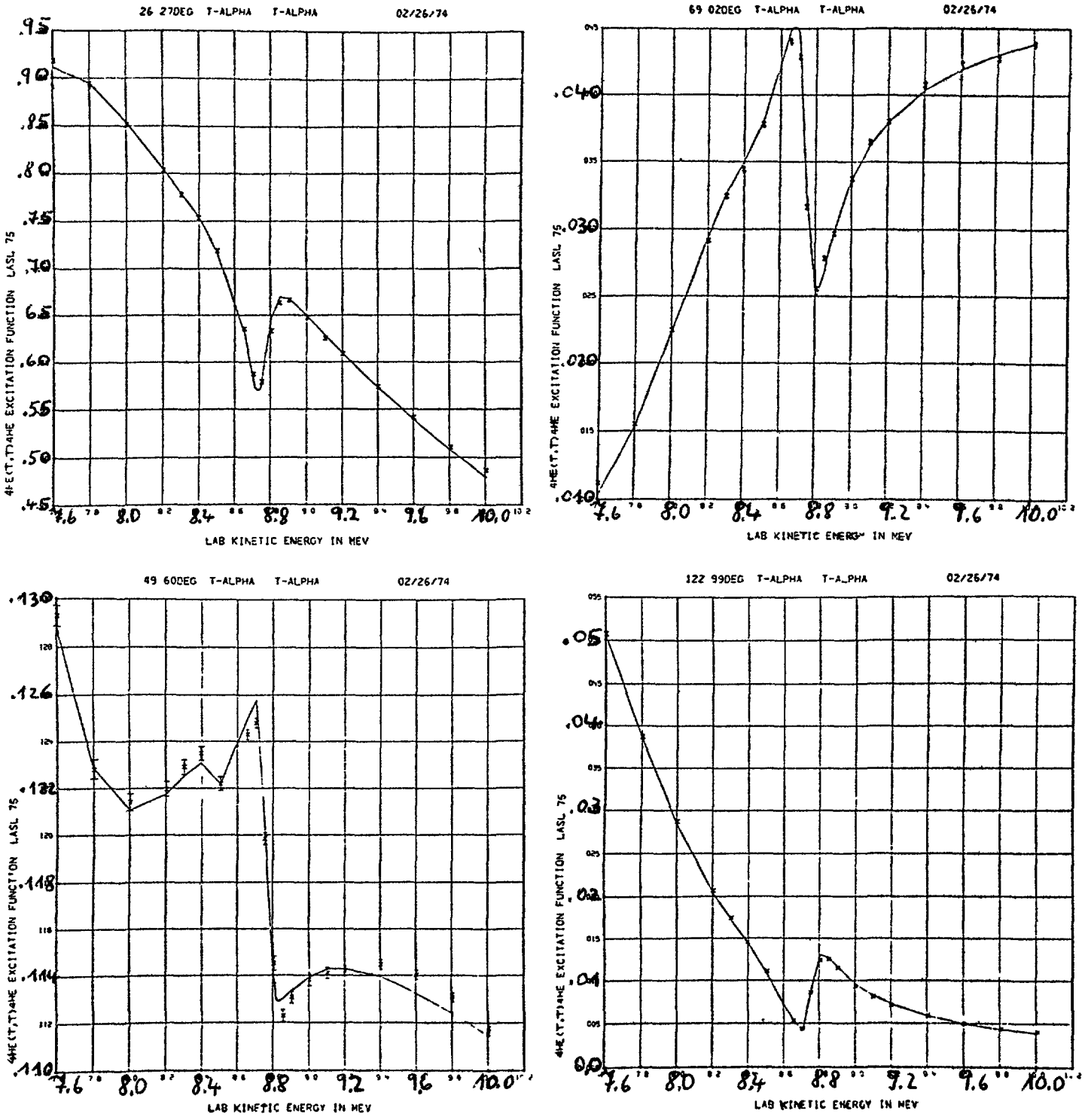
26 27DEG T-ALPHA T-ALPHA 02/26/74
69 02DEG T-ALPHA T-ALPHA 02/26/74
49 60DEG T-ALPHA T-ALPHA 02/26/74
122 99DEG T-ALPHA T-ALPHA 02/26/74
4HE(T,T)4HE EXCITATION FUNCTION LASL 75
LAB KINETIC ENERGY IN MEV

Fig. 2.

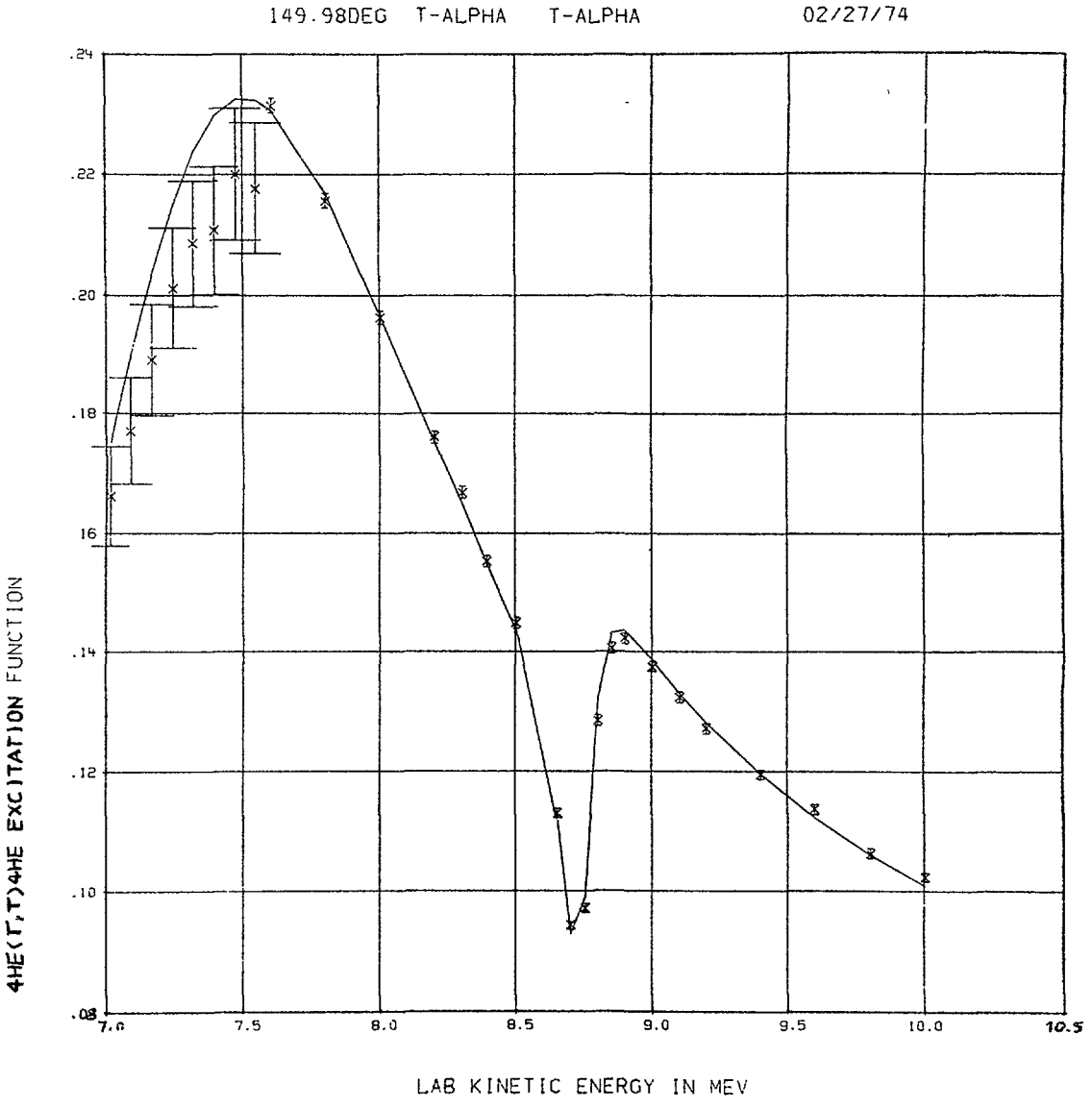
149.98DEG T-ALPHA T-ALPHA 02/27/74
4HE(T,T)4HE EXCITATION FUNCTION
.24
.22
.20
.18
16
.14
.12
.10
.08
7.0
7.5
8.0
8.5
9.0
9.5
10.0
10.5
LAB KINETIC ENERGY IN MEV

Fig. 3.

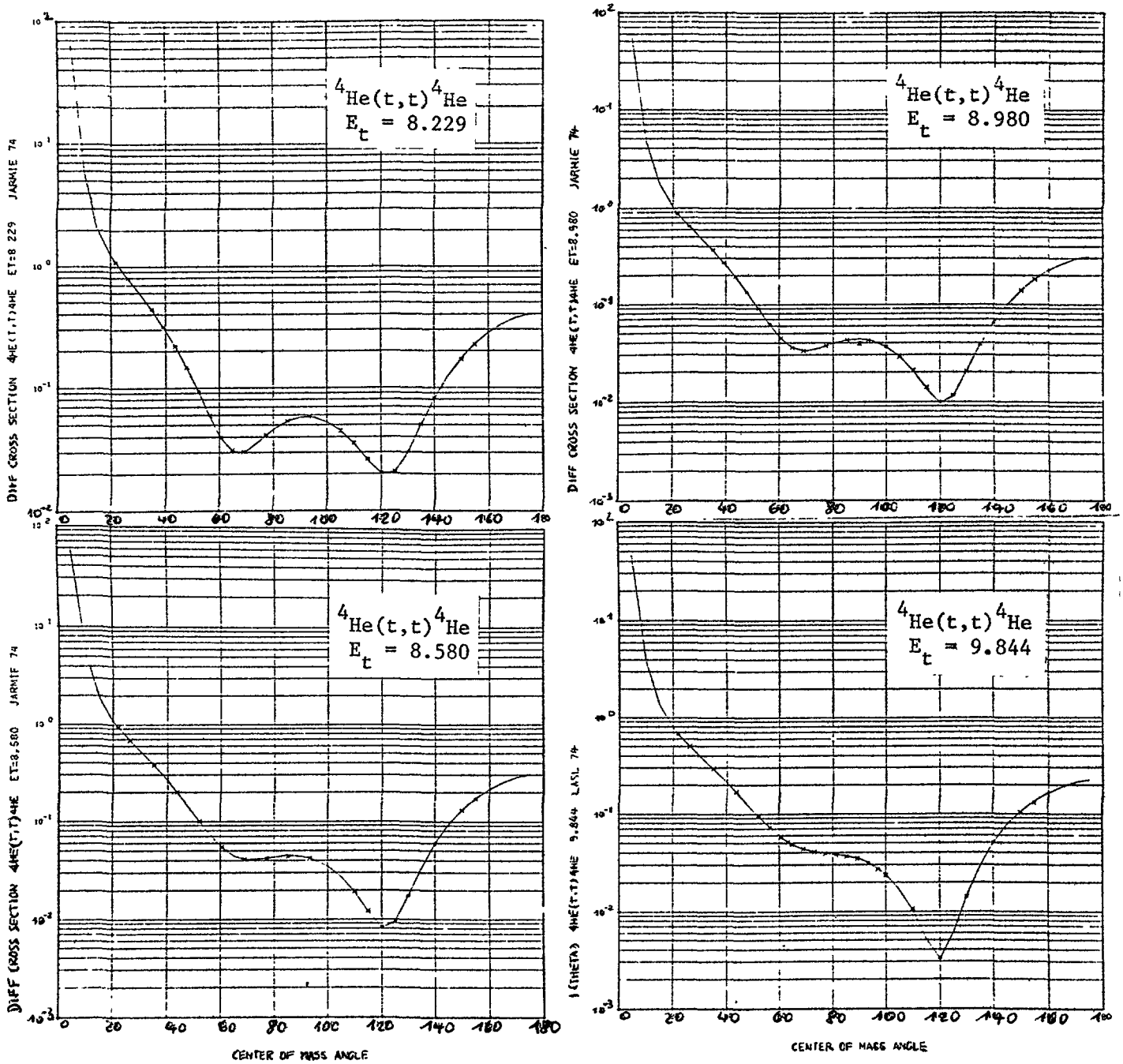
$^4He(t,t)^4He$
E_t = 8.229
$^4He(t,t)^4He$
E_t = 8.980
$^4He(t,t)^4He$
E_t = 8.580
$^4He(t,t)^4He$
E_t = 9.844
DIFF CROSS SECTION 4HE(T,T)4HE ET=8.229 JARMIE 74
DIFF CROSS SECTION 4HE(T,T)4HE ET=8.980 JARMIE 74
DIFF CROSS SECTION 4HE(T,T)4HE ET=8.580 JARMIE 74
I(THETA) 4HE(T,T)4HE 9.844 LASL 74
CENTER OF MASS ANGLE
CENTER OF MASS ANGLE

Fig. 4.

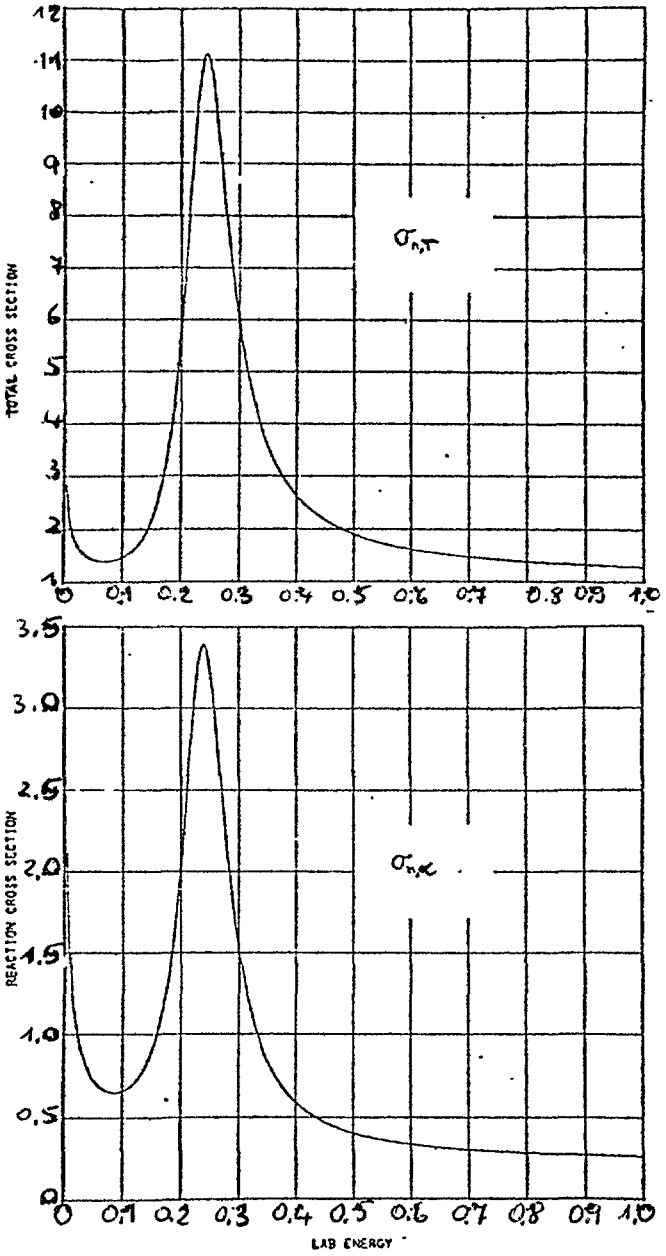

Fig. 5. Predicted values of the neutron total cross section (upper curve) and of the $^{6}Li(n,\alpha)$ reaction cross section (lower curve).

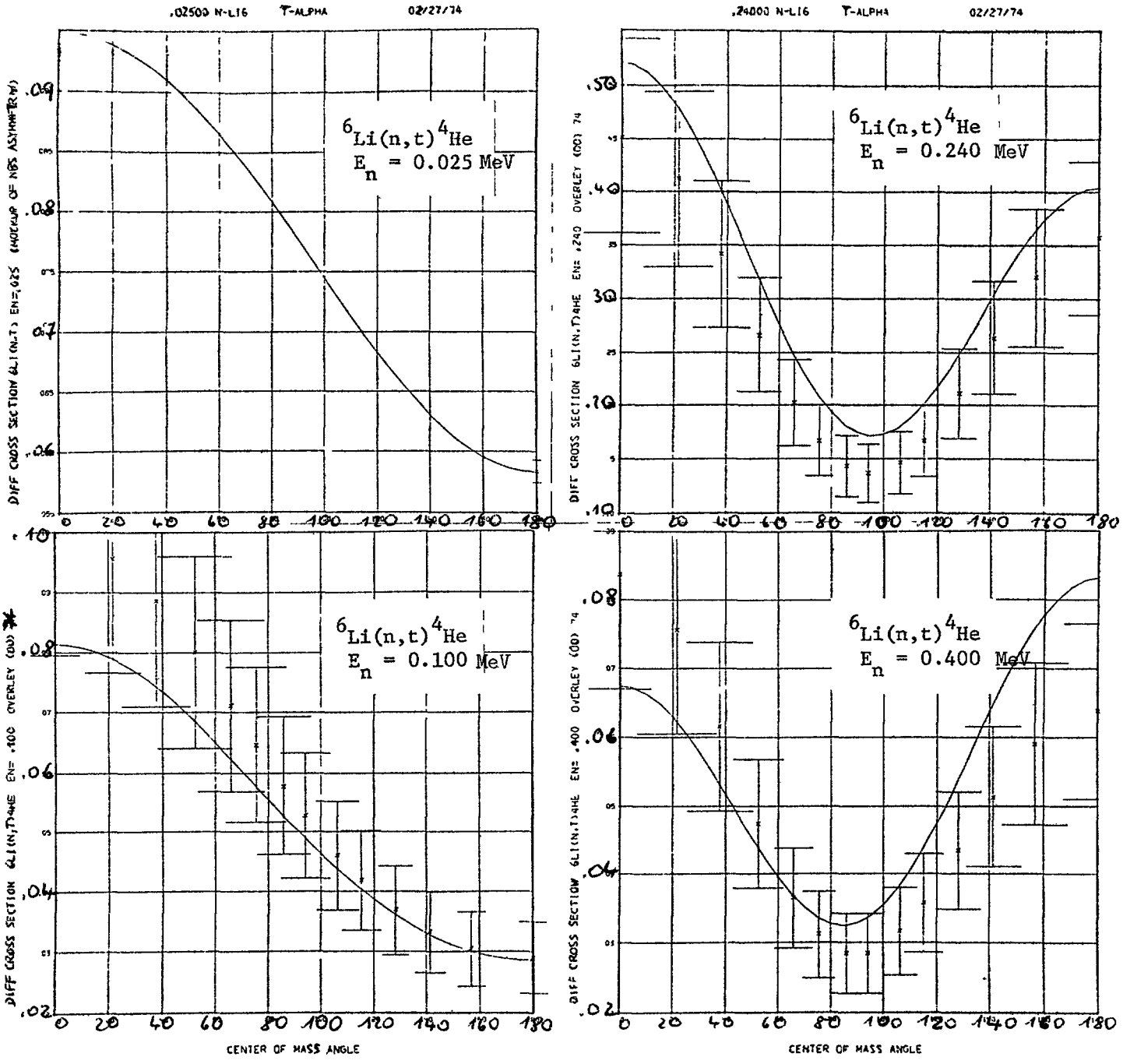
.02500 N-LI6 T-ALPHA 02/27/74
$^6Li(n,t)^4He$
E_n = 0.025 MeV
.24000 N-LI6 T-ALPHA 02/27/74
$^6Li(n,t)^4He$
E_n = 0.240 MeV
$^6Li(n,t)^4He$
E_n = 0.100 MeV
$^6Li(n,t)^4He$
E_n = 0.400 MeV
CENTER OF MASS ANGLE
CENTER OF MASS ANGLE

Fig. 6.

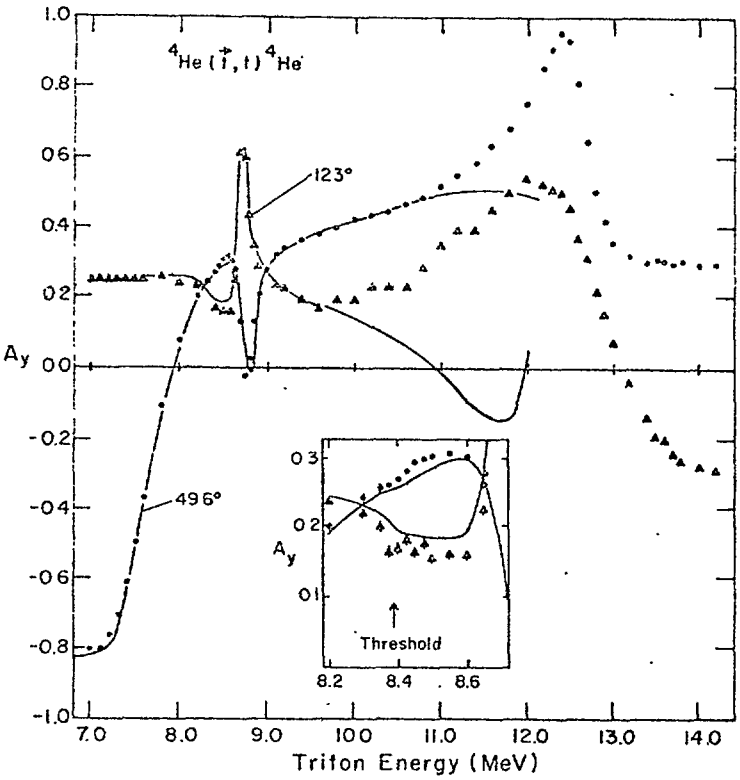
^{4}He ($\vec{t}$, t) ^{4}He
123°
49.6°
A_y
Threshold
Triton Energy (MeV)

(a)

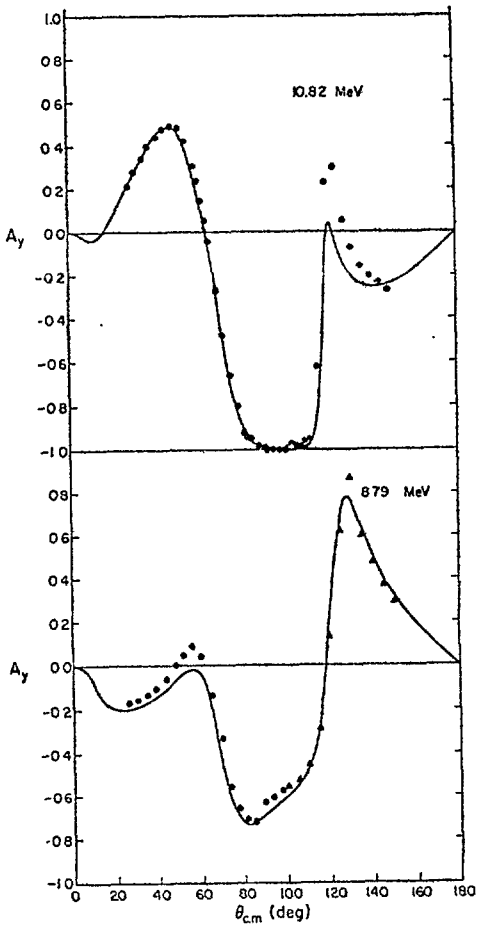
10.82 MeV
8.79 MeV
A_y
θ_{cm} (deg)

(b)

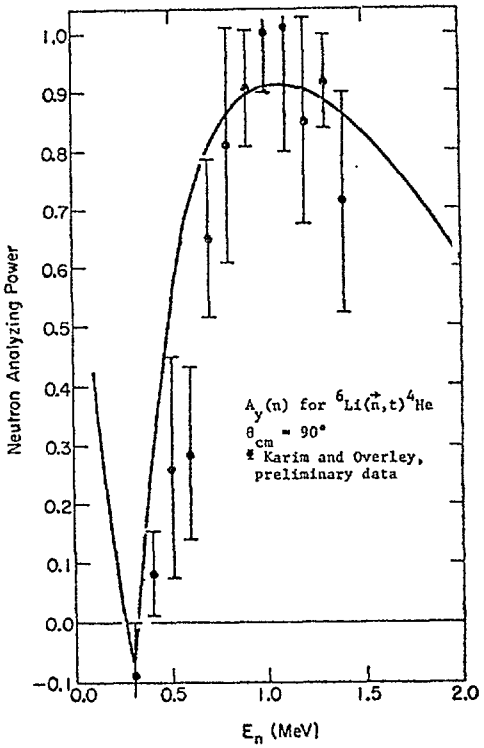
Neutron Analyzing Power
A_y(n) for ^{6}Li($\vec{n}$,t)^{4}He
θ_{cm} = 90°
* Karim and Overley, preliminary data
E_n (MeV)

(c)

Fig. 7.

Contributed Paper No. 2

PHOTON STRENGTH FUNCTIONS

Ingvar Bergqvist
Institute of Physics
University of Lund, Lund, Sweden

ABSTRACT

Methods for extracting photon strength functions are briefly discussed. We follow the Brink-Axel approach to relate the strength functions to the giant resonances observed in photonuclear work and summarize the available data on the E1, E2 and M1 resonances. Some experimental and theoretical problems are outlined.

1. INTRODUCTION

The main features of the photon strength distributions are well established. We know that most of the strength of the most important multipoles is localized to particular energy regions. The distributions exhibit resonance shapes and we label them as giant resonances. The basic properties of the giant E1 resonance (GDR) are well established and will be briefly reviewed. Experimental work is in progress to determine the localization and strength of the giant E2 resonance (GQR) as well as of the giant M1 resonance.

The energy region of primary interest in neutron reactions is around and below the neutron binding energy which is well below the peak of the GDR and GQR . Unfortunately, very little information from photonuclear work is available in this energy region and, in the general case, the photon strength has to be estimated. We shall follow the approach of Axel [1] for the extrapolation of the photon strength into the bound energy region. In applications to neutron radiative reactions a further assumption has to be made in order to describe γ-ray transitions to excited states. This assumption, referred to as the Brink hypothesis [2], states that each excited state has built on it a giant resonance identical to that for the ground state but shifted upward in excitation energy by the energy of the particular state. Employing these assumptions, a γ-ray strength function can be derived to form a basis for comparisons with experimental results on average strengths of radiative transitions.

This field has recently been surveyed in an excellent review paper by Bartholomew et al [3]. Important aspects of the concept have also been illuminated in recent conference reviews, e.g. Jackson [4] and Khanna and Bartholomew [5]. Comparisons with recent experimental results are in progress.

2. THE BRINK-AXEL APPROACH

The γ-ray strength function is defined [3] as the average reduced width for transitions of a particular multipole type. For a transition of multipole XL (L is the multipolarity) and energy E_γ from a level at E_λ of spin and parity J^π, the strength function is

$$f(E_\gamma) = \frac{\overline{\Gamma_{\gamma i}}}{E_\gamma^{2L+1}} \rho_J(E_\lambda)$$

where $\overline{\Gamma}_{\gamma i}$ is the partial γ-ray width averaged over states with spin and parity J^π in the neighbourhood of E_λ and $\rho_J(E_\lambda)$ is the level density for such states.

The strength function for ground state transitions can be related to the photo-absorption cross section, $\overline{\sigma}_{\gamma a}$ in b, by

$$f(E_\gamma) = 26 \cdot 10^{-5} \frac{\overline{\sigma}^J_{\gamma a}(E_\gamma)}{g_J E_\gamma^{2L-1}} \quad (\text{MeV})^{-(2L+1)}$$

where $g_J = \frac{2J+1}{2J_o+1}$ and $\sigma^J_{\gamma a}(E_\gamma)$ is the average absorption cross section of a nucleus with ground state spin J_o for the excitation of levels with spin J at energy $E_\lambda = E_\gamma$. The total observed absorption cross section, $\overline{\sigma}_{\gamma a}$, for the considered multiple XL is the sum of all contributing $\overline{\sigma}^J_{\gamma a}$. For E1 transitions one generally assumes [2] that

$$\overline{\sigma}^J_{\gamma aE1} = \frac{g_J}{3} \overline{\sigma}_{\gamma aE1}$$

The idea of the Brink-Axel approach is to apply the relation for transitions from the ground state to any excited state λ not only for transitions from the excited state λ to the ground state but also for those to other excited states. This implies that all levels are treated equally and only the average statistical properties of the levels are

considered. Single-particle effects, for example, which are of dominating importance in reactions of direct type, have to be dealt with separately.

The γ-ray strength function is, thus, in this approach proportional to the photon absorption cross section, $\sigma_{\gamma a}$, and a pre-requisite for the approach is that this cross section can be obtained from available giant resonance data.

3. THE GIANT E1 RESONANCE

Perhaps the most remarkable feature of the E1 resonance is its localized nature, despite the fact that it occurs in the continuum with many decay channels open. The localization as a function of mass number is schematically shown in fig 1 which also indicates the localization of the E2 and M1 resonances. (The figure is taken from a review article by Hanna [6]). The E1 resonance occurs at an energy of about $77/A^{1/3}$ MeV in medium and heavy nuclei. In light nuclei, however, the energy of the resonance falls off below the dashed line at $63/A^{1/3}$ MeV, which indicates the suggested position of the isoscalar GQR.

The resonance energy $E \approx 77/A^{1/3}$ is close to the value predicted from the hydrodynamical model. In this model the photon absorption cross section may consist of one or two Lorentz curves.

$$\sigma(E) = \sum_{i=1}^{2} \frac{\sigma_i}{1+(E^2-E_i^2)^2/E^2\Gamma_i^2}$$

$$\sigma_o \equiv \int\sigma(E)dE = \sum_{i=1}^{2} \frac{\pi}{2}\sigma_i\Gamma_i$$

The strength of the GDR is often given in terms of the Thomas-Reiche-Kuhns formula (referred to as the classical dipole sum rule)

$$\sigma_o \equiv \int\sigma dE = 60\frac{NZ}{A} \text{ MeV-mb}$$

The experimental results in terms of this dipole sum rule are shown in fig 2. The general trend of the data integrated over the resonance is that the cross section for heavy nuclei exceeds the classical sum rule by a factor of about 1.3. In the medium range the experimental value is close to the sum rule and for light nuclei it falls below it.

Two Lorentz curves are required to fit the photo absorption cross section for a deformed nucleus and it is well established that the area under the higher energy peak is twice that under the lower energy peak.

In some light and medium-weight nuclei the GDR is observed to be relatively wide and in some cases there is evidence for two peaks separated by 3-4 MeV. This broadening is attributed to the isospin splitting of the resonance into two components, $T_>$ and $T_<$. This effect should have important consequencies for neutron reactions because an incident neutron should excite only the $T_<$ states of the formed nucleus (the $T_>$ states are isospin forbidden). We shall follow the work of Fallieros and collaborators [7] to obtain estimates of the positions and relative strengths of the two components.

The $T_> = T+1$ and the $T_< = T$ components are displaced upward and downward with respect to the center of the dipole resonance by the symmetry energy term and the energy difference can be written as

$$\Delta E = E_> - E_< \simeq \frac{V}{A}(T+1); \quad T = \frac{N-Z}{2}$$

V is nearly the same as the strength of the isospin part of the optical potential. From the experimental data one obtains

$$V \simeq 60 \text{ MeV}$$

which has been shown by Fallieros and collaborators to correspond to a single-particle value around $V \simeq 100$ MeV.

The ratio of the strengths is given by

$$\frac{S(T_>)}{S(T_<)} \simeq \frac{1}{T} \left(\frac{1-1.5\ T/A^{2/3}}{1+1.5/A^{2/3}} \right)$$

From these formulas one obtains the energy splitting and strength ratio for the following examples (taken from Paul, ref [7])

	^{13}C	^{42}Ca	^{60}Ni	^{88}Sr	^{142}Nd	^{208}Pb
T	1/2	1	2	6	11	22
ΔE	6.9	2.9	3.0	4.8	5.1	6.6
$\frac{S(T_>)}{S(T_<)}$	1.4	0.8	0.4	0.08	0.03	0.003

We note that the energy separation is at least of the order of the width of the GDR and therefore the two components should be relatively easy to separate and identify. The $T_<$ component is expected to carry the dominating part of the GDR strength in heavy nuclei whereas the strength of the $T_>$ component, which should not be excited in neutron reactions, is appreciable in medium-weight nuclei and becomes at least as large as the $T_<$ strength in light nuclei.

In conclusion, the basic properties of the GDR are generally quite well established. The experimental photon absorption cross sections can be fitted with one or two Lorentz curves except for some (in particular light) nuclei which exhibit a more complex resonance structure. Thus, for estimates of the photon strength in the energy region of most interest in neutron reactions, i.e. close to the neutron binding energy and below, we strongly recommend to use the experimental data on GDR and Lorentz curves to provide predictions for the shape and magnitude of the strength function.

4. THE GIANT E2 RESONANCE

The observation some years ago of a compact isoscalar E2 resonance just below the E1 resonance in experiments on inelastic electron and proton scattering has started a considerable activity to establish the properties of this resonance. The results from various experiments are still contradic-

tory in many cases but some systematic trends seem to be possible to distinguish. In heavy nuclei, say A > 40, the E2 resonance is localized at about $63/A^{1/3}$ MeV in agreement with predictions of Bohr and Mottelson and recent shell-model calculations. It is expected that the resonance exhausts the isoscalar E2 sum rule (Gell-Mann - Telegdi sum rule)

$$\sigma_{-2} \equiv \int \frac{\sigma}{E^2}\, dE \simeq 0.22\, \frac{Z^2}{A^{1/3}} \quad \text{mb/MeV}$$

except for the strength related to the well-known first excited 2^+ state, which carries about 10% of the sum rule strength. However, only a fraction of this strength has been observed in several cases which indicates that the E2 strength might be spread over a wider energy region. In light nuclei, it now seems well established that the E2 strength is distributed over a very wide energy region extending from bound energies up to or above the E1 resonance.

5. THE GIANT M1 RESONANCE

Information on the giant M1 resonance is rather extensive for light and medium-weight nuclei but still scarce for heavy nuclei. The major strength comes from spin-flip transitions of nucleons with maximum orbital angular momentum and it is observed for light nuclei that this strength is concentrated to rather few levels - sometimes only one or two levels. The experimental results for heavy nuclei indicate that the M1 strength is spread in a similar way as the E1 strength but the data are incomplete and at present no systematic comparison can be made.

The M1 strength appears to be localized mainly in the energy region between about $30/A^{1/3}$ and $45/A^{1/3}$ MeV. From the results on light nuclei one might infer that the strength exhausts the M1 sum rule. This corresponds to an integrated strength which is roughly two orders of magnitude lower than that of the E1 strength. However, the localization of the M1 strength - on

the low-energy tail of the E1 resonance rather close to the neutron binding energy - may imply that it is important to consider this strength in neutron reactions. Its importance is closely related to the spreading of the strength but, as mentioned above, data are incomplete and much more work needs to be done in heavy nuclei.

6. EXPERIMENTAL METHODS

Several methods can be employed to experimentally test the validity of the concept of photon strength function and to determine the form and magnitude of the function in the photon energy region not readily available to photon absorption work.

The methods related to neutron reactions include high-resolution (GeLi) spectroscopy of γ-rays from neutron resonance capture in which partial radiation widths of primary transitions are determined. Thus, the absolute magnitude of the γ-ray strength can be obtained. However, the energy range is rather limited because of resolution and difficulties in multipolarity and primary assignments. The measurements have to be made for many neighbouring resonances to reduce Porter-Thomas fluctuations. Alternatively, the average γ-ray spectra following the capture of neutrons with an energy spread large enough to span many resonances, can be measured to give average relative intensities of transitions to particular final states. Absolute calibration can be achieved by normalizing to the thermal capture spectrum.

The gross-structure shape of a γ-ray spectrum, e.g. from neutron capture, can be utilized to yield information on the energy dependence of the γ-ray strength function over a wide energy region. Based on the assumption of a statistical γ-ray decay from any excitation energy region, a strength function can be found to give agreement with the observed spectral shape. The method has been observed to work surprisingly well in heavy nuclei. An extension of this method is the "sequential extraction method" in which

the γ-ray decay from each of a complete set of contiguous energy intervals is measured in the same experiment such as the (d,pγ) coincident experiments. Hence, it is possible to unfold the primary γ-ray spectrum for each energy interval and to deduce a relative strength function. To obtain absolute values of the strength function, normalization is made to the results from neutron resonance capture.

Other methods include studies of elastic and inelastic scattering of γ-rays and of photoneutron reactions just above the neutron separation energy.

RESULTS

The results from various methods to determine the γ-ray strength functions in nuclei with $A \gtrsim 90$ have recently been reviewed by Bartholomew et al [3]. In a few cases experiments with different methods have been performed on the same target nucleus. One such exampel is ^{181}Ta, for which the results are shown in fig 3. The strength functions shown by open circles in 3a and in 3b were obtained by fitting the experimental (n,γ) spectra from thermal capture and from 0.7 and 2.6 MeV neutron capture, respectively. The strength function, represented by solid triangles was obtained from the sequential extraction method using the (d,pγ) reaction and the solid points are from average γ-ray intensities of individual transitions following capture of a $\sim$ 2 keV broad beam of neutrons. The strength functions obtained from the different methods are consistent within the uncertainties inherent in each method. The departure observed for the two curves from fast neutron capture may reflect experimental difficulties related to appropriate background subtraction. New experiments with improved signal-to-background ratio are in progress in an attempt to solve this problem.

The overall agreement is quite good between the experimental strength function for Ta and the Lorentzian tail of the giant dipole resonance

(dashed curve). Similarly, for some of the other nuclei, which have been studied, the energy dependence of the strength function is observed to follow that of the Lorentz curve, although in some of these cases the absolute magnitudes do not agree. The reason for this discrepancy is not known.

Considerable departure in the energy dependence from the Lorentz curve is observed for nuclei in the range $190 \lesssim A \lesssim 208$ and also, but less obvious, for nuclei in $110 \lesssim A \lesssim 134$. A well-known example is ^{197}Au, for which the experimental results are summarized in fig 4. In 4a the strength function deduced from photon elastic scattering (solid points) and, above threshold, from photoneutron measurements (open circles and triangles) is shown. Figures 4b and 4c give the results for the reactions ^{197}Au(n,γ) and ^{197}Au(d,pγ). The open circles represent here the strength function extracted by the spectrum fitting method from (n,γ) spectra, the solid triangles by the sequential extraction method and the solid circles by the high-resolution work on individual γ-ray intensities following capture of neutrons from a $\sim$ 2 keV broad beam.

The strength functions obtained from the different methods are consistent in the region of overlap, i.e. $E_\gamma \geq 4.8$ MeV. At about 6 MeV the absolute magnitude of the strength function is consistent with the Lorentz curve (dashed line), however, below 5 MeV the extracted strength functions depart significantly below the Lorentzian. In this representation, taken from Bartholomew et al [3], there is evidence for a maximum or pigmy resonance, peaking at $E_\gamma \approx 6$ MeV in ^{197}Au and ^{198}Au. Results from other work show a more pronounced resonance shape than indicated in fig 4. The differences can probably be ascribed to experimental difficulties, in particular related to the determination of an appropriate background. Preliminary results from an (n,γ) experiment by Earle, Bergqvist and Nilsson with improved signal-to-background ratio indicate a more distinctive resonance

than shown in fig 4.

It has been suggested [8] that these irregularities in the strength function is a result of a threshold effect which appears when the energies of the neutron particle states with low orbital angular momentum are close to the neutron threshold. Numerical calculations of this effect based on the shell model are now being performed by Zimányi and Csernai.

The empirical strength functions deduced by spectrum fitting methods are mixtures of all multipoles. However, there is experimental evidence that the decay of levels excited by neutron capture is dominated by dipole transitions but in these methods there has been no attempt to separate the E1 and M1 contributions. The information on the energy dependence of the M1 strength is rather fragmentary. In some nuclei, resonance-averaged measurements exhibit an E_γ^5 energy dependence for M1 parallell to that for E1 radiation. A representative exemple is the result for Ta (by Bollinger, Erskine and Thomas quoted by Jackson [4]). Some other results indicate a peaking of the strength between 7 and 9 MeV. However, much more data are required to establish the properties of the M1 strength function.

Almost no data on the E2 strength are available.

NON-STATISTICAL EFFECTS IN NEUTRON CAPTURE

Most of the non-statistical effects that have been found in low-energy neutron capture are in s-wave capture for nuclei with A = 35-65 and p-wave capture for A = 90-100. For reviews of these effects, see Lane [8], Mughabghab [9] and Chrien [10]. The resulting γ-ray spectra are often dominated by a few γ-ray lines to levels with large neutron single-particle strength. It may seem meaningless in these cases to discuss the statistical concept of photon strength function. Nevertheless, we think that it should be worthwhile to investigate the applicability of the Brink-Axel approach also to nuclei with A < 90.

The neutron capture reactions at energies above about 5 MeV have been observed to proceed by direct and semidirect processes. Work is in progress to find an appropriate theoretical description of these effects (see ref [11]).

REFERENCES

[1] P. Axel, Phys. Rev. 126 (1962) 671

[2] D.M. Brink, Doctoral Thesis, Oxford University (1955)

[3] G.A. Bartholomew, E.D. Earle, A.J. Ferguson, J.W. Knowles and M.A. Lone, Advances in Nuclear Physics 7 (1974) 229

[4] H.E. Jacson, Proc. of the EANDC Topical Discussion on "Critique of Nuclear Models and their Validity in the Evaluation of Nuclar Data" Tokyo 1975, p. 119

[5] G.A. Bartholomew and F.C. Khanna, 2nd Symp. on Neutron Catpure Gamma Ray Spectroscopy and Related Topics, Petten 1974, p. 119

[6] S.S. Hanna, Proc. Int. Conf. on Nuclear Structure and Spectroscopy, Amsterdam 1974, Vol. 2 p. 249
Experimental data taken from
E.G. Fuller, H.M. Gerstenberg, H. Vander Molen and T.C. Dunn, Photonuclear Reaction Data, NBS Special Publication 380 (1973)

[7] Review papers by S. Fallieros and by P. Paul, Proc. Int. Conf. on Photonuclear Reactions and Applications, Asilomar 1973, p. 401 and 407

[8] A.M. Lane, 2nd Int. Symp. on Neutron Capture Gamma Ray Spectroscopy and Related Topics, Petten 1974, p. 31
J. Zimányi and B. Gyarmati, Int. Symp. on Correlation in Nuclei, Balatonfüred 1973, OMKDK Budapest 1974, p. 313
B. Gyarmati, A.M. Lane and J. Zimányi, Phys. Lett. 50B (1974) 316

[9] S.F. Mughabghab, 2nd Int. Symp. on Neutron Capture Gamma Ray Spectroscopy and Related Topics, Petten 1974, p. 53

[10] R.E. Chrien, 2nd Int. Symp. on Neutron Capture Gamma Ray Spectroscopy and Related Topics, Petten 1974, p 247

[11] I. Bergqvist, 2nd Int. Symp. on Neutron Capture Gamma Ray Spectroscopy and Related Topics, Petten 1974, p. 199

FIGURE CAPTIONS

1. Location of giant resonances (from ref. [6]).

2. Integrated absorption cross section normalized to the classical dipole sum rule (from Fuller et al. [6]). Solid points were obtained from integrating Lorentz line fits to neutron production cross section data. Open circles and squares are from total absorption cross section measurements with integration taken to 30 MeV for circles and to 140 MeV for squares.

3. Photon strength function for Ta (from ref. [3]) derived from Lorentz curves fitted to the observed giant dipole resonance (dashed curve) compared to the results of different experiments (see text).

4. Photon strength function for Au (from ref. [3]) derived from Lorentz curves fitted to the observed giant dipole resonance (dashed curve) compared to the results of different experiments (see text).

5. Energy dependence of the average intensities of γ-rays to individual states in ^{182}Ta (from ref. [4]).

Figure 1

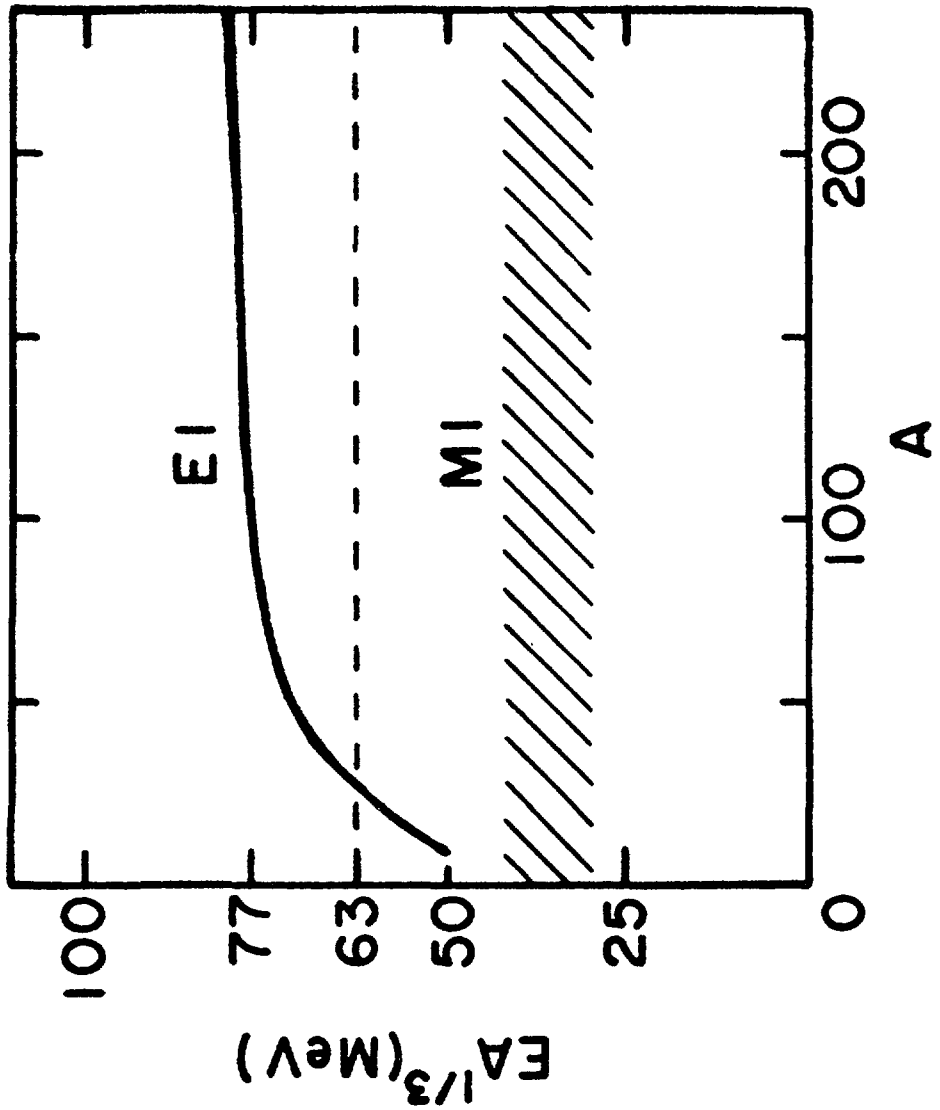

Figure 2

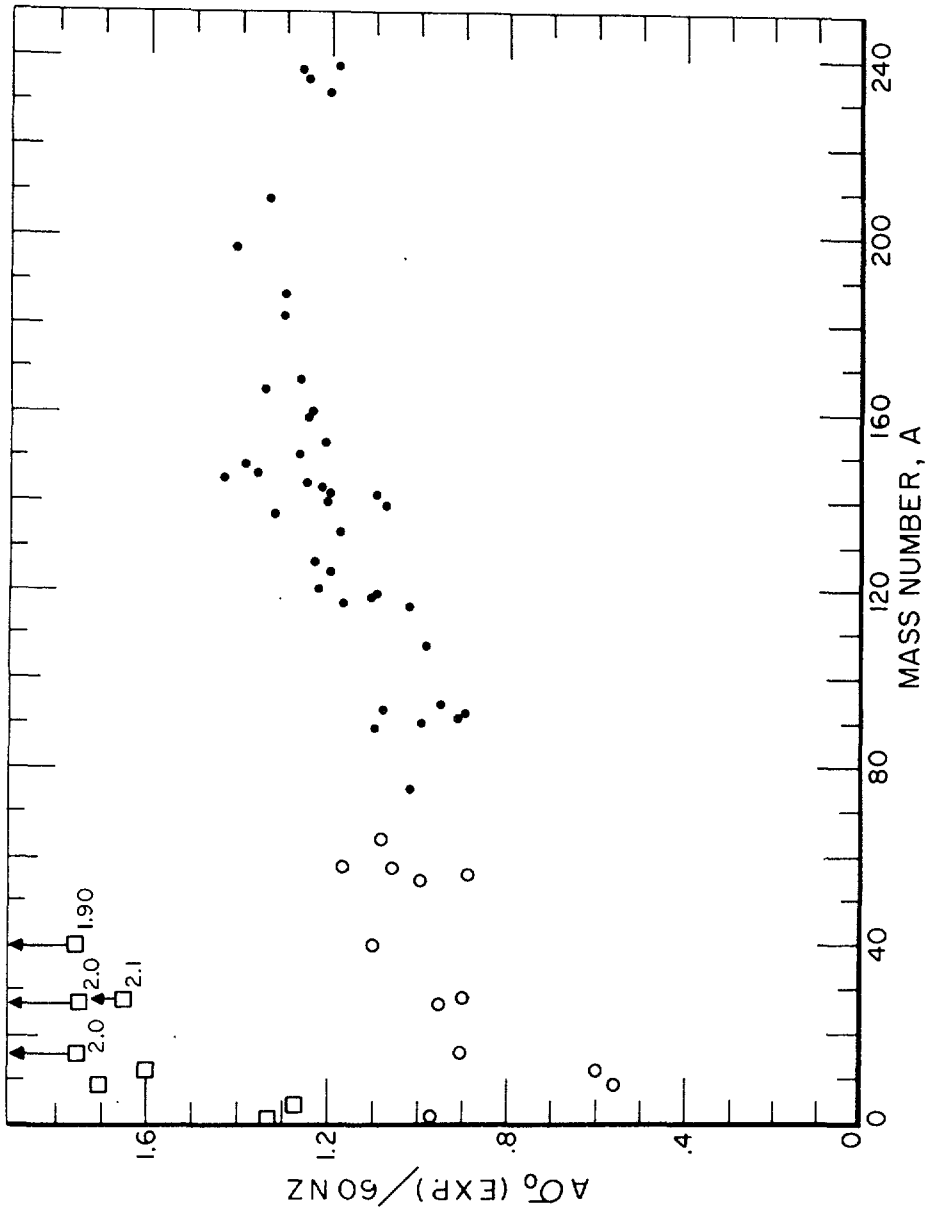
$A\sigma_o$ (EXP)/60NZ
0
.4
.8
1.2
1.6
0
40
80
120
160
200
240
MASS NUMBER, A
1.90
2.0
2.1
2.0

Figure 3

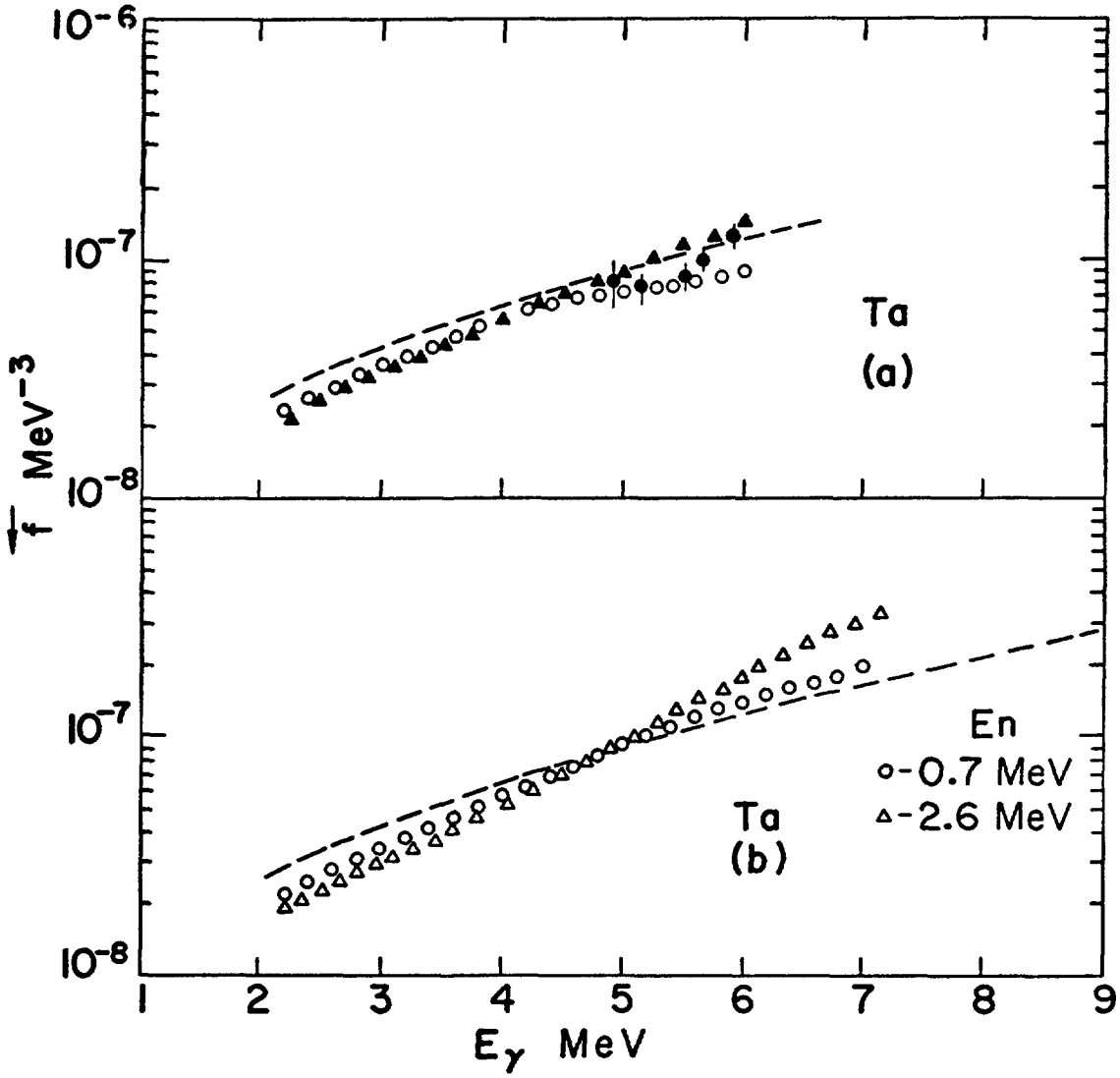
10⁻⁶
10⁻⁷
10⁻⁸
f MeV⁻³
Ta
(a)
10⁻⁷
10⁻⁸
En
o-0.7 MeV
Δ-2.6 MeV
Ta
(b)
1
2
3
4
5
6
7
8
9
Eγ MeV

Figure 4

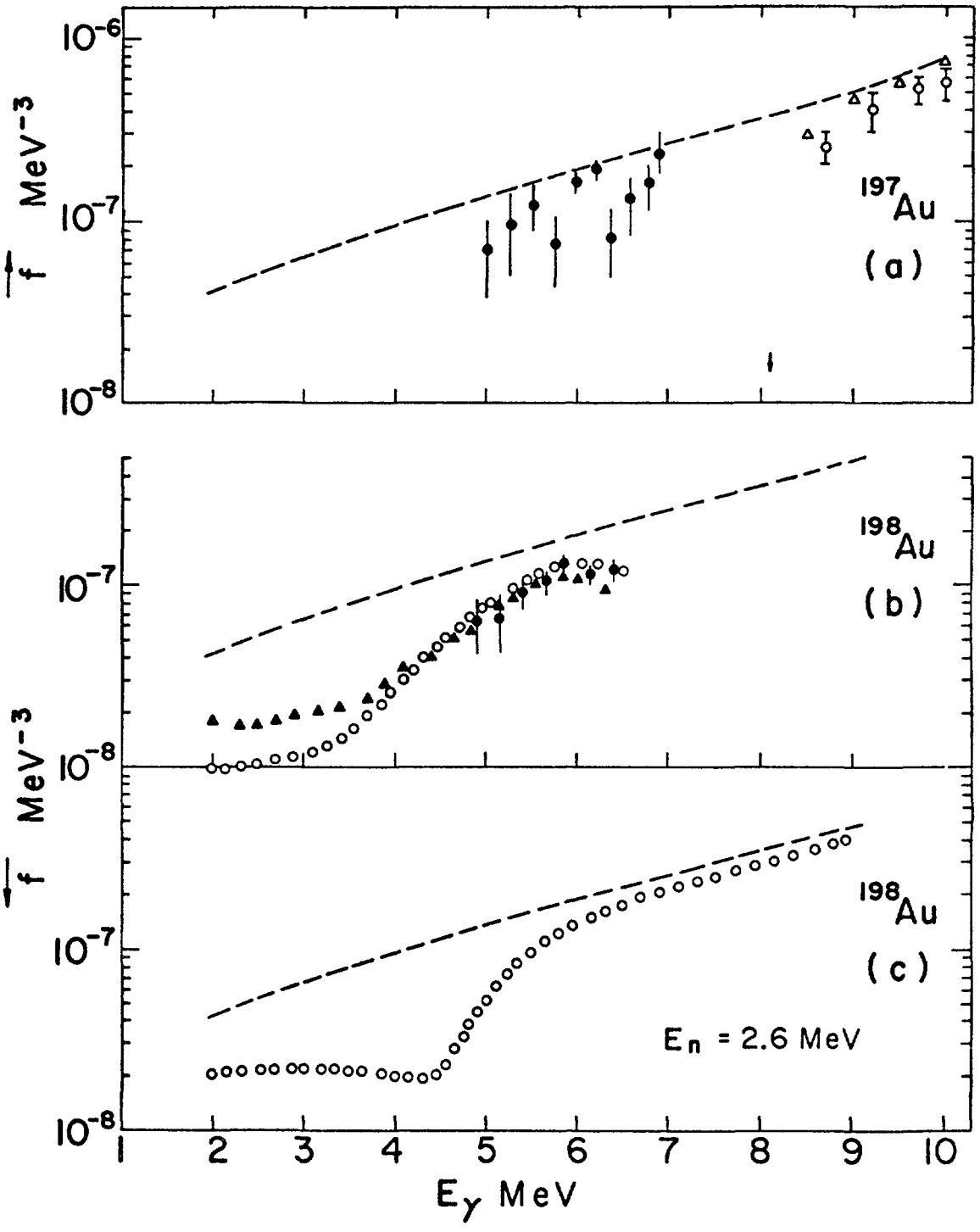
10^{-6}
10^{-7}
10^{-8}
$\bar{f}$ MeV^{-3}
^{197}Au
(a)
^{198}Au
(b)
^{198}Au
(c)
E_n = 2.6 MeV
1
2
3
4
5
6
7
8
9
10
E_γ MeV

Figure 5

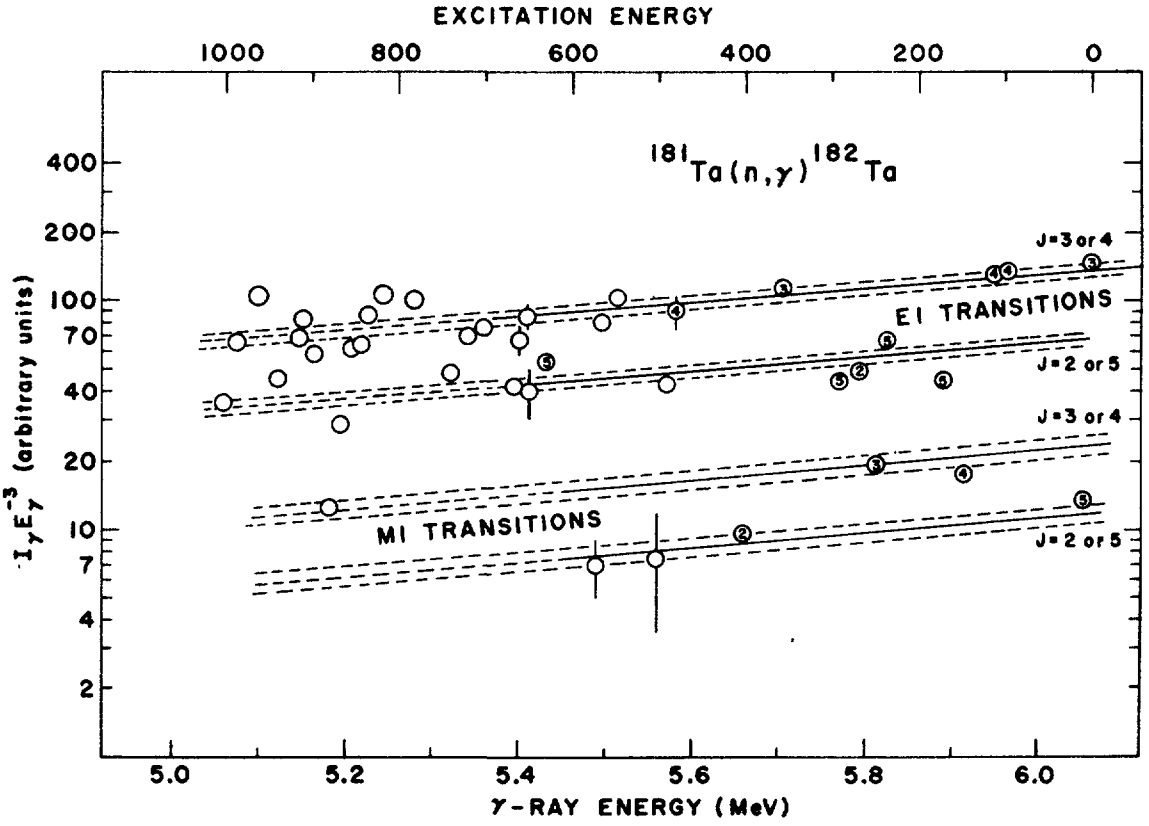

Next page(s) left blank

On Threshold Effects in the Statistical Distribution of Neutron Capture Widths

I. Rotter, H.W. Barz, Zentralinstitut für Kernforschung Rossendorf bei Dresden, GDR,
J. Höhn, Technische Universität Dresden, GDR.

Abstract

The following effects are investigated: (i) The existence of threshold states, i.e. states in the neighbourhood of decay thresholds which are not connected with states of the compound nucleus. (ii) The existence of a shift of the resonance states which is generated by a threshold and can lead to an accumulation of compound nucleus levels in the neighbourhood of thresholds. (iii) The existence of a mixing of the compound nucleus levels via the continuum which can lead to a systematic change of the widths and positions of the compound nucleus levels.

The calculations are performed for the $^{15}N+n$ reaction in the framework of the continuum shell model. The results obtained are discussed from the point of view of their influence on the statistical distribution of neutron capture widths.

1. Introduction

For statistical distributions of neutron widths the knowledge of the influence of dynamical effects on widths and positions of the decaying levels is necessary. Recently, a model calculation has been done [1] where the importance of single-particle resonances for the behaviour of the cross section near thresholds has been established. In order to investigate dynamical effects quantitatively calculations must be performed in which the complicated structure of the nuclear levels as well as the reaction mechanism are taken into account in a straightforward manner. Calculations of such a type are not carried out up to now. They can be done by using the coupled channel method [2] in the framework of the continuum shell model. This model is an extension of the usual shell model by including nucleon channels into the calculation from the very beginning. Resonance parameters like widths and positions of the resonance levels can be obtained. The results of

the calculations are exact in the framework of the model.

It is the aim of this paper to investigate the influence of the continuum on widths and positions of resonance levels in the continuum shell model (CSM) for the reaction ^{15}N+n. The single particle $d_{3/2}$ resonance is treated like a bound state up to a cut-off radius in order to define the space of bound states in analogy to the configuration space of the usual SM. The method of calculation is given in sect. 2 of the paper while the effects investigated and the results obtained are described in the following sections. Some conclusions are drawn in sect. 6.

2. The calculations

The basic equations of the model are given in refs. [2,3]. Using the projection technique, the whole wave function of the model is given by

$$\psi = \xi + \sum_R (\tilde{w}_R - \tilde{\phi}_R) \frac{1}{E_R - \frac{i}{2}\Gamma_R - E} \langle \tilde{\phi}_R^* | H_{QP} | \xi \rangle . \qquad (1)$$

Here, $H_{QP} \equiv QHP$, while $P+Q=1$ are the projection operators and H the Hamiltonian. The functions ξ and $\tilde{w}_R$ are solutions of the equations

$$(H_{PP} - E)\,\xi = 0 \qquad (2)$$

$$(H_{PP} - E)\,\tilde{w}_R = H_{PQ}\,\tilde{\phi}_R , \qquad (3)$$

resp. The wave functions $\tilde{\phi}_R$ are eigenfunctions of the operator

$$H_{QQ}^{eff} = H_{QQ} - H_{QP}\,\frac{1}{H_{PP} - E}\,H_{PQ} \qquad (4)$$

which is effective in the Q space. The eigenvalues of H_{QQ}^{eff} are denoted by $E_R - \frac{i}{2}\Gamma_R$. They contain the positions E_R and the widths

Γ_R of the resonance levels.

The method of numerical calculations consists in solving the usual SM problem

$$(H_{QQ} - E_{sh})\,\phi_R = 0, \qquad (5)$$

which gives the eigenvalues E_{sh} and the eigenfunctions ϕ_R of the operator H_{QQ}. Using these values, the equations (2) and (3) are solved with the coupled channel method [2,3].

The numerical calculations reported here are performed for the $^{15}N+n$ reaction. The SM structure for the intermediate nucleus ^{16}N and the target nucleus ^{15}N is obtained in the 1p-1h and 2p-2h configuration spaces and the 1h and 1p-2h configuration spaces, resp., by using a δ -force for the nucleon-nucleon interaction,

$$V(\vec{r}_1 - \vec{r}_2) = V_o\,(a + b\,P^{\sigma}_{12})\,\delta(\vec{r}_1 - \vec{r}_2). \qquad (6)$$

The parameters are $V_o = 500$ MeV/fm^3, $a = 1{,}0$, $b = 0.05$. The parameters of the Woods-Saxon potential are the same as in paper [2]. Together with the bound states the single-particle $d_{3/2}$ resonance is included in the Q-space up to the cut-off radius 7.5 fm, while the remaining part and the scattering states define the P-space. In some calculations, the SM energies E_{sh} of the resonance levels are chosen different from the eigenvalues of H_{QQ}. The SM wave functions ϕ_R, however, are not changed in all cases. The continuum is restricted to $l \leq 6$ in the coupled channel calculations.

3. Threshold states

Several years ago Baz [4] has shown that in the neighbourhood of thresholds the cross section of neutron scattering reactions may have a resonance - like behaviour which is not connec-

ted with the formation of an intermediate nucleus. The question whether those threshold states can be seen in the real cross section is not clarified up to now.

In fig. 1, the direct reaction cross section of the reaction $^{15}N_o(n,n)^{15}N_o$ corresponding to $J = 0^+$ is shown. The cross section is reduced at all energies where a new channel opens.

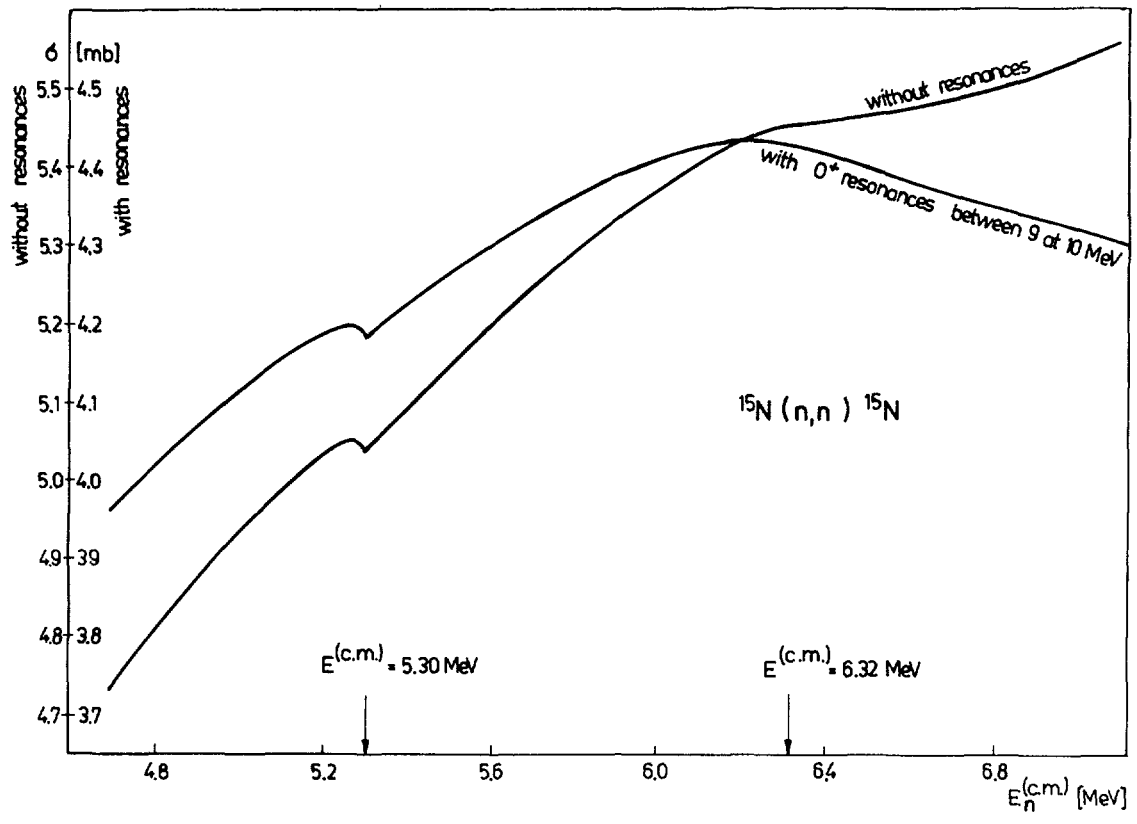

Fig. 1

The direct reaction part of the elastic $^{15}N+n$ ($J^{\pi} = 0^+$) scattering. The three inelastic channels correspond to the $5/2^+$ and $1/2^+$ states of ^{15}N at 5.30 MeV and to the $3/2^-$ state at 6.32 MeV.

The effect is, however, very small. It amounts to 0.3 % deviation in the cross section in the very neighbourhood of the thresholds

at 5.30 MeV. No effect at all could be seen in the inelastic channels of the same reaction and even in the elastic channel corresponding to $J = 1^-$.

The threshold effect in the direct reaction part will be diminished or amplified by threshold effects [5] in the widths $\Gamma(E)$. In fig. 1, the elastic cross section of $^{15}N_o(n,n)^{15}N_o$ is shown also for a case in which the resulting threshold effect at 5.30 MeV is maximal. The six 0^+ resonance levels which are included in the calculation are lying between 9 and 10 MeV. A resonance-like behaviour of the cross section results like in the case without resonances which is a pure threshold effect. It is, however, very small in comparison with real resonances.

The threshold effect in the elastic cross section of the neutron scattering on ^{15}N is connected in the main with the direct reaction part. It is small at the energies considered here. In nuclear reactions at higher energies in which the direct reaction part is larger the threshold effect may be larger and can lead to an additional resonance-like structure in the cross section. Surely, this structure will be covered by the high density of resonance states at these energies in realistic cases.

4. Shift of resonance states to thresholds

An effect of another type may occur in the neighbourhood of thresholds, namely a shift of the resonance states in direction to thresholds and an enlargement of their widths. An example is shown in fig. 2. Here, the threshold energy of the channel corresponding to the $3/2^-$ level of ^{15}N is arbitrarily changed. The resonance at 6.4 MeV is shifted to lower energies if the threshold is at 5.66 MeV and to higher energies if the threshold is at 7.44 MeV (dotted lines of fig. 2). The shifts are small, however, and the widths are changing only a little (table 1) although the spectroscopic factor of the 6.4 MeV resonance in relation to the channel corresponding to the $3/2^-$ level of ^{15}N is not small.

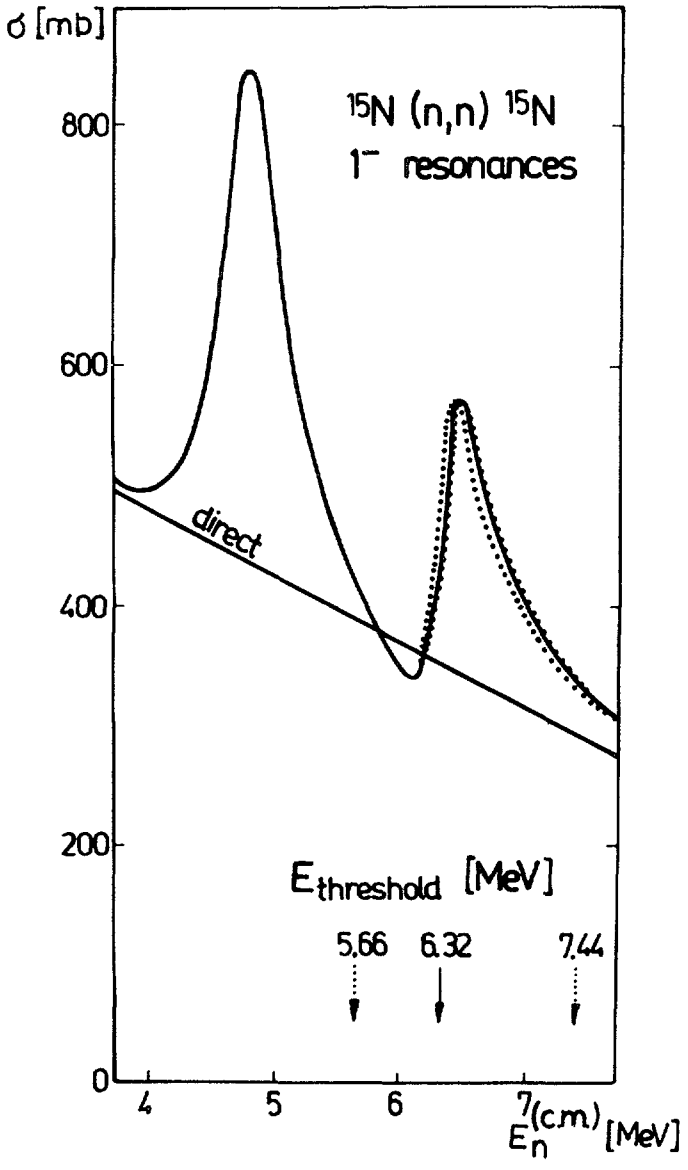

Fig. 2

The cross section of the ^{15}N+n reaction with two 1^- resonances. The calculations are performed with account of four channels corresponding to the $1/2^-$ ground state of ^{15}N, to the $5/2^+$ and $1/2^+$ states at 5.30 MeV and to the $3/2^-$ state at 6.32 MeV. The energy of the threshold corresponding to the $3/2^-$ state of ^{15}N has been chosen to be 6.32 MeV (experimental value, full line) as well as 5.66 MeV and 7.44 MeV (dotted lines).

Table 1

The shifts $E_R - E_{sh}$ and widths Γ_R of two 1^- resonance states in ^{16}N. The energy of the threshold corresponding to the $3/2^-$ state of ^{15}N is changed as in fig. 2.

$E_{threshold}^{(c.m.)}$	$E_R^{(c.m.)}=4.8$ MeV		$E_R^{(c.m.)}=6.4$ MeV	
	E_R-E_{sh}/MeV	Γ_R/keV	E_R-E_{sh}/MeV	Γ_R/keV
5.66	-0.220	282	-0.664	202
6.32	-0.219	281	-0.625	194
7.44	-0.219	279	-0.566	188

From these results it follows that thresholds have some influence on the position and the width of a resonance. The magnitude of the effect is, however, small in the case considered here. This is connected with the fact that the resonances have a complicated nuclear structure while the structure of the threshold is the simple particle + final nucleus structure in any case. The influence of a threshold on a resonance nearby depends not only on the energy but also on the overlap integral between the shell model wave functions of the threshold and of the resonance state. Therefore, it cannot be so large in the real case as one expects for resonances with a simple configuration.

5. The mixing of resonances via the continuum

The diagonal matrix elements

$$\langle \Phi_R / H_{QQ}^{eff} / \Phi_R \rangle = U_R - \frac{i}{2} V_R \qquad (7)$$

contain the energy U_R and the width V_R of the resonance level described by the SM wave function Φ_R. Here, the configuration

mixing of the discrete resonance states is taken into account like in a usual SM calculation. The channel coupling, i. e. the interaction of the resonance levels via the continuum, is considered in the eigenvalues $E_R - \frac{i}{2}\Gamma_R$ and eigenfunctions $\tilde{\Phi}_R$ following by a diagonalization procedure of H_{QQ}^{eff}.

In order to investigate the mutual mixing of the resonances via the continuum, the energies E_{sh} of some levels are changed arbitrarily relative to the energies of other levels. The distances between the levels are constant (200 keV). The wave functions Φ_R are taken from the SM calculation in every case without any change.

The widths V(E) and Γ (E) of a 0^+ resonance of ^{16}N are shown in fig. 3. The energies $E_{sh}^{(i)}$ of other 0^+ resonance levels are chosen in such a manner that $E_{sh}^{(1)} > E_{sh}^{(i)}$ (full line), $E_{sh}^{(1)} < E_{sh}^{(i)}$ (dashed line), and $E_{sh}^{(i)} < E_{sh}^{(1)} < E_{sh}^{(j)}$ (dotted and dash - dotted lines), respectively. As can be seen from these results, the width Γ of the resonance lying at the lowest energy is enlarged at the cost of the resonances lying at higher energies. This effect seems to be similar to the effect well known in structure calculations. Like in structure calculations, the lowest lying level is shifted to lower energies while the higher lying levels are shifted to higher energies so that the distance between the resonance levels enlarges by mixing via the continuum. This effect is larger if the resonances are more overlapping.
In fig. 4, the energies and widths of five 0^+ resonance levels are shown in the case in which the distance between them is changed. The shifts $U_R - E_{sh}$ and the widths V_R are independent of the distances between the resonances while $E_R - E_{sh}$ and Γ_R show the effects discussed above.

The results in fig. 3 show further that threshold effects are not important in the mixing of the resonances via the continuum. There can not be seen any enhancement of Γ in comparison with V in the neighbourhood of thresholds which would be larger than for other energies.

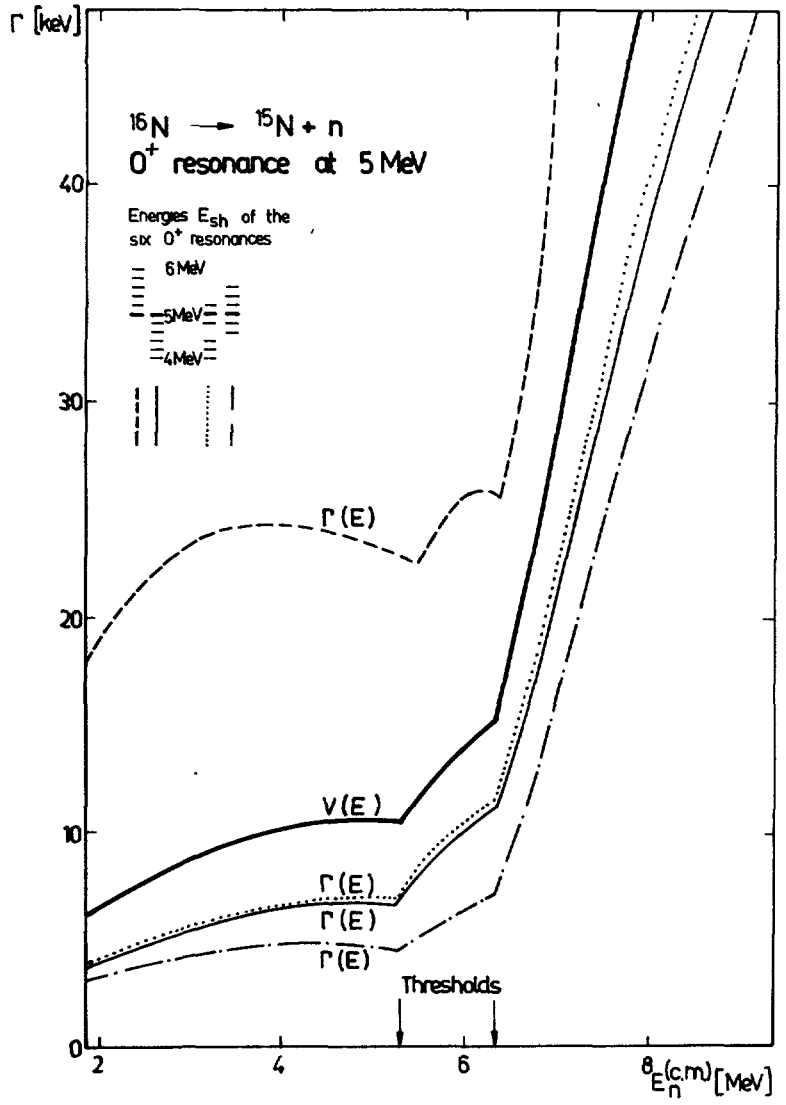

Fig. 3

The energy dependence of the widths V and Γ of a 0^+ resonance state in ^{16}N with account of four channels (s. fig. 2). The energies E_{sh} of five other 0^+ resonance states are given in the upper part of the figure. In the case of 5 MeV $\leq E_{sh} \leq$ 6 MeV, the energies $E_R^{(c.m.)}$ and widths Γ_R of all resonances are: 4.97 MeV - 23 keV, 5.03 MeV - 27 keV, 5.30 MeV - 88 keV, 5.53 MeV - 5 keV, 5.72 MeV - 4 keV, 5.99 MeV - 0.5 keV.

The mixing of the resonances via the continuum would be very different from that shown in figs. 3 and 4, if the single-particle $d_{3/2}$ resonance would not be included in the Q space of discrete states. The number of resonances would be changed as compared with the SM result and their energy shifts $E_R - E_{sh}$ and differences in the widths $\Gamma_R - V_R$ would be larger than in the calculations given here.

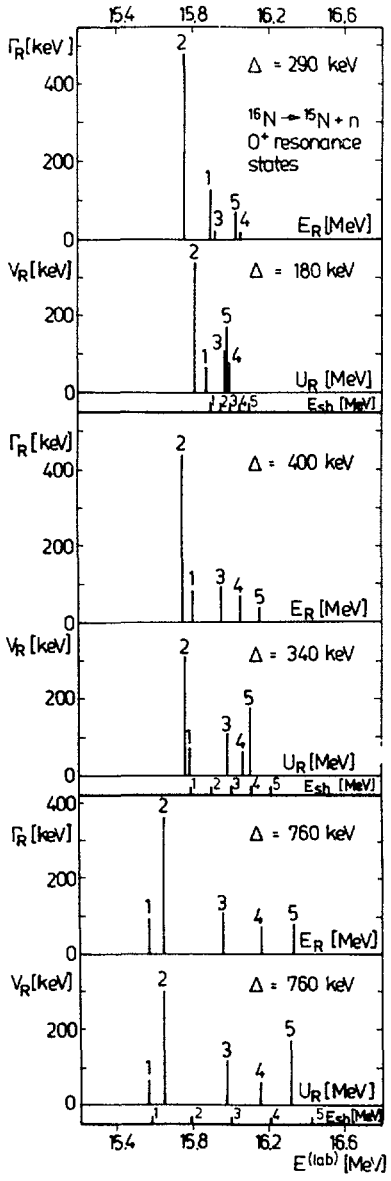

Fig. 4

The energies and widths of five 0^+ resonances in ^{16}N before the diagonalisation (U_R, V_R) and after the diagonalisation (E_R, Γ_R) of the operator H^{eff}_{QQ}. The distances between the SM energies E_{sh} are changed from 50 keV to 100 keV and 200 keV. The distance between the lowest and highest lying resonances is denoted by Δ. The calculation has been performed with account of four channels (fig. 2).

6. Conclusions

In this paper, the influence of the continuum on the resonance parameters of some resonance levels with realistic SM structure are investigated. The calculations, done for the ^{16}N nucleus in the framework of the CSM by using the coupled chan-

nel method, give results which are numerically exact. The results obtained may be summarized in the following manner.

(i) Threshold states are found in the direct reaction part of the cross section as well as in the partial cross section. The absolute magnitude of the effect is, however, very small.

(ii) A small shift of resonance levels towards thresholds can be observed as well as a small enhancement of the widths of these levels.

(iii) The influence of a threshold on a resonance nearby depends on the overlap integral between the wave functions of the threshold and of the resonance. The threshold does not enlarge this overlap integral even for resonances lying nearby.

(iv) The resonances are mixed via the continuum also in the case if the overlapping is vanishing small. All important parts of the wave functions inside the nucleus are taken into account by the cut-off-technique for single-particle resonances in diagonalizing H_{QQ} so that the mixing obtained here is additional to the configuration mixing obtained in a usual SM calculation. The mixing via the continuum enlarges effectively the widths of the low lying 0^+ resonance levels and reduces the widths of the 0^+ resonances lying at higher energies. Moreover, the low-lying levels are pushed down and the high-lying levels up.

From these results the conclusion can be drawn that threshold effects do not play any deciding role in the distribution of nucleon decay widths. Effects, however, which are coming from the continuum mixing may lead to systematic changes of the resonance parameters.

References

1. I. Lovas, E. Dénes, Phys. Rev. C7 (1973) 937

2. H.W.Barz, I. Rotter, J. Höhn, Phys. Letters 37B (1971) 4

3. I. Rotter, H.W. Barz, R. Wünsch, J. Höhn, Particles and Nucleus (USSR) 6 (1975) 435

4. A.I. Baz, Advances in Physics 8 (1959) 349

5. I. Rotter, H.W.Barz, J. Höhn, to be published

Contributed Paper No. 4

UNCERTAINTY ESTIMATES OF STATISTICAL THEORY CALCULATIONS OF NEUTRON CAPTURE CROSS SECTIONS OF FISSION PRODUCTS

H. Gruppelaar
Physics Department
Reactor Centrum Nederland
Petten, The Netherlands

Abstract

After a short outline of the statistical model used for the calculation of average radiative capture cross sections, the paper reviews the theory of the estimation of uncertainties originating from statistical fluctuations in the number of resonances per averaging interval, level width fluctuations and other fluctuations inherent to the statistical nature of the model.
Next, the influence of uncertainties of model parameters on the capture cross sections is discussed, and a survey is given of the difficulties which are encountered in the evaluation of these parameters and their uncertainties.
Finally, some remarks on the practical calculation of cross section covariances are given and some examples of calculations are presented.

1. INTRODUCTION

In nuclear mass regions where fast neutron radiative capture cross sections are not well known from experiments, such as in the fission-product mass range, one heavily relies on statistical model calculations. To estimate the uncertainty in these calculations one has to consider (i) the degree of validity of the model, (ii) the inherent uncertainties due to the statistical nature of the model, and (iii) uncertainties induced by errors in model parameters.

For a detailed comparison between theory and experiment an error analysis of the calculated cross section is necessary. In the field of fission-product cross section evaluation Schmittroth [1] has checked the model for capture calculations taking into account statistical model errors at high energies. In the present paper, however, the validity of the adopted model (sect. 2) is not questioned.

Experience with nuclides for which accurate capture measurements have been performed, shows that the adopted model seems to be adequate.†

Uncertainties due to the statistical nature of the model (sect. 3) are not only due to fluctuations in level widths and number of resonances per energy interval, but also arise from statistical estimates of the low-energy levels, spins and parities involved in the calculation. The first type of errors has been treated in refs. [2-4], the latter type of errors was considered in ref. [1]. In the present paper the theory described in these references is surveyed and some extensions and suggestions for practical calculations are given.

Errors in model parameters (sect. 4) often are the most important sources of uncertainties in the calculated capture cross sections. The sensitivity of the capture cross section for parameter variation of neutron- and radiation strength functions has been reported previously [3]. In this paper parameters associated with a more sophisticated model are considered. Also some problems connected to the estimation of parameters and their errors are mentioned. The sensitivity for optical-model parameter variations has been studied by MacKellar and Schenter [5].

Apart from a test of the validity of the model, an application of the work described in this paper might be the preparation of error files [6] connected to evaluated nuclear data files such as ENDF/B-IV. The demand for error files originates from questions with regard to sensitivity studies for safe and economic operation of nuclear systems. Another application is the interpretation of integral cross section measurements by means of adjustment of cross sections within the uncertainty limits [7,8]. In the last section some remarks on the practical calculation of variances and co-variances of capture cross sections are given and some examples are presented.

2. OUTLINE OF STATISTICAL MODEL

2.1. Average radiative capture cross section

It is supposed that (with the neglection of level-level interference) the radiative capture cross section averaged over an energy interval ΔE can be written as

$$\langle\sigma\rangle_{\Delta E} = \sum_{\ell jJ}{}' \langle\sigma_{\ell jJ}(E)\rangle_{\Delta E} \tag{1}$$

with partial cross sections

$$\langle\sigma_{\ell jJ}\rangle_{\Delta E} = \Big\langle \sum_{\mu} f_{\ell jJ}\big(\Gamma^{x}_{\mu}, E, E_{\mu}\big)\Big\rangle_{\Delta E}, \tag{2}$$

where the contribution of each resonance μ is expressed by the single level Breit-Wigner formula

$$f_{\ell jJ}\big(\Gamma^{x}_{\mu}, E, E_{\mu}\big) = \frac{\pi}{k^2}\,\frac{g_J\,\Gamma^{n}_{\mu\ell j}\,\Gamma^{\gamma}_{\mu J\pi}}{(E-E_{\mu})^2 + \frac{1}{4}\,\Gamma^{2}_{\mu J\pi}}\,. \tag{3}$$

---

†For a few nuclides non-statistical capture processes are important, see section 4.3.3 about the determination of the average value of the capture width.

A summation symbol Σ' (with a prime) means that quantum number selection rules have to be taken into account.
The symbol Γ^x is a short notation for *all* partial widths, which occur in the right-hand side of eq. (3). The other symbols in eqs. (1-3) have the usual meaning. Throughout this paper it is assumed that

$$\Delta E >> D_{J\pi} >> \langle \Gamma_{J\pi} \rangle, \tag{4}$$

where $D_{J\pi}$ is the mean level spacing and $\langle \Gamma_{J\pi} \rangle$ the average total width of the compound state. We interprete eq. (2) as follows:

$$\langle \sigma_{\ell j J} \rangle_{\Delta E} = \int_{\Delta E} dE\ \phi(E) \int_{-\infty}^{\infty} dE' q_{J\pi}(E') \langle f_{\ell j J}(\Gamma^x, E, E') \rangle \tag{5}$$

where $\phi(E)$ is a weighting function, usually taken as the constant $1/\Delta E$ and $q_{J\pi}(E)$ is the distribution function for the resonance energies, assumed to be equal to $1/D_{J\pi}$. The averaging signs in the right-hand side of eq. (5) have the meaning of an average over a Porter-Thomas distribution function $p(\Gamma^x)$, shortly denoted as

$$\langle f_{\ell j J}(\Gamma^x, E, E') \rangle = \int_0^{\infty} d\Gamma^x\ p(\Gamma^x)\ f_{\ell j J}(\Gamma^x, E, E'), \tag{6}$$

where the integration has to be performed over *all* widths Γ^x.
Eq. (5) can be written as

$$\langle \sigma_{\ell j J} \rangle_{\Delta E} = \int_{\Delta E} dE \frac{\phi(E)}{D_{J\pi}(E)} \left\langle \int_{-\infty}^{\infty} dE' f_{\ell j J}(\Gamma^x, E, E') \right\rangle =$$

$$= \int_{\Delta E} dE\ \phi(E)\ \frac{2\pi^2}{k^2 D_{J\pi}}\ g_J \left\langle \frac{\Gamma^n_{\ell j}\ \Gamma^\gamma_{J\pi}}{\Gamma_{J\pi}} \right\rangle . \tag{7}$$

The integrand of eq. (7) is roughly proportional to $\phi(E)E^{-\frac{1}{2}}$.
When ΔE is small eq. (7) can be approximated by

$$\langle \sigma_{\ell j J} \rangle_{\Delta E} = \frac{2\pi^2}{k^2 \Delta E} \langle n_{J\pi} \rangle_{\Delta E}\ g_J \left\langle \frac{\Gamma^n_{\ell j}\ \Gamma^\gamma_{J\pi}}{\Gamma_{J\pi}} \right\rangle, \tag{8}$$

where the neutron energy E is replaced by the average value

$$\overline{E} = \int_{\Delta E} dE\ E^{\frac{1}{2}} \phi(E) \Big/ \int_{\Delta E} dE\ E^{-\frac{1}{2}} \phi(E) \tag{9}$$

and $\langle n_{J\pi} \rangle_{\Delta E}$ is the average number of levels *in* ΔE with spin J and parity π:

$$\langle n_{J\pi} \rangle_{\Delta E} = \int_{\Delta E} dE\ q_{J\pi}(E) = \frac{\Delta E}{D_{J\pi}(\overline{E})} . \tag{10}$$

The notation of eqs. (1-10) is chosen to facilitate the treatment in section 3.

2.2. Width fluctuation factor

Eqs. (1,8) may be combined to obtain the Hauser-Feshbach formula with width fluctuation factor:

$$\sigma(\bar{E}) = \frac{\pi}{k^2} \sum_{\ell j J}' g_J \frac{T^n_{\ell j} \, T^\gamma_{J\pi}}{T_{J\pi}} (W_1)_{\ell j J}, \tag{11}$$

in which the relation between transmission coefficients and widths is supposed to follow the expression

$$T = 2\pi\Gamma/D. \tag{12}$$

The width fluctuation factor is defined as

$$W_1 = < \frac{\Gamma^n \Gamma^\gamma}{\Gamma} > / \frac{<\Gamma^n><\Gamma^\gamma>}{<\Gamma>}, \tag{13}$$

where mostly the fluctuations in the radiation widths are neglected. The *capture width* Γ^γ has to be distinguished from the *total radiation width* Γ^r which implicitly occurs in the denominator of eq. (13):

$$\Gamma^r = \Gamma - \sum_i \Gamma^n_i. \tag{14}$$

Each of the neutron widths Γ^n_i (including the incoming neutron width Γ^n) is supposed to be distributed according to a Porter-Thomas distribution with ν_i degrees of freedom. In sect. 3.1.1. an expression for W_1 is given.

3. STATISTICAL MODEL ERRORS

3.1. Fluctuations in resonance energies and widths

For use in this section eqs. (1-3,8) are recombined as follows:

$$\sigma(\bar{E}) = \sum_{J\pi} \sigma_{J\pi}(\bar{E}) = \sum_{J\pi} <\sigma_{J\pi}(E)>_{\Delta E} \tag{15}$$

with

$$<\sigma_{J\pi}(E)>_{\Delta E} = < \sum_\mu f_{J\pi}(\Gamma^x_\mu, E, E_\mu)>, \tag{16}$$

$$f_{J\pi} = \sum_{\ell j}' f_{\ell j J}, \tag{17}$$

such that

$$\sigma_{J\pi}(\bar{E}) = \frac{2\pi^2}{k^2 \Delta E} <n_{J\pi}>_{\Delta E} g_J < \frac{\Gamma^n_{J\pi} \, \Gamma^\gamma_{J\pi}}{\Gamma} > \tag{18}$$

with

$$\Gamma^n_{J\pi} = \sum_{\ell j}' \Gamma^n_{\ell j}. \tag{19}$$

Throughout this section it is assumed that $D_{J\pi}$ is independent of E.

The co-variance between average cross sections for two not *partially* overlapping intervals ΔE_1 and ΔE_2 is defined as

$$\mathrm{cov}(\sigma(\bar{E}_1),\sigma(\bar{E}_2)) = \sum_{J_1 J_2 \pi_1 \pi_2} \mathrm{cov}(\sigma_{J_1\pi_1}(\bar{E}_1),\sigma_{J_2\pi_2}(\bar{E}_2))\delta_{J_1 J_2}\delta_{\pi_1\pi_2}, \tag{20}$$

with

$$\mathrm{cov}(\sigma_{J\pi}(\bar{E}_1),\sigma_{J\pi}(\bar{E}_2)) = \Big\langle \sum_{\mu\nu} f_{J\pi}(\Gamma^x_\mu,E_1,E_\mu) f_{J\pi}(\Gamma^x_\nu,E_2,E_\nu)\Big\rangle_{\Delta E_1,\Delta E_2} +$$

$$- \Big\langle \sum_{\mu} f_{J\pi}(\Gamma^x_\mu,E_1,E_\mu)\Big\rangle_{\Delta E_1} \Big\langle \sum_{\nu} f_{J\pi}(\Gamma^x_\nu,E_2,E_\nu)\Big\rangle_{\Delta E_2}. \tag{21}$$

In the following part of this section the indices J and π are omitted. The occurrence of Kronecker delta symbols in eq. (20) follows from the absence of correlations between levels with different spin or parity. The first term of eq. (21) is written as

$$\int_{\Delta E_1} dE_1 \int_{\Delta E_2} dE_2\ \phi_1(E_1)\phi_2(E_2)\times$$

$$\int_{-\infty}^{\infty} dE_1' \int_{-\infty}^{\infty} dE_2'\ q(E_1',E_2')\langle f(\Gamma_1^x,E_1,E_1')f(\Gamma_2^x,E_2,E_2')\rangle, \tag{22}$$

where the joint-distribution function for the resonance energies is defined as

$$q(E_1',E_2') = \frac{1}{D}\,\delta(E_1'-E_2') + \frac{1}{D^2}\,\Psi\Big(\frac{E_1'-E_2'}{D}\Big) \tag{23}$$

with Ψ the two-level correlation function from random-matrix theory [9]. With the help of eqs. (22,23), each term of eq. (20) can be written as

$$\int_{\Delta E_1} dE_1 \int_{\Delta E_2} dE_2\ \phi_1(E_1)\phi_2(E_2)\Big[\int_{-\infty}^{\infty} \frac{dE_1'}{D}\,\langle f(\Gamma_1^x,E_1,E_1')f(\Gamma_1^x,E_2,E_1')\rangle +$$

$$- \int_{-\infty}^{\infty} dE_1' \int_{-\infty}^{\infty} dE_2'\ \Phi\Big(\frac{E_1'-E_2'}{D}\Big)\,\langle f(\Gamma_1^x,E_1,E_1')\rangle\langle f(\Gamma_2^x,E_2,E_2')\rangle/D^2\Big] \tag{24}$$

where

$$\Phi(r) = 1-\Psi(r) \tag{25}$$

is the so-called cluster function, which is equal to unity for r=0 and approaches zero for $|r| \gg 1$. The integrand in the first term of eq. (24) in between square brackets is only important for E_1 close to E_2; integration over E_1' leads to the approximation [3]:

$$\frac{4\pi^4}{k^4 D} g^2 < \left(\frac{\Gamma^n \Gamma^\gamma}{\Gamma}\right)^2 > \delta(E_1 - E_2). \tag{26}$$

The integrand of the second term of eq. (24) in between square brackets is only important for $E_1 \approx E_1'$ and $E_2 \approx E_2'$, such that $\Phi((E_1'-E_2')/D)$ can be replaced by $\Phi((E_1-E_2)/D)$ and the integration over E_1' and E_2' becomes trivial:

$$\Phi\left(\frac{E_1-E_2}{D}\right) \frac{4\pi^4 g^2}{k_1^2 k_2^2 D^2} < \frac{\Gamma_1^n \Gamma_1^\gamma}{\Gamma_1} > < \frac{\Gamma_2^n \Gamma_2^\gamma}{\Gamma_2} >. \tag{27}$$

Re-arrangement of terms gives the following expression for each term of eq. (20):

$$\int_{\Delta E_1} dE_1 \int_{\Delta E_2} dE_2 \; \phi_1(E_1)\phi_2(E_2) \left[\frac{4\pi^4 g^2}{k^4 D^2} \; D \; \mathrm{var}\left(\frac{\Gamma^n \Gamma^\gamma}{\Gamma}\right) \delta(E_1-E_2) + \right.$$

$$\left. \frac{4\pi^4 g^2}{k_1^2 k_2^2 D^2} < \frac{\Gamma_1^n \Gamma_1^\gamma}{\Gamma_1} > < \frac{\Gamma_2^n \Gamma_2^\gamma}{\Gamma_2} > \left\{ D\delta(E_1-E_2) - \Phi\left(\frac{E_1-E_2}{D}\right) \right\} / D^2 \right]. \tag{28}$$

The first term of eq. (28) may be interpreted as originating from fluctuations in the level widths. The second term of eq. (28) is related to the covariance of the number of levels n_1 and n_2 in two intervals [3]:

$$\mathrm{cov}(n_1, n_2) = \int_{\Delta E_1} dE_1 \int_{\Delta E_2} dE_2 \; \frac{1}{D^2} \left[D\delta(E_1-E_2) - \Phi\left(\frac{E_1-E_2}{D}\right) \right]. \tag{29}$$

Neglection of the energy dependence of $\phi(E)\sigma(E)$ in eq. (28) leads to the final expression for each term of eq. (20)

$$\mathrm{cov}(\sigma(\bar{E}_1), \sigma(\bar{E}_2))_{J\pi} = \frac{4\pi^4}{k^4 D^2} g^2 \frac{1}{<n>} \mathrm{var}\left(\frac{\Gamma^n \Gamma^\gamma}{\Gamma}\right) \delta_{\bar{E}_1 \bar{E}_2} +$$

$$\sigma(\bar{E}_1)\sigma(\bar{E}_2) \frac{\mathrm{cov}(n_1, n_2)}{<n_1> <n_2>}. \tag{30}$$

3.1.1. Width fluctuation variance

With the help of eq. (19) the variance in eq. (30) can be expressed as

$$\mathrm{var}\left(\frac{\Gamma^n_{J\pi}\Gamma^\gamma_{J\pi}}{\Gamma_{J\pi}}\right) = \sum_{\ell j}{}' \mathrm{var}\left(\frac{\Gamma^n_{\ell j}\Gamma^\gamma_{J\pi}}{\Gamma_{J\pi}}\right) + \sum_{\ell_1\neq\ell_2, j_1\neq j_2}{}' \left[< \frac{\Gamma^n_{\ell_1 j_1}\Gamma^n_{\ell_2 j_2}(\Gamma^\gamma_{J\pi})^2}{\Gamma^2_{J\pi}} > - < \frac{\Gamma^n_{\ell_1 j_1}\Gamma^\gamma_{J\pi}}{\Gamma_{J\pi}} > < \frac{\Gamma^n_{\ell_2 j_2}\Gamma^\gamma_{J\pi}}{\Gamma_{J\pi}} > \right], \tag{31}$$

Neutrons with $\ell_1 \neq \ell_2$ must differ at least two units of angular momentum in order to reach the compound state with the same parity. Consequently the product of the corresponding transmission coefficients is small at low neutron energies and the second sum of eq. (31) may be neglected.

The width fluctuation factor W_1 defined in eq. (13) can be calculated with the expression (which follows from ref. [24])

$$W_1 = <\Gamma> \int_0^\infty \frac{\exp(-<\Gamma^r>t)\,dt}{(1+\frac{2t}{\nu}<\Gamma^n>)\prod_i (1+\frac{2t}{\nu_i}<\Gamma^n_i>)^{\nu_i/2}}\,. \tag{32}$$

The relative variance of the widths can be expressed as $W_2^2 - W_1^2$ where W_k is defined as

$$W_k = <\left(\frac{\Gamma^n\Gamma^\gamma}{\Gamma}\right)^k>^{1/k} / \frac{<\Gamma^n><\Gamma^\gamma>}{<\Gamma>} \quad (k = 1,2). \tag{33}$$

For W_2^2 one easily obtains the relation

$$W_2^2 = -<\Gamma>^2 \frac{d}{d<\Gamma^n>}\frac{W_1}{<\Gamma>} =$$

$$= (\frac{2}{\nu}+1)<\Gamma>^2 \int_0^\infty \frac{t\,\exp(-<\Gamma^r>t)\,dt}{(1+\frac{2t}{\nu}<\Gamma^n>)^2 \prod_i (1+\frac{2t}{\nu_i}<\Gamma^n_i>)^{\nu_i/2}}. \tag{34}$$

3.1.2. Co-variance of n_1 and n_2

Expressions for the calculation of $\mathrm{cov}(n_1,n_2)$ follow from the asymptotic approximation [10] for the variance:

$$\mathrm{var}(n) = \frac{2}{\pi^2}(\ln<n>+a) \tag{35}$$

with $a \approx 2.18$. Requiring that for two adjacent intervals the variance can be calculated with

$$\mathrm{var}(n_1 + n_2) = \mathrm{var}(n_1) + \mathrm{var}(n_2) + 2\,\mathrm{cov}(n_1,n_2), \tag{36}$$

one finds for the covariance of two *adjacent* intervals

$$\mathrm{cov}(n_1,n_2) = -\frac{1}{\pi^2}\left(\ln\frac{\langle n_1\rangle\langle n_2\rangle}{\langle n_1\rangle+\langle n_2\rangle} + a\right). \tag{37}$$

Likewise the covariance for two intervals separated by a third interval can be calculated.

3.1.3. Ericson fluctuations

Due to the condition $\Delta E >> \langle\Gamma\rangle$ (eq. 4), which is always satisfied in reactor physics applications, Ericson fluctuations [25] are smeared out.

3.2. Fluctuations in the number of bound target levels

Above a certain excitation energy ε_p the target levels are not well known and the level density has to be prescribed by a continuous function of energy $\rho_o(\varepsilon)$. The average number of levels upto an energy E can be estimated by

$$\langle N^E\rangle = N_p + \int_{\varepsilon_p}^{E} \rho_o(\varepsilon)\,d\varepsilon, \tag{38}$$

where N_p is the number of levels below the pth excitation energy ε_p. Very roughly the capture cross section is inversely proportional to $\langle N^E\rangle$ and so is the relative variance of the capture cross section. As $\langle N^E\rangle$ increases exponentially with energy, the error is only of importance in a limited energy range just above ε_p. Schmittroth [1] has given an expression for the variance of bound levels neglecting correlations between levels and assuming $\varepsilon_p=0$ and a number of other approximations. We follow his treatment here.

For the error calculation in this section the capture cross section is approximated by:

$$\sigma(E) = \frac{C(E)}{\alpha^E + A^E(\varepsilon_p,\varepsilon_{p+1},\ldots)} = \frac{C(E)}{\alpha^E + \sum_{i\geq p} a^E(\varepsilon_i)}. \tag{39}$$

where A^E is a function of all excitation energies ε_i with $i\geq p$ and $a^E(\varepsilon_i)=0$ for $E<\varepsilon_i$. Assuming that the energies ε_i are independently distributed on the interval (ε_p,∞), each with a level density distribution function $\rho_o(\varepsilon_i)$, one finds *

$$\langle A^E\rangle = \int_{\varepsilon_p}^{E} a^E(\varepsilon)\rho_o(\varepsilon)\,d\varepsilon \tag{40}$$

and

$$\mathrm{cov}(A^{E_1},A^{E_2}) = \int_{\varepsilon_p}^{E_1} a^{E_1}(\varepsilon)a^{E_2}(\varepsilon)\rho_o(\varepsilon)\,d\varepsilon \quad (E_1 \geq E_2). \tag{41}$$

---

* In equ. (40) the function $\rho_o(\varepsilon)$ is supposed to be normalized according to equ. (38).

The average value of the cross section can be written as

$$\langle\sigma(E)\rangle = \frac{C(E)}{\alpha^E + \langle A^E\rangle} L, \tag{42}$$

where the "level fluctuation factor" L is equal to or less than 1. In most calculations this factor is taken as unity. The relative covariance between two cross sections is approximately equal to

$$\frac{\mathrm{cov}(\sigma(E_1),\sigma(E_2))}{\langle\sigma(E_1)\rangle\langle\sigma(E_2)\rangle} = \frac{\mathrm{cov}(A^{E_1},A^{E_2})}{(\alpha^{E_1} + \langle A^{E_1}\rangle)(\alpha^{E_2} + \langle A^{E_2}\rangle)}. \tag{43}$$

Analytical expressions for the integrals in eqs. (38, 40, 41) are obtained with the substitutions (adopted in calculations, see Sect. 5)

$$\rho_o(\varepsilon) = \frac{1}{T} \exp[(\varepsilon - \varepsilon_o)/T] \tag{44}$$

and

$$a^E(\varepsilon) = \frac{2m}{\hbar^2} (E-\varepsilon)\, \sigma_{cf}(E-\varepsilon), \tag{45}$$

where the compound formation cross section σ_{cf} in eq. (45) is approximated by the semi-empirical formula [11]

$$\sigma_{cf}(E) = \sigma_g(\mu E+\nu). \tag{46}$$

In eq. (46) σ_g is the geometrical cross section and μ and ν are simple functions of the nuclear mass.

3.3. Spins and parities of bound target levels

In the energy range *above* ε_p uncertainties in the cross section also arise from statistical estimates of the spins and parities I^π of the bound levels. A first impression of the effect of these errors is obtained by varying the spin of one bound level [12], which may lead to large errors (upto 40%) when the difference between I and the ground-state spin I_o is large and when the level density is low. Less pronounced effects are obtained for a change in parity of one level.

Schmittroth has calculated [1] the variance of the capture cross section due to uncertainties in I^π by means of a Monte-Carlo method, assuming the following distributions:

$$R_I = \left(\frac{2I+1}{2\sigma^2}\right) \exp\left[-\frac{(I+\frac{1}{2})^2}{2\sigma^2}\right] \tag{47}$$

$$P_\pi = 1/2, \tag{48}$$

where σ^2 is the spin cut-off parameter. Assuming that *all* spins and parities of excited target levels are unknown, errors of 20% to 30% have been found. However, in practice these errors are much smaller, since often one knows at least a few spins either exactly or within one unit of angular momentum.

In routine cross section calculations the inelastic scattering transmission coefficients are averaged over I and π above $E = \varepsilon_p$, using the distributions of eqs. (47,48). Problems in these calculations are the choice of σ^2 and the validity of eq. (48), which is too simple at low energies. Another problem, pointed out by Schmittroth [1] is the occurrence of a "spin and parity fluctuation factor" S, in the capture cross section, analogous to the factor L in eq. (42).

3.4. Low-energy level scheme of final nucleus

The level scheme of the final nucleus enters into the calculation when the γ-width is calculated (see sect. 4.4). Due to the large number of levels involved, the variance of $\langle\Gamma\gamma\rangle$ due to fluctuations in the number of levels and in the spins and parities is supposed to be small in comparison with other uncertainties such as the validity of the distribution functions.

4. ERRORS DUE TO UNCERTAINTIES IN MODEL PARAMETERS

4.1. Calculation of co-variance of the cross section

Assuming that the cross section is a function of a number of independent model parameters p_k, the covariance can be written as

$$\mathrm{cov}(\sigma(\bar{E}_1),\sigma(\bar{E}_2)) = \sum_k \frac{\partial\sigma(\bar{E}_1)}{\partial p_k} \frac{\partial\sigma(\bar{E}_2)}{\partial p_k} \mathrm{var}(p_k) \qquad (49)$$

A convenient way to estimate the quantity

$$\delta\sigma_k = \frac{\partial\sigma(\bar{E})}{\partial p_k} \mathrm{var}^{\frac{1}{2}}(p_k) \qquad (50)$$

is by varying the parameters p_k in $\sigma(\bar{E})$ over one standard deviation.

The parameters have to be chosen such that they are uncorrelated. This is only possible to a certain extent. Moreover, when the cross sections have to be evaluated for a *series* of nuclides which are going to be used together in certain applications [23], correlations between parameters of *different* nuclides have to be taken into account [3].

Often one has to deal with (large) asymmetrical errors. In these cases it might be better to assume a normal distribution for the logarithm of the parameter and/or the cross section.

The main job to be performed is the evaluation of parameters and their uncertainties. The most important parameters of the statistical model for radiative capture originate from the resolved resonance parameters and the low-energy level scheme. Often, problems are encountered in deriving average quantities from these experimental data. Moreover, in many cases experimental data are lacking and the model parameters have to be derived from theory or systematics. These circumstances make an error estimate difficult and often somewhat arbitrary.

In the process of parameter evaluation the (scarce) experimental cross section data also play an important role. Usually one or more parameters are manually adjusted to give a reasonable fit of the calculated cross sections with the experimental point cross sections. When *integral* measurements (such as reaction rates and reactivity worths) are available, an elaborate least-squares adjustment scheme can be used to obtain adjusted cross sections and parameters with their errors [8]. However, such a procedure is usually applied as a final step, after the determination of all cross section uncertainties with methods described in this paper.

A status report on fission product cross sections and model parameters has been given by Ribon and Krebs [13]. New fission-product cross section evaluations are underway in Japan (JAERI), U.S.A. (for ENDF/B-V) and in Europe (CNEN-Bologna, CEA-Saclay and Cadarache, RCN-Petten).

After these preliminaries some important parameters are considered in more detail in the next subsections, where the discussion is mainly based on experience with the so-called RCN-2 fission product cross section evaluation.

4.2. Neutron strength functions

At low neutron energies $T^{\gamma}_{J\pi}$ is much larger than $T^{n}_{\ell j}$, so the partial capture cross section $\sigma_{\ell jJ}(\bar{E})$ is approximately proportional to $T^{n}_{\ell j}$, where $\ell = 0$ or 1. At higher neutron energies $\sigma_{\ell jJ}(\bar{E})$ is roughly proportional to $T^{\gamma}_{J\pi}$, as the neutron transmission coefficients in the nominator and denominator of the expression for the capture cross section partially compensate each other.

From several studies [5,13] one may conclude that below about 50 keV it has to be preferred to calculate the neutron transmission coefficients from strength functions. Since at higher energies the sensitivity of the capture cross section for changes in the transmission coefficients is low, one can base the error calculation in the *entire* energy range on a suitable strength function model, rather than applying both a strength function model and an optical model in two energy ranges. Correlations between transmission coefficients are difficult to account for with an extended strength function model. On the other hand, the use of *two* models in different energy regions obstructs the calculation of correlations between cross sections in a low and high energy interval. In this paper an extended† strength function model has been adopted [39].

The s- and p-wave strength functions S_0 and S_1 and corresponding errors are determined from resolved resonance parameters, where the parity of each resonance often has to be estimated by means of a statistical analysis. The uncertainty in these parity assignments is a major source of errors in S_0 and S_1 for nuclides in the vicinity of A = 90. The variance in S_0, exclusively based on Porter-Thomas statistics, for a large number of resonances n, amounts to [14]

$$\mathrm{var}(S_0) = \frac{2}{n} S_0^2 \,. \qquad (51)$$

The p-wave strength function also follows from a fit to the total (or capture) cross section. Typical uncertainties for many

†The usually adopted relation between T^{n}_{ℓ} and S_{ℓ} does not fulfil the requirement $T^{n}_{\ell} \leq 1$ for all energies.

nuclides are 10% to 30% in S_0 and about 50% in S_1. The other strength functions are calculated from an optical model and supplied with large errors (a 100% error in S_2 results in a *maximum* error of about 15% in the capture cross section; see figs. 4,7-9, discussed in section 5).

4.3. Mean level spacings and spin cut-off parameters

In this and in the following sections the symbols E and ε are used for the neutron energy and the excitation energy, respectively.

4.3.1. Level density formula

The level density $\rho_{J\pi}(\varepsilon)$ is commonly described by the Gilbert-Cameron formula [15] (adopted in sect. 5),

$$\rho_{J\pi}(\varepsilon) = R_J P_\pi \rho_o(\varepsilon), \tag{52}$$

where for low excitation energies ρ_o is defined as in eq. (44) and for high energies (above ε_x) ρ_o is defined as

$$\rho_o(\varepsilon) = \exp\left[2\sqrt{aU}\right] / (12\sqrt{2}a^{1/4}\sigma U^{5/4}) \quad (\varepsilon \geq \varepsilon_x) \tag{53}$$

with

$$U = \varepsilon - P. \tag{54}$$

The symbol P in eq. (54) is for the pairing energy correction given by Gilbert and Cameron [15].

The square of the parameter σ in eq. (53) is the spin cut-off parameter, which also occurs in the expression for R_J, eq. (47) and which is related with the level density parameter a at energies $\varepsilon \geq \varepsilon_x$, according to the equation

$$\sigma^2(\varepsilon) = c\sqrt{aU}\, A^{2/3} \quad (\varepsilon \geq \varepsilon_x), \tag{55}$$

with c = 0.0888 [15] or c = 0.146 [16] (adopted in sect. 5).
For low energies the spin cut-off parameter $\sigma^2(0)$ may be estimated from the experimental low-energy level scheme. A linear relationship with excitation energy,

$$\sigma^2(\varepsilon) = \sigma^2(0) + (\sigma^2(\varepsilon_x) - \sigma^2(0))\, \varepsilon/\varepsilon_x, \quad (\varepsilon \leq \varepsilon_x) \tag{56}$$

could perhaps be used in the expression for R_J (adopted in sect. 5).

The parameters ε_o,T (eq. 44), a and ε_x follow from a fit of the Gilbert-Cameron formula to the mean s-wave level spacing D_{obs} at the neutron separation energy and to the low-energy level scheme (i.e. the parameters ε_p and N_p defined in sect. 3.2.).
From the independent parameters D_{obs}, $\sigma^2(0)$, ε_p, N_p, P and c, which describe the complete nuclear density formula, D_{obs} is by far the most important parameter in the uncertainty calculation of the capture cross section. In the following the indices c and t will be used to discriminate between compound and target nucleus parameters.

4.3.2. Compound nucleus parameters

Uncertainties in D^c_{obs} influence the capture cross section mainly via the capture transmission coefficient at the neutron separation energy, $T^\gamma_{J\pi}(0)$, which is inversely proportional to D_{obs} and which is used as a normalization for $T^\gamma_{J\pi}(E)$ at high neutron energies:

$$T^\gamma_{J\pi}(E) = T^\gamma_{J\pi}(0)\ g_{J\pi}(E) \tag{57}$$

with

$$T^\gamma_{J\pi}(0) = \frac{2\pi}{D_{obs}} <\Gamma^\gamma_{J\pi}(0)> \frac{R_J P_\pi}{R_{I_o+\frac{1}{2}} + R_{I_o-\frac{1}{2}}} \tag{58}$$

and

$$g_{J\pi}(0) = 1. \tag{59}$$

However, the level density $\rho^c_{J\pi}$ *also* occurs in the factor $g_{J\pi}(E)$, which describes the energy dependence of $T^\gamma_{J\pi}$. In sect. 4.4.1. an approximate expression for $g_{J\pi}(E)$ is given. It has to be noticed that a similar relation exists for $T^r_{J\pi}=2\pi\ \Gamma^r_{J\pi}/D_{J\pi}$, see eq. (14).

Due to the normalization requirement (57) the uncertainties in level density parameters other than D^c_{obs} have a relatively small impact on the capture cross section. This is particularly valid for $\sigma^2_c(0)$, ε^c_p, N^c_p and P^c, which enter only through $g_{J\pi}(E)$ into the expression for the cross section.

The effect of the parameter c which enters both into the expression for σ^2_c and in that for σ^2_t can be important: the large difference between the two values of c mentioned before [15,16] leads to a change in the capture cross section of 30% to 40% at 5 MeV. In figs. 1 and 2 the sensitivity of the calculated capture cross sections of ^{93}Nb and ^{98}Mo for a change of the parameter c from the value 0.146 to 0.0888 is shown. The calculations have been performed with the code FISPRO-RCN (see sect. 5.1.). The large effects shown in figs. 1 and 2 are not due to the target nucleus, since a decrease of σ^2_t would increase the capture cross section, in distinction to the effect of σ^2_c.

4.3.3. Target nucleus parameters

The level density of the target nucleus enters into the calculation above the neutron energy $E = \varepsilon^t_p$ (sect. 3.2.), where a part of the total neutron transmission coefficient can be calculated with the approximate expression [1] (adopted in sect. 5)

$$T_{J\pi}(E) = R_J \sum_\ell S_{\ell J} \int_{\varepsilon_p}^{E} \rho^t_o(\varepsilon)\ T^n_\ell(E-\varepsilon)d\varepsilon. \tag{60}$$

In this equation $S_{\ell J}$ mainly serves as an *orbital* angular momentum cut-off factor. Both R_J and $S_{\ell J}$ depend on σ^2_t.

The most interesting energy region of the capture cross section for applications in fast breeder reactors usually is below ε^t_x, where $\rho^t_o(\varepsilon)$ and σ^2_t are described by eqs. (44) and (56), respectively. Therefore important parameters are D^t_{obs}, N^t_p, ε^t_p and $\sigma^2_t(0)$. The influence of a non-equal parity distribution on eq. (60) has not been investigated in this paper.

The sensitivity of the cross section for a change in D^t_{obs} is large and increases with energy. A variation of ε^t_p (keeping N^t_p constant) also has a large effect on the capture cross section (see fig. 1). Therefore, *for the error calculation*, ε^t_p has to be chosen such that the probability of missing bound levels with excitation energies below ε^t_p is very low. The capture cross section is not very sensitive for a variation of $\sigma^2_t(0)$, although this sensitivity increases when the target ground-state spin is high. The reason that the capture cross section is not very sensitive to a variation in $\sigma^2_t(0)$ is due to the use of relation (56) in which the value of $\sigma^2_t(0)$ at ε^t_x is fixed at the value $c\sqrt{a(\varepsilon^t_x-P)}A^{2/3}$. In ref. [1] eq. (56) has not been used, but $\sigma^2_t(\varepsilon)$ was assumed to be equal to $\sigma^2_t(0)$ upto ε_x. This assumption leads to a rather large sensitivity of the capture cross section for $\sigma^2_t(0)$. In our case the parameter c is more important, although its effect mainly is expressed via σ^2_c.

4.3.4. Determination of parameters

The mean level spacing is determined from resolved resonance parameters. The variance in $D_{J\pi}$, based on the Wigner distribution * for level spacings, is given [14] by

$$\mathrm{var}(D_{J\pi}) = \frac{4-\pi}{\pi n} D^2_{J\pi}, \qquad (61)$$

where n is the number of level spacings used in the analysis. However, in practice the uncertainties are often much larger due to missed levels or due to unknown parities.

A major problem is the determination of D_{obs} when no resonance parameters are known. Up to now the best results are obtained from systematics of a as a function of the neutron number N for a fixed proton number Z. The mean level spacing determined in this way is usually not better known than within a factor of 2. Existing theoretical models, supplied with adjustable parameters, up to now do not improve this situation [13]. Often helpful to the evaluation of fission-product cross sections is the adjustment of D_{obs} to fit $\sigma(\bar{E})$ to measured cross-sections whenever this is possible. In this way the systematics of a may be improved.

The spin cut-off parameter $\sigma^2(0)$ can be determined from the experimental spin distribution by means of the following relation, obtained [1] from eq. (47) by the method of maximum-likelihood

$$\sigma^2(0) = \frac{1}{2n} \sum_{i=0}^{n} (I_i + \tfrac{1}{2})^2, \qquad (62)$$

where n is the number of levels with known spin. The error in $\sigma^2(0)$ is difficult to estimate. Assuming no uncertainties in the level scheme and neglecting the energy dependence, the relative variance is equal to 1/n.

The parameter c is an important quantity for the capture cross section at high energies. Its value is obtained from theoretical arguments [15,16].

---

* When Dyson statistics is used eq. (61) becomes

$$\mathrm{var}(D_{J\pi}) = \frac{8}{\pi^2 n^2} D^2_{J\pi}$$

4.4. Gamma parameters

4.4.1. Expression for the radiative capture width

The most sophisticated statistical model *adopted* in fast radiative capture calculations for the computation of the statistical capture width is expressed in the following relation [17] based on the Brink-Axel estimate

$$\langle\Gamma^{\gamma}_{J\pi}(E)\rangle = \frac{2}{3(\pi\hbar c)^2\rho_{J\pi}(B+E)}\left[\sum_i{}' (1-\delta_{\pi\pi_i})(B+E-\varepsilon_i)^2\sigma_L(B+E-\varepsilon_i) + \right.$$

$$\left. + \sum_{\pi'}(1-\delta_{\pi\pi'}) \int_{\varepsilon_p}^{B} (B+E-\varepsilon)^2\ \sigma_L(B+E-\varepsilon) \sum_I{}' \rho^c_{I\pi'}(\varepsilon)d\varepsilon\right], \qquad (63)$$

where the E1 photo absorption cross section is given by a sum over Lorentzian functions

$$\sigma_L(\varepsilon) = \sum_r \frac{\sigma_r\varepsilon^2\Gamma_r^2}{(\varepsilon_r^2-\varepsilon^2)^2+\varepsilon^2\Gamma_r^2}. \qquad (64)$$

The symbols E, B, ε denote the neutron energy, neutron binding energy and excitation energy, respectively. The parameters σ_r, ε_r, Γ_r are the giant resonance parameters corresponding to the peak cross section, peak energy and half maximum width, respectively.
In most calculations the summation over the "discrete" levels ε_i with spin I_i and parity $\pi_i = \pi$ is also replaced by an integration (eg. in ref. [37]). In the summation over final states the spins are restricted to $I_i = |J-1|$, J or J+1 for $J \neq 0$ and to $I_i = 1$ for $J = 0$.

With the assumption of equal parity distribution and no energy dependence of the spin cut-off parameter a convenient approximation for $\langle\Gamma^{\gamma}_{J\pi}(E)\rangle$ (adopted in sect. 5) is,

$$\langle\Gamma^{\gamma}_{J\pi}(E)\rangle \propto \frac{1}{\rho^c_o(B+E)} \int_o^B (B+E-\varepsilon)^2\ \sigma_L(B+E-\varepsilon)\ \rho^c_o(\varepsilon)d\varepsilon. \qquad (65)$$

In this equation the spin dependence is completely dropped, which is approximately correct: the spin dependence of $\langle\Gamma^{\gamma}_{J\pi}(E)\rangle$ is roughly given by

$$\exp\left[-(J+\tfrac{1}{2})^2\left(\frac{1}{2\sigma_c^2} - \frac{1}{2\sigma_b^2}\right)\right], \qquad (66)$$

where σ_c^2 is the spin cut-off parameter of the compound state and σ_b^2 is an effective spin cut-off parameter of the bound levels.

Assuming that eq. (65) holds andneglecting the energy dependence of the spin cut-off parameter the factor $g_{J\pi}(E)$ (see eq.57) is independent of J and π:

$$g_{J\pi}(E) = \frac{\int_o^B (B+E-\varepsilon)^2\ \sigma_L(B+E-\varepsilon)\ \rho^c_o(\varepsilon)d\varepsilon}{\int_o^B (B-\varepsilon)^2\ \sigma_L\ (B-\varepsilon)\ \rho^c_o(\varepsilon)d\varepsilon}. \qquad (67)$$

In conclusion: the J-dependence of $\langle\Gamma^{\gamma}_{J\pi}(E)\rangle$ is rather weak, but may become important when the level density is low. For nuclides with a low level density the parity dependence of $\langle\Gamma^{\gamma}_{J\pi}(E)\rangle$ is usually much stronger, as for most of these nuclides the parity distribution is not equal at low energies.

Similar equations as derived before follow for the total radiation width $\langle\Gamma^{\gamma}_{J\pi}\rangle$. In eq. (63) the probability that a γ-cascade proceeds via an unbound level has been neglected†. This so-called cascade process becomes important above a few MeV. Also neglected in eq. (63) are possible M1-components, and non-statistical capture effects (see sect. 4.4.3.).

4.4.2. Effect on the cross section

We assume that $\langle\Gamma^{\gamma}_{J\pi}(E)\rangle$ is normalized via relation (57) where $\langle\Gamma^{\gamma}_{J\pi}(0)\rangle$ may be obtained from: (i) complete calculation from eq. (63), (ii) normalization of eq. (63) with the experimental γ-width for s-wave capture $\langle\Gamma^{\gamma}_{\ell=0}\rangle$, (iii) experimental capture widths $\langle\Gamma^{\gamma}_{\ell=0}\rangle$ and $\langle\Gamma^{\gamma}_{\ell=1}\rangle$ and neglection or calculation of the J-dependence of the capture width.

In the error calculation we vary $\langle\Gamma^{\gamma}_{\ell=0}\rangle$ and $\langle\Gamma^{\gamma}_{\ell=1}\rangle$ simultaneously, thus assuming a complete correlation between $\langle\Gamma^{\gamma}_{\ell=0}\rangle$ and $\langle\Gamma^{\gamma}_{\ell=1}\rangle$. The sensitivity of the capture cross section for a change in the capture width is large and increases with energy.

The giant resonance parameters weakly influence the capture cross section between 5 MeV and 10 MeV. At still higher energies the giant resonance parameters become important for the description of the collective enhancement of the capture cross section [38].

4.4.3. Determination of parameters

For many nuclides the capture width has been measured for only a few resonances. However the spread in Γ^{γ} is not large, as many decay channels are involved. Difficulties in the determination of $\langle\Gamma^{\gamma}_{J\pi}(0)\rangle$ arise when there is a clear spin or parity dependence, while the spins and parities of the resolved resonances are not well known.

The use of theory to predict $\langle\Gamma^{\gamma}_{J\pi}(0)\rangle$ is difficult due to the uncertainties in the parity distribution of the low-lying levels. In ref. [37] an energy dependent expression for the parity distribution is given which might be helpful. Results for $\langle\Gamma^{\gamma}_{\ell=0}\rangle$, based on eq. (63), have been given in ref. [26], where also a comparison has been made with experimental widths and with other estimates obtained from semi-emirical formulas [27,28]. The three formalisms compared in ref. [26] give about the same results, with an uncertainty of roughly 25% in $\langle\Gamma^{\gamma}_{\ell=0}\rangle$ for nuclides in the fission-product mass range.

Another problem in the determination of $\langle\Gamma^{\gamma}_{J\pi}(0)\rangle$ originates from the existence of non-statistical components, in particular due to p-wave *valence* capture [18] around A= 90. The overwhelming evidence of these non-statistical effects in neutron capture has not yet resulted in codes for routine cross section evaluation. Weigmann and Rohr [28] have taken into account a simple expression for the valency neutron contribution in their semi-empirical description of the total radiative widths, based on the assumption that Γ^{γ} is completely correlated with

† In the calculations (sect.5) the $(n,2\gamma)$ cascade process has been taken into account.

the reduced neutron width:

$$\langle \Gamma^{\gamma}_{J\pi} \rangle_{val.} = s_{\ell} \, A^{2/3} \quad \beta_J \, D_{J\pi} \, S_{\ell}, \tag{68}$$

where β_J is the number of different final spin values for dipole emission from a compound state with spin J. The factor s_ℓ has been determined from a number of known experimental capture widths by subtracting the calculated statistical contributions. For p-wave capture in the mass range $88 \leq A \leq 125$ it has been found* that $s_1 = 3.82 \times 10^{-4}$ [28]. In the treatment of Weigmann and Rohr no "discrete" level scheme was considered in the calculation of the statistical part of $\langle \Gamma^{\gamma}_{\ell} \rangle$ and it has been assumed that $\langle \Gamma^{\gamma}_{\ell=1} \rangle = \langle \Gamma^{\gamma}_{\ell=0} \rangle$. However, from *statistical* calculations based on eq. (63) Reffo [29] has found that $\langle \Gamma^{\gamma}_{\ell=1} \rangle$ is much larger than $\langle \Gamma^{\gamma}_{\ell=0} \rangle$ in the mass range around A= 90. Probably s_1 would decrease therefore when eq. (63) and eq. (68) were used. When eq. (68) is used for the calculation of the valence capture part of the cross section the width fluctuation factor has to be omitted (in a first-order approximation), which gives an additional enhancement of the capture cross section.

In the case of the $^{93}Nb(n,\gamma)^{94}Nb$ reaction a *doorway state* reaction mechanism has been suggested [30,31]. In this case no correlations between Γ^{γ} and Γ^{n} for individual resonances have been observed, although there is a significant correlation between reduced (d,p) and (n,γ) strengths for transitions to the same final states. As it appears from fig. 3, there is also a clear enhancement of the capture cross section in between 10 and 30 keV. The capture cross section calculated with the strength function model, does not fit the experimental points measured by Kompe [32]. This is not due to the use of a too low p-wave neutron strength function, since the adopted value $S_1 = 7.0 * 10^{-4}$ is already 10 to 20% too high to fit the experimental total cross section points. The p-wave capture width, and the average s-wave level spacing, have been evaluated from resolved resonance parameters: $\langle \Gamma^{\gamma}_{\ell=1} \rangle = 195 \pm 18$ meV and $D_{obs} = 100 \pm 10$ eV. This example shows the type of difficulties which are encountered when non-statistical effects contribute.

Uncertainties in experimental giant resonance energies and widths are in the order of 1% and 5%, respectively. Semi-empirical descriptions of ε_r and Γ_r may also give a good estimate of these quantities [19,20]. Due to the normalization of eq. (57) the uncertainty in the peak cross sections σ_r may be neglected.

4.5. Level scheme parameters

As has been explained before, excitation energies, spins and parities of low-lying levels play a role in the determination of: (i) the "discrete" part of the total neutron transmission coefficient, (ii) the "discrete" part of the gamma width, (iii) the low-energy spin and parity distributions, (iv) the continuous level-density formulae (parameters ε_p and N_p) for the target and the compound nucleus.

In this work we assume that for $\varepsilon < \varepsilon_p$ there are *no* errors in the level scheme. For the error calculation this means that ε_p has to be taken rather low: in between 1 and 2 MeV.

---

* From recent calculations by Chrien et al. of valency capture widths for ^{98}Mo, a much higher value, $s_1 = 13 \cdot 10^{-4}$, follows. Second remark: Eq. (68) might be slightly improved by taking into account the E_γ^2 dependence by multiplying eq. (68) with the square of the neutron binding energy.

5. CALCULATIONS

5.1. Model restrictions†

For routine error calculations the model as programmed in the code FISPRO-RCN has been used. This code is an improved version of the code FISPRO [21] developed at Bologna and calculates the capture cross section according to eq. (11) with additional terms for cascade processes and direct and collective processes.

Some restrictions are made for the error calculation: (i) no uncertainties in the discrete level schemes, (ii) uncertainties mentioned in sects. 3.3. and 3.4. are neglected, (iii) $T^n_{\ell j}$ is independent of j and is calculated from strength functions (ℓ=0 to 4), (iv) uncertainties in P, ε_p, N_p, c (sect. 4.3.1.) are neglected; P is taken from ref. [15]; c = 0.146 [16], (v) $g_{J\pi}(E)$ is calculated according to eq. (67); only the parity dependence of $\langle\Gamma^\gamma_{J\pi}(0)\rangle$ is taken into account, (vi) the distributions (47,48) are used.

The following parameters are considered: S_ℓ (ℓ = 0 to 4), D^t_{obs}, D^c_{obs}, $\langle\Gamma^\gamma_{\ell=0}\rangle$, $\langle\Gamma^\gamma_{\ell=1}\rangle$, $\sigma^2_t(0)$, ε_r, Γ_r and K. The constant K is a multiplicative constant to fit the term for direct and collective capture at 14 MeV. The other parameters have been defined before. The parameter $\langle\Gamma^\gamma_{\ell=1}\rangle$ is supposed to be completely correlated with $\langle\Gamma^\gamma_{\ell=0}\rangle$.

The error calculation is performed for the average cross section $\langle\sigma\rangle_{\Delta E}$, where ΔE is determined by the group structure of the ABBN library [22]. Only one point per energy interval is calculated at the arithmetic mean energy $\bar{E}$.

5.2. Organization of the computations

The error calculation in the statistical energy range is performed with a system of four codes:

ERPREP	- prepares input for the following codes;
FISPRO-RCN	- code for cross section calculation;
FISW	- version of FISPRO-RCN for calculation of statistical model errors of sect. 3.1.;
ERCOM	- calculates statistical model errors of sect. 3.2., combines the output of all codes, calculates a correlation matrix and updates an error file.

The code ERPREP prepares the input for a large number of FISPRO-RCN runs: one run with the expectation values of the parameters and for each of the parameters listed above a run with the parameter varied over one standard deviation (the parameters $\langle\Gamma^\gamma_{\ell=0}\rangle$ and $\langle\Gamma^\gamma_{\ell=1}\rangle$ are varied simultaneously). In addition the input for the code FISW is produced.

The code FISW calculates, in addition to what the code FISPRO-RCN calculates, the width fluctuation factor W_2^2, according to eq. (34). For further processing the following quantities are stored on an intermediate file: i, ℓ, J, $\sigma_{\ell J}(\bar{E}_i)$, $D_{J\pi}$, $(W_1)_{\ell J}$, $(W_2^2)_{\ell J}$, for each value of i (energy index), ℓ and J.

In the code ERCOM these quantities are used to calculate the variances in the cross section due to fluctuating level widths according to the expression (see sect. 3.1.)

---

†Arguments for most of the model restrictions and the choice of parameters to be varied are given in previous sections.

$$\mathrm{var}(\sigma(\bar{E}_i)) = \sum_{\ell J} \sigma^2_{\ell J}(\bar{E}_i) \frac{D_{J\pi}}{\Delta\bar{E}_i} \left(\frac{W_2^2 - W_1^2}{W_1^2} \right)_{\ell J}. \qquad (69)$$

Likewise, the co-variances due to fluctuating numbers of resonances are calculated with the expression

$$\mathrm{cov}(\sigma(\bar{E}_i),\sigma(\bar{E}_j)) = \sum_{\ell J} \sigma_{\ell J}(\bar{E}_i)\sigma_{\ell J}(\bar{E}_j) \left(\frac{\mathrm{cov}(n_i,n_j)}{\langle n_i\rangle\langle n_j\rangle} \right)_{\ell J}, \qquad (70)$$

with $\langle n_i\rangle = \Delta E_i/D_{J\pi}$ and $\langle n_j\rangle = \Delta E_j/D_{J\pi}$ and $\mathrm{cov}(n_i,n_j)$, according to the recipes given in sect. 3.1.2.

The relative co-variances due to fluctuations in the number of bound target levels is (independently from the codes FISPRO-RCN and FISW) calculated in ERCOM as prescribed at the end of sect. 3.2. The quantities ε_p, ε_o, T, σ_g, μ, ν, $\bar{E}_i$ are used in this calculation.

All statistical model errors are combined to a co-variance matrix which is stored on an error file. For visual inspection the corresponding standard deviations and correlation coefficients are printed.

The quantities $\delta\sigma_k$ (eq. 50) are also processed by the code ERCOM through combination of results produced by FISPRO-RCN. These quantities are separately stored on the error file. Finally, the code ERCOM computes the total standard deviations in the capture cross section as well as the full correlation matrix.

Further processing (with other codes) takes place to update the error file with the co-variance matrix for the resolved resonance region, taking into account self-shielding effects [8]. After a correction to compensate for the neglection of the energy dependence of the product $\sigma(E)\phi(E)$ within each energy interval, the complete co-variance matrix for a mixture of fission-product nuclides can be calculated [8]. For this purpose it is possible to account for correlations between parameters of different nuclides, which becomes important when the uncertainty in lumped fission product mixtures is evaluated [23].

5.3. Results

In fig. 4 the components $\delta\sigma_k$ (eq. 50) which significantly contribute to the total standard deviation of the capture cross section of ^{103}Rh are plotted. Also indicated are the total standard deviation and the standard deviation due to statistical model errors. More details about the figure are given in the caption. The total standard deviation is rather low in this case, due to the fact that both $\langle\Gamma^\gamma\rangle$ and D^c_{obs} are well known. The largest error at low energies is due to the S_1-strength function. It is interesting to note the relatively small effects of the S_2-, S_3- and S_4-strength functions, in spite of the large uncertainties assigned. At high energies the main source of uncertainty is D^t_{obs}.

The correlation coefficients and total relative standard deviations of the capture cross section of ^{103}Rh are given in table 1. In the first part of the table the correlation coefficients and the total relative standard deviations due to statistical model errors as defined in sect. 3 are given separately, as a function of the ABBN

group number [22]. The strong correlations between the first four groups of table 1a are due to fluctuations in the number of bound levels. The other small, negative, coefficients originate from correlations between the number of resonances per energy group. When all errors are combined it appears (table 1b) that nearly all groups are strongly correlated. The negative correlation coefficients in table 1a are due to the parameter S_1 which generates a positive $\delta\sigma_k$ for low energies and a negative $\delta\sigma_k$ for high energies (see fig. 4).

The statistical model uncertainties in the calculation of the $^{103}Rh(n,\gamma)^{104}Rh$ cross section are rather small, due to the circumstance that resolved resonances are known upto E_{res} = 4.03 keV and that 24 bound target levels are known below ε_p^t = 1.294 MeV. To illustrate the possible effects of statistical model errors, a second calculation has been performed with E_{res} = 100 eV and ε_p^t = 0.2 MeV (only two excited states included). The results of this calculation are shown in figs. 5 and 6. It is seen that under this circumstance the statistical model errors predominate.

In figs. 7-9 the error components for the calculated capture cross section of ^{93}Nb, ^{139}La and ^{98}Mo have been plotted. The results for ^{93}Nb are quite similar with those for ^{103}Rh. It might be good to notice that uncertainties due to non-statistical effects (see section 4.4.3) are not included in the error calculation. In the case of ^{139}La the uncertainty in the capture width is rather high (Γ^γ is known only for two resonances), whereas the uncertainty in D_{obs}^t is relatively low as a result of the fact that some resonances have been measured in the $^{138}La(n,\gamma)^{139}La$ reaction. Consequently, the total standard deviation for the calculated capture cross section of ^{139}La is a rather flat function of energy. In the case of ^{98}Mo, large uncertainties are present in $\langle\Gamma^\gamma_{\ell=0}\rangle$, $\langle\Gamma^\gamma_{\ell=1}\rangle$, D^c_{obs} and D^t_{obs} due to uncertainties in the parity assignments of the resolved resonances. A large uncertainty in the capture cross section of ^{98}Mo is found, therefore.

In conclusion one could say that in a few favourable cases, where the resolved resonances and low-energy level schemes of both the target and the final nucleus are well known, a standard deviation of about 10% in the calculated capture cross section in between 10 keV and 1 MeV is feasible. However, non-statistical effects and systematical errors in the determination of the parameters may decrease the reliability of the statistical model calculation. Above the neutron energy of 1 MeV the statistical model has to be applied with great care, as several sources of statistical model errors, uncertainties in the distribution functions and errors in model parameters play a role. Above a few MeV also cascade processes and direct and collective processes have to be taken into account. Therefore the uncertainty in the calculated capture cross section at high energies will be larger than 40% in most cases. The correlations between average cross sections in two ABBN energy groups are large over at least three adjacent groups.

REFERENCES

[1] SCHMITTROTH, F., Neutron capture calculations for E_n=100 keV to 4 MeV, HEDL-TME73-79 (1973).

[2] SCHMITTROTH, F., Analysis of errors in computed integral cross section due to fluctuating resonance parameters, HEDL-TME72-99 (1972).

[3] DRAGT, J.B., GRUPPELAAR, H., Error analysis of neutron capture group cross sections for fast reactors, applied to fission products, RCN-192 (1973).

[4] GRUPPELAAR, H. in: Neutron capture gamma-ray spectroscopy, p. 760 (Conf. Petten, 1974), RCN, Petten, 1975.

[5] MACKELLAR, A.D., SCHENTER, R.E., Optical model for fast neutron capture cross section calculations, HEDL-TME 71-154 (1972).

[6] PEREY, F.G., Proc. Conf. on nuclear cross sections and technology, Washington D.C., 1975.

[7] GRUPPELAAR, H., DRAGT, J.B., JANSSEN, A.J., DEKKER, J.W.M., Proc. Conf. on nuclear cross sections and technology, Washington D.C., 1975.

[8] DRAGT, J.B., DEKKER, J.W.M., GRUPPELAAR, H., JANSSEN, A.J., subm. to Nucl. Sci. and Eng. (1975).

[9] MEHTA, M.L., Random matrices and the statistical theory of energy levels, Acad. Press, New York, 1967.

[10] DYSON, F.J., MEHTA, M.L., J. Math. Phys. 4 (1963) 701.

[11] DOSTROVSKY, I., FRAENKEL, Z., Phys. Rev. 116 (1959) 683.

[12] GRUPPELAAR, H. in: Nuclear data in science and technology, vol. 1, p. 553 (Symp. Paris, 1973), IAEA, Vienna, 1973.

[13] RIBON, P., KREBS, J. in: Fission product nuclear data (FPND), vol. 1, p. 235 (Panel Bologna, 1973), IAEA-169, Vienna, 1974.

[14] MUGHABGHAB, S.F., GARBER, D.I., Neutron cross sections, vol. 1, Resonance parameters, BNL-325, third ed., 1973.

[15] GILBERT, A., CAMERON, A.G.W., Can. J. of Phys. 43 (1965) 1446.

[16] FACCHINI, U., SAETTA-MENICHELLA, E., Energ. Nucl. 15 (1968) 54.

[17] REFFO, G., VACCARI, M., LARA: A FORTRAN IV code for the calculation of the compound nucleus contribution to the total radiative width in medium and heavy nuclei based on the Brink-Axel method, RT/FI(74) 17, 1974.

[18] LYNN, J.E., Theory of neutron resonance reactions, Oxford University Press, 1968.

[19] LEPRÊTRE, A. et al., Nucl. Phys. A219 (1974) 39.

[20] CARLOS, P. et al., Nucl. Phys. A219(1974) 61.

[21] BENZI, V., PANINI, G.C., REFFO, G., FISPRO II: A FORTRAN IV code for fast neutron radiative capture calculations. RT/FI(69) 44, 1969.

[22] ABAGYAN, L.P., BAZAZYANTS, N.O., BONDARENKO, J.I., NIKOLAEV, M.N., Group constants for nuclear reactor calculations, Consultants Bureau, New York, 1964.

[23] GRUPPELAAR, H. (comp.), RCN-1 pseudo fission product capture group cross sections, RCN-205, 1974.

[24] DRESNER, L., Resonance absorption of neutrons in nuclear reactors (diss. Princeton University), ORNL-2659, 1959.

[25] ERICSON, T., Phys. Rev. Lett. 5 (1960) 430.

[26] BENZI, V., REFFO, G., VACCARI, M. in: Fission product nuclear data (FPND), vol. III, p. 123 (Panel Bologna, 1973), IAEA-169, Vienna, 1974.

[27] MUSGROVE, A.R. de L., Interpolative formulae for average nuclear level spacing and total radiation width, AAEC/E211 (1970).

[28] WEIGMANN, H., ROHR, G. in: Nuclear physics with thermal and resonance energy neutrons, p. 194 (Symp. Petten, 1973), RCN-203 (1973).
[29] REFFO, G., CNEN, Bologna, private communication, 1975.
[30] RIMAWI, K., CHRIEN, R.E. in: Neutron capture gamma-ray spectroscopy, p. 369 (Conf. Petten, 1974), RCN, Petten, 1975.
[31] HASTE, T.J., THOMAS, B.W. in: Neutron capture gamma-ray spectroscopy, p. 294 (Conf. Petten, 1974), RCN, Petten, 1975.
[32] KOMPE, D., Nucl. Phys. A133 (1969) 513.
[33] YAMAMURO, N. et al., Proc. Conf. on nuclear cross sections and technology, Washington D.C., 1975.
[34] POENITZ, W.P., Fast neutron capture and activation cross sections of niobium isotopes, ANL/NDM-8 (1974).
[35] HOWERTON, H., SMITH, A., GUENTHER, P., WHALEN, J., Evaluated neutronic cross section file for niobium, ANL/NDM-6 (1974).
[36] BENZI, V., D'ORAZI, R., REFFO, G., VACCARI, M., Fast neutron radiative capture cross sections of stable nuclei with $29 \leq Z \leq 79$, RT/FI(72) 6.
[37] IGARASI, S., J. of Nucl. Sc. and Techn. 12 (1974) 67 (appendix).
[38] BROWN, G.E., Nucl. Phys. 57 (1964) 339.
[39] COQ, G. LE, FISINGA, programme de sections efficaces neutroniques, internal report CEA-Saclay (1970).

Table 1. Correlations and relative standard deviations for the capture cross section of ^{103}Rh.

a) Correlations and total standard deviations due to statistical model errors

	1	2	3	4	5	6	7	8	9	10	11	12	13	total	ΔE (keV)
1	1.000	.287	.088	.033										.001	6500-10500
2		1.000	.527	.219										.012	4000-6500
3			1.000	.596										.046	2500-4000
4				1.000										.059	1400-2500
5					1.000								-.001	.002	800-1400
6						1.000							-.001	.003	400-800
7							1.000						-.002	.003	200-400
8								1.000					-.002	.005	100-200
9									1.000				-.002	.009	47.5-100
10										1.000	-.002		-.003	.015	21.5-47.5
11											1.000	-.003	-.003	.025	10.0-21.5
12												1.000	-.011	.040	4.65-10.0
13													1.000	.132	2.15-4.65

b) Correlations and total standard deviations due to all types of errors

	1	2	3	4	5	6	7	8	9	10	11	12	13	total	ΔE (keV)
1	1.00	.98	.72	.21	.17	.24	.26	.26	.22	.14	.06	.03	.02	.72	6500-10500
2		1.00	.79	.29	.22	.24	.22	.20	.16	.09	.03	.00	.01	.73	4000-6500
3			1.00	.82	.71	.65	.55	.45	.35	.21	.09	.05	.13	.29	2500-4000
4				1.00	.95	.83	.65	.52	.40	.24	.11	.07	.19	.24	1400-2500
5					1.00	.93	.73	.58	.42	.22	.04	-.04	-.01	.19	800-1400
6						1.00	.87	.75	.59	.38	.18	.10	.09	.15	400-800
7							1.00	.98	.91	.76	.59	.50	.36	.10	200-400
8								1.00	.97	.87	.72	.63	.46	.10	100-200
9									1.00	.96	.86	.78	.58	.10	47.5-100
10										1.00	.97	.92	.70	.10	21.5-47.5
11											1.00	.99	.78	.12	10.0-21.5
12												1.00	.85	.13	4.65-10.0
13													1.00	.17	2.15-4.65

FIGURE CAPTIONS

fig. 1 Sensitivity of the calculated cross section of the $^{93}Nb(n,\gamma)^{94}Nb$ reaction for changes in ε_p^t and c.
The "normal" values of ε_p^t and c used in the calculation are ε_p^t = 1.15 MeV and c = 0.146 [16]. The parameters have been varied to ε_p = 1.28 MeV and c = 0.0888 [15], respectively. Other parameters used in the calculations are given in the caption of fig. 7.

fig. 2 Sensitivity of the calculated cross section of the $^{98}Mo(n,\gamma)^{99}Mo$ reaction for a change in c. The two values used for c are c = 0.146 [16] and c = 0.0888 [15]. Other parameters used in the calculations are given in the caption of fig. 9.

fig. 3 Evaluated capture cross sections of ^{93}Nb compared with experimental values. The experimental points are from Yamamuro et al. [33], Kompe [32] and Poenitz [34]. Evaluated curves are from Howerton et al. [35], Benzi et al. [36] and from RCN.
The dashed curve is calculated with a strength function model, with $S_0 = 0.36*10^{-4}$, $S_1 = 7.0*10^{-4}$, $S_2 = 0.57*10^{-4}$, $\langle\Gamma^\gamma_{\ell=0}\rangle$ = 146 meV, $\langle\Gamma^\gamma_{\ell=1}\rangle$ = 195 meV, D^c_{obs} = 100 eV.
(These parameters have also been used for figs. 1 and 7).
The discrepancy between the dashed curve and the measured points might be due to the existence of doorway states in the capture process. Above 50 keV the RCN-2 evaluated curve has been calculated with the statistical model where the transmission coefficients are calculated with the optical model, and the other parameters are as given in the caption of fig. 7.

fig. 4 Total standard deviations and error components of the calculated cross section of the $^{103}Rh(n,\gamma)^{104}Rh$ reaction.
The explanation of the symbols used in the inset of the figure is given in the text. The values of the parameters and their relative standard deviations (given in parenthesis) are as follows: $S_0 = 0.47*10^{-4}$ (15%), $S_1 = 6.50*10^{-4}$ (30%), $S_2 = 3.25*10^{-4}$ (100%), $S_3 = 3.25*10^{-4}$ (100%), $S_4 = 3.45*10^{-4}$ (100%), $\langle\Gamma^\gamma_{\ell=0,1}\rangle$ = 161 meV (6%), D^c_{obs} = 26.1 eV (-3%), D^t_{obs} = 48 eV (-70%), σ_t^2 = 6.5 (20%), ε_r = 16.1 MeV (1%), Γ_r = 7.4 MeV (5%), K = 1.23 (20%).
The first energy of the statistical calculation is at E_{res} = 4.03 keV; ε_p^t = 1.294 MeV. This figure corresponds to table 1.

fig. 5 Total standard deviations and error components of the calculated cross section of the $^{103}Rh(n,\gamma)^{104}Rh$ reaction, extending the statistical calculation to very low energies (E_{res} = 100 eV) and assuming that the target level scheme is unknown above ε_p^t = 0.2 MeV. All other parameters are as given in the caption of fig. 4.

fig. 6 Statistical model errors for the cross section of the $^{103}Rh(n,\gamma)^{104}Rh$ reaction, calculated with the same assumptions as given in the caption of fig. 5. The three components which contribute to the total standard deviations are due to fluctuations in: the level widths, number of resonances per averaging interval, and number of bound target levels involved.

fig. 7 Total standard deviations and error components of the calculated cross section of the $^{93}Nb(n,\gamma)^{94}Nb$ reaction. The values of the parameters and their relative standard deviations (given in parenthesis) are as follows: $S_0 = 0.36*10^{-4}$ (17%), $S_1 = 7.0*10^{-4}$ (50%), $S_2 = 0.57*10^{-4}$ (100%), $S_3 = 6.0*10^{-4}$ (100%), $S_4 = 2.7*10^{-4}$ (100%), $\langle\Gamma^{\gamma}_{\ell=0}\rangle$ = 146 meV (3.5%), $\langle\Gamma^{\gamma}_{\ell=1}\rangle$ = 195 meV (9.5%), D^{c}_{obs} = 100 eV (-10%), D^{t}_{obs} = 41 eV (-75%), ε_r = 16.5 MeV (1%), Γ_r = 4.7 MeV (5%), K = 0.75 (25%), σ^2_t = 12 (40%). The first energy of the statistical calculation is at E_{res} = 7.37 keV; ε^{t}_{p} = 1.15 MeV. The capture cross section of ^{93}Nb calculated with these parameters has been plotted in figs. 1 and 3.

fig. 8 Total standard deviations and error components of the calculated cross section of the $^{139}La(n,\gamma)^{140}La$ reaction. The values of the parameters and their relative standard deviations (given in parenthesis) are as follows: $S_0 = 0.64*10^{-4}$ (23%), $S_1 = 2.0*10^{-4}$ (100%), $S_2 = 3.3*10^{-4}$ (100%), $S_3 = 6.1*10^{-4}$ (100%), $S_4 = 2.8*10^{-4}$ (100%), $\langle\Gamma^{\gamma}_{\ell=0}\rangle = \langle\Gamma^{\gamma}_{\ell=1}\rangle$ = 50 eV (25%), D^{c}_{obs} = 290 eV (-9%), D^{t}_{obs} = 41 eV (-17%), ε_r = 15.1 MeV (1%), Γ_r = 5.0 MeV (5%), σ^2_t = 8.2(20%), K = 0.55 (24%). The first energy of the statistical calculations is at E_{res} = 10.5 keV; ε^{t}_{p} = 1.96 MeV.

fig. 9 Total standard deviations and error components of the calculated cross section of the $^{98}Mo(n,\gamma)^{99}Mo$ reaction. The values of the parameters and their relative standard deviations (given in parenthesis) are as follows: S_0 = $0.35*10^{-4}$ (40%), $S_1 = 7.0*10^{-4}$ (50%), $S_2 = 0.54*10^{-4}$ (100%), $S_3 = 3.94*10^{-4}$ (100%), $S_4 = 3.04*10^{-4}$ (100%), $\langle\Gamma^{\gamma}_{\ell=0}\rangle$ = 86 meV (17%), $\langle\Gamma^{\gamma}_{\ell=1}\rangle$ = 120 meV (20%), D^{c}_{obs} = 800 eV (-30%), D^{t}_{obs} = 1300 eV (-75%), ε_r = 15.8 MeV (1%), Γ_r = 6.0 MeV (5%), K = 1.6 (50%), σ^2_t = 6.6 (18%). The first energy of the statistical model calculation is at E_{res} = 5.39 keV; ε^{t}_{p} = 2.74 MeV. The capture cross section of ^{98}Mo calculated with these parameters has been plotted in fig. 2.

N.B. The energies at which the uncertainties are estimated do correspond with the arithmetic mean energy of the ABBN groups.

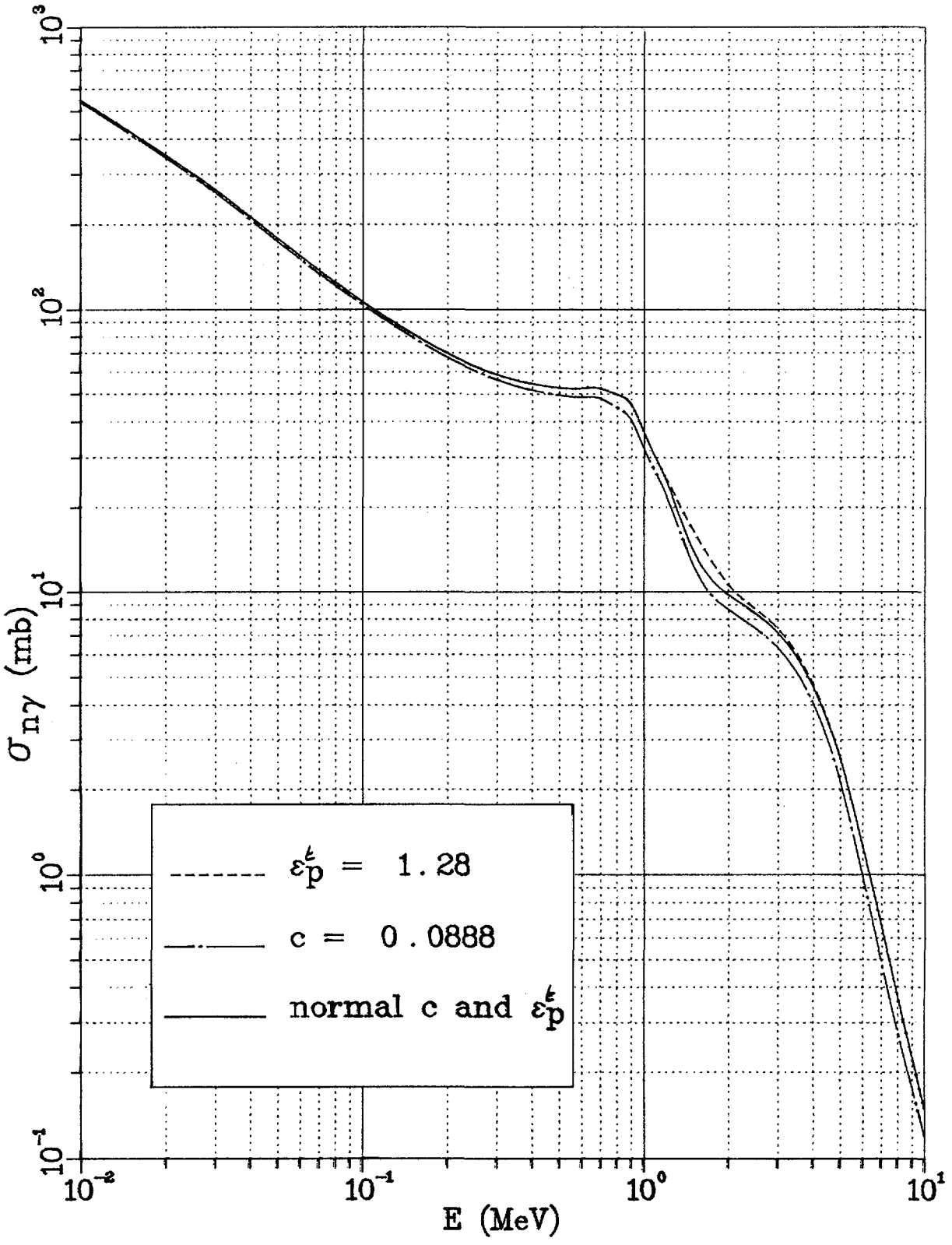
10^3
10^2
10^1
10^0
10^{-1}
$\sigma_{n\gamma}$ (mb)
10^{-2}
10^{-1}
10^0
10^1
E (MeV)
ε_p^t = 1.28
c = 0.0888
normal c and ε_p^t

Fig. 1.

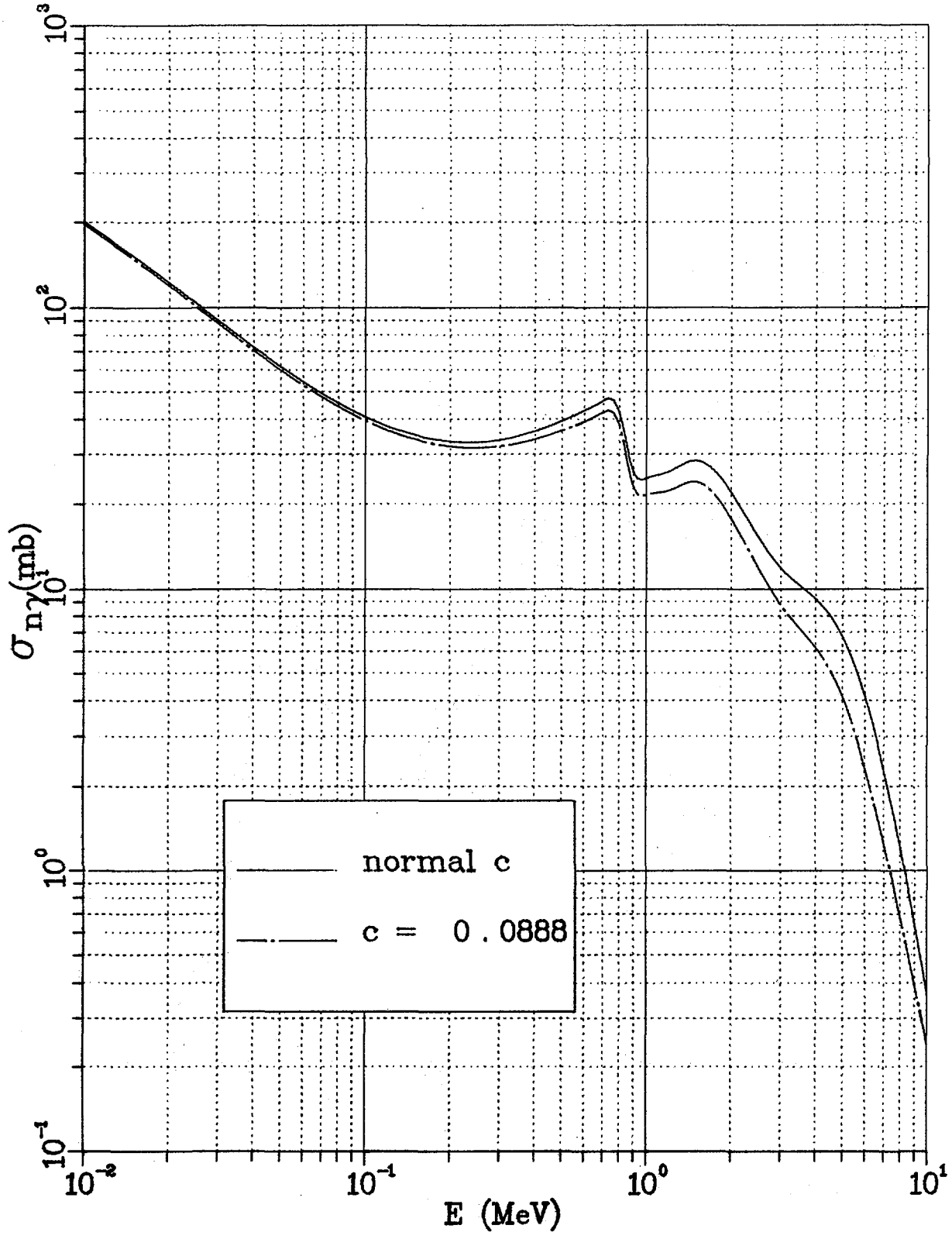
10^3
10^2
10^1
10^0
10^{-1}
$\sigma_{n\gamma}$(mb)
normal c
c = 0.0888
10^{-2}
10^{-1}
10^0
10^1
E (MeV)

Fig. 2.

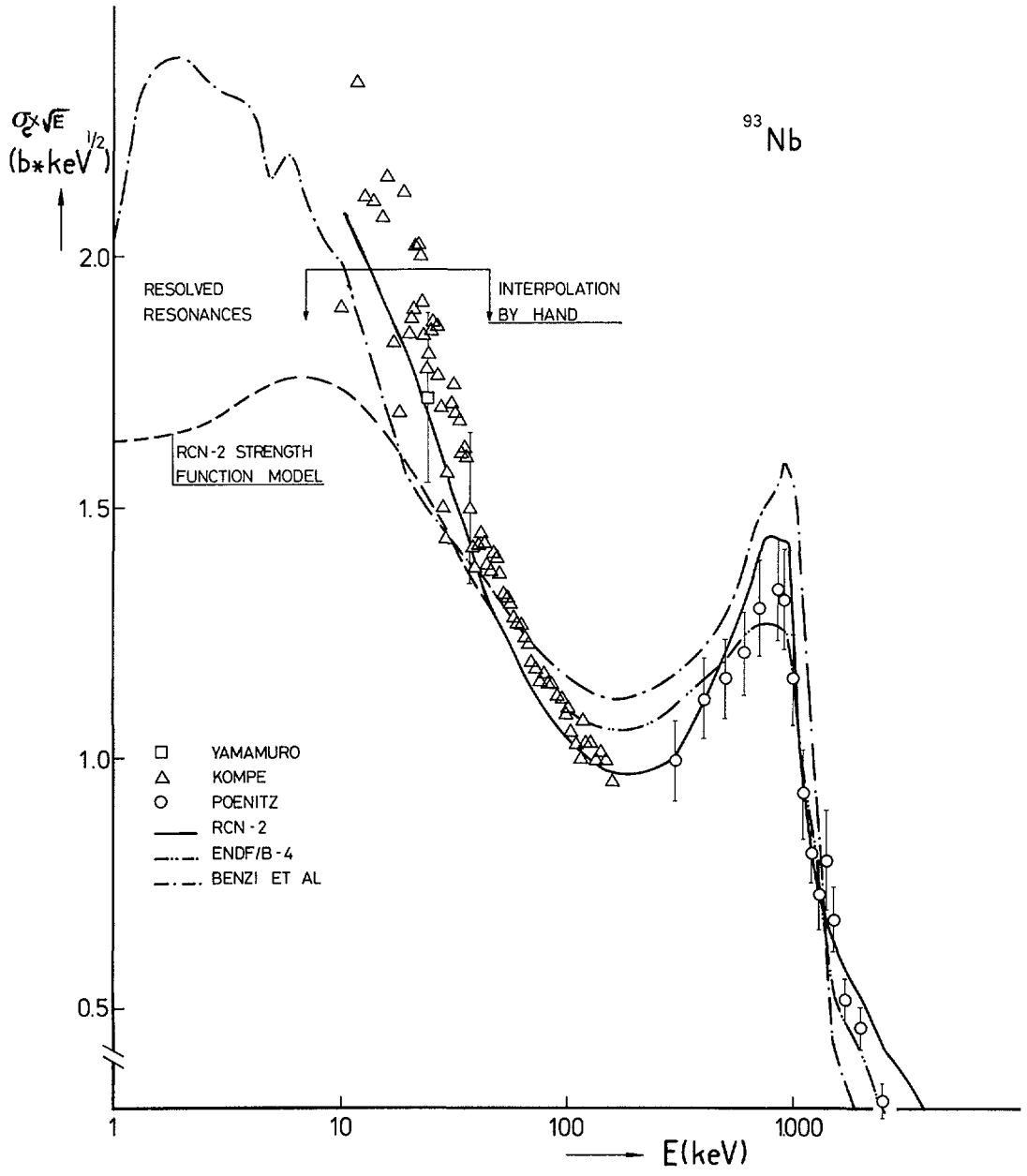
$\sigma_c \times \sqrt{E}$
(b*keV$^{1/2}$)
^{93}Nb
2.0
1.5
1.0
0.5
RESOLVED
RESONANCES
INTERPOLATION
BY HAND
RCN-2 STRENGTH
FUNCTION MODEL
YAMAMURO
KOMPE
POENITZ
RCN-2
ENDF/B-4
BENZI ET AL
1
10
100
1000
E(keV)

Fig. 3.

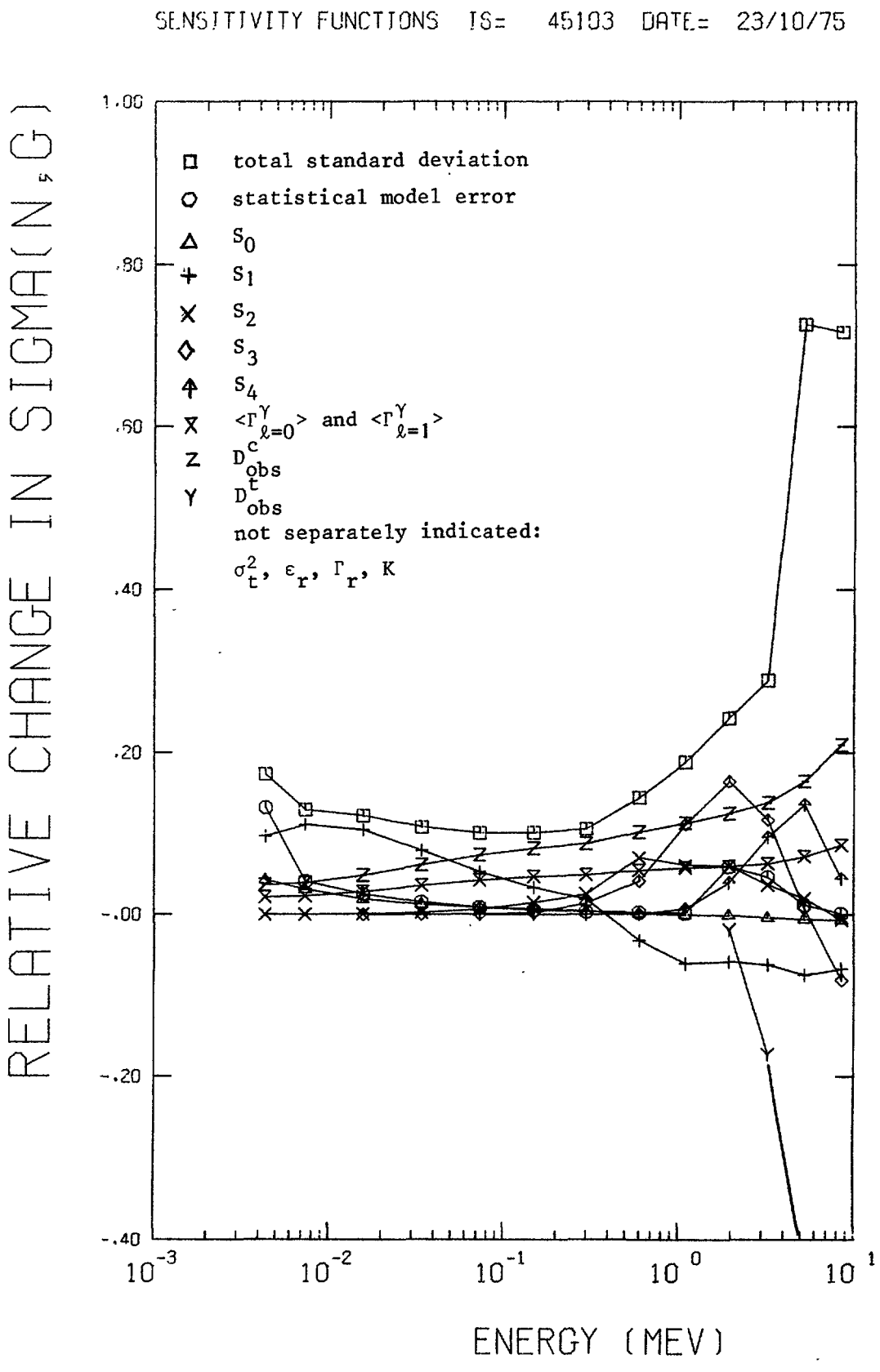
SENSITIVITY FUNCTIONS IS= 45103 DATE= 23/10/75
RELATIVE CHANGE IN SIGMA(N,G)
1.00
.80
.60
.40
.20
-.00
-.20
-.40
total standard deviation
statistical model error
S_0
S_1
S_2
S_3
S_4
$\langle \Gamma^{\gamma}_{\ell=0} \rangle$ and $\langle \Gamma^{\gamma}_{\ell=1} \rangle$
D^{c}_{obs}
D^{t}_{obs}
not separately indicated:
σ^2_t, ε_r, Γ_r, K
10^{-3}
10^{-2}
10^{-1}
10^{0}
10^{1}
ENERGY (MEV)

Fig. 4.

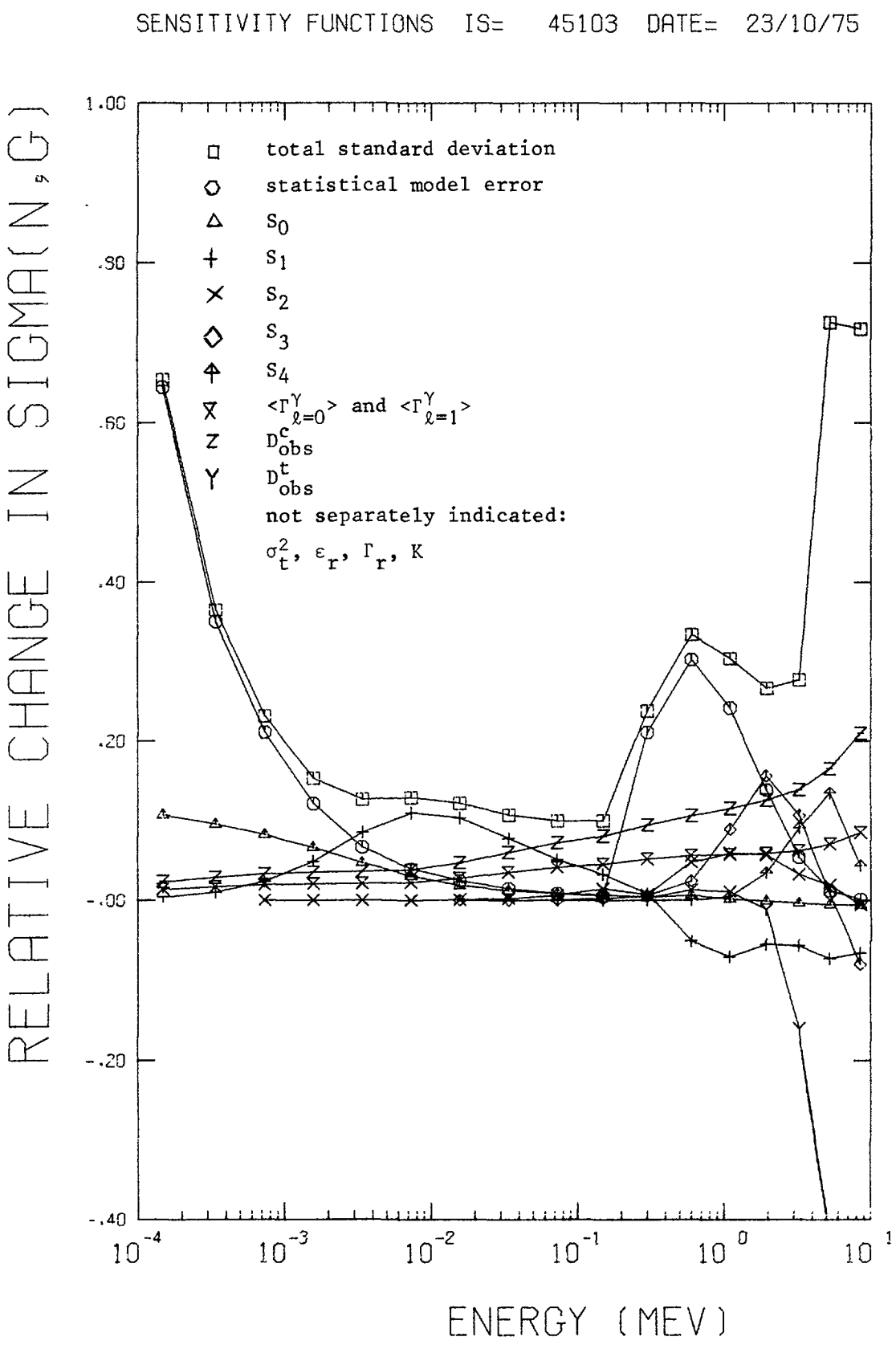
SENSITIVITY FUNCTIONS IS= 45103 DATE= 23/10/75
RELATIVE CHANGE IN SIGMA(N,G)
1.00
.80
.60
.40
.20
-.00
-.20
-.40
total standard deviation
statistical model error
S_0
S_1
S_2
S_3
S_4
$\langle\Gamma^{\gamma}_{\ell=0}\rangle$ and $\langle\Gamma^{\gamma}_{\ell=1}\rangle$
D^{c}_{obs}
D^{t}_{obs}
not separately indicated:
σ^2_t, ε_r, Γ_r, K
10^{-4}
10^{-3}
10^{-2}
10^{-1}
10^{0}
10^{1}
ENERGY (MEV)

Fig. 5.

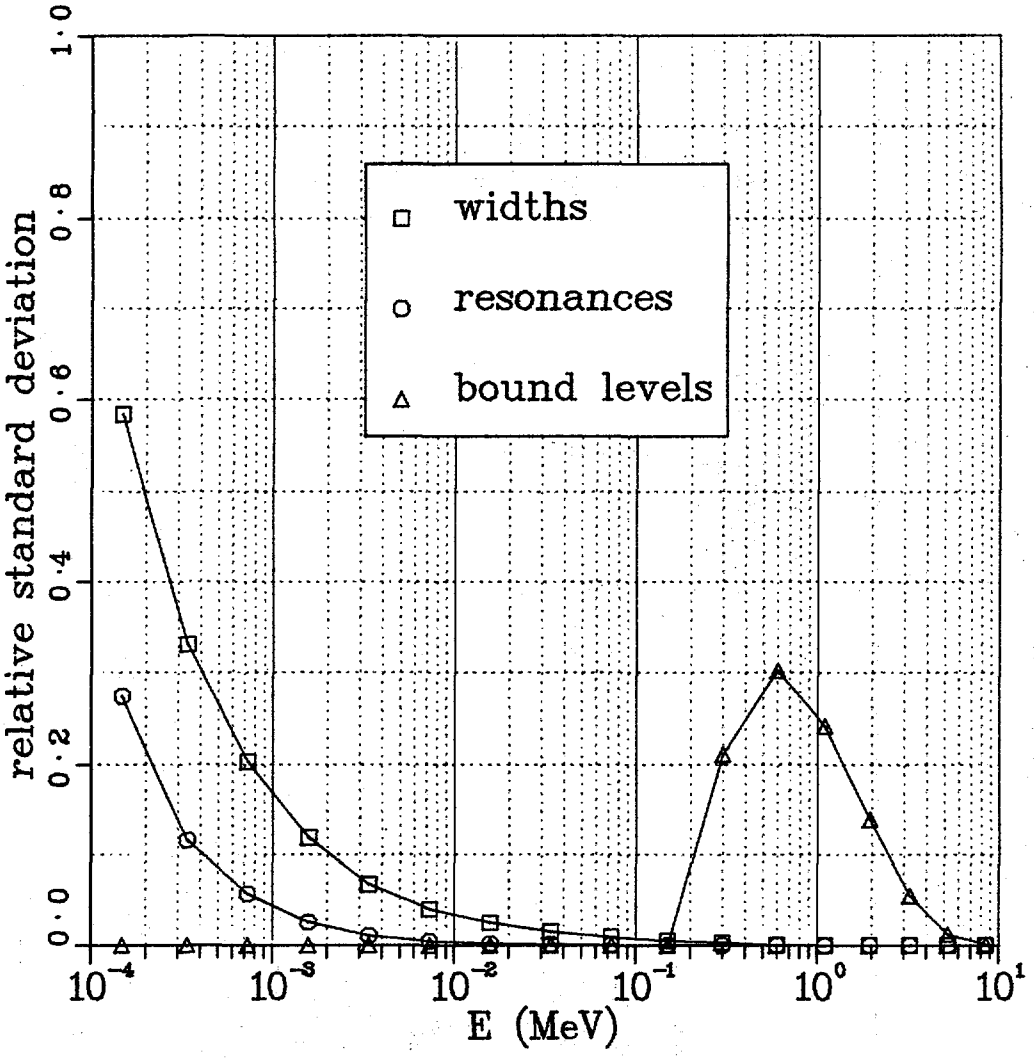
relative standard deviation
0·0
0·2
0·4
0·6
0·8
1·0
widths
resonances
bound levels
10^{-4}
10^{-3}
10^{-2}
10^{-1}
10^{0}
10^{1}
E (MeV)

Fig. 6.

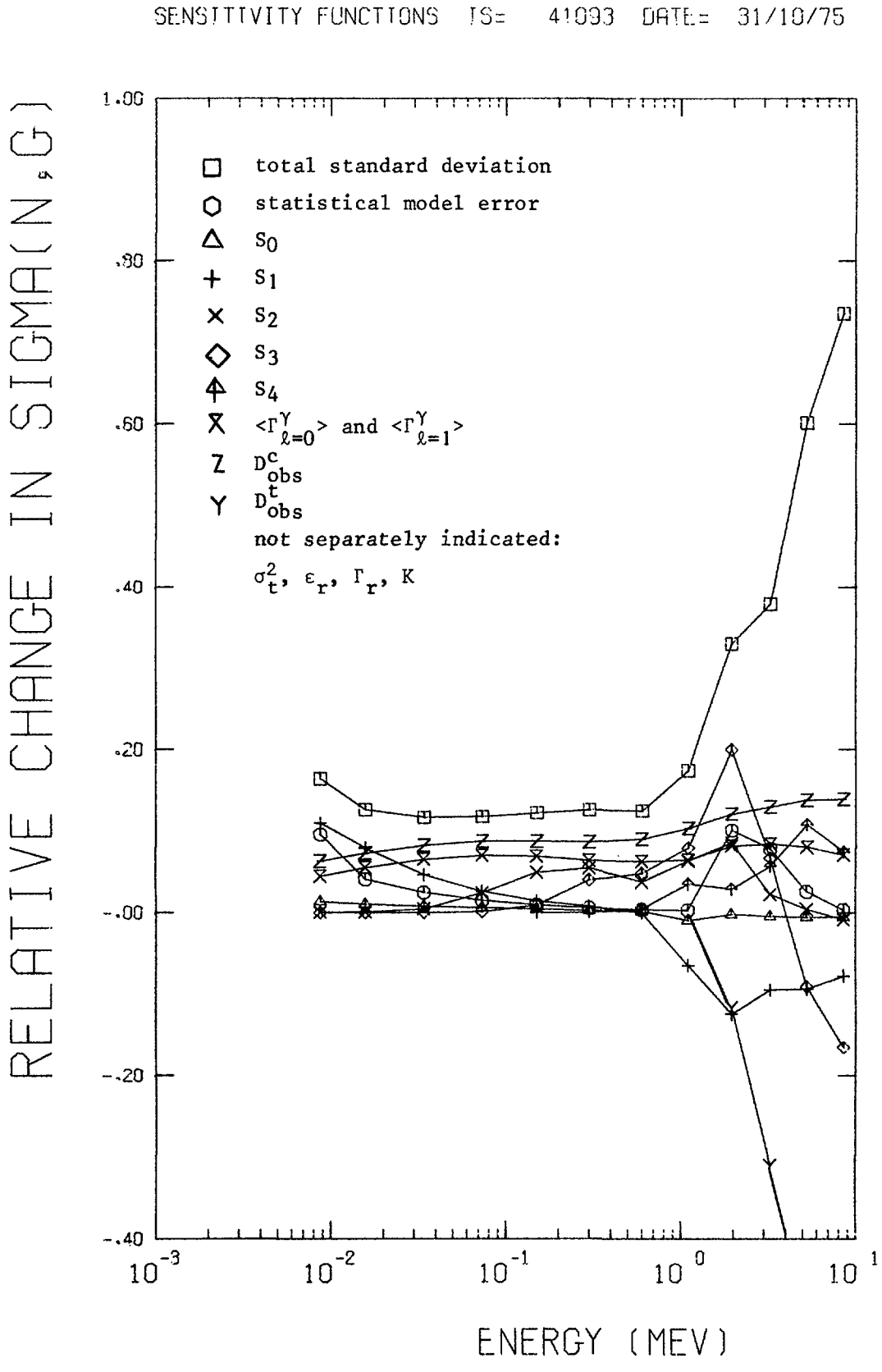
SENSITIVITY FUNCTIONS IS= 41093 DATE= 31/10/75
RELATIVE CHANGE IN SIGMA(N,G)
1.00
.80
.60
.40
.20
-.00
-.20
-.40
total standard deviation
statistical model error
S_0
S_1
S_2
S_3
S_4
$\langle\Gamma^{\gamma}_{\ell=0}\rangle$ and $\langle\Gamma^{\gamma}_{\ell=1}\rangle$
D^{c}_{obs}
D^{t}_{obs}
not separately indicated:
σ^2_t, ε_r, Γ_r, K
10^{-3}
10^{-2}
10^{-1}
10^{0}
10^{1}
ENERGY (MEV)

Fig. 7.

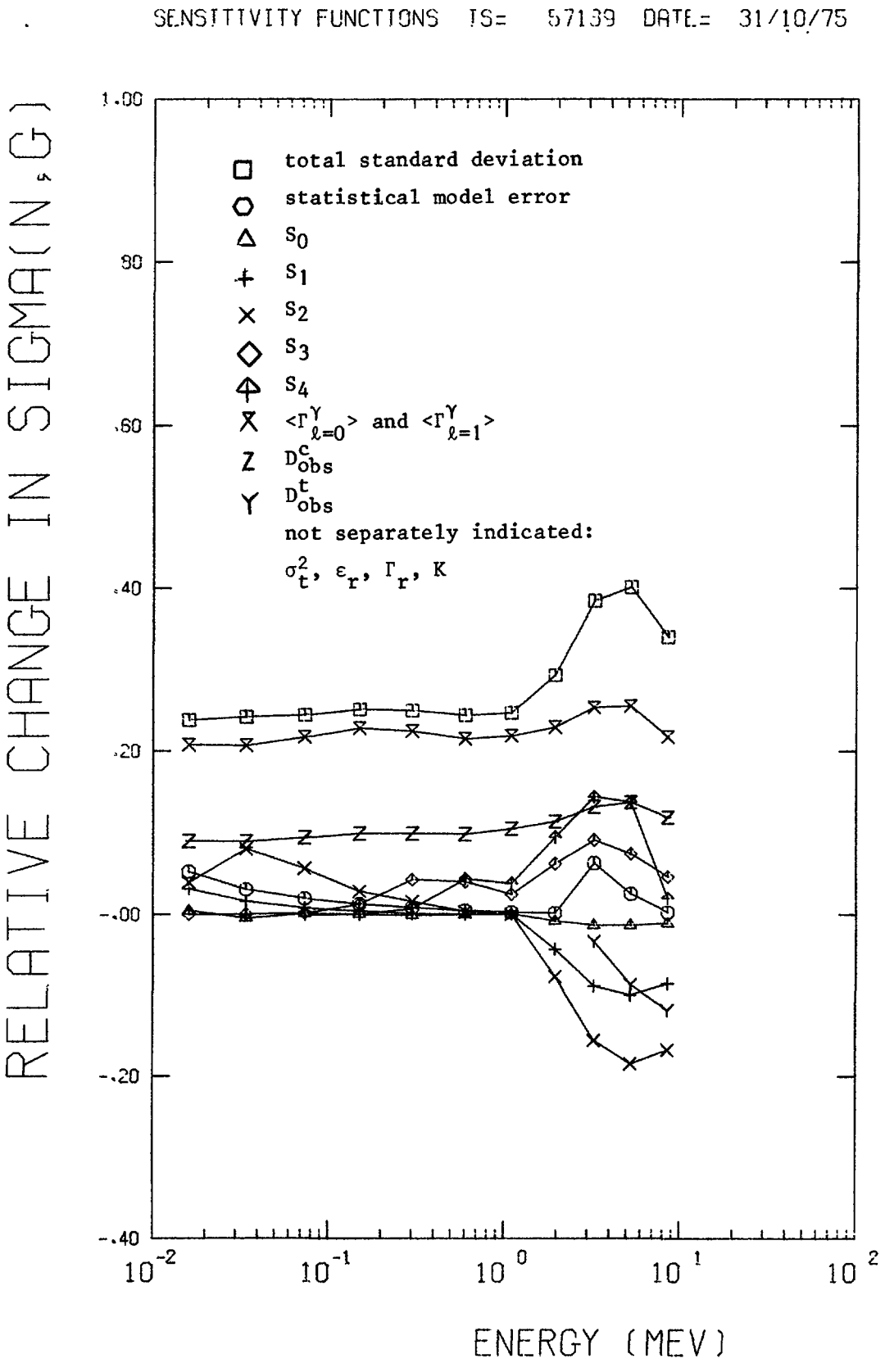
SENSITIVITY FUNCTIONS IS= 57139 DATE= 31/10/75
RELATIVE CHANGE IN SIGMA(N,G)
1.00
.80
.60
.40
.20
-.00
-.20
-.40
total standard deviation
statistical model error
S_0
S_1
S_2
S_3
S_4
$\langle\Gamma^{\gamma}_{\ell=0}\rangle$ and $\langle\Gamma^{\gamma}_{\ell=1}\rangle$
D^{c}_{obs}
D^{t}_{obs}
not separately indicated:
σ^2_t, ε_r, Γ_r, K
10^{-2}
10^{-1}
10^{0}
10^{1}
10^{2}
ENERGY (MEV)

Fig. 8.

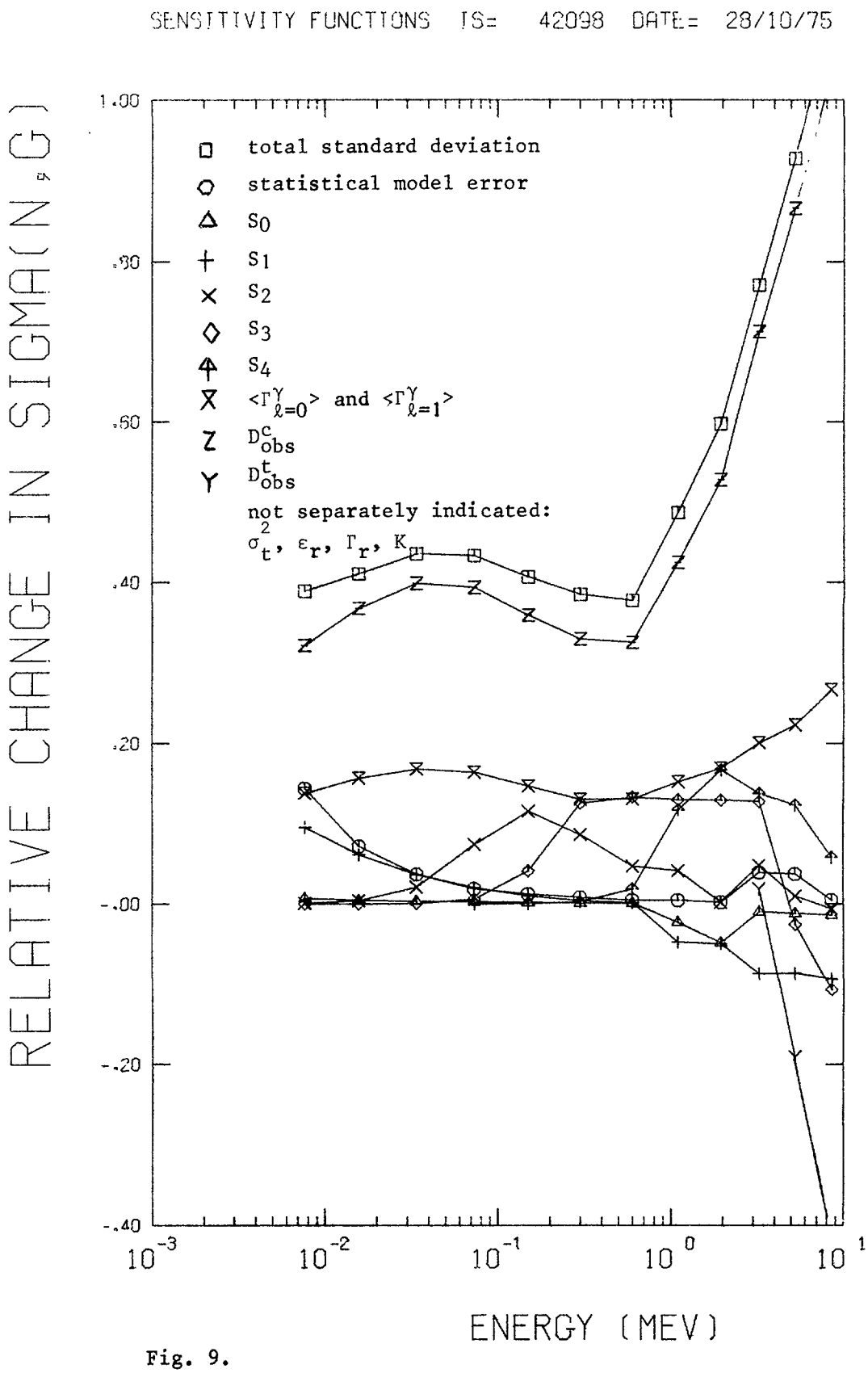
SENSITIVITY FUNCTIONS IS= 42098 DATE= 28/10/75
RELATIVE CHANGE IN SIGMA(N,G)
1.00
.80
.60
.40
.20
-.00
-.20
-.40
total standard deviation
statistical model error
S0
S1
S2
S3
S4
<Γγ ℓ=0> and <Γγ ℓ=1>
Dc obs
Dt obs
not separately indicated:
σ2t, εr, Γr, K
10-3
10-2
10-1
10 0
10 1
ENERGY (MEV)

Fig. 9.

Contributed Paper No. 5

Uncertainties and applications of the nuclear level density with inclusion of collective rotations.

A.S. Jensen
Institute of Physics, University of Aarhus
DK-8000 Aarhus C, Denmark

ABSTRACT

The collective rotations are included for small excitation energies in the level density of deformed nuclei by addition of a rotational band on top of each of the intrinsic levels. Estimates of the effect are given. Uncertainties of the calculations are studied in a realistic model. The calculations using different models are compared with level density observations. Examples of applications to fission probability calculations are discussed in connection with the comparison to available experimental data. The capability for predicting unknown data is thus indicated. Finally it is outlined how more flexible and thereby more useful level density expressions might be obtained.

Uncertainties and applications of the nuclear level density with inclusion of collective rotations.

A.S. Jensen
Institute of Physics, University of Aarhus
DK-8000 Aarhus C, Denmark

1. INTRODUCTION

There are several interrelated purposes of this paper. The first is to describe how to calculate the nuclear level density with collective rotations included. Thus in Sect. 2 the theory is briefly sketched and estimates of the effect of the collective rotations is given.

The second purpose is to estimate the uncertainties involved in the calculations. In Sect. 3 such estimates are given for the level density calculated from a reasonable single particle spectrum. The reliability is further investigated by comparison to available experimental values.

The third purpose is to illustrate the predicting power of models where the level density enters very directly. This is done in Sect. 4 where different measurements were analyzed using such models. This illucidates (with the results of Sect. 3) the possible applications limited by the uncertainties involved in the calculations.

The fourth purpose is to indicate improvements or different ways to proceed to obtain higher predicting power. In Sect. 5 is outlined a possibility of how this goal may be approached.

2. THEORY

The Hamiltonian describing the nuclear system is assumed of the form

$$\hat{H} = \sum_k \{ \sum_{i>o} \epsilon_i \, (a_i^+ a_i + a_{\bar{i}}^+ a_{\bar{i}}) - G_k \sum_{i,i'>o} a_i^+ a_{\bar{i}}^+ a_{\bar{i}'} a_{i'} \} \qquad (1)$$

where $a_i^+ \, (a_{\bar{i}}^+)$ is the creation operator for a particle (neutron or proton)

with single particle energy ϵ_i and with spin up (down) in the state labelled by i. If axial symmetry is assumed each single particle state has a given projection Ω_i of the angular momentum on the symmetry axis. The pairing strength G_k (k = neutron, proton) may be different for the two kind of particles.

2.1. Level density of spherical nuclei.

From the Hamiltonian in Eq. (1) the nuclear level density ρ may be evaluated in the saddle point approximation [1], [2]. The result is given by the familiar expression

$$\rho(E,N_n,N_p,K) = \frac{\exp(S)}{(2\pi)^2\sqrt{D}} \tag{2}$$

where the given average values of excitation energy E, number of neutrons N_n and protons N_p and projection K of the angular momentum are constraints on the system enforced by the corresponding Lagrangian multipliers β, λ_n, λ_p and γ. Both S and D are given as functions [2] of these solutions β, λ_n, λ_p and γ to the equations

$$E + E_o = \sum_k \{ \sum_{i>o} \epsilon_i (1-f_i^+(\epsilon_i-\lambda_k)/E_i) - \Delta_k^2/G_k \} \tag{3}$$

$$N_k = \sum_{i>o} (1-f_i^+(\epsilon_i-\lambda_k)/E_i), \qquad k= n,p \tag{4}$$

$$K = \sum_k \{ \sum_{i>o} \Omega_i f_i^- \} \tag{5}$$

If the pairing gaps Δ_k are finite they must satisfy the gap equations

$$2/G_k = \sum_{i>o} f_i^+/E_i \quad , \qquad k = n,p \tag{6}$$

When $T \equiv 1/\beta = 0$, $K = 0$ we have $E = 0$ defining E_o. The remaining quantities are given by

$$2f_i^{\pm} = \mathrm{Tanh}\,[\tfrac{1}{2}\beta(E_i+\gamma\Omega_i)] \pm \mathrm{Tanh}[\tfrac{1}{2}\beta(E_i-\gamma\Omega_i)] \tag{7}$$

$$E_i = \sqrt{(\epsilon_i-\lambda)^2+\Delta^2} \tag{8}$$

The procedure is now the following. The six equations (3) - (6) are for given E, N_k, K, G_k solved for β, λ_n, λ_p, γ, Δ_n, Δ_p. If no positive solutions for Δ_n and Δ_p can be found, one or both of Eqs. (6) are omitted and the corresponding Δ is assumed equal to zero.

Because of the pairing this procedure is only valid for doubly even nuclei. Considering the odd nucleus as an even nucleus plus one or two quasiparticles the systematic odd-even differences are accounted for [3]. Thus no special

attention is needed for odd systems.

The level density as function of the total angular momentum I may now be evaluated. Omitting all arguments of ρ except K the usual way to proceed [4] is to decompose $\rho(K)$ in parts of given I

$$\rho(K) = \sum_{I=K}^{\infty} \rho(K,I) \tag{9}$$

Under the assumption that ρ for a given I is independent of K i.e.

$$\rho(K=I_o,I) = \rho(K=I_o+1,I) \equiv \rho_{sym.}(I) \tag{10}$$

this leads to

$$\rho(K=I_o) - \rho(K=I_o+1) = \rho(K=I_o,I=I_o) = \rho_{sym.}(I=I_o) \tag{11}$$

When the K-distribution of ρ is Gaussian [1], [5] we find [2]

$$\rho_{sym.}(I) = \frac{2I+1}{2\sigma^2}\, \rho(K = I+\tfrac{1}{2}) \tag{12}$$

where the spin cut-off parameter is given as

$$\sigma^2 = \tfrac{1}{2} \sum_k \{ \sum_{i>o} \frac{\Omega_i^2}{\cosh^2(\frac{1}{2}\beta E_i)} \} \tag{13}$$

This derivation of Eq.(12) assumes that $\rho(K,I)$ is independent of the projection axis (here the symmetry axis) i.e. the system is assumed rotationally symmetric. Hence the label sym. on the resulting level density.

2.2. Level density of deformed nuclei.

For deformed nuclei rotational bands are built on top of each intrinsic state. For axial symmetric nuclei (considered so far) the rotational energy is given as

$$E_{rot.}(I,K) = \frac{\hbar^2}{2J_\perp}(I(I+1)-K^2) \tag{14}$$

where $J_\perp$ is the moment of inertia around an axis perpendicular to the symmetry axis. When the coupling between intrinsic and collective degrees of freedom is neglected the level density becomes [4]

$$\rho_{unif.}(E,I) = \sum_{K=-I}^{I} \rho(E-E_{rot.}(I,K),K) \tag{15}$$

We have now explicitely written also the energy argument in the level density of Eq.(2). Because this level density has contributions both from internal and collective degrees of freedom we label it unif. [3].

For small I-values we find [4] from Eqs.(12) and (15)

$$\frac{\rho_{unif.}}{\rho_{sym.}} \approx 2\sigma^2 \tag{16}$$

Depending on nucleus, deformation and excitation energy we have $\sigma^2 \simeq 10\text{–}100$.

Although we are not to consider non-axial systems it is maybe worth to give the effect on the level density. In this case K is not a conserved quantum number and the level density now becomes [4]

$$\rho_{n.a.}(I) = \sum_{\tau=1}^{2I+1} \rho(E-E_{rot.}(I,\tau)) \tag{17}$$

where τ labels the $2I+1$ different states with a given I. The argument K has disappeared and should in this case be removed from the preceding derivation. Again we obtain for small I-values

$$\rho_{n.a.}(I) \approx (2I+1)\rho(E) \tag{18}$$

which for a Gaussian K-distribution leads to

$$\frac{\rho_{n.a.}}{\rho_{sym.}} \approx 2\sigma^2 \frac{\rho(E)}{\rho(E,K=0)} \approx \sigma^3 \sqrt{8\pi} \tag{19}$$

For the non-spherical level densities Eqs.(15) and (17) the space reflection symmetry is assumed broken (pear-shape). If this symmetry is preserved the level densities should be reduced by a factor of two [4].

The inclusion of rotational states in this way introduces too many degrees of freedom. Double counting might therefore become a problem. To avoid this the coupling (i.e. the coriolis coupling) between intrinsic and rotational motion should be treated properly. The operator in this coupling term creating the particle-hole excitations is J_x (the angular momentum component along the rotation axis, the x-axis). The energies are consequently for the harmonic oscillator of the order $\hbar(\omega_y - \omega_z)$. When the nuclear temperature becomes comparable with this energy these particle-hole excitations are already counted among the intrinsic excitations. Thus they should not also be counted as collective rotational states. For actinides and rare earth nuclei a rough estimate of the corresponding excitation energy gives around 50 MeV for typical ground state deformations [6]. Very crudely we can in such cases say that below 50 MeV the rotations should be included as described, and above 50 MeV only intrinsic excitations should be counted. A proper treatment of the transition region is not formulated at the moment.

3. CALCULATED LEVEL DENSITIES COMPARED WITH OBSERVATIONS

The level density has been determined experimentally at the neutron separation energy for nuclei covering most of the periodic table. A comparison between calculations and these observations is therefore natural. Fortunately the neutron binding energy is about an order of magnitude smaller than the critical energy of around 50 MeV mentioned in Sect. 2.2, thus for deformed nuclei the rotations are expected to contribute fully as described above.

3.1. Results.

Only a few systematic investigations using different sets of single particle energies ϵ_i have appeared. One of them [3] obtains ϵ_i from an axial symmetric deformed average potential of the Woods-Saxon type. The functional form of the radius, depth and diffuseness parameters are taken from a Thomas-Fermi calculation [7]. The ground state deformations used are obtained by the shell correction method [8] for nuclei with mass number A between 140 and 253. The lightest nuclei considered ($100 \leq A \leq 140$) were all assumed spherical.

In fig. 1 we show the resulting ratio of the calculated and observed level density. The experimental values are taken from Lynn [9]. Systematic odd-even effects are reproduced as mentioned in sect. 2.1.

In the deformed region $\rho_{unif.}$ is on the average a factor four too small and except for a few nuclei we have $0.2 \leq \rho_{unif.}/\rho_{obs.} \leq 0.5$. The Pb-region is reproduced better by $\rho_{sym.}$ and also around ^{138}Ba there is a similar tendency. The transition from spherical to deformed nuclei in the region $190 \leq A \leq 208$ is clearly seen. For the lighter nuclei ($100 \leq A \leq 130$) $\rho_{sym.}$ underestimates the level density by a factor 100. This is surprising in view of the reasonable agreement for the other spherical nuclei around ^{208}Pb. In conclusion a very considerable improvement is obtained for deformed nuclei by inclusion of the rotational states. The discrepancy reduces from a factor of 100 to a factor 4.

In another investigation [10] ϵ_i was obtained from an average potential of the Nilsson type. For the spherical nuclei the parameters of Seeger and Perisho [11] was chosen and for the deformed nuclei a recent version of the Nilsson potential [12] was used. The equilibrium determined by the shell correction method was used.

Although also lighter nuclei were considered we shall here restrict ourselves to the same nuclei ($A \geq 100$) as in ref. [3]. The results exhibit no systematic odd-even effects allowing a presentation without reference to the odd or even character of the nuclei. With the observed values of Lynn [9] fig. 2 was then prepared.

The values of $\rho_{calc.}/\rho_{obs.}$ scatter around unity in all the different mass regions. The deformed nuclei ($150 < A < 185$ and $A > 228$) differ on the average only by a factor of two (up or down) from observations. The systematic underestimate seen in fig. 1 is not present. The "spherical" nuclei in the Pb-region show a strong variation with A. The increase towards the rare earth nuclei is opposite expectations based on the results in fig. 1. However, the Nilsson model single particle spectrum [12] removes this discrepancy [10].

For the nuclei of $A < 150$ this calculation seems to reproduce the average behavior of the observed level density. This is in contrast to the Woods-Saxon results.

3.2. Uncertainties in the calculations.

In ref. [3] uncertainties in the calculations were reported. For the small excitation energies the error introduced by the method of level density calculations described in sect. 2 is in the case of no pairing less than 25%.

An essential source of uncertainty is the parameters of the average potential leading to the single particle spectrum ϵ_i. A change of the radius of around 8% changes the level density by a factor less than 6. An increase of the spin-orbit coupling by 17% produces less than 30% change of the level density. An increase of the diffuseness by 50% changes the level density of spherical nuclei by up to a factor of 3; about the same (maybe slightly larger) result is expected for deformed nuclei when the ground state deformation is changed consistently.

The pairing strength G is also important. A variation corresponding to 15% change of the pairing gap produces less than 40% change in the level density. This is much less than the factor of 3 given in ref. [10]. The discrepancy may be due to the different pairing treatments and the different single particle spectra.

Such variations of the parameters together with their estimated uncertainties give us the uncertainty of the calculated level density. In ref. [3] an uncertainty range of about a factor of 3 is given.

The uncertainty range of the average potential parameters is also supposed to give limits within which other reasonable potentials should fall. It would therefore follow that the results described above in the two different models come out consistent with these limits. The overall larger (by a factor around four) level density from the Nilsson type potentials than from the Woods-Saxon potential may, in view of the very strong pairing dependence quoted in ref. [10], be considered within these inaccuracy limits for the heavier nuclei.

For the lighter nuclei, however, the discrepancy (compare figs. 1 and 2) is too big. It reflects a basic difference between the single particle spectra arising from the two different potentials. The Seeger and Perisho parameters [11] are adjusted to give good single particle levels and the reasonable level density resulting may therefore be anticipated. The question remains, however, why does the average potential based on the Thoms-Fermi calculations [7] so much underestimate the level density? or are the nuclei maybe not spherical? or are the contributions from the collective states like the vibrations unexpectedly large?

4. APPLICATION TO THE ANALYSES OF OBSERVATIONS

Partial decay widths frequently enter more or less directly in the measured quantities. For neutron emission we have

$$\Gamma_n(E,J) = \frac{1}{2\pi\rho_C(E,J)} \sum_I \sum_{j=|J-I|}^{J+I} \sum_{l=j-\frac{1}{2}}^{j+\frac{1}{2}} \int_o^{E-B_n} \rho_D(\epsilon,I) T_{lj}(E-B_n-\epsilon)\,d\epsilon \qquad (20)$$

where ρ_C and ρ_D are the level densities of compound and daughter nucleus, T_{lj} is the neutron transmission coefficient. The sums are over all final spins and the integration is over all possible final excitation energies of the daughter nucleus. Assuming $\rho(\epsilon,j)=N(2j+1)\rho(\epsilon)$ and T_{lj} independent of j we find

$$\Gamma_n = \frac{1}{2\pi\rho(E)} \cdot 2 \int_o^{E-B_n} \rho(\epsilon)\,d\epsilon \sum_{l=o}^{\infty} (2l+1) T_l(\epsilon) \qquad (21)$$

$$= \frac{1}{2\pi\rho(E)} \frac{4mR^2}{\hbar^2} \int_o^{E-B_n} (E-B_n-\epsilon)\rho(\epsilon)\,d\epsilon$$

where the inverse cross section is assumed equal to the geometrical

$$\sigma_{inv.} \equiv \pi\lambda\!\!\!^{-2} \sum_{l=o}^{\infty} (2l+1) T_l(\epsilon) = \pi R^2 \qquad (22)$$

The spin independent expression Eq.(21) for Γ_n is often used. Its validity seems to rely on the $2I+1$ dependence of the level density. This dependence breaks down for spin values above $\sim 5\hbar$ for the heavier nuclei. Because of the appearance of ρ both in numerator and denominator the errors tend to cancel and the expression Eq.(21) may still be fairly good for somewhat larger spin-values.

The dipole radiation width may be estimated from

$$\Gamma_\gamma(E,J) = \frac{C_\gamma \cdot A^{2/3}}{2\pi\rho_C(E,J)} \sum_{I=|J-1|}^{J+1} \int_o^{E} (E-\epsilon)^3 \cdot \rho_C(\epsilon,I)\,d\epsilon \qquad (23)$$

Where C_γ is a constant e.g. determined from the knowledge of Γ_γ at one energy. The spin dependence of Γ_γ is very weak and in analogy to Eq.(21) we may write

$$\Gamma_\gamma = \frac{3C_\gamma \cdot A^{2/3}}{2\pi\rho(E)} \int_o^{E} (E-\epsilon)^3 \rho(\epsilon)\,d\epsilon \qquad (24)$$

This approximation to Eq.(23) holds for spin values up to around $40\hbar$ in the heavier nuclei.

The fission width for one barrier is given by

$$\Gamma_f(E,J) = \frac{1}{2\pi\rho_C(E,J)} \int_o^{E-B_f} \frac{\rho_B(\epsilon,J)\,d\epsilon}{1+\exp\left(-\frac{2\pi}{\hbar\omega}(E-B_f-\epsilon)\right)} \qquad (25)$$

where ρ_B is the level density on top of the barrier, B_f is the barrier height and ω the frequency of the parabola with the same curvature as the barrier. The spin-dependent expression is obtained simply by omitting the argument J in

Eq.(25).

For a double hump fission barrier one often uses the approximation [13] to the total fission width Γ_f

$$\frac{1}{\Gamma_f} = \frac{1}{\Gamma_f^{(A)}} + \frac{1}{\Gamma_f^{(B)}} \tag{26}$$

where $\Gamma_f^{(A)}$ and $\Gamma_f^{(B)}$ refer to the first and second barrier, each calculated with an expression like Eq.(25). Because of the exponential dependence of Γ_f on B_f a small difference (0.5-1.0) MeV between the two barrier heights reduces Γ_f to that of the highest barrier.

4.1. Fission probability near threshold of ^{241}Cm.

The shell and pairing effects included in the width through the level densities may in certain cases be observed. For the reactions ^{238}Pu $(\alpha,2n)$ and ^{241}Am(p,2n), both passing the compound nucleus ^{241}Cm, the ratio Γ_n/Γ_f for ^{241}Cm has been extracted as function of energy from the measured excitation functions [14]. A bump around 5 MeV above the neutron binding energy of ^{241}Cm is observed.

Neglecting rotations we calculated Γ_n/Γ_f from the spin independent expressions Eqs.(21) and (25) both with and without pairing [14]. The results are compared with the experimental values in fig. 3. Clearly, the inclusion of pairing is crucial to obtain the observed bump. The explanation is the difference in shell structure between ground state and barrier deformation. This again is reflected in different values of the pairing gaps and how they disappear with excitation energy. Because pairing is essential for ρ for small excitation energies this in turn is reflected in the calculated Γ_n/Γ_f. The rotational contributions are not included but they are not expected to change the picture.

4.2. Fission probabilities above threshold.

In several cases for nuclei in the Pb-region, α and proton induced fission cross sections are measured over a large energy region [15]. Calculations neglecting shell and pairing effects in the fission probability always fail to reproduce the measurements in an energy region extending over more than around 10 MeV.

With Γ_n of Eq.(20) evaluated directly from the single particle spectrum of a Nilsson model [12] and Γ_f of Eq.(25) obtained with a uniform model assumption for ρ_B, Moretto et al. [16] were able to reproduce the measured fission probability. They neglected rotations in the level density but had 5 free parameters at their disposal. Thus implicitely the collective enhancement of ρ may be contained in such calculations.

An absolute comparison without parameters has been made by Freiesleben et al. [17]. They obtain the results shown in fig. 4 when rotations are included in ρ_B. The low energy behavior is reproduced for ^{210}Po but around 10 MeV above the barrier differences show up very strongly. Even allowing B_f as a free parameter would not improve the fit.

The conclusion is obviously that the statistical model yields an incorrect energy dependence or the calculated level densities are incorrect. If the latter is assumed either the single particle energies or the pairing strengths are not appropriate or other collective states contribute significantly. The answer has so far not been given.

4.3. Fission probability and lifetime measurements of ^{239}U.

The fission cross section of the reaction $^{238}U(n,f)$ has been measured [18] for compound nuclear excitation energies around the fission barrier. (This essentially determine Γ_f/Γ; $\Gamma = \Gamma_n+\Gamma_f+\Gamma_\gamma+$ .....) With the crystal blocking technique also the lifetime of the ^{239}U compound nucleus formed in the same reaction has been measured [19] for three neutron energies. (This essentially determines $\tau = \hbar/\Gamma$.)

When $E-B_n$ of the compound nucleus is small (like the case considered here) the continuous level approximation in Eq.(20) fails. Therefore the final states (in ^{238}U) were divided into a discrete region below 1 MeV, where the levels are known, and the statistical region above 1 MeV. Above 1 MeV we use the level density obtained from the Woods-Saxon potential (see Sect. 2) and the rotational states are included. We normalize $\rho_{unif.}$ of Eq.(15) (an extra factor of 1/2 due to the assumed space reflection symmetry is introduced) to the observed number of $\frac{1}{2}^+$ levels at the neutron binding energy. This (energy and spin independent) normalization factor N_n is around 4 (see fig. 1). The discrete levels contribute about 50% for an excitation energy of 6.5 MeV and practically nothing at 7.0 MeV. The normalization factor N_n only makes a difference when the discrete levels contribute significantly to Γ_n. Otherwise it disappears due to the ratio of level densities entering in Eq.(20).

The transmission coefficients were calculated using an optical model with parameters adjusted to give elastic cross sections [20]. This completes the description of the ingredients applied in the Γ_n-evaluation.

For Γ_f we introduce, as in the case of Γ_n, a discrete spectrum for the low energies above the fission barrier. It was chosen as rotational bands built on top of the lowest quasi particle states. To account for deficiencies in the level density ρ_B, (calculated from the single particle energies at the theoretical barrier deformation) a normalization factor N_f is applied (as in ρ_C and ρ_D where $N_n \approx 4$).

The energy dependence of the fission probability may now be reproduced with a suitable choice of the fission width parameters. We obtain a good fit with the values [21], [19]

$$\begin{aligned} B_f^{(A)} &= 6.1 \text{ MeV}, \quad \hbar\omega_A = 0.6 \text{ MeV}, \quad N_f^{(A)} = 35 \\ B_f^{(B)} &= 5.8 \text{ MeV}, \quad \hbar\omega_B = 0.5 \text{ MeV}, \quad N_f^{(B)} = 45 \end{aligned} \tag{27}$$

The barrier heights are slightly below values [22] obtained in systematic fission probability analyses. Also $\hbar\omega_A$ is on the low side. The N-values are very interesting. If we allow for a factor of around 4 (as in ρ_C and ρ_D) due to vibrations still a factor of 10 is needed. The outer barrier (B) being pear shaped (theory) reduces further the factor to 5 (see sect. 2.2.). This brings the value down close to the region of uncertainty due to level density inaccuracies and the uncertainties in the determination of $N_f^{(B)}$ itself. For the inner barrier (A), which has no pear shape (theory), the factor may rather be taken as an experimental indication of a non-axial deformation leading to a ρ_B enhancement. As seen from Eqs.(16) and (19) this could easily amount to a factor of 10.

The total decay width is now defined and the corresponding lifetime may be calculated as a function of energy. The result [21] is compared with experimental lifetime [19] in fig. 5. They differ by about a factor of two which partly may be due to the different averaging procedures used in the calculated and experimental lifetime extraction [19].

Since both the compound cross section σ_C and the $^{238}U(n,\gamma)$ cross section $\sigma_{n,\gamma}$ are known experimentally we may obtain the total width from calculations of Γ_γ by the relation [19]

$$\Gamma = \frac{\sigma_C}{\sigma_{n,\gamma}} \cdot \Gamma_\gamma \qquad (28)$$

The corresponding lifetime (dashed curve in fig. 5) fall between the calculated and observed points. Thus confirming the consistency of the hole picture.

The effects of the rotational enhancement of the level density normally enter only weakly in these width calculations, the reason being that only ratios of level densities are needed. For Γ_n the effect may be difficult to recognize because ρ_C and ρ_D are similar. It may be easier for Γ_f when ρ_C and ρ_B are different mostly due to different symmetry properties, e.g. spherical ground state and axial symmetric barrier or axial symmetric ground state and non-axial symmetric barrier. Because of the parameters entering in Γ_f, e.g. B_f, most of the effect may be hidden in such effective parameter determinations. In order to get a more complete picture systematic investigations of many nuclei are needed. The measured fission probabilities should be refitted when the different symmetry properties indicated from energy surface calculations are taken into account [23].

4.4. Conclusion.

The examples of fission probabilities shown here serve as illustration of the predicting power (or lack) of the theoretical models considered.

Prediction of already known data is possible if a few parameters are left for fitting, e.g. in the analyses of Moretto et al. [16]. In absolute calculations, e.g. Freiesleben et al. [17], the experimental results are in general not reproduced. Thus the power of absolute predictions of existing experimental results already is not very good.

However, in small energy regions where additional information (e.g. the level density at the neutron binding energy, transmission coefficients etc.) are available, the predictions seem quite possible.

In the actual calculations described above the level density is only reliable to within the accuracy given in sect. 3. But also other quantities entering the expressions are uncertain, e.g. barrier heights and deformations and how they change with excitation energy and spin. Predictions of experimental results must take all this into account. Since experimental quantities involve ratios of level densities, they are possibly better determined than the level density itself.

The power of predicting unknown data must consequently rely heavily on all entering quantities and the ability to extrapolate them. Here the reliability and extrapolation of the level density seems already to present a problem due to the uncertainty of the single particle spectrum ϵ_i (or the average potential giving ϵ_i).

5. HOW TO PROCEED?

In the level density the essential parameters are ϵ_i. But in the statistical region, i.e. many excited states, probably only gross properties of the ϵ_i-spectrum are important. The most obvious is the average single particle energy spacing g_o around the Fermi energy. It has been used extensively, but is now known to be insufficient. Also the degree of bunching is very important for the level density. A measure of the bunching is the shell correction δW.

It would be very valuable if the level density could be parametrized directly in terms of g_o, δW and maybe other quantities characteristic of the ϵ_i-spectrum. The computer-time would be reduced and the essential properties of the level density and their consequences would appear in a more transparent way. Γ_n, Γ_f and Γ_γ would become possible or at least easier to predict.

Estimates of the level density would then only rely on these average properties of the single particle spectrum. They might be easier to extrapolate (but presumably of the same degree of difficulty as the average potential parameters leading to ϵ_i) or they might be determined by additional information about the process in question.

On a phenomenological basis an attempt of this kind was already made by Ignatyuk et al. [24]. They used the ordinary Fermi gas expression with an energy dependent level density parameter a given by

$$a(E) = \tilde{a}\left(1 + \frac{f(E)}{E} \cdot \delta W\right) \tag{29}$$

$$f(E) = 1 - \exp(-\gamma E) \tag{30}$$

This expression represents for large E-values a translation of the energy scale corresponding to the shell correction δW [25]. The mass dependent

parameters $\tilde{a}$ and γ are then given by the best fit to the observed level densities at the neutron binding energy. The improvement over the expression without the δW-terms is significant.

This level density was then applied [26] to the fission probability of nuclei in the Pb-region. For excitation energies below 50 MeV the experimental results are reproduced.

The expression of Eq.(29) enters in the intrinsic level density and Ignatyuk et al. [24] did not include any collective enhancement. Recently this was attempted [27] as described in sect. 2. The level density data for the deformed actinide and rare earth region and the spherical Pb-region were used to determine the parameters $\tilde{a}$ and γ. Subsequent calculation of the fission probability of ^{212}Po gives too strong an energy dependence.

The same procedure was then carried out [27] with the function of Eq.(30) replaced by

$$f(E) = 1 - \exp(-\gamma \sqrt{E}) \qquad (31)$$

Below 70 MeV the fission probability of ^{212}Po is then reproduced within a factor of two. Because it varies by five orders of magnitude in the excitation energy region of interest, such a fit is not trivially obtained.

The importance of the functional form of $f(E)$ or in other words the influence on the level density of the shell structure is demonstrated by this example. To find $f(E)$ in a more systematic way one could calculate the level density in realistic models, i.e. with shell and pairing effects and from this extract the function. Such procedure hopefully would lead to the above mentioned simple parametrization of the level density in terms of gross properties of the level spectrum.

Since the simplicity is obtained with essentially no cost of lesser accuracy (so far an assumption, although I believe it is possible) this is an enormous advantage in the analyses of existing data. Also unkown data may be predicted with "error bars" from the known uncertainties of the parameters in the level density.

ACKNOWLEDGEMENTS

Useful comments of T. Døssing are appreciated.

REFERENCES

[1] BOHR, A. and MOTTELSON, B., Nuclear Structure Vol 1 (Benjamin, New York)

[2] MORETTO, L.G., Nucl.Phys. A185 (1972) 145

[3] DØSSING, T., JENSEN, A.S., Nucl.Phys. A222 (1974) 493

[4] BJØRNHOLM, S., BOHR, A., MOTTELSON, B., Proc.IAEA Symp., New York 1973

[5] ERICSON, T., Adv. of Physics 9 (1960) 425

[6] DØSSING, T., cand.scient. Thesis, N.B.I., University of Copenhagen (1974)

[7] MYERS, W.D., Nucl.Phys. A145 (1970) 387

[8] BRACK, M., DAMGAARD, J., JENSEN, A.S., PAULI, H.C., STRUTINSKY, V.M., WONG, C.Y., Rev.Mod.Phys. 44 (1972) 320

[9] LYNN, J.E., The Theory of Neutron Resonance Reactions (Clarendon Press, Oxford, 1968)
and private communication.

[10] HUIZENGA, J.R., BEHKAMI, A.N., SVENTEK, J.S., ATCHER, R.W., Nucl.Phys. A223 (1974) 577 and
HUIZENGA, J.R., BEHKAMI, A.N., ATCHER, R.W., SVENTEK, J.S., BRITT, H.C., FREIESLEBEN, H., Nucl.Phys. A223 (1974) 589

[11] SEEGER, P.A., PERISHO, R.C., Los Alamos Scientific Laboratory Report, LA-3751 (1957)

[12] NILSSON, S.G., TSANG, C.F., SOBICZEWSKI, A., SZYMANSKI, Z., WYCECH, S., GUSTAFSON, C., LAMM, I.L., MØLLER, P., NILSSON, B., Nucl.Phys. A131 (1969) 1

[13] BJØRNHOLM, S., STRUTINSKY, V.M. Nucl.Phys. A136 (1969) 1

[14] METAG, V., LEE, S.M., LIUKKONEN, E., SLETTEN, G., BJØRNHOLM, S., JENSEN, A.S., Nucl.Phys. A213 (1973) 397

[15] KODAI-JOOPARI, A., Ph.D. Thesis, University of California, Lawrence Radiation Laboratory, report, UCRL-16489 (1966)

[16] MORETTO, L.G., THOMPSON, S.G., ROUTTI, J., GATTI, R.C., Phys.Lett. 38B (1972) 471

[17] FREIESLEBEN, H., BRITT, H.C., HUIZENGA, J.R., Proc. IAEA Symp., New York 1973

[18] LAMPHERE, R.W., Nucl.Phys. 38 (1962) 561 and
Phys.Rev. (1956) 1654

[19] ANDERSEN, J.U., NIELSEN, K.O., SKAK-NIELSEN, J., HELLBORG, R., PRASAD, K.G. Nucl.Phys. A241 (1975) 317

[20] PEREY, C.M., PEREAY, F.G., Nucl.Data A10 (1971-72) 539

[21] HANSEN, E.C., JENSEN, A.S., private communication (1974)

[22] BACK, B.B., BRITT, H.C., HANSEN, OLE, Leroux, B., GARRETT, J.D., Phys.Rev. C10 (1974) 1948

[23] GAVRON, A., BRITT, H.C., KONECNY, E., WEBER, J., WILHELMY, J.B., Phys.Rev. Lett. 34 (1975) 827

[24] IGNATYUK, A.V., SMIRENKIN, G.N., TISHIN, A.S., Obninsk preprint (1973)

[25] WILLIAMS, F.C., CHAN, G., HUIZENGA, J.R., Nucl.Phys. A187 (1972) 225

[26] IGNATYUK, A.V., ITKIS, M.G., OKOLOVICH, V.I., RUSKINA, G.Ya., SMIRENKIN, G.N., TISHIN, A.S., Obninsk preprint (1973)

[27] HAGELUND, H., JENSEN, A.S., private communication (1975)

FIGURE CAPTIONS

Fig. 1 The ratio of calculated to observed level density at the neutron separation energy as function of the mass number A . The calculations are those of ref. [3] where a Woods-Saxon potential was applied. The rotational contribution is included for the closed points and not for the open points. The squares are the doubly even nuclei, the circles odd-odd nuclei and the crosses are the odd nuclei. The tilted crossed have an odd proton.

Fig. 2 The same as fig. 1 with the calculations from ref. [10] where Nilsson type potentials were used (see text). As in fig. 1 the rotational contribution is included for the closed points and not for the open points. No distinction referring to the odd or even character of the nucleus was made.

Fig. 3 The quantity Γ_n/Γ_f for the fissioning system ^{241}Cm as a function of the excitation $E^* - S_2$ above the neutron binding S_2 . These results are from ref. [14]. The full drawn curve is the extracted experimental result and the dotted continuation is an interpolation connecting to the high energy value [14]. The dashed and the dot-dashed curves are calculations with and without pairing, respectively. A height B_f = 5.0 MeV of the first and highest barrier of ^{241}Cm was used.

Fig. 4 The ratio Γ_f/Γ_n for ^{210}Po as a function of excitation energy taken from ref. [17]. The curves with level densities based on the single particle spectra for an asymmetric and a symmetric second saddle point deformation are calculated with the rotations included. The fission barrier height of 22.1 MeV is obtained using the experimental ground state masses and no additional free parameters are allowed. The points are measured values [17].

Fig. 5 The lifetime as a function of the excitation energy of the compound nucleus ^{238}U. The figure is taken from ref. [19] where the Aarhus Studsvik measurements (triangles) are reported. Also the more uncertain Moscow-results are shown (full circles).

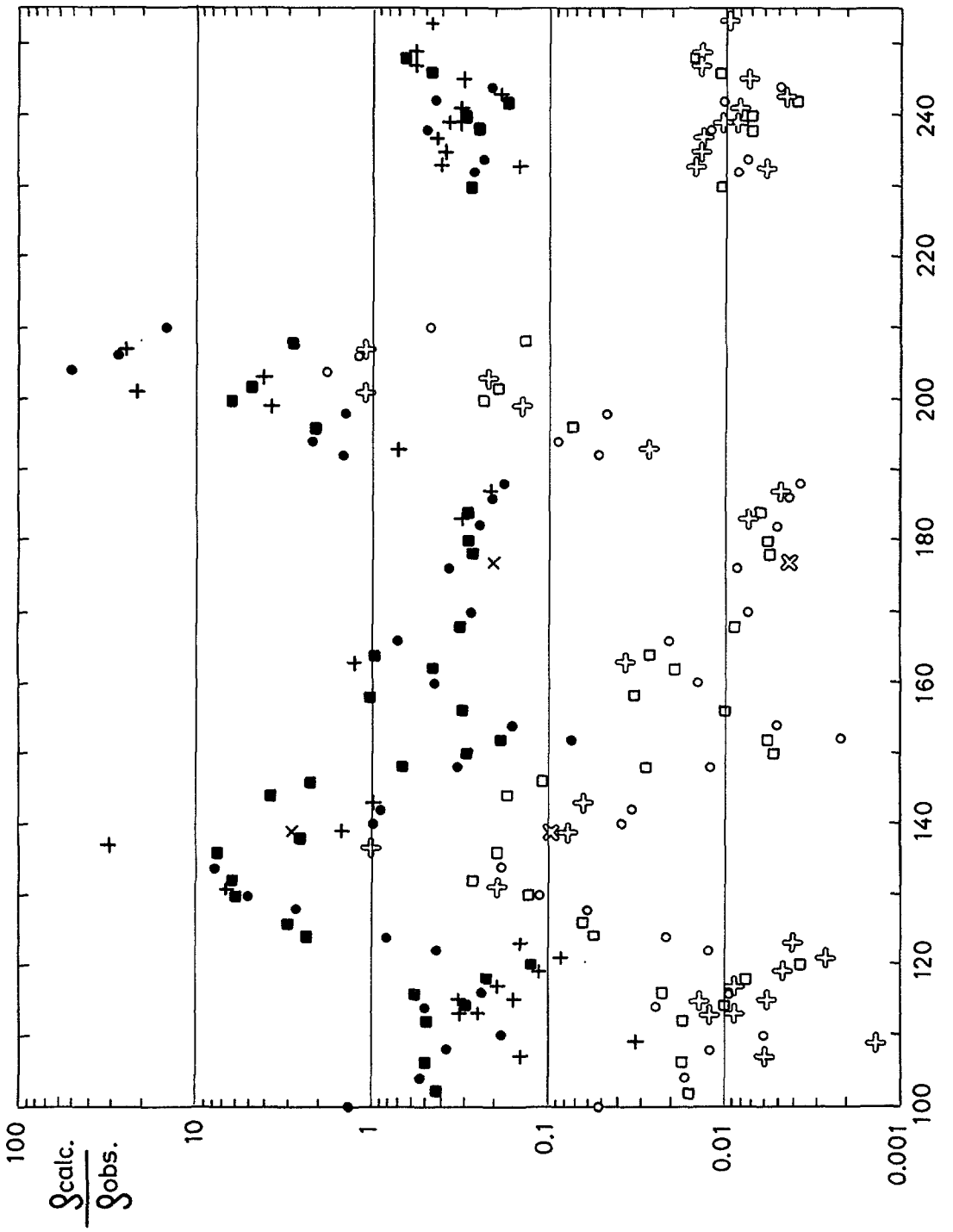

Figure 1

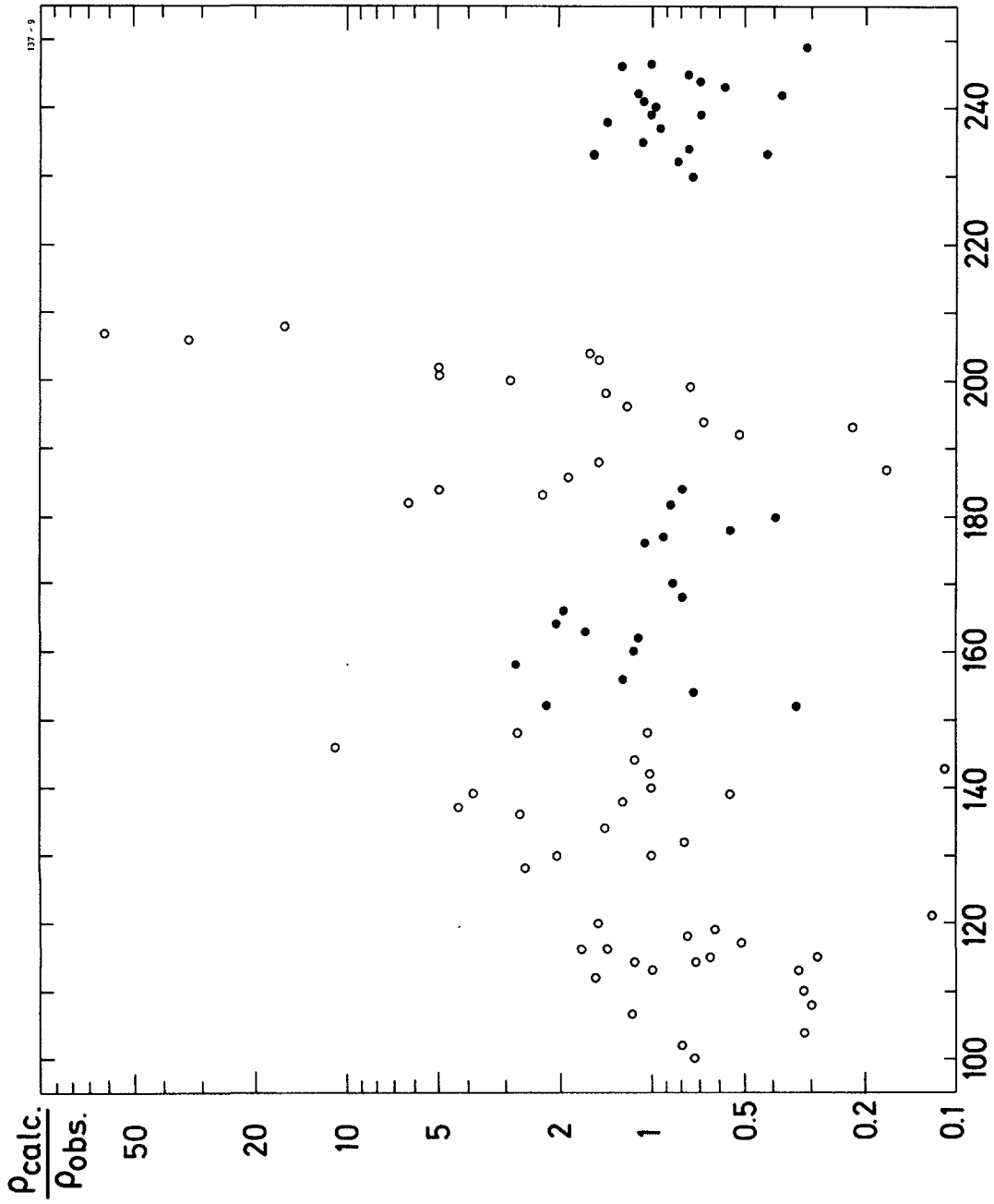
137 - 9
ρcalc./ρobs.
50
20
10
5
2
1
0.5
0.2
0.1
100
120
140
160
180
200
220
240

Figure 2

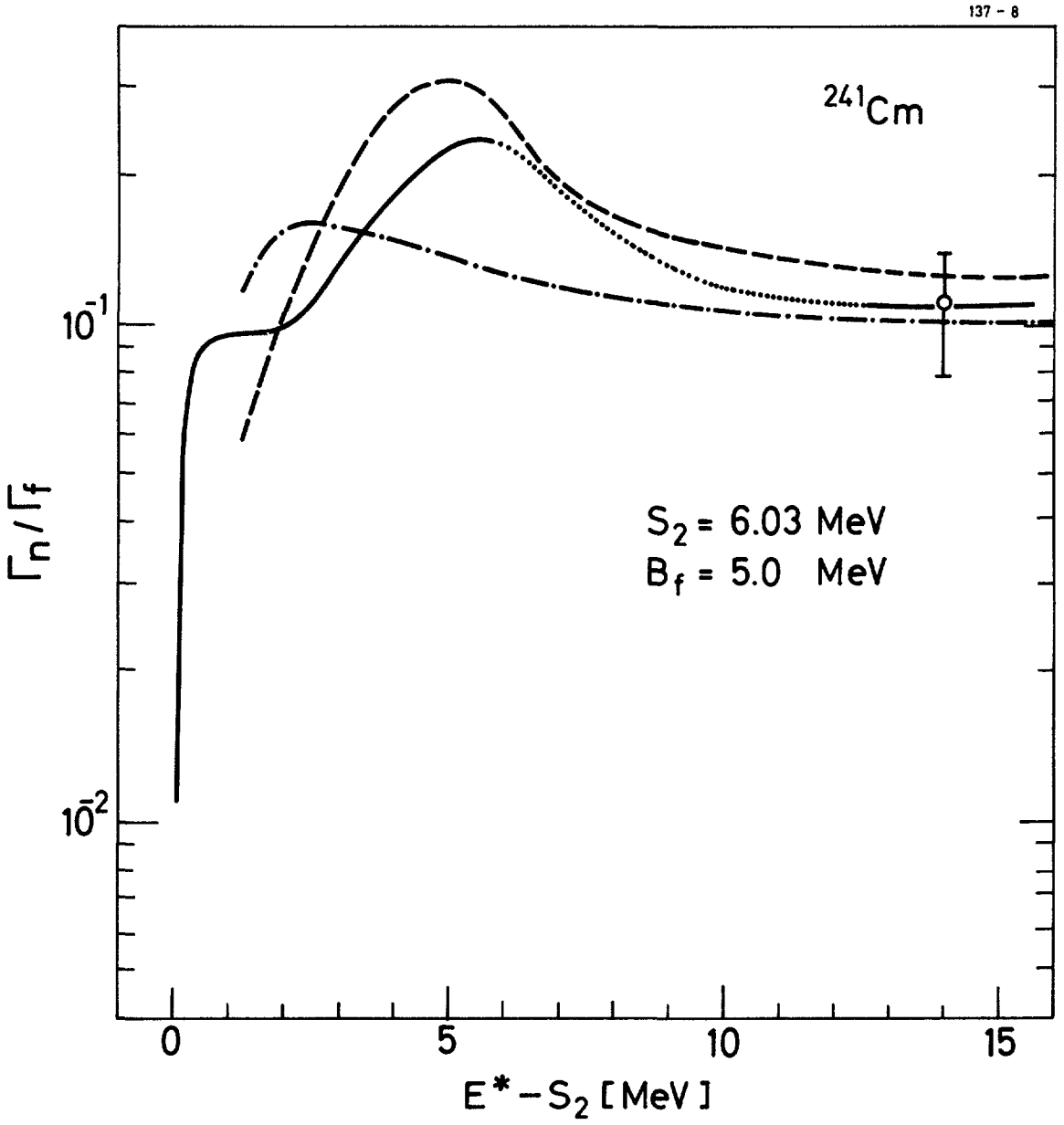
137 - 8
^{241}Cm
S_2 = 6.03 MeV
B_f = 5.0 MeV
Γ_n / Γ_f
10^{-1}
10^{-2}
0
5
10
15
$E^* - S_2$ [MeV]

Figure 3

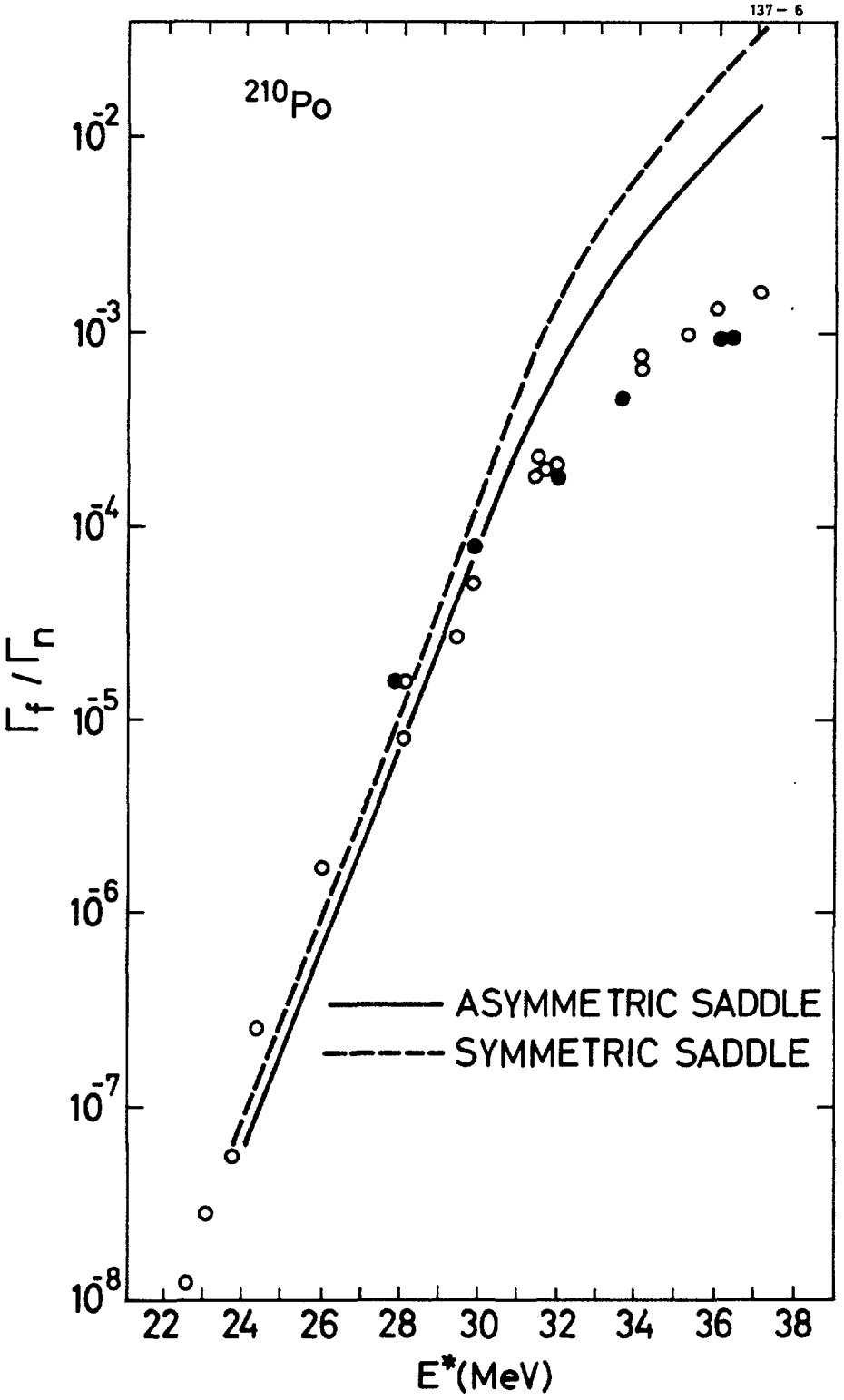
137 - 6
^{210}Po
10^{-2}
10^{-3}
10^{-4}
10^{-5}
10^{-6}
10^{-7}
10^{-8}
Γ_f / Γ_n
ASYMMETRIC SADDLE
SYMMETRIC SADDLE
22
24
26
28
30
32
34
36
38
E*(MeV)

Figure 4

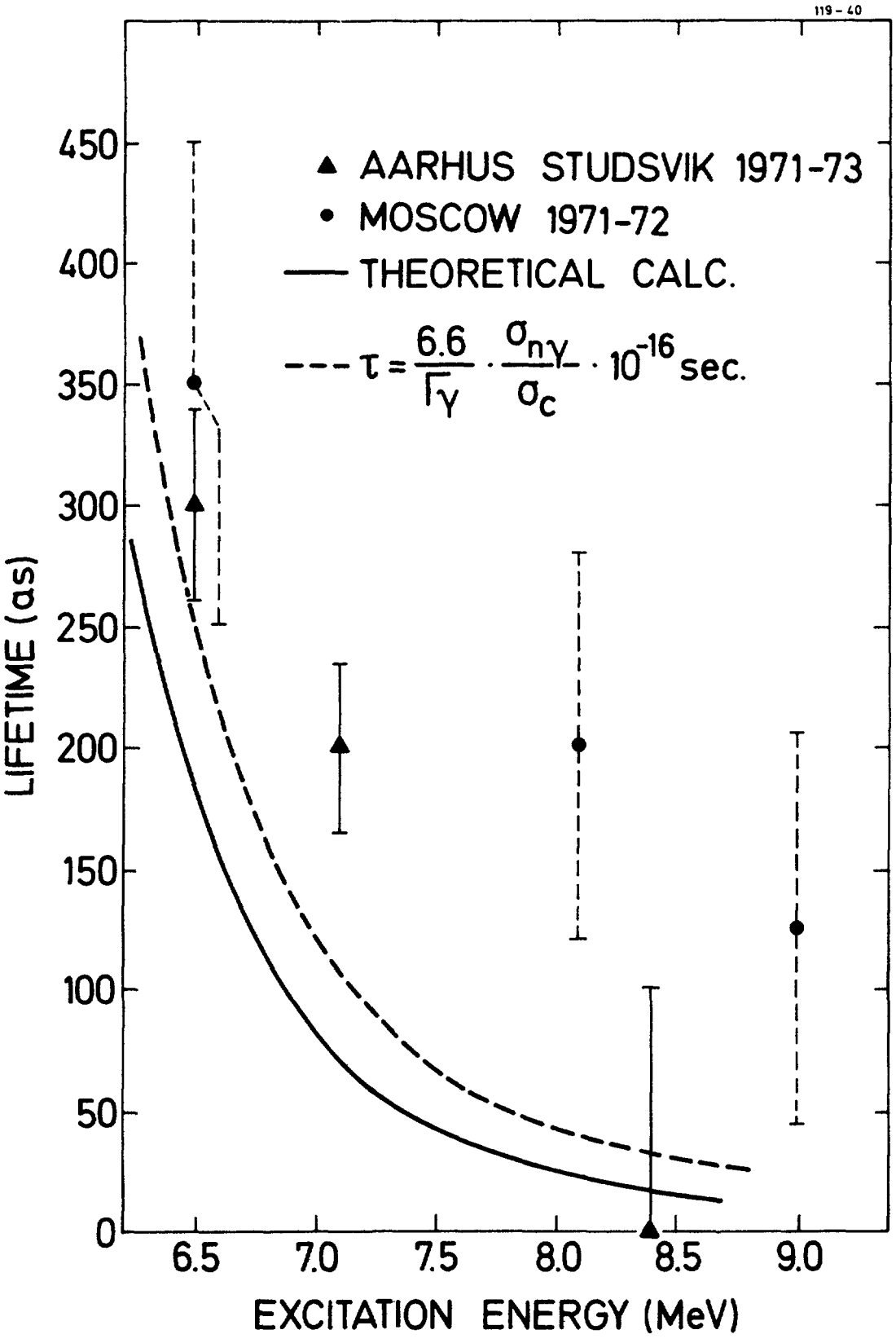

Figure 5

Next page(s) left blank

Contributed Paper No. 6

ON A NEW SEMIEMPIRICAL NUCLEAR LEVEL DENSITY FORMULA WITH SHELL EFFECTS

V.S. RAMAMURTHY, S.K. KATARIA and S.S. KAPOOR

Bhabha Atomic Research Centre,
Trombay, Bombay 400 085, India

A B S T R A C T

A new semi-empirical nuclear level density formula is proposed, which takes into account the influence of nuclear shell structure on level densities and its excitation energy dependence. The formula is tested against experimental level spacings of nearly 120 nuclei and is shown to perform nearly as good as a detailed microscopic calculation starting from a set of shell model levels, at the same time retaining the inherent simplicity of phenomenological formulae.

1. INTRODUCTION

Nuclear level densities play a central role in any statistical analysis of nuclear reactions. Experimental information on nuclear level densities as obtained from analysis of neutron and charged particle resonances, inelastic scattering and reactions, particle evaporation spectra etc. extend neither over a wide range of excitation energies nor over all nucleon numbers over the periodic table. In view of this, in any practical calculation, one often resorts to theoretical estimates of nuclear level densities.

Two different approaches have been employed in the past for theoretical calculations of nuclear level densities. In the first approach, one retains the traditional Bethe expression for level density, with the level density parameter $\underline{a}$ obtained by suitable interpolation/extrapolation techniques from available experimental informations, as for instance given by Newton[1] or by Gilbert and Cameron[2]. However, this approach suffers from one serious drawback. That is, in all these formulae, shell effects are taken into account only in an empirical way. Consequently, since the constants of these formulae are determined from experimental data confined to a narrow range of excitation energies, any attempt to extrapolate these formulae to other excitation energy ranges are subject to large errors. It has in fact been shown[3] on the basis of a detailed calculation starting from a shell model single particle energy level scheme that the Bethe form of the level density formula cannot satisfactorily describe the excitation energy dependence of shell effects on nuclear level density by treating $\underline{a}$ as an energy independent free parameter. In particular,

the rapid washing out of shell effects on the thermodynamic properties of nuclei is a feature, which is now well established but which is ignored by the existing level density formulae.

In the second and more recent approach,[4] one numerically computes the level density starting from a set of shell model single particle energy levels. This approach has a sounder theoretical basis than the first approach and takes into account in a natural way the influence of nuclear shell and pairing effects on the level density and its wiping out with excitation energy. Consequently, this approach has found a wider use in the last few years. There exist however a few inherent drawbacks in this approach. First is, of course, the availability of shell model level schemes for all nuclei, coupled with the need of a considerably larger computation effort. While this, in itself, is not a big constraint, because of a large number of single particle level schemes currently available in literature and easy accessibility of fast computers, this is a step which the average non-specialist user will like to gladly dispense with. The second drawback of this procedure is more intrinsic. In any shell model calculation, the quantity on which the calculated level density crucially depends, is the density of single particle levels at the Fermi surface. This is not a quantity which is crucially adjusted in any calculation of shell model energy level scheme. In fact, differences to the extent of 10-20% are known to exist between the calculated average single particle energy level density at the Fermi surface corresponding to various level schemes currently being used in literature for the calculation of nuclear shell

correction energies to the deformation potential energies. It is therefore necessary to adopt some sort of normalization procedure which ensures that the shell independent parts of the calculated level densities are consistent with any Liquid Drop Model (LDM) estimate. The need for such a normalization in microscopic calculations of nuclear moments of inertia parameters from shell model single particle level schemes has already been pointed out in an earlier work.[5] Normalization to the LDM values is a well established procedure in deformation potential energy calculations. The third and the most important drawback of microscopic calculations of level densities from shell model single particle level scheme is as follows. All microscopic calculations of level densities currently made starting from shell model levels are done in the independent particle model approximation. However, it has been shown[6] that if one takes into account the fact that the shell model potential is a self consistent potential generated by two body interactions, significant differences in the calculated level densities as a function of excitation energy result. In view of these inherent uncertainties in a microscopic calculation and the inadequacy of the earlier simpler prescriptions we propose in the present work a new semi-empirical method of calculating nuclear level densities, which while retaining the simplicity of the earlier semi-empirical methods, treats nuclear shell effects in a more realistic manner.

2. BASIC THEORETICAL CONSIDERATION

The traditional Bethe expression for nuclear level densities is based on the independent particle model of the nucleus with equispaced

single particle energy levels.

In its simplest form, the nuclear density of states is given by

$$\omega = C \exp[S] \qquad (1)$$

where S is the thermo dynamic entropy of the nucleus and the preexponential factor C is a slowly varying function of the excitation energy. For equispaced levels

$$S = 2\sqrt{a E_x}$$

$$C = \frac{\sqrt{\pi}}{12} \frac{1}{a^{1/4} E_x^{5/4}} \qquad (2)$$

where Ex is the excitation energy and a is a parameter related to the density of single particle states g.

$$a = \frac{\pi^2}{6} g$$

For a system of non-interacting Fermions, confined to nuclear volumes, a is proportional to the mass number A of the nucleus.

The spin dependent level density ρ is obtained from ω through the relation

$$\rho(E_x, I) = \frac{(2I+1)}{\sqrt{8\pi}\,\sigma^3} \omega(E_x) \exp[-I(I+1)/2\sigma^2] \qquad (3)$$

where I is the angular momentum and σ is the spin cut off factor. In general in addition to the entropy S, both the pre-exponential factor C and σ^2 are shell and pairing dependent. However the predominant energy dependence of ρ comes only through the entropy S. In the present work, we have therefore restricted our analysis to the entropy S. C and σ^2 have been estimated in the conventional way, as given,

for instance, in ref. (7).

It is well known[8] that nucleon levels in actual nuclei exhibit appreciable fluctuations from the equispaced level scheme and these fluctuations are the source of the shell effects in nuclear masses and other observables.

Let us consider only one kind of nucleons, say neutrons. Let $G(\epsilon) = \sum_i \delta(\epsilon - \epsilon_i)$ represent the actual single particle level density for these nucleons, where ϵ_i are a suitable set of shell model levels. In the spirit of the Swiatecki - Strutinsky approach[9] we can write $G(\epsilon)$ as

$$G(\epsilon) = g(\epsilon) + \delta g(\epsilon) \tag{4}$$

where $g(\epsilon)$ represents the overall smooth behaviour of the level scheme, while $\delta g(\epsilon)$ is the local fluctuation. For energies close to the Fermi energy, $g(\epsilon)$ can be well approximated by a constant, g_0. It has been shown earlier[9] that the fluctuations $\delta g(\epsilon)$ can be well represented by a fast converging Fourier series expansion of the form.

$$\delta g(\epsilon) = \sum_m g_m \cos(m\omega\epsilon - \phi_m) \tag{5}$$

Closed expressions for the entropy and excitation energy as a function of the temperature for such a level scheme have been obtained by Gilbert.[9]

$$S = \frac{\pi^2}{3} g_0 T + \sum_m \frac{g_m \cos(m\omega\mu - \phi_m)}{m^2\omega^2 T}\left[\frac{m^2\pi^2\omega^2T^2\cos(m\pi\omega T)}{\sinh^2(m\pi\omega T)} - \frac{m\pi\omega T}{\sinh(m\pi\omega T)}\right] \tag{6}$$

$$E_x = \frac{\pi^2}{6} g_0 T^2 + \sum_m \frac{g_m \cos(m\omega\mu - \phi_m)}{m^2\omega^2}\left[\frac{m^2\pi^2\omega^2T^2\cos(m\pi\omega T)}{\sinh^2(m\pi\omega T)} - 1\right] \tag{7}$$

A detailed analysis[10] of results of microscopic calculations of entropies and excitation energies of nuclei starting from shell model levels has shown that in most cases, only the contribution from the fundamental term is important in equations (6) and (7). On the assumption that the effect of the temperature dependence of the chemical potential μ on entropy and excitation energy is small at the temperatures under consideration, one can write

$$S = \frac{\pi^2}{3} g_0 T + \frac{A_1}{T} f(BT) \qquad (8)$$

$$E_x = \frac{\pi^2}{6} g_0 T^2 + A_1 h(BT) \qquad (9)$$

where $A_1 = \frac{g_1}{\omega^2}\cos(\omega\mu - \phi_1)$

$B = \pi\omega$

$$f(BT) = \frac{B^2T^2\cosh(BT)}{\sinh^2(BT)} - \frac{BT}{\sinh(BT)}$$

$$h(BT) = \frac{B^2T^2\cosh(BT)}{\sinh^2(BT)} - 1$$

As $T \to \infty$, $f \to 0$, and $h \to -1$

$$\therefore E_x \to \frac{\pi^2}{6} g_0 T^2 - A_1$$

$$S \to \frac{\pi^2}{3} g_0 T$$

One can therefore identify A_1 as the shell correction, Δ_S to the ground state energy of the nucleus.

The above considerations therefore suggest a simple prescription for a complete representation of the thermodynamic entropy of a nucleus as a function of excitation energy

$$S = \frac{\pi^2}{3} g_0 T + \frac{\Delta_S}{T} f(BT) \qquad (10)$$

$$E_x = \frac{\pi^2}{6} g_0 T^2 + \Delta_S h(BT) \qquad (11)$$

g_0 is related to the LDM value of the level density parameter $\underline{a}$ as

$$\underline{a} = \frac{\pi^2}{6} g_0 = cA$$

The constant B which represents the fundamental frequency of oscillation of $\delta g(\epsilon)$ is expected to be of the order of the major shell spacing $\hbar\omega_0$ for spherical nuclei. It is known that

$$\hbar\omega_0 \simeq \frac{30-40}{A^{1/3}} \text{ MeV}$$

We can therefore write

$$B = \frac{\pi^2 A^{1/3}}{B_0} \text{ MeV}^{-1}$$

where Bo is a mass independent parameter.

Eqs. (10) and (11) form the basis of the method proposed here for a theoretical estimate of the level density of any nucleus as a function of its excitation energy. With the temperature T as an implicit parameter, these equations give the entropy as a function of excitation energy, provided the mass independent parameters c = $\underline{a}$/A and Bo and the ground state shell correction energy Δ_S of the nucleus are known. The effect of nucleon pairing can be accounted for approximately by defining an effective excitation energy

$E_x^{eff} = E_x - \Delta_p$ where Δ_p is the pairing energy of the last two protons/

neutrons for even Z/ even N nuclei. Δ_p is zero for odd-odd nuclei.

3. DETERMINATION OF PARAMETERS

Extensive experimental data on nuclear level densities have been obtained from neutron resonance studies. For the present analysis which is confined mainly to spherical nuclei, we have used the results of compilation of Baba[7] . The experimental level spacings, after correction for the angular momentum dependence, pre exponential factor and the pairing energy making use of relations (1) - (3), were converted into the thermodynamic entropies of nuclei. Eqs. (10) and (11) were then fitted to the experimental data in the least square sense to obtain the best values of the parameters c = a/A and Bo. The values of the ground state shell correction energy for the different nuclei were taken from the mass formula of Seeger and Howard[11]. Figs. (1) and (2) show plots of the calculated mean square deviations between the calculated and the experimental entropies, against the unknown parameters C and Bo. It is seen that a well defined set of parameters can be chosen on the basis of minimum mean square deviation. The best values of parameters are

$$c = 0.146 \ (MeV^{-1})$$

$$Bo = 18 \ MeV^{-1}$$

It is heartening to note that the best values of the parameters are realistic. The value Bo = 18 MeV^{-1} corresponds to a major shell spacings of $\frac{36}{A^{1/3}}$ MeV, in very good agreement with the values used in literature[11].

In order to test the consistency of the proposed formula and the experimental data, the input data were divided into three groups, even-even, even-odd and odd-odd nuclei and the above analysis was carried out

for each group. These results are also shown in Figs. (1) and (2). It is seen that the same value of E_0 is obtained for each group. The maximum deviation in the best value of a is less than 4%. The root mean square deviation obtained for the best set of parameters is about 0.8 between the calculated and the experimental entropies for even-even nuclei and somewhat larger for odd-odd and odd mass nuclei. A deviation of this order compares favourably with those obtained by detailed microscopic calculations[4].

4. CONCLUSION

We have proposed here a simple nuclear level density formula which takes into account nuclear shell effects in a realistic way. The parametrization chosen is based on the results of earlier microscopic calculations of the thermodynamic properties of nuclei and is capable of reproducing the excitation energy dependence of shell effects on the thermodynamic properties. The merit of the present method therefore lies in its greater reliability for extrapolation to higher excitation energies, where it is necessary to take into account the washing out of shell effects with excitation energy. This is a feature which is not contained in earlier level density formulae. The better quality of fit obtained for even-even nuclei as compared to odd-odd and odd mass nuclei indicates that there is still some scope for improvement in the way in which pairing effects are taken into account. Attempts are in progress to find a better parametrization to include pairing effects, which can simulate the results of microscopic BCS calculations.

We are thankful to Shri M. Prakash for many helpful discussions.

REFERENCES

1. NEWTON, T.D., Can. J. Phys. 34 (1956) 804.

2. GILBERT, A., CAMERON, A.G.W., Can. J. Phys. 43 (1965) 1446.

3. RAMAMURTHY, V.S., Ph.D. Thesis, Bombay University (1971).

4. HUIZENGA, J.R., BEHKAMI, A.N., SVENTEK, J.S., ATCHER, R.W., Nucl. Phys. A223 (1973) 577.

5. KAPOOR, S.S., RAMAMURTHY, V.S., Physics and Chemistry of Fission, Rochester, Vol. II (1973) 375.

6. KATARIA, S.K., Annual Report of Nuclear Physics Division, 1973 BARC-768 (1974) 74.

7. BABA, A., Nucl. Phys. A159 (1970) 623.

8. NIX, J.R., Ann. Rev. Nucl. Sci. 22 (1972) 65.

9. GILBERT, A., UCRL - 18095 (1968).

10. RAMAMURTHY, V.S., KATARIA, S.K., KAPOOR, S.S., Nuclear and Solid State Physics Symposium, Calcutta 1975.

11. SEEGER, P.A., HOWARD, W.M., Nucl. Phys. A238 (1975) 491.

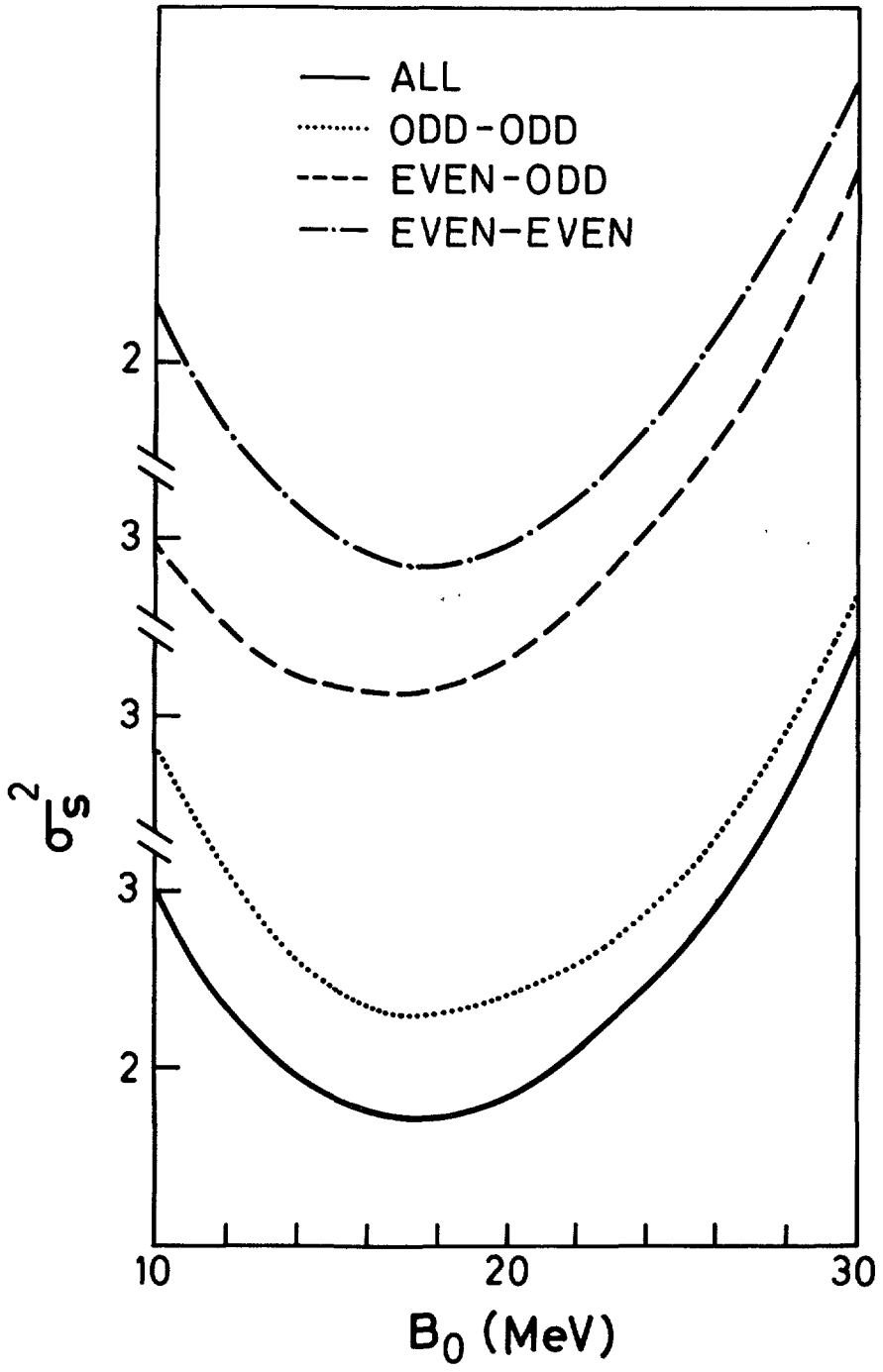

Fig. 1. Plot of the Calculated mean square deviation in entropies versus Bo.

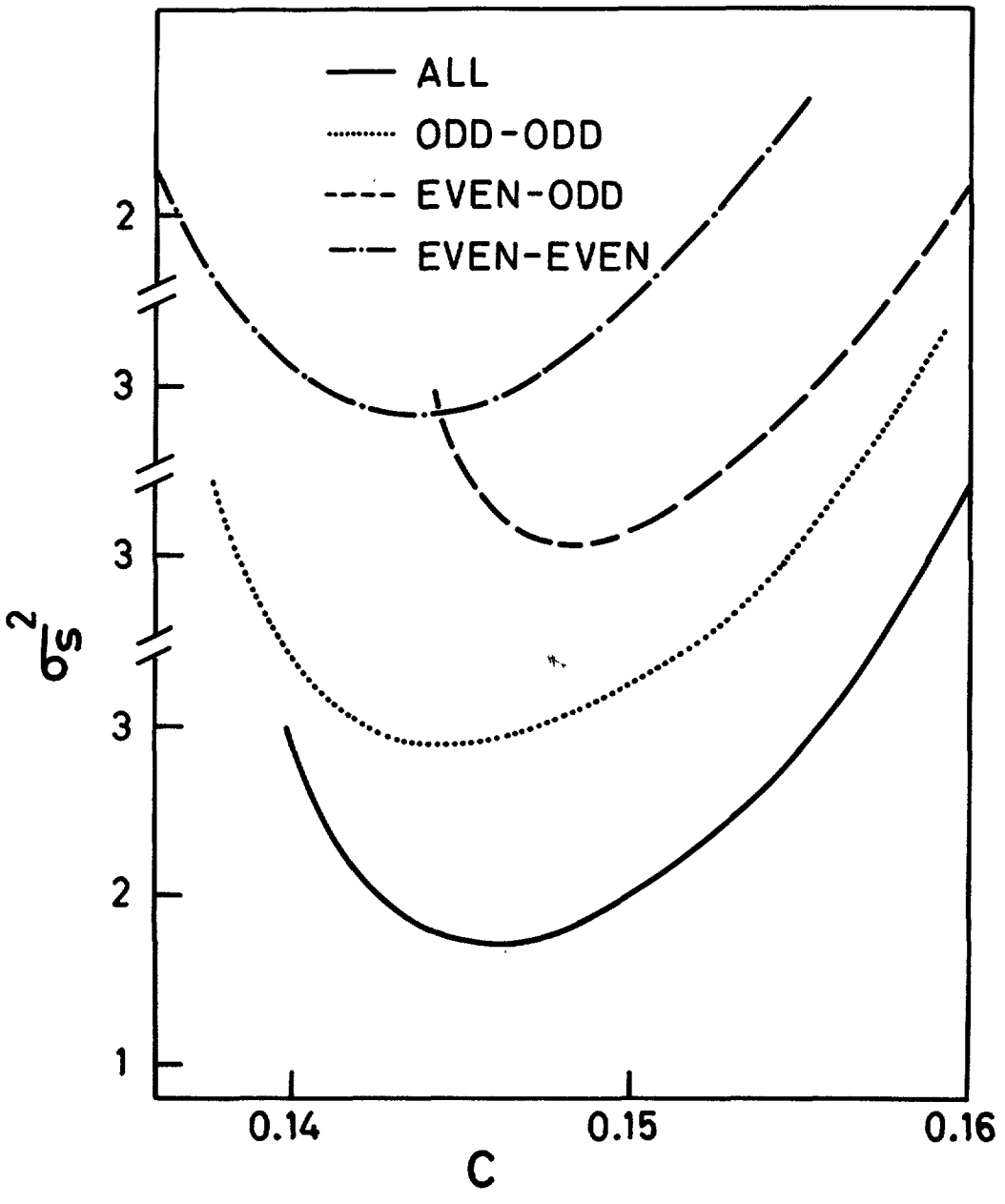

Fig. 2. Plot of the calculated mean square deviation in entropies versus c.

Next page(s) left blank

Contributed Paper No. 7

NEUTRON OPTICAL POTENTIALS

D. Wilmore
AERE, Harwell, Didcot, Oxfordshire, UK.

and

P.E. Hodgson
Nuclear Physics Laboratory, Oxford

ABSTRACT

The purpose of this paper is to provide a guide to the use of optical model computer programs to analyse and calculate neutron data.

After a brief discussion of the physical basis of the optical model a survey is given of the most widely used optical model and Hauser-Feshbach computer programs. The range of applicability and reliability of the major optical potentials proposed is assessed by comparison with available experimental data and some observations and suggestions are made for the optimum choice of optical potentials for given purposes of neutron data calculations.

1. INTRODUCTION

The purpose of this review is to provide a guide to the use of optical model computer programs to analyse and calculate neutron data, together with the best neutron potentials for such calculations.

The physical basis of the optical model is briefly discussed in section 2 and the optical potential is defined in section 3, and some available computer programmes are listed. Section 4 is devoted to a description of various potentials which have been proposed, and indication of the degree of their success is given.

2. PHYSICAL CONSIDERATIONS

The optical model of elastic scattering arises from a very simplified picture of complicated nuclear interactions which involve large numbers of particles. It is therefore hardly surprising that the range of its validity is limited and care should be excercised in its use. It gives cross-sections (called 'shape elastic') varying smoothly with energy that are directly comparable with the experimental data at higher energies. At lower energies there is in addition a contribution coming from the formation and decay of the compound nucleus that shows itself by marked resonance structure as in Fig. 1. This structure cannot be calculated in

detail, but the Hauser-Feshbach theory does allow us to calculate the energy averaged cross-section from this process. This can then be simply added to the shape elastic cross-section to give a total cross-section that can be compared with the experimental data:

$$\sigma \text{ (Total)} = \sigma \text{ (Shape elastic)} + \sigma \text{ (Compound elastic)}$$

This relation holds at every angle.

The resonance structure is only visible if the resolution of the detecting apparatus is high enough, so absence of resonance does not necessarily imply that the compound nucleus contribution is absent. It is thus always necessary to calculate the compound nucleus cross-section, unless it is already known from previous work to be negligible. A detailed account of the physical basis and formalism of the optical model may be found in [2] and [3].

The description given here assumes that the nucleus may be treated in a completely statistical manner, but in many cases there are strong terms which couple particular states in which many nucleons act collectively. In these cases the optical model becomes inadequate and a treatment involving coupled channels becomes necessary. A knowledge of the coupling terms involves the theory of the particular collective motion concerned, and many such calculations have been performed for rotational and vibrational nuclei. The presence of collective effects in such nuclei implies that the underlying resonant structure involves strong corellations, and the development of a theoretical basis for the fluctuation cross-sections in such conditions has proved extremely difficult, and it is only recently that hopes for its solution have appeared.

3. OPTICAL MODEL CALCULATIONS

We first of all consider the standard optical model calculation of the cross-section for elastic scattering of a neutron by a nucleus. The potential is usually defined by the expression

$$V(r) = Vf_1(r) + i\,W_v\,f_2(r) + i\,W_s g(r) + U_s \frac{df_s(v)}{dr} \left(\frac{\hbar}{m\pi}\right)^2 \underline{L}.\underline{\sigma}$$

where $$f_i(v) = \frac{1}{1+\exp\left(\frac{r-R_i}{a_i}\right)}, \quad R_i = r_i A^{1/3}$$

and $$g(r) = \frac{4}{a} \frac{\exp\left(\frac{r-R}{a}\right)}{\left\{1+\exp\left(\frac{r-R}{a}\right)\right\}^2}$$

If this potential is inserted in the Schrodinger equation, standard mathematical techniques [2,3,4] enable the differential cross-section and polarisation as a function of scattering angle, together with the total cross-section for non-elastic interactions (the reaction cross-section) and the total cross-section to be calculated. Many electronic computer programs have been written to carry out this calculation

rapidly and accurately given the parameters of the potential V(r).

In this review we are concerned with how to carry out such calculations to give any neutron cross-sections that may be required. To do this one first needs a computer program together with the appropriate parameters.

3.1 The computer program

Very many programs have now been written to carry out simple optical model calculations, and some of these are listed in Table I. These may usually be obtained on application to the authors and put on the nearest available computer.

Before using a program to calculate unknown cross-sections it is essential to ensure that it is working correctly. This may be done by repeating standard calculations whose results are available either in graphical or (preferably) in numerical form. This test should be carried out in the region of parameter space (energy and nucleus) for which calculations are to be made because programs are written with particular regions in mind, and may give inaccurate results in other regions.

At low incident energies there is often a substantial contribution to the cross-section coming from compound nucleus reactions. The cross-sections of these reactions may be calculated by the Hauser-Feshbach formalism, and several computer programs to do this are listed in Table II. Provided the cross-sections are averaged over sufficiently large energy intervals, the total cross-section at any angle is just the sum of the compound and direct components, so the data may easily be analysed (see section 4.3).

4. OPTIMUM OPTICAL POTENTIALS

The searches for potentials which give a good representation of the nuclear scattering have generally been of an empirical nature, but have been guided by the knowledge of what forces might be expected in a complicated situation from known nucleon potentials. Thus one might expect that the potential would roughly follow the density distribution of nucleons within the nucleus, although the resulting potential would be modified by the nucleon-nucleon potential. Such effects as the exclusion principle must also be taken into account.

There are three main approaches which have been made to determine the optical potential. The first was empirical and consisted of postulating physically reasonable forms for the terms which are expected to appear, and then performing large numbers of fits to experimental data, adjusting the various parameters which occur in the potential. Over the last two decades numerous analyses of experimental data for nuclear scattering have been made, and the resulting potentials published. Sometimes the potentials are optimised to fit data for a single nucleus at one energy and sometimes they are chosen to give the best overall fit to a wide range of data. This approach led to a large number of potentials which could fit particular sets of data, but because of various ambiguities between different parameters, data from one situation cannot always be used elsewhere.

Perey and Buck [5] suggested that the main dependence of the optical model potentials on energy would come from the non-local nature of the forces. They were able to obtain a single potential of this form which they fixed by reference to lead data. It was found that this potential and the equivalent local potential derived from it by Wilmore and Hodgson [6], fitted the data over a wide range (see section 4.1 and Table III). It was subsequently discovered that the potential could not be used successfully at low energies and was not able to fit the neutron s-wave phase shift around A = 100 (see Fig. 2). Moldauer [7] was able to find a potential, after extensive analysis of experimental results, which was able to fit the data below 1 Mev (see Table III). Engelbrecht and Fiedeldey [8] looked for a potential which would extend the range at the high energy limit. They found a set of data, based upon the energy dependent local equivalent of the non local potential, which accounts for data between 1 and 200 Mev (see Table III). Over the restricted range of 1-25 Mev however, the Perey-Buck potential remains better.

The third approach, that of Greenlees, Pyle and Tang [9], was to say that the potential could be, in a large measure, fixed by taking a very simplified model in which the nucleon potential was simply folded into the nucleon distribution. Thus $V(r) = \int f(r')v(r-r')dr'$ where $f(r)$ is the nucleon distribution within the nucleus, and $v(r-r')$ is the nucleon-nucleon interaction. This approach has had considerable success in the analysis of proton data at high energies.

For convenience of reference some of these overall neutron potentials are listed in table III.

When calculating an unknown cross-section, it is advisable to start with one or more of these overall potentials, and in some cases, as will be apparent from the examples given below, the results are already quite reliable. If accurate data for nearby nuclei and energies are available, it may be worthwile altering the parameters of the appropriate overall potential to optimise the fit to these data, before going on to use it to calculate the unknown cross-section.

To show the accuracy that may be expected when these potentials are used to calculate unknown cross-sections, we now present a series of comparisons between cross-sections calculated using them and the experimental data.

4.1 Total cross-sections

Figs. 4-16 show the cross-sections as a function of energy for the original Perey Buck non-local calculations as a function of energy and mass number. The total cross-sections are fitted well by the parameters but the reaction cross-section are not well described at low energies, particularly for the lighter nuclei. Fig. 3 shows the results of Manero [10] compared with the energy dependent equivalent local potential for Fe^{56}. The fit here is remarkably good. The question arises as to how far the optical model may be pushed beyond its range of applicability and Manero et al. have also compared the calculations with experiments on calcium and carbon Fig. 4-5. Calcium seems to be a more difficult case and Fig. 4 shows an 8% difference between the experimental and theoretical results. For the carbon nucleus marked fluctuations are seen, so that the model is really beyond the range where it might be expected to give good results, and yet the

agreement shown in Fig. 5 is no worse than that found for the calcium case. Glasgow and Foster [11] carried out an extensive comparison of experimental results with calculations using the Perey Buck non local potential, for a large number of nuclei between 3 and 15 Mev. Their results, which are displayed in Figs. 6-15, show that above the resonance fluctuation region, the agreement is generally within 3%, except in the region of strongly deformed nuclei, where differences of up to 7% are observed.

4.2 Neutron strength functions and total reaction cross-sections

The s-wave, p-wave and d-wave strength functions [12] are shown in Figs. 2, 17 and 18 as a function of mass number, in comparison with the results of calculations using the potentials of Perey and Buck. The considerable disagreement around mass 100 is the s wave strength has already been commented upon, but there is also a discrepancy around mass 150 which may be accounted for by collected effects. The p-wave and d-wave functions do not show good agreement, but the experimental determination is more difficult and the errors are greater. Also there may be individual shell effects which are more important for particular orbitals, but affect the average cross-sections less markedly.

The reaction cross-sections have been compared with the potentials of Perey and Buck, and Becchetti and Greenlees [13]. The results shown in Figs. 19-20, show that quite good agreement may be obtained if estimates of the compound elastic contribution are allowed for at low energies.

4.3 Elastic scattering

Provided that the energy is sufficiently high for the compound elastic contribution to be negligible, the differential cross-sections for the elastic scattering of neutrons from about 5 to 30 Mev are quite well given by some standard potentials, as shown in Figs. 21-32 and 37.

In the absence of the necessity for a coupled channel treatment, the elastic cross-section is often obtained by using the Hauser-Feshbach theory to calculate the contribution from the fluctuation or compound elastic cross-section. The cross-section is then given by

$$\sigma(\text{total} = \sigma(\text{shape elastic}) + \sigma(\text{compound elastic})$$

and for this result to hold, it is necessary that the average is carried over an energy interval greater than the average width of the fluctuations. Above a few Mev the compound nucleus contribution becomes negligible and may be neglected. Often estimates may be obtained at low energies, by assuming that the contribution is isotropic. Experimental information at some energies then gives information to determine its energy dependence. Such calculations are shown in Figs. 26-32, for calcium [6,14]. The 14.6 Mev experimental results for calcium were used as a basis for a parameter fit to try to improve on the local equivalent of the Perey Buck potential. Fig. 32 shows that in this case little improvement can be made.

Zyp and Jonker [15] used the potentials of Rosen [16] and of Becchetti and Greenlees [13] to analyse the polarisation data for 3.2 Mev neutrons, scattered from a wide range of targets, and the results are shown in Fig. 33. It was found that the potential of Rosen, which was derived from a consideration of polarisations,

gives a better fit than other potentials, but the elastic scattering cross-sections are fitted less well by Rosen potential than by the others.

4.4 Inelastic scattering

The inelastic scattering of neutrons introduces further parameters into the model of the nucleus. To calculate the compound elastic scattering cross-sections, a knowledge of the correllation between level widths is needed. Some results of such calculations are shown in Figs. 34-36. The results of Gilboy and Towle [17] for iron, show quite good agreement between theory and experiment, but this can only be obtained by neglecting the width fluctuation correction. The results of McDaniel, Brandenberger, Glasgow and Leighton [18], used a value of the Moldauer [19] correlation parameter Q = 0.5. They found that their results for Zr^{92} and Mo^{96} were even worse for other values. The calculations of Brandenberger [20] for Pb^{206} do however show good agreement with experiment.

5. CONCLUSIONS

There are many readily available computer programs that can be used to calculate various neutron cross-sections. The most widely used are listed in tables I and II. Many overall neutron optical potentials have been found that give cross-sections in fair agreement with the experimental data. Some of these potentials are listed in table III and some indication of their range of applicability and general reliability may be obtained from the figures in this paper. The overall potentials may be improved for some nuclei, but it is generally found that such parameter changes, although giving benefits for a few neighbouring nuclei, will give a worse agreement over most of the range of nuclear masses.

REFERENCES

1. Barnard, E., Devilliers, J., Reitmann, D., Moldauer, P., Smith, A. and Whalen, Nucl.Phys. A229 (1974) 189.

2. Hodgson, P.E., The Optical Model of Elastic Scattering, Clarendon Press, Oxford, (1963).

3. Hodgson, P.E., Nuclear Reactions and Nuclear Structure, Clarendon Press, Oxford, (1971).

4. Buck, B., Maddison, R.N., and Hodgson, P.E., Phil.Mag. 5 (1961) 1181.

5. Perey, F.G. and Buck, B., Nucl.Phys. 32 (1962) 353.

6. Wilmore, D. and Hodgson, P.E., Nucl.Phys. 55 (1964) 673.

7. Moldauer, P.A., Phys.Rev.Lett. 9 (1962) 17, Phys.Rev. B135 (1964) 642.

8. Engelbrecht, C.A. and Fieldeldey, H., Ann.Phys. 42 (1967) 262.

9. Greenlees, G.W., Pyle, G.J., Tang, Y.C., Phys.Rev.Lett. 17 (1966) 33, Phys.Rev. 171 (1968) 1115, Phys.Lett. B 26 (1968) 658.

10. Manero, F., Armitage, B.H., Freeman, J.M., and Montague, J.H., Nucl.Phys. 59 (1964) 583.

11. Glasgow, D.W. and Foster, D.G., Phys.Rev. C3 (1971) 604.

12. Kompe, D., Nucl.Phys. 133 (1969) 513.

13. Becchetti, F.D. and Greenlees, G.W., Phys.Rev. 182 (1969) 1190.

14. Wilmore, D., The Calculation of Neutron Cross Sections from the Non-local Optical Model, AERE-R4649, EANDC (UK) 36 'U'.

15. Zijp, E. and Jonker, C.C., Nucl.Phys. A222 (1974) 93.

16. Rosen, L., Beery, J.G., Goldhaber, A.S. and Auerbach, E.H., Ann.Phys. 34 (1966) 96.

17. Gilboy, W.B. and Towle, J.H., Nucl.Phys. 64 (1965) 130.

18. McDaniel, F.D., Brandenberger, J.D., Glasgow, G.P. and Leighton, H.G., Phys.Rev. C10 (1974) 1087.

19. Moldauer, P.A., Rev.Mod.Phys. 36(1964) 1079.

20. Brandenberger, Ohlsen, Smith, Okhysen and Spahn, Private communication to one of the authors; Ohlsen Ph.D. Thesis (1966), University of Texas; Brandenberger Ph.D. Thesis (1966), University of Texas.

21. Buck, B. and Perey, F., Phys.Rev.Lett. 8 (1962) 444.

22. Zafivatos, C.D., Oliphant, T.A., Levin, J.S. and Cranbergh, Phy.Rev.Lett. 14 (1965) 913.

23. A List of Computer Programs for Neutron Cross Section Calculations and Analysis, O.E.C.D. report, NEANDC-97"U".

24. Bucher, W. and Hollandsworth, C.E., Phys.Lett. 58B(1975)277.

FIGURE CAPTIONS

1. Measured neutron total (vertical bars) and angle integrated elastic scattering (circles) cross-sections of titanium [1]. The solid curve indicates the total cross-section calculated from the optical model.

2. Experimental data on neutron s-wave strength functions compared with spherical and deformed optical-model phase shifts [21].

3. Total neutron cross-section for iron as a function of neutron energy. The open circles show the results of optical model calculations using the equivalent non-local potential [6,14] in comparison with the experimental data [10].

4. Total neutron cross-section for calcium as a function of neutron energy. The open circles show the results of optical model calculations using the equivalent non-local potential [6,14] in comparison with the experimental data [10].

5. Total neutron cross-section for carbon as a function of neutron energy. The open circles show the results of optical model calculations using the equivalent non-local potential [6,14] in comparison with the experimental data [10].

6. Neutron total cross-sections for light nuclei [11], in comparison with optical model predictions.

7. Neutron total cross-sections for the 2s-1d shell nuclei [11] compared with optical model results.

8. Neutron total cross-sections for various $1f_{7/2}$ nuclei, with the exception of $_{20}{}^{1a}{}^{44}$ [11].

9. Neutron total cross-sections for $1f_{5/2}$ and $2p_{\frac{1}{2}}$ nuclei [11] compared with optical model results.

10. Neutron total cross-sections for $2p_{\frac{1}{2}}$ and $1g_{9/2}$ nuclei [11] compared with optical model results.

11. Neutron total cross-sections for $1g_{7/2}$ and $2d_{5/2}$ nuclei [11] compared with optical model results.

12. Neutron total cross-sections for various $2d_{5/2}$ and $1h_{11/2}$ nuclei [11] compared with optical model results.

13. Neutron total cross-sections for various $2d_{3/2}$ and $3s_{\frac{1}{2}}$ nuclei [11] compared with optical model results.

14. Neutron total cross-sections for various $2d_{3/2}$ and $3s_{\frac{1}{2}}$ nuclei [11] compared with optical model results.

15. Neutron total cross-sections for various $1h_{9/2}$ and $2f_{7/2}$ nuclei [11] compared with optical model results.

16. Calculations of the total cross-sections using the non-local potential [5].

17. Calculations of p-wave strength functions from the non local potential [5], compared with the experimental results [12].

18. Calculations of d-wave strength functions from the non-local potential [5], compared with experiment [12].

19. Calculations of the reaction cross-section using the non-local potential [5].

20. Calculations of the total and reaction cross-sections from the Becchetti and Greenlees potential [13].

21. The differential elastic scattering cross section for 7 Mev neutrons on Bi^{209} compared with non-local optical model predictions [22].

22. Elastic scattering cross-sections of 7 Mev neutrons on uranium [6,14].

23. Elastic scattering cross-sections of 14 Mev neutrons on uranium [6,14].

24. Elastic scattering cross-sections of 14 Mev neutrons on iron [6,14].

25. Elastic scattering cross-sections of 14-5 Mev neutrons on iron [6,14].

26. The estimation of the compound nucleus contribution to the elastic scattering cross-section in Ca [6,14].

27. Elastic scattering cross-sections of 1 Mev neutrons on calcium [6,14].

28. Elastic scattering cross-sections of 2 Mev neutrons on calcium [6,14].

29. Elastic scattering cross-sections of 3.5 Mev neutrons on calcium [6,14].

30. Elastic scattering cross-sections of 4.1 Mev neutrons on calcium [6,14].

31. Elastic scattering cross-sections of 6 Mev neutrons on calcium [6,14].

32. Elastic scattering cross-section of 14.6 Mev neutron on calcium [6,14], showing improvement to be obtained by parameter fitting.

33. Polorisations [15] for various nuclei compared with results from the potentials of Rosen (solid curves) and Becchetti and Greenlees (dashed curves).

34. Differential inelastic scattering cross-sections of iron compared with Hauser-Feshbach theory predictions [17].

35. Differential cross-section for inelastic neutron scattering from Pb^{206}, compared with Hauser Feshbach theory predictions [20].

36. The differential inelastic cross-sections for 1.5 Mev neutrons compared with theoretical calculations [18].

37. Differential cross-sections at small angles [24] compared with calculations using the equivalent non-local potential [6, 14].

TABLE 1. Optical model programs (see reference [23]).

Name of Program	Author	Features
ECIS	Raynal	Coupled Channels with search.
SASSI	Benzi	Spherical Optical Model with Compound Nuclear Cross Sections.
SMOG	Benzi	Spherical Optical Model with polarisations.
ADAPE	Fabbri	Adiabatic coupled channels.
DANGFASI (DUMBO)	Fabbri	Coupled Channels with polarisations, phase shifts.
CERBERO	Fabbri	Spherical Optical Model, Compound Nucleus Cross Sections, charged particle Cross Sections, Moldauer Formalism.
SURF	Fabbri	Coupled Channels, Photo Reaction Cross Sections.
MIDI	Fabbri	Coupled Channels, Radiative Capture.
MIMOC	Fabbri	Coupled Channels, Microscopic Model, Phase Shifts.
RES	Fabbri	Coupled Channels, Microscopic Model, Resonance Parameters.
ELEISE-3	Igarasi	Optical Model, Compound Nucleus Cross Sections, Non-local Potential, Charged Particle Cross Sections, Moldauer Formalism, Evaporation Model, Search.
STAX-2	Tomita	Optical Model, Compound Nucleus Cross-Sections, Moldauer Formalism, Search
INS-ELASTIC	Kawai	Optical Model.
OMW	Wilmore	Optical Model, Search.
OMPS	Hill	Optical Model, Search.
ABACUS-NEARREX	Zawadzki	Optical Model, Compound Nucleus Cross Sections.
2 (and 4)-PLUS	Dunford	Coupled Channels.
JUPITER (1 and 2)	Tamura	Coupled Channels, adiabatic coupled channels.
OPTIC	Goldman	Optical Model.
SCAT	Melkanoff	Optical Model.
ABACUS-II	Auerbach	Optical Model, Search.
GENOA	Perey	Optical Model with Search.
JIB3, DWUCK	Perey	Optical Model with Search, Compound Nucleus.
SNOOPY, FTAU	Perey	Optical Model with Search, Compound Nucleus.
DWBA-VENUS	Tamura	DWBA
MARS	Tamura	Coupled Channels Born Approximation.
JULIE/SALLY	Bassel	DWBA

TABLE II

Programs for compound nuclear cross-sections (see reference [23]). Many of the optical model programs listed in Table I also contain facilities for the calculation of compound nuclear cross-sections.

Name of Program	Author	Features
HFW	Wilmore	Hauser Feshbach, fluctuations, continua of states.
COMNUC	Dunford	Moldauer formalism, fission.
HF-XS	Grench	Hauser Feshbach, radiative capture.
LIANA	Smith	Hauser Feshbach, fluctuations.
HELENE	Penny	Hauser Feshbach.
TRNRX	Mathur	Hauser Feshbach, γ-ray angular distribution.
HAFEVER	Friedman	Hauser Feshbach
NEARREX	Moldauer	Hauser Feshbach, fluctuations, capture.
MANDY/BARBARA	Sheldon	Hauser Feshbach, fluctuations.
RES.AV-IXS	Tucker	Hauser Feshbach, fluctuations.
HFS	Wills	Hauser Feshbach.

Potential	Equivalent Non-local [6,14] Wilmore/Hodgson	Moldauer [7]	Engelbrecht & Fieldeldey [8]	Becchetti & Greenlees [13]
V	$47.01-0.267E-0.00018E^2$	46	$46\ \exp(-0.67x-0.02x^2)$	$54-0.32E+24\ \frac{N-Z}{A}+0.4\ \frac{Z}{A^{1/3}}$
W_v	0	0	0	$Max(0.22E-2.7,0)$
W_s	$9.52-0.053E$	$W_G = 14$	$W_G = 12.6x\ \exp(-0.4x^{1.28})$	$Max(0,11.8-.25E+12\ \frac{N-Z}{A})$
U_s	0	7	$7\ \exp(-0.67x-0.02x^3)$	6.2 with $r_s=1.01$ & $a_s=0.75$
R_1	$1.322-0.00076A+4.10^{-6}A^2-8.10^{-9}A^3$	$0.6 + 1.16A^{1/3}$	$0.6 + 1.16A^{1/3}$	1.17
a_1	0.66	0.62	0.62	0.75
R_2	$1.266-0.00037A+2.10^{-6}A^2-4.10^{-9}A^3$	$R_G = 1.1 + 1.16A^{1/3}$	$R_G = 1.1 + 1.16A^{1/3}$	1.32
a_2	0.48	b = 0.5	b = 0.5	$0.51+0.7\ \frac{N-Z}{A}$
Comments	1-25 MeV	a) < 1 MeV b) Imaginary potential of the form $W_G\ \exp\{-(r-R_G)^2/b^2\}$	a) x = 0.01E b) Imaginary potential of the form $W_G\ \exp\{-(r-R_G)^2/b^2\}$	a) E < 50 MeV b) A > 40

TABLE III

SOME COMMONLY USED NEUTRON POTENTIALS

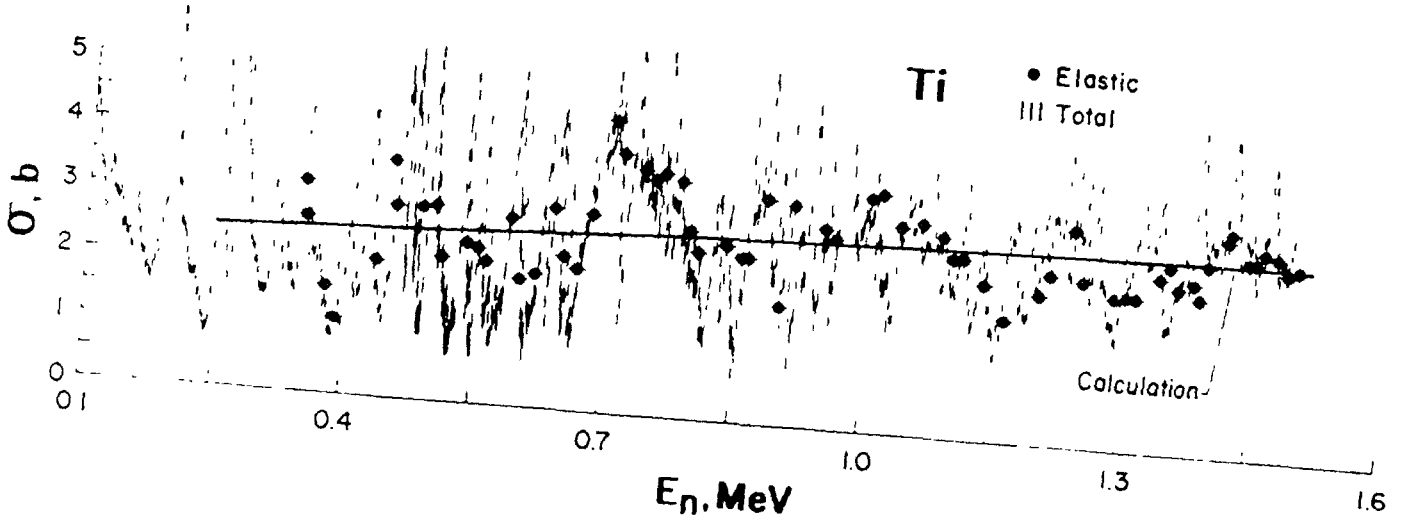
Ti
● Elastic
III Total
Calculation
σ, b
5
4
3
2
1
0
0.1
0.4
0.7
1.0
1.3
1.6
En, MeV

Fig. 1

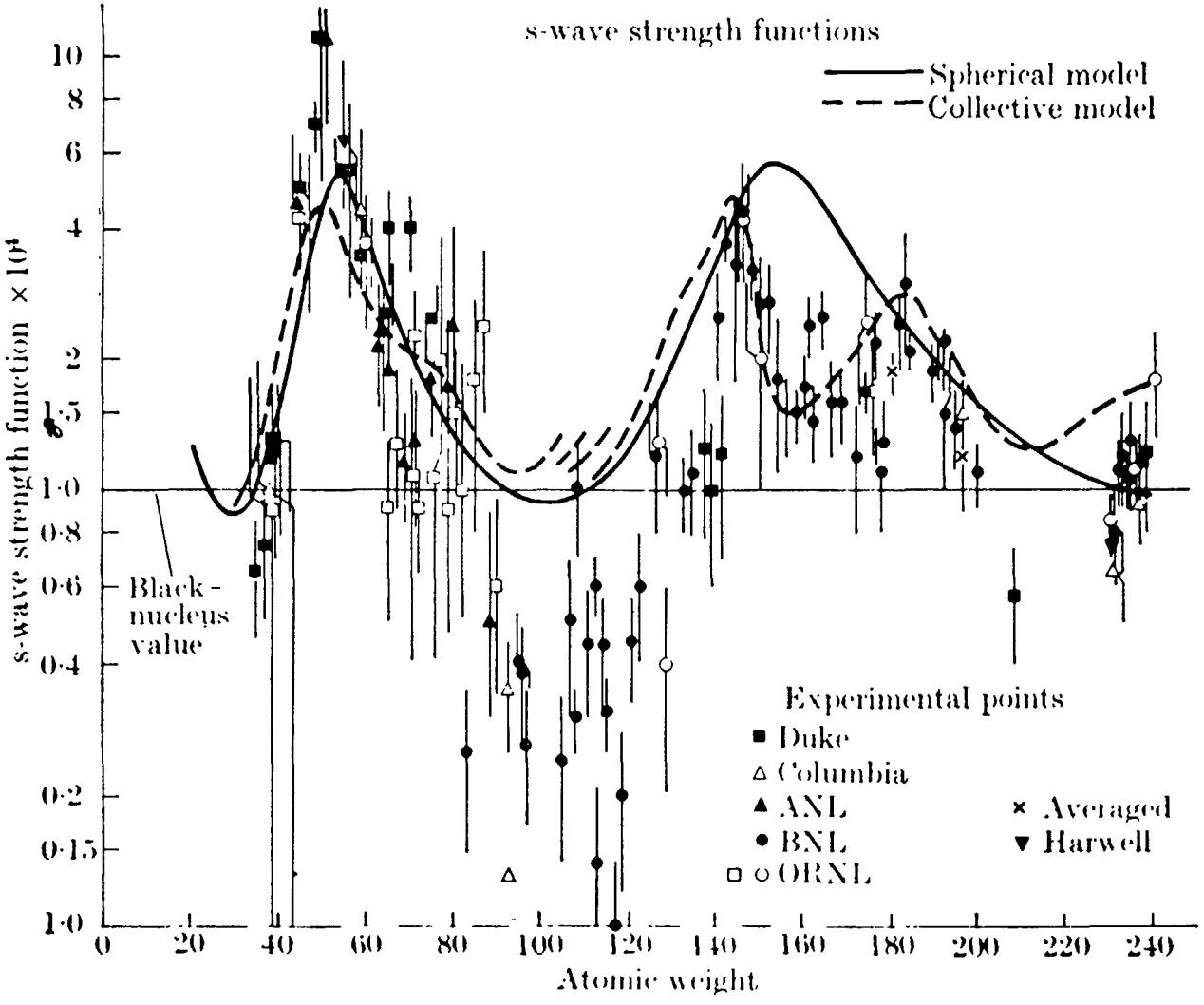
s-wave strength functions
Spherical model
Collective model
s-wave strength function × 10⁴
10
8
6
4
2
1·5
1·0
0·8
0·6
0·4
0·2
0·15
0·10
Black-nucleus value
Experimental points
Duke
Columbia
ANL
BNL
ORNL
Averaged
Harwell
0
20
40
60
80
100
120
140
160
180
200
220
240
Atomic weight

Fig. 2

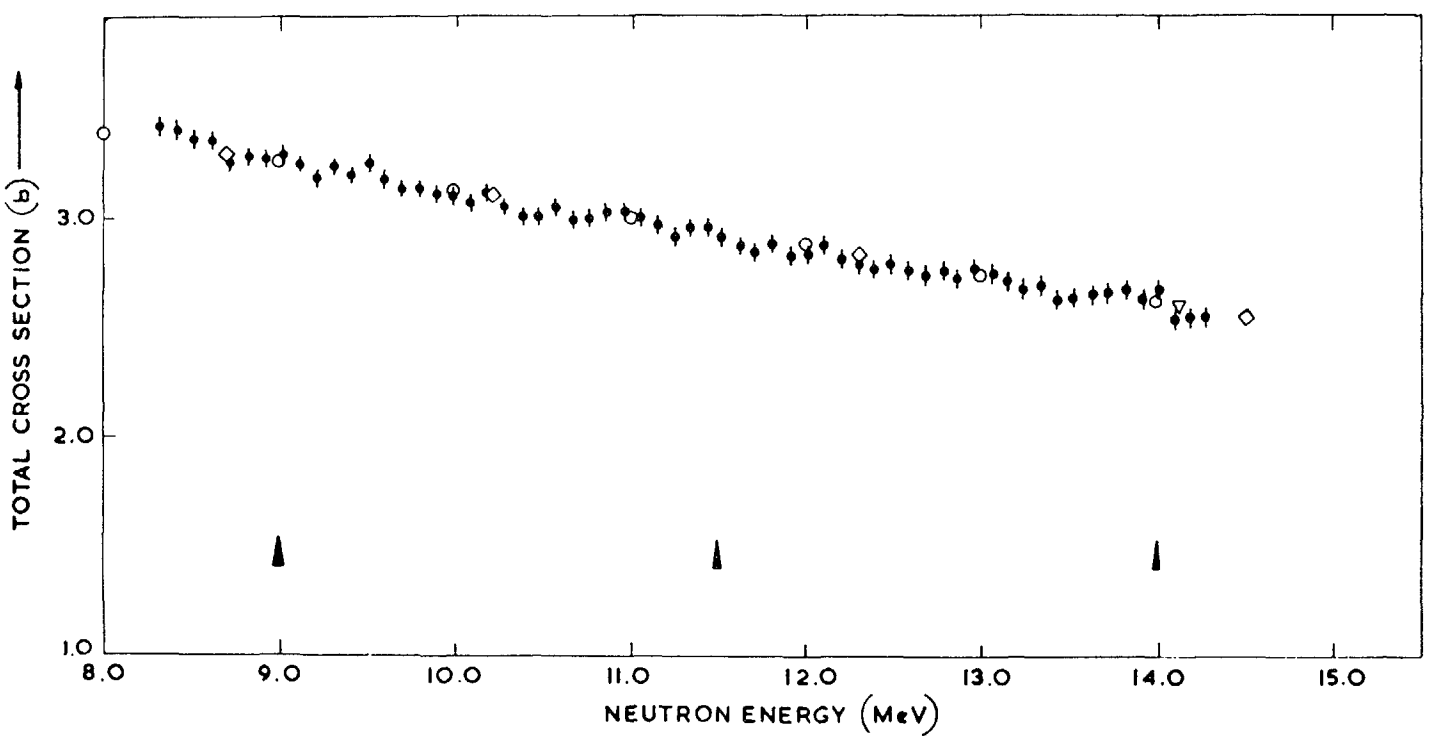
TOTAL CROSS SECTION (b)
3.0
2.0
1.0
8.0
9.0
10.0
11.0
12.0
13.0
14.0
15.0
NEUTRON ENERGY (MeV)

Fig. 3

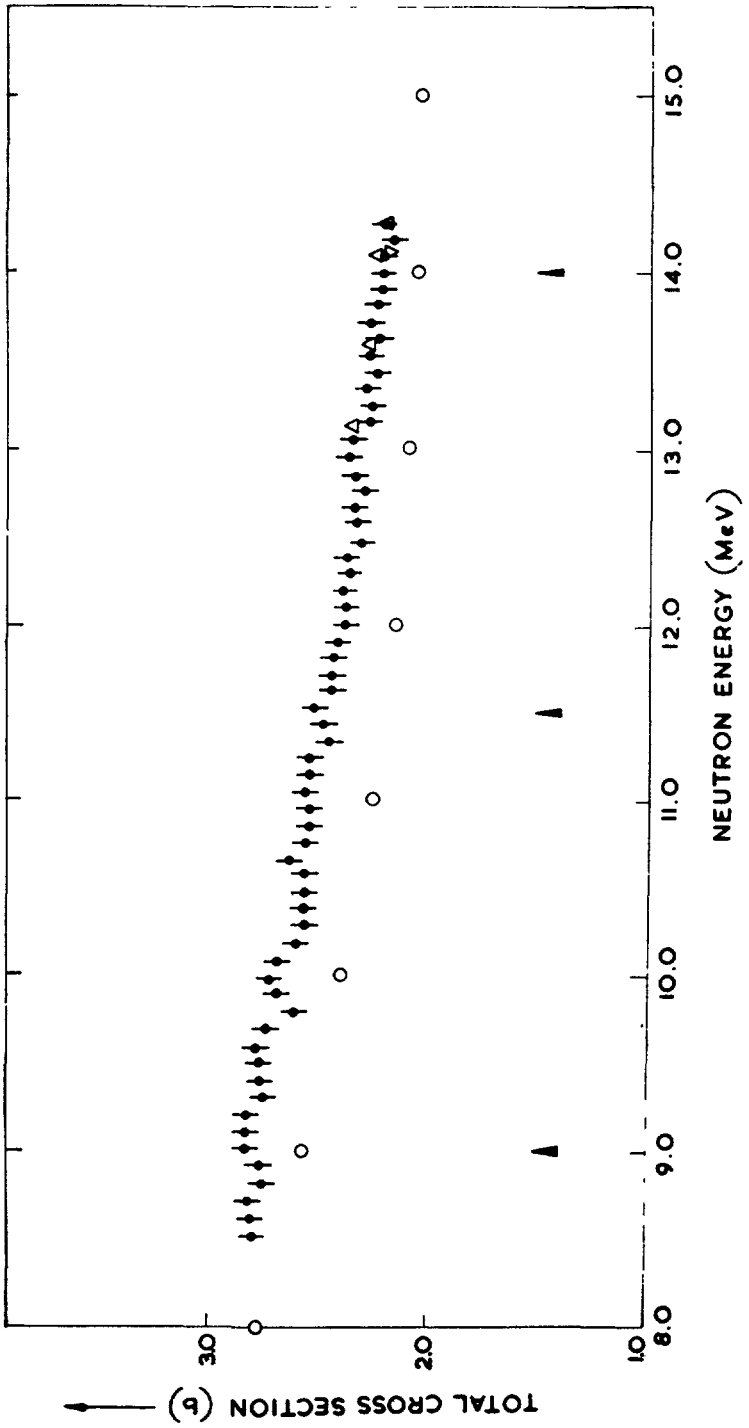
TOTAL CROSS SECTION (b)
3.0
2.0
1.0
8.0
9.0
10.0
11.0
12.0
13.0
14.0
15.0
NEUTRON ENERGY (MeV)

Fig. 4

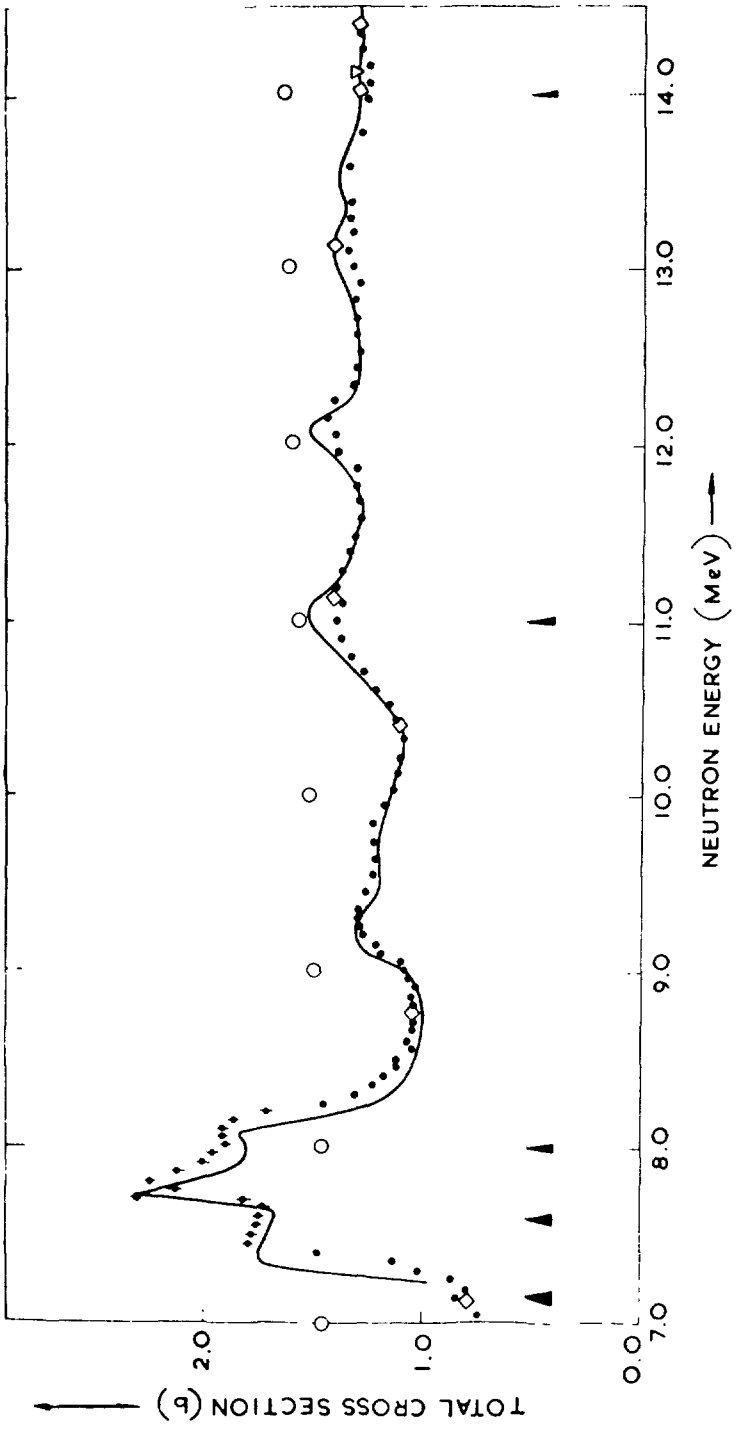
TOTAL CROSS SECTION (b)
0.0
1.0
2.0
7.0
8.0
9.0
10.0
11.0
12.0
13.0
14.0
NEUTRON ENERGY (MeV)

Fig. 5

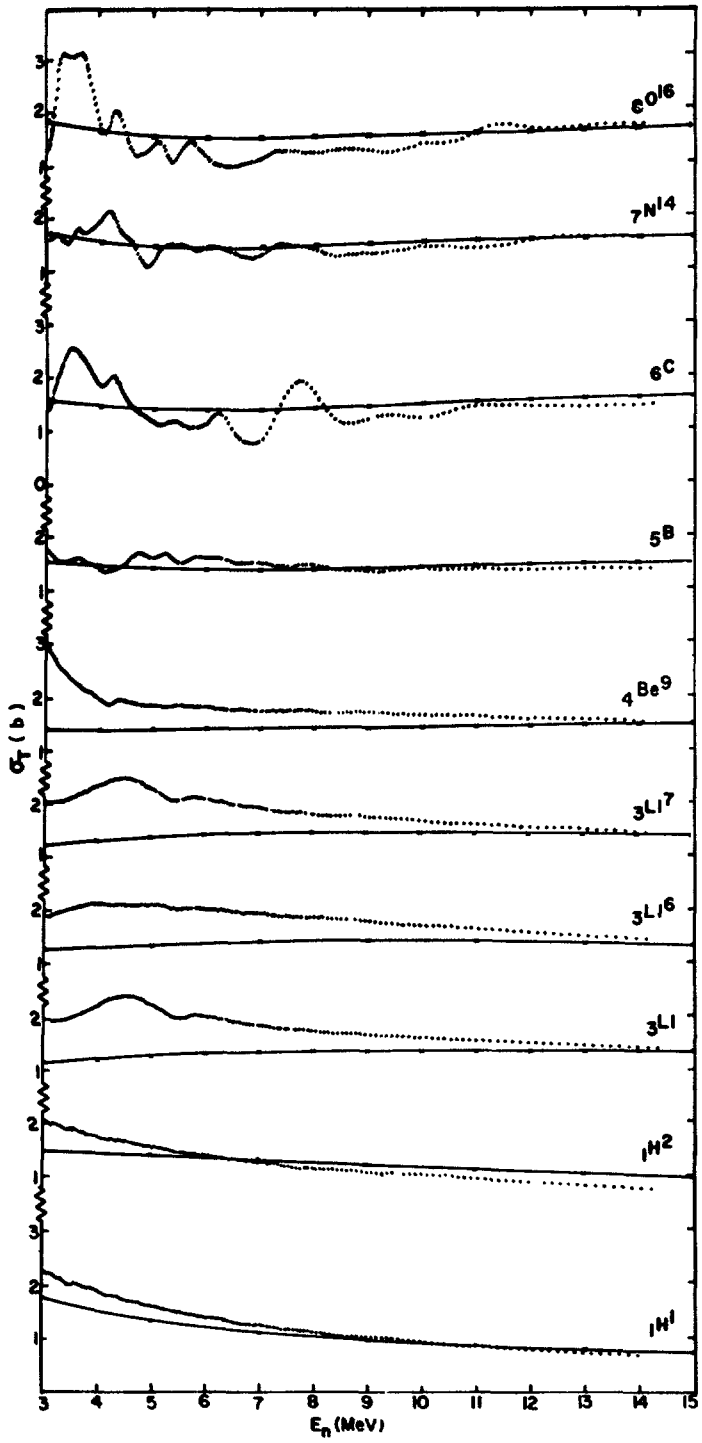

Fig. 6

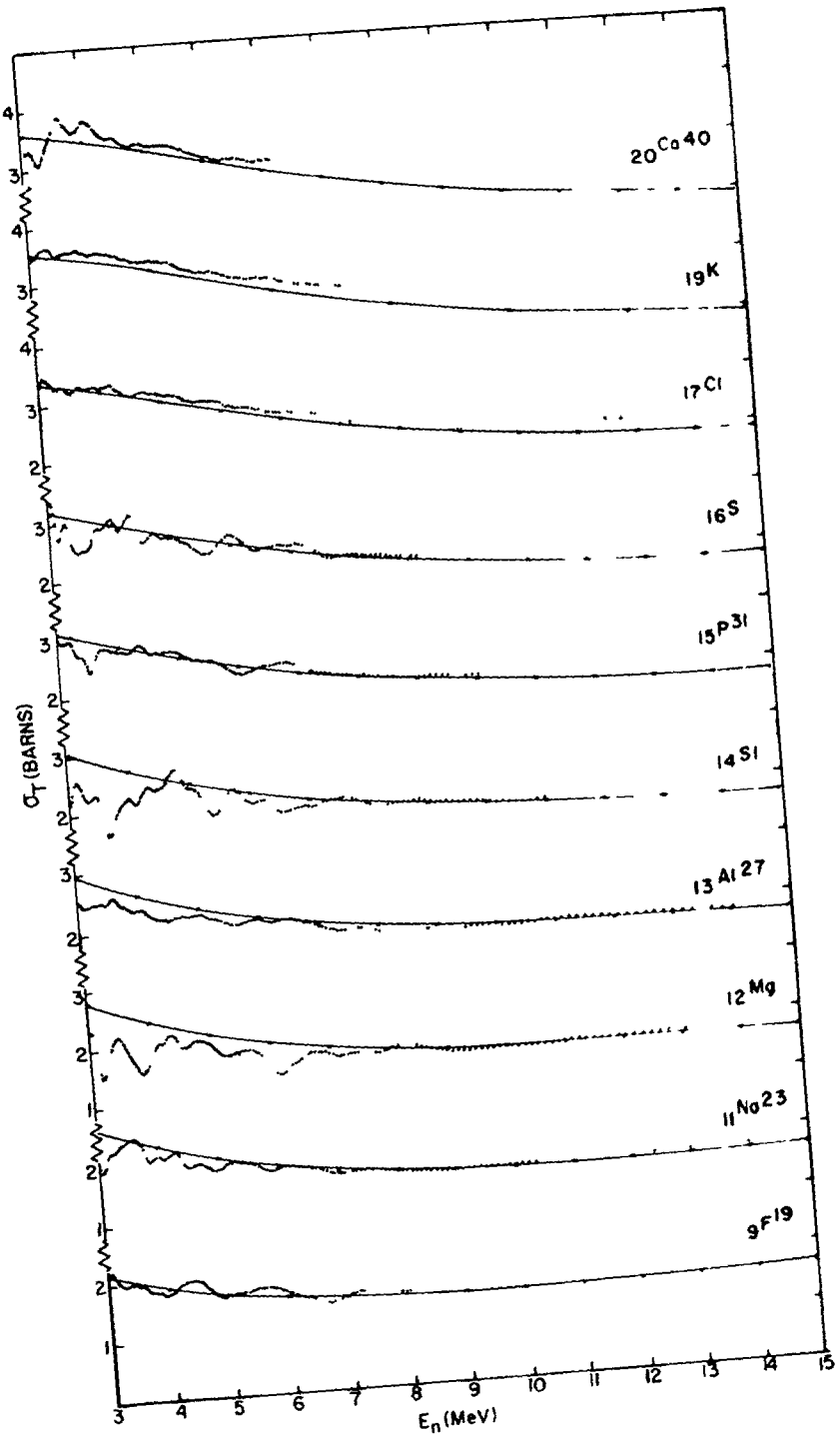
20^{Ca40}
19^{K}
17^{Cl}
16^{S}
15^{P31}
14^{Si}
13^{Al27}
12^{Mg}
11^{Na23}
9^{F19}
σ_T (BARNS)
E_n(MeV)

Fig. 7

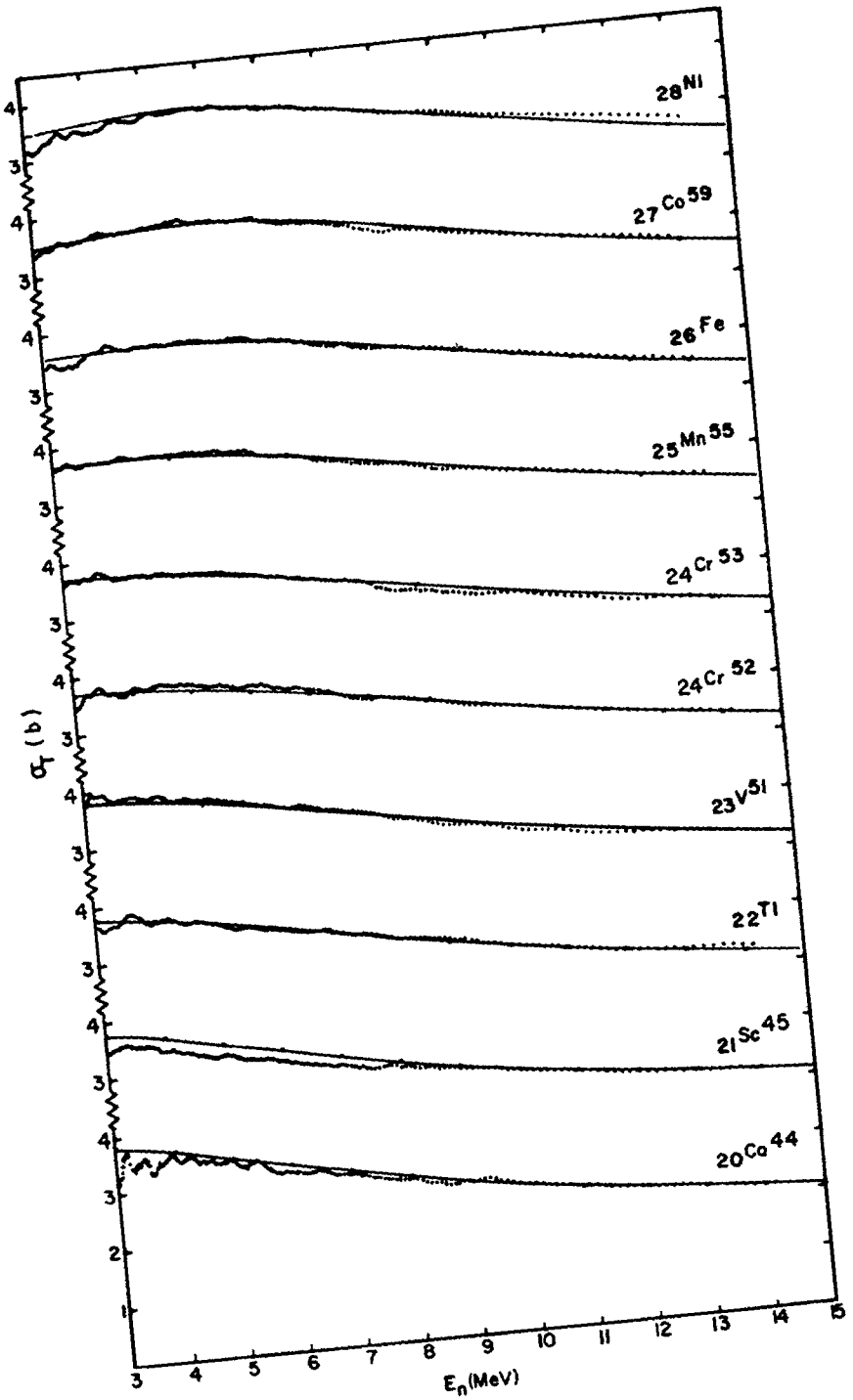
28Ni
27Co59
26Fe
25Mn55
24Cr53
24Cr52
23V51
22Ti
21Sc45
20Ca44
σT (b)
En(MeV)

Fig. 8

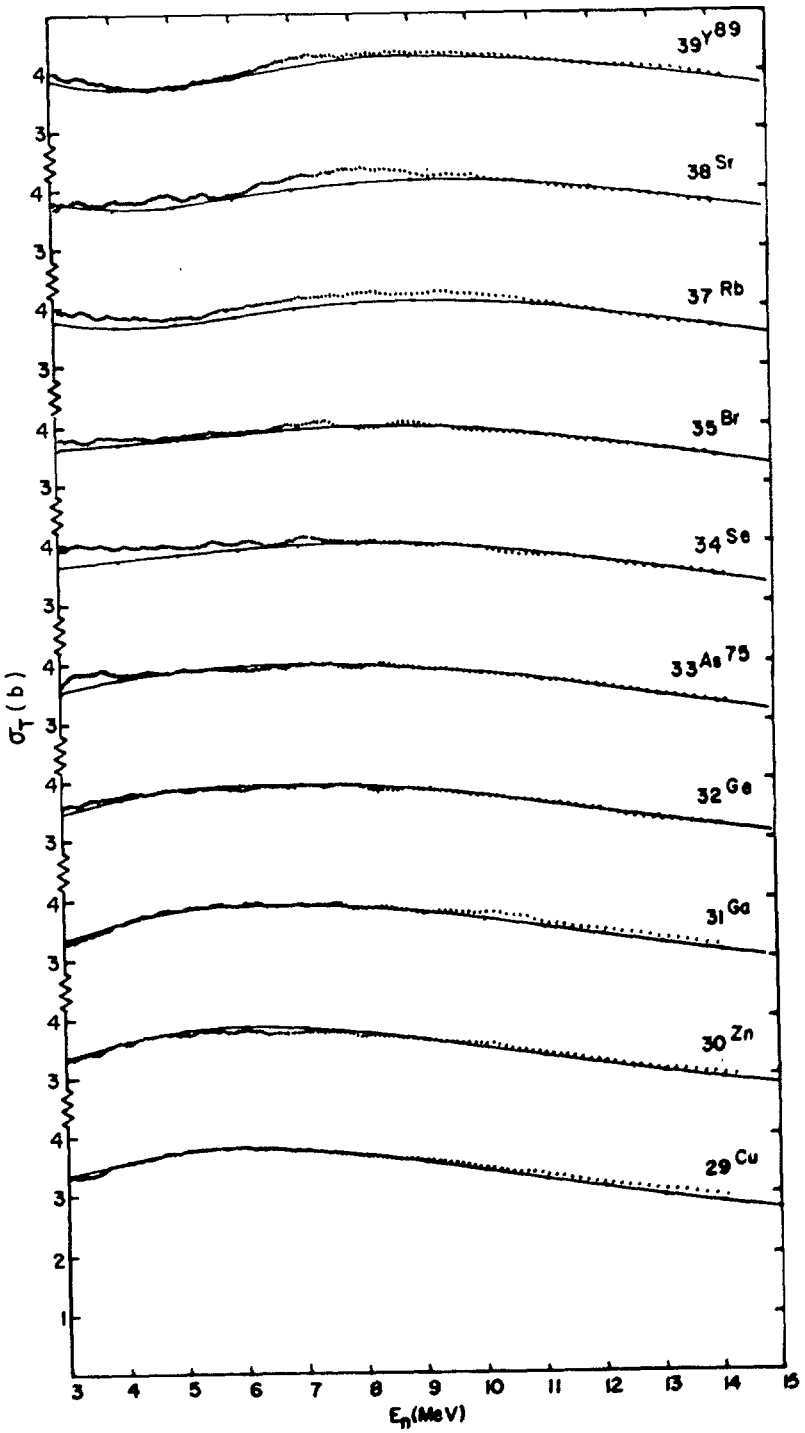
39Y89
38Sr
37Rb
35Br
34Se
33As75
32Ge
31Ga
30Zn
29Cu
σT (b)
En(MeV)
1
2
3
4
5
6
7
8
9
10
11
12
13
14
15

Fig. 9

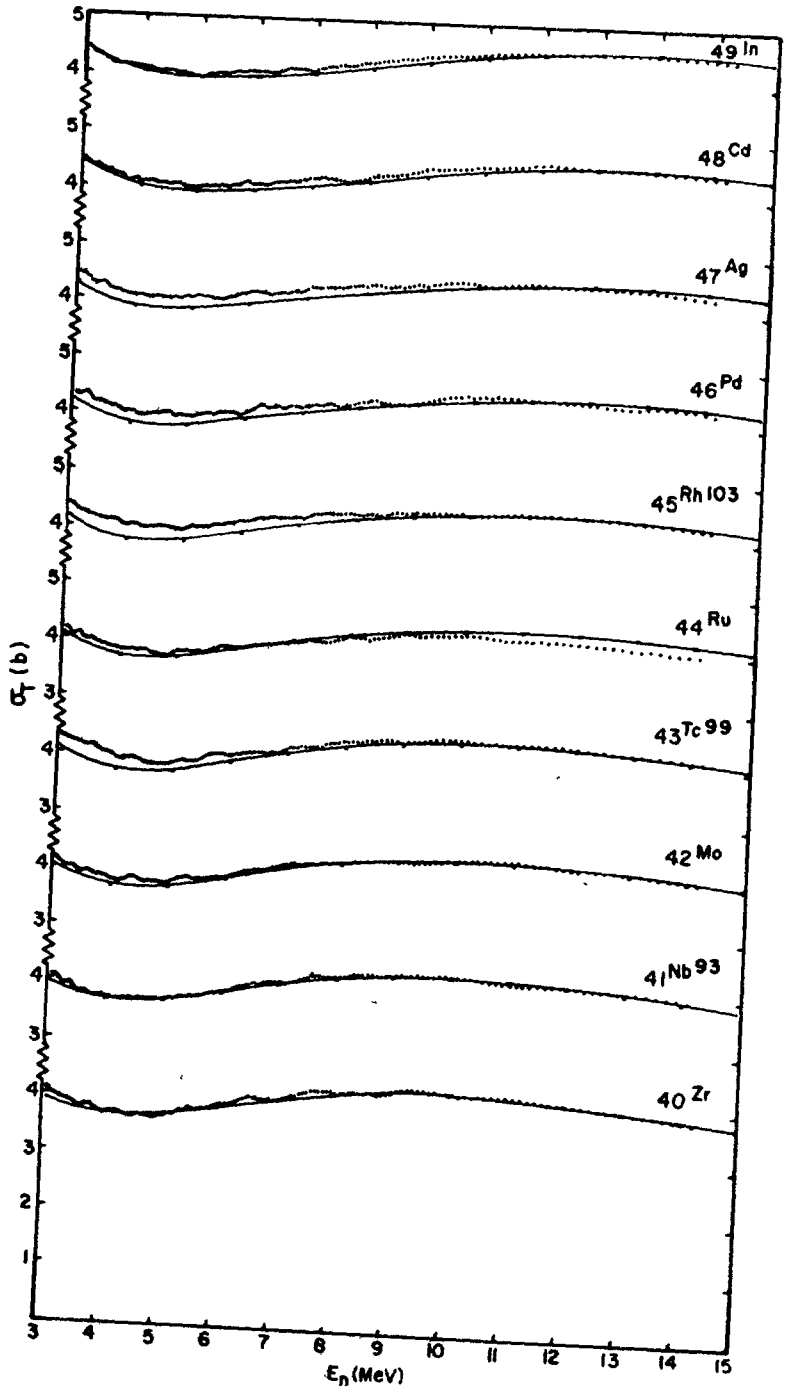
49 In
48 Cd
47 Ag
46 Pd
45 Rh 103
44 Ru
43 Tc 99
42 Mo
41 Nb 93
40 Zr
σT (b)
En (MeV)

Fig. 10

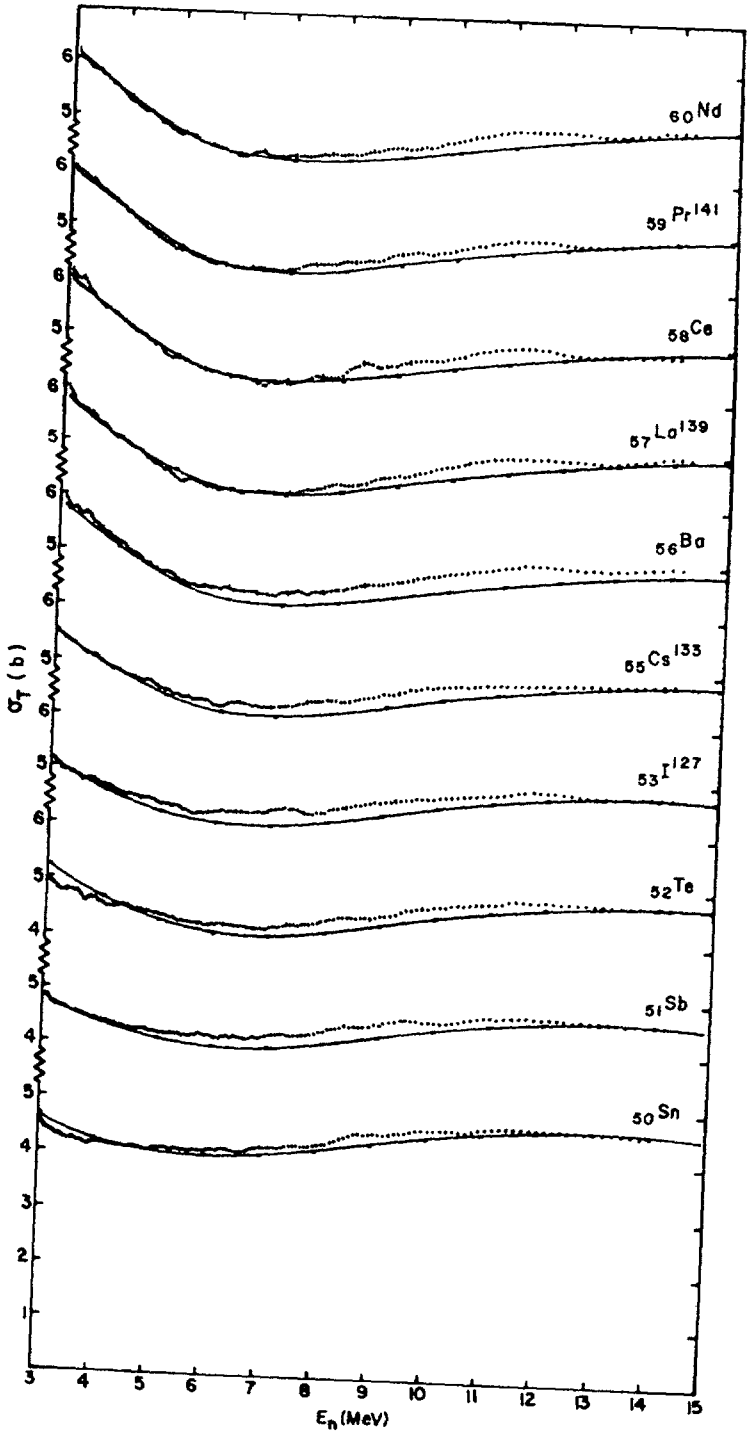
60Nd
59Pr141
58Ce
57La139
56Ba
55Cs133
53I127
52Te
51Sb
50Sn
σT (b)
En (MeV)

Fig. 11

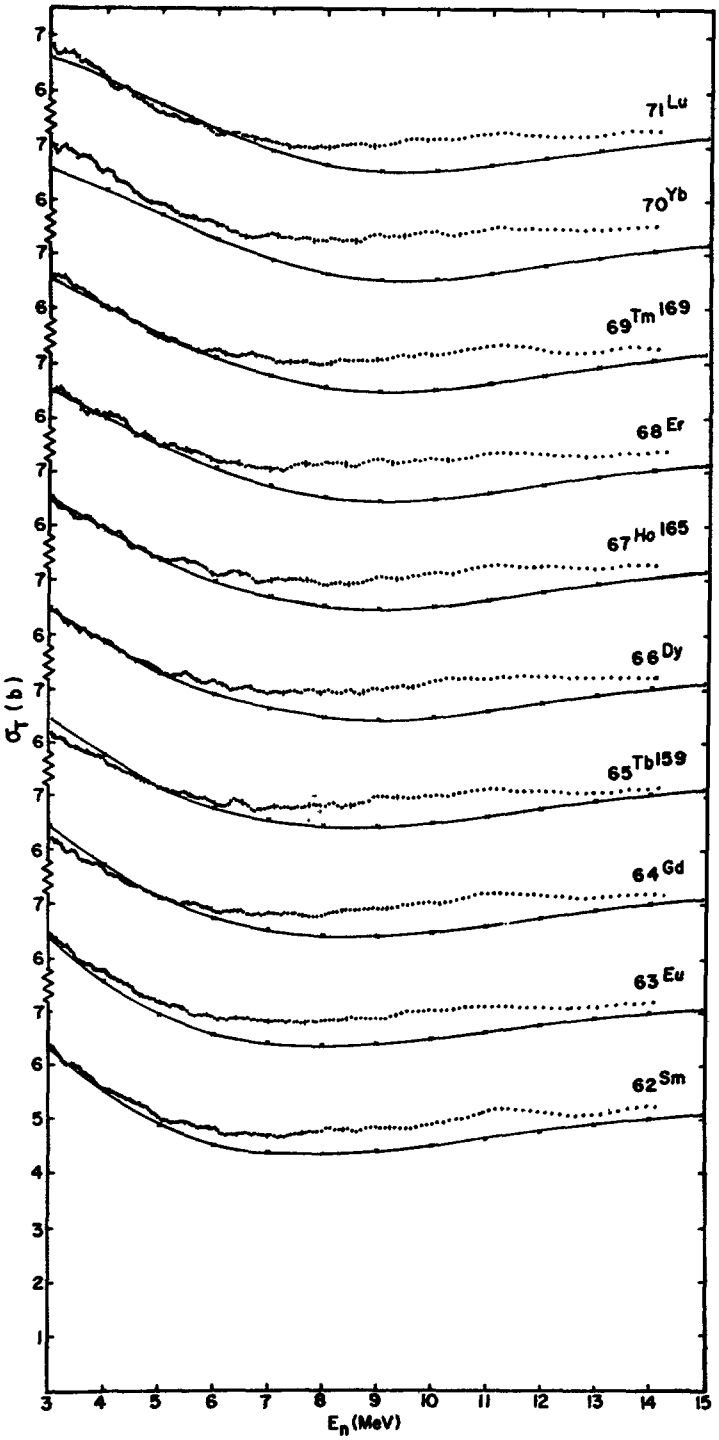
71 Lu
70 Yb
69 Tm 169
68 Er
67 Ho 165
66 Dy
65 Tb 159
64 Gd
63 Eu
62 Sm
σT (b)
En (MeV)

Fig. 12

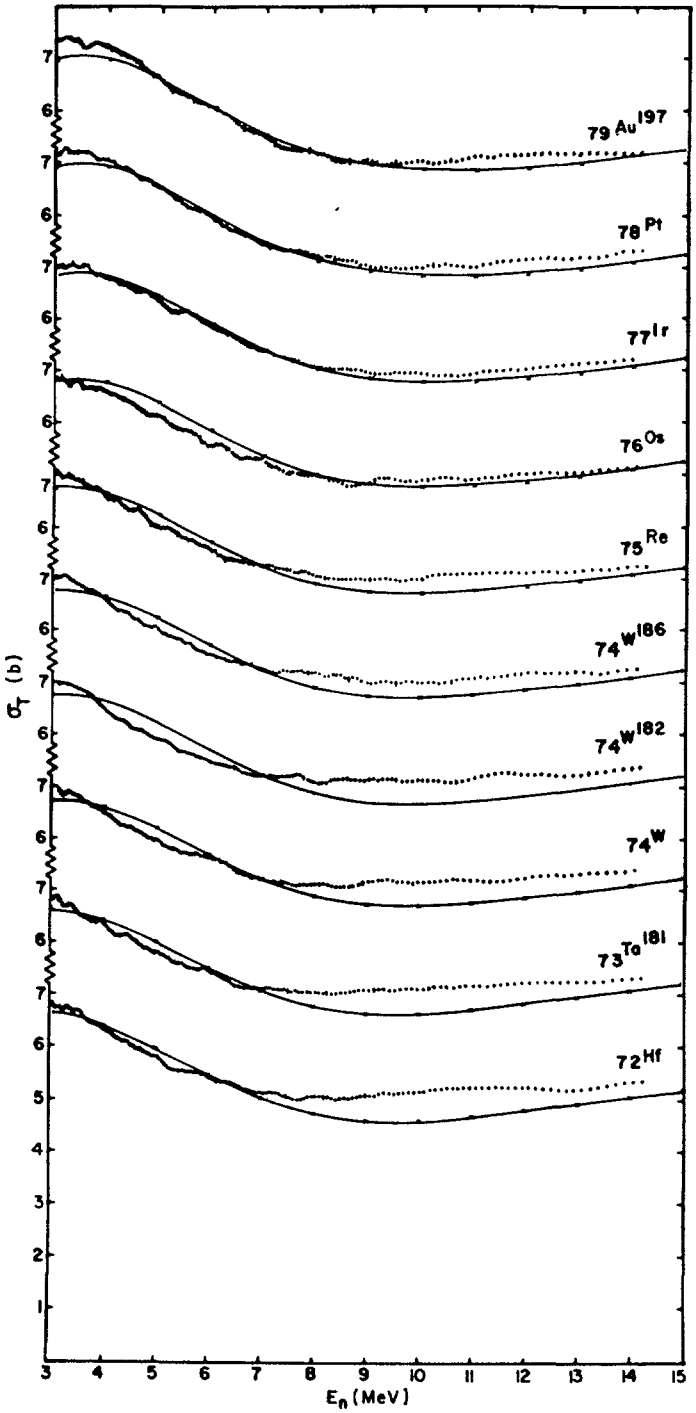
79 Au 197
78 Pt
77 Ir
76 Os
75 Re
74 W 186
74 W 182
74 W
73 Ta 181
72 Hf
σT (b)
En (MeV)

Fig. 13

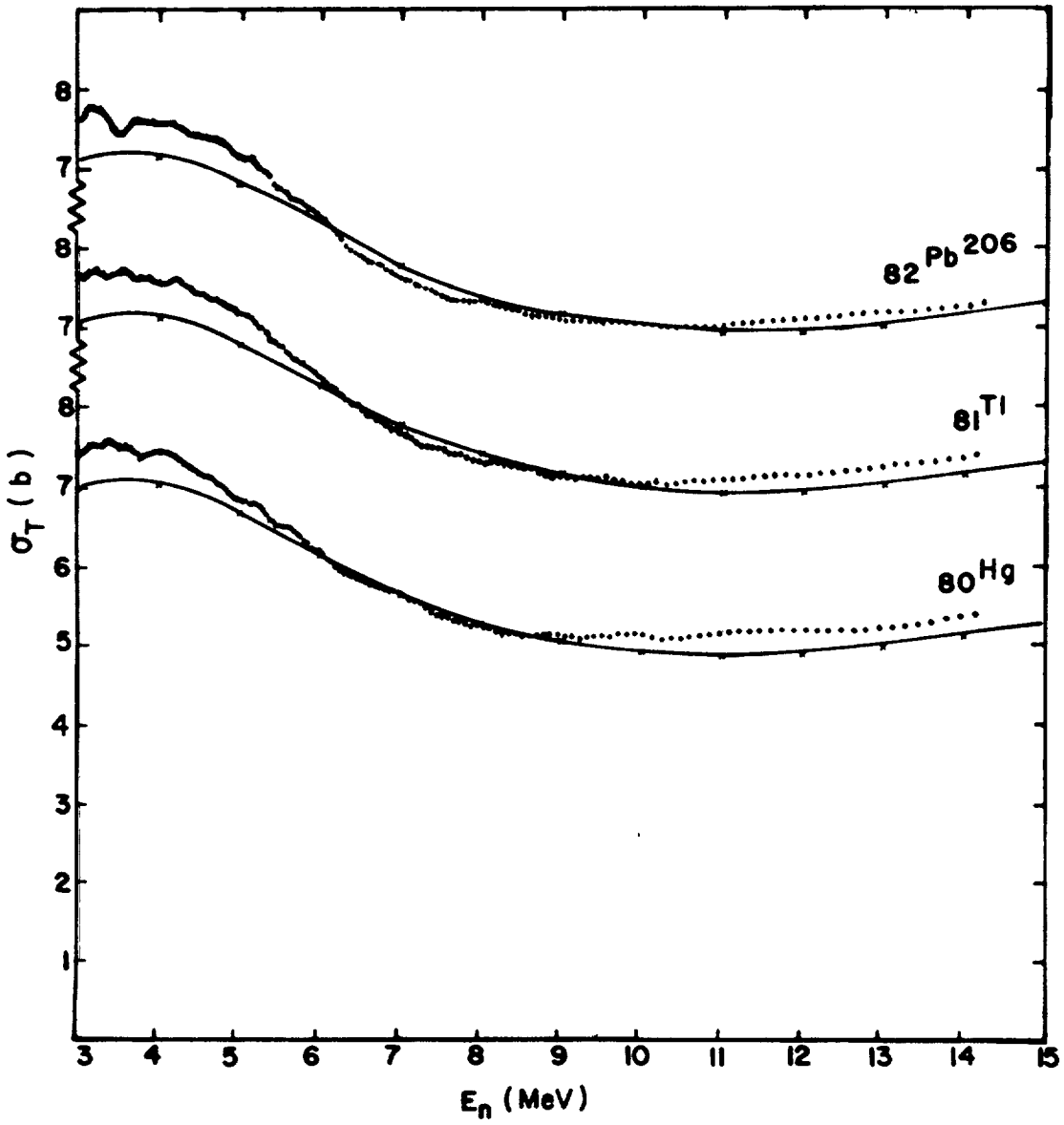

Fig. 14

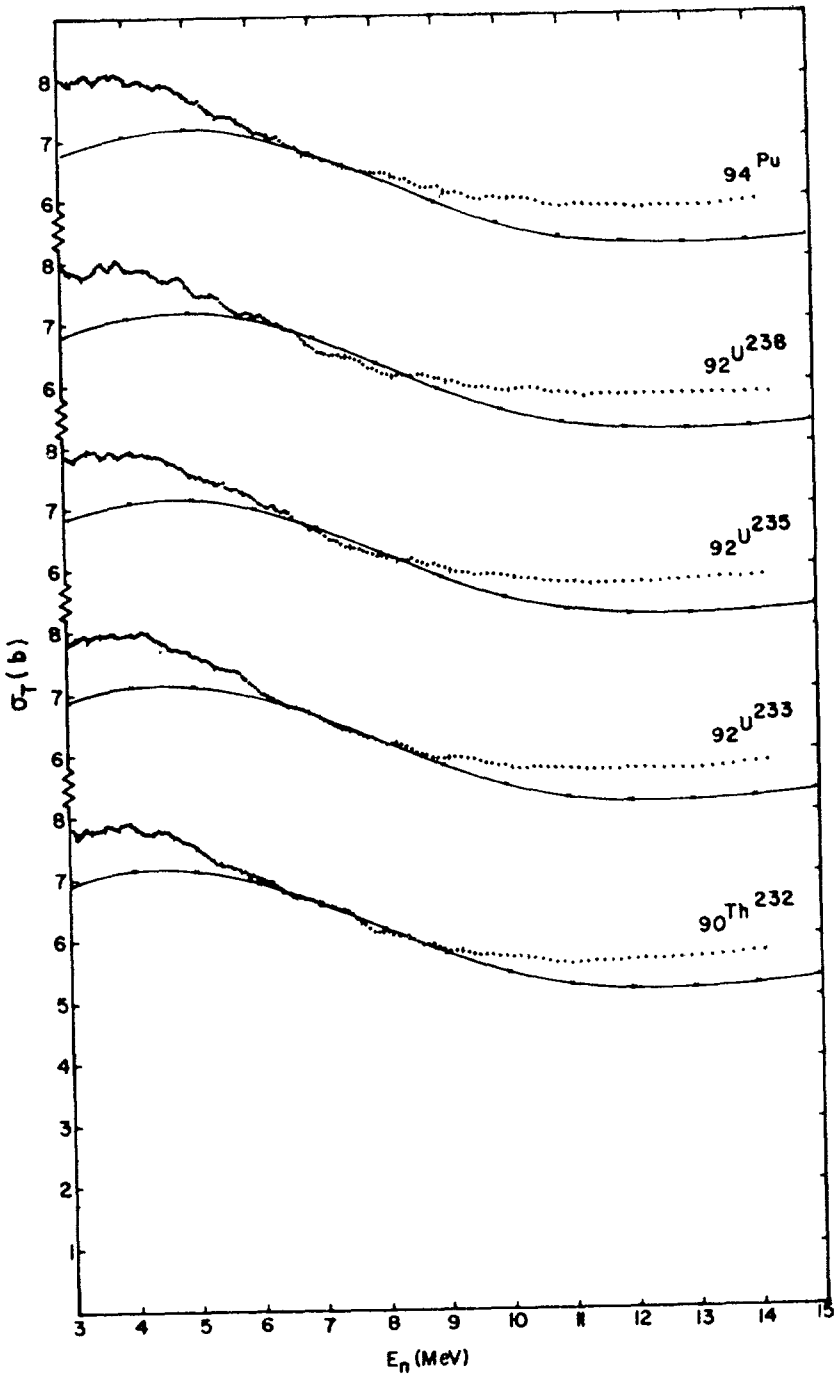

Fig. 15

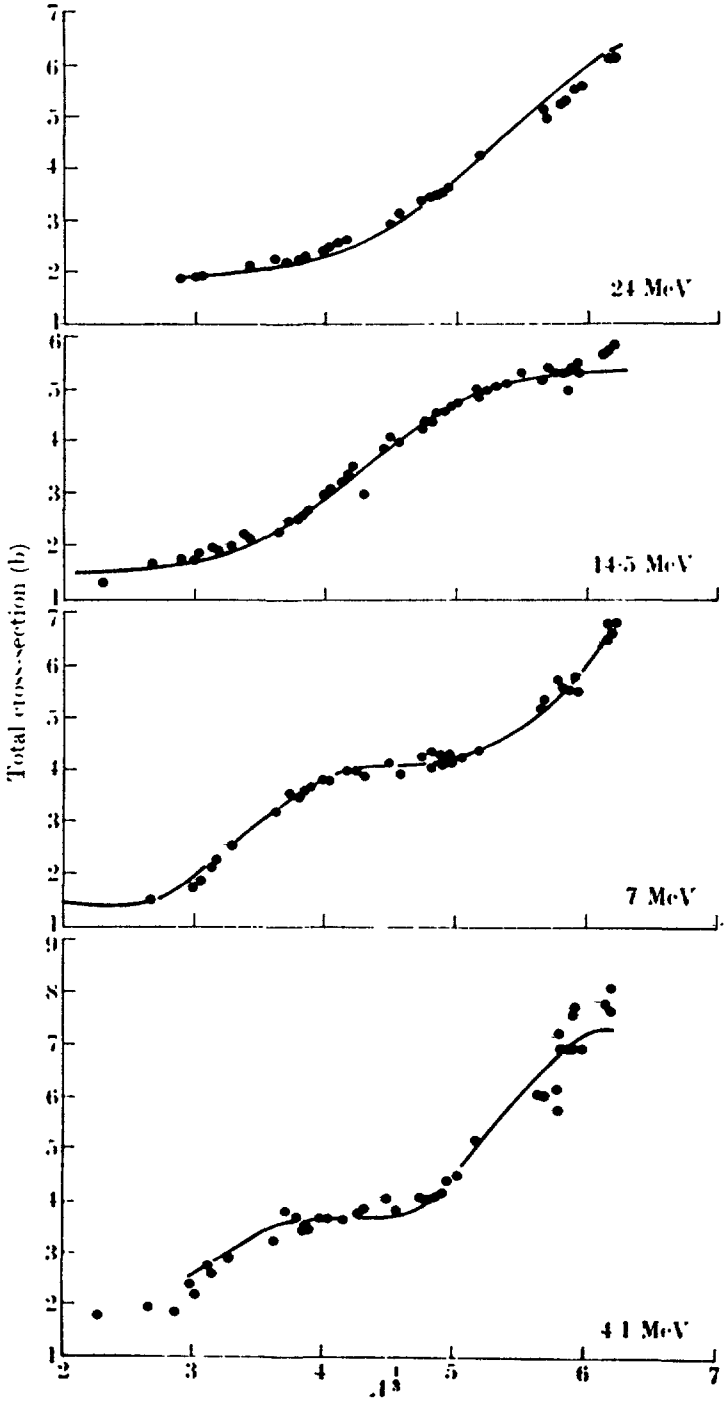

Fig. 16

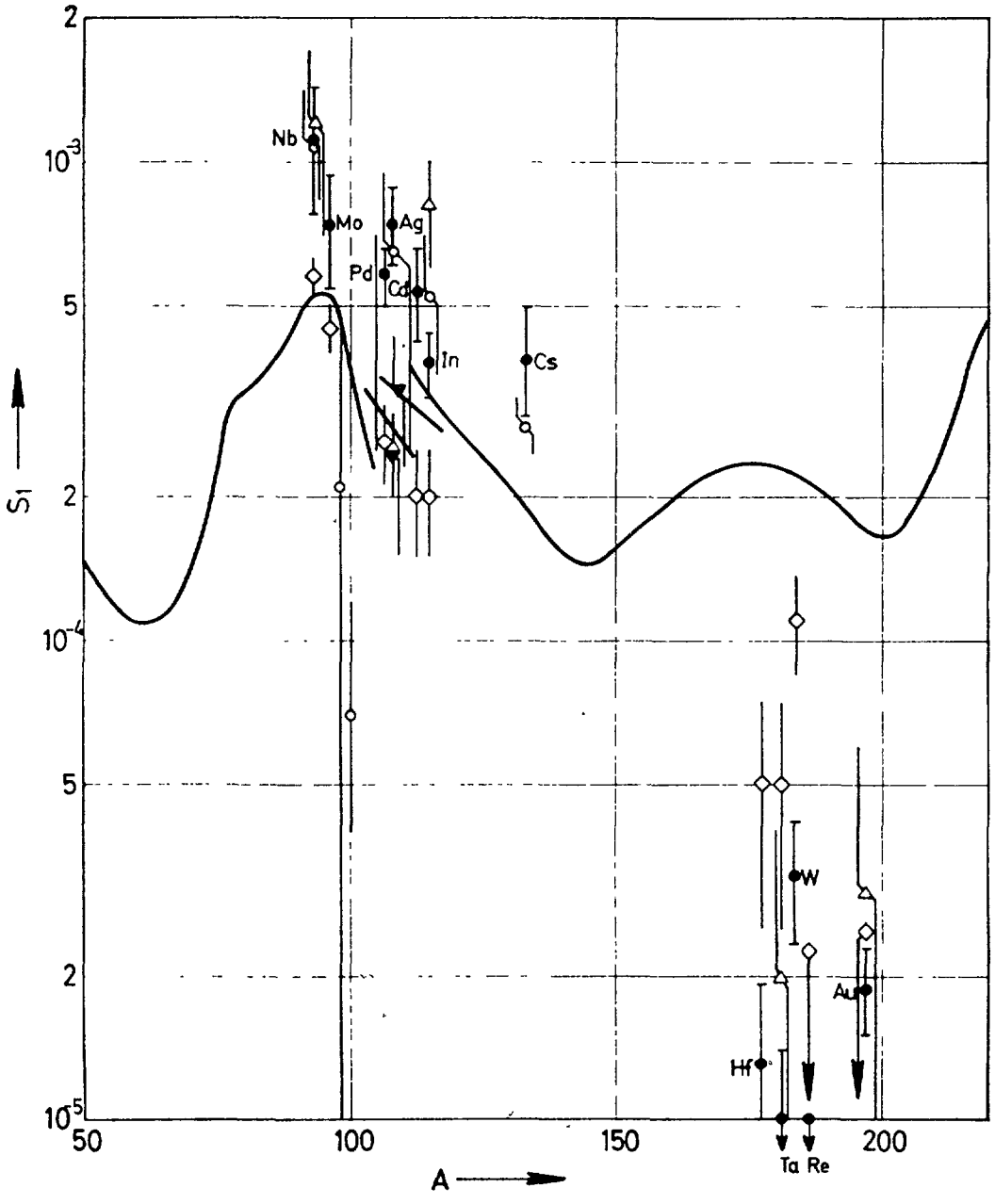
2
10⁻³
5
2
10⁻⁴
5
2
10⁻⁵
S₁
Nb
Mo
Ag
Pd
Cd
In
Cs
W
Au
Hf
Ta Re
50
100
150
200
A

Fig. 17

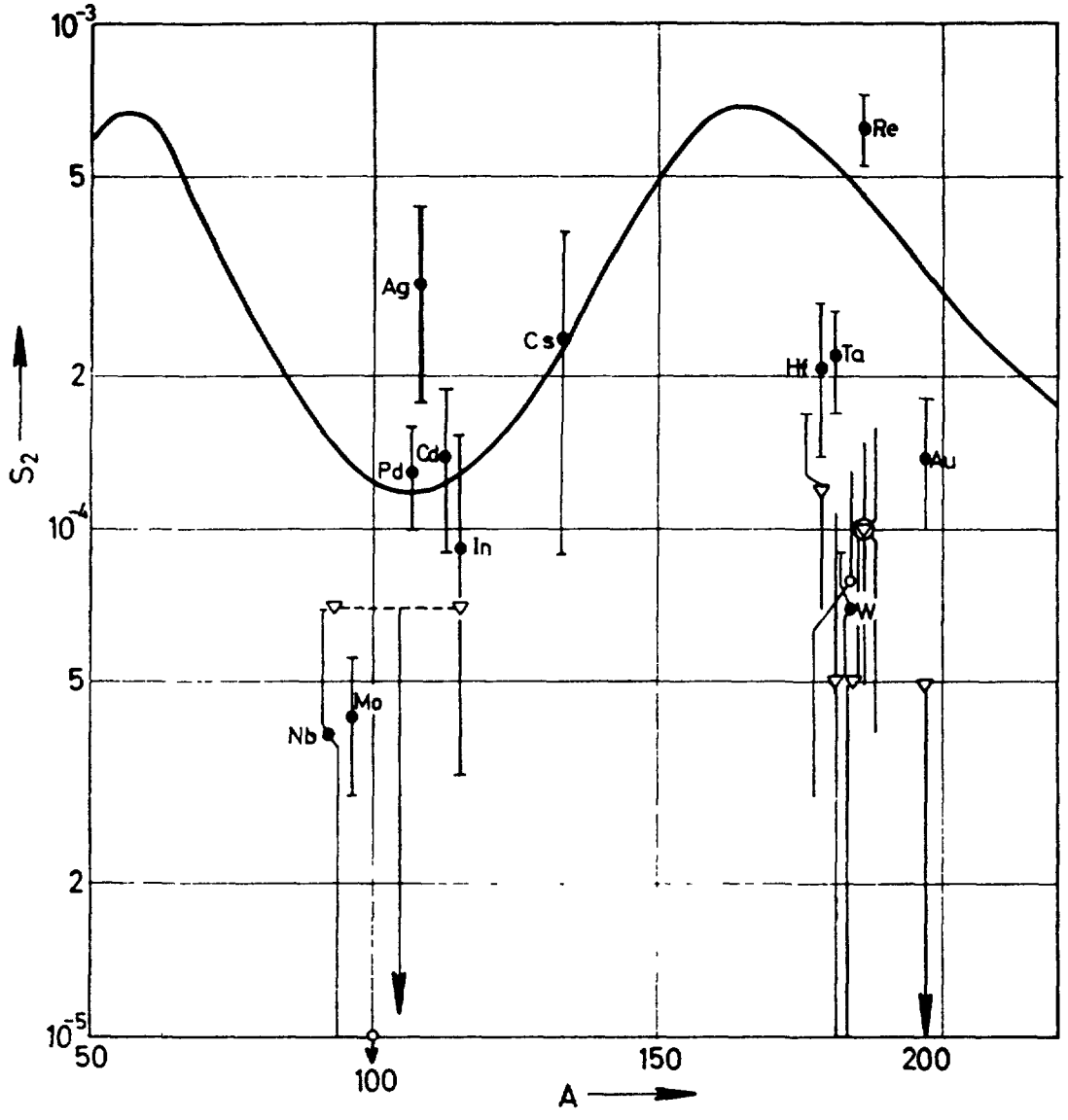
10^{-3}
5
2
10^{-4}
5
2
10^{-5}
S_2
50
100
150
200
A
Re
Ag
Cs
Hf
Ta
Pd
Cd
In
Au
W
Mo
Nb

Fig. 18

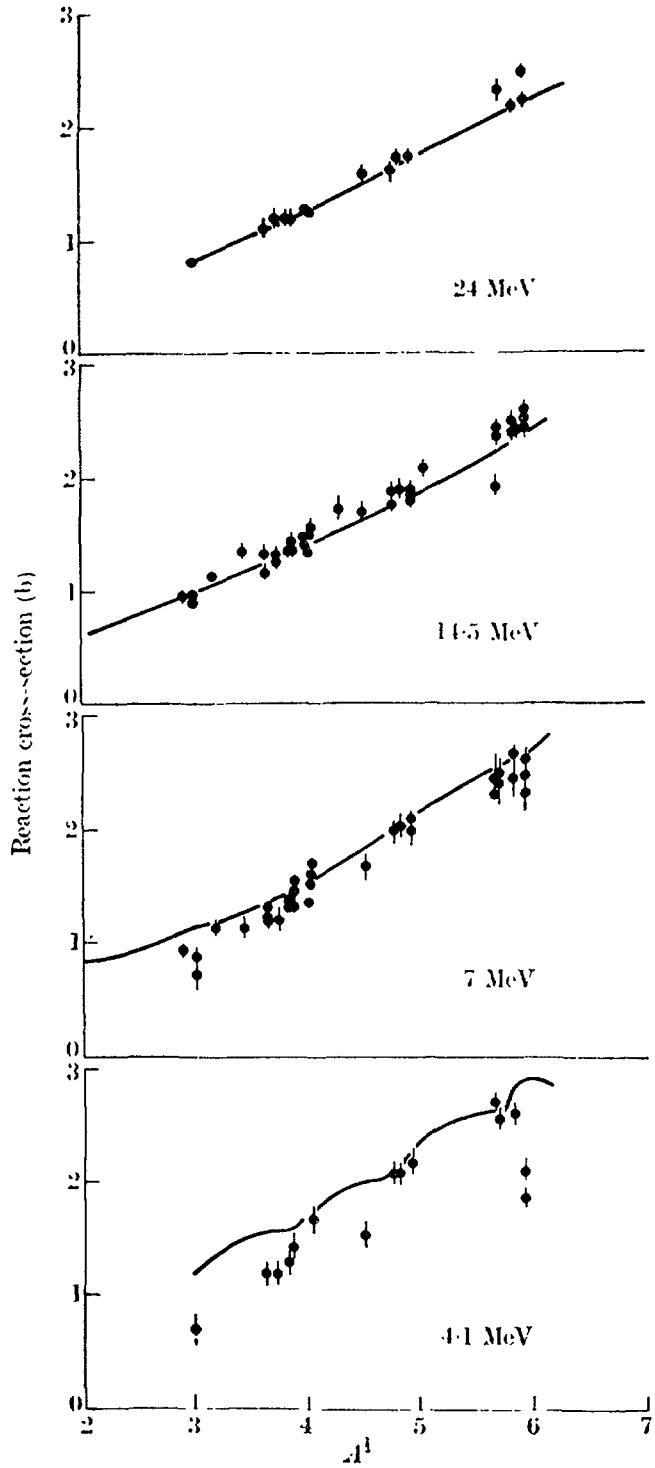

Fig. 19

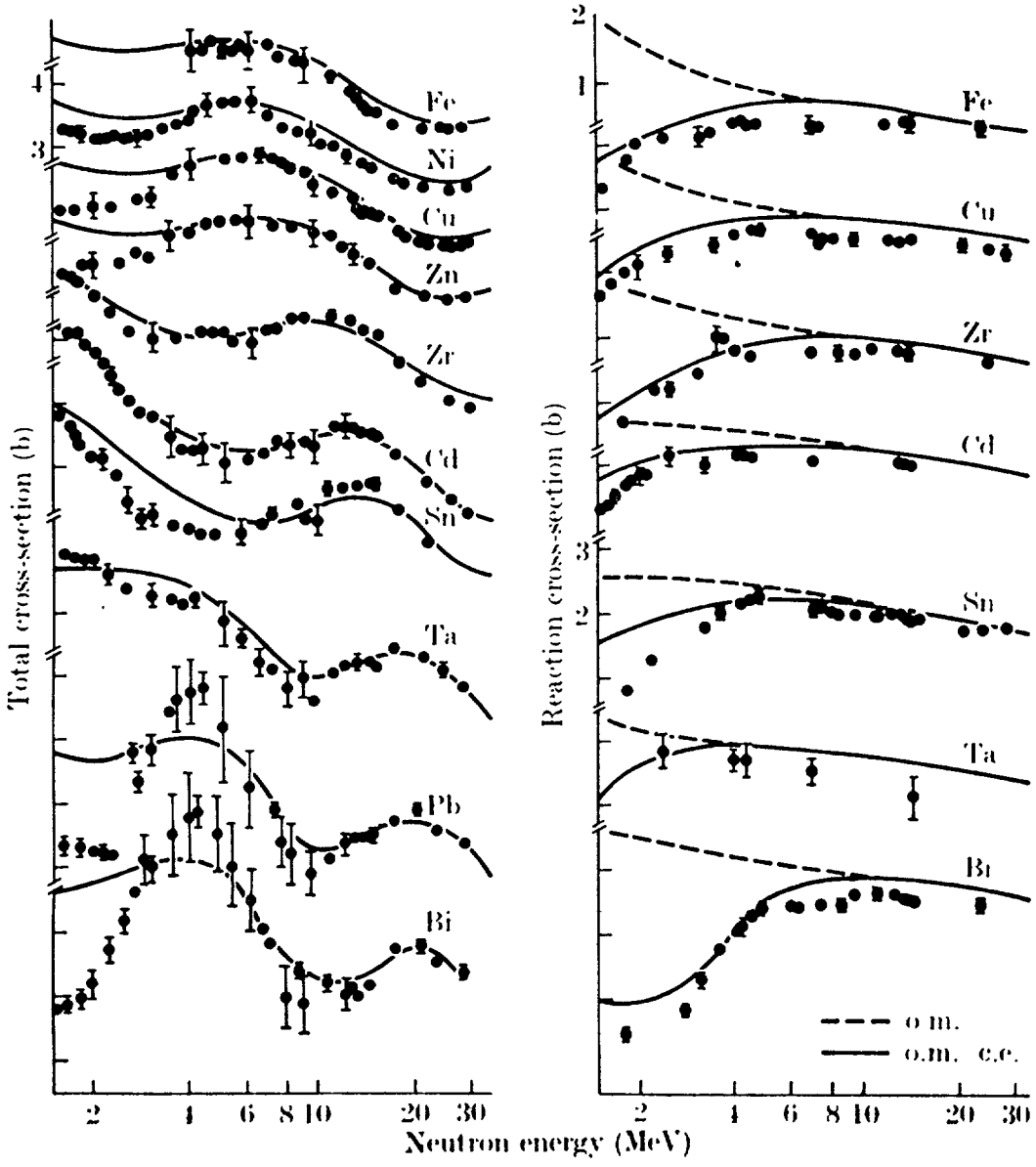
Total cross-section (b)
Reaction cross-section (b)
Fe
Ni
Cu
Zn
Zr
Cd
Sn
Ta
Pb
Bi
o.m.
o.m. c.c.
2
4
6
8
10
20
30
Neutron energy (MeV)

Fig. 20

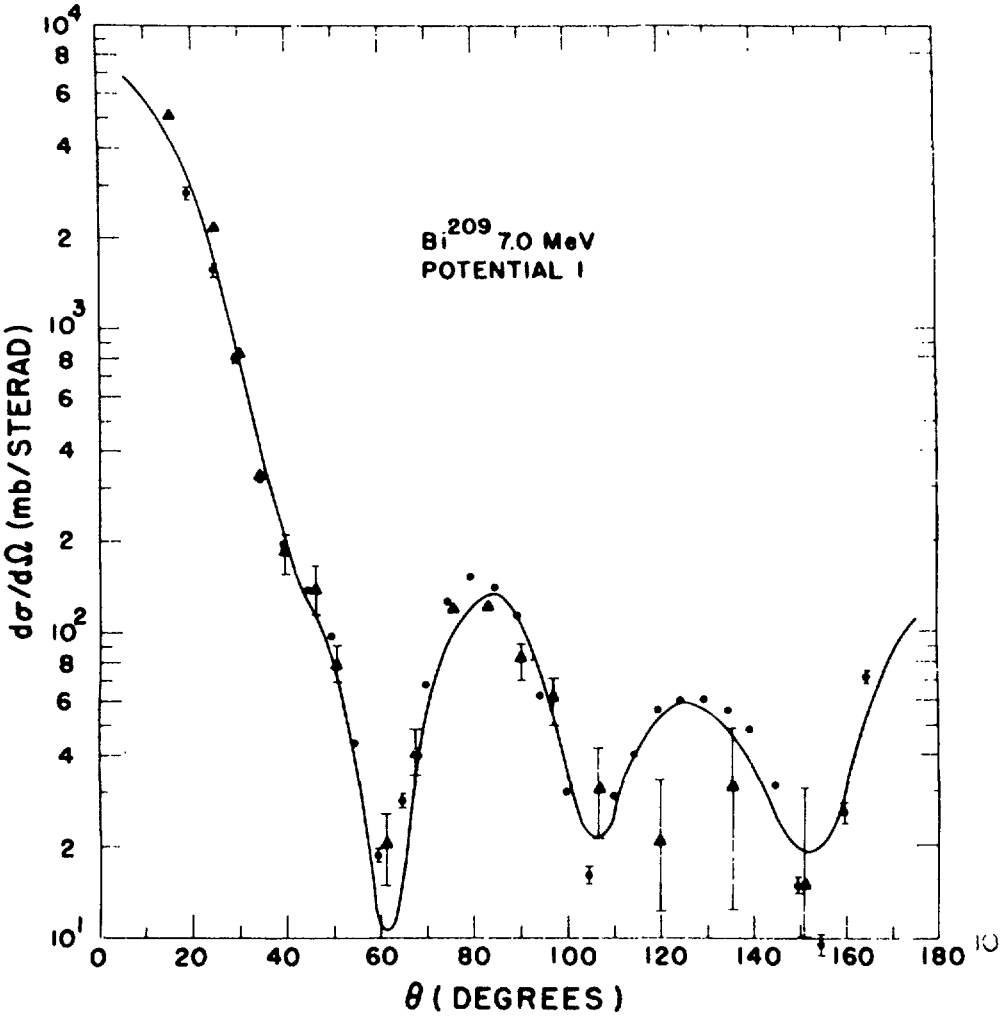
Bi209 7.0 MeV
POTENTIAL I
dσ/dΩ (mb/STERAD)
θ (DEGREES)
10^4
8
6
4
2
10^3
8
6
4
2
10^2
8
6
4
2
10^1
0
20
40
60
80
100
120
140
160
180

Fig. 21

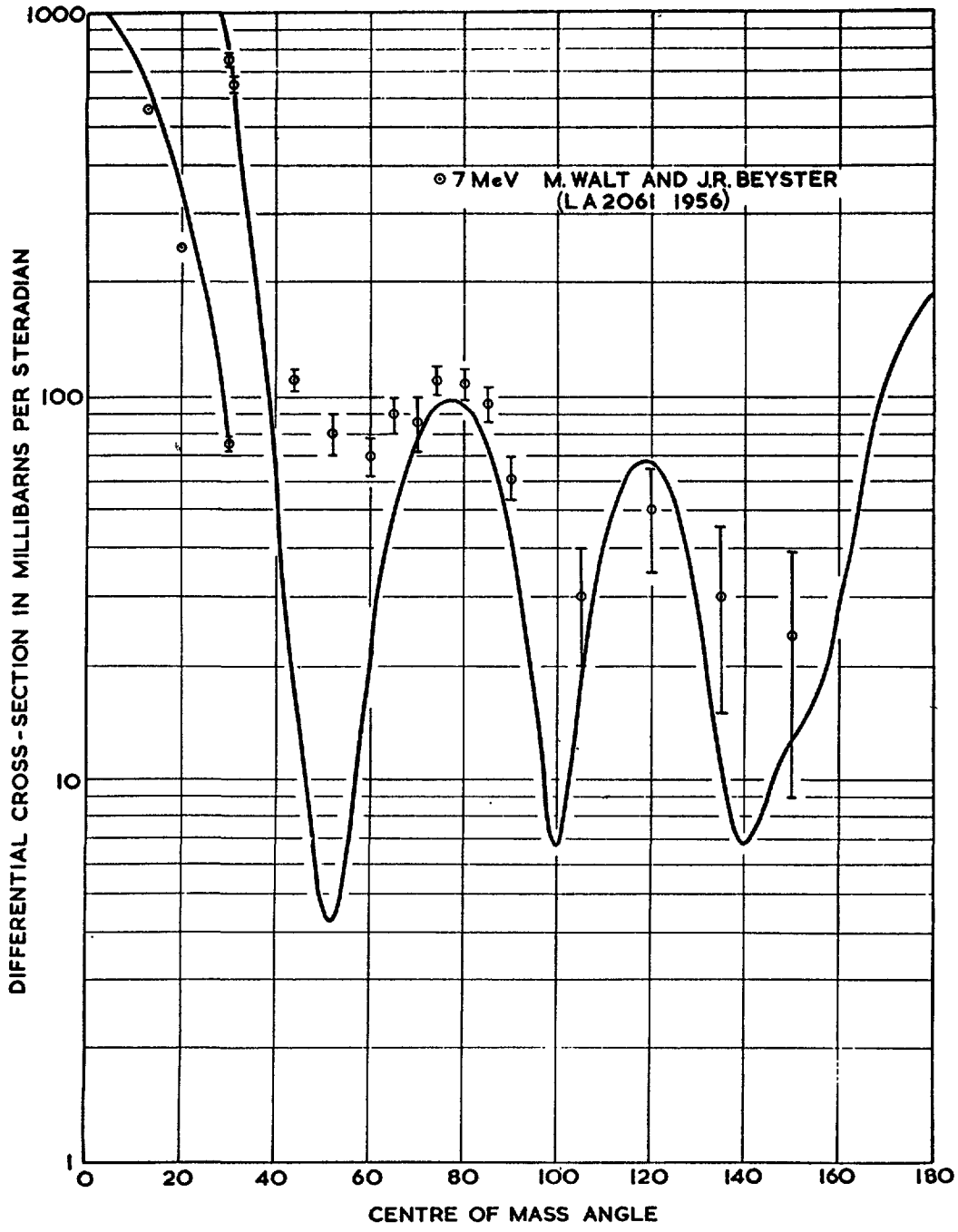
⊙ 7 MeV M. WALT AND J.R. BEYSTER
(L A 2061 1956)
DIFFERENTIAL CROSS-SECTION IN MILLIBARNS PER STERADIAN
1000
100
10
1
0
20
40
60
80
100
120
140
160
180
CENTRE OF MASS ANGLE

Fig. 22

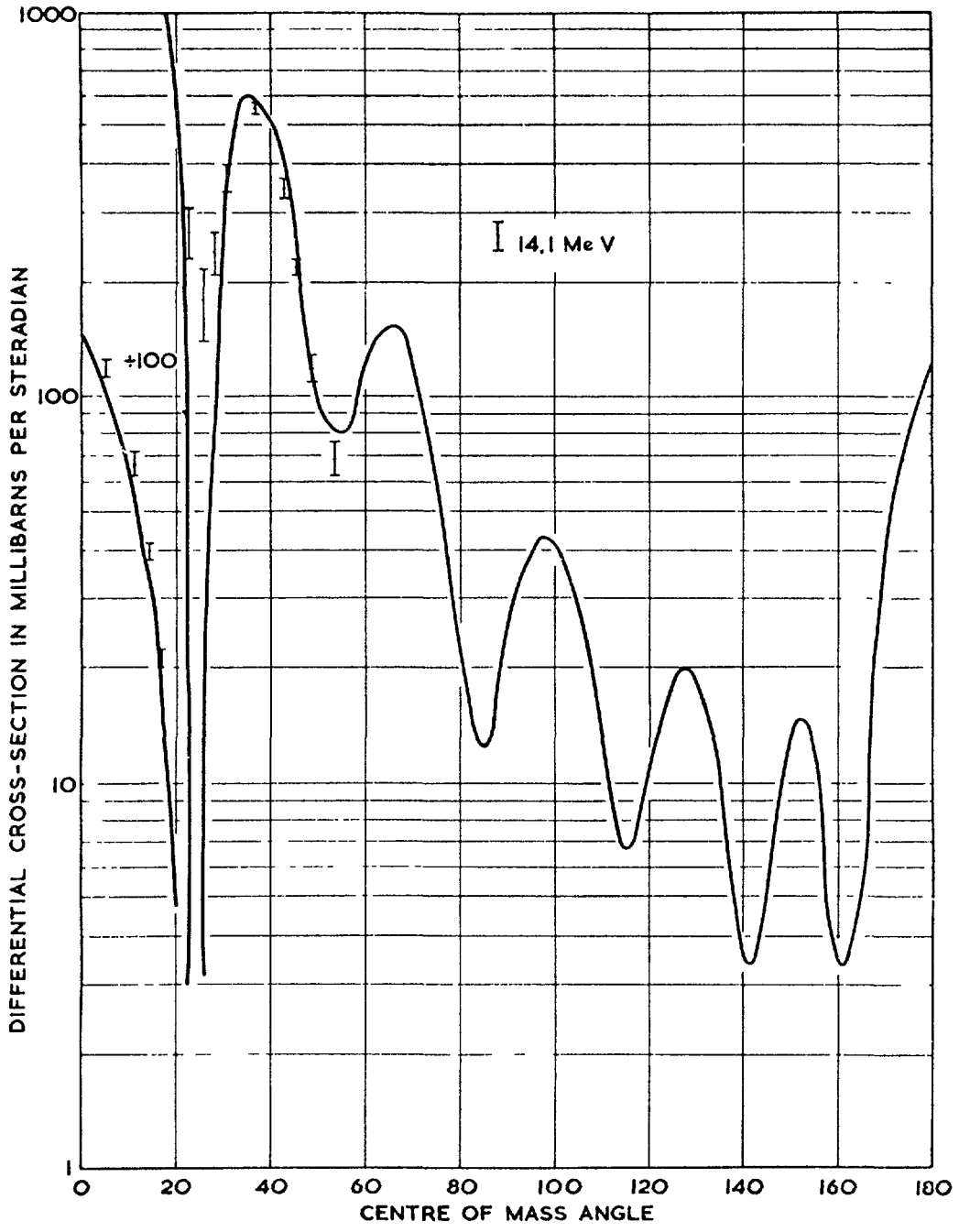
1000
100
10
1
DIFFERENTIAL CROSS-SECTION IN MILLIBARNS PER STERADIAN
14.1 Me V
÷100
0
20
40
60
80
100
120
140
160
180
CENTRE OF MASS ANGLE

Fig. 23

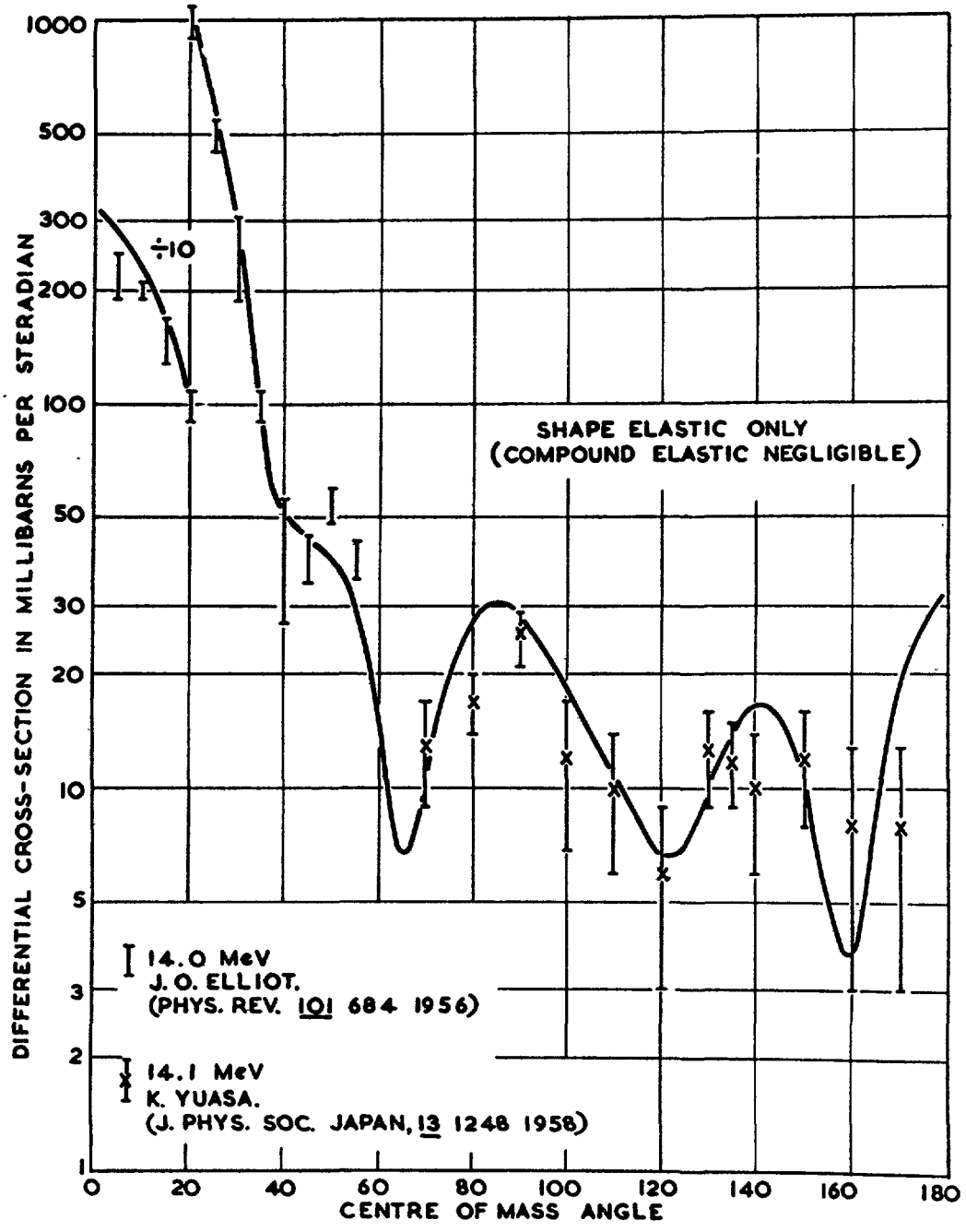
DIFFERENTIAL CROSS-SECTION IN MILLIBARNS PER STERADIAN
1000
500
300
200
100
50
30
20
10
5
3
2
1
÷10
SHAPE ELASTIC ONLY
(COMPOUND ELASTIC NEGLIGIBLE)
14.0 MeV
J. O. ELLIOT.
(PHYS. REV. 101 684 1956)
14.1 MeV
K. YUASA.
(J. PHYS. SOC. JAPAN, 13 1248 1958)
0
20
40
60
80
100
120
140
160
180
CENTRE OF MASS ANGLE

Fig. 24

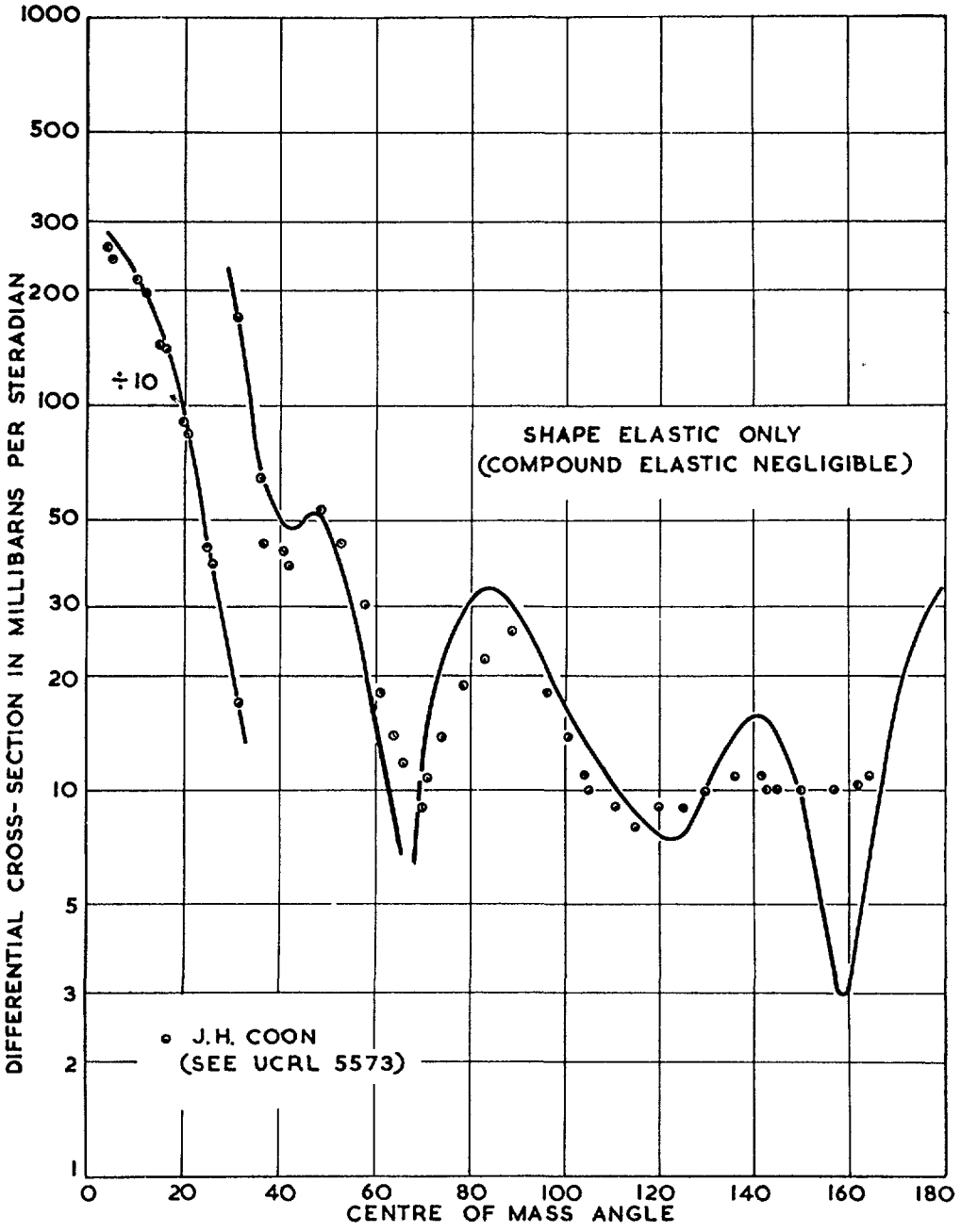
DIFFERENTIAL CROSS-SECTION IN MILLIBARNS PER STERADIAN
1000
500
300
200
100
50
30
20
10
5
3
2
1
÷10
SHAPE ELASTIC ONLY
(COMPOUND ELASTIC NEGLIGIBLE)
J.H. COON
(SEE UCRL 5573)
0
20
40
60
80
100
120
140
160
180
CENTRE OF MASS ANGLE

Fig. 25

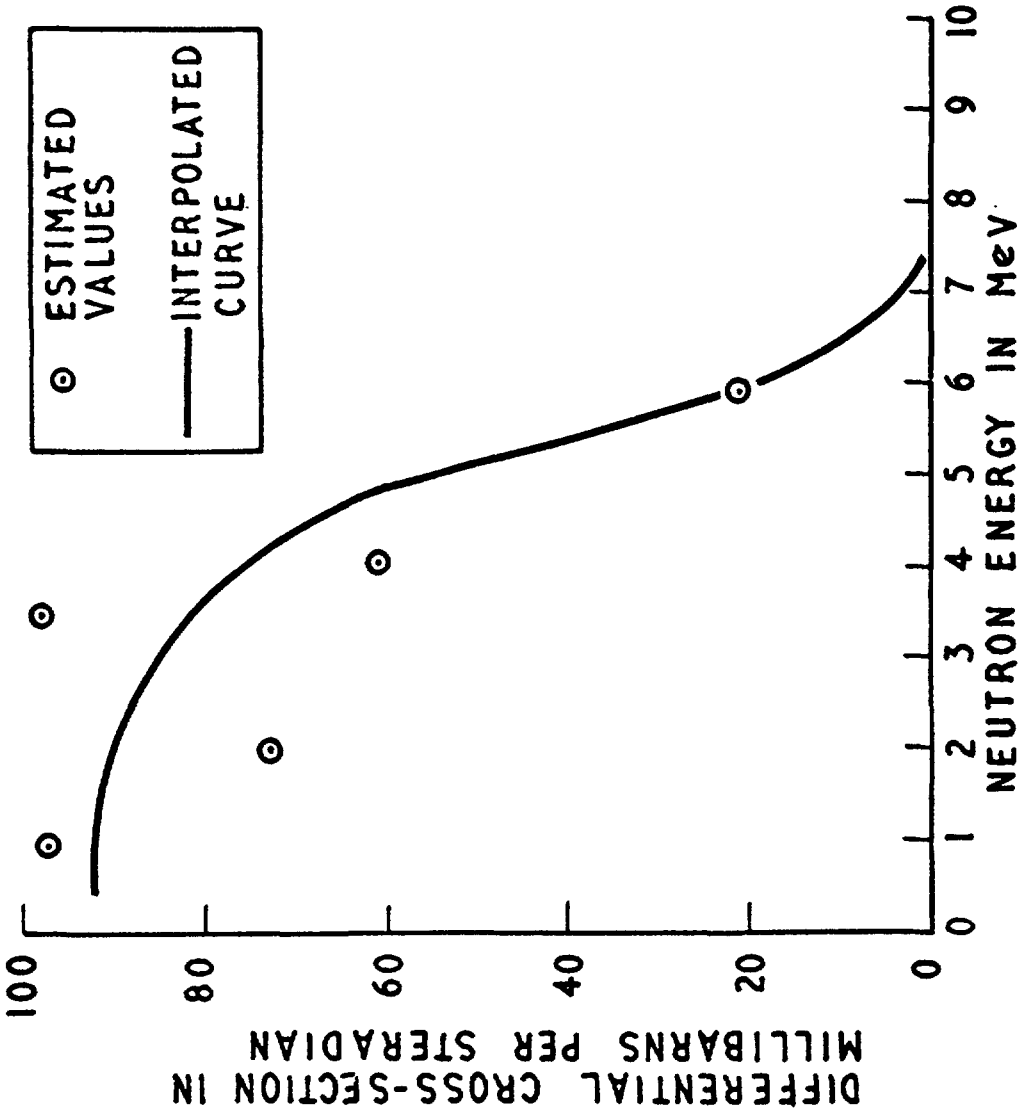
ESTIMATED VALUES
INTERPOLATED CURVE
DIFFERENTIAL CROSS-SECTION IN MILLIBARNS PER STERADIAN
100
80
60
40
20
0
0
1
2
3
4
5
6
7
8
9
10
NEUTRON ENERGY IN MeV

Fig. 26

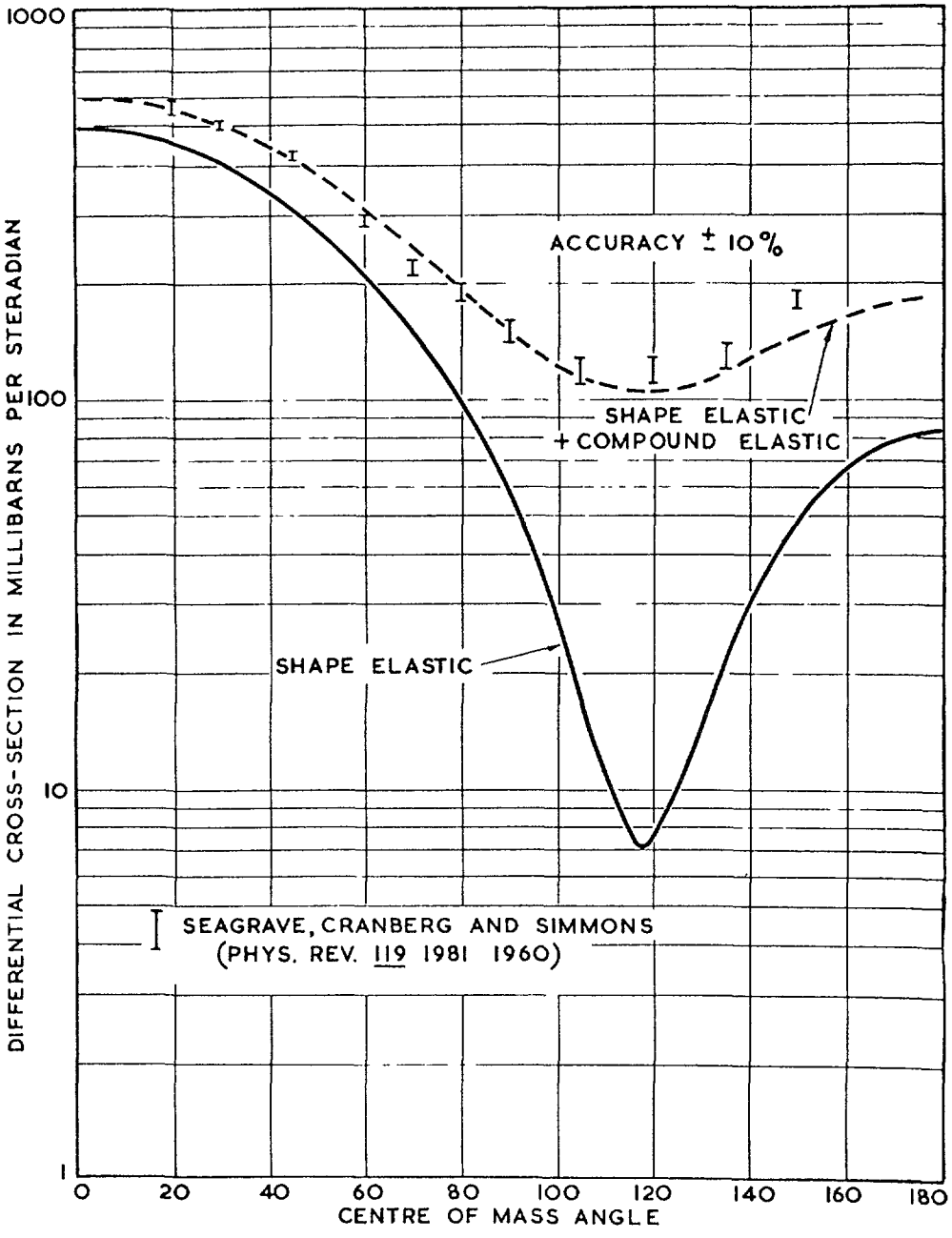
1000
100
10
1
DIFFERENTIAL CROSS-SECTION IN MILLIBARNS PER STERADIAN
ACCURACY ± 10%
SHAPE ELASTIC
+ COMPOUND ELASTIC
SHAPE ELASTIC
SEAGRAVE, CRANBERG AND SIMMONS
(PHYS. REV. 119 1981 1960)
0
20
40
60
80
100
120
140
160
180
CENTRE OF MASS ANGLE

Fig. 27

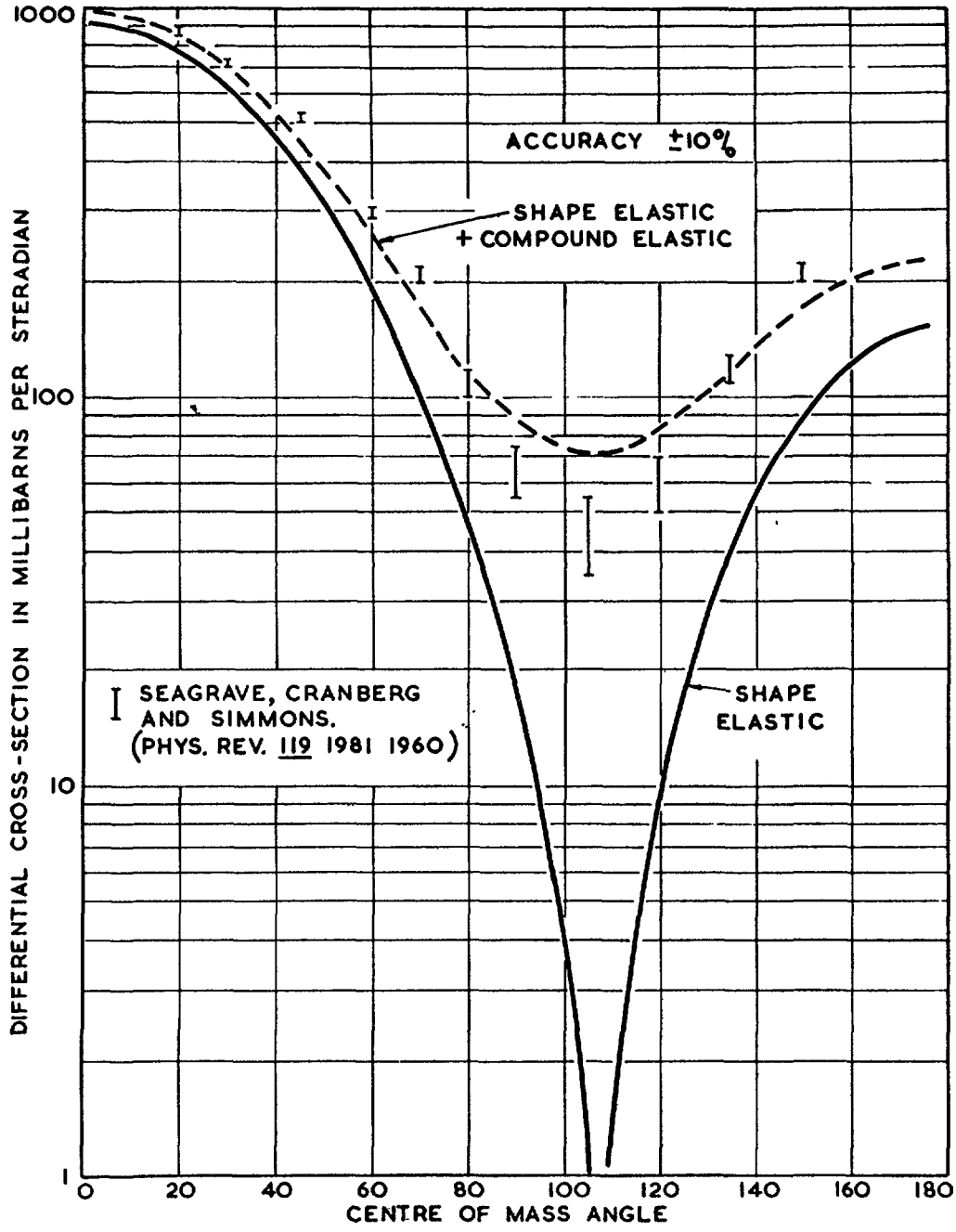
1000
100
10
1
DIFFERENTIAL CROSS-SECTION IN MILLIBARNS PER STERADIAN
ACCURACY ±10%
SHAPE ELASTIC
+ COMPOUND ELASTIC
SHAPE
ELASTIC
I SEAGRAVE, CRANBERG
AND SIMMONS.
(PHYS. REV. 119 1981 1960)
0
20
40
60
80
100
120
140
160
180
CENTRE OF MASS ANGLE

Fig. 28

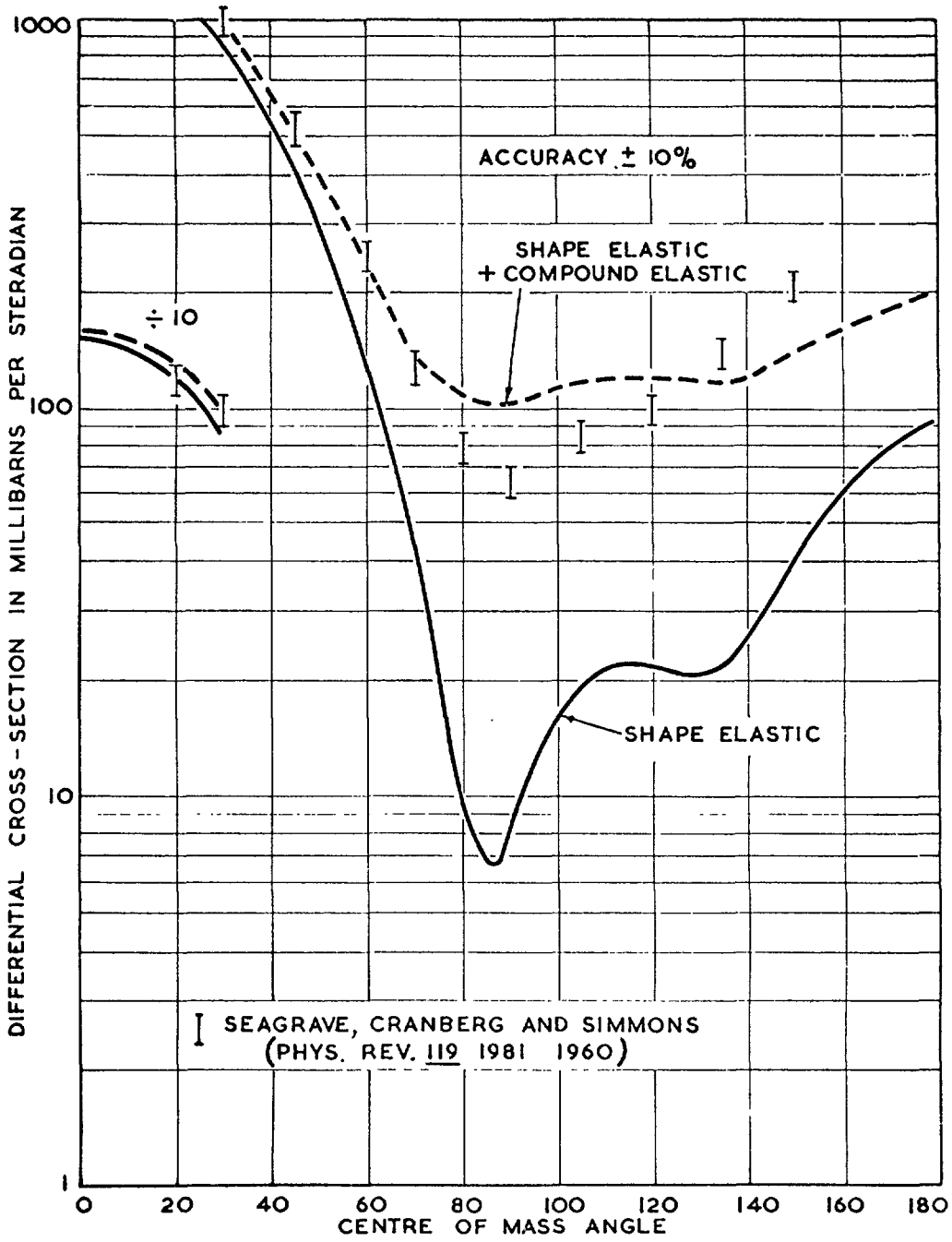
1000
100
10
1
DIFFERENTIAL CROSS-SECTION IN MILLIBARNS PER STERADIAN
ACCURACY ± 10%
SHAPE ELASTIC
+ COMPOUND ELASTIC
÷ 10
SHAPE ELASTIC
SEAGRAVE, CRANBERG AND SIMMONS
(PHYS. REV. 119 1981 1960)
0
20
40
60
80
100
120
140
160
180
CENTRE OF MASS ANGLE

Fig. 29

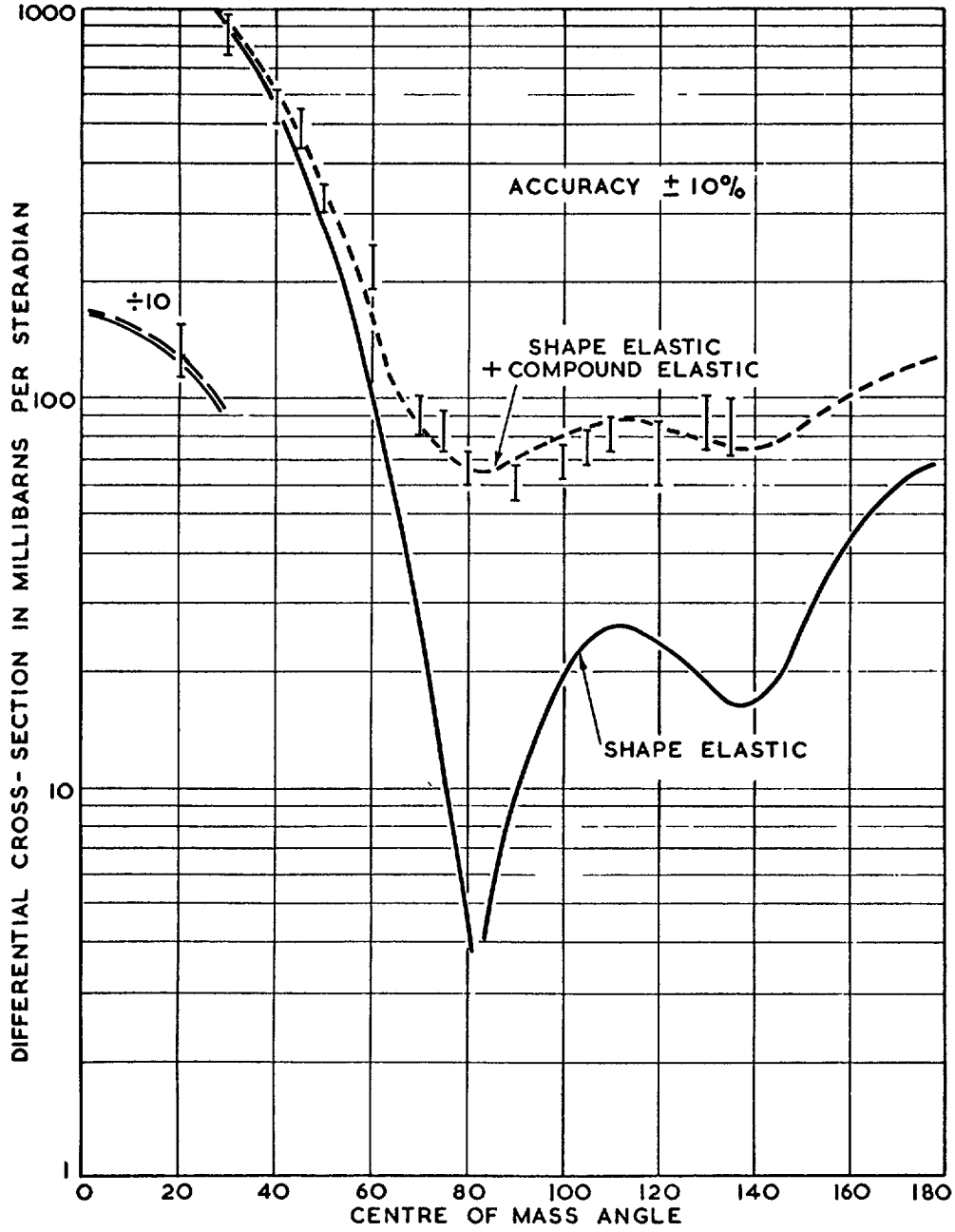
1000
100
10
1
DIFFERENTIAL CROSS-SECTION IN MILLIBARNS PER STERADIAN
ACCURACY ± 10%
÷10
SHAPE ELASTIC
+ COMPOUND ELASTIC
SHAPE ELASTIC
0
20
40
60
80
100
120
140
160
180
CENTRE OF MASS ANGLE

Fig. 30

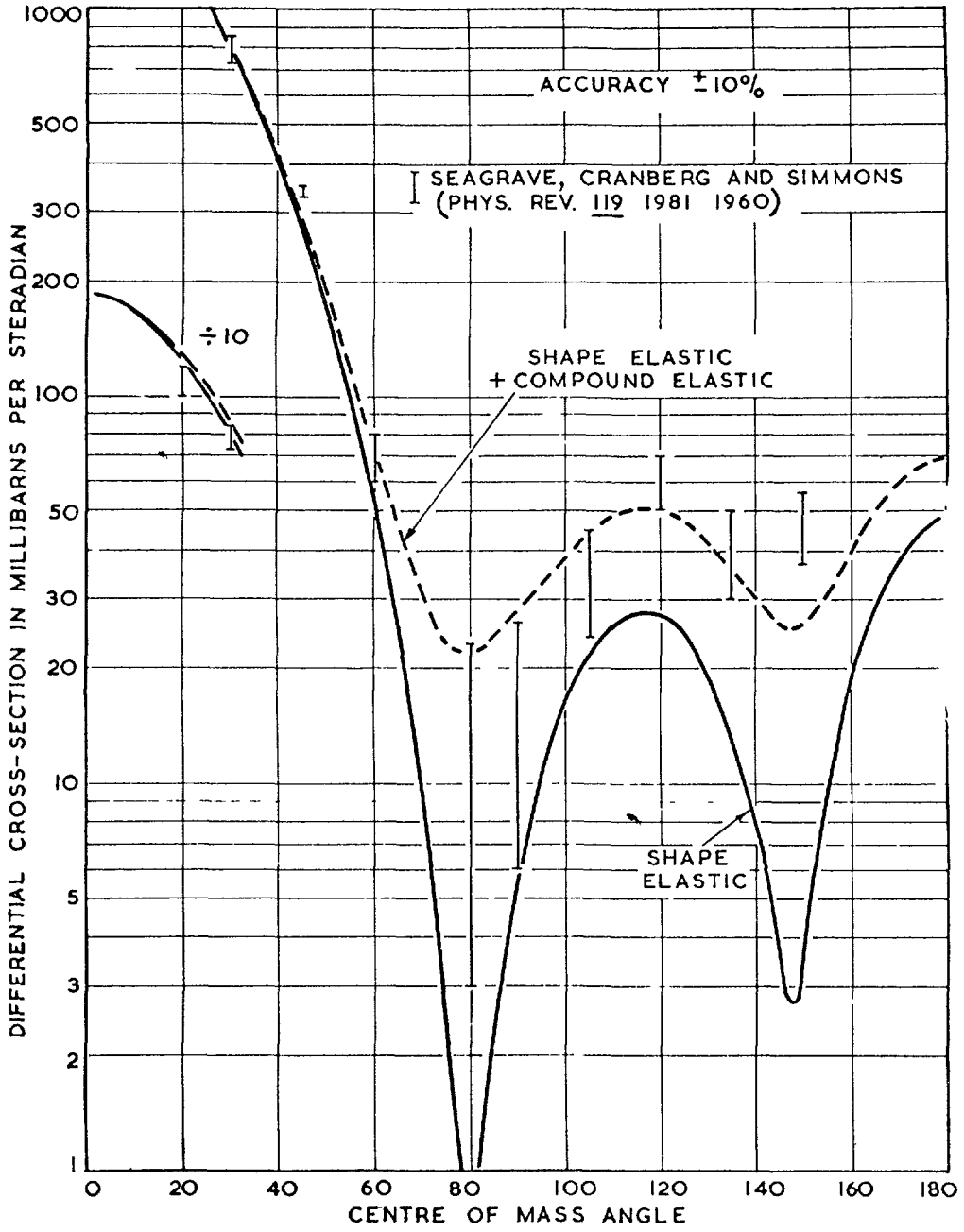
ACCURACY ±10%
SEAGRAVE, CRANBERG AND SIMMONS
(PHYS. REV. 119 1981 1960)
÷10
SHAPE ELASTIC
+ COMPOUND ELASTIC
SHAPE
ELASTIC
DIFFERENTIAL CROSS-SECTION IN MILLIBARNS PER STERADIAN
CENTRE OF MASS ANGLE
1000
500
300
200
100
50
30
20
10
5
3
2
1
0
20
40
60
80
100
120
140
160
180

Fig. 31

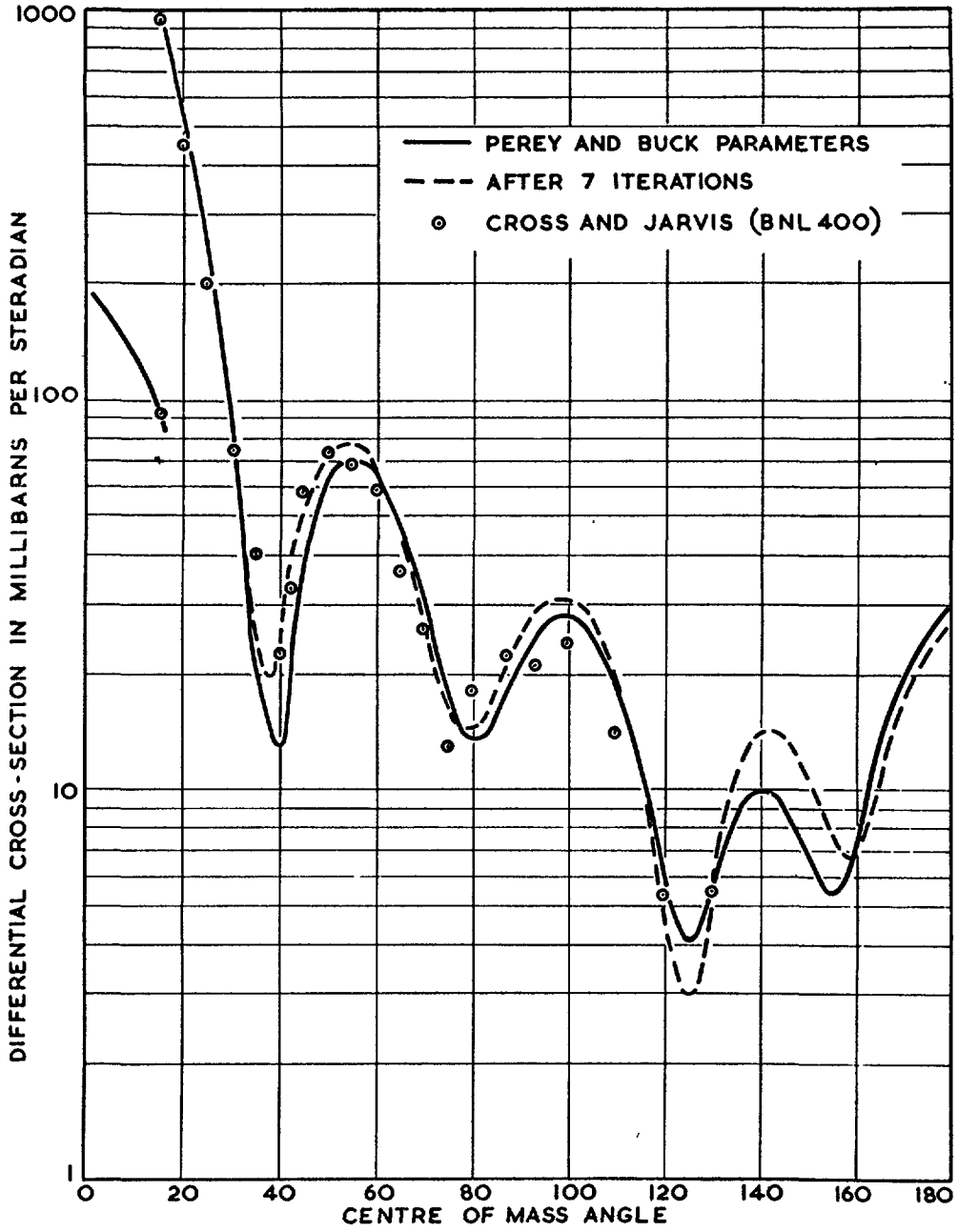
1000
100
10
1
DIFFERENTIAL CROSS-SECTION IN MILLIBARNS PER STERADIAN
PEREY AND BUCK PARAMETERS
AFTER 7 ITERATIONS
CROSS AND JARVIS (BNL 400)
0
20
40
60
80
100
120
140
160
180
CENTRE OF MASS ANGLE

Fig. 32

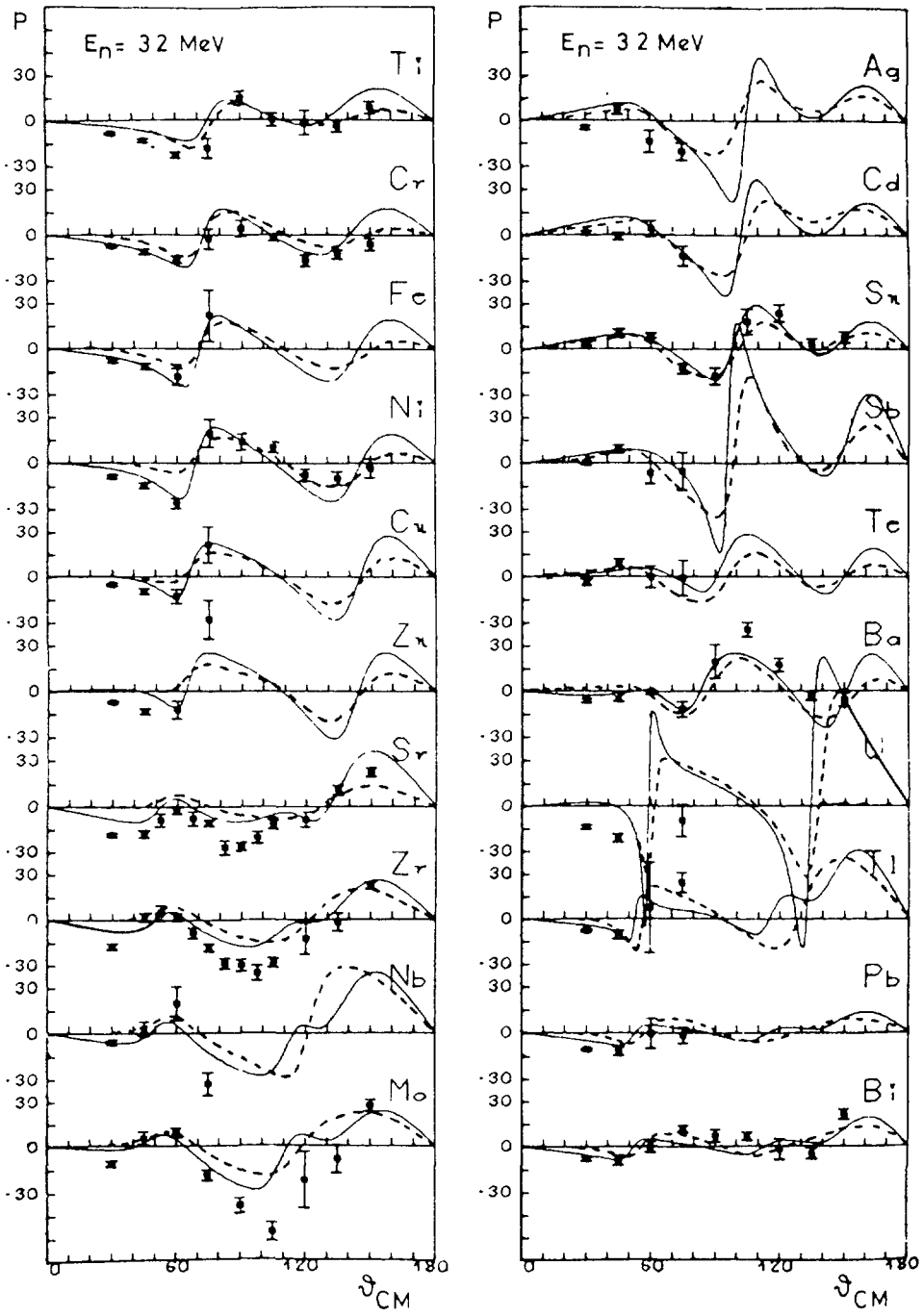
P
E_n= 32 MeV
Ti
Cr
Fe
Ni
Cu
Zn
Sr
Zr
Nb
Mo
Ag
Cd
Sn
Sb
Te
Ba
I
Tl
Pb
Bi
30
0
-30
0
60
120
180
ϑ_{CM}

Fig. 33

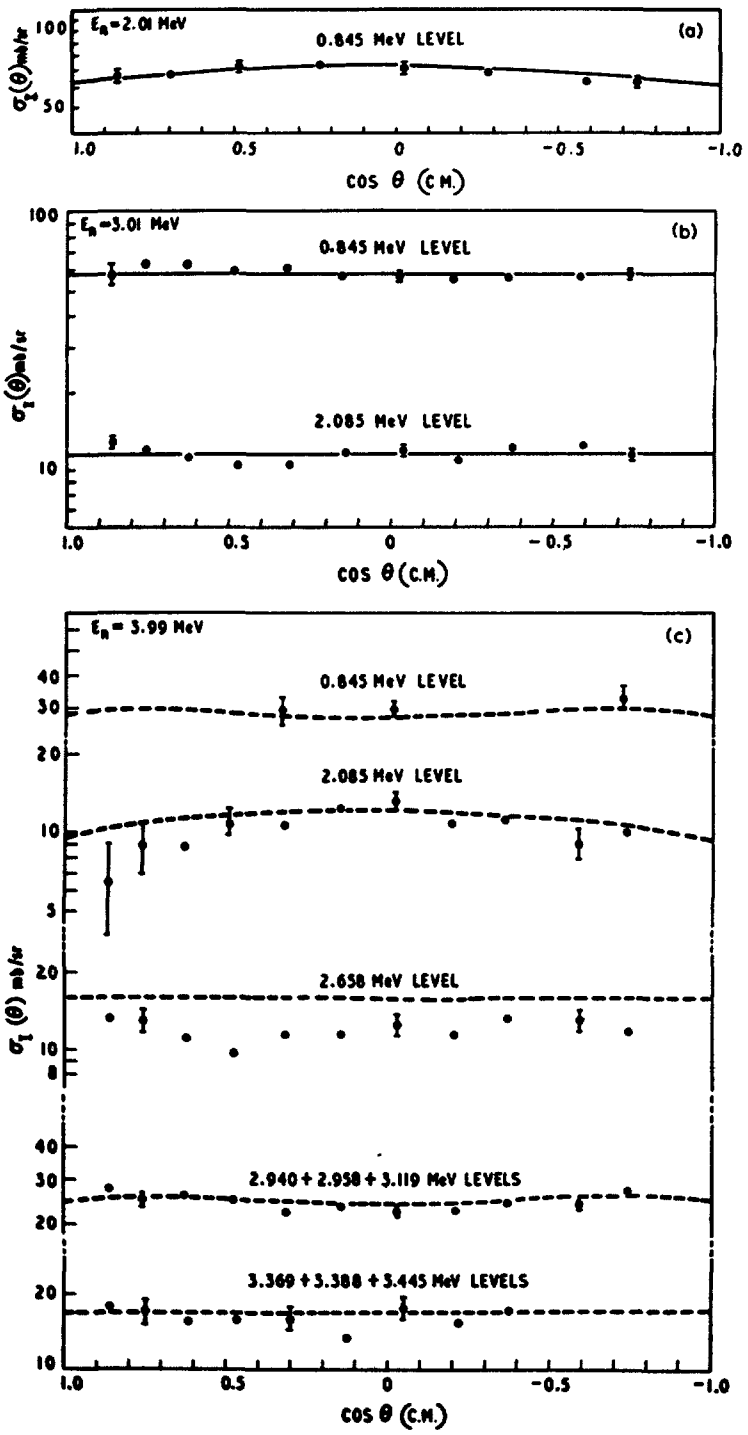
E_n=2.01 MeV
0.845 MeV LEVEL
(a)
$\sigma_1(\theta)$mb/sr
100
50
1.0
0.5
0
-0.5
-1.0
COS θ (C.M.)
E_n=3.01 MeV
0.845 MeV LEVEL
2.085 MeV LEVEL
(b)
$\sigma_1(\theta)$mb/sr
100
10
1.0
0.5
0
-0.5
-1.0
COS θ (C.M.)
E_n = 3.99 MeV
(c)
0.845 MeV LEVEL
2.085 MeV LEVEL
2.658 MeV LEVEL
2.940 + 2.958 + 3.119 MeV LEVELS
3.369 + 3.388 + 3.445 MeV LEVELS
$\sigma_1(\theta)$ mb/sr
40
30
20
10
5
8
1.0
0.5
0
-0.5
-1.0
COS θ (C.M.)

Fig. 34

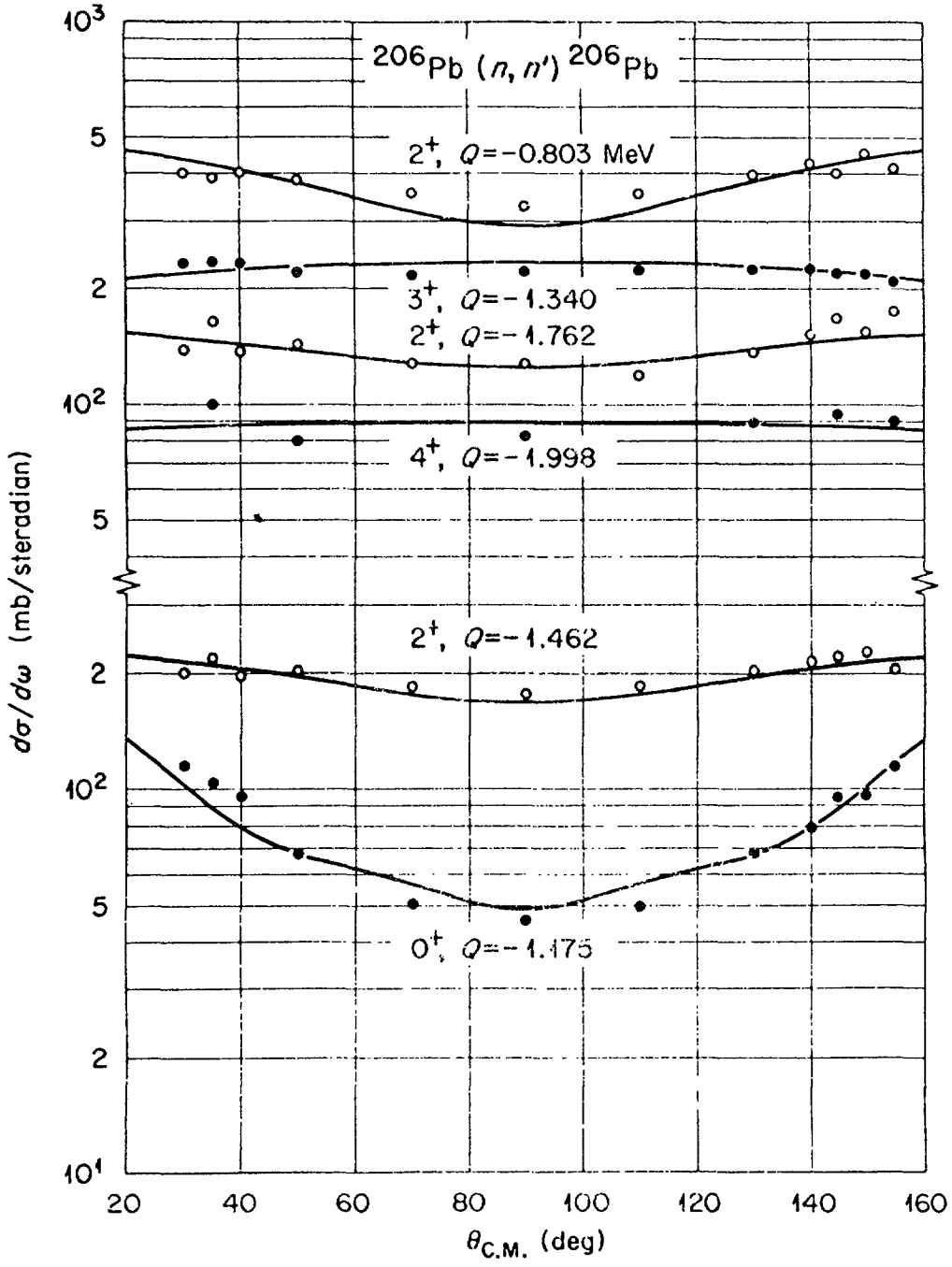
206Pb (n, n') 206Pb
2+, Q=-0.803 MeV
3+, Q=-1.340
2+, Q=-1.762
4+, Q=-1.998
2+, Q=-1.462
0+, Q=-1.175
dσ/dω (mb/steradian)
θC.M. (deg)
10³
5
2
10²
5
2
10²
5
2
10¹
20
40
60
80
100
120
140
160

Fig. 35

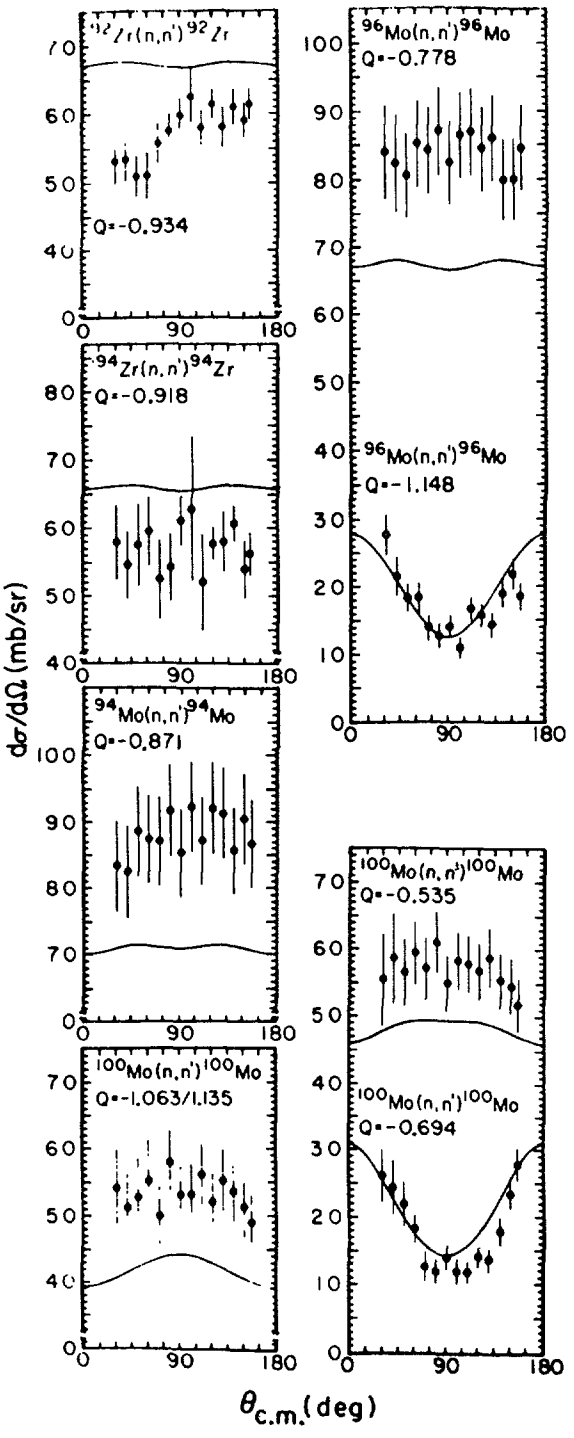
$^{92}Zr(n,n')^{92}Zr$
Q=-0.934
$^{94}Zr(n,n')^{94}Zr$
Q=-0.918
$^{94}Mo(n,n')^{94}Mo$
Q=-0.871
$^{100}Mo(n,n')^{100}Mo$
Q=-1.063/1.135
$^{96}Mo(n,n')^{96}Mo$
Q=-0.778
$^{96}Mo(n,n')^{96}Mo$
Q=-1.148
$^{100}Mo(n,n')^{100}Mo$
Q=-0.535
$^{100}Mo(n,n')^{100}Mo$
Q=-0.694
dσ/dΩ (mb/sr)
$\theta_{c.m.}$(deg)

Fig. 36

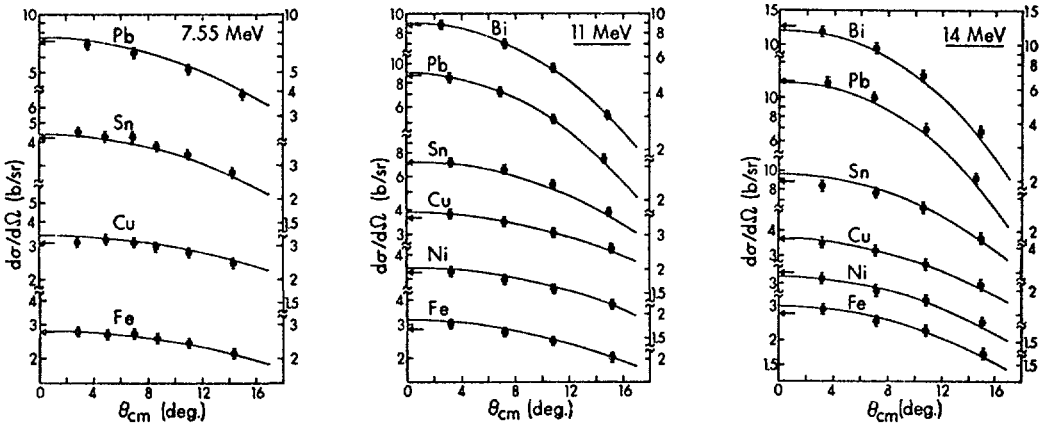
Pb
7.55 MeV
Sn
Cu
Fe
dσ/dΩ (b/sr)
θcm (deg.)
Bi
11 MeV
Pb
Sn
Cu
Ni
Fe
dσ/dΩ (b/sr)
θcm (deg.)
Bi
14 MeV
Pb
Sn
Cu
Ni
Fe
dσ/dΩ (b/sr)
θcm (deg.)

Fig. 37

Contributed Paper No. 8

Applications of the Statistical Theory to the Prediction and Evaluation of Neutron Cross Sections for Reactors - Evaluation of ^{241}Am Cross Sections -

Sin-iti Igarasi

Japan Atomic Energy Research Institute

Tokai-mura, Naka-gun,

Ibaraki, Japan

ABSTRACT

Neutron cross sections of ^{241}Am are evaluated in the energy region from 1 keV to 15 MeV. The cross sections are estimated by using optical and statistical model calculations, because the existing experimental data for this nuclide are very scarce, except for the fission cross section. The experimental data are used to obtain an empirical formula of smoothed fission cross section. The cross sections on (n,2n) and (n,3n) reactions are calculated with a simple formula proposed by Pearlstein. These cross sections are treated as the elements of the competing processes in calculation of compound elastic, inelastic scattering and capture cross sections.

1. Introduction

In recent work[1] of the author, modified cross section formulas were proposed in the statistical model calculations to establish the equality between the sum of the partial cross sections and the total cross section obtained by the optical model calculations, even if the partial cross sections were taken by using various kinds of the nuclear models or by experiments. From the viewpoint of the cross-section evaluation, the obtained cross sections must be constructed so that this equality is satisfied. In this paper, the cross-section evaluation on ^{241}Am is presented as an example of applications of the statistical model calculations with the modified formulas.

Existing experimental data for ^{241}Am are very scarce. The fission cross section is only available for the cross-section evaluation. In this work, the numerical data were obtained from CCDN and by surveying the literature. Brief description on the experimental data of the fission cross section will be given in section 2.

Descriptions of the optical potential and the cross-section formulas are given in section 3. Since ^{241}Am is a deformed nucleus, the coupled-channel calculations[2] must be applied. In this work, however, spherical optical potential was used. Discussions will be given on this circumstance.

In section 4, the evaluation method is presented for the fission, (n,2n) and (n,3n) reaction cross sections which were treated as the elements of the competing processes in the statistical model calculations. Results of the present evaluation are shown in graphs and tables.

2. Present Status of the Experimental Data

According to CINDA 74[3], there are few experiments above 1 keV, except for the fission cross section measurements. A few experiments have been performed for investigation of the spontaneously fissioning isomers. For the present evaluation, the following experiments on fission cross section measurements only were usable.

(i) Nobles et al.[4,5] presented data at 13 points in the energy region from 0.49 to 7.34 MeV. The measurement was performed with gas scintillation counter. The data were normalized to $^{235}U(n,f)$ cross section. Though this experiment is very old, the data near 6 MeV are valuable for estimating (n,n'f) cross section.

(ii) Protopopov et al.[6] measured the data at 14.6 MeV with ionization chamber. The cross section is rather small, i.e. 2.35 ± 0.15 barns.

(iii) Kazarinova et al.[7] presented two data points at 2.5 and 14.6 MeV. The cross section at 14.6 MeV is 2.95 ± 0.15 barns which is larger than that of Protopopov et al.

(iv) Seeger et al.[8,9,10] measured with underground nuclear explosion technique in the region from 20 eV to 1.0 MeV. The data points above 1 keV are about 750. They used the standard cross sections of $^{6}Li(n,\alpha)$ reaction below 10 keV and of $^{235}U(n,f)$ above 10 keV. Systematic error was estimated at 7.1% and statistical error was at 10 to 300% or more. The data below about 100 keV may be too large.

(v) Fomushkin et al.[11] measured with 14.5 MeV neutrons and with fission neutrons. In the former experiments, they obtained a value of 2.53 ± 0.12 barns with integration of the fission fragment angular distributions and a value of 2.3 ± 0.15 barns with the ionization chamber. The standard cross section used was $^{238}U(n,f)$ cross section.

(vi) Bowman et al.[12,13] measured with Livermore 30-MeV linac. The data were obtained in the region from 0.5 to 6.0 MeV, with ^{239}Pu(n,f) standard cross section. The errors were estimated at 5%.

(vii) Shpak et al.[14] presented 43 data points from 8 keV to 3.3 MeV with the errors of 5 to 40%. The data were obtained with glass plate detectors and were normalized to the standard ^{239}Pu(n,f) cross section. The data below 500 keV are smaller than those obtained by Seeger et al.

(viii) Fomushkin et al.[15] measured data at 14 points with glass plate detector. The standard cross section was ^{235}U(n,f) cross section.

(ix) Iyengar et al.[16] obtained data with solid-state track detectors in the region from 0.32 to 2.1 MeV. The data seem to be rather small.

(x) Iyer et al.[17] measured a value of 2.7 ± 0.47 barns at 14.1 MeV. The standard was ^{238}U(n,f) cross section.

The data of the fission cross section surveyed above are shown in Fig. 1, from 1 keV to 15 MeV, with a symbol.

3. Optical Potential and Cross Section Formulas

Optical model of the nucleus is very useful to compute the total and absorption cross sections and the transmission coefficients which play very important role in the statistical model calculations. For deformed nucleus such as ^{241}Am, the deformed optical potential[2] had better be used. In this evaluation, however, spherical optical potential was used, because there are no proper methods to calculate all the necessary quantities in the framework of the coupled-channel calculations with the deformed potential and, because there are no experimental data to verify precisely the results of the calculations. Moreover, the coupled-channel calculations require much more computer time than the spherical optical model calculations.

In this evaluation, the parameters of the spherical optical potential were determined in the following manner. Above about 2 MeV, the total cross section was assumed to be reproduced by the coupled-channel calculation with the deformed optical potential given by Tanaka[18]. Deformation parameter β_2 was given as 0.24[19]. Effect of β_4 (= - 0.015) was investigated in detail, but it was negligibly small. However, the effect of β_4 should not be ignored in general[18,20].

Below 2 MeV, the potential parameters given by Tanaka are not suitable, because his potential has unreasonably small imaginary part in the low energy region. Taking account of the experimental data of ^{235}U and ^{239}Pu, the total cross section of ^{241}Am was assumed to be 12 - 13 barns near 100 keV, 15 - 16 barns near 10 keV and 25 - 26 barns near 1 keV. The potential parameters of the spherical optical model were determined so that the total cross section satisfied the above conditions from 1 keV to 15 MeV. Besides, the absorption cross section should be larger than 2.6 barns at 15 MeV, because the fission cross section shown in Fig. 1 is about 2.5 barns.

Under these conditions, automatic parameter search was performed by a computer code which looks for a suitable parameter set of the spherical

optical potential so that the calculated total cross sections fit to the experimental data. After many trials, the best set of the parameters was determined as

$$\left.\begin{aligned} V &= 40.5 + 0.5E_n \quad (\text{MeV}) \\ W_s &= 8.2 + 0.5\sqrt{E_n} \quad (\text{MeV}) \\ V_{so} &= 7.0 \quad (\text{MeV}) \\ r_0 &= 1.32 \quad (\text{fermi}) \\ a &= b = a_{so} = 0.47 \quad (\text{fermi}) \end{aligned}\right\} \tag{3.1}$$

where the potential form was

$$V(r) = V \cdot f_1(r, a, r_0) + iW_s \cdot f_2(r, b, r_0) + V_{so}\left(\frac{\hbar}{m_\pi c}\right)^2 \frac{1}{r}\left|\frac{df_1(r, a_{so}, r_0)}{dr}\right| \cdot (\vec{\sigma}\cdot\vec{l}) \,, \tag{3.2}$$

$$f_1(r, a, r_0) = \left\{1 + \exp[(r - r_0 A^{1/3})/a]\right\}^{-1} \,, \tag{3.3}$$

and

$$f_2(r, b, r_0) = 4\exp[(r - r_0 A^{1/3})/b] \times \left\{1 + \exp[(r - r_0 A^{1/3})/b]\right\}^{-1} \,. \tag{3.4}$$

Using the above potential, the total cross section (σ_{tot}), shape elastic scattering cross section (σ_{se}) and the absorption cross section (formation cross section of the compound nucleus plus direct reaction cross section) (σ_a) were calculated as well as the neutron transmission coefficients. Compound elastic scattering cross section (σ_{ce}), inelastic scattering cross section (σ_{in}) and neutron capture cross section ($\sigma_{n,\gamma}$) were obtained with the following formulas[1,21,22],

$$\sigma_{n,n'}(E_n)=\frac{\pi}{k_n^2}\sum_{J\pi\ell j\ell' j'} g^J\left\{\frac{\langle\Theta^{J\pi}_{n j\ell}\rangle\cdot\langle\Theta^{J\pi}_{n' j'\ell'}\rangle}{\langle\Theta^{J\pi}\rangle}S^{J\pi}_{n j\ell;n' j'\ell'}\right.$$
$$\left.\times\left(1+\frac{\Delta\Theta^{J\pi}_{\gamma}}{\langle\Theta^{J\pi}\rangle}\right)-\frac{1}{4}\delta_{n j\ell;n' j'\ell'}Q^{J\pi}(\langle\Theta^{J\pi}\rangle)\cdot\langle\Theta^{J\pi}_{n j\ell}\rangle^2\right\}\cdot(1-\alpha), \quad (3.5)$$

$$\sigma_{n,\gamma}(E_n)=\frac{\pi}{k_n^2}\sum_{J\pi\ell j} g^J\frac{\langle\Theta^{J\pi}_{n j\ell}\rangle}{\langle\Theta^{J\pi}\rangle}\left\{\langle\Theta^{J\pi}_{\gamma 1}\rangle+\langle\Theta^{J\pi}_{\gamma 2}\rangle\right.$$
$$\left.\times\left[\frac{\Delta\Theta^{J\pi}_{\gamma}}{\langle\Theta^{J\pi}\rangle}S^{J\pi}_{n j\ell;\gamma 2}-1+S^{J\pi}_{n j\ell;\gamma 2}\right]\right\}(1-\alpha), \quad (3.6)$$

where index n' stands for the emitted neutron with energy $E_{n'}$ and state of residual nucleus with spin I' and parity π'. Therefore, the compound elastic scattering cross section σ_{ce} is equal to $\sigma_{n,n}(E_n)$ and the inelastic scattering cross section σ_{in} is the sum of $\sigma_{n,n'}(E_n)$;

$$\sigma_{in}(E_n)=\sum_{n'(\neq n)}\sigma_{n,n'}(E_n)=\sum_{E_{n'}I'\pi'}\sigma_{n,n'}(E_n I\pi\rightarrow E_{n'}I'\pi'). \quad (3.7)$$

For overlapping levels of the residual nucleus, Eq. (3.7) must be rewritten with the level density $\rho_{I'\pi'}(\varepsilon)$;

$$\sigma_{n,n'}(E_n)=\sum_{n'(\neq n)}\sigma_{n,n'}(E_n)+\sum_{I'\pi'}\int_{E_c}^{E_n}d\varepsilon\,\rho_{I'\pi'}(\varepsilon)\sigma_{n,n'}(E_n,I,\pi\rightarrow E_n-\varepsilon,I',\pi'). \quad (3.8)$$

Quantities $\langle\Theta^{J\pi}_{n j\ell}\rangle$ and $\langle\Theta^{J\pi}_{\gamma i}\rangle$ in Eqs. (3.5) and (3.6) are connected with the neutron and γ-ray transmission coefficients $\langle T^{J\pi}_{n j\ell}\rangle$ and $\langle T^{J\pi}_{\gamma i}\rangle$ as follows[1,22],

$$\left.\begin{aligned}\langle\Theta^{J\pi}_{n j\ell}\rangle-\frac{1}{4}Q^{J\pi}(\langle\Theta^{J\pi}\rangle)\cdot\langle\Theta^{J\pi}_{n j\ell}\rangle^2&=\langle T^{J\pi}_{n j\ell}\rangle,\\ \langle\Theta^{J\pi}_{\gamma i}\rangle-\frac{1}{4}Q^{J\pi}(\langle\Theta^{J\pi}\rangle)\cdot\langle\Theta^{J\pi}_{\gamma i}\rangle^2&=\langle T^{J\pi}_{\gamma i}\rangle,\\ &(i=1\text{ and }2),\end{aligned}\right\} \quad (3.9)$$

where $Q^{J\pi}$ represents the effect of the resonance interference. Two γ-ray

coefficients $\langle T_{\gamma 1}^{J\pi} \rangle$ and $\langle T_{\gamma 2}^{J\pi} \rangle$ are given in the integral form[23] with the level density of the compound nucleus,

$$\left.\begin{aligned} \langle T_{\gamma 1}^{J\pi} \rangle &= C_0^{J\pi} \int_{E_n}^{E_n+B_n} d\varepsilon_\gamma \varepsilon_\gamma^3 f_\gamma(\varepsilon_\gamma) \rho_c(E_n+B_n-\varepsilon_\gamma) \quad , \\ \langle T_{\gamma 2}^{J\pi} \rangle &= C_0^{J\pi} \int_{0}^{E_n+B_n} d\varepsilon_\gamma \varepsilon_\gamma^3 f_\gamma(\varepsilon_\gamma) \rho_c(E_n+B_n-\varepsilon_\gamma) , \end{aligned}\right\} \tag{3.10}$$

and the quantity $\Delta\Theta_\gamma^{J\pi}$ in Eqs. (3.5) and (3.6) is defined as

$$\Delta\Theta_\gamma^{J\pi} = \langle \Theta_{\gamma 2}^{J\pi} \rangle - \langle \Theta_{\gamma 1}^{J\pi} \rangle . \tag{3.11}$$

The correction factors for the width fluctuation $S_{nj\ell;n'j'\ell'}^{J\pi}$ and $S_{nj\ell;\gamma 2}^{J\pi}$ are given in the conventional integral forms[1].

A factor α representing the effects from the competing processes is defined as

$$\alpha = \Delta\sigma / \sigma_a \quad , \tag{3.12}$$

where $\Delta\sigma$ means the sum of the cross sections of all competing processes which cannot be obtained by Eqs. (3.5) and (3.6). In this paper, $\Delta\sigma$ is the sum of the fission cross section $\sigma_{n,f}$, (n,2n) and (n,3n) reaction cross sections. In the next section, evaluation or estimation of these cross sections will be presented.

4. Evaluation of the Cross Sections

In this section, the present evaluation and its results are presented. In order to compose the cross section $\Delta\sigma$ mentioned previously, the fission, (n,2n) and (n,3n) cross sections are estimated.

For fission cross section, the evaluation was performed on the basis of the experimental data[4-17] shown in Fig. 1. In order to express the cross section in a mathematical formula, the following form was assumed,

$$\sigma_{n,f}(E_n)=\sum_{\lambda}\frac{C_\lambda}{(E_n-E_\lambda^R)^2+R_\lambda}+\sum_{k}\frac{B_k}{1+\exp[\alpha_k(E_k^B-E_n)]} \quad (4.1)$$

The first term in Eq. (4.1) stands for the sum of the resonance components and the second expresses the sum of the high energy components of the fission cross section. Here, a formula of penetrability[24] for the barrier with threshold (or barrier) energy E_k^B was assumed to be

$$P_f(E_n)=\frac{1}{1+\exp[\alpha_k(E_k^B-E_n)]} \quad (4.2)$$

Fission probability was given in the high energy region as follows,

$$\frac{\sigma_{n,f}(E_n)}{\sigma_c(E_n)}=\frac{\beta_k}{1+\exp[\alpha_k(E_k^B-E_n)]} \quad (4.3)$$

The formation cross section $\sigma_c(E_n)$ of the compound nucleus is assumed here to change slowly with the incident neutron energy in MeV region.

Derivation of the second term in Eq. (4.1) is given as follows. Using Eq. (4.3), the cross section should be expressed as

$$\sigma_{n,f}(E_n)=\sigma_c(E_n)\left[\frac{\beta_c}{1+\exp[\alpha_c(E_c^B-E_n)]}+\left\{1-\frac{\beta_c}{1+\exp[\alpha_c(E_c^B-E_n)]}\right\}\cdot\frac{\beta_T}{1+\exp[\alpha_T(E_T^B-E_n)]}\right] \quad (4.4)$$

where E_C^B and E_T^B are the barrier energies for the compound and target nuclei, respectively. The second term in Eq. (4.4) stands for (n,n'f) cross section. The barrier energy E_C^B is about 900 keV in the measure of the incident neutron energy and E_T^B is about 6 MeV. Hence, the second term is negligible near $E_n = E_C^B$, and has the form of $\text{const.}/\{1+\exp[\alpha_T(E_T^B - E_n)]\}$ near $E_n = E_T^B$.

It was tried to determine the parameters in Eq. (4.1) using the least-squares method. In the preliminary stage of this trial, weight for each data point $\sigma_{ex}(E_n)$ was given as the inverse square of the error, $\Delta\sigma_{ex}(E_n)$, assigned in the original reports. When the error was not given in the report, the error of 10% was assumed for each data point. Six levels of the resonances were assumed in this stage; 1.5, 3.0, 10.0, 15.0, 30.0 and 150.0 keV. However, unrealistic results were achieved in the calculation with these assumptions. For example, some resonance energies were negative.

In the final stage after some trial, weight for the data was modified as follows: for a data point $\sigma_{ex}(E_0)$ at energy E_0, the farthest data $\sigma_{ex}(E_1)$ from the data of interest was looked for in the interval of $E_0 - 0.05E_0$ to $E_0 + 0.05E_0$. The weight for the data point $\sigma_{ex}(E_0)$ was assigned as the inverse of $|\sigma_{ex}(E_0) - \sigma_{ex}(E_1)|^2 + \Delta\sigma_{ex}(E_0)^2$. The number of resonance levels was also reduced to four. Under these conditions, the calculations were performed, and special results were obtained in the region from 1 keV to 15 MeV. However, the deduced barrier energy E_T^B for (n,n'f) was about 8 MeV, that is unrealistic. This is due to the data of Nobles et al.[4,5] which are smaller than the majority of the data above 1 MeV. Nevertheless, these data of Nobles et al. are very valuable in the region around 6 MeV, because no data presents the rise for (n,n'f) process except them. Hence, in order to utilize these data and to get an adequate value of E_T^B, they were renormalized so that the cross section value of 1.39 barns at 2.42 MeV changed into 1.7 barns. Symbol X in Fig. 2 shows these renormalized

values. They were still small, but could not be risen more because they must not be larger than the data at 14 MeV. Moreover, selection of reliable data at 14 MeV was made, as well as rejection of the data transcribed from the graphs. It is due to this selection that the number of data points in Fig. 2 is smaller than that in Fig. 1 in MeV region.

Result of the least squares fit thus obtained is shown in Fig. 2, as well as a band of 95% confidence coefficient. A resonance level near 160 keV was necessary to make the cross section curve rise reasonably in the region from 60 keV to 400 keV. In fact, the smaller cross section values shown in Fig. 3 were obtained by ignoring this resonance. The cross section curve in Fig. 2 seems plausible as the expectation value of the average cross section. The parameters in Eq. (4.1) thus obtained are shown in Table 1. The energies of fission threshold are 6.43 MeV and 6.55 MeV for the compound and target nuclei, respectively. If the structure be the intermediate resonance, widths of the four levels are 5.05, 8.90, 8.95 and 24.6 keV. Taking σ_c = 2.7 barns, the parameters β_c and β_T in Eq. (4.4) are given as 0.686 and 0.849. Parameter α_c = 7.72 is plausible, because the corresponding quantity $\hbar\omega_c$ is 2π / 7.72 = 0.814 MeV. However, α_T = 0.704 is too small. If there had been more experimental data in the region from 6 to 10 MeV, more reliable value should be obtained for the parameter α_T.

According to Pearlstein[25], (n,2n) and (n,3n) reaction cross sections are calculated by the following simple formulas,

$$\sigma_{n,2n}(E_n) = \sigma_{ne}(E_n) \cdot P_M(E_n) \cdot P_{2n}(E_n), \tag{4.5}$$

and

$$\sigma_{n,3n}(E_n) = \sigma_{ne}(E_n) \cdot P_M(E_n) \cdot P_{3n}(E_n), \tag{4.6}$$

where $\sigma_{ne}(E_n)$ is non-elastic cross section, $P_M(E_n)$ is neutron emission probability,

$$P_{2n}(E_n)=\frac{\int_0^{E_n-S_n}\varepsilon\sigma_{inv}(\varepsilon)\exp\left[\sqrt{4a(E_n-\varepsilon)}\right]d\varepsilon-\int_0^{E_n-S_{2n}}\varepsilon\sigma_{inv}(\varepsilon)\exp\left[\sqrt{4a(E_n-\varepsilon)}\right]d\varepsilon}{\int_0^{E_n}\varepsilon\sigma_{inv}(\varepsilon)\exp\left[\sqrt{4a(E_n-\varepsilon)}\right]d\varepsilon}, \tag{4.7}$$

and

$$P_{3n}(E_n)=\frac{\int_0^{E_n-S_{2n}}\varepsilon\sigma_{inv}(\varepsilon)\exp\left[\sqrt{4a(E_n-\varepsilon)}\right]d\varepsilon}{\int_0^{E_n}\varepsilon\sigma_{inv}(\varepsilon)\exp\left[\sqrt{4a(E_n-\varepsilon)}\right]d\varepsilon} \tag{4.8}$$

Neutron separation energy S_n from the residual nucleus is about 6.7 MeV[26] and two-neutron separation energy S_{2n} is about 12.6 MeV[26]. Inverse cross section $\sigma_{inv}(\varepsilon)$ is assumed constant, and the integrals can be performed analytically. Pearlstein adopted a level density parameter a of Newton's form[27]. These quantities were adopted in this paper.

Two quantities σ_{ne} and P_M were modified here from those by Pearlstein. In high energy region, the compound elastic scattering cross section σ_{ce} becomes very small. Hence, σ_{ne} may be equal to the formation cross section of the compound nucleus σ_c. In this paper, since the direct reaction is not considered, the cross section σ_c is equal to the cross section σ_a which is obtained by the optical model calculation. In the present calculation, σ_a is about 2.7 barns near 10 MeV.

From the meaning of the quantity P_M, it should be defined as

$$P_M=1-\frac{\sigma_{compt.}}{\sigma_{ne}}, \tag{4.9}$$

where $\sigma_{compt.}$ stands for the sum of the charged particle emission cross sections. In this case, the fission cross section is only the component of $\sigma_{compt.}$. Taking account of the second plateau value of the fission cross section, $\sigma_{compt.}$ was assumed as 2.57 barns. With these values, (n,2n) and (n,3n) cross sections were easily obtained.

As mentioned in the previous section, the cross section $\Delta\sigma$ was obtained as the sum of the fission, (n,2n) and (n,3n) cross sections calculated in this section. Using this $\Delta\sigma$, the compound elastic, inelastic scattering and capture cross sections were calculated by using Eqs. (3.5) and (3.6). These calculations were performed with many parameters such as energy, spin and parity for each discrete level[19,28] of the residual nucleus, level density parameters[29] for the residual and compound nuclei, average level spacing[30] and γ-ray width[30] at zero neutron energy, and neutron separation energy[26]. The levels above 0.85 MeV in the residual nucleus were assumed here as the overlapping levels. These parameters are shown in Tables 2 and 3.

In this evaluation, Brink-Axel type profile function was used in the calculation of the γ-ray transmission coefficients. The energy and width of the giant resonance in the photoreaction were taken as 12.84 MeV and 5.0 MeV. Detailed descriptions were given in Ref. 1 about the γ-ray transmission coefficients, profile function and level density formulas used here.

Results of the present evaluation are shown in Fig. 4. The capture cross section below 10 keV reveals $1/v$ form being due to s-wave neutron capture. Above several ten keV, the p-wave neutron capture becomes dominant. These are one order larger than those of ^{235}U or ^{239}Pu. This may be due to the effects of the fission cross sections. Though the fission cross section of ^{241}Am is probably overestimated here in the low energy region, it is still small in comparison with that of ^{235}U or ^{239}Pu. Therefore, true values of the capture cross section may be larger than those obtained here.

5. Concluding Remarks

As an example of application of the statistical model calculations, the evaluation of ^{241}Am cross sections was presented. In this evaluation, no experimental data were utilized, except for the fission cross section. The fission, (n,2n) and (n,3n) cross sections were estimated by taking account of the experimental data and of the magnitudes of the absorption cross sections. The fission cross section, in particular, was obtained by an empirical formula with which the smooth trend of the experimental data was reproduced. These cross sections were used in order to make up a parameter representing an effect of the competing processes whose cross sections cannot be calculated by the cross section formulas for calculating the compound elastic, inelastic scattering and capture cross sections. That the sum of all partial cross sections is equal to the total cross section obtained by the optical model is assured in this calculation method.

This is an example showing that the statistical model calculations are practically useful to obtain a reliable cross section set in some cases. This method is applicable to estimate the cross sections of some transactinium nuclides and of fission product nuclides. For these nuclides, there are few experimental data. From the viewpoint of the reactor applications, these are not necessarily the highest important matters for the moment. Hence, the data with accuracies of about 20 to 30% may be usable to estimate the reactor characteristics. In this sense, the optical and statistical models are very useful, because they can be applied easily to obtain the data with a certain degree of accuracy, on average, in a wide energy range and for many nuclides.

From the viewpoint of consistent nuclear model calculations, however, it is desirable that the calculations be based on the same fundamental nuclear model. Hence, it should be attempted to unify the statistical, direct and collective model calculations by an appropriate way.

References

1) Igarasi, S., J. Nucl. Sci. Tech. 12 (1975) 67

2) Tamura, T., Rev. Mod. Phys. 37 (1965) 679

3) CINDA, an Index to the Literature on Microscopic Neutron Data, IAEA, (1974)

4) Nobles, R.A., Henken, R.L., Smith, R.K., Phys. Rev. A99 (1955) 616

5) Data presented in BNL-325 (1955) and NEUDADA library

6) Protopopov, A.N., Selitskii, Yu.A., Solovev, S.M., Sov. Atom. Energy 6 (1960) 36

7) Kazarinova, M.I., Zamyatnin, Yu.S., Gorbachev, V.M., Sov. Atom. Energy 8 (1961) 125

8) Seeger, P.A., Hemmendinger, A., Diven, B.C., Nucl. Phys. A96 (1967) 605

9) Seeger, P.A., Hemmendinger, A., Diven, B.C., LA-3586 (1966)

10) Hemmendinger, A., Proc. of Conference of Nuclear Data for Reactors, Paris (1966) 219

11) Fomushkin, E.F., Gutnikova, E.K., Zamyatnin, Yu.S., Maslennikov, B.K., Belov, V.N., Surin, V.M., Nasyrov, F., Pashkin, N.F., Sov. J. Nucl. Phys. 5 (1967) 689

12) Bowman, C.D., Auchampaugh, G.F., Fultz, S.C., Hoff, R.W., Phys. Rev. 166 (1968) 1219

13) Bowman, C.D., Auchampaugh, G.F., Proc. of Conference on Nuclear Data for Reactors, Paris (1966) 149

14) Shpak, D.L., Ostapenko, Ju.B., Smirenkin, G.N., INDC(CCP) 8 (1970) 4

15) Fomushkin, V.F., Gutnikova, E.K., INDC(CCP) 7U (1970)

16) Iyengar, K.N., Iyer, R.H., Kapoor, S.S., Nadkarni, D.M., Sagu, M.L., Proc. on Nucl. Phys. and Solid State Phys. Sympos. 2 (1970) 67

17) Iyer, R.H., Sampathkumar, R., BARC 474 (1970)

18) Tanaka, S., Proc. of the EANDC Topical Discussion on Critique of Nuclear Models and Their Validity in the Evaluation of Nuclear Data, JAERI-M 5984 (1975) 212

19) Erskine, J.R., Kyle, G., Chasman, R.R., Friedman, A.M., Phys. Rev. C11 (1975) 561

20) Harada, K., Igarasi, S., A Report Presented to the Specialists Meeting on Inelastic Scattering, held at Harwell, April 14 to 16 (1975)

21) Hauser, W., Feshbach, H., Phys. Rev. 87 (1952) 366

22) Moldauer, P.A., Phys. Rev. 123 (1961) 968

23) Lane, A.M., Lynn, J.E., Nucl. Phys. 11 (1959) 646

24) Hill, D.L., Wheeler, J.A., Phys. Rev. 89 (1953) 1102

25) Pearlstein, S., Nucl. Sci. Eng. 23 (1965) 238

26) Wapstra, A.H., Gove, N.B., Nuclear Data Tables A9 No. 4-5 (1971)

27) Newton, T.D., Can. J. Phys. 34 (1956) 804

28) Porter, F.T., Ahmad, I., Freedman, M.S., Milsted, J., Friedman, A.M., Phys. Rev. C10 (1974) 803

29) Gilbert, A., Cameron, A.G.W., Can. J. Phys. 43 (1965) 1446

30) Mughabghab, S.F., Garber, D.I., BNL-325, 3rd ed. Vol. 1 (1973)

Appendix

Computer codes used in this evaluation are CASTHY, TOTAL, JUPITOR and two small ones by which an empirical formula of the smoothed fission cross section was obtained, and (n,2n) and (n,3n) cross sections were calculated. In this Appendix, brief descriptions are presented concerning CASTHY and TOTAL whose users manuals are not yet prepared.

A computer code CASTHY is made based on the formulas given in Ref. 1. Using this code, the excitation functions of total, capture, elastic and inelastic scattering cross sections are calculated. Effect of the γ-ray cascade in the compound nucleus is also taken into account. At present, however, it is treated only approximately.

A code TOTAL is made for automatic search of the optical potential parameters by using the least squares method concerning the total cross section. The data of 50 points and the parameters of 15 at most are treated in one run. Many subroutines of this code are transcribed from ELIESE-3 (JAERI 1224 (1972)). In particular, in a subroutine for the automatic parameter search, the data area of the angular distributions of the elastic scattering cross section in ELIESE-3 is replaced by the data area of the total cross section in TOTAL. For details the reader is referred to the report JAERI 1224.

Figure Captions

Fig. 1. Experimental data of ^{241}Am fission cross section. The data are taken mainly from NEUDADA Library.

Fig. 2. The best fit curve of ^{241}Am fission cross section. The confidence band obtained in this work is also given. Symbol X stands for the renormalized values of the data of Nobles et al.

Fig. 3. An example of the cross section curve obtained by neglecting the resonance near 160 keV.

Fig. 1

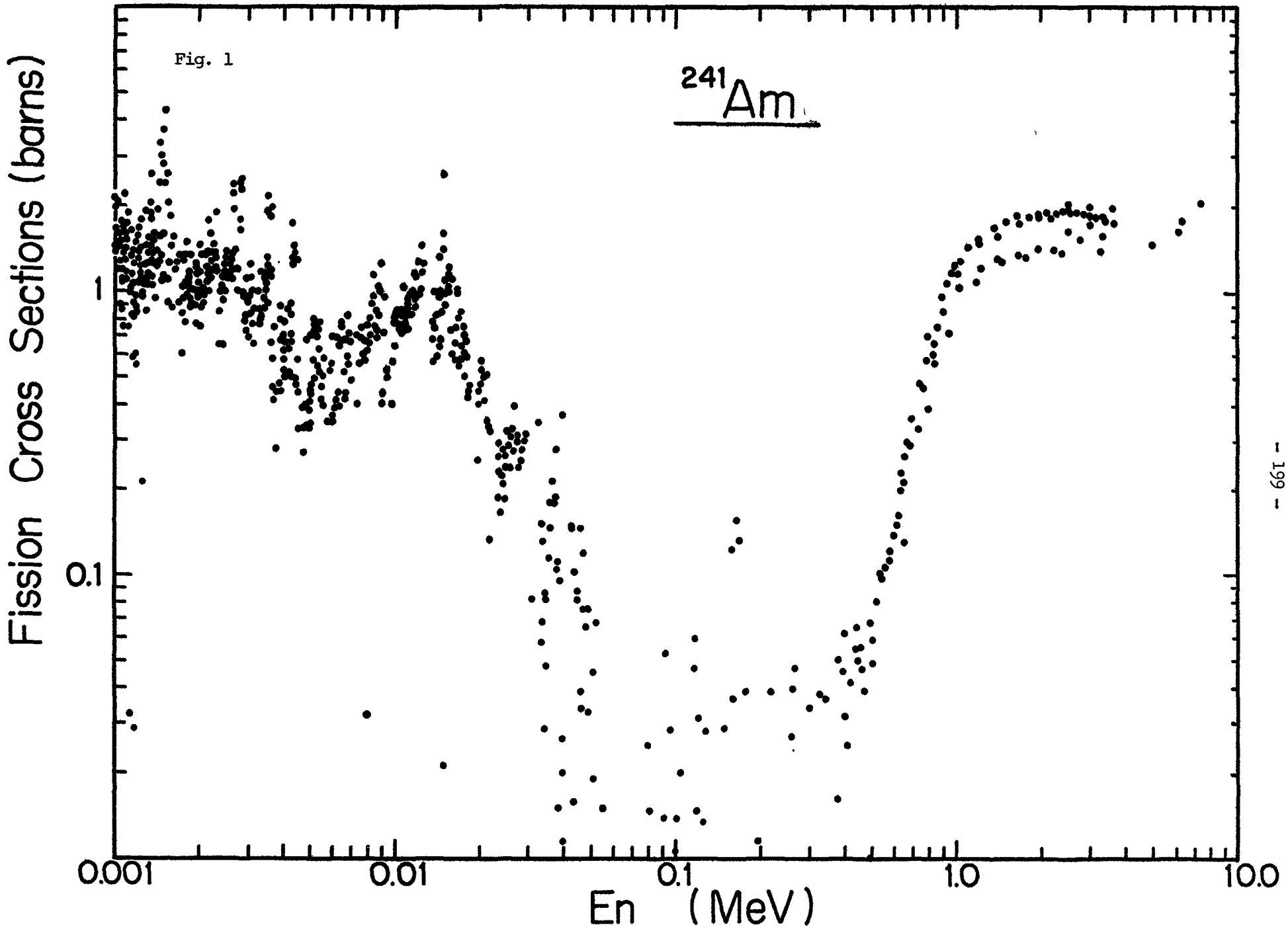
241Am
Fission Cross Sections (barns)
1
0.1
0.001
0.01
0.1
1.0
10.0
En (MeV)

Fig. 2

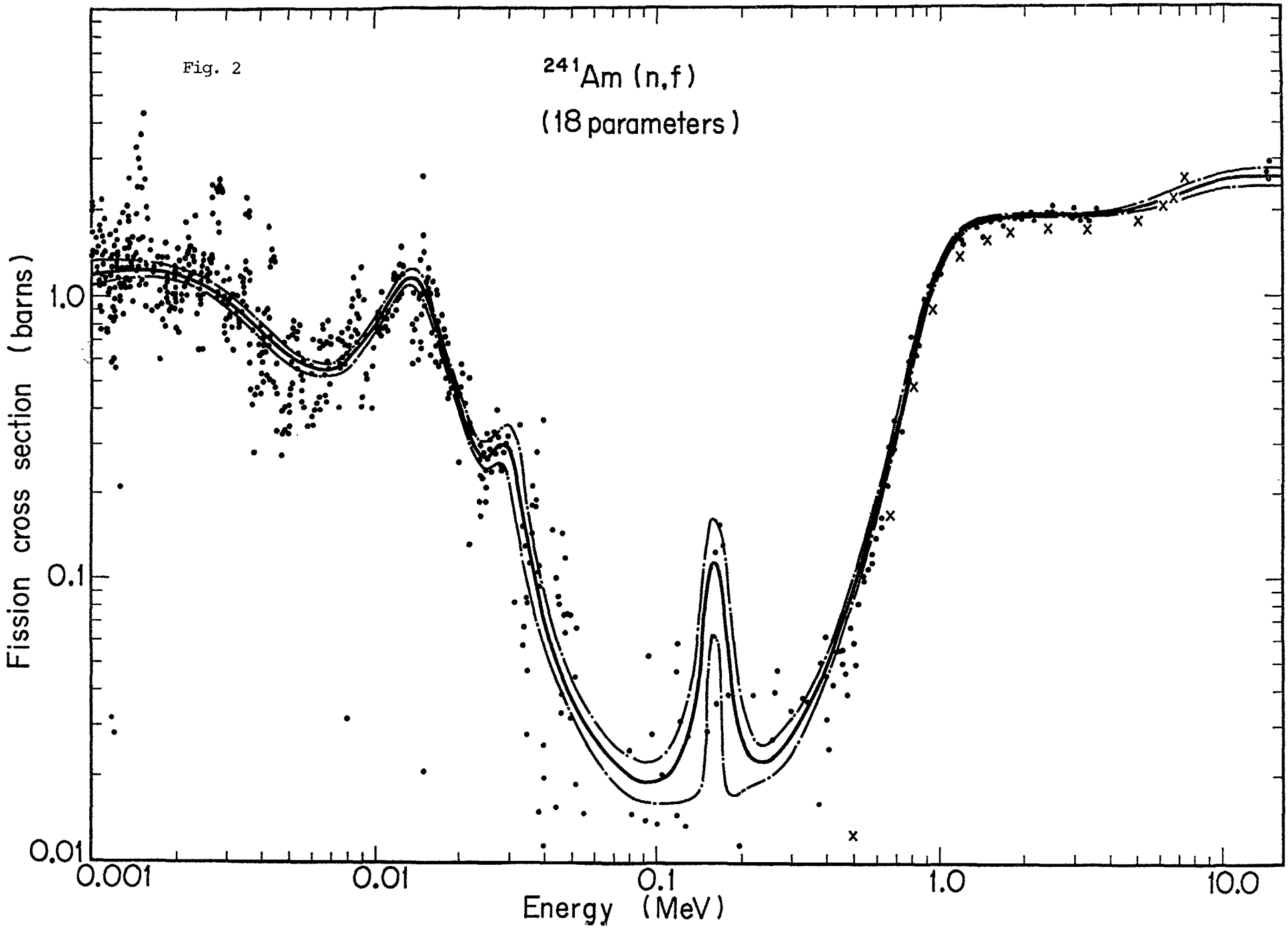
^{241}Am (n,f)
(18 parameters)
Fission cross section (barns)
1.0
0.1
0.01
0.001
0.01
0.1
1.0
10.0
Energy (MeV)

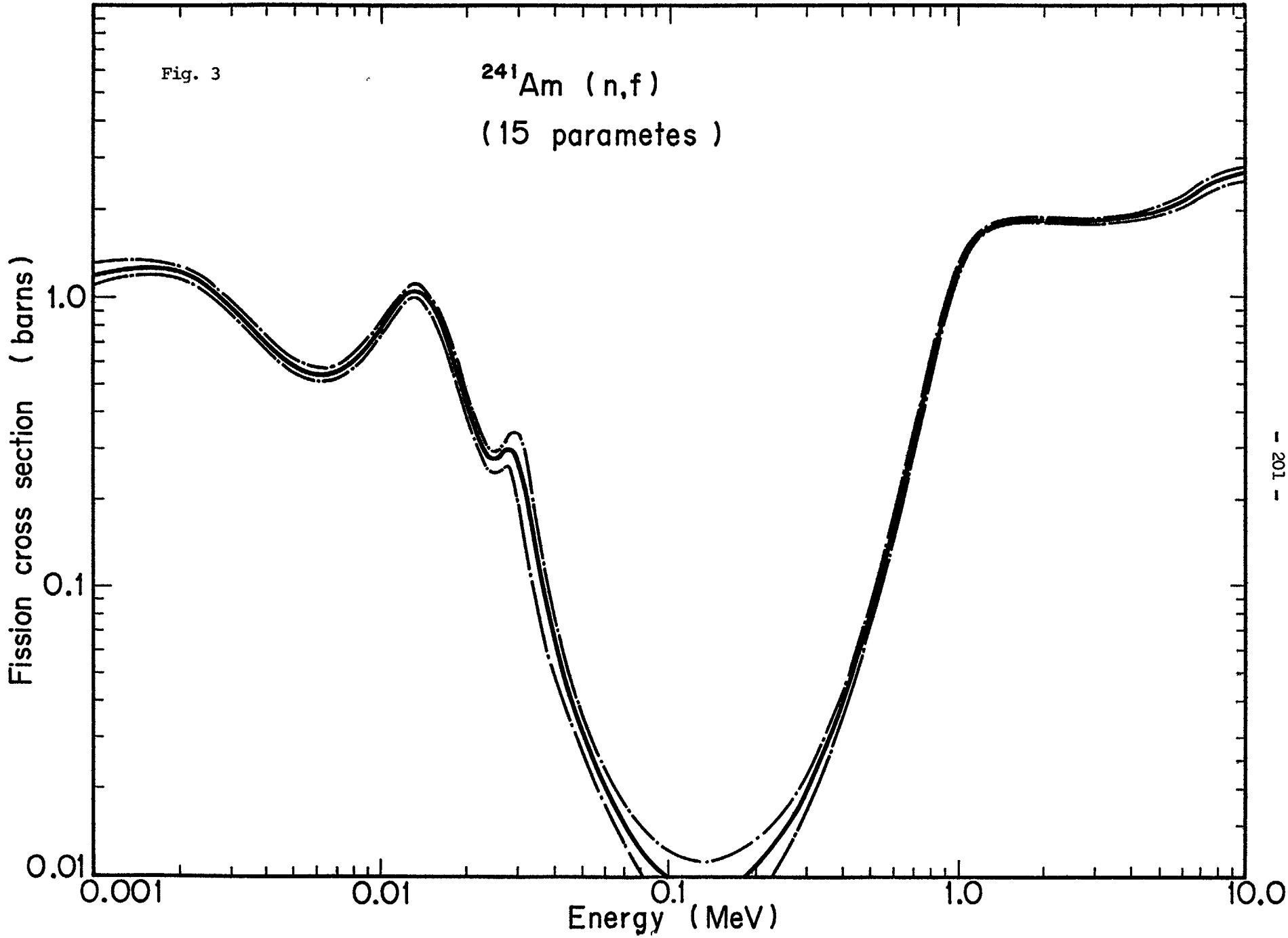
Fig. 3
241Am (n,f)
(15 parametes)
Fission cross section (barns)
1.0
0.1
0.01
0.001
0.01
0.1
1.0
10.0
Energy (MeV)

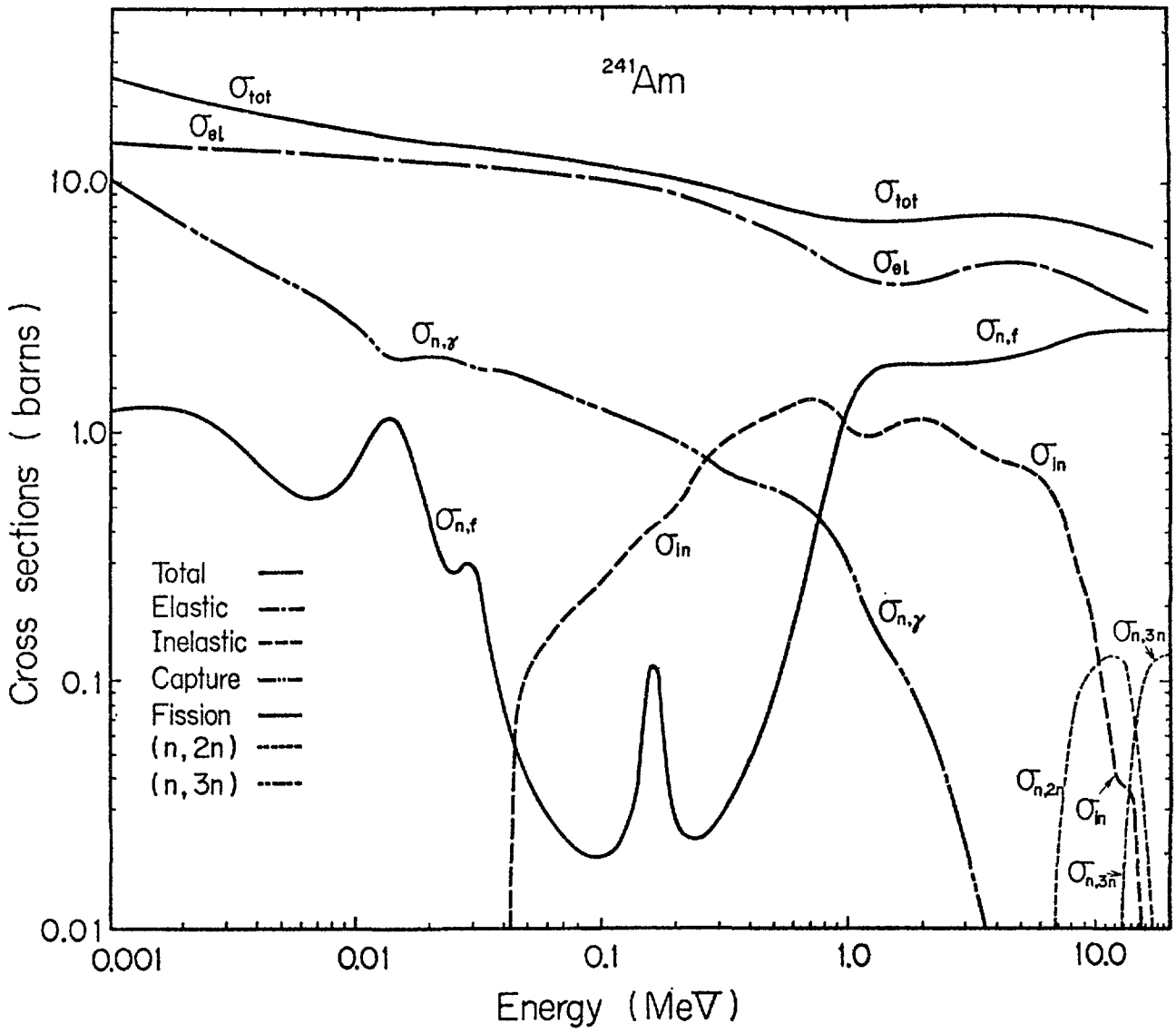

Fig. 4. Evaluated neutron cross sections of ^{241}Am.

Table 1. Parameters obtained as the best fit values.

(a) Resonance Parameters.

λ	E^R(MeV)	C(MeV^2·barns)	R(MeV^2)
1	1.39×10^{-3}	7.07×10^{-6}	6.36×10^{-6}
2	1.36×10^{-2}	2.16×10^{-5}	1.98×10^{-5}
3	2.92×10^{-2}	3.94×10^{-6}	2.00×10^{-5}
4	1.64×10^{-1}	1.63×10^{-5}	1.51×10^{-4}

(b) Barrier Parameters.

k	E^B(MeV)	(MeV^{-1})	B(barns)
c	0.903*	7.72	1.85
T	6.55	0.704	0.720

* Since neutron separation energy from the compound nucleus is 5.53 MeV, the barrier energy for the compound nucleus is estimated as 5.53 + 0.903 = 6.43 MeV from its ground state.

Table 2. Level Scheme of ^{241}Am

Level	Energy(MeV)	Spin and Parity
gr.	0.0	$5/2^-$
1	0.042	$7/2^-$
2	0.095	$9/2^-$
3	0.158	$11/2^-$
4	0.206	$5/2^+$
5	0.235	$7/2^+$
6	0.272	$9/2^+$
7	0.323	$11/2^+$
8	0.380	$13/2^+$
9	0.475	$3/2^-$
10	0.504	$5/2^-$
11	0.549	$7/2^-$
12	0.625	$1/2^+$
13	0.636	$3/2^-$
14	0.652	$1/2^-$
15	0.653	$3/2^+$
16	0.682	$11/2^-$
17	0.732	$11/2^+$
18	0.822	$13/2^+$

Table 3. Level Density Parameters*), Level Spacing and γ-ray Width

(i) Compound Nucleus

$a=26.532\ (MeV^{-1})$ $\Delta=0.0$

$E_x=3.1198\ (MeV)$ $C_o=5766.83\ (MeV)$

(ii) Residual Nucleus

$a=26.069\ (MeV^{-1})$ $\alpha_M=17.559\ (MeV^{-1/2})$

$\Delta=0.43\ (MeV)$ $E_x=3.5524\ (MeV)$

$C_o=5642.73\ (MeV)$

(iii) Level Spacing and γ-ray Width

$\langle D_{obs}\rangle=0.74\ (eV)$ $\langle \Gamma_\gamma\rangle=0.041\ (eV)$

*) Notations are referred to Appendix of Ref.1.

Contributed Paper No. 9

SYSTEMATIC OPTICAL AND HAUSER-FESHBACH MODEL INTERPRETATION OF MEASURED ELASTIC AND INELASTIC NEUTRON SCATTERING DATA

T. Wiedling, E. Ramström and B. Holmqvist

Neutron Physics Laboratory, AB Atomenergi, Studsvik,

Nyköping, Sweden

ABSTRACT

The elastic and inelastic neutron scattering processes play predominant roles in nuclear fission reactors and will without doubt also be most important in future fusion reactors. The elastic and, in particular, the inelastic neutron scattering processes dominate the energy loss of the primary fission neutrons and largely determine the character of the reactor neutron spectrum. The energy of the neutrons released in a deuterion-tritium-fueled fusion reactor is converted to thermal energy partly by scattering processes in the blanket, where, when tritium loaded, also the tritium breeding process takes part. The scattering processes are thus of importance in connection with the regeneration of tritium. Accurate experimental investigations of neutron scattering processes and the analyses and theoretical interpretation of the observed effects are evidently very interesting from the applied neutron physics point of view.

The purpose of this paper is to give a short introduction to the application of the optical model and the Hauser-Feshbach model for estimating neutron elastic and inelastic scattering cross sections to be used in the reactor technology in connection with core, shielding and safety problem calculations. The discussions will concentrate on the practical aspects of the numerical calculations of the cross sections and comparisons with experimental results.

1. INTRODUCTION

1.1. Applications of neutron scattering data

The elastic and inelastic neutron scattering processes play predominant roles in nuclear fission reactors and will also be most important in future fusion reactors. Elastic and, in particular, inelastic neutron scattering are the main processes contributing to the energy loss of the primary fission neutrons and largely determine the character of the reactor neutron spectrum. Thus in a fast reactor the inelastic scattering in the fuel itself is by far the strongest slowing down mechanism. Also in the thermal reactor the inelastic scattering contributes substantially to this effect. For the same reason the scattering in the reactor structure and the shield are most important, and thus also for the choice of proper materials. The energy of the neutrons released in a deuterium-tritium fueled fusion reactor is converted to thermal energy partly by scattering in the lithium loaded blanket where also the tritium breeding process takes place. The scattering processes are thus of importance in connection with the regeneration of tritium. However, in the present status of the fusion reactor technology the study of neutron processes occurring in fission reactors may be considered to have a higher priority than the investigation of those of the fusion reactor.

Neutron scattering takes place not only in the reactor fuel and the elements of the reactor structure, but also in the fission products of the fuel. Since many of these fission products are radioactive, their nuclear properties are not easily measured in the laboratory. Information on the neutron-nucleus interactions of these products can thus be obtained only by calculations based on the knowledge and experience gained from experimental and theoretical studies of stable isotopes.

Uncertainties in neutron cross section data of reactor fuels and structural materials directly affect the safety and economy of a reactor design, and the consequences of the lack of precision in fundamental nuclear reactor data have been discussed on several occasions [1-6]. It may be mentioned that Greebler et al. [3] have shown that a 15 per cent uncertainty in the inelastic scattering cross section of steel above an energy of 0.8 MeV would introduce the same effect on the predicted breeding ratio of a 1000 MWe fast breeder reactor as does 30 per cent uncertainty in the ^{240}Pu neutron capture cross section in the energy range 0.1 - 100 keV. Such error sources may cause substantial uncertainties in the calculated reactor operating costs. Another example of uncertainty effects is given by Shure [7] who studied the effects of uncertainties in the neutron inelastic cross section of iron on an iron-water shield and demonstrated that a 10 per cent change in the iron cross section changes the predicted flux of neutrons entering the water shield by about 30 per cent.

1.2. Scope of the present review

The accuracy of cross sections required for a reactor physics calculation depends on several factors like isotope, type of reaction, magnitude of cross section, position of the isotope in the reactor, reactor type, and nature of the calculation. The World Request List for Nuclear Data Measurements (WRENDA) [8] can advantageously be used as a guide to get an indication of the accuracies of cross sections requested for calculations on fission and fusion reactor systems. Specifically for neutron elastic and inelastic scattering cross sections applicable within the fission reactor programs, WRENDA specifies accuracies mostly of the order of 5 to 10 per cent. However, there are exceptions from these values, as for instance for the neutron inelastic cross sections of iron and nickel, the proposed accuracy for which is 3 per cent, and it is doubtful whether so high a precision is

obtainable with the techniques at present available.

Accurate experimental investigations of neutron scattering processes and the analyses and theoretical interpretations of the observed effects are evidently of a very great importance from the applied neutron physics point of view. These studies contribute to the knowledge of the pure scattering interactions, but also provide a tool for calculating the cross sections of other neutron-nucleus processes of interest for applications like those of the nonelastic and neutron absorption processes, as well as the total cross sections.

The purpose of this paper is to give a short introduction to the application of the optical model and the Hauser-Feshbach model for estimating neutron elastic and inelastic scattering cross sections to be used in the reactor technology in connection with core, shielding and safety problem calculations. Since this paper will concentrate on the practical aspects of the numerical calculations of the cross sections and comparisons with experimental results, there will be no detailed discussion of nuclear theories. Thus the optical model will be applied quite straight-forward by proceeding from a central potential and neglecting the physically more correct non-locality and other refinements of the theory, however interesting they may be from the pure nuclear physics point of view. With the same attitude in mind the inelastic neutron scattering process will be treated on the basis of the experience gained from simultaneous experimental studies and model calculations of excitation functions.

There exists a large amount of data from a number of measurements on neutron scattering [9]. However, the lack of comprehensive data sets has resulted in a demand for systematic experimental investigations. In recent years there have also been extensive systematic programs at Argonne, Oak Ridge, and Studsvik [10-15]. The ANL program has until recently been restricted to the energy range below 1.5 MeV neutron energy. The ORNL inter-

est has been in the 5 to 8 MeV range, and the Studsvik efforts were made in the 1.5 to 8 MeV interval.

Comprehensive investigations are now in progress at several laboratories [16] using an appreciably improved technique, and will certainly make important contributions to our knowledge of neutron scattering, elastic as well as inelastic.

Extensive reviews of the theoretical nuclear models for neutron elastic and inelastic scattering have recently been presented by Hodgson [17-19].

The experimental neutron elastic scattering data which form the basis of the present discussion were collected at Studsvik mainly during a ten year period before 1970. Until that time they were the most comprehensive set of data in the energy interval 1.5 to 8 MeV. The optical model calculations made in connection with the collection of these data were also comparatively extensive. It is worthwhile to draw attention to the recent comprehensive studies at Studsvik of inelastic neutron scattering of a number of elements in the energy range 2 to 4.5 MeV [15]. Results and experience from these investigations will be reviewed.

2. NUCLEAR THEORY BASIS

2.1. Elastic neutron scattering

The theoretical interpretation of the first systematic experimental investigation of neutron elastic scattering, i.e. the one by Walt and Barschall [20] who measured the differential cross section of a large number of elements at 1 MeV, was accomplished on the basis of the nuclear optical model by Feshbach, Porter and Weisskopf [21]. Calculations of cross sections performed with a complex square well potential, V = U+iW, showed that a general agreement was obtained with the experimental results. However, the simple square well potential is a somewhat unphysical picture of the nucleon-nucleus interaction. Instead an analytical expression of the shape of the

potential chosen should preferably be based on a phenomenological approach founded on physical arguments. With this in mind the real part, U, of the potential could be expected to be uniform in the nuclear interior in accordance with the short range and saturation properties of the nucleon-nucleon forces and to have an exponential fall-off with increasing radius. The imaginary part, W, is expected to be a combination of volume and surface terms. Owing to the Pauli exclusion principle the absorption of nucleons is reduced when the density is large, causing the surface peaking. The features described above can be represented by the Saxon-Woods and the derivative of the Saxon-Woods form factor, i.e. $f(r) = \{1+\exp[(r-R)/a]\}^{-1}$ and $g(r) = 4\{1+\exp[(r-R)/b]\}^{-2}\exp[(r-R)/b]$, where R is the nuclear radius and a and b are surface diffuseness parameters.

The optical potential discussed above is valid for zero spin nuclei. For non-zero spin nuclei a number of additional interactions are possible, of which the spin-orbit effect is the most important. Thus one usually introduces a spin-orbit interaction term in the potential. The local central optical potential is then described by the expression

$$-V(r) = Uf(r)+iWg(r)+U_{SO}(\hbar/\mu_{\pi}c)^2 1/r(d/dr)\,|f(r)|\,\bar{\sigma}\cdot\bar{\ell}$$

where the last term represents the spin-orbit interaction with the depth U_{SO}. The constant μ_{π} denotes the pion mass, $\bar{\sigma}$ and $\bar{\ell}$ the Pauli spin operator and the orbital angular momentum operator, respectively.

The nuclear optical model has up to now been treated on the assumption that it has a local character. As Brueckner has shown [22] the optical potential has, however, a non-local character and may be expected to be energy dependent. The non-locality of the basic forces has later been discussed by Watson [23]. The non-locality formalism and its application to neutron data have been worked out by Perey and Buck [24], Wilmore and Hodgson [25] and Engelbrecht and Fiedeldey [26], among others.

Lane [27] suggested an isobaric spin dependence of the real part of the optical potential. This effect was demonstrated in the neutron-nucleus interaction by Holmqvist [12] by an analysis of neutron elastic scattering data. A comprehensive treatment of the whole optical model complex has recently been presented by Hodgson [17,18].

An essential characteristic of the optical model is its ignorance of the detailed mechanism of the nucleon-nucleus interaction. Features depending on particular properties associated with the level structure of the nucleus are thus not described by the model. Also important for a satisfactory optical model description of a nucleon-nucleus interaction is the excitation of many levels of the compound nucleus to average out characteristic properties of specific levels. Such a condition is met in experiments with particle beams of large energy spread relative to the mean level spacing of the compound nucleus. The number of excited levels must be large enough not to show up any effects from individual resonances or small groups of resonances. All effects must be wholly statistical in nature. This condition is usually fulfilled for medium and heavy nuclei at an incident energy above a few MeV.

Perturbating interactions may arise in the nucleon-nucleus system when the nucleus is non-spherical, causing coupling effects between the elastic channel and the non-elastic channels. The pure optical model is not applicable to such a system. It is certainly not valid either for such a high nucleon energy that there will be a strong coupling between the incident nucleon wave function and that of individual constituents of the nucleus.

2.2. Inelastic neutron scattering

The inelastic scattering of neutrons from nuclei can take place either as a compound nucleus reaction or as a direct reaction. The compound nucleus reaction can be described as proceeding in two independent phases, i.e. the formation of the compound system and the disintegration of this system into

the products of the reaction. The theoretical description of the formation of the compound nucleus can be based on the optical model making it possible to calculate the cross section of this process, i.e. the total absorption cross section. The distribution of the total absorption cross section between the different decay modes which are open at a particular excitation energy of the compound nucleus can be estimated by the statistical model proposed by Hauser and Feshbach [28]. When formulating this theory it was assumed that the contribution of each total angular momentum and parity of the system to the average partial reaction cross' section could be written as the product of the average cross sections for compound nucleus formation and decay, respectively. However, according to Porter and Thomas [29] the level widths fluctuate in resonances and therefore the assumption of independence of formation and decay of the compound nucleus on the average is no longer valid. Furthermore, it is known that compound nucleus resonances interfere in a statistically describable manner. Taking these two effects into account Moldauer [30] derived an expression believed to be more general than the original one of Hauser and Feshbach for the description of the neutron-nucleus interaction. Moldauer introduces a correlation parameter, Q_α, the value of which is dependent on the properties of the compound nucleus. In the limit of infinitely many overlapping resonances the value of Q_α goes to zero, while in the case of isolated resonances Q_α approaches one. In the many channel limit, where there are competing decay channels, the fluctuations of the level widths about their average values can be disregarded. Recently it has been shown by Moldauer [31] that the simple estimates of the correlations among the resonance parameters, which form the basis for the introduction of the correlation parameter, are not adequate. However, in many cases the formalism introduced by Moldauer has been found empirically successful in describing experimental scattering data.

In a direct inelastic reaction the incoming neutron is thought to interact with only a few nucleons in the target nucleus knocking one neutron out of the system and leaving the target nucleus in an excited state. The cross sections for neutron inelastic scattering taking place through this process are usually calculated by the distorted-wave Born approximation (DWBA) [32] and the coupled-channel approximation [33]. The latter formalism is the one used most frequently. It is, for instance, applied in cases where there are open channels corresponding to inelastic scattering to rotational states. Furthermore, the coupled-channel model is applicable for nuclei with collective states excited via low lying states. The coupled-channel calculations have been discussed in detail by Tamura [34].

There are no sharp boundaries between the energy regions or the mass regions in which the compound nucleus reaction and the direct reaction are operative. However, as is well known, the effects of the different processes can be observed experimentally in the different shapes of the angular distributions of the neutrons, since the compound nucleus formation gives an isotropic or slightly anisotropic but symmetric angular distribution, whereas that of the direct reaction is anisotropic. The results of inelastic neutron scattering measurements [15] indicate that for medium weight and heavy nuclei the process takes place primarily via compound nucleus formation, at least for neutron energies below about 5 MeV.

3. NUCLEAR MODEL DESCRIPTIONS OF EXPERIMENTAL NEUTRON SCATTERING OBSERVATIONS

3.1. Elastic scattering

3.1.1. Problems of interpretation of experimental observations

The local potential of the nuclear optical model is characterized by a number of parameters describing the interaction of the nucleon-nucleus sys-

tem. A potential of the previously given analytical form including the Saxon-Woods and derivative Saxon-Woods form factors has as many as seven parameters: the potential depths, radii, and diffuseness parameters of the real and imaginary parts, and the potential depth of the spin-orbit term. It has often been emphasized that the large number of parameters makes the nuclear optical model difficult to use with confidence. With such a large number of parameters it has been argued that it would be possible to get a description of any experimental scattering data whatsoever, and accordingly there would be no physical basis for the interpretation of the results. It is true that experimental results can be described by several different parameter sets, but at least the most extreme ones can be disregarded for reasons of fundamental physics.

By the use of high speed computers laborious nuclear optical model calculations can be made in order to determine the numerical values of the parameters. The introduction of automatic search procedures facilitates the adjustment of the parameters to give the best fits, described by an index of quality χ^2, to experimental elastic scattering angular distribution data. The minimum value of χ^2 in the parameter space can be acquired by a search code to minimize the quantity

$$\chi^2 = \frac{1}{N} \sum_{i}^{N} \left\{ \frac{[d\sigma(\theta_i)/d\Omega]_{se} - [d\sigma(\theta_i)/d\Omega]_{exp}}{\Delta[d\sigma(\theta_i)/d\Omega]_{exp}} \right\}^2$$

which leads to an objective and quantitative comparison between experiment and calculation. $[d\sigma(\theta_i)/d\Omega]_{se}$ and $[d\sigma(\theta_i)/d\Omega]_{exp}$ are the calculated and experimental differential cross sections, respectively, $\Delta[d\sigma(\theta_i)/d\Omega]_{exp}$ is the experimental uncertainty and N is the number of observations.

One of the most serious difficulties in using the multiparameter search procedure is the existence of several minima in the parameter space. A specific minimum value of χ^2 may not be the "extreme" one. The minima may in some

cases by comparatively closely spaced, i.e. there are only small differences between the numerical values of the parameter sets, giving roughly the same χ^2-values. Also the choice of numerical input values of the parameters can have an influence on the resulting numerical parameter values. Sometimes, therefore there may be some doubt about the uniqueness of a calculated parameter set. In this connection the well known (U,r_{oU}) and (W,b) ambiguities should be recalled. The (U,r_{oU}) coupling is often discussed in terms of the relation Ur_{oU}^n. It is characteristic of this ambiguity that within small limits of U and r_{oU} the variation of one of these parameters is related to a variation of the other one in such a way that the product Ur_{oU}^n remains essentially constant. In the special case of a square well potential the value of the exponent n is equal to 2, and this value can suitably be used when checking calculations with a potential of the Saxon-Woods shape. The (U,r_{oU}) ambiguity has been overcome by Holmqvist [12] by choosing the volume integral of the potential as a measure of the strength itself. The volume integral is defined by the expression $J = 4\pi \int_0^\infty f(r)r^2dr$. This technique has been used with advantage to smooth out the scattering in the parameter values caused by the more or less statistical distribution obtained in the parameter search routine and attributable to minimum values of χ^2 of the same significance.

It is necessary to be very critical when examining optical model data, particularly if one considers only a limited experimental material. It is important to stress that more general conclusions concerning the validity and generality of the results of the search procedure are possible only if a large homogeneous experimental set of data is available, collected with high accuracy for many elements in a large energy interval. A proper experimental data bank certainly gives the opportunity to test the optical model with confidence and reliability and to study its ambiguities. For a comprehensive experimental data set one could expect an overrepresentation

of the "correct" minimum values and thus also of the most significant parameter sets.

With regard to the statistical nature of the optical model it is a question whether it should to be used in attempts to draw conclusions concerning specific neutron-nucleus interactions, for instance in limited mass regions of special character. The best use of the nuclear optical model is probably only for descriptions of the general behaviour of the nucleon-nucleus system.

3.1.2. Experience of optical model parameter calculations

The results of a series of calculations of optical model parameters will be reported in order to demonstrate some properties of the search procedure when the parameter values are adjusted to obtain best agreement between calculated and measured elastic scattering cross sections. Already in the previous paragraph it was mentioned that the choice of the numerical values used as input parameters in a search procedure may have an influence on the resultant minimum values. It is thus important to investigate this problem in some detail. An investigation of this type can be performed in a number of ways but because of the enormous computer time which may easily be spent, some suitable boundaries must be chosen. For this reason the study has been limited and concentrated to an investigation of the importance and influence of the choice of the numerical input value of one of the parameters, i.e. the radius (r_{oU}) of the real part of the potential when carrying out a multiple parameter search procedure. This is a suitable choice of parameter from the physics point of view since the nuclear radius is a fundamental nuclear characteristic the magnitude of which is well known from a number of different experiments. Without being extreme in any sense the computer input value of the real part of the radius was in one series of calculations chosen well below the one usually considered to be an ordinary value. In two other series of calculations the radius parameter was of more common size.

The computer codes (ABACUS II and ABACUS-NEARREX) available limited the number of variable parameters to five. The minimum value of χ^2 was searched for in the (U,r_{oU},a,W,r_{oW}) space. The parameters b and U_{SO} were kept constant. Even if valuable information on the (W,b) coupling was lost by the constancy of b, this was not considered a serious limitation in this study. The strength of U_{SO} has, within rather wide limits, little influence on the shape of an angular distribution and on the cross sections, and thus there is no drawback in choosing a fixed value. The parameters of the optical model potential represent measures of the experiments and the χ^2 is a quantity used to judge the results of the calculated fits in a way not influenced by any human bias. As a criterion two fitting procedures are considered to be of the same quality if the ratio between the χ^2 values is not larger than 2, which is a very conservative choice. Otherwise the one with the larger value is rejected. However, the calculations give not only angular distribution fits but also total elastic and total cross section values. Thus, the decision whether a calculated parameter set is to be accepted or not can be founded not only on the minimum value of χ^2 but, if necessary in extreme cases, also on comparisons between the observed and calculated elastic scattering angular distributions and observed and calculated total elastic scattering and total cross sections. These specific optical model calculations were applied to neutron elastic scattering angular distributions measured at 8 MeV neutron energy for a number of elements ranging in mass number from 27 to 209. Experimental details can be found in a number of previous publications [12-14].

Calculations have been performed for each element with computer input values of the r_{oU}-parameter of 1.0, 1.2 [12,13] and 1.3 fm, respectively. All other input parameter values, i.e. those of U, W, a and r_{oW}, were the same for each run and for each element. The numerical data of the calculations on some elements, light as well as heavy, are shown in Table 1. Apart

from the optical model parameter values the table gives the calculated and experimental elastic and total cross sections. Absorption cross sections are also included for the sake of completeness. As is observed for several cases, three parameter sets fit the data equally well according to the χ^2-values. But the input value r_{oU} = 1.0 fm gives for the light and medium heavy elements (Al, Mn, Fe, Co, Cu) U-values which are high and r_{oU}-values which are low relative to the two other data sets. In some cases this effect seems to be compensated by a somewhat larger diffuseness parameter a. The discriminator, i.e. χ^2, of a parameter set does not, for these elements, have the sensitivity necessary to permit a distinct choice of parameter set. For the heavy elements (As, Cd, Au, Pb_r) there is a much more efficient χ^2-discrimination, often in combination with remarkably small U and r_{oU} values, i.e. U in the 30 to 40 MeV range and r_{oU} less than 1 fm. The reason why r_{oU}^{input} = 1.0 fm gives a sharp discrimination for many of these elements is probably effects on the search procedure of the more complicated diffraction patterns of their angular distributions.

Angular distributions calculated with the optical model parameter data sets obtained with r_{oU}^{input} = 1.0 and 1.2, are shown for the elements Al, Mn, Fe and Co in Fig. 1. As is seen, there are only slight differences between the curves of each element, as could also be expected from the χ^2-values and other data of Table 1.

3.1.3. Elastic scattering cross section calculations with generalized sets of optical model parameters

Neutron data are requested for many nuclei and for a range of neutron energies [9]. It is an ambitious but not a very interesting task to measure all these data. Since it is possible to specify the accuracy of data needed

for technological applications it is from many points of view, economical as well as practical, important to study, analyse and present existing knowledge of neutron cross sections so that such a Sisyphean labour can be eliminated. Thus global sets of optical model parameters have been presented by, among others, Wilmøre and Hodgson [25] and Holmqvist and Wiedling [13]. By giving the parameter sets in simple algebraic forms the proper parameters are easily calculated and the required cross sections can be calculated with a suitable computer program within the accuracy, i.e. 10 to 20 per cent, required for many, if not most, of the structural materials used in present day fission reactor design.

Since the optical model, as a matter of course, describes only the overall properties of the nucleon-nucleus interaction and no specific nuclear structure effects are taken into account, i.e. it is completely statistical, systematic deviations are to be expected between experimental and calculated cross sections for nuclei with characteristic internal properties. These deviations may become even more pronounced if one uses a global set of potentials to describe the neutron-nucleus interaction pattern.

The results of neutron scattering measurements at Studsvik have been used in an attempt to obtain generalized parameter sets of the optical potential. The experimental data consists of elastic scattering angular distributions of a number of elements ranging from Al to Bi in the neutron energy interval 1.5 to 8 MeV. Five-parameter search procedures were used to get the numerical values of U, W, r_{oU}, r_{oW} and a. The parameters b and U_{SO} were given the values 0.48 fm and 8 MeV, respectively. On the basis of these results parameter sets with the following algebraic characteristics [13] were obtained

$$U = 44.44+0.1987A-1.893\times10^{-3}A^2+4.527\times10^{-6}A^3$$

$$W = 5.89+9.376\times10^{-2}A-7.343\times10^{-4}A^2+1.408\times10^{-6}A^3$$

$r_{oU} = 1.183+0.0003A$

$r_{oW} = 1.183+0.0004A$

(The potential depths are given in MeV and the radii in fm.) The main task has not been to provide a tool to describe the observations of the neutron-nucleus process with the nuclear model most appropriate for each specific case, since this has not been necessary with regard to the requested cross section accuracy. Accordingly, within the studied neutron energy range the optical model parameters U and W which, from the point of view of the non-local optical potential are expected to be energy-dependent, are energy-independent in the studied energy interval within the experimental and computational accuracies.

Elastic scattering angular distributions and total cross sections have been calculated for a number of elements by use of the expressions for U, W, r_{oU} and r_{oW}. Fig. 2 shows some corresponding angular distributions, those of the 5-parameter search procedure, and the experimental cross sections for a range of elements at 3 MeV neutron energy. Total calculated and experimental [35, 36] cross sections are compared in Fig. 3. An examination of the results shows in general good agreement between experiments and calculations and the results for the total cross sections should be observed in particular. The deviations between the total cross sections are, with a few exceptions, less than a few per cent.

The experimental information which Wilmore et al. [25] used to deduce their parameters was less homogeneous than that of the Studsvik data library, but on the other hand their analyses were extended into a larger energy range. Examples of angular distributions of elastically scattered neutrons calculated with the Wilmore-Hodgson expressions, including a spin-orbit term (U_{SO} = 10 MeV) which they did not originally use, are shown for

Co at 6.09 MeV and Pb at 8.05 MeV in Fig. 4. Also included in the figure are angular distributions calculated by the 5-parameter search routine by use of the Studsvik generalized optical model parameters, as well as the experimental differential cross sections. There are good fits to the experimental angular distributions of the Studsvik calculations and somewhat less good to the Wilmore-Hodgson potentials. Comparisons of the total and total elastic calculated cross sections calculated with Studsvik and Wilmore-Hodgson's sets show for these two cases maximum spreads of less than 10 per cent. The two parameter sets evidently show satisfactory agreement at least for the presented cases.

3.2. Inelastic scattering

3.2.1. Problems of interpretation of experimental observations

There are a number of problems in connection with the interpretation of experimental inelastic scattering observations and the model descriptions of the results. Thus cross section calculations according to the Hauser-Feshbach (HF) statistical model demand a rather detailed knowledge of the characteristics of the target nucleus. There must be information available about the excitation energies, spins and parities of all levels which it is energetically possible to excite in the target nucleus at the specified neutron energy as well as about the nuclear optical potential of the nucleon-nucleus system for the calculation of the transmission coefficients. The information on the level properties is usually obtained from the results of other types of nuclear physics experiments even if comparisons between calculated and experimental excitation functions make it possible in principle to settle the spins and parities of the levels, at least when applying the pure Hauser-Feshbach model contrary to the Hauser-Feshbach-Moldauer (HFM) [30] concept which does not, a priori, give a recipe for a definite choice of level data.

Since the parameters of the optical model potential are used to derive the transmission coefficients, the magnitudes of the parameters will have a direct influence on the coefficients and, accordingly, on the calculated cross sections. Thus, it is of general interest to know how sensitive the results of the cross section calculations are to changes in the optical model parameters. This problem has been investigated by Almén-Ramström [15] for some elements by changing the values of the parameters U, W, r_{oU}, r_{oW}, and a one at a time in the HF calculations. The results obtained for Fe at 3 MeV neutron energy show that changes of 2 and 5 per cent in the real potential depth will affect the inelastic scattering cross sections of most neutron groups by appreciably less than 5 and 20 per cent, respectively. The corresponding value is 4 per cent for a change of 10 per cent in the imaginary potential depth. Changes of the values of U and W of 5 and 10 per cent, respectively, are comparatively large if it is considered that the potential depths of the Studsvik sets [13] range for U from about 48 to 44 MeV and for W from 7.8 to 6.2 MeV in the mass region Al to Bi. The uncertainty of a calculated cross section can thus be considered to be comparatively little influenced by inaccuracies in the potential depths.

As mentioned above, the energies, spins and parities of all levels up to the bombarding energy have to be known when HF calculations are to be made. However, when the number of levels is comparatively large, for instance at high excitation energies, a level density function is the only nuclear structure information required. The level density distribution as expressed in the formalism of Gilbert and Cameron [37] may suitably be used for this purpose. If no computer code with the option to include an expression for the level density in the target nucleus is available, there are difficulties in performing reliable HF calculations for a target nucleus for which no proper knowledge exists about the levels with regard to energies, spins

and parities. However, experience has shown [15] that these difficulties can be partly overcome if the details are known for those levels for which the cross sections are wanted and for about ten of the closest lying higher levels. The characteristics of levels with even higher energies have also some influence on the results of the calculations. These sources cause an uncertainty of the order of a few per cent in the results of the model calculations.

3.2.2. Results of a study of the usefulness of the Hauser-Feshbach model

The usefulness of a model for the description of the inelastic scattering process has to be investigated by systematic comparisons of calculated and experimental cross sections. Recently such an investigation of the Hauser-Feshbach statistical model has been performed in a study of inelastic scattering from eighteen elements in the energy range 2.0 to 4.5 MeV [15]. The main result of this investigation is that the bulk of the observations are well described by the HF formalism adjusted according to Moldauer's original but somewhat inadequate model picture [30]. Thus it is an obvious result that in cases where there are few open competing decay channels for the compound nucleus, the cross sections calculated with the HFM formalism with $Q_\alpha = 0$ usually give a good description of the experimental data but when the number of open channels increases, the cross sections calculated with the pure HF formalism compare favourably with the experimental data. At the lowest primary neutron energy studied, i.e. 2.0 MeV, where for some of the nuclei the number of open decay channels is limited, the inelastic scattering cross sections calculated with $Q_\alpha = 0$ are lower than those calculated with the pure HF formalism by at most 50 per cent. This figure decreases when the number of open decay channels for the compound nucleus increases with increasing primary neutron energy. Thus for instance for 17 open channels, the cross sections calculated with $Q_\alpha = 0$ are less than 20

per cent lower than those calculated with the pure HF formalism. Some exceptions from the general trend have been observed for a few excitation functions for some levels in odd-mass nuclei with collective states in the investigated excitation energy region.

Some specific results will be briefly discussed. Fig. 5 shows experimental cross sections for vanadium as well as the excitation functions calculated with the pure Hauser-Feshbach formalism (solid line) and the Moldauer formalism with the correlation parameters $Q_\alpha = 0$ (dashed line) and $Q_\alpha = 1$ (point-dashed), respectively. The experimental cross sections are well described by those calculated with $Q_\alpha = 0$ for incident neutron energies below about 4 MeV, while at higher energies, where the number of open channels increases, the cross sections calculated with the pure Hauser-Feshbach formalism describe the data well. ^{89}Y (Fig. 5) is an example of an isotope for which the experimental excitation functions for most but not all of the studied levels are in good agreement with the calculated cross sections. Thus the experimental data for the 1.51, 1.74 and 2.22 MeV levels are consistent with those calculated with $Q_\alpha = 0$ in the whole investigated energy range. However, the calculated cross sections for the 0.900 MeV level, the spin and parity of which are well known [38], are almost a factor of two larger than the experimental data. Furthermore, the calculated excitation function cross sections of the group composed of the 2.53, 2.57 and 2.62 MeV levels are about 50 per cent larger than the cross sections of two experimental points. One explanation of the observed discrepancies may be that ^{89}Y has collective states within the investigated excitation energy region resulting from coupling of the 39th $p_{1/2}$ proton to excited states of the $^{88}_{38}Sr_{50}$ core which have been shown to be collective in nature to some extent [39]. However, in the calculations only wave functions for single-particle nuclear states are used. Further detailed studies are necessary in order to

get a complete understanding of the observed effects.

3.2.3. Applications of the optical model and Hauser-Feshbach formalism

As mentioned previously neutron scattering takes place in the fission products of the reactor fuel besides in the reactor fuel itself and in the elements of the reactor structure. Thus the neutron cross sections for the fission products will affect the reactivity of the reactor. However, these cross sections are not always easy to measure, since many of the fission products are radioactive. Thus information on these quantities has to be obtained from calculations with the optical model and the Hauser-Feshbach formalism. In order to make these calculations with confidence, existing theoretical models must be checked for reliability on nuclei of a different character.

When deriving the set of generalized optical model parameters mentioned previously [13], only results from a few measurements on nuclei in the atomic mass region covered by the fission products were taken into account. This is also the case for the systematic investigation of neutron inelastic scattering discussed above [15]. Thus in order to test the usefulness of this set of generalized parameters for nuclei in the mass range covered by the fission products, calculations of inelastic scattering cross sections have recently been made by Ramström [40] in the energy range from threshold up to about 1.5 MeV for some fission products, i.e. ^{98}Mo, ^{100}Mo, ^{103}Rh, ^{133}Cs, ^{139}La and ^{141}Pr. The results show that the experimental data for most of the investigated levels are well described within the quoted experimental uncertainties. Exceptions are a few levels in ^{100}Mo and ^{139}La. Calculations were also made using the Igarasi potential [41]. However, the experimental inelastic scattering cross sections are as a rule better described by those calculated with the Studsvik potential than with the Igarasi potential.

4. COMPUTER PROGRAMS

A number of computer codes exist for calculations of neutron cross sections using the optical model as well as the Hauser-Feshbach formalism. Only one of them, viz. ABACUS-NEARREX [42], which is widely used, will be very shortly commented upon as regards its potentialities. ABACUS (in the versions ABACUS II and ABACUS-NEARREX) is the program mainly used in the calculations discussed in this report.

The ABACUS-NEARREX (the ANL version) is a computer code for optical model calculations of total, shape elastic and absorption cross sections. The optical potential is chosen in its ordinary form. Different types of form factors are available to describe the radial shapes of the real, imaginary and spin-orbit parts of the potential. Furthermore, the imaginary part can be of both surface and volume absorption character. It is most important that a search routine is included in the program, making it possible to vary automatically up to five of the potential parameters in order to get the best fit between calculated and experimental cross sections. Provision is made for the computation of compound elastic and inelastic neutron cross sections according to the Hauser-Feshbach formalism [28], including, if desired, the Moldauer [30] corrections, as well as of radiative capture and fission cross sections. For technical reasons, such as the size of the computer memory and the running time of the computer, the program can handle only a limited number of levels. At present it is possible to include up to 50 levels in the Studsvik version of the program. For nuclei in which more levels are excited pure Hauser-Feshbach calculations can be performed with a computer program HAFEX [43] using the transmission coefficients calculated with ABACUS-NEARREX. In order to reduce the number of levels for which the transmission coefficients have to be calculated for nuclei with many close-lying states, the levels in different excitation energy intervals may in this program be grouped according to their spins and parities.

Another method to calculate the inelastic cross sections if the number of excited states is comparatively large in the target nucleus is to describe the distribution of levels by a level density formula. This computer facility is important for the calculation of compound nucleus cross sections at such high neutron energies that there is no detailed knowledge of the level scheme of the target nucleus. This option is not included in ABACUS-NEARREX, but is in some other codes, for instance HELENE [44].

Beside the ABACUS-NEARREX computer code there are a large number of optical model programs. The following may be mentioned: MAGALI (Saclay), GENOA 2 (ORNL), ADAPE (CNEN, Bologna), 2-PLUS (AI) and JUPITER (ORNL). The last three programs have been developed for deformed nucleus optical model calculations.

The experience from test runs of existing versions of major computer codes widely used in different laboratories has shown that they may be inconsistent with one another. The problem seems to be a matter of the computational procedure and is probably widespread, since calculations carried out with the same parameters and programs but different computers fail to give the same results. It is evident that considerable attention should be paid to this problem. It is recommended that computer code versions should be checked by running specific standard test programs.

5. CONCLUDING REMARKS

The problems connected with the production and use of neutron scattering data have been treated in such a way as to present the results and conclusions in a manner easy to understand by the user of cross section data in applied fields of nuclear physics.

The neutron elastic and inelastic scattering studies, some results and experiences of which have been discussed in the previous paragraphs, have been performed in an attempt to check existing nuclear theories and models.

Such studies are necessary at the present state of the art of theoretical nuclear physics in order to give the user of neutron data simple tools to estimate cross sections with the necessary accuracy, since the optical model and the Hauser-Feshbach model, when specifically used to calculate scattering cross sections, are virtually useless for this purpose unless some information founded on experimental results and experience is stored in the fundamental expressions of the models. Some such information is stored in the parameters of the nuclear optical potential, the numerical values of which were deduced by extensive studies and intercomparisons of experimental results and numerical calculations. By this technique it has been possible to estimate the magnitudes of several of the parameters. The estimation of cross section values of the accuracy required for reactor physics applications has been simplified by the design of global sets of expressions of the parameters. The accuracy which can be obtained by using such a set in a large mass or energy region is of course limited by the statistical amount of experimental data available. The experimental data must be of high quality and be well distributed in respect of atomic mass number and energy. With regard to measurements of cross sections to be used for this purpose it may be necessary to judge whether the experiments should be made in such detail that single isotopes have to be studied or whether, to satisfy the requirement of high-quality experimental and calculated data, the natural elements can serve the purpose. This is an important point, since enriched isotopes of specific elements are usually difficult to obtain for many laboratories.

Problems in generalizing the parameter sets associated with nuclear structure effects may be overcome by limiting the data descriptions to those mass ranges which can be expected to be of highest technological priority and deducing separate optical model data sets for each of these regions. It would be possible to get model sets giving the highest cross section accu-

racy needed for each applied purpose in reactor physics. This approach to the problem may, of course, be satisfactory for the user of data, but not from the pure physics point of view, neither experimentally nor theoretically. To meet these latter requirements it is necessary to study the scattering processes in detail with the utmost precision in order to find out the properties of every single isotope. This is a very ambitious and interesting task but the question is whether it is necessary in order to meet the needs of future applications of neutron elastic and inelastic scattering cross sections for fission and fusion reactor physics. The user of the data must have the competence to specify a realistic value of the accuracy required for each specific nucleus. This accuracy may differ from isotope to isotope depending on its application.

The calculations of reliable neutron inelastic scattering cross sections are in some respects more complicated than those of elastic scattering. There are a number of reasons for this circumstance associated with the model picture of the scattering process, i.e. the creation of a compound nucleus and its decay via a number of channels related to individual levels with different characteristics such as single particle configurations, nuclear deformations and rotational bands. Often a vast amount of information on energies, spins and parities has to be known for a whole band of individual levels otherwise accurate cross sections cannot be calculated. Such information on level data can only be obtained by the combined efforts of experimental and theoretical nuclear physics. Recent view-points on and problems associated with the theoretical description of inelastic scattering observations have been discussed by Moldauer [45] at this meeting.

The present discussion of neutron scattering processes has been limited to applications in the fission reactor field, with the natural overlap to fusion reactor problems. This approach has been considered natural and adequate since the main application of neutron data is and has been in reac-

tor physics. The bulk of existing systematically collected experimental scattering data have also been produced on requests from the reactor physics community. There is, however, still a large volume of information lacking which, with regard to its use in calculations for fission reactors may be estimated with adequate accuracy by application of the present knowledge of the behaviour of the nuclear models. On the other hand cross sections for fusion reactor development are needed to a large extent at energies up to 14 MeV, i.e. far above those of the fission reactor, and thus simultaneous systematic experimental and theoretical studies are necessary in order to develop adequate model descriptions applicable in this field.

REFERENCES

[1] OKRENT, D., Conf. on Neutron Cross Section Technology, March 22-24, 1966, Washington D.C., Conf-660303 Book 1 (1966) 430.

[2] GREEBLER, P., HUTCHINS, B.A., Conf. on Neutron Cross Section Technology, March 22-24, 1966, Washington D.C., Conf-660303 Book 1 (1966) 357.

[3] GREEBLER, P., HUTCHINS, B.A., COWAN, C.L., Second Int. Conf. on Nuclear Data for Reactors, June 15-19, 1970, Helsinki, IAEA Vienna Vol. I (1970) 17.

[4] GREEBLER, P., HUTCHINS, B.A., WOLFE, B., Proc. Conf. on Neutron Cross Sections and Technology, March 4-7, 1968, Washington D.C., NBS Special Publication 299 Vol. 1 (1968) 291.

[5] KOUTS, H.J.C., Bull. Am. Phys. Soc. Series II 20 (1975) 134.

[6] UOTINEN, V.O., ROBERTSON, J.D., TULENKO, J.S., Bull. Am. Phys. Soc. Series II 20 (1975) 134.

[7] SHURE, K., Nucl. Sci. Eng. 19 (1964) 17.

[8] WRENDA 75, World request list for nuclear data measurements, INDC(SEC)-46/U+R+F+S (1975).

[9] CINDA 75, An index to the literature on microscopic neutron data, IAEA, Vienna, 1975.

[10] SMITH, A.B., et al., Phys. Rev. 135B (1964) 76; Nucl. Phys. A93 (1967) 609; Phys. Rev. C1 (1970) 581; Argonne National Laboratory Report ANL/NDM-7 (1974).
BARNARD, E., et al., Nucl. Phys. A118 (1968) 321; ANL/NDM-3 (1973).
GUENTHER, P.T., et. al., ANL/NDM-1 (1973); ANL/NDM-4 (1974).
VONACH, W.G., SMITH, A.B., Nucl. Phys. 78 (1966) 389.
LISTER, D., SMITH, A.B., Phys. Rev. 183 (1969) 954.

[11] KINNEY, W.E., Oak Ridge National Laboratory Report ORNL-TM-2052 (1968).
PEREY, F.G., KINNEY, W.E., ORNL-4441 (1969); ORNL-4518 (1970);

ORNL-4519 (1970); ORNL-4539 (1970); ORNL-4551 (1970); ORNL-4552 (1970).
KINNEY, W.E., PEREY, F.G., ORNL-4517 (1970); ORNL-4549 (1970); ORNL-4550 (1970); ORNL-4780 (1972).

[12] HOLMQVIST, B., Arkiv Fysik 38 (1968) 403.

[13] HOLMQVIST, B., WIEDLING, T., Atomic Energy Company Report AE-430 (1971); J. Nucl. Energy 27 (1973) 543.

[14] HOLMQVIST, B., WIEDLING, T., Nucl. Phys. A188 (1972) 24.
CORCALCIUC, V., HOLMQVIST, B., WIEDLING, T., Nucl. Phys. A232 (1974) 436.
ETEMAD, M.A., Atomic Energy Company Report AE-481 (1973); AE-482 (1973); AE-485 (1974).

[15] ALMÉN-RAMSTRÖM, E., Atomic Energy Company Report AE-503 (1975).

[16] HOLT, R.J., SMITH, A.B., WHALEN, J.F., Bull. Am. Phys. Soc. Series II 20 (1975) 145.
GUENTHER, P., SMITH, A.B., Bull. Am. Phys. Soc. Series II 20 (1975) 171.
WIEDLING, T., Neutron Physics Laboratory Annual Progress Report July 1, 1974 - June 30, 1975. Atomic Energy Company Report S-501 (1975).
MICHAUDON, A., Centre d'Études de Bruyères-le-Châtel. Compte rendu d'activite du service de physique nucleaire pour l'annee 1974, CEA-N-1798 (1975).

[17] HODGSON, P.E., The optical model of elastic scattering, Clarendon Press, Oxford, 1963.

[18] HODGSON, P.E., Nuclear reactions and nuclear structure, Clarendon Press, Oxford, 1971.

[19] HODGSON, P.E., Theories of neutron inelastic scattering, EANDC(UK) 76"AL".

[20] WALT, M., BARSCHALL, H.H., Phys. Rev. 93 (1954) 1062.

[21] FESHBACH, H., PORTER, C.E., WEISSKOPF, V.F., Phys. Rev. 96 (1954) 448.

[22] BRUECKNER, K.A., Proc. Int. Conf. on the Nuclear Optical Model, Tallahassee (Eds. A.E.S. Green, C.I. Porter, D.S. Saxon, Tallahassee) (1959) 145.

[23] WATSON, K.M., Phys. Rev. 89 (1958) 575.

[24] PEREY, F.G., BUCK, B., Nucl. Phys. 32 (1962) 353.

[25] WILMORE, D., HODGSON, P.E., Nucl. Phys. 55 (1964) 673.

[26] ENGELBRECHT, C., FIEDELDEY, H., Ann. Phys. 42 (1967) 262.

[27] LANE, A.M., Nucl. Phys. 35 (1962) 676.

[28] HAUSER, W., FESHBACH, H., Phys. Rev. 87 (1952) 366.

[29] PORTER, C.E., THOMAS, R.G., Phys. Rev. 104 (1956) 483.

[30] MOLDAUER, P.A., Phys. Rev. 135B (1964) 642; Rev. Mod. Phys. 36 (1964) 1079.

[31] MOLDAUER, P.A., Phys. Rev. 11C (1975) 426.

[32] TOBOCMAN, W., Theory of direct nuclear reactions, Oxford University Press, Oxford, 1961.

[33] BOHR, A., MOTTELSON, B.R., Kgl. Dan. Videnskab. Selskab. Mat. Fys. Medd. 27 16 (1953).

[34] TAMURA, T., Rev. Mod. Phys. 37 (1965) 679.

[35] FOSTER, D.G., Jr., GLASGOW, D.W., Phys. Rev. 3C (1971) 576.

[36] CIERJACKS, S., FORTI, P., KOPSCH, D., KROPP, L., NEBE, J., UNSELD, H., KFK 1000/EUR 3963e/EANDC(E)-111"U" (1968).

[37] GILBERT, A., CAMERON, A.G.W., Can. J. Phys. 43 (1965) 1446.

[38] GOLDHABER, M., DER MATEOSIAN, E., SCHARFF-GOLDHABER, G., SUNYAR, A.W., DEUTSCH, M., WALL, N.S., Phys. Rev. 83 (1951) 661.

[39] SHAFROTH, S.M., TREHAN, P.N., VAN PATTER, D.M., Phys. Rev. 129 (1963) 704.

[40] RAMSTRÖM, E., To be published.

[41] IGARASI, S., et al., Japan Atomic Energy Research Institute Report JAERI-M 5752 (1974).

[42] MOLDAUER, P.A., ENGELBRECHT, C.A., DUFFY, G.J., Argonne National Laboratory Report ANL-6978 (1964).

[43] ERIKSSON, J., Private communication.

[44] PENNY, S.K., Oak Ridge National Laboratory Report ORNL-TM-2590 (1969).

[45] MOLDAUER, P.A., these Proceedings, review paper 2.

TABLE I Numerical parameter data, cross sections and χ^2-values from 5-parameter optical model search procedures for Al, Mn, Fe, Co, Cu, Zn, As, Cd, Au and Bi for input parameter values of r_{oU} of 1.0, 1.2 and 1.3 fm at 8.05 MeV neutron energy. Also experimental total elastic (σ_{el}^{exp}) [13] and total (σ_T^{exp}) [35] cross sections are given.

Element		Al			Mn			Fe			Co			Cu		
r_{oU}^{input}	f_m	1.0	1.2	1.3	1.0	1.2	1.3	1.0	1.2	1.3	1.0	1.2	1.3	1.0	1.2	1.3
U	MeV	57.04	49.9	49.76	52.54	50.5	47.66	54.33	49.3	48.56	56.24	51.3	53.76	49.7	47.5	44.58
W	MeV	7.02	7.14	7.37	8.11	8.04	7.99	10.58	10.45	10.44	9.56	10.04	9.44	10.12	10.11	10.01
r_{oU}	fm	1.05	1.22	1.217	1.16	1.19	1.23	1.151	1.23	1.232	1.131	1.19	1.163	1.19	1.22	1.277
r_{oW}	fm	1.27	1.24	1.24	1.16	1.17	1.17	1.23	1.20	1.20	1.14	1.17	1.108	1.22	1.18	1.18
a	fm	0.71	0.65	0.64	0.66	0.65	0.62	0.655	0.64	0.638	0.67	0.66	0.639	0.70	0.68	0.679
σ_T	b	1.728	1.78	1.78	3.18	3.21	3.25	3.18	3.31	3.31	3.24	3.36	3.26	3.55	3.58	3.79
σ_A	b	0.99	1.01	1.02	1.31	1.32	1.34	1.43	1.47	1.47	1.39	1.46	1.37	1.59	1.57	1.63
σ_{se}	b	0.74	0.77	0.76	1.88	1.89	1.91	1.74	1.85	1.84	1.84	1.90	1.89	1.97	2.01	2.16
σ_{ce}	b	0	0	0	0	0	0	0	0	0	0	0	0	0	0	0
σ_{el}	b	0.74	0.77	0.76	1.88	1.89	1.91	1.74	1.85	1.84	1.84	1.90	1.89	1.97	2.01	2.16
χ^2		5.81	6	6.9	7.2	8	8.0	2.3	2	2.3	2.4	4.8	2.4	1.16	0.73	1.45
σ_T^{exp}	b	1.68±0.05			3.32±0.09			3.31±0.09			3.52±0.08			3.63±0.05		
σ_{el}^{exp}	b	0.81±0.04			1.94±0.14			1.76±0.09			1.82±0.09			2.00±0.10		

Element		Zn			As			Cd			Au			Pb_{rad}		
r_{oU}^{input}	f_m	1.0	1.2	1.3	1.0	1.2	1.3	1.0	1.2	1.3	1.0	1.2	1.3	1.0	1.2	1.3
U	MeV	35.23	49.4	47.37	39.74	48.95	47.42	30.87	49.49	49.3	37.00	45.48	43.01	48.94	44.5	44.75
W	MeV	12.25	10.8	11.05	9.81	9.73	9.92	8.24	9.55	9.47	6.33	6.29	7.24	5.83	6.21	5.98
r_{oU}	fm	0.66	1.20	1.231	0.79	1.224	1.243	0.95	1.20	1.21	0.89	1.23	1.29	1.17	1.25	1.247
r_{oW}	fm	1.27	1.19	1.184	1.24	1.17	1.182	1.32	1.27	1.27	1.32	1.27	1.27	1.33	1.28	1.28
a	fm	0.69	0.70	0.689	0.672	0.668	0.668	0.67	0.68	0.68	0.62	0.65	0.636	0.68	0.65	0.652
σ_T	b	2.86	3.62	3.66	2.67	3.79	3.88	3.55	3.97	3.96	5.30	4.93	5.21	5.54	5.51	5.50
σ_A	b	1.41	1.62	1.63	1.42	1.62	1.66	1.91	1.99	1.99	2.32	2.32	2.53	2.50	2.46	2.45
σ_{se}	b	1.44	2.00	2.02	1.25	2.18	2.22	1.65	1.98	1.96	2.98	2.60	2.68	3.03	3.04	3.05
σ_{ce}	b	0	0	0	0	0	0	0	0	0	0	0	0	0	0	0
σ_{el}	b	1.44	2.00	2.02	1.25	2.18	2.22	1.65	1.98	1.96	2.98	2.60	2.68	3.03	3.04	3.05
χ^2		12.1	5	5.8	116	18	21	6.8	2.4	2.7	195	0.7	28	4.7	2	1.5
σ_T^{exp}	b	3.68±0.08			4.00±0.05			4.25±0.10			5.19±0.10			5.57±0.12		
σ_{el}^{exp}	b	1.82±0.09			2.37±0.11			1.62±0.2			2.30±0.2			2.70±0.2		

FIGURE CAPTIONS

Fig. 1 Elastic neutron scattering angular distributions of Al, Mn, Fe and Co at 8.05 MeV calculated with optical model parameter sets obtained in 5-parameter search procedures with input values of r_{oU} of 1.0 (dashed lines) and 1.2 fm (solid lines). The circles represent experimental cross sections [12,13].

Fig. 2 Angular distributions of elastically scattered 3 MeV neutrons calculated with the optical model formalism by the 5-parameter search routine (solid lines) and using Studsvik generalized optical model parameters (dashed lines) [13]. The circles represent experimental cross sections [12].

Fig. 3 Comparisons between experimental and calculated total cross sections. The calculations were made with the Studsvik generalized optical model parameters. The experimental cross sections are those of Foster et al. (open circles) [35] and Cierjacks et al. (filled circles) [36].

Fig. 4 Neutron elastic scattering angular distributions of Co and Pb at 6.09 MeV and 8.05 MeV, respectively, calculated with Studsvik (solid lines) and Wilmore-Hodgson (dashed lines) optical model parameters. The circles represent experimental cross sections [12,13].

Fig. 5 Inelastic neutron scattering excitation functions in the energy range 2 to 4.5 MeV for levels in V and Y. The solid lines represent pure HF calculations. The dashed and point dashed lines are modified HF calculations with Q_α = 0 and 1, respectively.

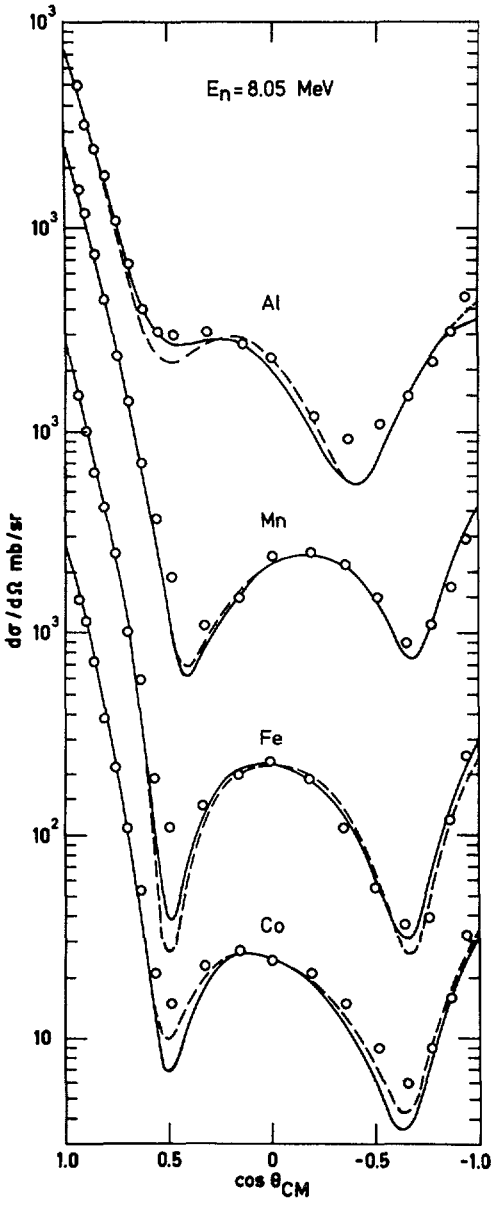

Fig. 1 Elastic neutron scattering angular distributions of Al, Mn, Fe and Co at 8.05 MeV calculated with optical model parameter sets obtained in 5-parameter search procedures with input values of r_{oU} of 1.0 (dashed lines) and 1.2 fm (solid lines). The circles represent experimental cross sections [12,13].

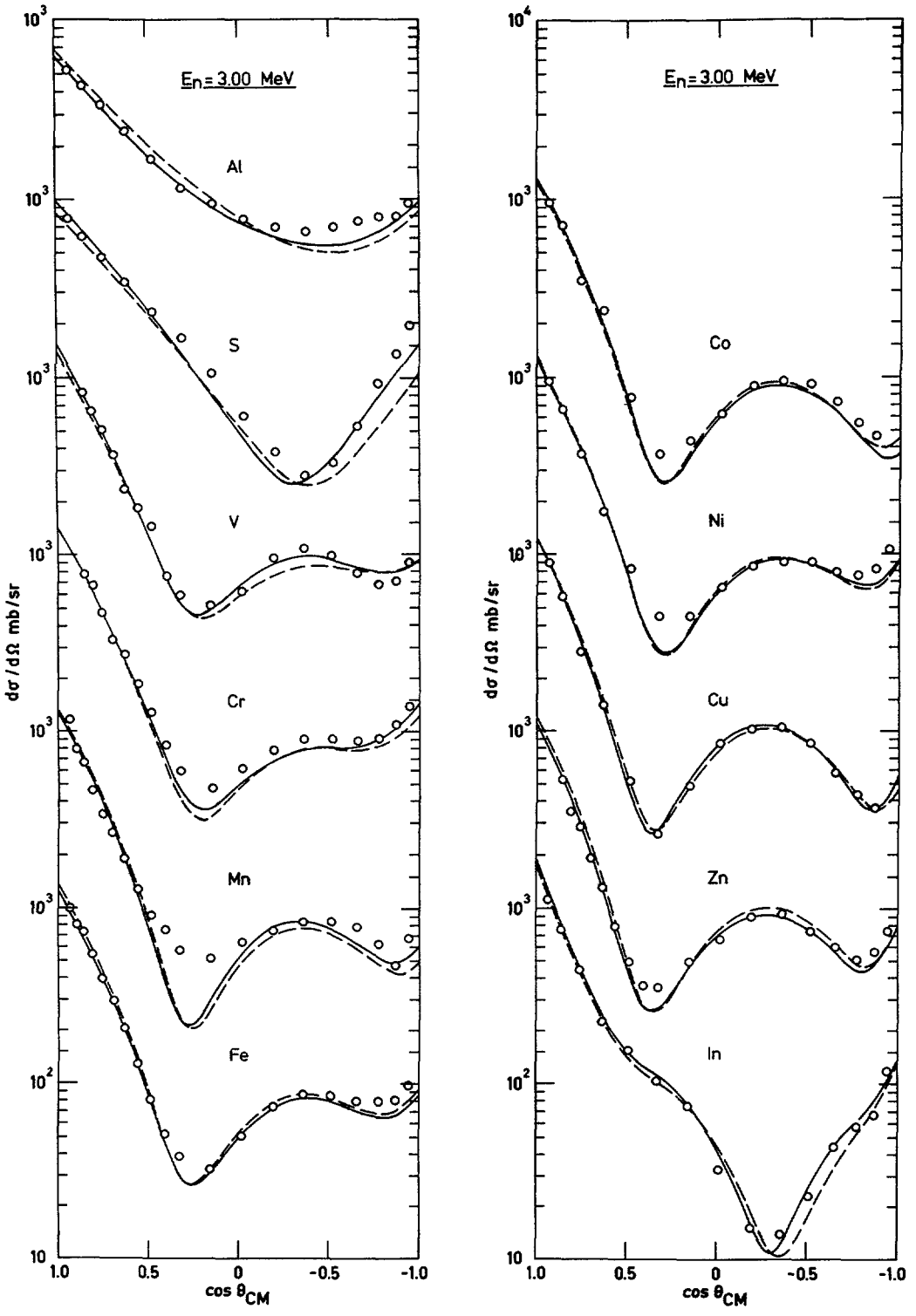

Fig. 2 Angular distributions of elastically scattered 3 MeV neutrons calculated with the optical model formalism by the 5-parameter search routine (solid lines) and using Studsvik generalized optical model parameters (dashed lines) [13]. The circles represent experimental cross sections [12].

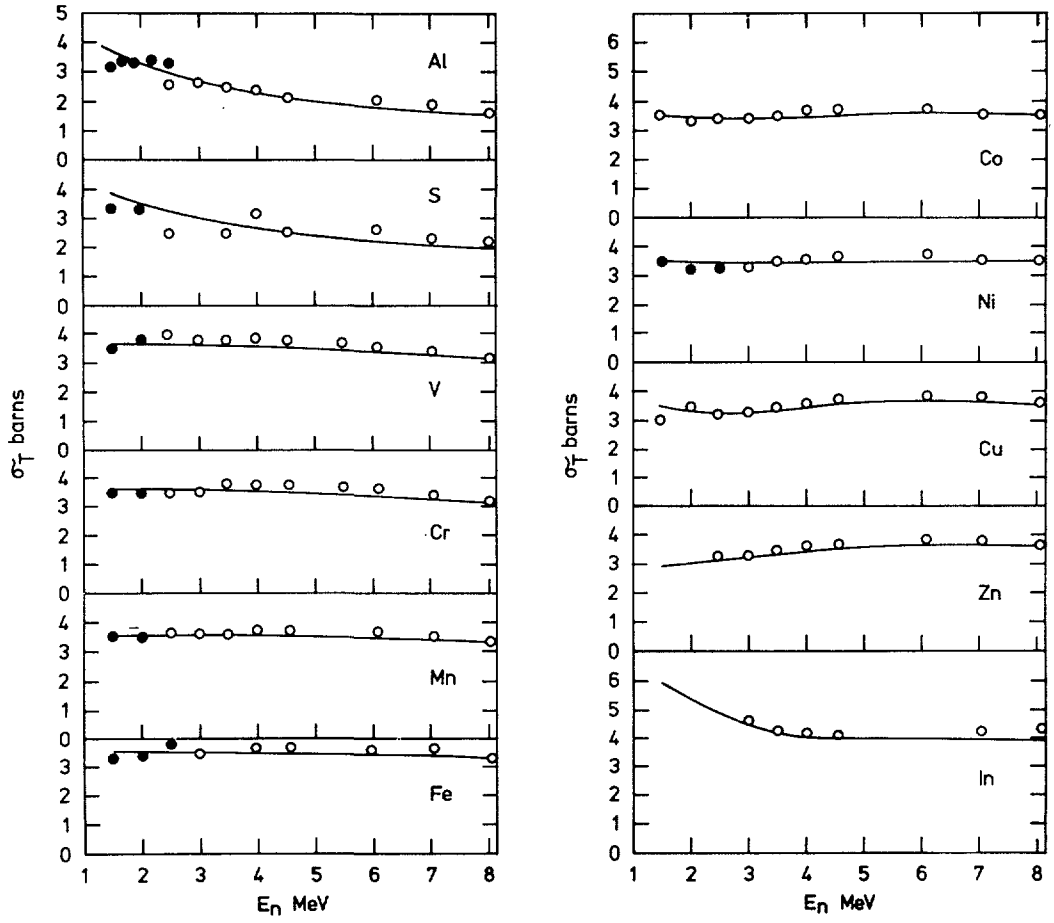

Fig. 3 Comparisons between experimental and calculated total cross sections. The calculations were made with the Studsvik generalized optical model parameters. The experimental cross sections are those of Foster et al. (open circles) [35] and Cierjacks et al. (filled circles) [36].

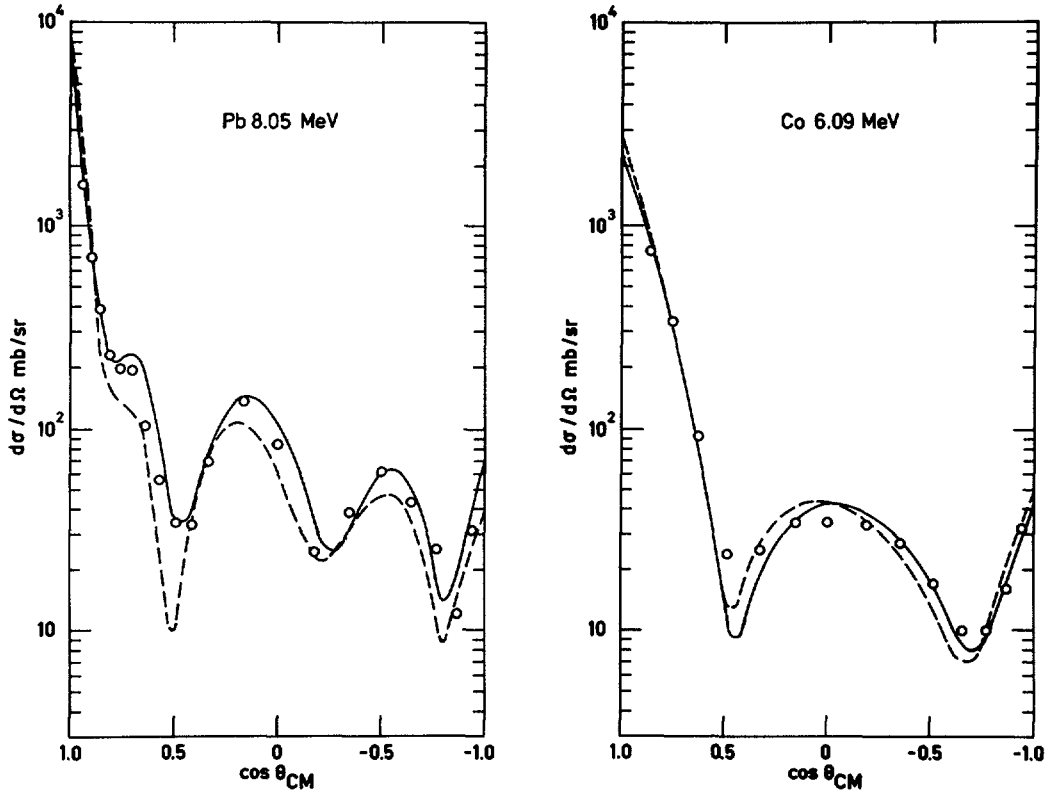

Fig. 4 Neutron elastic scattering angular distributions of Co and Pb at 6.09 MeV and 8.05 MeV, respectively, calculated with Studsvik (solid lines) and Wilmore-Hodgson (dashed lines) optical model parameters. The circles represent experimental cross sections |12, 13|.

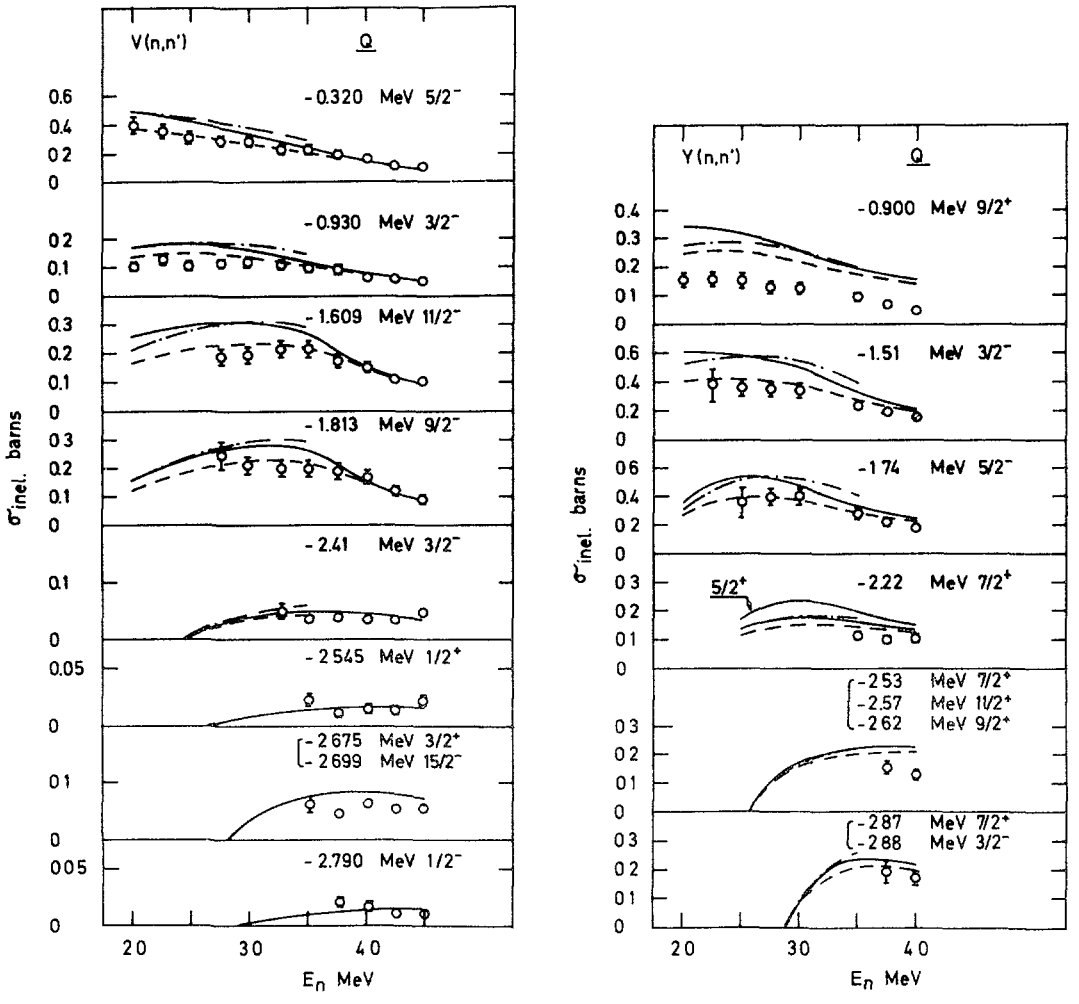

Fig. 5 Inelastic neutron scattering excitation functions in the energy range 2 to 4.5 MeV for levels in V and Y. The solid lines represent pure HF calculations. The dashed and point dashed lines are modified HF calculations with Q_α = 0 and 1, respectively.

AE:s kontorstryckeri
Nyköping 1975

Contributed Paper No. 10

ANALYSIS OF DIFFERENTIAL ELASTIC AND INELASTIC SCATTERING CROSS SECTIONS BY THE HAUSER-FESHBACH THEORY

T. Schweitzer, D. Seeliger, K. Seidel, S. Unholzer
Section of Physics, Technical University Dresden, GDR

Abstract:

The differential elastic and inelastic scattering cross sections of 3.4 MeV neutrons for the elements Na, Mg, Al, Si, P, V, Mn, Fe, Co, Pb and Bi have been determined experimentally. The measured angular distributions are compared with optical model and Hauser-Feshbach theory calculations performed with the program ELISA.

1. INTRODUCTION

At the Technical University Dresden an extensive investigation program on inelastic scattering in the neutron energy range around 3 MeV is carried out. As yet, differential elastic and inelastic scattering cross-sections at 3.4 MeV for 11 elements have been measured.

The main purposes of this work are the following:

- to test the reaction mechanism at comparatively low incident energy by comparison with the statistical theory of nuclear reactions,
- to obtain an absolute and consistent description of both elastic and inelastic scattering channels over a wide mass number region
- and, last not least, to get accurate nuclear data for application.

The present paper presents some preliminary results of this work.

2. EXPERIMENTAL RESULTS

The measurements were carried out on the 500 keV pulsed beam DD-neutron generator of the Technical University. Scattered neutrons were measured with the time-of-flight method in the energy range from 1 - 3.4 MeV between 15° and 150°. A more dedaited description of the experimental method is given elsewhere [1].

The main part of data handling and analysis was carried out with computer techniques on the BESM-6 computer.

Experimental results are corrected for detector efficiency, neutron flux attenuation, multiple scattering, isotopic composition of the scattering sample, finite dimensions of scatterer and other effects. Statistical errors of the peak areas have been estimated to be less than 1% for the elastic scattering and better than 5% for inelastic scattering. Systematic errors of the angular distribution data are mostly due to geometrical uncertainties in the distance between target and scattering sample and to uncertainties in the unfolding of time-of-flight peaks (between 1 and 30 %) which in some cases overlap strongly. Such errors are stated in the figures 1 to 4.

Moreover the absolute calibration of the experiment is subject to some errors, which influence all points of the angular distribution in the same manner. A maximum inaccuracy of 8 % in the determination of incident neutron flux is caused by the ignorance of the true distribution function of deuterium molecules in the target matter and by uncertainties in the cross sections of the D(d,n) and D(d,p) reactions. The error of detector efficiency was estimated to be around 5 %, caused by inaccuracies in the light yield curves for compton electrons and recoil protons.

But this values represent the upper limit of systematic errors in the cross sections. Comparison with standard data shows, that the total errors in σin are between 10 and 15 %.

3. THEORETICAL ANALYSIS

The experimental cross sections have been compared with theoretical predictions, which consist of calculations of the shape elastic scattering cross sections by the optical model and of the compound reaction components by Hauser-Feshbach theory with Moldauer fluctuation corrections. Both type of calculations were carried out with the computer program ELISA [2], which includes the following possibilities:

- calculations in the framework of a usual spherical optical potential;
- calculations of compound nuclear processes in the framework of Hauser-Feshbach statistical theory, either with or without Moldauer fluctuation corrections. In these calculations, besides the discrete levels of final nuclei, a continuous part of final states, with definite level density parameter a and spin cut-off factor σ , may be included.
- Calculations are possible for spins 0, 1/2 and 1 of incoming or outgoing particles.

In the present work optical potential parameters from Holmqvist [3] were used for all calculations, so that no fitting procedure was needed. In the statistical theory calculations the open proton and alpha channels have been taken into account.

4. RESULTS AND DISCUSSION

In figs. 1-4 comparison between experiment and theory is shown for some typical representatives of light, medium and heavy nuclei.

Altogether, the computed elastic differential cross sections are in good accordance with experimental results. In all cases besides the shape elastic reaction a considerable compound elastic part must be added to the cross section. In the case of ^{28}Si the compound elastic part seems to be overestimated by the statistical theory (see fig. 2).

The calculated inelastic cross section is in good agreement with the experimental results for the first 2^+-state of ^{24}Mg (see fig. 1). It seems, that no essential contributions of other reaction mechanisms in this case are evident.

For ^{28}Si (see fig. 2) there are striking deviations between calculations and experiment for both elastic and inelastic (2^+ level at 1.77 MeV) cross sections. If we assume, that the compound nucleus formation cross section is overestimated by a factor 2, than we get a satisfactory description of elastic scattering. But in this case the existing discrepancies for inelastic scattering are increased, leading to the assumption, that for the excitation of the 2^+ state an other (direct) reaction mechanism is responsible. A reason for this behaviour is probably due to the considerable deformation of the ^{28}Si ground state. Further investigations of this point are needed.

The differential elastic scattering cross section for ^{56}Fe (see fig. 3) is in a good agreement with calculations, whereas the experimental inelastic cross section for the first 2^+ state at 0,84 MeV is considerably higher than the results of calculations by the statistical theory. We assume that this is due to direct excitation processes.

Also for the heavy nucleus ^{209}Bi (fig. 4) elastic scattering is well described by the program employed. In the case of inelastic scattering the situation is different for the two excited levels: For the first excited $7/2^-$ state at 0.91 MeV both shape and magnitude of statistical theory calculation are in

satisfactory agreement with experiment. A small probably direct contribution is evident. The calculations, corresponding to the second state at 1.61 MeV are based on the spin-parity assigument $J^{\pi} = 13/2^{+}$ [4]. Theoretical predictions only in this one case are higher than experimental cross sections, and the shape of angular distributions is also different. Further calculations are needed, especially with other J^{π} -assignments.

5. SUMMARY

- It was shown by some examples, that the differential elastic scattering cross section at 3.4 MeV neutron energy may be well described by the computer program ELISA, including both shape elastic and compound elastic contributions. The Holmqvist optical parameters have been found to be a very useful parameter set for this purpose.
- The experimental differential inelastic scattering cross sections in general are not completely reproduced by the statistical Hauser-Feshbach theory including Moldauer fluctuation corrections. We assume, that additional direct contributions must be taken into account, even in this comparatively low energy region around 3 MeV. Further theoretical investigations are needed to confirm this assumption.

REFERENCES

[1] SCHWEITZER, Th., et al., ZfK-Report, ZfK-283 (1974) 7
SCHWEITZER, Th., et al., Mat. IV. Symposium on Interactions of Fast Neutrons with Nuclei,
Gaussig, Nov. 1974 (to be publ. in Wiss. Zeitschr. TU Dresden, 1975)
KAISER, U. et al., TU Dresden Report, TU-Informationen 05-4o-75, 1975

[2] KIESSIG, G., Dissertation TU Dresden 1975

[3] HOLMQVIST, B. and WIEDLING, T.,
Journal of Nuclear Energy Vol 27 pp 543 (1973)

[4] TANAKA, S. et al., Nucl. Phys. A179 513-523 (1972)

FIGURE CAPTIONS

Fig. 1 Differential elastic and inelastic scattering cross sections in the center of mass system for ^{24}Mg at 3.4 MeV incident energy.
Theoretical curves (full lines) are calculated with the program ELISA [2] including optical model and statistical Hauser-Feshbach calculations with Holmqvist's optical model parameter set [3].
a) elastic scattering; T - total elastic, S - shape elastic and C - compound elastic contributions.
b) inelastic scattering with excitation of the 1-st state.

Fig. 2 The same as on Fig. 1, but for ^{28}Si

Fig. 3 The same as on Fig. 1, but for ^{56}Fe

Fig. 4 The same as on Fig. 1, but for ^{209}Bi; in this case the first (open circles) and second (full points) excited states have been measured and calculated (broken line and full line, respectively).

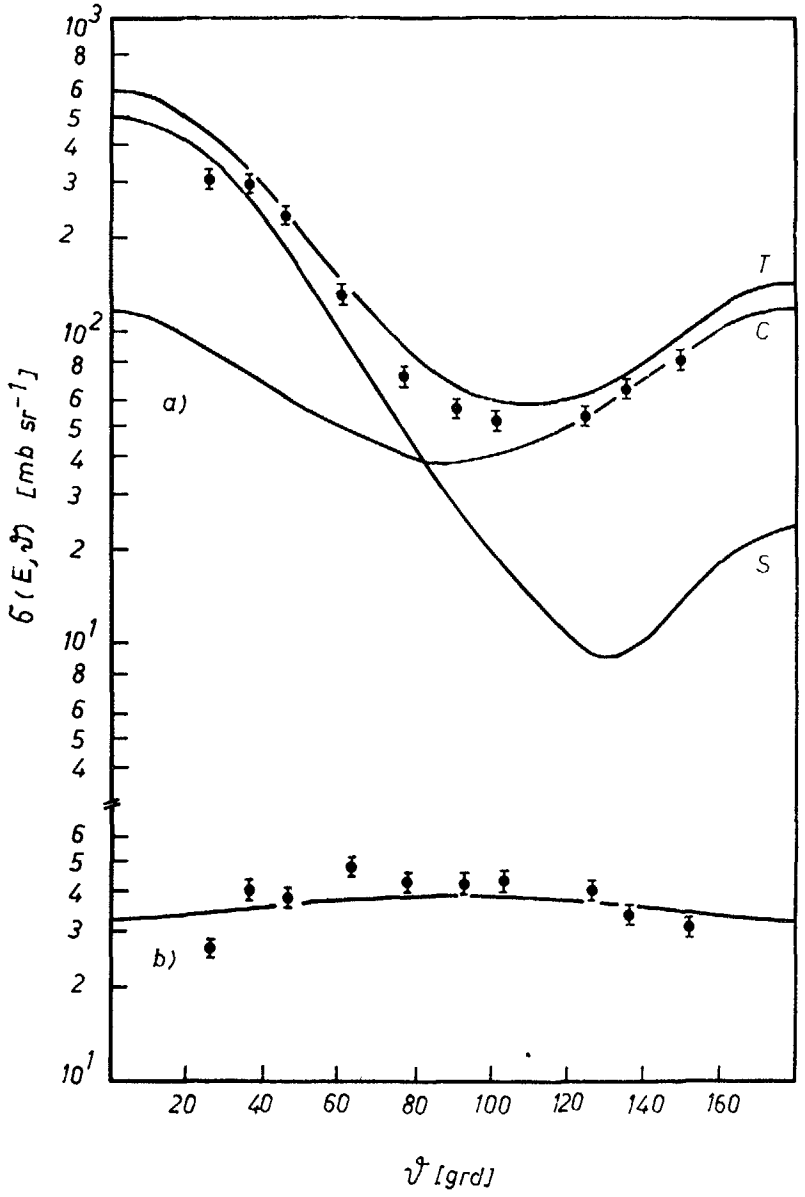
10^3
8
6
5
4
3
2
10^2
8
6
5
4
3
2
10^1
8
6
5
4
6
5
4
3
2
10^1
T
C
S
a)
b)
20
40
60
80
100
120
140
160
$\sigma(E,\vartheta)$ [mb sr^{-1}]
ϑ [grd]

Fig. 1

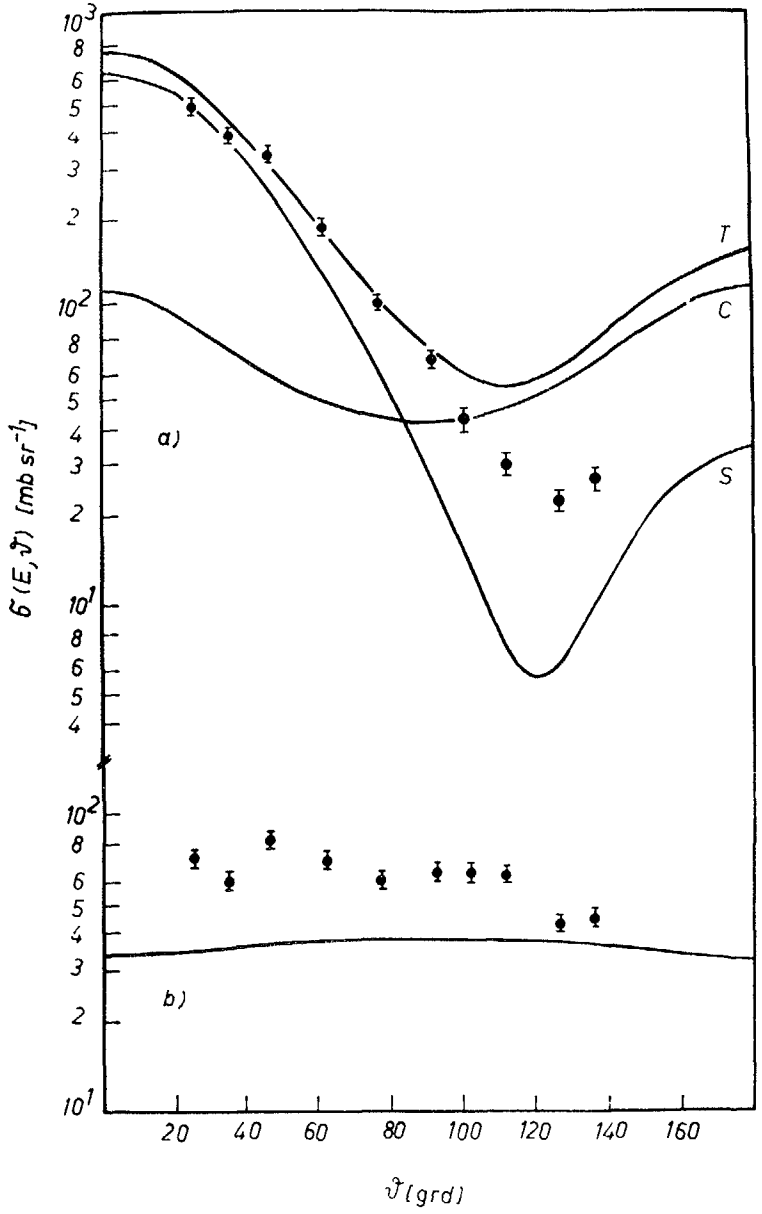
10^3
8
6
5
4
3
2
10^2
8
6
5
4
3
2
10^1
8
6
5
4
10^2
8
6
5
4
3
2
10^1
T
C
S
a)
b)
20
40
60
80
100
120
140
160
$\sigma(E,\vartheta)$ [mb sr^{-1}]
ϑ (grd)

Fig. 2

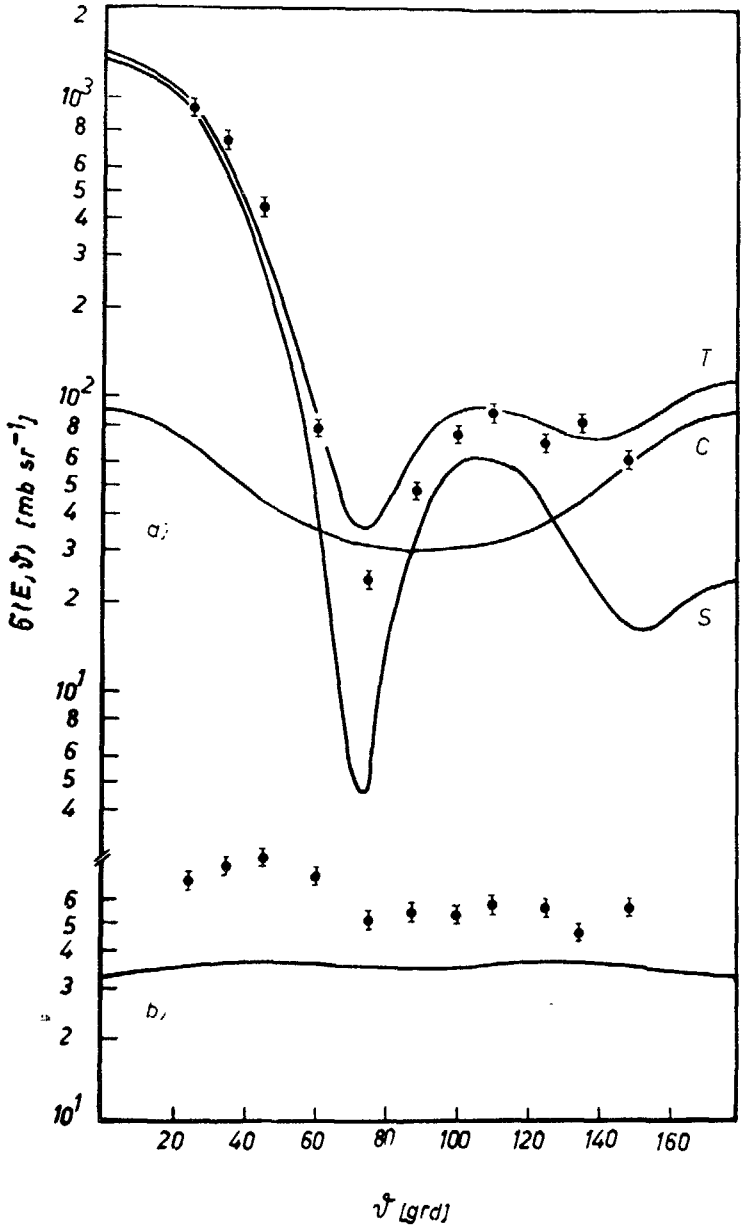

Fig. 3

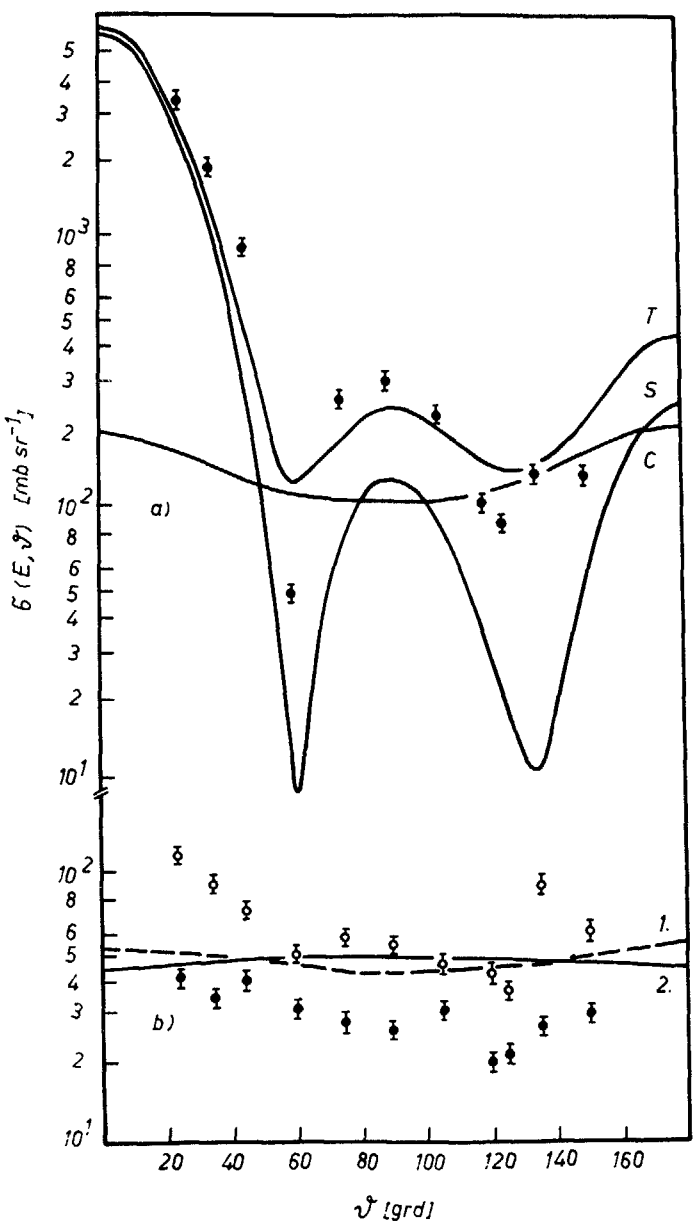

Fig. 4

Contributed Paper No. 11

NUCLEAR MODEL CODES AVAILABLE AT THE NUCLEAR ENERGY AGENCY COMPUTER PROGRAM LIBRARY (NEA-CPL).

ENRICO SARTORI (IAEA OFFICER AT THE NEA-CPL)
LUIS GARCIA DE VIEDMA (HEAD OF THE NEA-CPL)

ABSTRACT

This paper briefly outlines the objectives of the NEA-CPL and its activities in the field of Nuclear Model Computer Codes. A short description of the computer codes available from the CPL in this field is also presented.

- - - - - -

In 1964 the Nuclear Energy Agency (NEA) of the Organization for Economic Co-operation and Development (OECD) established a Computer Program Library at Ispra, Italy. Thirteen European countries plus Japan and Australia contribute to the financing of the CPL, which from the very beginning has operated in close collaboration with centres providing similar services in North America, namely the United States Code Center (USCC) at Argonne National Laboratory and the Radiation Shielding Information Center (RSIC) at Oak Ridge National Laboratory. In addition, a number of other countries maintain links with the CPL through the International Atomic Energy Agency (IAEA).

The major objective of the CPL is to avoid excessive duplication of effort in programming by making existing computer codes more widely available, and to achieve through the collection, testing and re-distribution of computer programs in the field of reactor physics and technology, an improved use of these programs and an accelerated development of new and more advanced codes based on the exchange of users' experience and proposals for improvement (1).

The collaboration established by the CPL with nuclear centres through a very well tried and tested circuit of liaison officers, has always insured a good input of the programs available in this field. Thereafter, the program packages are made available to other CPL member establishments upon request, on a free of charge basis.

The CPL user community is kept informed of Library activities through a series of publications such as Computer Program Abstracts, Index of Nuclear Programs and Newsletters. Seminars are also organized by the Library to encourage the discussion of topics of general interest to the nuclear community in relation to computer applications, the aim being to stimulate the exchange of information on well defined subject matter and to act as a guideline for the CPL on the direction to be taken in the selection of program material.

The original subject scope of the CPL covered the field of computer codes in Reactor Physics, however at the recommendation of the NEACRP (Committee on Reactor Physics) and the NEANDC (Nuclear Data Committee), it was agreed that the subject scope of the Library be widened to include (among other fields) Nuclear Model Computer Codes, on the understanding that only a limited number of programs be originally selected for dissemination by the Library, due to the high costs involved.

To assist with the selection of those codes which were thought to be particularly useful and for which there existed a potentially wide-ranging interest, the members of the NEANDC supplied the CPL with information and the availability status of computer codes developed in their countries. This information was further analyzed and processed by Prof. V. Benzi, CNEN, Bologna, and eventuated in the publication of a "List of Computer Programs for Neutron Cross Section Calculations and Analysis" (2) which included information in coded form of the most important features of these selected codes. Included in this list were approximately forty Optical Model and thirty Statistical Model Codes. The NEANDC has since been requested by the CPL to make a further selection of these codes.

In the meantime, the CPL has commenced its collection of some of these codes and to date about fifteen codes in the fields of Optical and Statistical Model Calculations are available from the Library. A short description of these, together with some related programs can be found in part 2.

It is hoped that the participants of this specialist meeting can give the CPL an indication of further programs to be included in its collection. It should also be added that the CPL intends to devote one of its future seminars to the discussion of Nuclear Model Calculations with particular emphasis being placed on the features and performances of the various programs in this field, and any suggestions as to the specific codes to be made the topic of this discussion would also be very welcomed.

COMPUTER CODES IN THE FIELD OF OPTICAL MODEL AND STATISTICAL MODEL CALCULATIONS AVAILABLE FROM THE NEA-CPL

Each header contains the following information:

Name of the program, contributing organization, country of origin and programming language.

SAUD-EX, CNEN, Italy. Fortran-2.

Evaluates the neutron radiative capture cross section by means of the statistical model, using the Lane-Lynn scheme. Neutron S- and p-waves only are taken into account and the competition of the inelastic scattering with the capture process is not considered. The Porter-Thomas distribution is assumed for the reduced neutron width. The application range is from 1 to 100 keV. (4).

FISPRO, CNEN, Italy. Fortran-4.

Evaluates the fast neutron radiative capture cross section of fission products according to the Hauser-Feshbach theory as developed by Margolis. The dependence of the level density on the excitation energy is based on a gaslike model. Rough estimations of cross-sections for one-phonon, two-phonon evaporation, direct and semi-direct capture can be made. Neutron penetrabilities are either given on input cards or are computed according to the strong interaction ($l \leq 4$) and to the spherical optical model ($l \leq 9$). Maximum number of excited levels is 19 and maximum neutron orbital angular momentum is 9. (5).

HAFEVER, USCC, USA. Fortran-4.

Calculates the energy exchange inelastic scattering cross section (integrated over angle) according to the Hauser-Feshbach theory as modified by Goldman, which includes the effect of spin-orbit coupling on the transmission coefficients. Penetrabilities must be provided in the input. The target nucleus is originally in the ground state. The maximum number of energy levels of the target nucleus is 20 and maximum neutron orbital angular momentum is 14. (6).

NEARREX, USCC, USA. Fortran-4

Computes neutron-induced, average fluctuation (or compound nucleus) cross-sections. Provision is made for the computation of compound-elastic and inelastic radiative capture and fission cross-sections as well as other processes, such as proton emission. It can also be used to compute proton induced average cross sections. Hauser-Feshbach theory as modified by Moldauer is used. The residual states can be any one of the ground or excited states of the target nucleus, for which excitation energies, spins and parities must be specified. The average resonance parameters for each of these neutron channels are computed as a function of the compound transmission coefficients, specified as input. Equidistant spacing model is used for the level density. The angular momentum dependence of the level density is of Gaussian form. Each neutron partial wave is assumed to be distributed according to the Porter-Thomas distribution (7).

THRESH, USCC, USA. Fortran-4

Calculates neutron induced reaction cross sections from 0 to 20 MeV and fission-spectrum averages for nuclides having 21 to 50 protons. Reaction products considered are 2n, 3n, p, d, t, He3, α, np, nd, nt, n He3, nα, pn, 2p, pα, α n, α p, dn. A statistical model with empirically determined parameters is employed (Evaporation Model) The model is based on the fact that the high energy non-elastic cross section is well known and that the competition for charged particles and neutron emission for neutron induced reactions is a relatively smooth function of the neutron-excess over protons in the target nucleus. Binding energies, if calculated by the program, are calculated from Hillman's empirical mass formula.

Fitting parameters and binding energies are supplied by the program but may optionally be defined by the user. (8).

CASCADE, USCC, USA. Fortran-4.

Solves the intranuclear gamma-ray cascade equation to determine secondary particle emission probabilities. Competing processes considered are gamma-ray emission, neutron emission and fission. The gamma ray cascade takes into consideration that particle emission is possible when gamma-rays with energy less than that of the incident particle are emitted.

/Contd..

CASCADE, USCC, USA. Fortran-4. (Contd..)

The neutron cascade may occur when the compound nucleus is in such a highly excited state that a neutron is emitted leaving channels other than gamma-ray channels open.

A coupled set of inhomogeneous Volterra equations of the second kind describing the energy dependence of the probability for particle termination of a gamma-ray cascade is solved numerically. Branching ratios determined from these probabilities may be used as input to the COMNUC program. Only dipole radiation is permitted, no discrete channels are permitted. Only continuum particle emission is considered. (9).

COMNUC, USCC, USA. Fortran-4.

Calculates neutron reaction cross sections using statistical model for decay of the compound nucleus. Competing reaction types permitted are elastic, discrete and continuum inelastic, gamma-ray emission, capture, fission and (n, 2n). Hauser-Feshbach theory as modified by Moldauer is used to determine competition in the decay of the compound nucleus. The continuum fission model assumes that fission may occur for various orders of deformation. The deformation is assumed to occur adiabatically so that the level density for the undeformed compound nucleus can be used. The calculation of gamma-ray emission probability follows the single particle model of Weisskopf. The radiation is assumed to be a mixture of dipole and quadrupole. All nuclear level densities required are calculated according to the formulation of Cook. Direct reaction components may be provided by card input. These are combined with calculated compound nucleus cross sections. Transmission coefficients can be supplied on card or a simple spherical optical model can be used. Branching ratios calculated by CASCADE may be input by COMNUC. (9).

SMOG, CNEN, Italy. Fortran-2.

Evaluates the total-, the reaction-, the shape-elastic total and differential cross sections, the phase strength functions and transmission coefficients by means of the optical model. Woods-Saxon, Gauss and square well potentials including spin-orbit coupling can be selected. The Fox-Goodwins method is used for numerical integration. Maximum angular momentum is 20. (10).

SASSI, CNEN, Italy. Fortran-2.

Calculates the neutron total and reaction cross-sections, as well as the angular distributions for shape-elastic and compound-nucleus processes (elastic and inelastic). The spherical optical model and the Hauser-Feshbach statistical model as modified by Goldman to include spin orbit effects is used. The Fox-Goodwins method is used for numerical integration. Maximum angular momentum is 50. Maximum number of excited levels is 30. (11).

ELIESE-1, JAERI, Japan. Fortran-2.

Calculates any kind of cross sections for elastic and inelastic scattering of neutrons, protons and alpha particles. The optical model and Hauser-Feshbach's method in the compound nuclear process is used. Fox-Goodwin's two point method is used for numerical integration of wave functions. The only process competing with inelastic scattering considered is (n, p). Contributions from highly excited levels in the continuum region are not included. Maximum number of excited levels is 30. Experimental and calculated angular distributions of scattered particles may be compared by means of the χ^2 deviation. (12).

ELIESE-3, JAERI, Japan. Fortran-4.

Calculates elastic cross section and its angular distribution, the inelastic scattering cross section for each discrete nuclear level and its angular distribution, the total inelastic scattering and compound-nucleus formation cross section for particles with spin 0, 1/2, 1. The reaction cross sections concerning absorption and emission of particles with spin 0, 1/2, 1 can be calculated. Optical model and Hauser-Feshbach theory are used. Moldauer's method can be used in the calculation of the compound nuclear process. Hauser-Feshbach's method is extended to calculate the cross section for the excitation of the overlapping levels of the residual nucleus. A resonance interference option is also included. A constant nuclear temperature representation of nuclear level densities is used at low excitation energies and the Fermi-gas formula is adopted at high excitation energies. Gaussian and Yukawan non-local kernels are available. Polarization, asymetry, rotation, depolarization and tensor polarization of scattered particles can be calculated. Fox-Goodwin's method is used for calculating wave functions. Automatic search for up to 15 potential parameters, limited to the elastic scattering calculation is available (13).

STAX-2, JAERI, Japan. Fortran-4

Calculates neutron elastic and inelastic scattering and compound-nucleus formation cross-sections, transmission coefficients. Optical model and Moldauer's theory are used. The optical potentials used are Woods-Saxon for real part, derivative Woods-Saxon for imaginary part and Thomas form for spin-orbit. The wave equation is solved by the Noumerov's method. Searches for potential parameters are made with respect to any combination of the following integral or differential cross sections; total elastic and inelastic for the first excited level. Searches are made by means of the Gauss -Newton method. Largest value of orbital angular momentum is 10, maximum number of excited levels is 25. (14.)

2 PLUS, USCC, USA. Fortran-4

Solves the problem of scattering of charged or uncharged nucleons by a nucleus represented by a deformed nuclear potential. The model assumes that the target nucleus has a 0+ ground state and a 2+ first excited level, which are strongly coupled by the deformed potential. (Coupled Channel Calculations) All other levels are treated in the weak coupling limit (spherical potential). A Hauser-Feshbach compound nucleus calculation has been included so that lower energy neutron scattering may be calculated. A coupled set of sevel, complex second-order differential equations is solved by difference techniques. The asymptotic scattering solution boundary conditions are applied by using a matrix inversion method. The basic three- dimensional problem is reduced to one dimension by a spherical harmonics expansion. The output contains total, potential elastic, potential inelastic (2+), reaction and compound nucleus cross sections as well as elastic and inelastic angular distributions. Maxima of 12 levels including ground state and 30 terms in the Legendre expansion are permitted. Comparison of theoretical and experimental data is permitted by means of a χ^2-test. (15).

JUPITOR 1, USCC, USA. Fortran-4.

Is used to perform coupled-channel calculations to evaluate the cross-sections for the scattering of nuclear particles by various collective nuclei. Spin of the projectile can be either 0, 1/2, 1 for non-adiabatic or 0, 1/2 for adiabatic coupled channel calculations. Targets can be either vibrational (spherical) or rotational (permanently deformed) and of either even or odd atomic numbers. When the target is deformed, excitation of states belonging to higher (vibrational) bands can be considered. Coulomb excitation can be included and the form factor can be either real or complex. A maximum of six states and 30 partial waves can be coupled at one time. The maximum number of orbital angular momentum is 69, in solving the coupled differential equations the prediction-correction method due to Stormer is used. (16).

RELATED PROGRAMS.

LYNNE, USCC, USA. Fortran-4

Performs a multipole expansion of the Woods-Saxon potential. The numbers generated are suitable for microscopic calculations of inelastic scattering from nuclei, which use a Wood-Saxon interaction between the projectile and the target nucleons.

PEGGY, USCC, USA. Fortran-4.

A least squares search program which analyses in terms of phase shifts, the elastic scattering of spin 0 and 1/2 particles by spin 0 nuclei. Real or complex phase shifts may be used with or without spin-orbit-coupling. Differential cross section and polarization angular distributions may be analyzed either separately or simultaneously.

RAMES, USCC, USA. Fortran-4

Computes both local and non-local radial integrals of a variety of radial operators using single-particle wave functions, which are eigenstates of motion in Woods-Saxon potential well.

ATHENA-4, USCC, USA. Fortran-4.

Computes form factors for inelastic scattering calculations using single particle wave functions that are eigenstates of motion in either Woods-Saxon potential or harmonic oscillator well. Two-body forces of Gauss, Coulomb, Yukawa and a sum of cut-off Yukawa radial dependences are available.

BESFIT, USCC, USA. Fortran-4.

Calculates differential elastic scattering cross sections using a Bessel function expansion, based on a diffraction model. Constant terms may either be supplied as input data or obtained by a least squares fitting of the data.

REFERENCES

(1) L. Garcia de Viedma: "Nuclear Energy Agency Computer Program Activities".
Proc. Conf. "Information Systems: Their Interconnection and Compatibility", Varna, 1974. IAEA (1975).

(2) NEANDC-97U, January 1974.

(3) M.F. James: "A Brief Outline of Methods of Calculation of Neutron Cross-Sections". NEA-CPL Newsletter No. 5 June 1966.

(4) V. Benzi et al: CNEN Internal Report 60-SU-03 (1973).

(5) V. Benzi et al: CNEN RT/F1(69)44(1969).

(6) M.A. Friedman et al: A PDA-141 (1960).

(7) P.A. Moldauer et al: ANL-6978 (1964).

(8) S. Pearlstein: BNL 16271 (1971).

(9) C.L. Dunford: A1-AEC-12931 (1970).

(10) V. Benzi et al: CNEN Internal Report 61-SU-04 (1961).

(11) V. Benzi et al: CNEN RT/F1(71)6 (1971).

(12) S. Igarasi: JAERI-1096 (1965).

(13) S. Igarasi: JAERI-1224 (1972).

(14) Y. Tomita: JAERI-1191 (1969).

(15) C.L. Dunford: NAA-SR-11706 (1966).

(16) T. Tamura: ORNL-4152 (1965).

Contributed Paper No. 12

NEUTRON EMISSION SPECTRA ANALYSIS WITH PRE-EQUILIBRIUM AND EQUILIBRIUM STATISTICAL THEORY

D. Hermsdorf, A. Meister, S. Sassonov, D. Seeliger, K. Seidel
Section of Physics, Technical University Dresden, GDR

Abstract:

The results of neutron emission spectra analysis at 14 MeV incident energy in the framework of equilibrium and pre-equilibrium statistical models are summarized.

1. INTRODUCTION

During the past years an extensive program of measurements of differential inelastic scattering cross-sections for 14 MeV neutrons in a wide mass number range was carried out at the Technical University Dresden. Resulting voluminous amount of neutron data for more than thirty elements have been collected in a special report [1]. It was a rather hard work because of complicated experimental techniques on one side and the necessity to use a lot of corrections and data handling processes on the other side. The whole research program was designed to obtain maximum accuracy of the absolute cross sections.

Based on the first experimental results of this program in 1970 we started interpretation of neutron emission spectra in the framework of, at that time, new preequilibrium models. First results we presented at the Neutron Conference in Kiev in 1971, afterwards updated results were presented at some other conferences (for example [2]). The present paper contains a summary of the most important results from this work, which provided new interesting details in our knowledge of the mechanism of nucleon inelastic scattering in the medium energy region.

2. PRE-EQUILIBRIUM MODELS

First, a brief review of the statements and expressions of the various exciton model modifications used for our interpretations of neutron scattering is given. A detailed explanation of models as well as detailed bibliography are avoided. Interested people are referred to the two reviews by Blann [3] and by Seidel, Reif, Toneev and Seeliger [4].

2.1. General formulation

With the aid of master equations of the exciton model we can follow the time evolution of a reaction:

$$\begin{aligned}\frac{d}{dt}P(p,h,t) = {} & P(p-1,h-1,t)\,\lambda_+(p-1,h-1) + \\ & + P(p+1,h+1,t)\,\lambda_-(p+1,h+1) - \\ & - P(p,h,t)\left[\lambda_+(p,h) + \lambda_-(p,h) + \right. \\ & \left. + \sum_i \int_0^{E-B_i} W_i(p,h,\epsilon)\,d\epsilon\right]\end{aligned} \tag{1}$$

In eq. (1) the following notations have been used

- P - occupation probability of n = p+h exciton states;
- $\lambda_\pm$ - decay constants for transitions between n and n $\pm$ 2 exciton states of the intermediate system;
- W_i - emission probability for a particle i at excitation $B_i + \epsilon$ above the Fermi energy;
- E - full excitation energy $E = \epsilon_0 + B_0 = \epsilon + B_i + U$,
- ϵ_0, ϵ - kinetic energy of incoming and outgoing particles;
- B_0, B_i - the respective binding energies.

The preequilibrium particle spectrum $N_i(\epsilon)$ may by expressed as

$$N_i(\epsilon)\,d\epsilon = \int_0^{T_{eq.}} \sum_{\substack{n=n_0 \\ \Delta n=+2}}^{\bar{n}} P(n,t)\,W_i(n,\epsilon)\,d\epsilon\,dt\,, \tag{2}$$

where $T_{eq.}$ is the equilibration time. Finally, the total preequilibrium cross-section for (α,β) process is given by

$$\begin{aligned}\sigma^N_{\alpha,\beta} = \int_0^{E-B_\beta} \sigma^N_{\alpha,\beta}(\epsilon)\,d\epsilon = {} & \\ = \sigma_\alpha(\epsilon_0) \int_0^{E-B_\beta} \sum_n W_\beta(n,\epsilon)\,\tau_n\,d\epsilon\,,\end{aligned} \tag{3}$$

with the mean life-time of an n-exciton state

$$\tau_n = \int_0^{T_{eq.}} P(n,t)\, dt \qquad (4)$$

and the cross section $\sigma(\epsilon_0)$ for the formation of the first p-h-state.

Let us consider the most important physical quantities, which determine results of calculations by the general equations (1) - (4).

2.2. Particle emission

The nucleon emission probability from p,h-state is given by the well-known principle of detailed balance in nuclear reactions

$$W_{nucl.}(p,h,\epsilon)\, d\epsilon = \frac{2}{\pi^2 \hbar^3}\, \mu\, \epsilon\, \sigma_{inv}(\epsilon)\, \frac{\omega(p-1,h,U)}{\omega(p,h,E)} \qquad (5)$$

where $\omega(p, h, E)$ is the density of p,h-states, which is usually calculated from the expression given by Ericson

$$\omega(p,h,E) = \frac{g(gE)^{p+h-1}}{p!\,h!\,(p+h-1)!} \qquad (6)$$

2.3. Transition rates

The decay constants for transitions $n \rightarrow n + \Delta n$ at excitation energy E is given by the time-dependent perturbation theory

$$\lambda_{\Delta n} = \frac{2\pi}{\hbar} \langle |M|^2 \rangle\, \omega_f^{\Delta n} \qquad (7)$$

where $\omega_f^{\Delta n}$ is the density of accessible final states for transitions $\Delta n = \pm 2$ as given by Williams (factor $^1/2$ by Oblozinsky et al.)

$$\omega_f^{+} = \frac{g(gE)^2}{2(p+h+1)} \qquad \omega_f^{-} = \frac{g}{2}\left[ph(p+h-2)\right] \qquad (8)$$

2.4. Approximations

Solution of the set of coupled differential equations (1) demands voluminous calculations with a large computer. Therefore in most cases it is convenient, to use simple analytical formulas, which are derived from (1) through additional physical assumptions.

i) It may be seen from (8), that during the first steps of interactions in the intermediate system the transition probability λ_- is very small:

$$\lambda_+ \gg \lambda_- \quad \text{if} \quad n \ll \bar{n} = (2gE)^{1/2}$$

Neglecting λ_--transitions, from equations (1) and (2) we get the following preequilibrium particle spectra

$$N_i(\epsilon)\,d\epsilon = \sum W_i(n,\epsilon)\,d\epsilon \cdot \tau_n$$

$$\tau_n = \int_0^{\tau_{eq.}} P(p,h,t)\,dt \approx \frac{D_n}{\lambda_+(p,h,E) + \sum_i \int_0^{\epsilon - B_i} W_i(p,h,\epsilon)\,d\epsilon} \tag{9}$$

where D_n is the depletion factor, which reduces the population of each state according to the amount of particle emission from simpler states. D_n is given by

$$D_n = \prod_{n'=n_0+2}^{n} \left[1 - \sum_i \int_0^{E-B_i} W_i(n'-2,\epsilon)\,d\epsilon\right] \tag{10}$$

ii) Blann's hybrid model contains the following approximations: The transition rate in (9) is replaced by the collision rate λ_{coll} of the particles in the continuum, which is derived from considerations of nuclear matter. Blann recommends following equation for λ_{coll} as a function of particle energy ϵ :

$$\lambda_{coll} = \langle v \rangle \rho \bar{\sigma} = 1{,}4 \cdot 10^{21}(\epsilon + B_0) - 6 \cdot 10^{10}(\epsilon + B_0)^2 \ \text{sec}^{-1} \tag{11}$$

The second point of the hybrid model is, that emission probability from p,h-state W_i, is replaced by the decay constant $\lambda_{em}(\epsilon)$ for transitions into continuum for a particle at excitation $\epsilon + B_i$ above the Fermi energy.

$$\lambda_{em}(\epsilon) = \frac{(2s_i+1)\mu_i \epsilon \sigma_{inv}}{\pi^2 \hbar^3 g} \tag{12}$$

From eqs. (9) - (12) we get the preequilibrium decay probability in the hybrid model approximation as

$$N_i(\epsilon)\,d\epsilon = \sum_{\substack{n=n_0 \\ \Delta n=+2}}^{\bar{n}} R_i(n)\,\frac{\omega(n-1,U)}{\omega(n,E)}\left[\frac{\lambda_{em}(\epsilon)}{\lambda_{coll}(\epsilon)+\lambda_{em}(\epsilon)}\right] \tag{13}$$

where $R_i(n)$ is the number of all particles of the type i in the n-exciton-state.

iii) The most simple expressions for preequilibrium decay probability we get from (9) with the additional assumption, that emission probability during the equilibration process is neglectible

$$\sum_i \int_0^{\epsilon - B_i} W_i(n,\epsilon)\,d\epsilon \ll \lambda_+$$

This assumption leads from eq. (9) to

$$N_i(\epsilon)\,d\epsilon = \sum_{n_0}^{\bar{n}} \frac{W_i(n,\epsilon)}{\lambda_+(n,\epsilon)}\,d\epsilon \tag{14}$$

and from eqs. (5), (6), (7), (8) and (14) we can derive the well-known formula

$$N_i(\epsilon)\,d\epsilon = \frac{(2s_i+1)\mu\,\epsilon\,\sigma_{inv}(\epsilon)}{2\pi^3\hbar^2 g^4 \langle |M|^2\rangle E^3} \times \times \sum_{n_0}^{\bar{n}} (U/E)^{n-2}\,(n+1)^2(n-1)\,d\epsilon \tag{15}$$

which assumes that $\langle |M|^2 \rangle$ does not depend upon n. Assuming a constant life-time of exciton states $\tau_n = \tau_0 = \text{const.}$, the following expression is derived

$$N_i(\epsilon)\,d\epsilon = \frac{(2s_i+1)\,\mu\,\epsilon\,\sigma_{inv}(\epsilon)}{2\pi^3\hbar^2 g E} \times \times \sum_{n_0}^{\bar{n}} (U/E)^{n-2}\,(n+1)(n-1)\,\tau_0\,d\epsilon \tag{16}$$

As shown in fig. 1 eqs. (2), (13), (15) and (16) correspond to similar, but not identical preequilibrium spectra-shapes. If the different spectra are normalized in the high energy region - differences up to ± 25 % between them occur in the low energy region.

3. RESULTS FROM ANALYSIS OF EXPERIMENTAL NEUTRON SPECTRA

3.1. Spectra shape

The first we tried to do was the description of the shape of neutron emission spectra in a wide energy and mass-number range. Because of the strong time decoupling of preequilibrium and equilibrium reaction modes the following expression has been used for comparison with experiments

$$\sigma_{nn'}(\epsilon) = \sigma^{N}_{nn'}(\epsilon) + \sigma^{G}_{nn'}(\epsilon), \qquad (17)$$

where the first term implies the preequilibrium spectra shape, according to eq. (16),

$$\sigma^{N}_{nn'}(\epsilon) = K_1 \epsilon \sigma_{inv}(\epsilon) \sum_{n_0}^{\bar{n}} \left(\frac{U}{E}\right)^{n-2} (n+1)(n-1) \qquad (18)$$

The second term describes the well-known equilibrium part of emission spectra, given by the statistical theory of nuclear reactions:

$$\sigma^{G}_{nn'}(\epsilon, a) = K_{2,a} \epsilon \sigma_{inv}(\epsilon) U^{-5/4} \exp\left[2(aU)^{1/2}\right] \qquad (19)$$

(Fermi gas model)

or

$$\sigma^{G}_{nn'}(\epsilon, T) = K_{2,T} \epsilon \sigma_{inv}(\epsilon) \exp\left[U/T\right] \qquad (20)$$

(constant temperature model)

In a χ^2-fit to the integrated (over the solid angle) experimental spectra the free parameters of eq. (17) K_1, K_2 and a (or T) have been varied independently.

The following results have been obtained:

- It was shown, that inclusion of preequilibrium emission is a useful and simple way to describe the shape of experimental neutron emission spectra in a wide energy and mass number range. As yet, there is no other way to do it. The shapes of

preequilibrium and equilibrium spectra become strongly different with increasing mass-number. Therefore, the χ^2-fit has a sharp minimum for the fit parameters K_1, K_2 and a (or T) (see fig. 2) and experimental spectra can be divided with definite accuracy (which is determined by the accuracy of the employed models) in the two reaction modes. At least it is a simple method to parametrize neutron spectra.

- After integration of separated preequilibrium spectra $\sigma^N_{nn'} = \int \sigma^N_{nn'}(\epsilon)\,d\epsilon$ we obtained the mean mass-dependence of preequilibrium emission cross-section $\sigma^N \sim A^{1/3}$

  Most of the cross-section values are within the range

  $$\sigma^N_{nn'} = (130 \pm 30)\ A^{1/3}\,[\text{mbarn}].$$

  By several reasons it seems, that the resulting preequilibrium cross-section is somewhat overestimated.

- It is well-known, that from neutron spectra level density parameters were obtained by many authors. Therefore, we examined the influence of preequilibrium emission on these parameters. We compared a parameters, obtained in a narrow high excitation energy range $U \approx 10 + 11$ MeV from the equilibrium model only, and those from the analysis with eq. (17) in whole excitation range $U \approx 0 + 12$ MeV, including preequilibrium processes. In the second case small contributions of secondary neutrons had to be subtracted from experimental spectra. The results in fig. 3 indicate a strong deviation between both parameter sets increasing with mass-number. The parameters from the analysis including preequilibrium emission are in general agreement (deviations 10-20 %) with level density parameters from neutron resonances and fluctuation analysis. This analysis confirms the remarkable contributions of comparatively slow preequilibrium neutrons, which are predicted by the exciton models. A the same time it shows, that the existing exciton-models altogether somewhat overestimate the preequilibrium spectra in the low energy part. This is demonstrated in fig. 4 for the gallium spectrum. The lowest preequilibrium spectrum is an idealized one, which gives the

best a parameter. The other spectra correspond to approximations (16) (indicated with "τ") and (15) (indicated with "M^2"). The worst spectrum in this sense is predicted by the hybrid model (13) (not shown).

- Assuming that the high energy "tails" consist of preequilibrium neutrons only, from the slope of the experimental spectra the initial numbers of excitons n_0 may be obtained by means of the equation

$$n_0 - 2 = \frac{d\left[\ln\left(\sigma_{nn'}^{exp}(\epsilon)/\epsilon\right)\right]}{d\left[\ln\left(U/\epsilon\right)\right]} - R \quad . \tag{21}$$

The results of such exercise are in surprisingly good agreement with predictions of exciton model, the mean behaviour is well described by (fig. 5)

$$n_0 = 3{,}2 \pm 0{,}2 \ ,$$

supporting the principal consistency of exciton models. This is also in agreement with an analog analysis of nucleon-induced reactions, whereas most of the α-induced reactions give n_0-values near 5, [3, 4].

3.2. Transition rates

The problem of calculating absolute spectral yield by the exciton models is mainly one of calculating the intranuclear transition rates $\lambda_+(7)$ between intermediate states. Therefore, it seems very interesting to get these values (or the equivalent matrix elements $\langle |M|^2 \rangle$ from various reaction channels at the same excitation energy. The consistency of the models demands, that we get the same matrix element $\langle |M|^2 \rangle$ independent of the type of outgoing reaction channel.
For this purpose the preequilibrium emission spectrum for the 3-exciton state from eq. (9)

$$N_{n'}(\epsilon)\,d\epsilon = W_{n'}(3,\epsilon)\,\frac{d\epsilon}{\lambda_+(3,E) + \sum_i \int W_i(3,\epsilon)\,d\epsilon} \tag{22}$$

was compared with the experimental observed absolute "high

energy tail" of the spectra. In this way we can obtain absolute transition probabilities λ_+ as shown on fig. 6. It is remarkable, that within ± 50 % the λ_+-values are constant over the whole mass number range.
The average extracted values are (at E≈21-22 MeV)

$$\langle \lambda_+(3) \rangle = (5{,}9 \pm 0{,}7)\ 10^{21}\,[s^{-1}]$$
$$\langle \tau_3 \rangle = \lambda_+^{-1}(3) = (1{,}7 \pm 0{,}2)\ 10^{-22}\,[s]$$
$$\langle \Gamma_3 \rangle = (3{,}9 \pm 0{,}4)\,[MeV]$$
$$\langle |M|^2 \rangle = (18 \pm 2)\ A^{-3}\ MeV^2$$

In an independent work Colli et al. [5] from analysis of total (n,p) cross-sections at 14 MeV obtained a very similar transition rate

$$\lambda_+(3) = 4{,}9 \cdot 10^{21}\,[s^{-1}]$$
$$\langle |M|^2 \rangle = 15{,}2\ A^{-3}\,[MeV^2]$$

Thus both reaction channels at 14 MeV incident energy are well described by the same transition probability (or matrix element). This result is also in agreement with an analysis of (p,n)-excitation function by Birattera et al. [6], which gave the result

$$\langle \lambda_+(3) \rangle = 6 \cdot 10^{21}\,[s^{-1}].$$

Existing theoretical approaches considerably deviate from experimental values:

- $\langle \lambda_+(3) \rangle = \frac{1}{2}\lambda_{coll} = 14 \cdot 10^{21}\,[s^{-1}]$
  from nucleon-nucleon collisions in nuclear matter (see eq.(11),
- $\langle \lambda_+(3) \rangle = 24 \cdot 10^{21}\,[s^{-1}]$
  from an everaging procedure over all accessible p-h-configurations by Gadioli et al. [7],
- $\langle \lambda_+(3) \rangle = 7 \cdot 10^{21}\,[s^{-1}]$
  from the imaginary part of the optical model [2].

3.3. Absolute cross-sections

One of the main purposes of any nuclear reaction theory is the a-priori prediction of absolute cross sections without any free perameters.

The hybrid model does not imply any free parameter, but analysis of many experiments has shown, that the used collision rates from nuclear matter theory are too high. An improvement of the agreement with experiment is obtained by an additional factor $^1/K$ on the right side of eq. (11), wheras $K \approx 5 \ldots 10$. We found, that the hybrid model is a useful tool for absolute calculation of neutron spectra, if an additional factor $K \approx 10$, constant for the whole mass-number scale, is introduced.

An a-priori absolute calculation of neutron spectra without any free parameters (with an accuracy of about $\pm$ 15 %) we obtained with an approach of Toneev and coworkers [8]. As in other approaches, Toneev starts from relation

$$\lambda_{coll} = \langle v \rangle \rho \langle \sigma \rangle = \langle v \rangle \Lambda^{-1} \qquad (23)$$

between density of nucleons ρ, the average velocity $\langle v \rangle$, the effective cross-section of interaction between nucleons $\langle \sigma \rangle$ and the mean free path Λ of them. Usually, the collision rate is taken equal to the transition rate for the 1p Oh-state

$$\lambda_{coll}(\epsilon_0) = \lambda_+(1, 0, \epsilon_0 + B_0), \qquad (24)$$

whereas transition rates for more complex states are calculated by eqs. (7) and (8). In Toneev's approach $\lambda_{coll.}$ is calculated for all n-exciton states, taking into account the cross-section as a function of interacting particle energy $\langle \varepsilon_{coll} \rangle$ and the restrictions by the Pauli principle (by the factor $\eta < 1$):

$$\langle \sigma \rangle = \eta \left(\frac{\varepsilon}{\varepsilon_F} \right) \sigma \left(\langle \varepsilon_{coll} \rangle \right) \qquad (25)$$

The interacting energy $\langle \varepsilon_{coll} \rangle$ is composed of the average energy of an excited particle $\langle \varepsilon_F + {}^E/n \rangle$ and the kinetic energy of the collision partner $({}^3/5)\varepsilon_F$. Therefore, the free nucleon-nucleon interaction cross-section becomes a function of n. A solution of master equations (1) has been carried out by the Monte-Carlo method, which takes into account all transitions $\lambda_{\Delta h}$ between intermediate states as well as emission of particles of any type (including α-particles). Some examples of

calculated spectra are shown on Fig. 7 - as one can see, an excellent absolute agreement between experiment has been obtained.

A summary of all calculations is seen in the Fig. 8. The total pre-equilibrium cross section $\sigma^N_{nn'}$, calculated this way (with $\sigma_\alpha(\varepsilon_o)$ in (3) from optical model nonelastic cross section) are denoted with full points. Values of $\sigma^N_{nn'}$, fitted to the experimental spectra (by chosing an optimal $\sigma_\alpha(\varepsilon_o)$) are shown as open circles. Both values are very similar, indicating the high accuracy of absolute calculations. The absolute pre-equilibrium model (without any experiment) yields the same mass systematic $\sigma^N \sim A^{1/3}$ as was found from experiment by the fitting procedure (17). This is another essential argument supporting the validity of exciton models.

3.4. Timing of the (nn') process

From application of exciton models we learned much about the dynamics of inelastic scattering. The main point is, that by the master equations (1) both pre-equilibrium and equilibrium emission spectra are calculated on a unique base, from which arises, without any additional assumptions, the division of reaction events into two, corresponding to the time, strongly different groups.

At the beginning of the nuclear interaction $\lambda_+ \gg \lambda_-$ (for $n \ll \bar{n}$) is valid, whereas in the later phase of the reaction process both transition probabilities are almost equal $\lambda_+ \approx \lambda_-$ (for $n \approx \bar{n}$).

A more precise, with respect to eq. (7), relation between the exciton number and the transition probability $\lambda(n)$ was given by Gadioli et al. [7]:

$$(26) \quad \lambda(n) = \lambda_+(n) + \lambda_-(n) = \left(1 + \frac{(n^2-1)(n+1)(n-2)}{11.5\,A^2}\right)\frac{4}{n+1}\,\lambda_+(3)$$

From eq. (26) we calculated the life-time τ_n of exciton states as a function of n for a A=100 nucleus at 22 MeV excitation energy. The result is the following: The life-time of the 3-exciton states is about $1.5 \cdot 10^{-22}$s. During the first interactions the life-time rapidly increases because of decreasing density of accessible final states. At $n \approx 13$ the transition probability λ_- becomes remarkable. After some ten interactions, with an relaxation time of about $\tau_{relax} \simeq 5 \cdot 10^{-21}$s, an equilibrium distribution of particles and holes is reached with an average time interval between two-particle interactions (transitions) of about $3 \cdot 10^{-22}$s. In the next figure (Fig. 9) the total emission probability per 10^{-22} seconds I(t) as a function of time is shown.

$$(27) \quad I(t) = \sum_i \int_0^{E-B_i} \sum_n P(n,t)\, W_i(n,\varepsilon)\, d\varepsilon$$

Intermediate system starts with a high emission probability $I(0) = 0.15 \cdot 10^{-22}$s., which rapidly decreases with increasing time (i.e. exciton number n). After the relaxation time $t > \tau_{relax}$ the emission probability is almost constant $I(t) \approx 3 \cdot 10^{-5}/10^{-22}$s. for a long time up to 10^{-18}s. Between 10^{-18}s. and 10^{-17}s. I(t) drops to zero. We conclude, that the dominating part of all emission events arises within the time intervals $0 < t < 5 \cdot 10^{-21}$s. and $10^{-18} < t < 10^{-17}$s., corresponding to pre-equilibrium and equilibrium reaction mechanism, respectively.

Let us estimate the life-time of compound nucleus τ_{CN} by the statistical model:

$$(28) \quad \frac{1}{\tau_{CN}} = \frac{m(2s+1)}{\pi^2 \hbar^3 \rho_{CN}(E)} \int_0^{\varepsilon_{max}} \varepsilon\, \sigma_{inv}(\varepsilon)\, \rho(U)\, d\varepsilon$$

Taking $\rho_{CN}(E)$ from the constant temperature model with T=0.9 MeV and the average inverse cross section $\langle \sigma_{inv}(\varepsilon_i) \rangle = 2$ barn, we get from (28) $\tau_{CN} \approx 3 \cdot 10^{-18}$s., in agreement with the results of eq. (27).

4. CONCLUSIONS

The various modifications of the exciton model are found to be useful for description of neutron inelastic scattering, as well as it was shown for other reaction channels [3, 4]. The main advantage of this model is its simplicity and physical transparency. With this model, in addition to the well-known statistical theory of nuclear reactions, it is possible to calculate angular integrated spectra of emitted particles and excitation functions. Of course, there are some shortcomings of this model: It does not describe angular distributions and there are some indications, that this model in its present state overestimates the low-energy part of pre-equilibrium spectra.

REFERENCES

[1] HERMSDORF, D., MEISTER, A., SASSONOV, S., SEELIGER, D., SEIDEL, K. and SHAHIN, F., ZfK-277 (1974)

[2] SEELIGER, D. et al., Mat. Neutron Conf., Kiev, 1971, part I. p. 243;
HERMSDORF, D. et al., Mat. Intern. Summerschool, Predeal, 1972;
HERMSDORF, D. et al., Kernenergie 16 (1973) 252 and Journal of Nuclear Energy 27 (1973) 774;
HERMSDORF, D., et al., Mat. Intern. Conf. Nucl. Phys., Munich, 1973;
SEELIGER, D. et al., Mat. Neutron Conf., Kiev, 1973, part I, p. 258 and p. 269
SEELIGER, D. et al., Mat. Symposium Interact. Fast Neutrons with Nuclei, Gaußig, 1973; ZfK 271
SEIDEL, K. et al., Mat. Intern. Symp. Smolenice 1974

[3] BLANN, M., Preequilibrium Models for Nuclear Reactions Rep. Univ. Roch., 1974, UR-NSRL-92

[4] SEIDEL, K., SEELIGER, D., REIF, R., TONEEV, W.D., Predravnovesnij raspad v jadernich reacijach Review Journal "ETCHAJA", Dubna, accepted for publication

[5] BRAGA-MARCAZZAN, G.M. et al., Phys. Rev. C6 (1972) 1398

[6] BIRATTERA, C., et al., Nucl. Phys, A201 (1973) 579

[7] GADIOLI, E. et al., Nucl. Phys. A217 (1974) 589

[8] GUDIMA, K.K. et al., OJJaJ P 4-7821, Dubna, 1974

FIGURE CAPTIONS

Fig. 1 Comparison between different shapes of pre-equilibrium spectra, according to eqs. (2), (15) and (16), distinguished as full line, dashed line and dash-dotted line, respectively.

Fig. 2 Sensitivity of the χ^2-fit of eq.(17) to experimental neutron emission spectra for nuclei with different mass numbers; a) Nb b) Si c) Ta d) Ti; All quantities are normalized to best fit numbers.

Fig. 3 Level density parameters obtained from neutron spectra, fitted by Weisskopf-Ewing formula only (open circles) and taking into account pre-equilibrium emission, according to eq. (17) (full points); results from neutron resonances and fluctuation analysis (crosses) are shown for comparison.

Fig. 4 Analysis of integrals over the solid angle neutron emission spectrum for Ga by eq. (17); dashed curves give equilibrium spectra and dash-dotted curves pre-equilibrium spectra; the different shapes of pre-equilibrium spectra correspond to eqs. (15) and (16) (denoted with "M^2" and "τ", respectively); the'best shape', with respect to the a-value, is denoted with "a".

Fig. 5 Initial number of excitons n_o, extracted from the shape particle emission spectra for different reactions [4]; open circles - from present analysis of (nn')-spectra; squares and triangles - from proton-induced reactions and crosses - from α-induced reactions.

Fig. 6 Absolute transition probabilities $\lambda_+(3)$ at $E \simeq 21$-22 MeV excitation energy (in units 10^{21} s^{-1}) extracted from neutron emission spectra of nuclei in a wide mass-number range.

Fig. 7 Absolute calculation of neutron and proton emission spectra for ^{181}Ta+n with the program WRPEC from Toneev et al. [8].

Fig. 8 Mass-dependence of the total pre-equilibrium cross section $\sigma^{N}_{nn'}$,[mb]; open circles - with the choice of an optimal $\sigma_{\alpha}(\varepsilon_0)$, full points - with $\sigma_{\alpha}(\varepsilon_0)$ from the optical model.

Fig. 9 Total emission probability I(t) per 10^{-22}s.

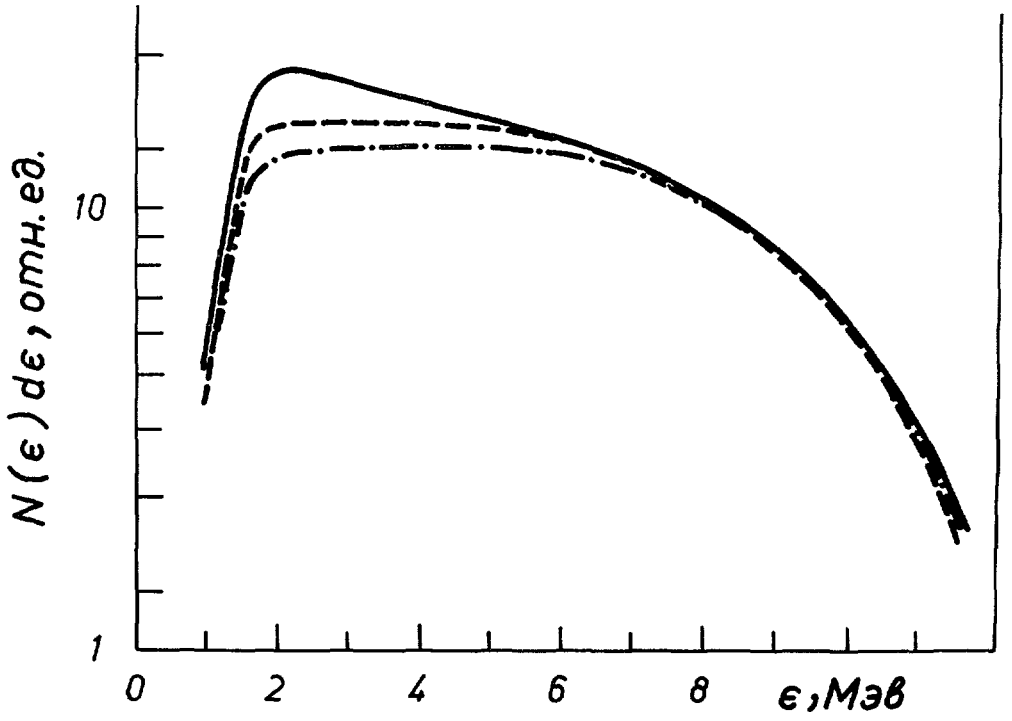

Fig. 1

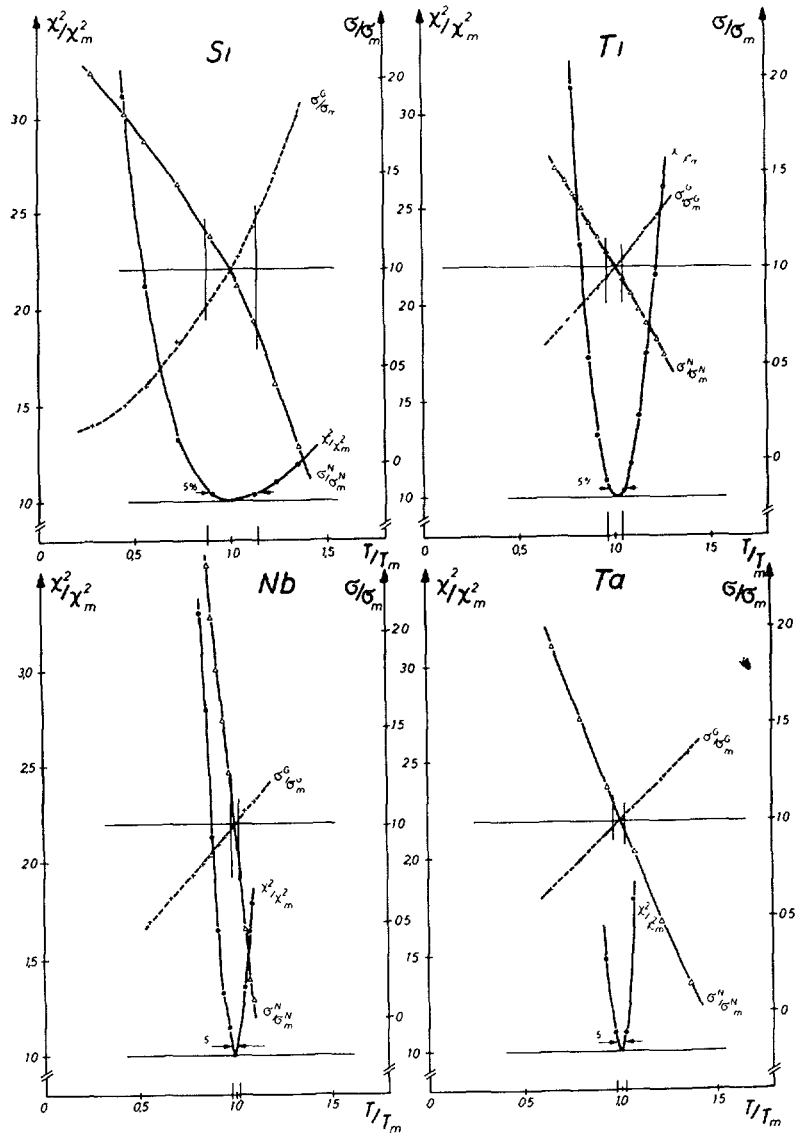

Fig. 2

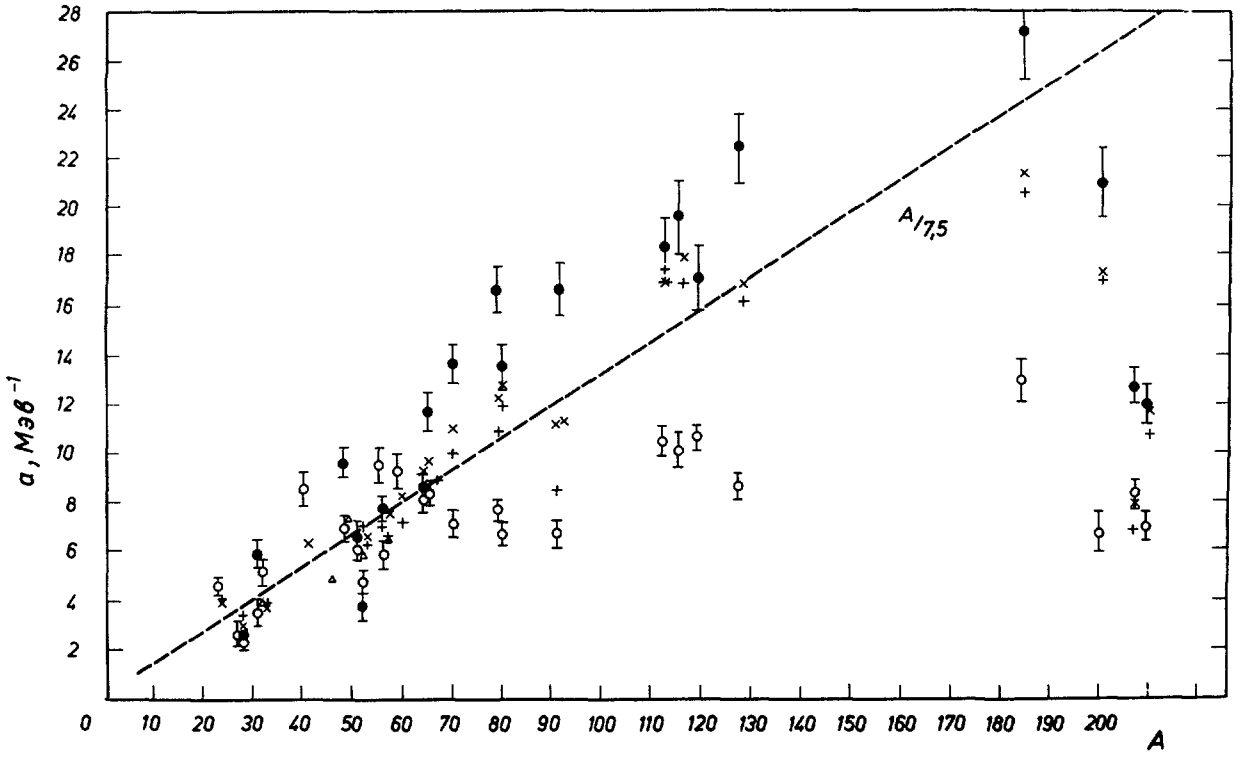

Fig. 3

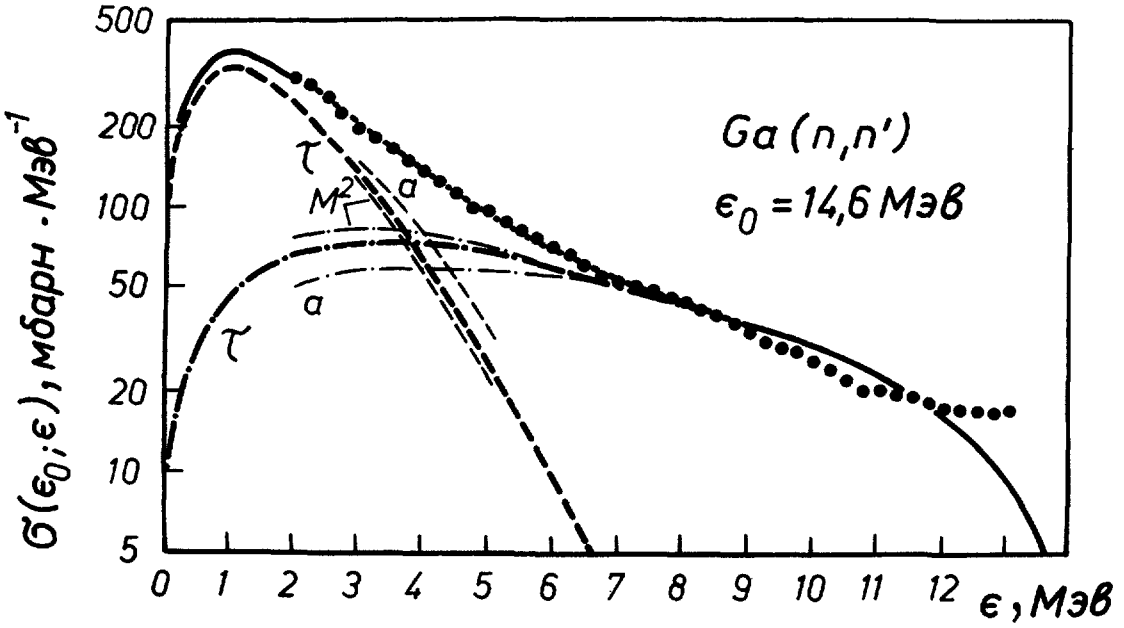

Fig. 4

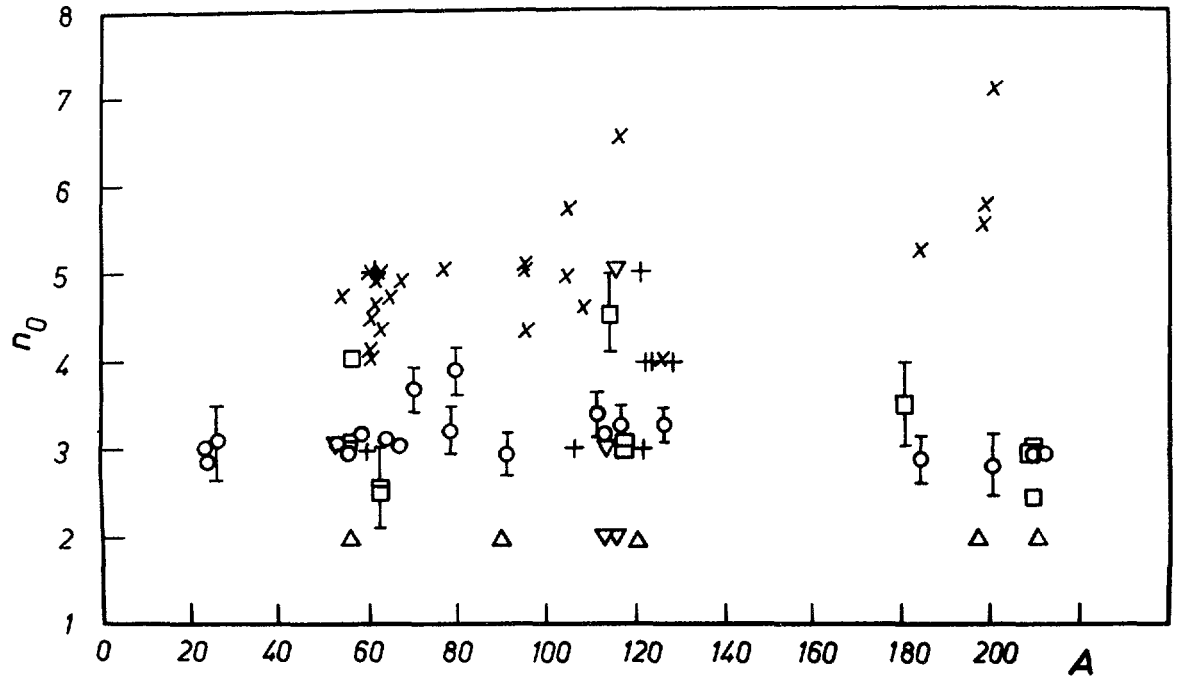

Fig. 5

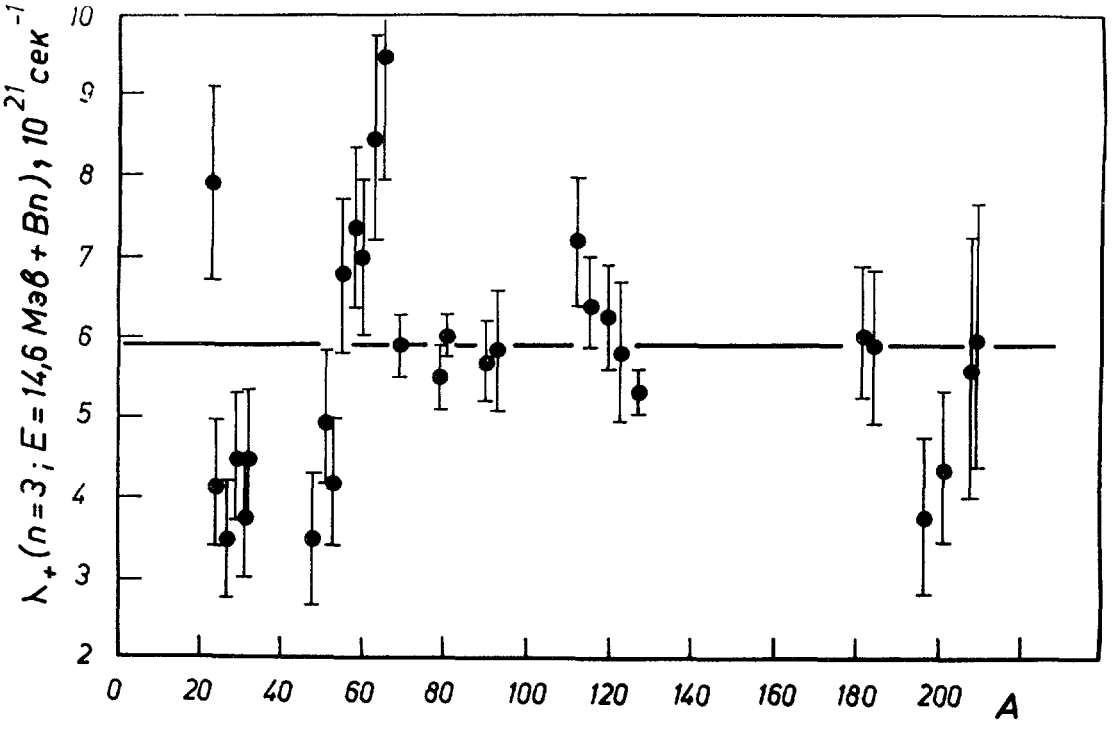

Fig. 6

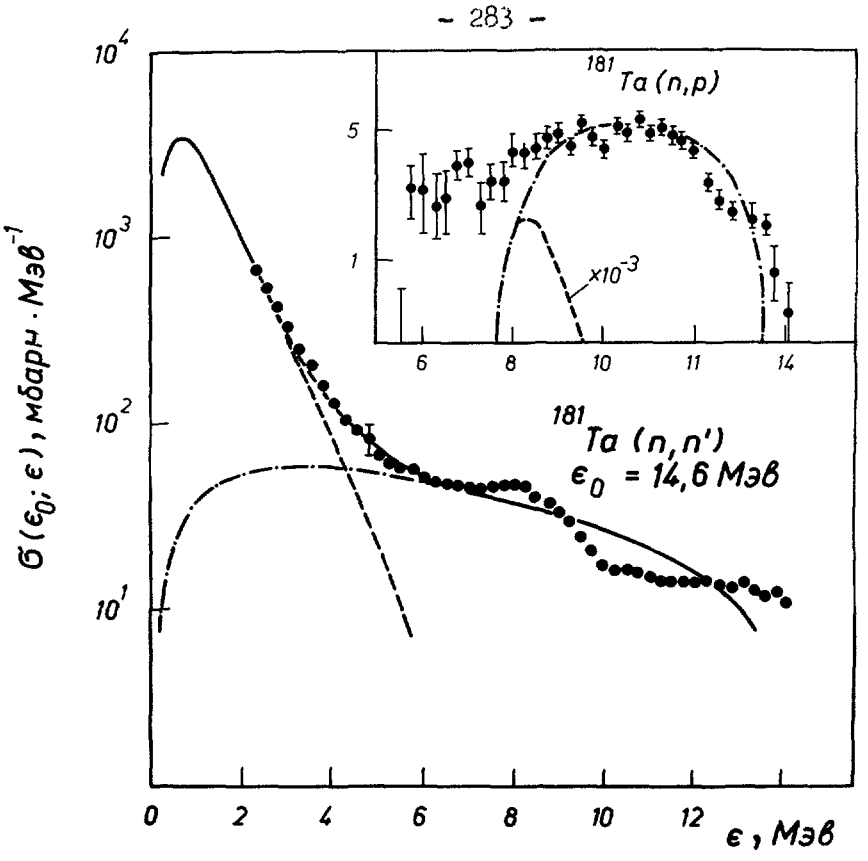
10^4
10^3
10^2
10^1
$\sigma(\epsilon_0;\epsilon)$, мбарн · Мэв$^{-1}$
^{181}Ta (n,p)
5
1
$\times 10^{-3}$
6
8
10
11
14
^{181}Ta (n,n')
ϵ_0 = 14,6 Мэв
0
2
4
6
8
10
12
ϵ, Мэв

Fig. 7

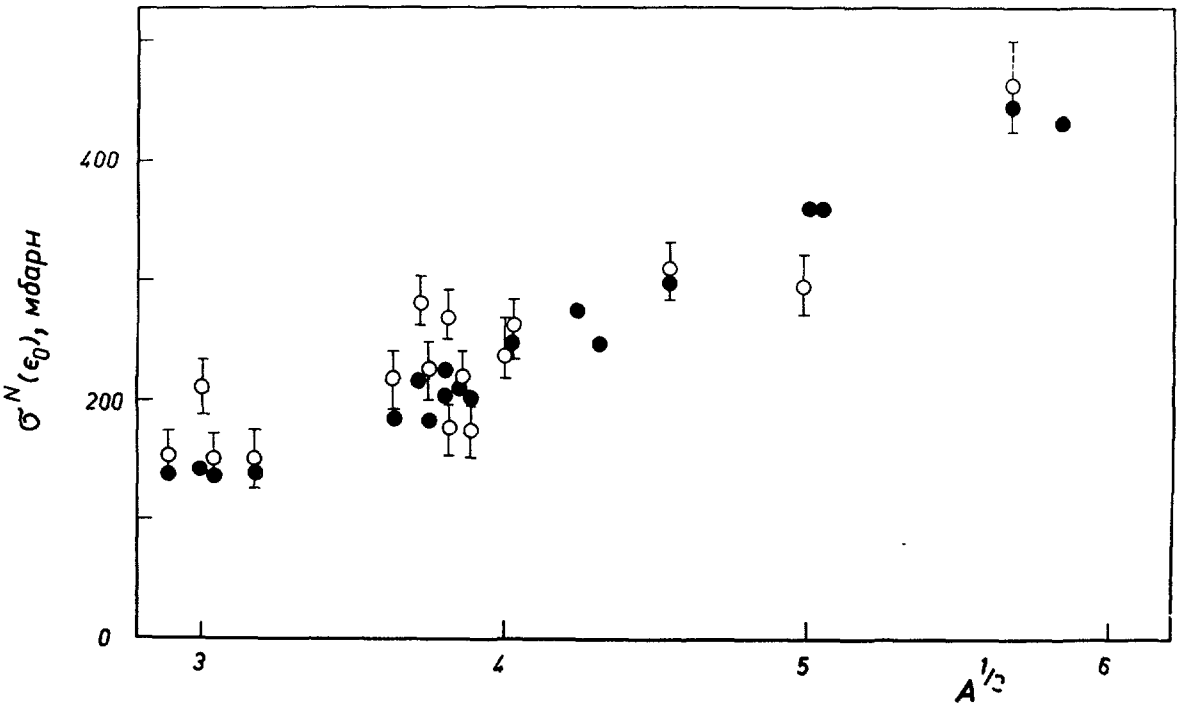
400
200
0
$\sigma^N(\epsilon_0)$, мбарн
3
4
5
6
$A^{1/3}$

Fig. 8

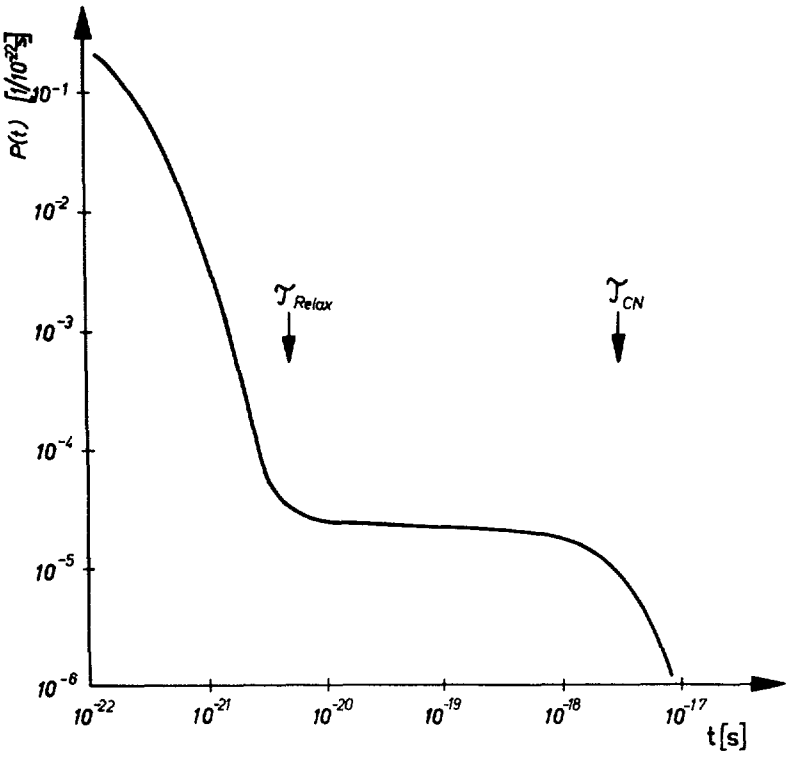
P(t) [1/10^22]
10^-1
10^-2
10^-3
10^-4
10^-5
10^-6
τ Relax
τ CN
10^-22
10^-21
10^-20
10^-19
10^-18
10^-17
t[s]

Fig. 9

75-8678
Translated from Russian

Contributed Paper No. 13

CALCULATION OF PRE-EQUILIBRIUM PROCESSES IN (n,2n), (n,np) AND (n,pn) REACTIONS

K. Seidel, D. Seeliger, and A. Meister,
Technical University of Dresden,
German Democratic Republic

ABSTRACT

The authors consider the influence of pre-equilibrium processes on the cross-sections of (n,2n), (n,np) and (n,pn) reactions for an initial nuclear energy of 14 MeV. The influence of the main structural effects of nuclei on equilibrium and pre-equilibrium cross-sections are discussed for a model nucleus. Lastly, a comparison is made between the cross-sections calculated for a number of specific nuclei, both with allowance for pre-equilibrium processes and, as previously done, without such allowance.

1. INTRODUCTION

Pre-equilibrium processes play an important part in many nuclear processes where the initial energy is between a few MeV and 100 MeV. Using pre-equilibrium decay models it is generally possible to arrive at a qualitative description of these processes [1].

The work described here is a study of the role of these processes in reactions accompanied by multiple emission of nucleons. The calculations are all performed for an initial neutron energy of 14 MeV, since most of the experiments have been performed at this energy, at least for the (n,2n) reaction. For the (n,pn) and (n,np) reactions there are very few experimental data available, even at this energy.

One aim of the work is to study the mechanisms of these reactions, including the interaction of structure and mechanism, and the other is to develop a new method of calculating (n,2n), (n,pn) and (n,np) reaction cross-sections, which are difficult to determine experimentally but are of practical importance. The new method should be more accurate than the equilibrium, statistical theory of nuclear reactions. The work is a continuation of that described in Ref. [2], in which the method was first used.

2. MODEL

After the bombardment of a nucleus by a neutron, the compound system, starting with a small number of degrees of freedom (two particles plus one hole correspond to n = 3 excitons), is gradually transformed into a more complex configuration (for each transition $\Delta n = 2$), until a state of statistical equilibrium is reached, i.e. the state of the compound nucleus [3]. There is a specific probability of the emission of a nucleon from each pre-equilibrium state with n quasiparticles. This emission will lead to a unit decrease in A and n and to a decrease in the excitation energy. The nucleus (Z,N) will therefore give rise to a nucleus (Z-1,N) in the case of emission of a proton or (Z,N-1) in the case of emission of a neutron and so on. Absolute spectra for both types of nucleons from all intermediate nuclei are calculated as long as the excitation energy does not become less than the nucleon binding energy. The calculations are performed on the basis of the hybrid model [3], according to which the probability ${}_nP_x^{\pi}(E)$ of pre-equilibrium emission of a nucleon of type x from a state with n excitons is equal to

$$ {}_nP_x^{\pi}(E) = {}_np_x \left[\frac{\varrho_{n-1}(U)}{\varrho_n(E^*)}\right]\left[\frac{\lambda_{em}(E)}{\lambda_{em}(E) + \lambda_+(E)}\right] \qquad (1) $$

where ${}_np_x$ is the number of nucleons of type x in state n;

$\varrho_{n-1}(U)$, $\varrho_n(E^*)$ represent the densities of states with n-1 and n quasiparticles in the final and intermediate nucleus, respectively, as obtained by combination of equidistant, single-particle levels;

λ_{em} is the probability of emission, obtained from σ_{inv} by means of the detailed balance principle; and

λ_+ is the probability of an intranuclear transition with $\Delta n = 2$.

In accordance with Ref. [3], λ_+ is calculated on the basis of the probability of nucleon collision in the nuclear matter, which gives the expression:

$$ \lambda_+(E) = \frac{1}{K}\left[1{,}4 \cdot 10^{21}\ (E+B) - 6{,}0 \cdot 10^{18}\ (E+B)^2\right] s^{-1} \qquad (2) $$

where K is a parameter which is independent of energy;

B is the nucleon binding energy.

The equilibrium spectrum $P_x^p(E)$ of particles of type x is calculated from the comprehensive statistical theory of nuclear reactions [4]:

$$P_x^p(E) = \frac{(2s+1)\, m\, E\, \sigma_{inv}(E)\, \varrho_R(U)}{\sum_r m_r g_r \int_0^{E_{max}} E_r\, \sigma_{inv,r}(E_r)\, \varrho_r(U_r)\, dE_r} \qquad (3)$$

where $\varrho_R(U)$ is the level density of the residual nucleus, given in terms of the Fermi-gas model [5] by:

$$\varrho_R(U) \sim \frac{1}{(U_{eff}+t)^2} \exp\left[2(a\, U_{eff})^{1/2}\right] \qquad (4)$$

The influence of shell effects on the density $\varrho_R(U)$ can be taken into account by using experimentally determined density parameters (a). As well known, allowance for the pairing effect is made by introducing an effective excitation energy $U_{eff} = U - \Delta$.

Given the known cross-section of formation of an initial system with n = 3, we thus obtain absolute spectra of the emitted nucleons and after summation with respect to energy we get the cross-sections of the (n,n'), (n,p), (n,2n), (n,np), (n,pn) etc. reactions.

All the parameters, except K in (2), can be regarded as well known. The value of K is obtained by comparing the calculation based on pre-equilibrium decay models with the (n,n') experimental spectra [6] in the high-energy range where pre-equilibrium emission predominates. Fig. 1 shows that in a wide range of mass numbers (A), K = 12 can be regarded as a suitable parameter.

3. CALCULATIONS FOR MODEL NUCLEAR SYSTEMS

The cross-sections for equilibrium and pre-equilibrium decay depend in complex manner on such quantities as binding energy, density parameter, shell structure, pairing energy etc. In order properly to appreciate both the importance of taking into account pre-equilibrium decay, and the influence of structural effects on the cross-sections, we performed various calculations for a model compound system with the following parameters:

Initial energy of incident neutron = 14 MeV;

Binding energy of all nuclei $B_n = B_p = 7$ MeV;

Density parameter of all nuclei $a = 13.3\ \text{MeV}^{-1}$, which corresponds to a mass number $A \approx 100$, since for the Fermi-gas model $a = \frac{A}{7.5}\ \text{MeV}^{-1}$;

Pairing energy for all nuclei $\Delta = 0$;

Cross-sections of the inverse reaction σ_{inv} are calculated using the optical model for A = 100 as in Refs [7] and [8].

Figure 2 shows emission spectra for the first neutron and proton with and without consideration of pre-equilibrium decay models. The presence of pre-equilibrium decay has a strong effect on the shape of the spectra, the cross-sections, and also on the branching of decay of the compound system for both channels. Owing to the emission of a large number of nucleons of high energy the mean energy of excitation of the final nucleus is reduced and, as a result, the probability of emission of secondary nucleons is reduced.

Figure 3 shows the (n,p), (n,n'), (n,pn), (n,np) and (n,2n) cross-sections obtained by using the comprehensive statistical model (left-hand side) and by taking into account pre-equilibrium decay models (right-hand side). In the second case, the first figure in parentheses is the pre-equilibrium cross-section and the second figure the equilibrium cross-section.

It is interesting to note that the pre-equilibrium cross-sections for emission of secondary nucleons are relatively small. However, the presence of pre-equilibrium processes in the emission of primary nucleons has a marked effect on the total cross-section of processes with emission of two nucleons. The (n,pn) and (n,np) cross-sections are 2.1 and 1.3 times greater, respectively. The (n,2n) cross-section is reduced by a factor 0.86. The total probability of neutron emission is reduced by 8% while the probability of proton emission is increased by a factor of 4.9!

In view of the arbitrary choice of parameters, these figures must of course be regarded as a sort of average representation of the influence of pre-equilibrium decay on the reaction cross-sections.

We shall now consider the influence of structural parameters on the cross-sections. Similar calculations were performed with successive variation of the nucleon binding energy, the density parameter (shell effect) or the effective excitation energy (pairing effect). The results are shown in Table 1. The first column indicates which of the above-mentioned effects is being considered.

As regards the shell effect we can expect that in the pre-equilibrium stage of the reaction with n = 3 the mean excitation energy for each exciton is $\frac{21}{3} = 7$ MeV, which is considerably higher than the value (of the order of

1 MeV) for the gap in the single-particle level scheme. In the equilibrium state the number of excitons in our system is $\bar{n} \approx 18 \ldots 19$, i.e. the mean energy per exciton is of the same order of magnitude as the width of the gap between shells. Accordingly, the influence of the shell structure must be relatively weak in pre-equilibrium processes and very strong in equilibrium processes (cf. also [9]). The figuresgiven in the second line were obtained with the density parameters of the residual nuclei after proton emission reduced by 2 MeV^{-1} compared with the parameter in the first line. This means that proton emission is reduced by a factor of approximately 10 if the calculation is based solely on the statistical model. There is also a correspondingly marked reduction in the (n,pn) and (n,np) cross-sections. The fact that there are pre-equilibrium processes with proton emission means that there is a reduction of only 8% in the total probability of proton emission while the (n,pn) and (n,np) cross-sections are reduced by factors of 0.72 and 0.48, respectively. If no account were taken of pre-equilibrium decay models, the reduced a parameter would lead to (n,pn) and (n,np) cross-sections reduced by factors of 0.09 and 0.13, respectively, while the (n,2n) cross-section would be increased by 0.5%.

The figures in the third line were obtained by applying a similar shell effect in the neutron system. In this case, too, the presence of pre-equilibrium processes will smooth out the shell structure effects in the cross-sections. The probability of neutron emission is decreased and proton emission is increased.

The next three lines demonstrate the occurrence of the pairing effect. In accordance with expression (4), shifts of Δ = 2, 1 or 0 MeV are introduced for residual nuclei of types even-even, odd-even (or even-odd) or odd-odd, respectively. In decay of the compound nucleus for even-even target nuclei the probability of emission of a primary neutron is reduced in favour of higher probability of proton emission, since in the latter case the residual nucleus is of the odd-odd type. There is a corresponding increase in the (n,pn) cross-section and decrease in the (n,2n) and (n,np) cross-sections. Depending on whether or not pre-equilibrium decay models are taken into account, the cross-sections of these processes differ by 0.7, 0.84 and 2.1, respectively.

In the case of target nuclei of the even-odd type the (n,np) and (n,pn) cross-sections are reduced. In that of odd-even nuclei the (n,2n) cross-section is reduced while the (n,np) cross-section is increased by a factor of about 10!

Finally, the last line of Table 1 gives the cross-sections for the case of underestimated binding energy $B_n = B_p = 5$ MeV. The excitation energy $E^* = 21$ MeV remains unchanged; this is actually equivalent to an increase in the energy of the incident neutrons. In this case, the effect of pre-equilibrium processes is even more pronounced than in the first case - the probability of proton emission is increased by a factor of 6.2, while the probability of neutron emission is decreased by a factor of 0.83.

Summarizing the calculations performed, it can be said that taking account of pre-equilibrium decay models results in a considerable change in the cross-sections of processes with emission of one or two nucleons. An effect of this order of magnitude can be expected from the structural effects studied. In calculating (n,2n), (n,pn) and (n,np) processes, therefore, it is essential to take into account the possibility of pre-equilibrium emission of particles and to use individual parameters B, a and Δ for each nucleus concerned.

4. CALCULATIONS FOR SPECIFIC NUCLEI

In real nuclei the effects considered above are mixed and partly interconnected, for instance the filling of a shell is usually reflected both in the density and the binding energy. It is therefore generally not possible to predict the effect of pre-equilibrium emission on the cross-sections of the processes in which we are interested. For this reason we shall examine 13 isotopes in the range $58 \leqslant A \leqslant 209$, taking careful account of binding energy, density parameters, and pairing energy in each nucleon-emission event.

The cross-sections for compound-system formation and the inverse-process cross-sections are taken from the optical model [7, 8]. The emission of compound particles is taken into account by a slight reduction in the probability of the first compound system being formed. In the second stage of the reaction the emission of complex particles is ignored. The binding energies are taken from the table of Q values in Ref. [10]. The density parameters are taken from the semi-empirical formula in Ref. [11] and from the experimental values obtained in the analysis of neutron resonances in Ref. [12]. The pairing energies for calculating the density from expression (4) were taken from Ref. [13]. In the pre-equilibrium decay models, account has so far not been taken of the effect of nucleon pair correlation on density.

The results of the calculations are given in Fig. 4. The upper part of the figure shows the (n,2n) cross-sections with and without consideration of

pre-equilibrium decay models. In all cases, except for the ^{58}Ni nucleus, the expected reduction of 14-29% is found in the (n,2n) cross-section. For a constant incident neutron energy 14 MeV, the effect of considering the pre-equilibrium decay models decreases with increasing mass number. Reference [2] was followed not long ago by the work of Holub and Cindro [14], which showed that actually the experimental cross-sections of the (n,2n) process are somewhat lower than the value obtained from calculations based on the statistical theory of nuclear reactions. It must be emphasized that not very long ago this process was regarded as a "standard example" of a model of successive evaporation of two neutrons.

The increase in the ^{58}Ni(n,2n) cross-section from 0.7 mbarn to 1.6 mbarn can be explained by the relatively high threshold of the (n,2n) reaction and the large cross-section for equilibrium emission of protons.

The cross-sections of the (n,np) reactions show a marked increase, especially for heavy nuclei. This is due to the fact that most of the secondary protons are emitted in the pre-equilibrium stage of the reaction. The mechanism of the (n,np) reaction thus differs fundamentally from the assumptions based on the statistical theory of nuclear reactions.

When we consider the lighter nuclei, another effect is observed. The Coulomb barrier becomes more transparent for protons, and the proton-binding energy is less, in the general case, than the neutron-binding energy. There is a range of excitation energies in which only proton emission is possible, and the compound nucleus lives for a relatively long time before it decays via the proton channel. In this case, taking account of pre-equilibrium decay models results in only a small change in the (n,np) cross-section. In the case of ^{90}Zr the (n,np) cross-section decreases slightly while in that of ^{58}Ni, ^{69}Ga and ^{79}Br it increases slightly. With ^{80}Se, the pronounced increase in the cross-section is due to the fact that the threshold of the (n,np) reaction is higher than that of the (n,2n) reaction. There is thus no energy range in which only secondary emission of protons takes place. The effect of pre-equilibrium processes is therefore more pronounced.

The cross-sections of (n,pn) reactions are given in the lower part. In the fairly heavy nuclei, owing to the Coulomb barrier, the emission of a primary proton takes place almost exclusively via pre-equilibrium processes.

In the range $A<100$, taking pre-equilibrium decay models into account results in a smaller and less obvious change in the cross-section value. The direction of the change in the cross-section depends on the extent to which the reduction in the probability of compound nucleus formation (due to

pre-equilibrium emission of nucleons and leading to a reduction in the emission of primary protons from the compound nucleus) is offset by the emission of low-energy, pre-equilibrium, primary protons, after which the "evaporation" of a secondary neutron is possible.

For ^{58}Ni and ^{112}Cd, taking account of pre-equilibrium decay models generally means a decrease in the number of primary, low-energy protons, i.e. the (n,pn) cross-section is reduced. In the case of ^{80}Se, as a result of the high energy of the proton bond, the (n,pn) cross-section shows an increase since the emission of low-energy protons occurs primarily in the pre-equilibrium stage of the reaction.

The calculations for specific nuclei outlined above illustrate the complicated influence of nucleus structure effects and of process flow mechanism on the total cross-sections of (n,2n), (n,pn) and (n,np) reactions. The same applies of course to the particle spectra. Figure 1 represents an analysis of the neutron spectra. Taking account of pre-equilibrium decay models is necessary not only for a correct description of the high-energy part, which consists primarily of pre-equilibrium neutrons, but also to get a correct absolute value for the spectrum of secondary neutrons.

CAPTIONS TO FIGURES

Fig. 1. Comparison between experimental and calculated (parameter K in equation (2) equal to 12) neutron spectra for various nuclei in the range $79 \leqslant A \leqslant 200$.

Symbols: — • — spectrum for pre-equilibrium decay models

— — — spectrum of primary neutrons from statistical theory

— - — spectrum of secondary neutrons

——— total calculated spectrum.

Fig. 2. Primary neutron and primary proton spectra with (———) and without (— — —) consideration of pre-equilibrium decay models; excitation energy $E^* = E_0 + B_n = 21$ MeV; cross-section for formation of compound system = 1720 mbarn. The energy range is indicated in which the emission of secondary nucleons is possible.

Fig. 3. Branching scheme for probabilities of neutron and proton emission; $A = Z + N = 100$; $E^* = 21$ MeV; $B_p = B_n = 7$ MeV; $a = 13.3$ MeV^{-1}. Left side: without consideration of pre-equilibrium decay models; Right side: with consideration of pre-equilibrium decay models.

Fig. 4. Effect of consideration of pre-equilibrium decay on cross-sections for multiple emission of nucleons for specific nuclei and for a model compound system (A = 100).

Table 1

Calculated decay cross-sections (σ mbarn) and emission of neutrons (n) and protons (p) for a compound system with the following parameters: cross-section for formation 1720 mbarn; A = 100; E^* = 21 MeV. A comparison is made between cross-sections obtained without consideration of pre-equilibrium decay and cross-sections obtained with consideration of this type of emission, the table giving the corresponding sums of pre-equilibrium + equilibrium components for each channel. The influence of structural effects on the cross-sections in question are studied by varying the parameters B, a and Δ.

	$B_p=B_n$ (MeV)	a (MeV^{-1})	Δ (MeV)	σ (mbarn)	
				n from (Z,N)	p from (Z,N)
Standard system	7	I3,3	0	I7I0 → 782+887	9,7 → 46+5
p-shell effect	7	a=II,3 exc. a(Z,N-γ)=I3,3 for γ=0,I,2.	0	I7I9 → 782+892	0,95 → 46+0,5
n-shell effect	7	a=II,3 exc. a(Z-γ,N)=I3,3 for γ=0,I,2	0	I656 → 782+859	64 → 46+33
Pairing effect (even-even target)	7	I3,3	0,I,2	I662 → 782+862	58 → 46+30
Pairing effect (odd-even target)	7	I3,3	0,I,2	I7I2 → 782+888	8,I → 46+4,2
Pairing effect (even-odd target)	7	I3,3	0,I,2	I7I2 → 782+890	8,I → 46+2,4
Binding energy E^* = 21 MeV	5	I3,3	0	I707 → II80+450	I2,8 → 87+3,4

Table 1 (continued)

σ (mbarn)			Neutron emission	Proton emission
n from (Z,N-1) n,2n	p from (Z,N-1) n,np	n from (Z-1,N) n,pn	σ_{nM} (mbarn)	σ_{pM} (mbarn)
I700 → 37+I432	0,45 → 0,28+0,30	7,I → 0,29+I4,5	34I7 → 3I53	I0,5 → 5I
I709 → 37+I443	0,06 → 0,28+0,04	0,78 → 0,29+I0,3	3429 → 3I65	I,0 → 47
I65I → 37+I406	0,2I → 0,28+0,I4	48 → 0,29+36	3355 → 3I20	64 → 79
I645 → 37+I342	0,I9 → 0,28+0,I2	3I → 0,29+2I	3338 → 3044	58 → 76
I704 → 37+I434	0,003 → 0,28+0,002	2,3 → 0,29+2,8	34I8 → 3I44	8,I → 50
I645 → 37+I27I	8,2 → 0,28+5,7	6,4 → 0,29+I3	3363 → 2993	I6 → 54
I704 → 2I2+I303	3,I → 7,6+I,6	I2,7 → 8,I+58	4943 → 4II4	I6 → 99

REFERENCES

[1] SEIDEL, K., SEELIGER, D., REIFF, P., TONEEV, V.D., "Pre-equilibrium decay in nuclear reactions" (in Russian), Fizika elementarnykh chastits i atomnogo yadra, JINR, Dubna (1975).

[2] SEIDEL, K., SEELIGER, D., MEISTER, A., International Symposium on Neutron Induced Reactions, Smolenice CSSR 1974; TU Dresden-Informationen 05-9-74

[3] BLANN, M., Phys. Rev. Lett. 27 (1971) 337; BLANN, M., and MIGNERY, A., Nucl. Phys. A 186 (1972) 245

[4] WEISSKOPF, V. D. and EWING, D. H., Phys. Rev. 57 (1940) 472

[5] LE COUTEUR, K. J. and LANG, D. W., Nucl. Phys. 13 (1959) 32

[6] HERMSDORF, D., MEISTER, A., SASSONOFF, S., SEELIGER, D., SEIDEL, K. and SHAHIN, F., ZfK - 277 (1974)

[7] LINDNER, A., IFK - 17, EANDC (E) 73 "U" (1966)

[8] PEREY, F. G., Phys. Rev. 131 (1963) 745
KIESSIG, G., programme ELIESE, unpublished

[9] STRUTINSKY, V. M., Nucl. Phys. A 95 (1967) 420

[10] MAPLES, G., GOTH, G. W. and CERNY J., Nucl. Data A 2 (1966) 429

[11] SEELIGER, D. and SEIDEL, K., Wiss. Zeitsch. d. TU Dresden 21 (1972) 714

[12] FACCHINI, U. and SAETTA-MENICHELLA, E., Energia Nucleare 15 (1968) 54

[13] NEMIROWSKY, P. E. and ADAMCHUK, YU. V. Nucl. Phys. 39 (1962) 551

[14] HOLUB, E. and CINDRO, N., Phys. Letters 56 B (1975) 143

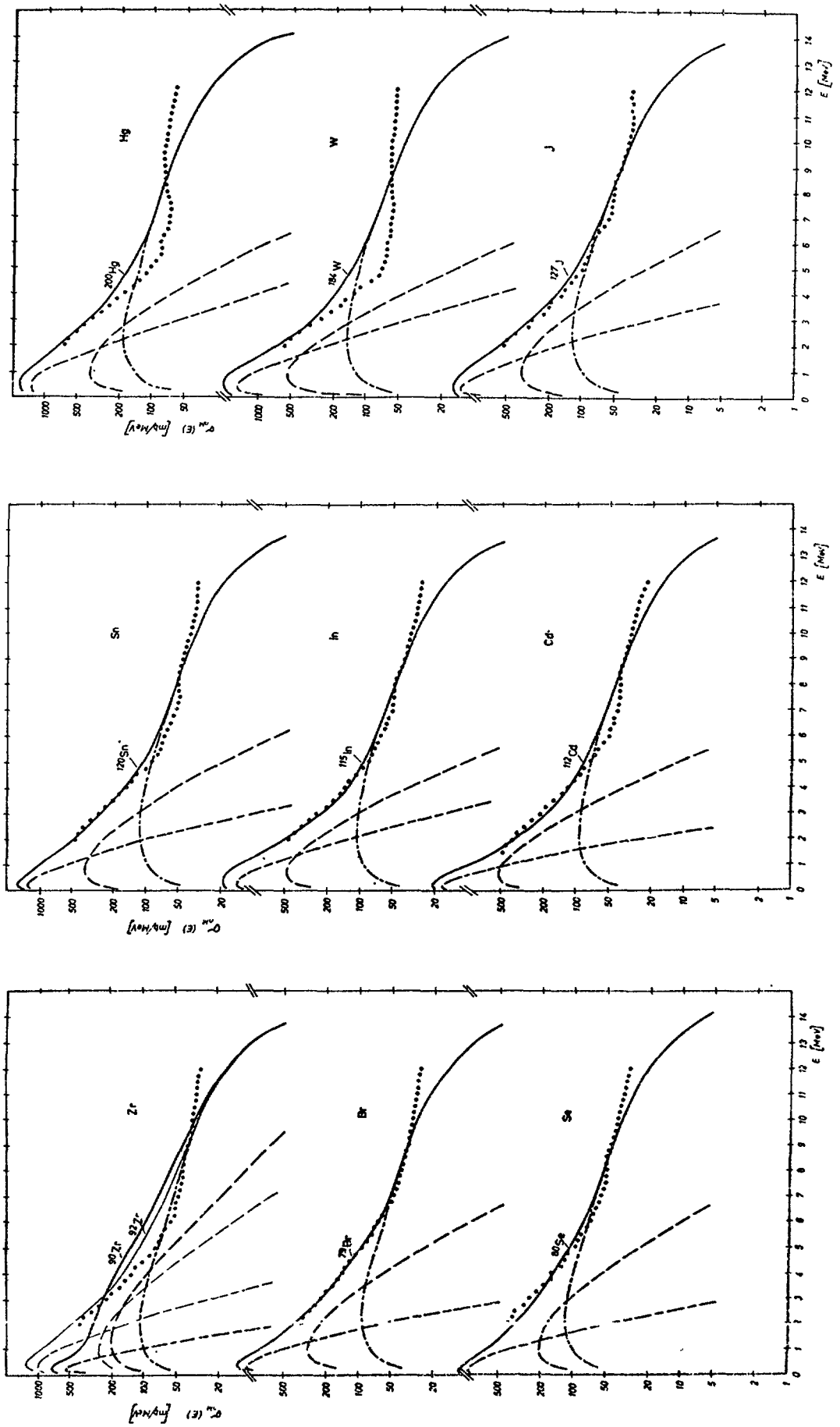
Hg
200Hg
W
184W
J
127J
Sn
120Sn
In
115In
Cd
112Cd
Zr
90Zr
92Zr
Br
79Br
Se
80Se
E [MeV]
σγn (E) [mb/MeV]

Fig. 1

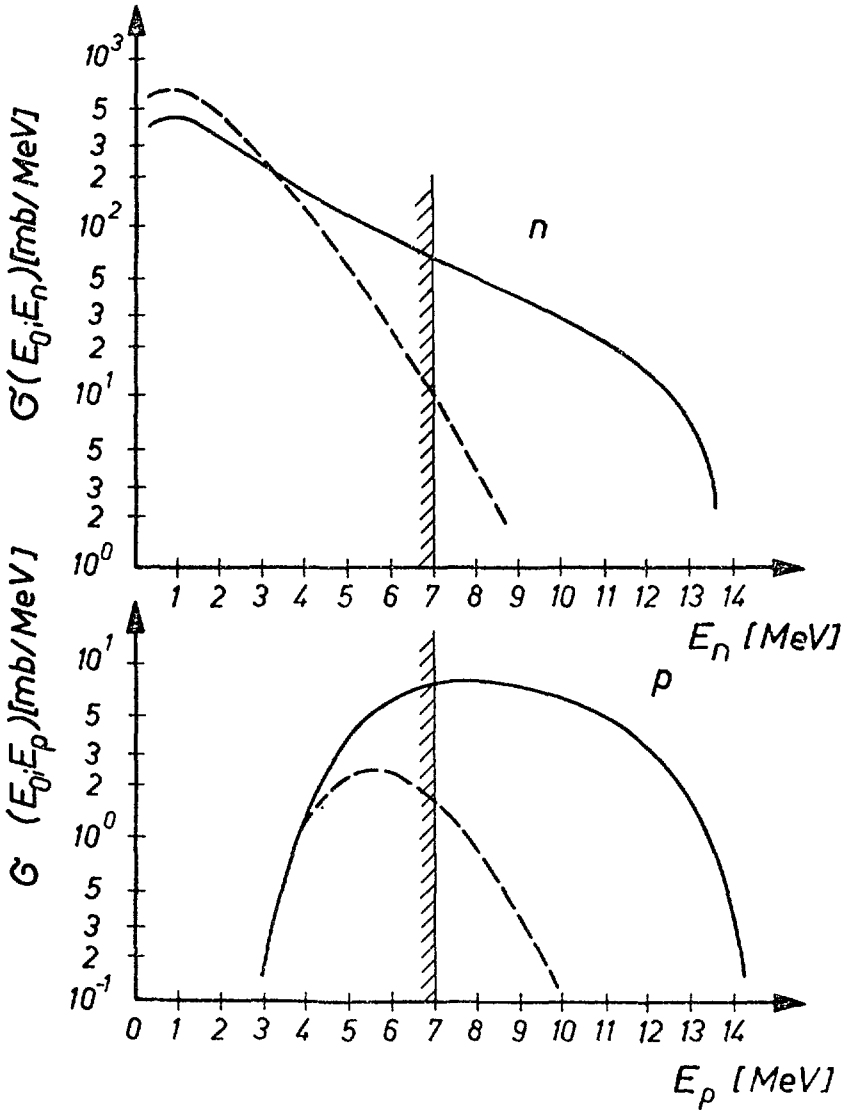
$\sigma(E_0;E_n)$ [mb/MeV]
10^3
5
3
2
10^2
5
3
2
10^1
5
3
2
10^0
n
1 2 3 4 5 6 7 8 9 10 11 12 13 14
E_n [MeV]
$\sigma(E_0;E_p)$ [mb/MeV]
10^1
5
3
2
10^0
5
3
2
10^{-1}
p
0 1 2 3 4 5 6 7 8 9 10 11 12 13 14
E_p [MeV]

Fig. 2

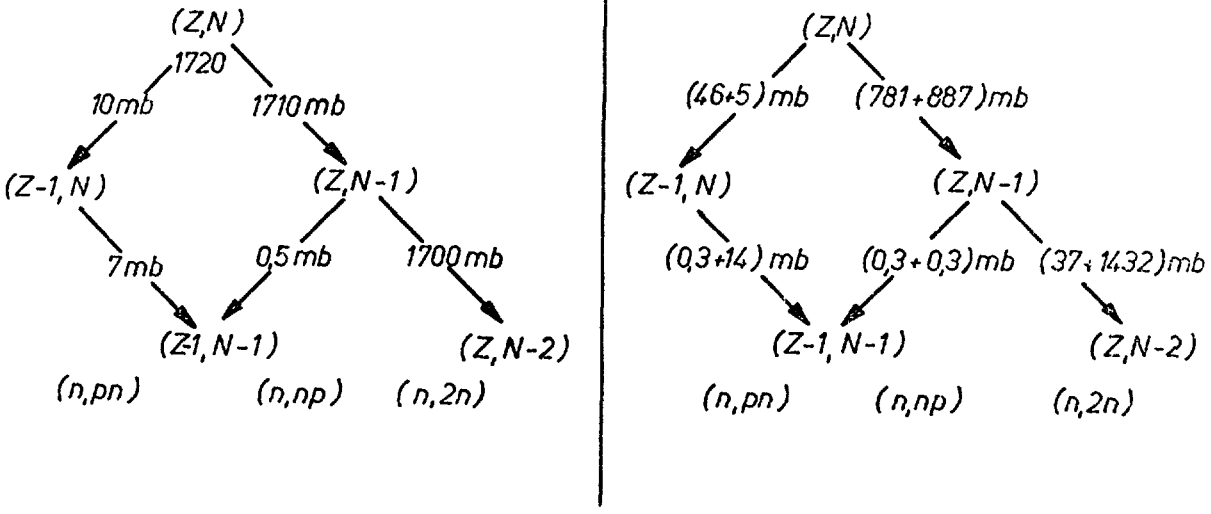

Fig. 3

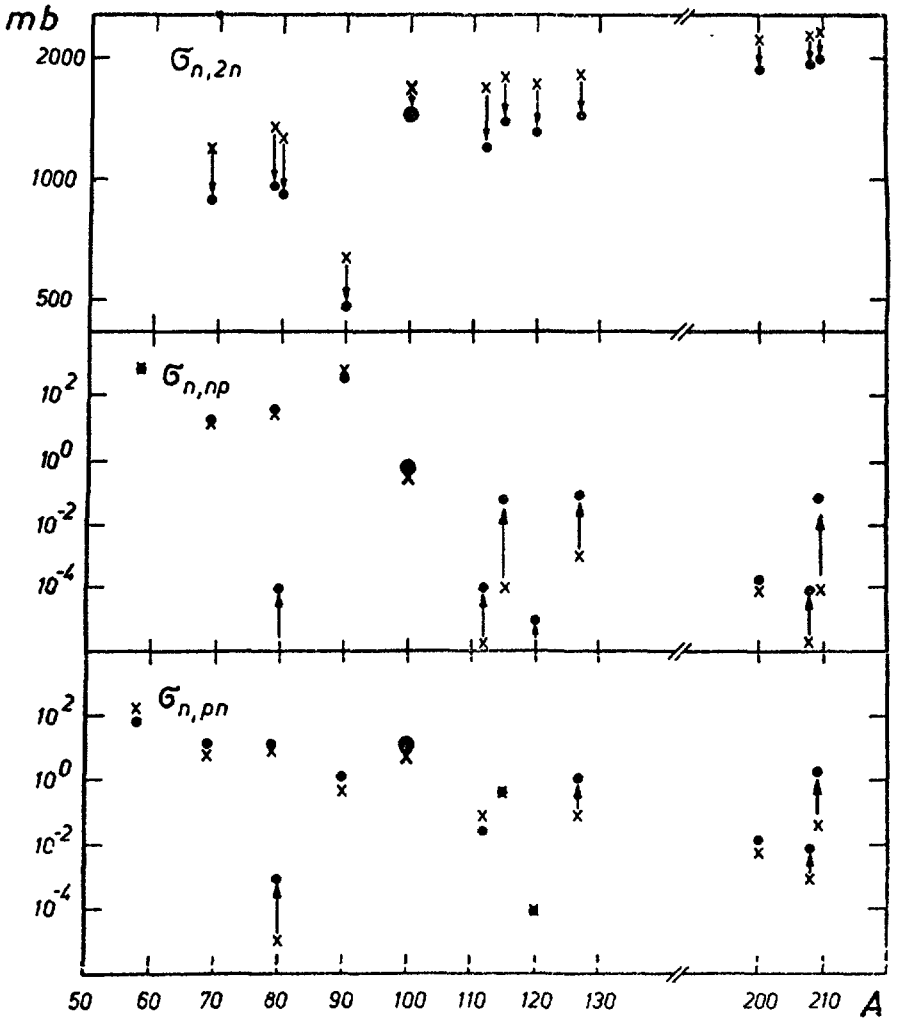

Fig. 4

Next page(s) left blank

Contributed Paper No. 14

THE USE OF THE PRÉ-EQUILIBRIUM MODEL IN THE EVALUATION OF ^{93}Nb + n CROSS SECTIONS

D. Hermsdorf, G. Kießig, D. Seeliger
Section of Physics, Technical University Dresden, GDR

Abstract:

Based on a critical analysis of experimental data as well as calculations in the framework of different nuclear reaction models, the reaction cross sections for ^{93}Nb+n at neutron incident energies from 30 keV up to 20 MeV were evaluated. The present paper demonstrates, that statistical models including particle emission from pre-equilibrium states have proved to be valuable tools for evaluation purposes.

1. INTRODUCTION

Niobium represents a material of still growing interest to fusion reactors because it is preferred for the design of the neutron blanket surrounding the fusion plasma. An accurate knowledge of the cross sections of such materials composing the blanket is essential for estimating breeding, heat generation, radiation demage and radioactivity. Derived data requirements can be fulfilled only partially by experimental data, and some of the wanted data have not been evaluated up to now. This situation exists although since the initial evaluations by Howerton [1] and Allen and Drake [2] the cross sections have undergone several revisions and re-evaluations [3, 4]. Also further independent evaluations [5, 6] and compilations [7] were carried out. Therefore a re-evaluation of niobium cross sections founded on recent measurements published in the period from 1969 to April 1975 was accomplished, as well as calculations in the frame of some nuclear reaction models. Results of this work have been reported elsewhere [8].

The aim of the present work is, to show by some examples the utility of pre-equilibrium models for neutron data evaluation work.

2. THEORETICAL MODELS USED FOR EVALUATION

2.1 Survey of used programs and models

A main feature of this evaluation is the use of nuclear reaction models, which enable us to calculate different reaction channels in a unique and consistent manner and with the use of a unique set of nuclear structure parameters for different model calculations. In this sense the following reaction models and computer programs have been applied:

- The Hauser-Feshbach program ELISA [9] for calculations

of σ_{nT}, σ_{nn^*}, σ_{nn}, as well as $\sigma_{n,\alpha}$ and $\sigma_{n,p}$ in the energy range 0.03 MeV to 5 MeV. The total spectroscopic information available up to an excitation energy of about 1.5 MeV (16 or 10 isolated levels in the neutron and proton channel, respectively) was treated exactly, whereas the continuum region was taken into account by a nuclear level density dependent part.

- Optical model calculations of σ_{nT} and σ_{nn}, also by means of the program ELISA, in the energy range up to 20 MeV.
- Calculations by means of complete statistical models including pre-equilibrium and equilibrium particle emission in the energy range above 9 MeV with the programs GLUNE [10] and WPREC [11] for all reaction channels. As partially shown in section 3., especially GLUNE, based on Blann's hybrid model [12], proved very successful for consistent calculations of the excitation functions of $\sigma_{nn'}$, $\sigma_{n,2n}$, $\sigma_{n,3n}$, σ_{np}, $\sigma_{n,pn}$ and $\sigma_{n,np}$ as well as neutron and proton emission spectra. The formalism of exciton models has been applied also for description of the (n,α) reaction channel using the "preformation" factor, introduced by Colli et al. [13].
- Based on the complete statistical model (Weisskopf-Ewing-formalism) there are some known computer programs for data evaluation purposes and a variety of different empirical formulae. We used some of them for comparison, especially Pearlstein's program THRESH [14] has been tested extensively.

We used the following set of parameters for different model calculations:

- Nuclear level density parameters a [15];
- Q-values [16];
- pairing energies [17];
- optical potential parameters [4, 18] and transmission

coefficients calculated therefrom (inverse cross sections);
- nuclear level schemes [19].

2.2 Pre-equilibrium calculations

In 1966 Griffin [20] suggested a simple quantitative model of nuclear reactions in order to explain the high-energy part of nucleon spectra in reactions at moderate excitation energy. Afterwards Griffin's exciton model was continuously modified and improved. However, its basic assumptions, simplicity and physical transparency, were preserved up to now.

A formulation of present state of exciton model is given in an other contribution to this meeting [21], so that we can shorten its description and explanation of symbols in this paper.

In the hybrid model [12], a special variant of the exciton model, the probability of emitting a nucleon of type i in the channel energy range ϵ to $\epsilon + d\epsilon$ is given as

$$(1)\quad N_i(\epsilon)d\epsilon = \sum_{\substack{n=n_0 \\ \Delta n=2}}^{\bar{n}} \left[R_i(n)\,\frac{\omega(n-1,U)}{\omega(n,E)}\right]\left[\frac{\lambda_{em}(\epsilon)}{\lambda_{coll}(\epsilon)+\lambda_{em}(\epsilon)}\right]\cdot D_n$$

The first set of square brackets represents the probability to find a nucleon of the required type and energy in a p-particle- h-hole state. The second set of brackets contains the probability, that the excited particle of type i will decay into continuum at the rate $\lambda_{em}(\varepsilon)$ before it interacts internally with the rate $\lambda_{coll}(t)$ to give an (n+2)-exciton state. Finally, D_n - is the depletion factor which represents the fraction of initial population surviving the deexcitation by particle emission prior to the considered n-exciton state.

One of the most important features of the hybrid model is the replacement of internal transition rates λ_+ by the collision rate λ_{coll} of the particle in the continuum,

which is derived from considerations of nuclear matter. Blann recommends the following expression

$$(2)\quad \lambda_{Coll} = 1.4\cdot 10^{21}(\varepsilon+B_i) - 6\cdot 10^{10}(\varepsilon+B_i)^2\ [s^{-1}]\ ,$$

where B_i - is the binding energy of the particle i. The decay rate to continuum easily can be calculated by the principle of detailed balance. And so, with the hybrid model, in principle, can be calculated without any free parameters both absolute cross sections and excitation functions of nuclear reactions with outgoing nucleons. Really, the collision rate λ_{coll} must be multiplied with an adjustable parameter **1/K**, where $k \approx 5...10$. Only in this case hybrid model gives satisfactory absolute pre-equilibrium cross section values at excitation energy about 20 MeV. In the present work all calculations with the hybrid model were carried out with a constant factor k=5, which gives the best overall apreement between different reaction channels. The intermediate state densities used in this work are those of the equidistant spacing type

$$(3)\quad \omega(p,h,E) = \frac{g(gE)\,p+h-1}{p!\,h!\,(p+h-1)!}\ ,$$

where density of single particle states g is calculated from level density parameters a [15] by the well-known Fermi gas expression

$$(4)\quad a = \frac{\pi^2}{6}\,g\ .$$

3. DISCUSSION OF RESULTS FOR VARIOUS REACTION CHANNELS

3.1 Inelastic scattering

Deviations from the simple evaporation spectrum (constant temperature T or constant a) become remarkable at incident energies higher than 7 MeV. Experimental spectra can be well described taking into account neutron emission from pre-equilibrium states (see also contribution [21] to this meeting). Figs. 1 and 2 show, for example, experimental and calculated neutron emission spectra at 14 MeV and 9 MeV incident energy. In both cases calculations with k=5 give a good fit to experimental data. At 14 MeV a considerable part of emitted neutrons are due to (n,2n) processes (see contribution [22] to this meeting). The situation for the (nn')-channel is the following: Above 9 MeV the $\sigma_{nn'}$ cross section decreases rapidly mainly due to the competition of (n,2n)-reactions. Taking into account pre-equilibrium emission this general situation keeps unchanged, but, the $\sigma_{nn'}$ cross sections become significantly higher than it would be expected by the complete statistical reaction theory only. For instance, at 14 MeV pre-equilibrium emission cross-section for the first neutron is about $\sigma^{N}_{nn'} \simeq 400$ mb [21], that leads to a decrease of $\sigma_{n,2n}$ cross section by about 150 - 200 mb [22] and corresponding increase of the total $\sigma_{nn'}$ cross section by the same amount. Since the total $\sigma_{nn'}$ cross section at 14 MeV in the present evaluation was estimated to be about 350 mb, we can conclude, that pre-equilibrium emission causes an essential part of the total $\sigma_{nn'}$ cross section. Its importance increases with increasing energy.

Unfortunately, there are no direct measurements of (nn')-cross section at energies higher than 9 MeV. But the neutron emission spectra (Fig. 1) have proved a valuable tool for adjustement of neutron emitting reactions altogether.

3.2 Reaction (n,2n)

The resulting evaluation of (n,2n) excitation function is shown in Fig. 3. The calculation with GLUNE, including pre-equilibrium emission fits well experimental data as well as mass-systematics. At 14 MeV it gives by about 10% reduced (n,2n) cross section for niobium in comparison with the calculation in the framework of complete statistical model [14, 23]. The reduction of $\sigma_{n,2n}$ is mainly due to the higher loss of excitation energy through pre-equilibrium emission of first neutrons. Cross sections of pre-equilibrium emission of two neutrons are rather small (6 mb at 14 MeV up to 30 mb at 20 MeV). A more detailed discussion of the influence of pre-equilibrium emission on cross sections $\sigma_{n,2n}$, $\sigma_{n,pn}$ and $\sigma_{n,np}$ is presented in another contribution to this meeting [22].

The recent measurement of (n,2n) excitation function by Frehaut [24] is also in good agreement with the present evaluation, supporting our conclusions.

3.3 Reaction (n,p)

The calculated (n,p) excitation function is shown in Fig. 4. There is only one experimental point at 14 MeV, which seems to be to small by a factor 2. More experiments are requested, to prove the calculations. The present calculation shows the increase with energy of the importance of pre-equilibrium emission. The resulting behaviour of pre-equilibrium and equilibrium contributions to (np)-process is similar to the results obtained by Decowski et al. [24] from analysis of experimental (n,p) excitation functions for several nuclei. Generally speaking, due to Coulomb barrier effects, the influence of pre-equilibrium processes on charged particle emission is much higher, than on neutron emission.

The present calculation is similar to the evaluation by Smith et al. [4], which is based on mass-systematics of typical (np)-excitation functions.

3.4 Reaction (n,α)

The original hybrid model [12]did not include α-particle emission. Therefore, the present evaluation is based on theoretical considerations in the frame of pre-equilibrium emission of pre-formed α-particles developed by Colli et al. [13] in the framework of exciton model. But, there is no principal limitation of the hybrid model, as shown by Obložinsky [25], including thatcomplex-particle emission in the hybrid model is also possible. Results are shown in Fig. 5. The present evaluation is in good agreement with experimental data. The importance of pre-equilibrium processes in this case seems to be obvious.

4. SUMMARY AND CONCLUSIONS

The evaluation of niobium neutron cross sections was carried out to meet the nuclear data requirements. This was tried to

achieve by use of very recent measurements and new nuclear reaction models. In this way these models have been examined for their suitability and accuracy. Especially it has been paid attention to apply different models and computer codes for a consistent description of several reaction channels at onçe by use of the same nuclear structure parameters. Models including pre-equilibrium particle emission have proved their importance in all reaction channels at neutron energies higher than 9 MeV. Simplicity and universality of exciton model and its modifications favour the application of this phenomenological nuclear reaction theory for the evaluation work.

REFERENCES

[1] HOWERTON, R.I., UCRL-5351, 1958
[2] ALLEN, M.S., DRAKE, M.K., GA-8133, 1967
[3] BLOW, S., LIPSCOMBE, B.A., AERE-M2230, 1969
[4] SMITH, A.B., et al., ANL-AP/CTR/TM-4, 1973
[5] POPOV, V.J., et al., Byull. Centra Yad. Dann. 4 (1967) 169
[6] BAZAZYANTS, N.O., et al., Yad. Konst. 8 (1972) 61
[7] ALLEY, W.E., LESSLER, R.M., UCRL-50484 (Rev. 1), 1972
[8] HERMSDORF, D., et al., Neutron cross section evaluation for ^{93}Nb in the energy range from 30 keV to 20 MeV, 3rd Conf. Neutron Physics, Kiev, 1975, (to be published)
[9] KIESSIG, G., Thesis, Technical Univ. Dresden, 1975
[10] HERRMANN, U., SEIDEL, K., SEELIGER, D., 3rd Intern. Seminar on Interaction of Fast Neutrons with Nuclei, Gaussig, Nov. 1973 (Proc. Conf. ZfK-271 (1974) 80)
[11] GUDIMA, K.K., OSOSKOV, G.A., TONEEV, V.D., Rep. JINR, P4-7821, Dubna 1974
[12] BLANN, M., MIGNEREY, A., Nucl. Phys. A186 (1972) 245
[13] MILAZZO-COLLI, L., BRAGA-MARCAZZAN, M.G., Nucl. Phys. A210 (1973) 297
[14] PEARLSTEIN, S., J. Nucl. Energ. 27 (1973) 81
[15] SHUBIN, Yu.N., Byull. Centra Yad. Dann. 4 (1967) 304
[16] MATTAUCH, J.E., et al., Nucl. Phys. 67 (1965) 32
[17] GILBERT, A., CAMERON, A.G.W., Canad. J. of Phys. 43 (1965) 1446
[18] HOLMQVIST, B., WIEDLING, T., J. Nucl. Energ. 27 (1973) 543
[19] VAN HEERDEN, I.J., et al., Z. Phys. 260 (1973) 9
[20] GRIFFIN, J.J., Phys. Rev. Lett. 17 (1966) 478
[21] HERMSDORF, D., et al., Neutron emission spectra analysis with pre-equilibrium and equilibrium statistical theory, these Proceedings, Contributed Paper 12
[22] SEIDEL, K., et al., Calculation of pre-equilibrium processes in (n,2n), (n,np) and (n,pn) reactions, these Proceedings, Contributed Paper 13
[23] PAULSEN, A., WIDERA, R., Z. Phys. 238 (1970) 23

[24] DECOWSKI, P., et al., 3rd International Seminar on Interaction of Fast Neutrons with Nuclei, Gaussig 1973 (Proc. Conf. ZfK-271 (1974) 71)
[25] OBLOŽINSKY, P., acta phys. slov. 25 (1975) 214

Figure captions

Fig. 1 Evaluation of neutron emission spectrum from ^{93}Nb+n at 14 MeV incident energy. Full line represents calculation with the program GLUNE [10], dash-dotted curve shows the pre-equilibrium contribution in this spectrum.

Fig. 2 The same as Fig. 1, but for 9 MeV incident energy.

Fig. 3 Evaluation of (n,2n)-excitation function. Full line represents calculation with the program GLUNE; dashed curve gives calculation by the equilibrium statistical model [23] only; dotted line represents evaluation by Smith et al. [4].

Fig. 4 Evaluation of (n,p)-excitation function. Full line represents calculation with the program GLUNE; dashed curve shows equilibrium and dash-dotted curve pre-equilibrium contribution to (n,p)-reaction.

Fig. 5 Evaluation of (n,α)-excitation function. Calculations were carried out following the method suggested by Colli et al. [13]. Notation of the curves is the same as in Fig. 4.

NEUTRON EMISSION SPECTRUM , E0 = 14 MEV

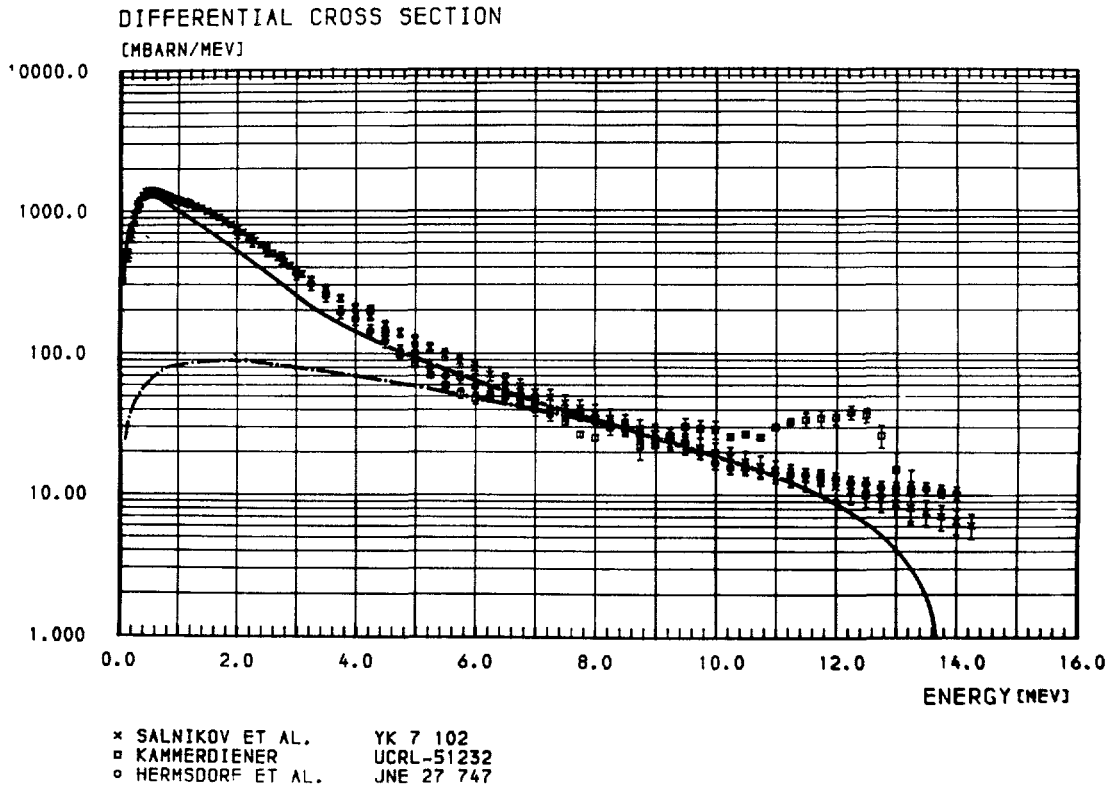

Fig. 1

NEUTRON EMISSION SPECTRUM , E0 = 9 MEV

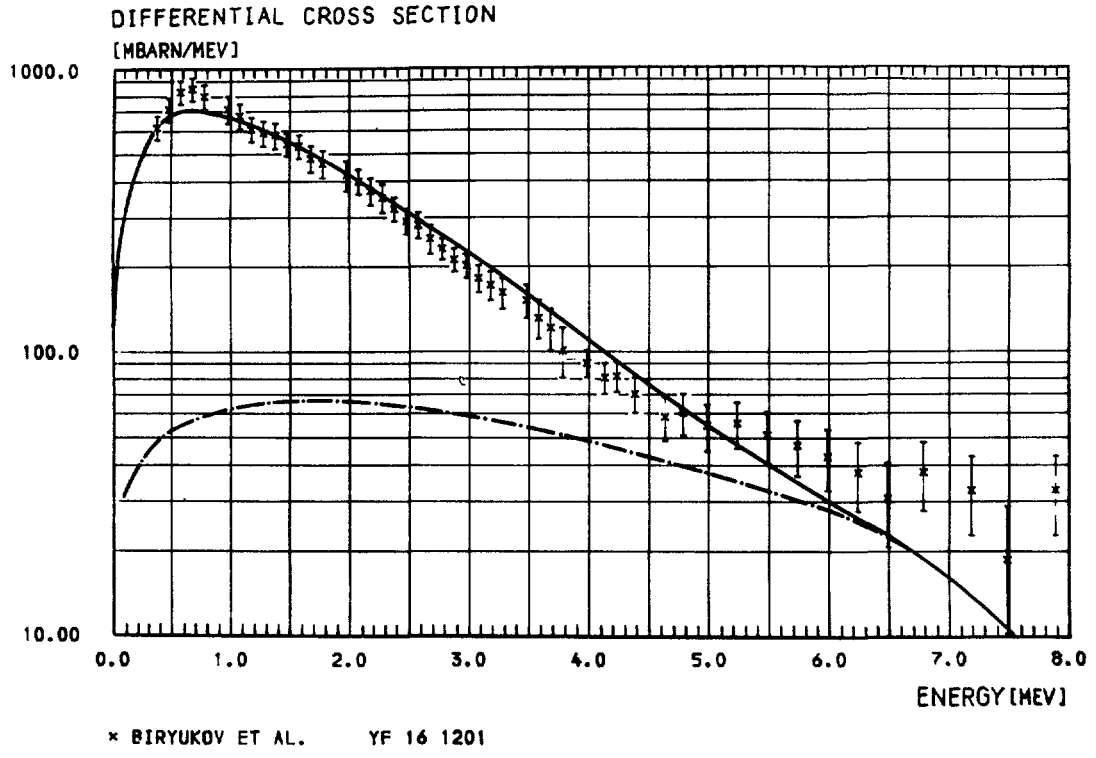

Fig. 2

93-NB(N,2N) EXCITATION FUNCTION

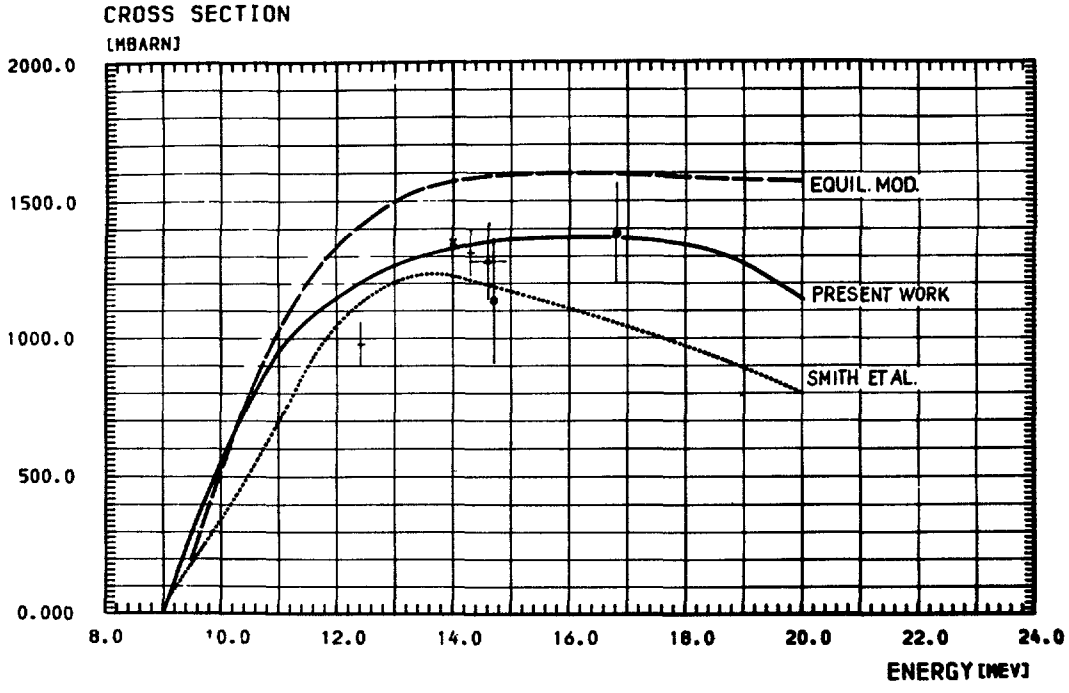

+ MATHER ET AL. AVRE-0-72/72
× HAERING ET AL. ZP 244 352
□ PAULSEN ET AL. ZP 238 23
○ CARTER 66 WASH 2 682
▲ HERMSDORF ET AL. JNE 27 747

Fig. 3

93-NB(N,P) EXCITATION FUNCTION

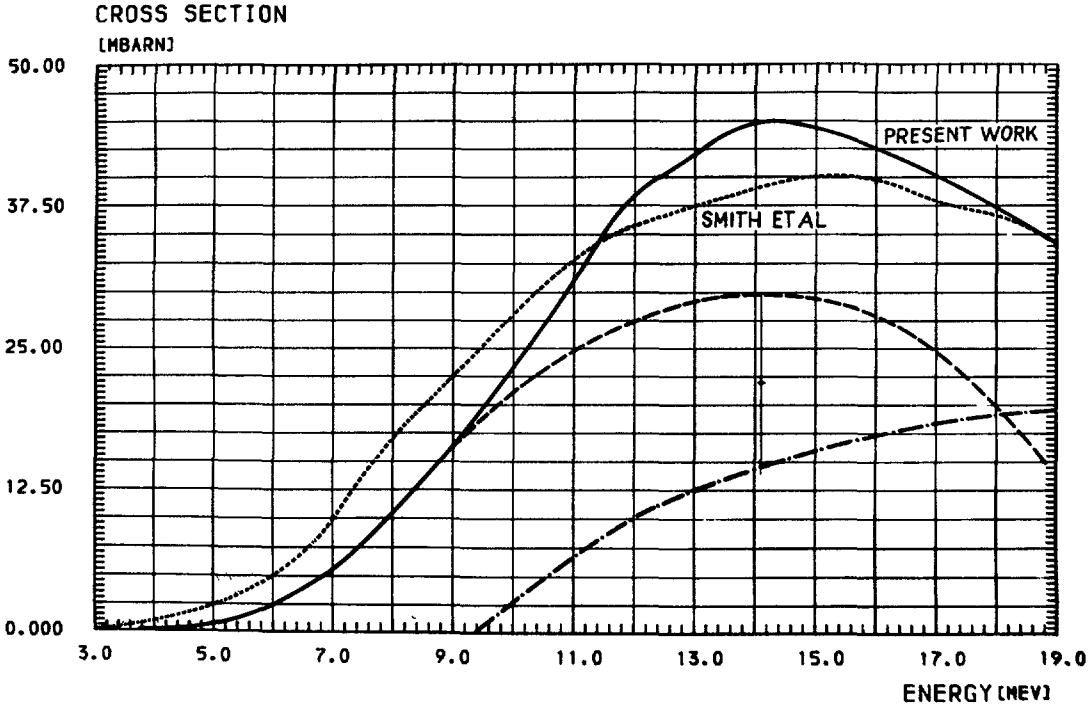

+ VERBINSKI ET AL. PR 108 779

Fig. 4

93-NB(N,ALPHA) EXCITATION FUNCTION

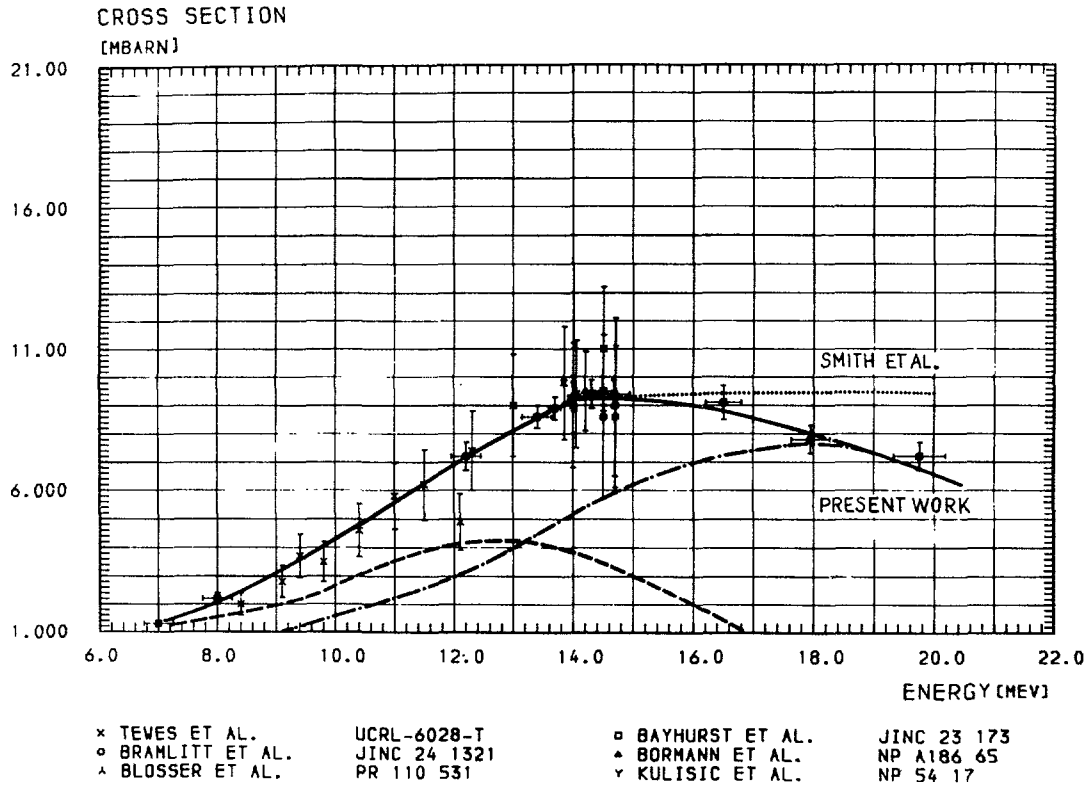

Fig. 5

Contributed Paper No. 15

Absolute values geometry dependent effects and the direct component in the pre-equilibrium analysis of inelastically scattered neutrons

Helmut Jahn

Institut für Neutronenphysik und Reaktortechnik
Kernforschungszentrum Karlsruhe und Fakultät für
Physik der Universität Karlsruhe
Fed.Rep.Germany

Abstract

The pure hybrid model and the geometry dependent hybrid model for pre-equilibrium nuclear reactions have been developed by Blann to calculate excitation functions as well as angle integrated scattered particle energy distributions of the inelastic scattering cross-sections of nucleons on nuclei with absolute values resulting for the cross sections. Both models are applied to the $^{56}Fe(n,n')$ process. In case of the pure hybrid model an extra direct component has to be added to fit the empirical data while the geometry dependent hybrid model reproduces the empirical data quite well without any adjustment and without an extra direct term. Indications are presented that the lowest exciton number term of the geometry dependent hybrid model can be understood as a certain average over the direct component. But more theoretical as well as empirical investigations have to be carried through in order to reach a definite clarification of these problems.

The influence of the pre-equilibrium component on the neutron leakage spectrum from a homogenous iron assembly is investigated.

1. Success and limitation of the Exciton Model

Cline and Blann[1] have discussed the detailed behaviour of an equilibrating compound nucleus by integrating an appropriate set of master equations. In this way they succeeded to describe the equilibrating process by a sequence of transitions between different numbers of excited particles and holes, so-called excitons. Only the increase or decrease by a particle-hole pair has been considered. To describe the single transition steps between the succeeding exciton numbers they used formulas of Williams[2] for the transition rates of which the expression describing an increase of the exciton numbers is

$$\lambda_{+}(n,E) = \frac{2\pi}{\hbar}|T|^2 \frac{g^3E^2}{n+1} \tag{1}$$

g is the one-particle level density, E the excitation energy of the equilibrating compound nucleus and

$$n = p + h \tag{2}$$

is the number of excitons which is the sum of the number p of particles and the number h of holes. The transition matrix element $|T|^2$ which is very difficult to calculate has been left unknown. It has been assumed to be independent of the exciton number n and the energy E and is simply treated as a constant parameter to be adjusted.

Cline and Blann[1] were able to show that a rigorous numerical solution of their master equations could very well be approximated by a closed form expression for the angle integrated spectral probability distribution of energy ε of an emitted nucleon which can be written as:

$$P(\varepsilon)d\varepsilon = \left\{P_{eq.}(\varepsilon) + P_{pr}(\varepsilon)\right\}d\varepsilon \tag{3}$$

In eq. (3) $P_{eq}(\varepsilon)$ is the simple Weisskopf evaporation formula which is given by

$$P_{eq}(\varepsilon) = C\frac{(2S+1)}{\pi^2\hbar^3} m\varepsilon\sigma(\varepsilon)\frac{\omega(U)}{\omega(E)} \tag{3a}$$

with the Fermi gas nuclear state density

$$\omega(E) = \frac{1}{\sqrt{48}E} e^{2\sqrt{\frac{\pi^2}{6}gE}} \tag{3b}$$

and the corresponding expression for $\omega(U)$ where U is the excitation energy of the residual target nucleus given by

$$U = E - \varepsilon - B \tag{3c}$$

with the binding energy B of the emitted nucleon. C in eq.(3a) and the one nucleon equidistant level density g are constants to be adjusted.

Furthermore $P_{pr}(\varepsilon)$ in eq.(3) is the energy distribution of nucleons emitted before equilibrium has been reached which can be written as

$$P_{pr}(\varepsilon)d\varepsilon = \sum_{\substack{n=n_0 \\ (\Delta n=2)}}^{\bar{n}} \left(\frac{\rho_{n-1}(U)g}{\rho_n(E)}\right)\left(\frac{\lambda_c(\varepsilon)}{\lambda+(n,E)}\right) d\varepsilon \tag{3d}$$

where $\rho_n(E)$ or $\rho_{n-1}(U)$ are the density distributions of the n or n-1 exciton states usually given by the Ericson expression

$$\rho_n(E) = \frac{g(gE)^{n-1}}{p!h!(n-1)!} \tag{3e}$$

and $\lambda_c(\varepsilon)$ is emission rate of the nucleons into the continuum given by the expression

$$\lambda_c(\varepsilon) = \frac{(2S+1)}{\pi^2\hbar^3} \frac{m\varepsilon\sigma(\varepsilon)}{g} \tag{3f}$$

In this expression (3f) m, s and $\sigma(\varepsilon)$ are mass, spin and inverse absorption cross section of the emitted nucleon.

Expression (3d) can simply be understood as the sum over the product of two factors:

The first factor in the first set of brackets in (3d) is the fraction of n-exciton states having a particle in the channel energy range ε to $\varepsilon+d\varepsilon$, so that the residual nucleus would have an excitation energy U.

The second factor in the second set of brackets in (3d) is the probability that the excited particle of interest having the energy range ε to $\varepsilon+d\varepsilon$ will decay into the continuum provided

$$\lambda_c(\varepsilon) << \lambda+(n,E) \tag{3g}$$

Inserting (1), (3f) and (3e) into (3d) gives the expression

$$P_{pr}(\varepsilon)d\varepsilon = \frac{(2S+1)m\varepsilon\sigma(\varepsilon)}{4\pi^3\hbar^2 g^4 E^3 |T|^2} \sum_{\substack{n=n_o \\ (\Delta n=2)}}^{\bar{n}} \left(\frac{U}{E}\right)^{n-2} (n+1)^2 (n-1)d\varepsilon \tag{3h}$$

which inserted into (3) according to Cline and Blann[1] reproduces quite well a variety of experimental (α,p); (α,n); (p,p') and (p,n) data in the range between 16 and 45 MeV bombarding energy with a proper choice of n_o and with $|T|^2$ properly adjusted (see Figs. 1 and 2).

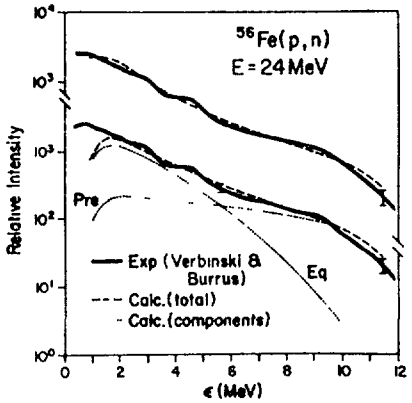

Fig. 1 Experimental (ref. [1]) and calculated neutron spectra for the ^{56}Fe+p reaction at 24 MeV of excitation. The heavy solid curves show the experimental spectrum and the dashed curves show the calculated results. The upper and lower sets of curves are for calculations made with and without the inclusion of multiple particle emission, respectively. The dotted curves show the pre-equilibrium and first-particle-out equilibrium component spectra, labelled Pre and Eq, respectively. A value of $n_o = 3$ was used in the calculations.

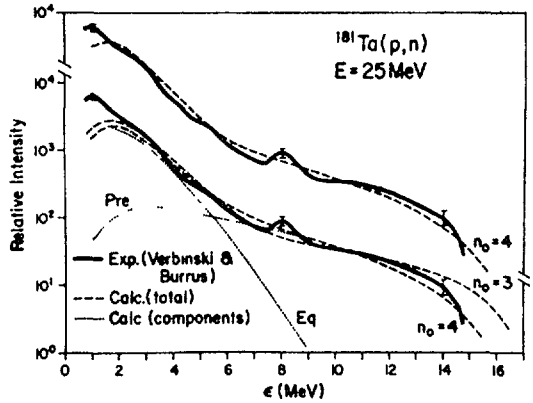

Fig. 2 . Experimental (ref. [1]) and calculated neutron spectra for the ^{181}Ta+p reaction at 25 MeV of excitation. The solid, dashed and dotted curves have the same significance as in fig. 1 except that values of $n_o = 3$ and $n_o = 4$ was used in the calculations. Component spectra are shown only for $n_o = 4$.

An extension to 14 MeV - (n,p) cross sections has been carried out by Braga - Marcazzan, Gadioli - Erba, Milazzo - Collin and Sona[3] of Milan, who have found an A^{-3} behaviour of the transition matrix-element $|T|^2$. And the Dresden-Group of Giera, Hermsdorf, Meister, Seeliger, Seidel and Wohlfahrt[4] have demonstrated how well this description works for the case of the 14-MeV-(n,n')-processes.

On the other hand Cline and Blann[1] have pointed out that the fraction of pre-equilibrium particle emission as defined by

$$f = \frac{\int_0^\infty P_{pr}(\varepsilon)\,d\varepsilon}{\int_0^\infty \left\{P_{eq}(\varepsilon)+P_{pr}(\varepsilon)\right\}d\varepsilon} \qquad (4)$$

can very well reach the value of 0,20 to 0,56 at 16 - 45 MeV excitation energies as can be seen from tables 1 and 2.

TABLE 1.

Data analyzed and the resulting parameter values for nucleon-induced reactions

Reaction system	Compound nucleus	Emitted particle	Lab. angles for data [a])	Excitation energy (MeV)	n_0 [b])	f_n [c])	f_p [c])	f [c])
^{56}Fe+p	^{57}Co	n	0° → 170° (5)	24	3	0.29 (0.29)	0.16 (0.16)	0.19 (0.19)
^{115}In+p	^{116}Sn	n	0° → 170° (6)	27	4 5	0.13 0.18	0.75 0.76	0.14 0.19
^{118}Sn+p	^{119}Sb	n	60° 60°	16 19	3 3			
^{181}Ta+p	^{182}W	n	0° → 170° (6)	25	3 4	0.088 (0.15) 0.15 (0.18)	0.98 (0.98) 0.97 (0.98)	0.093 (0.16) 0.15 (0.19)
^{208}Pb+p	^{209}Bi	n	0°, 170° 0° → 170° (7)	18 21	3 3	0.27 0.068	0.96 0.86	0.28 0.072
^{209}Bi+n	^{210}Bi	n	20° → 160° (8)	18	2 3	0.20 0.20	1.00 1.00	0.20 0.20
^{nat}Fe+p	Co	p	90°	17	3			
^{56}Fe+p	^{57}Co	p	90°	17	4			
^{nat}Cu+p	Zn	p	90°	19	2 3			
			90°	22	2 3			

[a]) The numbers in parentheses indicate the number of angles for which data were included in the analysis.

[b]) n_0 is the initial exciton number.

[c]) f_n, f_p and f are the fractions of the first-particle-out neutron, proton and nucleon yields, respectively, which are due to pre-equilibrium particle emission. The numbers in parentheses are for analyses in which multiple particle emission was considered.

TABLE 2.
Data analyzed and the resulting parameter values for ^{4}He ion induced reactions

Reaction system	Compound nucleus	Emitted particle	Lab. angles for data [a])	Excitation energy (MeV)	n_0 [b])	f_n [c])	f_p [c])	f [c])
^{59}Co+α	^{63}Cu	p	30° → 150° (5)	35	5	0.29	0.29	0.29
		p	30° → 150° (7)	45	5	0.50	0.48	0.48
^{58}Ni+α	^{62}Zn	p	30° → 150° (5)	32	4	0.28	0.18	0.21
		p	30° → 150° (5)	43	4	0.38	0.30	0.32
^{93}Nb+α	^{97}Tc	p	30° → 150° (5)	32	5	0.35	0.45	0.38
		p	45° → 135° (3)	43	5	0.38	0.49	0.41
^{124}Sn+α	^{128}Te	p	30° → 150° (3)	33	4 5		0.72 0.87	
^{nat}Pt+α	Hg	p	45° → 135° (5)	40	5 6	0.056 0.14	0.90 0.98	0.060 0.15
^{197}Au+α	^{201}Tl	p	30° → 150° (3)	28	7	0.28	0.88	0.28
^{59}Co+α	^{63}Cu	n	45° → 135° (4)	45	(5) [d])	0.57	0.54	0.56
^{93}Nb+α	^{97}Tc	n	45° → 135° (4)	43	(5) [d])	0.49	0.60	0.52
^{197}Au+α	^{201}Tl	n	45° → 135° (4)	40	(7) [d])	0.25		

[a]) See table 1
[b]) See table 1
[c]) See table 1 (but multiple particle emission included in all these results).
[d]) Values assumed in order to estimate fractions of pre-equilibrium particle emission.

These tables show that the fraction of pre-equilibrium proton emission can even reach the value of 1.00. But for the case of proton emission and high atomic number there is much suppression of equilibrium protons by the Coulomb barrier increasing with atomic number which does not affect the pre-equilibrium protons because of their higher energies. Thus the increase of the fraction of pre-equilibrium proton emission f_p with atomic number from the value of 0,16 for the ^{57}Co compound nucleus up to the value of 1.00 for the ^{210}Bi compound nucleus is mainly caused by the Coulomb barrier increasing with the atomic number. Therefore Cline and Blann[1] have concluded that it is more meaningful to look at the integrated pre-equilibrium neutron cross section plus the pre-equilibrium proton cross section divided by the total compound-nucleus cross section. This quantity they have named as f, and it can be seen from tables 1 and 2 that f is not much different from the fraction of pre-equilibrium neutron emission f_n. Values of f correspondingly corrected for the Coulomb barrier have also been calculated by

Blann[6] from the $^{54}Fe(p,p')$ experimental data of Bertrand and Peelle[5] above 30 MeV excitation energy and have been plotted in Fig.3 together with f-values calculated from the $^{51}V(p,n)$ experimental data of Grimes et al.[14] for excitation energies below 30 MeV. As tables 1 and 2 Fig. 3 shows for excitation energies below 30 MeV again f-values up to 0.2. But for excitation energies in the range between 30 and 70 MeV even f-values from 0.3 up to 0.8 are obtained.

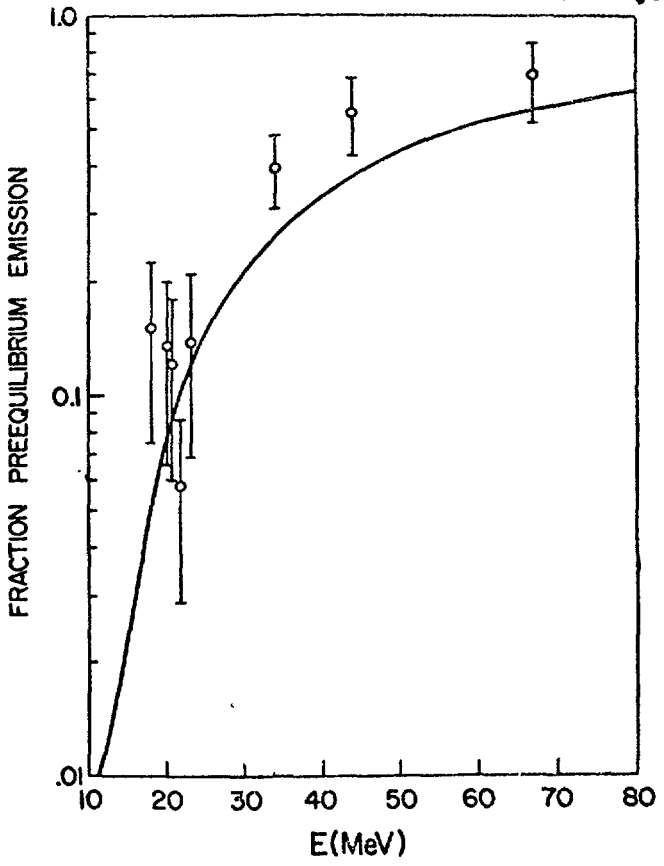

Fig. 3 Fraction preequilibrium emission as a function of complex state excitation energy from experimental measurements and from the Hybrid Model for $n_o = 2$. The experimental measurements below 30 MeV were based on ^{51}V (p,n) values from ref. 14, those above 30 MeV on ^{54}Fe (p,p') values from ref. 5) Corrections were estimated for unmeasured particles as discussed in the text.

This range of f-values from 0.2 up to 0.8 for a range of 18-70 MeV excitation energies cannot be obtained from the description of Cline and Blann[1] mentioned above and represented by eq.(3) as long as $|T|^2$ is assumed to be constant. This has been shown by Blann and Mignerey[7] whose f-values resulting from the method of Cline and Blann[1] are represented by the dashed curve of Fig.4. It shows f-values always smaller than 0.1 even at energies up to 100 MeV for a model nucleus of 100 nucleons when $|T|^2$ is adjusted at 15 MeV excitation and with $n_\sigma = 4$.

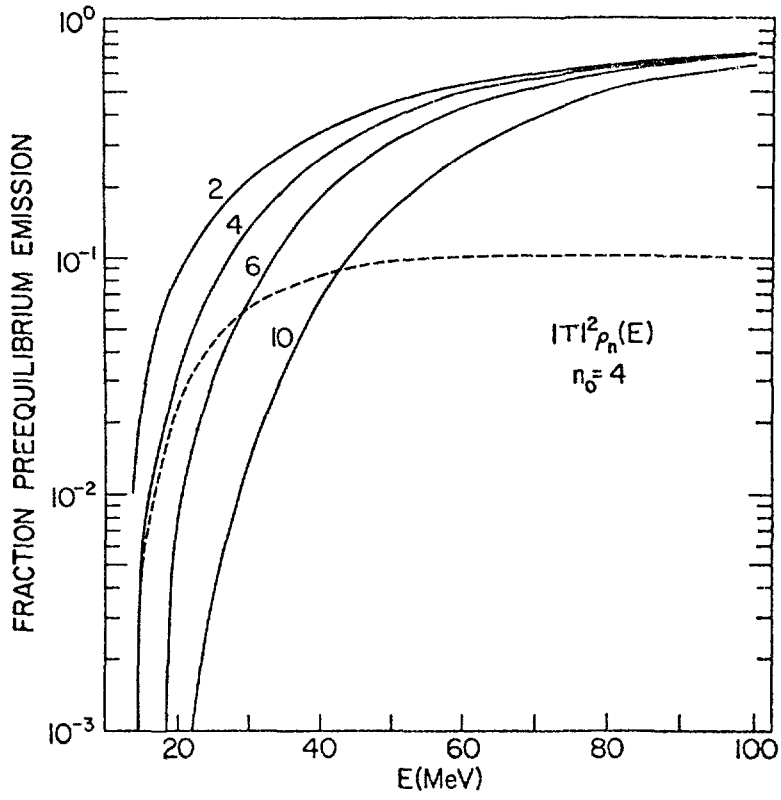

Fig. 4 Predicted variation of the fraction preequilibrium emission versus excitation energy and initial exciton number according to the Hybrid Model. The exciton numbers are shown above the curves calculated for that number. It was assumed that all initial excitons were particles, half neutrons and half protons, for a mass 100 nucleus. The dashed curve shows the results of a calculation using the Exciton Model energy dependence, with the assumption that $|T|^2$ is independent of excitation energy, and normalized to the Hybrid Model result at 15 MeV excitation (from ref.[7]).

As the reason for this failure concerning the dependence of the fraction of pre-equilibrium emission from the excitation energy Blann and Mignerey have recognized the assumption that $|T|^2$ in eq.(1) and (3) is a constant independent of excitation energy. This has the consequence that the lifetime of an n-exciton configuration goes like

$$\tau_n = \frac{1}{\lambda^+(n,E)} \sim E^{-2} \tag{5}$$

Thus the lifetime for an n-exciton configuration and, as a consequence, the pre-equilibrium particle emission is more and more suppressed at higher excitation energies. Moreover at these higher excitation energies the lifetime τ_n for an n-exciton configuration predicted by (1) or (5) would become so small that a collision cross-section in excess of a free nucleon-nucleon cross-section would be implied which is a rather unphysical behaviour.

2. Improvement by the "Hybrid Model"

Because of these just mentioned difficulties concerning the Exciton Model Blann has undertaken a new approach to calculate the transition rate λ_+ which does not make use of the formula (1) of Williams. Instead Blann has calculated λ_+ as a collision probability per unit time for collisions of a nucleon to be emitted with the nucleons of a Fermi gas. Each collision is connected with an absorption of the incident nucleon together with an excitation of the hitted nucleon. Only those collisions can take place by which a hitted nucleon is lifted into a level above the Fermi energy. Moreover the collisions are described by means of the free nucleon-nucleon scattering cross section of which the empirical laboratory energy dependence below 100 MeV is represented as proportional to the reciprocal collision energy and as constant above 100 MeV. As the result for the thus calculated transition rate λ_+ Blann[8] obtains for a nucleon energy $\varepsilon+B$ above the Fermi energy up to 100 MeV:

$$\lambda_+(\varepsilon) = \left[1.4\cdot 10^{21}(\varepsilon+B) - 6\cdot 10^{10}(\varepsilon+B)^2\right]\mathrm{sec}^{-1} \tag{6}$$

For

$$E \gg U \tag{7}$$

we obtain using (3c):

$$\lambda_+(E) = \left[1.4\cdot 10^{21}E - 6\cdot 10^{10}E^2\right]\mathrm{sec}^{-1} \tag{8}$$

and thus for the lifetime of an excitation between two collisions we get

$$\tau_n = \frac{1}{\lambda_+} \sim E^{-1} \tag{9}$$

which shows a smaller decrease with increasing excitation energy as compared to eq. (5). For this reason using the new λ_+ of eq. (6) and (8) Blann and Mignerey[7] have obtained higher values for the fraction of pre-equilibrium particle emission with increasing excitation energy than they had obtained before with the Williams-expression of eq. (1). These improved results are also shown in Fig. 4 (solid curve) from which we can see that the fraction of pre-equilibrium particle emission now can reach values of the order of magnitude of the experimental data as shown in tables 1 and 2.

The λ_+-expressions of eq. (6) and (8) do no more contain any adjustable parameter. Therefore the description using these new λ_+ expressions of eq. (6) and (8) has been called by Blann the "Hybrid Model". It also follows from the λ_+-expressions (6) and (8) that (3g) does no longer hold over the whole range of energies to be considered. Thus $\lambda_c(\varepsilon)$ is now taken into account in the denominator of the emission probability in the expression for the energy spectrum of the emitted nucleon for the hybrid model given by:

$$(10) \qquad P_{prx}(\varepsilon)d\varepsilon = \frac{1}{E}\sum_{\substack{n=n_o \\ \Delta n=2}}^{\bar{n}} \frac{nPx}{p} \frac{\rho_{n-1}(U)g}{\rho_n(E)} \frac{\lambda_c(\varepsilon)}{\lambda_c(\varepsilon)+\lambda_+(\varepsilon)} D_n d\varepsilon = \sum_{n=n_o}^{\bar{n}} nPx(\varepsilon)d\varepsilon$$

where D_n is the depletion factor

$$(11) \qquad D_n = \prod_{n_o+2<n'<n}^{n} \left(1-\sum_x \int_o^{\varepsilon_{max}} {}_{n'}P_x(\varepsilon)d\varepsilon\right)$$

and ${}_nP_x$ is the number of particles in an n-exciton state of type x to be emitted. An absolute emission cross section has also been obtained by multiplying (10) with the absorption cross-section of the optical model σ_{x_o} abs.(ε_o) for absorption of a particle of type x_o with energy ε_o. The absolute cross-section for emission of a particle of type x with energy ε after a collision by a particle of type x_o with energy ε_o then is:

$$(12) \qquad d\sigma_{x_o x}(\varepsilon_o,\varepsilon) = \sigma_{x_o abs.}(\varepsilon_o)P_{prx}(\varepsilon)d\varepsilon$$

Rather good results of the hybrid model compared with 42 MeV experimental (α,p)-data are shown by Fig.5. Also Fig.6. shows a rather good agreement of the 55 MeV-(α,p)-data of Chevarier et al. of Lyon[9]. It shows also an even-odd-effect of the n_o-value which according to Blann comes from a pairing correction of the one-nucleon level density g.

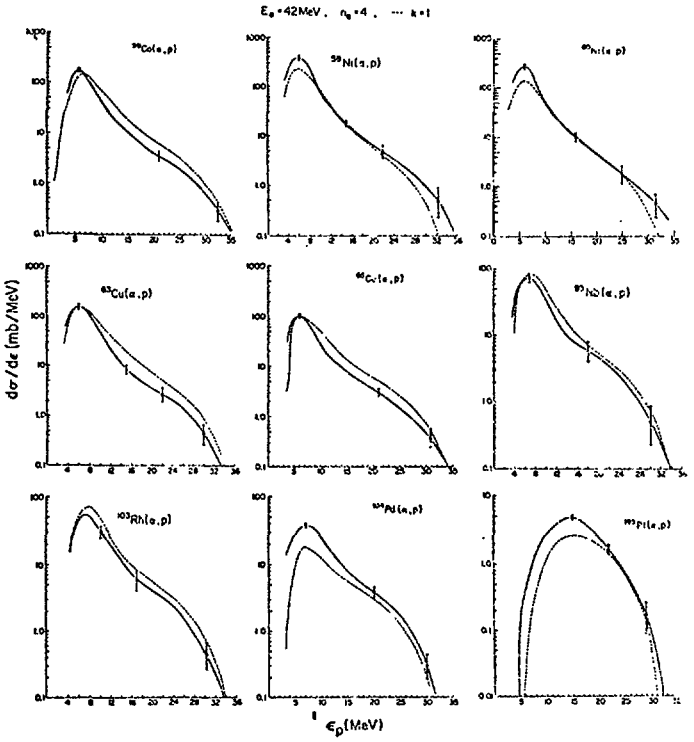

Fig. 5 Experimental and calculated (α,p) spectra on several targets. The experimental results (ref 7) are shown as solid curves with several error bars and are for incident ^{4}He energies of 42 MeV.

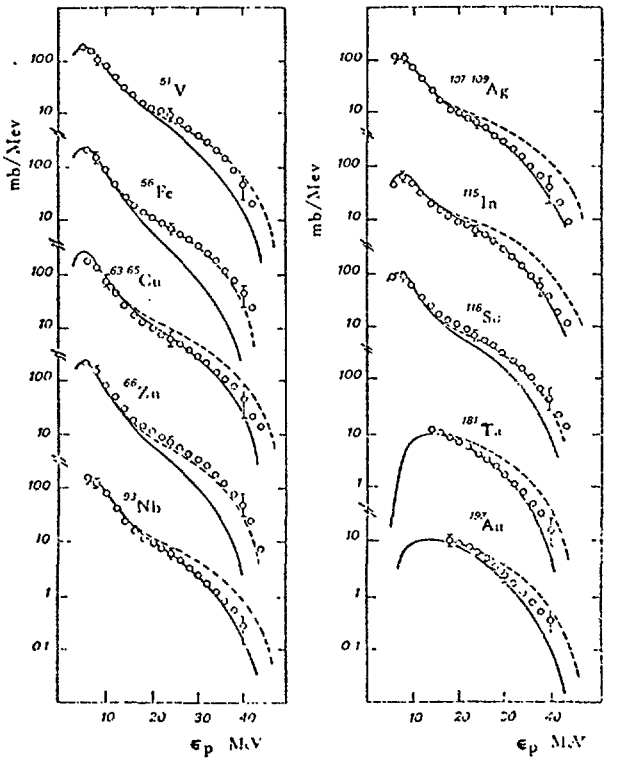

Fig. 6 Experimental and calculated (α,p) spectra for 55 MeV incident α energy (from ref.9). The points represent experimental angle integrated cross sections (ordinate) versus the proton kinetic energy. The solid curves represent hybrid plus compound results for n_o=5; the dashed curves are for hybrid model calculations with n_o= 4.

3. Introduction of geometry dependence

But even still bigger problems with the n_o-values arise if the hybrid model is applied to the 197 Au(p,p') spectrum data of Bertrand and Peelle[5] at 62-MeV bombarding energy. Fig. 7 shows that only for n_o = 2 the calculated values (dashed curve) are close to the experimental data (solid curve) while for n_o = 3 the calculated values (dotted curve) are only 10 -- 20 % of the experimental data at high energies.

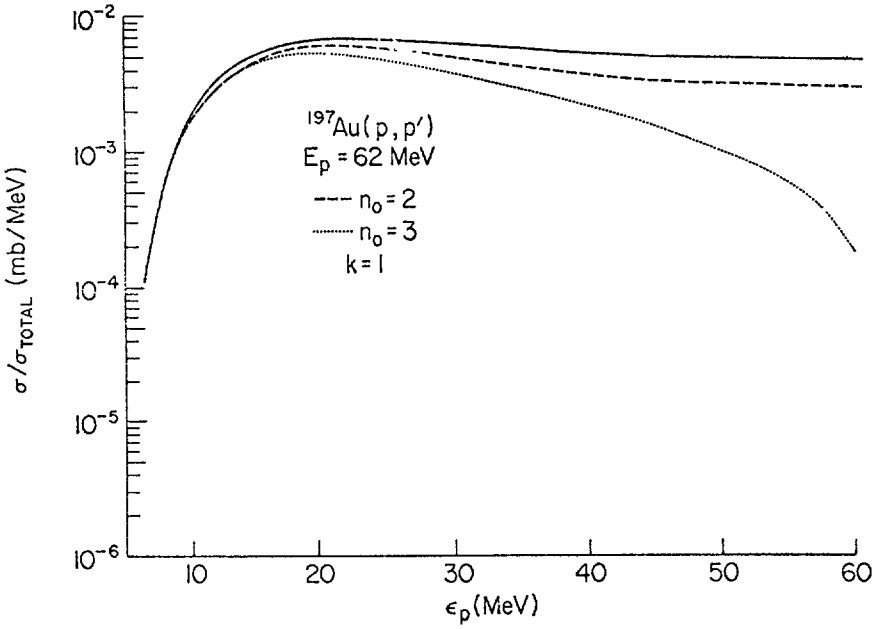

Fig. 7 Experimental and calculated $^{197}Au(p,p')$ spectrum for 62 MeV incident protons. Experimental results (ref. 5) are given by the solid curve; calculated results by the dashed line for $n_o = 2$ and by the dotted line $n_o = 3$.

Now it can hardly be understood how $n_o = 2$ should come about as the first exciton excitation resulting from the first collision of a nucleon incident on a target nucleus within the framework of the above considered models. Therefore Blann had the idea to assume that the initial interactions might take place primarily in the nuclear skin region. Then the hole degree of freedom would get lost, and the initial state might be characterized as a two particle excited state. But this would mean that the geometry of the reaction has entered into the calculation by assuming a surface interaction, and this indicates the failure of pure phase-space arguments in treating all of the pre-equilibrium components as introduced with eqs. (3d), (3e) and (10). The phase-space arguments may be valid when the average excited particle energies have dropped below some value; this may partly be the explanation for the better results for these models when applied to ^{4}He induced reactions as shown in Figs. 5 and 6.

As the consequence of this kind of consideration Blann[10] has introduced the geometry effect for the nucleon induced reactions by taking into account that the nuclear density distribution within the nucleus is not uniform but can be represented according to Hofstadter as:

$$d(R) = d_s\left[e^{(R-c)/z}+1\right]^{-1} \tag{13}$$

where

$$c = 1.07 \cdot A^{1/3}\,\text{fm}, \tag{13a}$$

$$z = 0.55\ \text{fm} \tag{13b}$$

and d_s is the saturation density in the center of the nucleus. Using the impact parameter

$$R_\ell = \lambda\!\!\!^{-}\,\ell \tag{14}$$

with

$$\lambda\!\!\!^{-} = \frac{\hbar}{\sqrt{2m\epsilon_o}} = \text{de-Broglie wave length of the incoming particle} \tag{14a}$$

$$\ell = \text{quantum number of orbital angular momentum of the incoming particle} \tag{14b}$$

the nucleus is divided into shells of Radius R_ℓ of which the density decreases with R_ℓ according to

$$d(R_\ell) = d_s\left[e^{(R_\ell-c)/z}+1\right]^{-1} \tag{15}$$

Blann then concludes that only those parts of the nuclear density have to be introduced into the calculations for the ℓ-th partial wave which are met as an average by a nucleon crossing the nucleus on its way from the impact parameter R_ℓ up to the Radius

$$R_s = cA^{1/3} + 5z \tag{16}$$

at the nuclear suface at which the density is $\approx \frac{1}{150}$ of its maximum value. This average density is given by

$$(17) \qquad \langle d_\ell(R) \rangle = \frac{1}{R_s - R_\ell} \cdot \int_{R_\ell}^{R_s} d(R)\,dR$$

and should be introduced according to Blann into every density dependent quantity of what is called by Blann the "geometry dependent hybrid model".

The first quantity to be considered is the Fermi energy which for the case of a uniform density d_s is given by the expression

$$(18) \qquad E_F = \frac{h^2}{2m} \left(\frac{3}{2}\pi^2 d_s\right)^{2/3}$$

For the geometry dependent case then according to Blann there should be the smaller geometry dependent Fermi energy

$$(19) \qquad E_F(R_\ell) = E_F \left[\frac{\langle d_\ell(R) \rangle}{d_s}\right]^{2/3}$$

because of the smaller geometry dependent density $\langle d_\ell(R) \rangle$ of eq.(17). But, since the potential depth is mainly given by the Fermi energy, with (19) the decrease of the potential depth toward the nuclear surface is obtained. Now in this way it can easily be seen from eq. (19) that the potential depth will become so small near the nuclear surface that deviations from the exciton state density expression eq. (3e) for unlimited potential depth of Ericson for $\rho_n(E)$ can no more be neglected. Blann was able to take into account the limited potential depth for the two-particle one-hole state density expression to be inserted into eq. (10) with the result:

$$(20) \qquad \rho_{1p1h}(U) = gE_F(R_\ell);\ U>E_F(R_\ell)$$

and

$$(21) \qquad \rho_{2p1h}(E) = \frac{1}{4}g^2 E_F(R_\ell)\left[2E-E_F(R_\ell)\right];\ E>E_F(R_\ell)$$

For n>3 Blann continued to use the Ericson expression of eq. (3e) because for these higher exciton numbers the average energy per exciton would be small enough, so that the influence of the limited potential depth could be neglected.

For the non-geometry dependent hybrid calculations mentioned above the one-nucleon equidistant level density expression

$$g = \frac{3A}{2E_F} \tag{22}$$

was used. Inserting the geometry dependent Fermi energy of eq. (19) into eq. (22) the geometry dependent one-nucleon level density expression

$$g(R_\ell) = \frac{E_F}{E_F(R_\ell)}\, g \tag{23}$$

is obtained which was used by Blann in ref[10].

However the result of eq. (23) shows a one-nucleon level density increasing towards the nuclear surface which is a rather unphysical behaviour. A different result is obtained on the basis of the realistic Fermi gas one-nucleon level density

$$g = \frac{2Vm^{3/2}}{\pi^2\hbar^3}\left(\frac{\varepsilon+B+E_F}{2}\right)^{1/2} \tag{24}$$

where V is the volume of the nucleus, m the mass of the nucleon and $\varepsilon+B+E_F$ its energy above the bottom of the potential. The geometry dependent one-nucleon level density then is

$$g(R_\ell) = \frac{2Vm^{3/2}}{\pi^2\hbar^3}\left(\frac{\varepsilon+B+E_F(R_\ell)}{2}\right)^{1/2} \tag{25}$$

On the other hand V is given by mass number A and saturation density d_s according to

$$V = \frac{A}{d_s} \tag{26}$$

and the saturation density d_s is given by the full Fermi energy E_F according to

$$d_s = \frac{2}{3\pi^2\hbar^3}(2mE_F)^{3/2} \tag{27}$$

We therefore can express the geometry dependent one-nucleon level density $g(R_\ell)$ by the geometry-dependent Fermi energy $E_F(R_\ell)$ of eq. (19) and the full Fermi energy E_F according to

$$g(R_\ell) = \left(\frac{\varepsilon+B+E_F(R_\ell)}{E_F}\right)^{1/2} g \tag{28}$$

with g of eq. (22). Eq. (28) was introduced by Blann in ref.[6].

Blann also has introduced a geometry dependence for the intranuclear transition rate $\lambda_+(\varepsilon)$ of eq. (6) and (8). The results of eq. (6) and (8) had been obtained from the average cross section $\langle\sigma(\varepsilon+B+E_F)\rangle$ for scattering of a nucleon in nuclear matter giving a mean free path in nuclear matter of

$$MFP(\varepsilon+B+E_F) = \frac{1}{d_s \langle\sigma(\varepsilon+B+E_F)\rangle} \tag{29}$$

The rate of intranuclear transitions, $\lambda_+(\varepsilon)$, then is given by dividing the nucleon velocity v by the mean free path:

$$\lambda_+(\varepsilon) = \frac{v}{MFP(\varepsilon+B+E_F)} = d_s \langle\sigma(\varepsilon+B+E_F)\rangle \sqrt{\frac{2(\varepsilon+B+E_F)}{m}} \tag{30}$$

This expression of eq. (30) for $\lambda_+(\varepsilon)$ is proportional to the saturation density d_s of nuclear matter. If geometry dependence is taken into account d_s is to be replaced by the average density $d_\ell(R)$ of eq. (17). The geometry dependent $\lambda_+(\varepsilon,R_\ell)$ then becomes

$$\langle\lambda_+(\varepsilon,R_\ell)\rangle = \frac{\langle d_\ell(R)\rangle}{d_s} \lambda_+(\varepsilon) \tag{31}$$

There is still another method introduced by Blann[10] to calculate the intranuclear transition rate $\lambda_+(\varepsilon)$. This method uses the relationship between the mean free path of a nucleon travelling through nuclear matter and the imaginary part W of the optical model. Such a relationship has been found by Kikuchi and Kawai[11] to be given by

$$MFP(\varepsilon+B+E_F) = \frac{\hbar}{W}\sqrt{\frac{\varepsilon+B+E_F}{2m}} \tag{32}$$

where use is made of the well confirmed assumption

(33) $$W \ll E_F$$

For the intranuclear transition rate $\lambda_+(\varepsilon)$ we then obtain like in eq. (30)

(34) $$\langle\lambda_+(\varepsilon)\rangle = \frac{v}{MFP(\varepsilon+B+E_F)} = \frac{2W}{\hbar}$$

and for the geometry-dependent case in analogy to eq. (17) W has to be replaced by

(35) $$\langle W_\ell(R)\rangle = \frac{1}{R_s-R_\ell}\int_{R_\ell}^{R} W(R)dR$$

so that the geometry-dependent intranuclear transition rate becomes

(36) $$\langle\lambda_+(\varepsilon,R_\ell)\rangle = \frac{2\langle W_\ell(R)\rangle}{\hbar}$$

Now it can be seen from the expressions (20), (21), (23), (28), (36) and (3f) if inserted altogether into (10) that we are having an ℓ-dependent emission probability $P^{(\ell)}_{prx}(\varepsilon)$ for the geometry-dependent case. Therefore (12) has to be replaced by

(37) $$d\sigma_{x_o x}(\varepsilon_o,\varepsilon) = \pi\lambda^2 \sum_{\ell=0}^{\infty}(2\ell+1)T_{x_o\ell}(\varepsilon_o)P^{(\ell)}_{prx}(\varepsilon)d\varepsilon$$

where the $T_{x_o\ell}(\varepsilon)$ are the transmission coefficients by which the absorption cross-section σ_{x_o} abs.(ε_o) is composed according to

(38) $$\sigma_{x_o}\,\text{abs.}(\varepsilon_o) = \pi\lambda^2 \sum_{\ell=0}^{\infty}(2\ell+1)T_{x_o\ell}(\varepsilon_o)$$

Results obtained by Blann[10] from these considerations of geometry dependence are shown in Figs. 8 and 9 for the ^{54}Fe(p,p') angle integrated absolute spectral probability distributions of energy of the emitted proton for bombarding energies of 62 and 39 MeV.

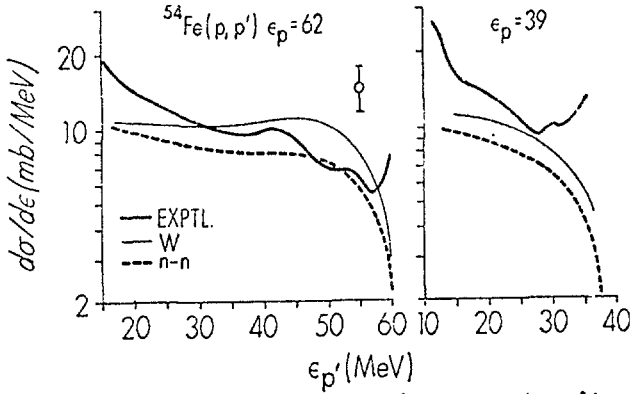

Fig. 8: Calculated and experimental (p,p') spectra from ^{54}Fe targets bombarded with 39 and 62 MeV protons. The heavy solid curve is the experimental result of ref. [5]. All calculated curves are the results of the geometry dependent hybrid model with parameters averaged over the incident particle trajectory and with the equidistant one-nucleon level density.

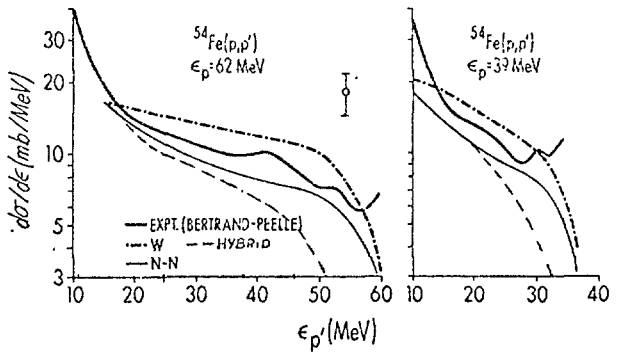

Fig. 9: (p,p') spectra as in Fig. 8, but the calculated spectra are obtained with the realistic Fermi gas one nucleon level density. Only the dot-dash and the thin solid curve are obtained with geometry dependence while for the dashed curve all parameters were evaluated for properties averaged over the entire nucleus as corresponding to the non-geometry dependent pure hybrid model.

The difference between the calculated curves of Fig. 8 and Fig. 9 is caused by having used the two different one-nucleon level densities as mentioned above. In Fig. 8 the equidistant one-nucleon level density with geometry dependence of equation (23) is used while in Fig. 9 use is made of the realistic Fermi gas level densities of (24) with (26) and (27) as corresponding to the non-geometry dependent pure hybrid model and of eq. (28) for taking into account the geometry dependence. In both figures the heavy solid curve represents experimental results of Bertrand and Peelle [5]. In Fig. 8 the dashed curve is obtained by calculating the transition rate λ_+ from the collisions of the nucleon to be emitted with the nucleons of a Fermi gas according to equations (6) and (31) where via eq. (31) the geometry dependence has been taken into account. The corresponding curve in Fig. 9 is the thin solid curve. On the other hand the thin solid curve of Fig. 8 represents results where λ_+ is obtained with the imaginary part W of the optical model with geometry dependence according to eq. (36). To this the corresponding curve in Fig. 9 is the dot-dash curve while the dashed curve in Fig. 9 is also obtained from the imaginary part of the optical model but by integrating from zero to Rs in eq. (35) and using all parameters non-geometry dependent as corresponding to the pure hybrid model. The results of Fig. 9 obtained with the realistic Fermi gas one nucleon level density show some improvement concerning the agreement with the experimental results as compared to the results of Fig. 8 obtained with the equidistant one nucleon level density. Fig. 9 shows that for the high energy tail the curves for the geometry dependent case are lifted as compared to the curves

for the pure non-geometry dependent Hybrid case. Thus the effect as discussed in connection with Fig. 7 is obtained but now by introducing the geometry dependence while maintaining $n_o = 3$ instead of using the unphysical choice $n_o = 2$ as in the case of the dashed curve of Fig. 7.

4. Application of the pure hybrid and geometry dependent hybrid model to the 14.7 MeV $^{56}Fe(n,n')$-process.

a) Attempt with the pure hybrid model

Calculations have been carried through to reproduce the 14 MeV $^{56}Fe(n,n')$ angle integrated emission cross section for the energy distribution of the emitted neutrons using the geometry dependent hybrid model with the equidistant one-nucleon level density according to eq. (23). The thus obtained calculated values for the emission cross section amounted to only a fraction of the experimental values at high emission energies where the evaporation component can be neglected. For instance at 10 MeV emission energy only about one fourth of the experimental value could be reached by the emission cross section calculated as indicated above. This calculated pre-equilibrium component of the emission cross section could be increased by a factor of 1.64 by integrating from zero to Rs in eq. (17), (19), (23), (35) and (36) thus choosing all parameters non geometry dependent as corresponding to the pure hybrid model. The thus obtained results as presented in ref.[13] are shown in Fig. 10.

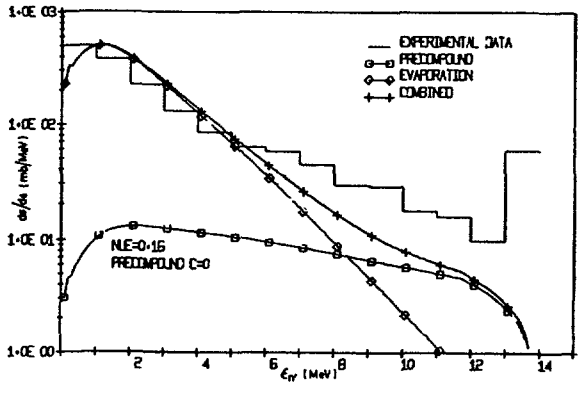

Fig. 10: Inelastic scattering cross-section of 14 MeV neutrons on ^{56}Fe reproduced using the pure hybrid model with equidistant Fermi gas one nucleon level density.

The step curve in Fig. 10 is obtained by Hansen et al.[14] from experimental data. The equilibrium or evaporation component has been choosen to be

$$(39) \qquad \left(\frac{d\sigma(\varepsilon_o,\varepsilon)}{d\varepsilon}\right)_{equi} = 4\pi C'\sigma(\varepsilon)\varepsilon e^{-\frac{\varepsilon}{T}} \; ; \quad T = \sqrt{\frac{\varepsilon_o}{\nu A}} \text{ MeV}$$

where ε_o is the bombarding energy and ν and C' are constants to be adjusted to get agreement of the low energetic part of the calculated curve with the step curve as seen in Fig. 10 with the constant $\nu = 0{,}16\ \text{MeV}^{-1}$. The inverse absorption cross section $\sigma(\varepsilon)$ is taken from a Karlsruhe version of the Perey-Buck[19] program for the optical model. This has also been done with respect to the absorption cross section $\sigma_{x_o}\text{abs}(\varepsilon_o)$ needed from the optical model for the pre-equilibrium component according to eq. (12) in the pure hybrid case.

Fig. 10 still shows a considerable deficit of the high energy tail of the calculated curve as compared to the step curve. For instance at 10 MeV energy of the emitted neutron the value of the emission cross section of the calculated curve is about three times smaller than the average value of the experimental gained step curve.

b) Direct component from PWBA-analysis of angular distribution

A hint about how to account for this discrepancy shown in Fig. 10 between the theoretical and experimental curves for the emission cross section of the 14 MeV ^{56}Fe(n,n')-process has been taken from the angular distribution of the emitted neutron measured by Hermsdorf et al.[15] as shown in Fig. 11.

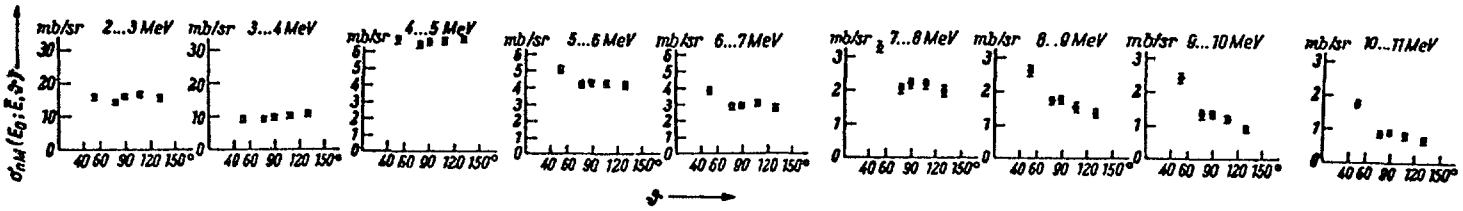

Fig. 11 Angular distribution of 14,7 MeV neutrons scattered inelastically Fe as measured by Hermsdorf et al.[15].

Fig. 11 shows energy average results with averaging energy intervals of 1 MeV. It could be shown in ref. [13] that these results could be reproduced rather well by means of the ansatz:

$$(40)\qquad \frac{d^2\sigma(\varepsilon_o,\varepsilon,\theta)}{d\Omega d\varepsilon} = \frac{1}{4\pi}\left(\frac{d\sigma(\varepsilon_o,\varepsilon)}{d\varepsilon}\right)_{equi} + \frac{1}{4\pi}\left(\frac{d\sigma(\varepsilon_o,\varepsilon)}{d\varepsilon}\right)_{\substack{Blann\\ absolut}} + \left(\frac{d^2\sigma(\varepsilon_o,\varepsilon,\theta)}{d\Omega d\varepsilon}\right)_{direct}$$

On the right hand side of eq. (40) the first term is the equilibrium component of Fig. 10 as presented by eq. (39), the second term is the pre-equilibrium component of Fig. 10 as explained in connection with Fig. 10 and the third term as the only angular dependent term is choosen to be an expression corresponding to the plane-wave-Born-approximation (PWBA) as

$$(41)\qquad \left(\frac{d^2\sigma(\varepsilon_o,\varepsilon,\theta)}{d\Omega d\varepsilon}\right)_{direct} = \text{const}\sqrt{\frac{\varepsilon}{\varepsilon_o}}(2\ell'+1)\sum_L C_{\ell\ell'}(L,0;0,0)\{j_L(QR)\}^2$$

In (41) $Q = |k_o - k|$ is the absolute value of the difference between the wave number vectors of the incident and scattered neutron, L is the quantum number of angular momentum transmitted between the neutron and the target nucleus by means of the scattering process by which a nucleon of angular momentum quantum number ℓ in the ground state of the target nucleus is lifted into the quantum number ℓ' of the excited state with $\ell + \ell' > L > |\ell - \ell'|$. The angular distribution belonging to the transmission of the angular momentum L is given in (41) by the square of the spherical Bessel function $j_2(QR)$ with the corresponding Clebsch-Gordan-coefficient $C_{\ell\ell'}$.

Almost the same expression as (41) is valid for collective excitations of the target nucleus by a direct scattering process with the only difference that L then has the meaning of angular momentum quantum number of the corresponding collective state. Thus only this one L occurs in the expression corresponding to (41) instead of the summation over L.

Often also in the case of single nucleon excitation only one term in the summation over L in (41) is mostly used in the literature assuming that mainly one angular momentum L is transmitted. Thus the square of the spherical Bessel functions appears as the typical shape, which is closely related to the direct reactions. In case of ^{56}Fe the highest proton shell is 1 f 7/2 and the highest neutron shell is 2 p 3/2 in the ground state. The next unoccupied proton shell would be 2 p 3/2, the next unoccupied neutron shell would be 1 f 5/2. To lift a proton as well as a neutron into the next upper shell would mean $\Delta\ell = 2$ in both cases. On the other hand 2^+ excited states from collective or shell model seniority excitations are present together with a number of 4^+ states as can be seen from the work of Mani[16]. Because of these 2^+ states and the $\Delta\ell$=2 structure mentioned above the attempt has been made[13] to fit the angular distribution values measured by Hermsdorf et al.[15] with the term L=2 alone with $\{j_2(QR)\}^2$ in the above expression (41). This is introduced into (40) and averaged over the energy regions of the scattered neutrons from 2-3 MeV till 10-11 MeV as has been done by Hermsdorf et al. for the measured values (see Fig.10). The obtained results are shown in Fig. 11 for the energy regions 7-8 MeV and 10-11 MeV of the scattered neutrons.

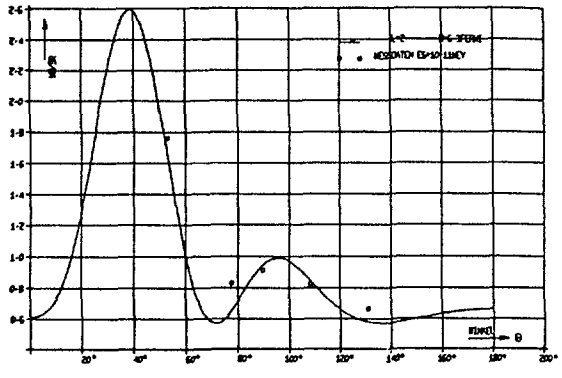

10 - 11 MeV

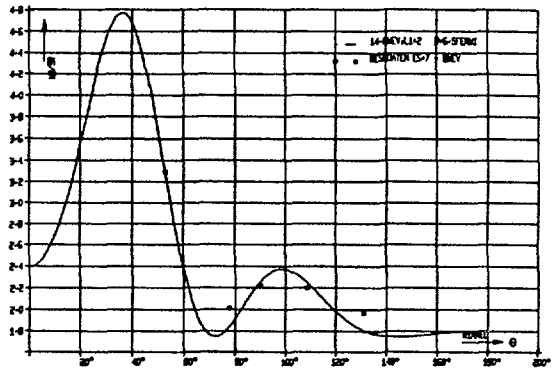

7 - 8 MeV

Fig.11a PWBA-fit of angular distributions of 14.7 MeV neutrons scattered inelastically on ^{56}Fe. The background is from the pure hybrid model with the equidistant Fermi gas one nucleon level density.

The diagrams of Fig. 11a show that the measured values of the angular distribution of the inelastically scattered 14,7 MeV neutrons are fitted rather well by the $\{j_L(QR)\}^2$-behaviour of the square of the spherical Bessel function with index L = 2. The same is true for the other energy regions. This should be considered while taking into account that the errors of measurement amount to up to 10 %. The still remaining deviations according to their trend correspond to quite those deviations which are to be expected and are found also otherwise between the PWBA- and the measured values. This means that the measured curves use to be more flat than the PWBA-curves while the positions of the maxima and minima are essentially maintained. Thus by means of the preceding and the following fits we have demonstrated that the angular distribution values measured by Hermsdorf et al.[15] show the typical shape of direct reactions which is closely related to the shape of the square of the spherical Bessel functions. For this case of the $\{j_2(QR)\}^2$-fit with L = 2 as the only angular momentum transmitted by the reaction between the neutron and the target nucleus the integration over the scattering angular space for every region of energy of the scattered neutron has been carried out. The smoothed results of this integration are represented by the mounting curve of Fig. 12 as the direct component. This combined with the equilibrium and pre-equilibrium component of Fig. 10 according to eq. (40) gives a rather good fit of the step curve obtained by Hansen et al.[14] from the empirical data as is shown by Fig. 12.

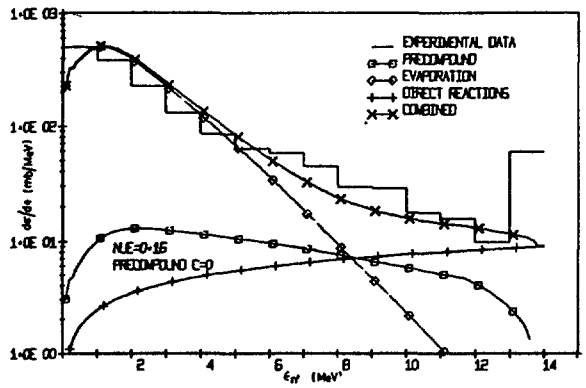

Fig. 12: Comparison between measured and calculated angular integrated inelastic cross-sections, where the fit includes the direct part. (ν = 0,16; see equ. (40)).

Thus the deficit of the calculated equilibrium + pre-equilibrium components for the pure hybrid case shown by Fig. 10 for the high energy tail as compared to the step curve has now been filled by the direct component desribed above as shown by Fig. 12.

As the next step [17] in the 14 MeV $^{56}Fe(n,n')$ pre-equilibrium calculations a change has been carried through from the equidistant one-nucleon Fermi gas level density (22) to the realistic Fermi gas level density (24) with (26) and (27). This realistic Fermi gas level density is again non-geometry dependent and thus also the other parameters are choosen non-geometry dependent as λ_+ according to eq. (35) and (36) if integrated from zero to Rs. This means that again the pure non-geometry dependent hybrid model is used but with realistic instead of equidistant one-nucleon level density. The effect on the calculated results for the 14 MeV Fe(n,n')-process caused by this change is that the pre-equilibrium component is lifted again by a factor of about 1.3 to 1.64 as compared to the pre-equilibrium component of Fig. 10. This has the consequence that at a neutron emission energy of 10 MeV the calculated spectral emission cross section is still smaller than the experimental obtained value of the step curve but now by a factor of about 2 instead of the factor 3 of Fig. 10. This can be seen in detail from Fig. 13

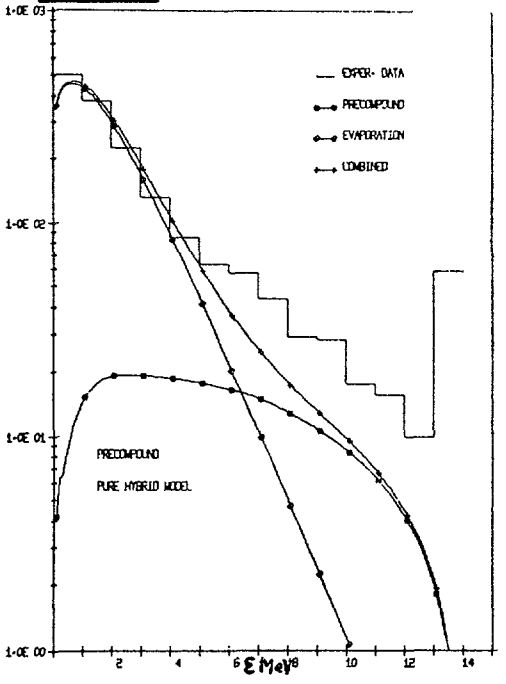

Fig. 13: Inelastic scattering cross-section of 14 MeV neutrons on ^{56}Fe reproduced using the pure hybrid model with realistic Fermi gas one-nucleon level density.

There is still another change in Fig. 13 as compared to Fig. 10. This change is concerned with the equilibrium component of Fig. 13 which no longer is adjusted as in Fig. 10. In Fig. 10 the equilibrium component was calculated using the expression (39) in which the constant factor C' had to be adjusted to fit the low energy part of the experimental step curve. Instead of using eq. (39) the equilibrium component in Fig. 13 was obtained from the Hauser Feshbach expression for continuous channels (see Review Paper 2 of Moldauer.) The special version of the Hauser Feshbach expression for continuous channels used in Fig. 13 is obtained from that one which otherwise is used in the Hauser-Feshbach computer programm HELENE [18]. So instead of (39) the following expression was used for the equilibrium component of Fig. 13:

$$(42a)\quad \left(\frac{d\sigma(\varepsilon_o,\varepsilon)}{d\varepsilon}\right)_{equi} = \pi\lambda^2 \frac{\sum_\ell (2\ell+1) T_\ell(\varepsilon_o) \sum_{\ell'} T_{\ell'}(\varepsilon)}{D} \frac{\omega(\varepsilon_o-\varepsilon)}{2}$$

with

$$(42b)\quad D = \sum_{\ell'',\nu''} T_{\ell''}(\varepsilon_o - E_{o\nu''}) + \sum_{\ell''} \int_0^{\varepsilon_o-\varepsilon_c} T_{\ell''}(\varepsilon) \frac{\omega(\varepsilon_o-\varepsilon)}{2} d\varepsilon$$

where the T_ℓ are the transmission coefficients of the neutron channel defined as in (37) and (38) and calculated again from the previously mentioned Karlsruhe version of the Perey-Buck [19] program for the optical model. Moreover $\omega(\varepsilon_o-\varepsilon)$ is the level density of the target nucleus with the excitation energy of the target nucleus given by

$$(42c)\quad \varepsilon_o - \varepsilon = U$$

So far as $\omega(U)$ is concerned an expression has been used which is taken from the work of Gilbert and Cameron [20] and is also used in the Hauser-Feshbach computer program HELENE [18]. For the here considered case this expression is given by

$$\omega(U) = \begin{cases} \omega_1(U) = e^{\frac{U-U_0}{T}} & ; U \leq U_x \\ \omega_2(U) = \dfrac{e^{2\sqrt{a(U-\Delta)}}}{12\sqrt{2c}\,(U-\Delta)^{3/2}} & ; U \geq U_x \end{cases} \tag{42d}$$

with

$$c/a = 0.0888A^{2/3} \text{ and } a/A = 0.00917S+0.120 \text{ MeV}^{-1} \tag{42e}$$

The other constants in (42d) and (42e) are for ^{56}Fe (see Gilbert and Cameron):

$$T = 1.26 \text{ MeV}; \; U_o = 0.8 \text{ MeV}; \; U_x = 9.2 \text{ MeV} \tag{42f}$$

$$S = 0.06 \text{ MeV}^{-1}; \; \Delta = 2.81 \text{ MeV}, \; \varepsilon_c = 5.2500 \text{ MeV}$$

Fig. 13 shows that the low energy branch of the experimental step curve is remarkably well reproduced with the help of the equilibrium contribution given by eq. (42a-f) without any adjustment. In order to fill the deficit at the high energy tail again a direct component according to the PWBA expression of eq. (41) has been added and again the attempt has been carried through to fit the angular distribution measured by Hermsdorf et al.[15] with L = 2 only. This fit is shown in Fig. 14.

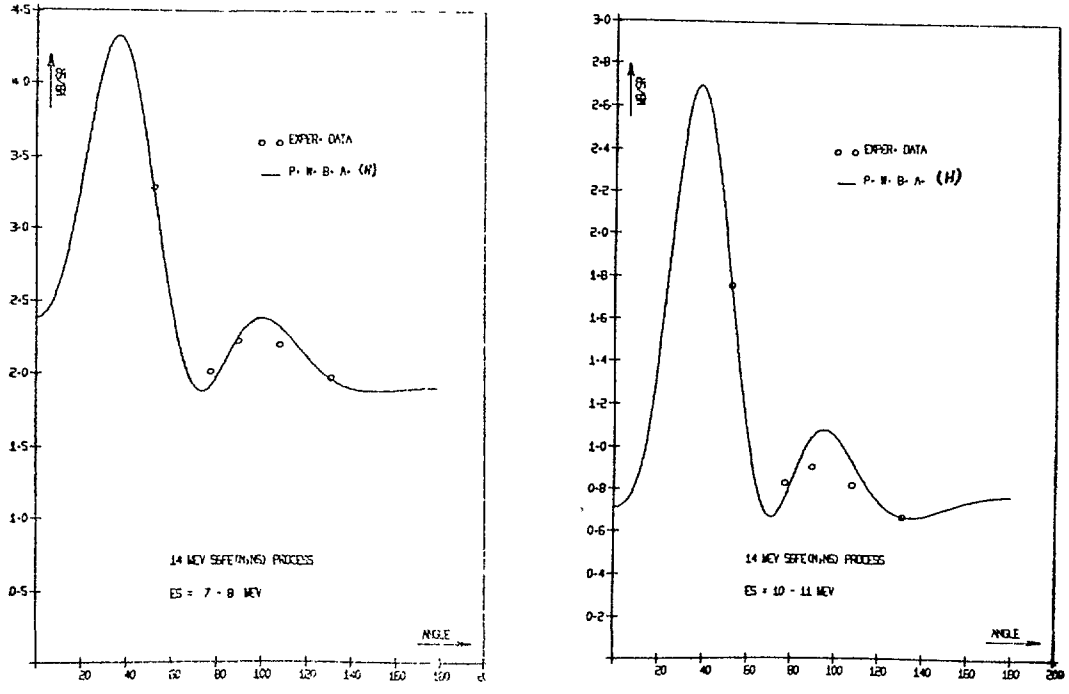

Fig. 14 PWBA-fit of angular distributions of 14.7 MeV neutrons scattered inelastically by ^{56}Fe. The background is from the pure hybrid model with the realistic Fermi gas one nucleon level density.

Fig. 14 shows that with the background from the pure hybrid model with the realistic Fermi gas one-nucleon level density the measured values of the angular distribution are fitted almost as well by the $\{j_2(QR)\}^2$ behaviour as in Fig. 11 with the background from the pure hybrid model with the equidistant Fermi gas one-nucleon level density. With the angle integrated results of Fig. 14, the angle integrated direct component is then obtained and its combination with the equilibrium and pre-equilibrium components of Fig. 13 is shown in Fig. 15

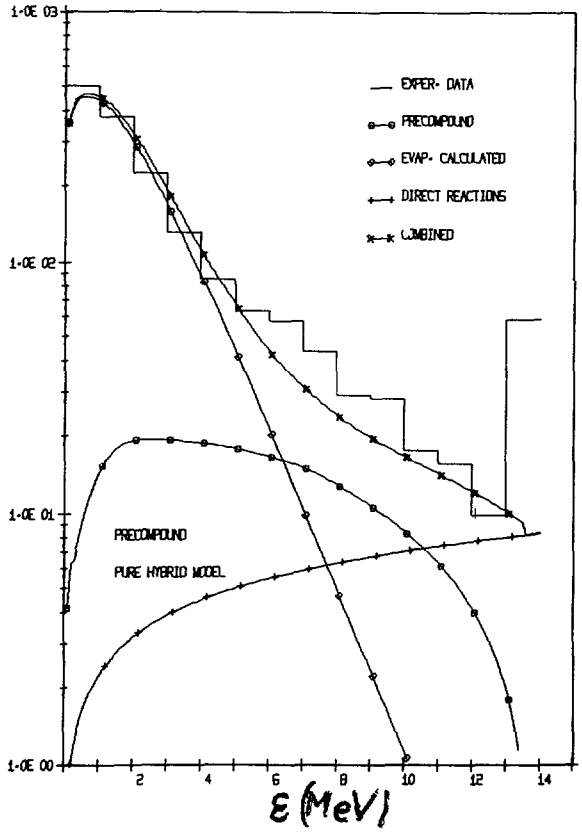

Fig. 15 Comparison between measured and calculated angular integrated inelastic cross-sections, where the combined curve includes the direct component and where the pre-equilibrium component is obtained from the pure hybrid model with realistic Fermi gas one nucleon level density.

Again as in Fig. 12 it is shown in Fig. 15 that the deficit at the high-energy tail of the energy distribution of the inelastic neutron scattering cross section is filled by the direct component also in the case where the pre-equilibrium component is obtained from the pure hybrid model with realistic Fermi gas one-nucleon level density.

c) Geometry dependent hybrid model with realistic Fermi gas one nucleon level density

The 14 MeV $^{56}Fe(n,n')$ pre-equilibrium calculations have been carried on[17] by introducing the geometry dependence into the hybrid model with realistic Fermi gas one-nucleon level density. This has been done by introducing the geometry dependent potential depth for the exciton number $n_o = 3$ according to the equations (19), (20) and (21) and by introducing the geometry dependence of the realistic Fermi gas one-nucleon level density according to eq. (28). The geometry dependence of λ_+ has been taken into account according to the equations (35) and (36). The results are shown in Fig. 16:

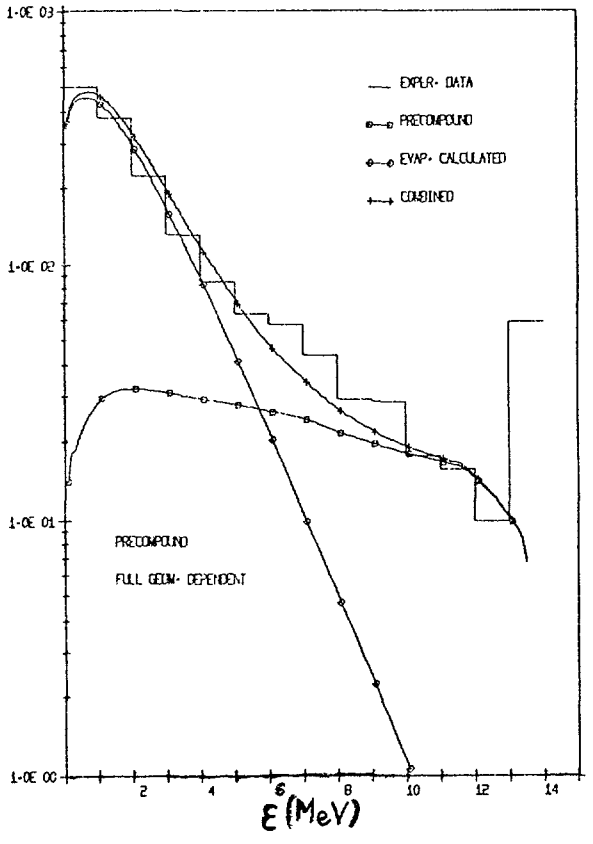

Fig. 16 Comparison between measured (step curve) and calculated (smooth curve) angular integrated inelastic cross sections of neutrons on ^{56}Fe. The calculated pre-equilibrium component is obtained from the geometry dependent hybrid model with realistic Fermi gas one nucleon level density.

In Fig. 16 the equilibrium component as well as the pre-equilibrium component are represented by the smooth curves as in the preceding figures. The equilibrium component has been obtained from equations (42a-f) as in Fig. 13. Thus in Fig. 16 both curves are obtained from absolute values without any adjustment to the empirical step curve of Hansen et al.[14]. This fact that the curves of Fig. 16 are based on absolute values is quite remarkable in view of the rather good agreement between the combined calculated curve and the empirical step curve. It therefore would be very interesting to investigate whether this good agreement can also be obtained by this program if applied to other nuclei without any adjustment. This would mean that this program as applied in Fig. 16 could be used to predict energy distributions of the inelastic neutron scattering cross sections on nuclei on which measured results are not yet available (see ref[17]).

It should be remarked that (n,2n)-processes and other tertiary reactions are not included in these calculations. There are indications that their contributions to the here considered energy distribution of the neutron emission cross-section decreases very rapidly from about 20 % at 2 MeV neutron emission energy to smaller than 10 % at 3 MeV neutron emission energy and can be neglected above a neutron emission energy of 4 MeV.

In Fig. 16 sufficient agreement with the empirical step curve has been reached by the combined curve of the calculated equilibrium component + pre-equilibrium component alone without an extra direct component as was the case for the results presented in Figs. 12 and 15. From this the conclusion could be drawn that the direct component should be contained in the pre-equilibrium component of Fig. 16 which has been calculated as explained on the basis of the geometry-dependent hybrid model with realistic Fermi gas one-nucleon level density. This is in agreement with the name"direct reaction term" used by Blann in ref.[10] for the first step $n_o=3$ geometry-dependent exciton contribution of which the geometry dependence is given by the equations (19)-(21), (38), (35) and (36). Especially the limited hole depth introduced for the geometry dependent $n_o=3$ term by the equations (19)-(21) causes the geometry dependent $n_o=3$ term to be originated mainly from the surface region of the nucleus where a direct reaction would mainly take place at the here considered energies. Thus accordingly the geometry dependent $n_o=3$ term should be considered as the angle

integrated direct component. The angular dependence then should be calculated as before by the PWBA expression (41). But const. in equation (41) should not anymore be adjusted to fit the experimental measured points. But instead it should be calculated as an $\varepsilon_o,\varepsilon$-dependent factor $F(\varepsilon_o,\varepsilon)$ by equating the angle integrated PWBA expression (41) with the absolute value of the geometry dependent $n_o=3$ term of the pre-equilibrium component (see equations (10) and (37)) calculated with geometry dependent Hybrid model. Accordingly equation (40) has to be replaced by

$$(43)\quad \frac{d^2\sigma(\varepsilon_o,\varepsilon,\theta)}{d\Omega d\varepsilon} = \frac{1}{4\pi}\left(\frac{d\sigma(\varepsilon_o,\varepsilon)}{d\varepsilon}\right)_{equi} + \frac{1}{4\pi}\left(\frac{d\sigma(\varepsilon_o,\varepsilon)}{d\varepsilon}\right)_{\substack{\text{Blann absolute realistic}\\ \text{geometry dependent } n\geq 5}} + \left(\frac{d\sigma^2(\varepsilon_o,\varepsilon,\theta)}{d\Omega d\varepsilon}\right)_{\substack{direct\\ n_o=3}}$$

where eq. (42a-f) has to be introduced into the first term of the right hand side of eq. (43), while eq. (37) with (3e), (19), (28), (35) and (36) into the second term and the last term is equal to (41) but with const. on the right-hand side replaced by the factor $F(\varepsilon_o,\varepsilon)$ which has to be determined according to

$$(44)\quad \int\left(\frac{d\sigma^2(\varepsilon_o,\varepsilon,\theta)}{d\Omega d\varepsilon}\right)_{\substack{direct\\ n_o=3}} d\Omega = \left(\frac{d\sigma(\varepsilon_o,\varepsilon)}{d\varepsilon}\right)_{\substack{\text{Blann absolute realistic}\\ \text{geometry dependent } n_o=3}}$$

where the right-hand side has to be taken from eq. (37) with (19)-(21), (28), (35) and (36). Examples for the angular distributions obtained with equations (43) and (44) are presented in Fig. 17:

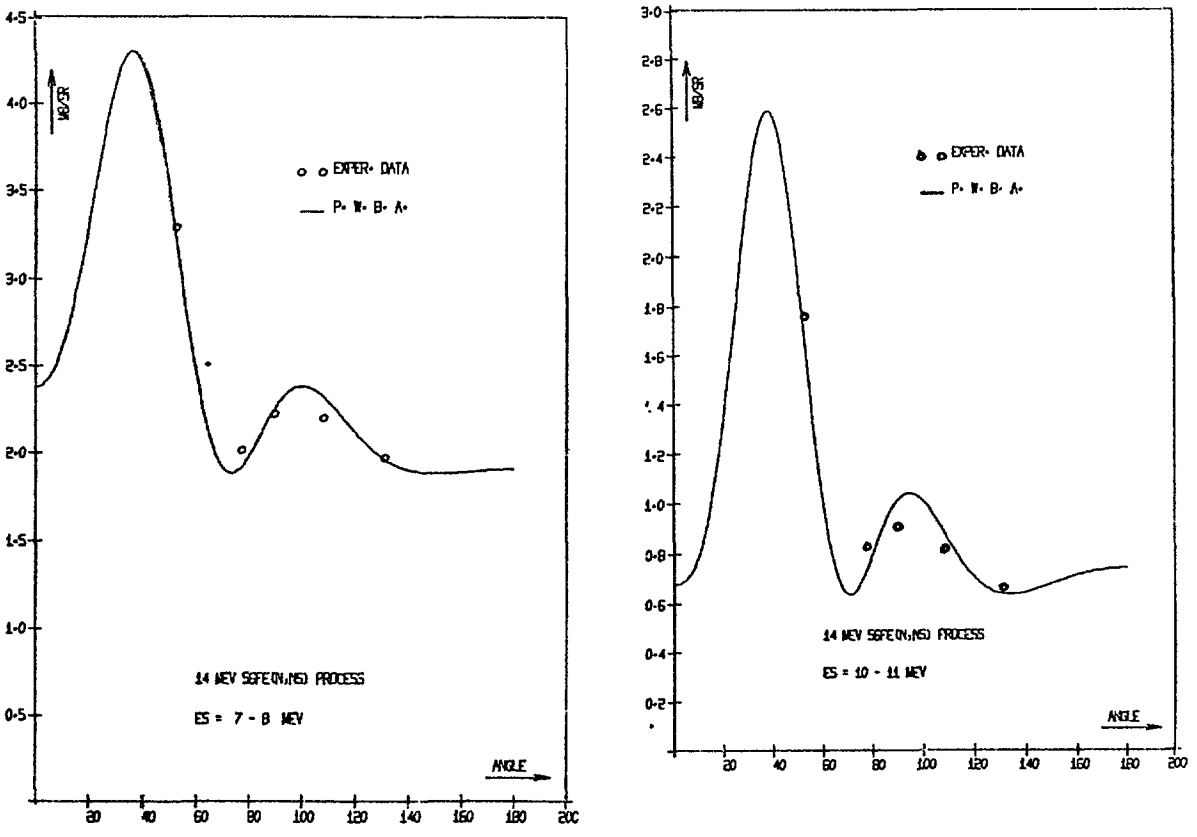

Fig. 17 Angular distribution of 14 MeV neutrons scattered inelastically on ^{56}Fe. The curves represent a PWBA distribution with equilibrium + $n \geq 5$ pre-equilibrium background where the angle integrated PWBA component is equated with the $n_0 = 3$ component of the geometry dependent hybrid model.

Fig. 17 shows that the calculated curves now agree with the measured values almost as well as in Fig. 11a and even better than in Fig. 14. But in Fig. 11a and Fig. 14 the calculated curves where adjusted to the measured points while in Fig. 17 the calculated curves represent absolute values obtained on the basis of the equations (43) and (44) without any adjustment to the measured points.

5. Microscopic DWBA-calculations and the pre-equilibrium description of the high energy tail of the 14,5 ^{56}Fe(n,n')-process

On the preceding pages we have shown that the high energy tail of the angle integrated scattered neutron energy distribution of the inelastic scattering cross section of neutrons on ^{56}Fe can be predicted by the geometry-dependent hybrid model yielding absolute values so that no adjustment to the empirical points was needed. Moreover no information about the special nuclear structure of the target nucleus as wave functions of the ground and excited states and their excitation energy spectra is needed for this geometry-dependent hybrid model description of the angle integrated scattered neutron energy dependent inelastic cross section. This description only needs information of the type of general nuclear systematics as A-dependence of the nuclear density distribution and information from the optical model.

As a counterpart to this geometry-dependent hybrid model description there is a description which is explicitly based on knowledge about the wave functions of the ground and excited states of the target nucleus and their excitation energy spectra using DWBA calculations to obtain the high-energy tail of the angle integrated scattered nucleon energy distributed inelastic scattering cross section of nucleons on nuclei.

For the 14,5 ^{56}Fe(n,n')-process this description has been carried through by Fu[21] using the ^{56}FeDWBA analysis of Mani[16]. Mani uses for each investigated level of the target nucleus the DWBA formula with first-order collective form factors β_ℓ of the target nucleus which gives for the inelastic-scattering cross section of protons leading to an excitation of this level of angular momentum ℓ:

$$\sigma_\ell(p,p') = \beta_\ell^2 \sigma_{DW}(\ell,p,p') \tag{45}$$

where $\sigma_{DW}(\ell,p,p')$ has to be calculated from the optical model for proton scattering and β_ℓ^2 has to be adjusted to the experimental measured cross section. Since β_ℓ is the deformation parameter of the target nucleus it must be the same for the DWBA formula of direct inelastic scattering of neutrons

$$\sigma_\ell(n,n') = \beta_\ell^2 \sigma_{DW}(\ell,n,n') \tag{46}$$

where $\sigma_{DW}(\ell,n,n')$ has to be calculated from the optical model for neutron scattering. Thus if β_ℓ is known from the $^{56}Fe(p,p')$ DWBA analysis of inelastic proton scattering it can be used to calculate the $^{56}Fe(n,n')$DWBA cross section for neutron scattering according to (46). The cross sections thus obtained for the excitation of the first 15 discrete levels of ^{56}Fe are the discrete points four of which are shown as crosses in Fig. 18. By averaging the 15 discrete points over the 1 MeV energy intervalls 9-10,10-11,11-12, 12-13 and 13-14 MeV the step curve shown by Fig. 18 in this region is obtained. The first 15 levels of ^{56}Fe are those who are below the continuum cut off energy ε_c of equation (42). In order to avoid a discontinuity above the continuum cut off energy a pre-equilibrium cross section was adjusted by Fu[21] to the step curve at the continuum cut-off energy in such a manner that the calculated reproduction of the secondary neutron energy spectrum was smoothly extended from the step curve into the continuum. This pre-equilibrium component together with the equilibrium component calculated from the code HELENE[18] gives the calculated values of the secondary neutron energy distribution above the contiuum cut-off energy as shown in Fig. 18:

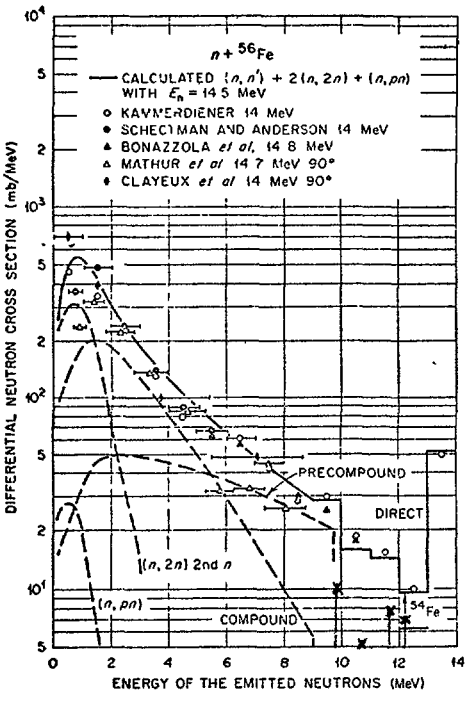

Fig. 18: Angle integrated differential cross section of secondary neutrons from iron bombarded by 14.5 MeV neutrons. The calculated curves contain direct DWBA results, the equilibrium component from the computer code HELENE and an adjusted pre-equilibrium component from an older exciton model version of Blann[22].

The pre-equilibrium component in Fig. 18 is taken from an older exciton model version of Blann[22] which is obtained from equations (3d-f) by assuming $\lambda_+(n,E)$ = const independent of n and E.

This description of Fig. 18 has the disadvantage that detailed nuclear structure information about the first 15 levels of the target nucleus such as level angular momentum ℓ was necessary to obtain the direct part to which the pre-equilibrium component was adjusted. This method doesn't allow to predict the high-energy tail of the energy dependence of the angle integrated inelastic differential cross section of secondary nucleons from a target nucleus bombarded by nucleons without the above mentioned detailed nuclear structure information about the special target nucleus. On the other hand this treatment would suggest to understand the lowest exciton number term of the pre-equilibrium component as an averaged or summarized direct component since at the continuum cut-off energy only the lowest exciton number term of the pre-equilibrium component is predominant. This agrees with the conclusion which is expressed by the equations (43) and (44) and by Fig. 17 and which also has been reached by Cohen, Holden and Rao[23] and by Lewis[24] from the DWBA analysis of experimental data for (p,p') and (d,d') reactions and which also is the basis of the contributed paper of Arndt and Reif to this meeting.

In contrast to the above considered DWBA method there is the fact that the geometry dependent hybrid model yields absolute values for the scattered particle energy-dependent inelastic cross section without nuclear structure information about the special target nucleus as explained around Fig. 16. This fact could be meaningful for the absolute values of the DWBA calculated direct inelastic cross sections in view of the above stated correspondence between the direct component and the lowest exciton nuclear term of the pre-equilibrium component.

The evaluation of Fig. 18 is contained in the ENDF/B-IV library but only for natural iron. For the other nuclei such as Cr or Ni pre-equilibrium models do not yet have been used for the evaluation of the secondary neutron energy distribution on the ENDF/B-IV file. On the other hand it should be easy to extend the geometry dependent hybrid evaluation as applied to iron in Fig. 16 also to other nuclei which are interesting in this context (see ref.[17]).

6. More rigorous theoretical derivations

More rigorous theoretical derivations have been presented. One is based by Grimes, Anderson, Pohl, McClure and Wong[25] and by Feshbach[26] on the concept of doorwaystates of the work by Feshbach, Karman and Lemmer[27]. The other by Agassi, Weidenmüller[28,32] and Mantzouranis[29] is based on the statistics of the interaction matrixelements characterising the microscopic behaviour of nuclei. Both derivations arrive at equations similar to those obtained by Blann for the description of the pre-equilibrium processes. But a closer look at the single steps of the derivations shows that apparently the direct reaction processes have been separated in both cases before treating the equilibration problem. This would mean that the direct reaction processes are not contained in the descriptions of the pre-equilibrium processes as given in both cases. On the other hand Mantzouranis, Agassi and Weidenmüller[30,31] have included the angular distributions of the pre-equilibrium nucleons into their generalized master equation description the calculated results of which agree rather well with the measured results for angular distributions and spectra of pre-equilibrium nucleons in a variety of cases in which no direct component has been separated from the empirical data. Thus still more clarification appears to be desirable about the distinction between pre-equilibrium and direct processes in nuclear reactions.

7. Applications

Measurements of neutron leakage spectra in the energy range 0,1 to 15 MeV from homogeneous assemblies have been made in order to provide test cases for neutron transport codes and input neutron cross-sections. Cylindrical[33] and spherical[34] assemblies have been used made of iron, uranium, niobium, beryllium and carbon. For the case of iron which is an important material in fast reactors, calculations of the neutron leakage spectrum for the cylindrical[33] as well as for the spherical[34] case have been carried through on the basis of microscopic neutron input data and various transport codes. The calculated results have been compared with the measured results for both cases. Fig. 19 shows the results for the cylindrical case.

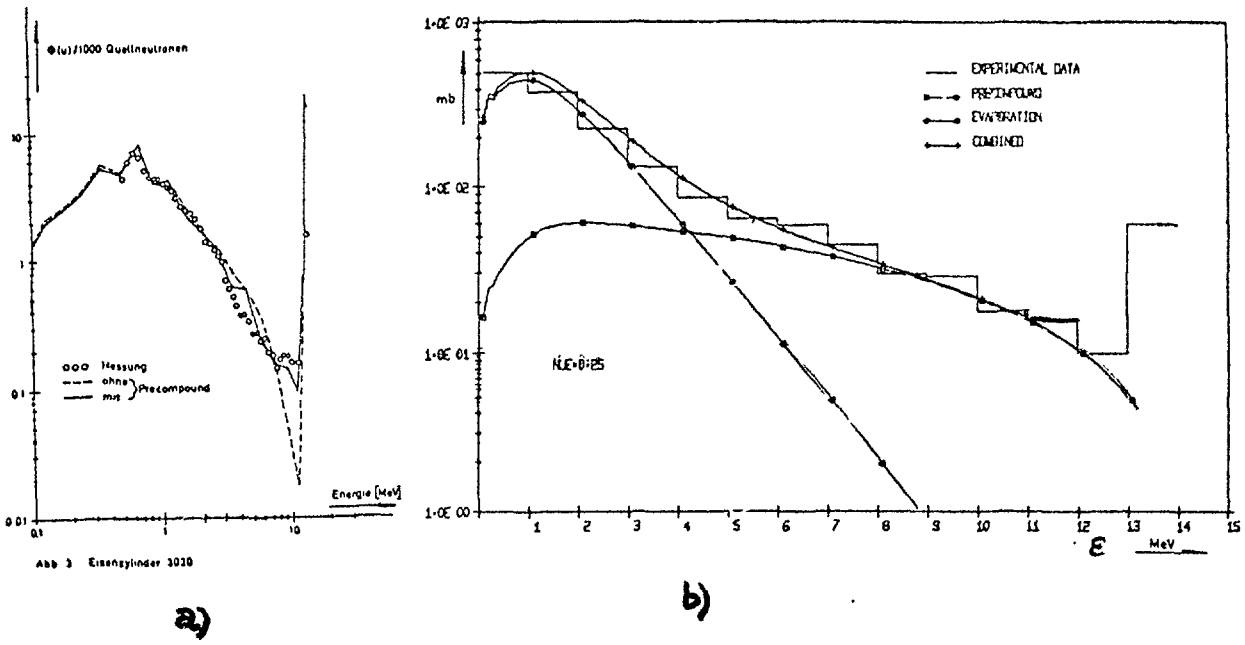

Fig. 19: a) Measured and calculated neutron leakage spectrum of an iron cylinder bombarded by 14 MeV Neutrons.

b) Microscopic scattered neutron energy dependent inelastic cross section of 14 MeV neutrons of Fig. 3 of ref[13].

The calculated curves in Fig. 19a) are obtained with a modified version of the Karlsruhe Monte Carlo code KAMMCØ[35]. For the dashed curve the evaporation formula (39) with $\nu=0.1$ is used for the distribution of the inelastic scattered neutrons while in the solid curve the precomponend processes are taken into account as shown in the combined curve of Fig. 19b). Accordingly Fig. 19a) shows that above 3 MeV neutron energy of the leakage spectrum the influence of the pre-equilibrium component becomes remarkable. This is important for shielding problems of fast reactors and expecially for the inner wall problem of the fusion reactor.

Acknowledgements

Enlightening discussions with M. Blann as well as the efficient contributions of my colleagues C.H.M. and I. Broeders to this report are gratefully acknowledged. Without their support this work could not have been accomplished.

References

1. C.K. Cline and M. Blann, Nucl. Phys. A172 (1971) 225
2. F.C. Williams, Jr., Phys. 31b (1970) 184
3. G.M. Braga Marcazzan, E. Gadioli-Erba, I. Milazzo-Colli and P.G. Sona, Phys. Rev. 6 (1972) 1398
4. Seeliger, D., these Proceedings, Review Paper 6
5. F.E. Bertrand and R.W. Peelle, ORNL 4469 (1970), ORNL 4638 (1971)
6. M. Blann, Proceedings of the Romanian Summer School in Nuclear Physics, Predeal, Romania, Sept. 4-13 (1974)
7. M. Blann and A. Mignerey, Nucl. Phys. A186 (1972) 245
8. M. Blann, Phys. Rev. Lett. 27 (1971) 337
9. A. Chevarier, N. Chevarier, A. Demeyer, G. Hollinger, P. Pertosa and Tran Minh Duck, Phys. Rev. C8 (1973) 2155
10. M. Blann, Phys. Rev. Lett. 28 (1972) 757, Nucl. Phys. A213 (1973) 570
11. K. Kikuchi and M. Kawai, Nuclear matter and nuclear reactions (North-Holland, Amsterdam, 1968)
12. G.D. Harp and J.M. Miller, Phys. Rev. C3 (1971) 1847; G.D. Harp, I.M. Miller and B.I. Berne, Phys. Rev. 165 (1968) 1166
13. H. Jahn, C. Broeders and I. Broeders, Proceedings of the Conference on Nuclear Cross Sections and Technology, Washington D.C., March 3-7, 1975, 350
14. L.F. Hansen, I.D. Andersen, P.S. Brown, R.I. Howerton, I.L. Kamerdiener, C.M. Logan, E.F. Plechaty and C. Wong, Nucl. Sci. Eng. 51, 278 (1973)
15. D. Hermsdorf, S. Sassonoff, D. Seeliger und K. Seidel, Kernenergie 17, 259(1974)
16. G.S. Mani, Nucl. Phys. A165 (1971), 225
17. C. Broeders, I. Broeders, H. Jahn, to be published
18. S.K. Penny, HELENE, ORNL-TM-2590 (1969)
19. F. Perey, ORNL 3429, (1963)
20. A. Gilbert, A.G.W. Cameron, Can. Journ. Phys. 43, (1965), 1446
21. C.F. Fu, Proceedings of the Conference on Nuclear Cross Sections and Technology, Washington, D.C., March 3-7, 1975, 328
22. M. Blann, Phys. Rev. Lett 21 (1968) 1357
23. B.L. Cohen, J.E. Holden and G.R. Gao, Phys. Rev. C9 (1974) 1025
24. M.B. Lewis, Phys. Rev. C9 (1974) 1878
25. S.M. Grimes, J.D. Anderson, B.A.Pohl, J.W. McClure and C. Wong Phys. Rev. C3(1971) 645; C4(1971) 607
26. H. Feshbach, Rev. Mod. Phys. 46(1974)1
27. H. Feshbach, A.K. Kerman and R.H. Lemmer Am. Phys. (N.Y.) 1967, 41, 230
28. D. Agassi, H.A. Weidenmüller, Phys. Lett. 56 B(1975) 305
29. D. Agassi, H.A. Weidenmüller, G. Mantzouranis, MPIH-1975-V11
30. G. Mantzouranis, D. Agassi, H. Weidenmüller, Phys. Lett. 57B (1975) 220
31. G. Mantzouranis, H.A. Weidenmüller and D. Agassi MPIH-1975-V20
32. H.A. Weidenmüller, Proceedings of the Conference on High Excited States in Nuclei, Jülich, 23-26 Sept. 1975

33. H. Borgwaldt, C.H.M. Broeders, I. Broeders, H. Jahn, M. Lalovic, D. Rusch, Reaktortagung, Nürnberg 1975

34. R.H. Johnson, I.J. Dorning, B.W. Wehing, Proceedings of the Conference on Nuclear Cross Section and Technology, Washington D.C., March 3-7, 1975, BB1, CB3

35. G. Arnecke, H. Borgwaldt, V. Brandl, M. Lalovic, KFK 1270/4 (1970)

Contributed Paper No. 16

DIRECT INELASTIC NUCLEON SCATTERING TO HIGHER EXCITED STATES

E. Arndt and R. Reif
Section of Physics, Technical University Dresden, GDR

Abstract:

The spectra of inelastically scattered nucleons and the corresponding angular distributions are calculated up to higher excitation energies in the framework of the DWBA within a microscopic approach. The method offers the possibility of a new approach to evaluate an appreciable part of the spectra and the angular distributions in a unified manner.

Recent experimental investigations of inelastic proton and deuteron scattering with bombarding energies of 17 MeV and 12 MeV exhibit a strong correlation of the transition strength of both reactions up to excitation energies of the nucleon separation energy [1]. From these results one can conclude that - apart from excitations of low-lying collective states - direct processes contribute to the smooth background of the continuous spectra to a large extent also for higher inelasticity. This offers the possibility to calculate the high energy part of the spectra and the angular distribution within the framework of the well developed first-order DWBA method.

On this line the spectra and angular distributions for different excitation energies of the reactions $^{116}Sn(p,p')$, E_p = 17 MeV and $^{40}Ca(n,n')$, E_n = 14 MeV have been calculated within a microscopic approach to the scattering process. The differential cross section is composed of elementary excitations (2quasi-particle excitations in ^{116}Sn [2] or 1p1h-transitions in ^{40}Ca [3]). These are summed up incoherently for $^{116}Sn(p,p')$ using a Lorentz distribution for the squared coefficients of the nuclear wave function [5]. Multipolorders of L=2 up to L=6 have been taken into account. In the case of ^{40}Ca the formfactor of the dominating excitations of the negative parity states resolved in the inelastic proton scattering have been computed with nuclear wave functions in the Tamm-Dancoff approximation and broadened according to the experimental resolution of the neutron experiment. In both cases a two-body potential of Gaussian shape with a range of 1.7 fm has been used as an effective interaction between the incoming nucleon and the target nucleons. The optical parameters have been taken from refs. [5] and [6] for $^{116}Sn+p$ and $^{40}Ca+n$, respectively. The theoretical values are compared with the experiments of refs. [7] and [8] and results obtained within the Hybrid model with intranuclear transition rates derived from the optical model. Examples are given in Figs. 1 and 2.

The results may be summarized as follows:

1) The calculated relative spectra for a definite scattering angle resembles in shape the $n_o=3$ component of the pre-compound spectrum from the geometry-dependent hybrid model.

2) The gross structure observed in the experiment is indicated qualitatively and results from the energy distribution of quasi-particle energies.

3) Normalizing the strength of the effective interaction to the collective 3^- excitation in ^{40}Ca the absolute spectrum of inelastically scattered neutrons is reproduced within a factor of two up to excitation energies of about 7 MeV.

4) The forward-peaked angular distribution in the high-energy pre-compound region is reproduced.

5) For higher excitation energies transition strength is missing because of the neglect of higher-order terms as well as the re-emission from quasi-bound states. Accordingly, the theoretical angular distributions are too much forward-peaked for these excitation regions.

Similar results have been obtained with collective model approach in ref. [9] and with simplifying assumptions on the formfactor and using plane waves instead of distorded waves in ref. [10].

REFERENCES

[1] COHEN, B.L. et al., Phys. Rev. C9 (1974) 1025
[2] CLEMENT, D.M., BARANGER, E.U., Nucl. Phys. A120 (1968) 25
[3] GILLET, V., SANDERSON, E.A., Nucl. Phys. A91 (1967) 292
[4] REIF, R., acta phys. slov. 25 (1975) 208
[5] MAKOFSKE, W. et al., Phys. Rev. 174 (1968) 1429
[6] ROSEN, L. et al., Ann. Phys. (N.Y.) 34 (1965) 96
[7] KALBACH-CLINE, C. et al., Nucl. Phys. A222 (1974) 405
[8] HERMSDORF, D. et al., ZfK-277 (1974)
[9] LEWIS, M.B., Phys. Rev. C9 (1974) 1878
[10] LUKJANOV, A.A. et al., Jad. Fiz. 21 (1975) 67

FIGURE CAPTIONS

Fig. 1 DWBA spectra compared with the n=3 component of the pre-equilibrium spectrum from the geometry dependent hybrid model and the experimental data [7]. The parameters of the Lorentz distribution of 2quasi-particle excitations were Δ=0.5 and Γ=0.5 MeV. The theoretical curves are normalized independently.

Fig. 2 Experimental and DWBA angular distribution for different excitation energies.

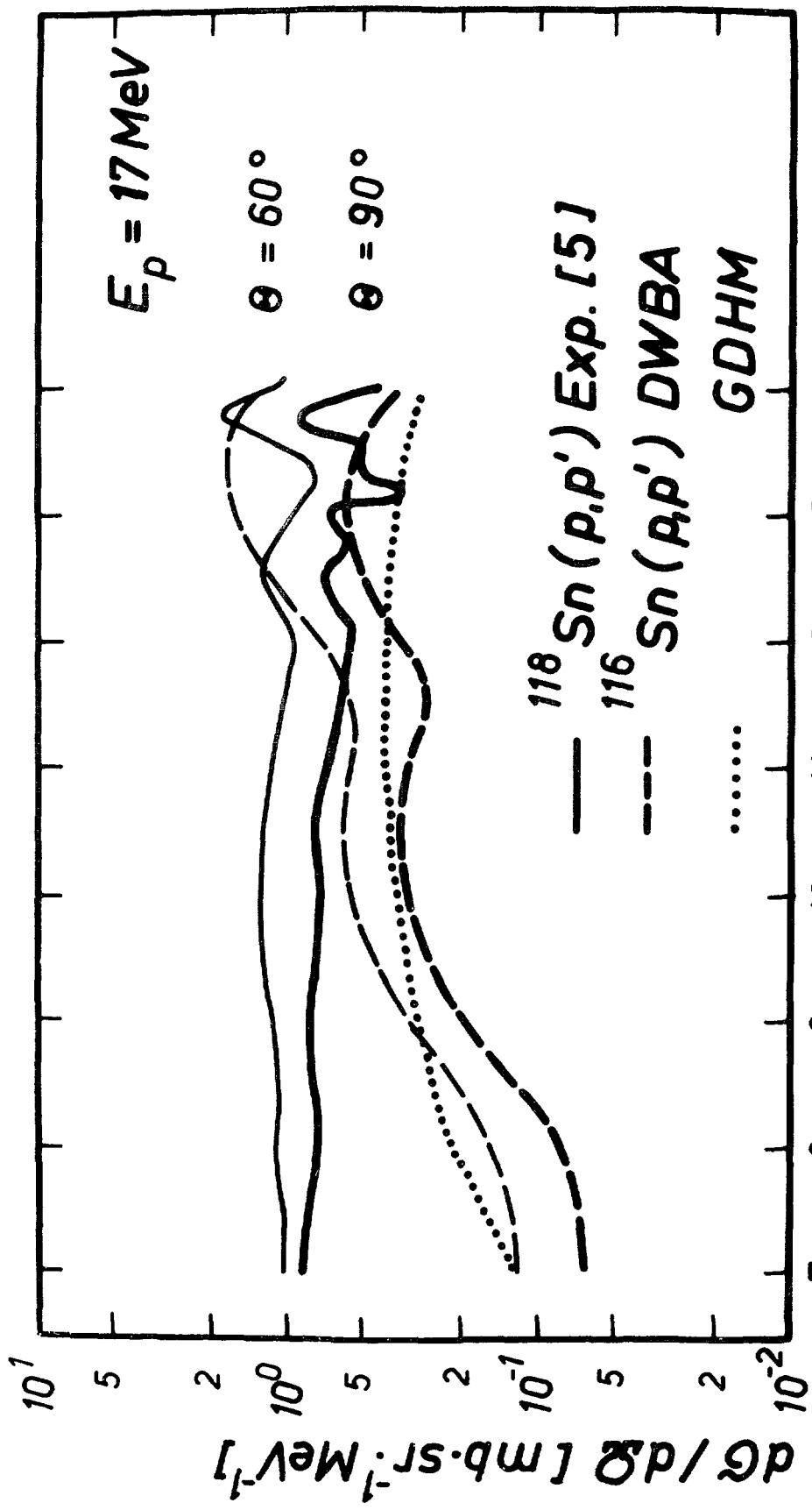
$E_p = 17$ MeV
$\theta = 60°$
$\theta = 90°$
$^{118}Sn(p,p')$ Exp. [5]
$^{116}Sn(p,p')$ DWBA
GDHM
$d\sigma/d\Omega$ [mb·sr^{-1}MeV^{-1}]
E[MeV]
10^{1}
5
2
10^{0}
5
2
10^{-1}
5
2
10^{-2}
7
8
9
10
11
12
13
14

Figure 1

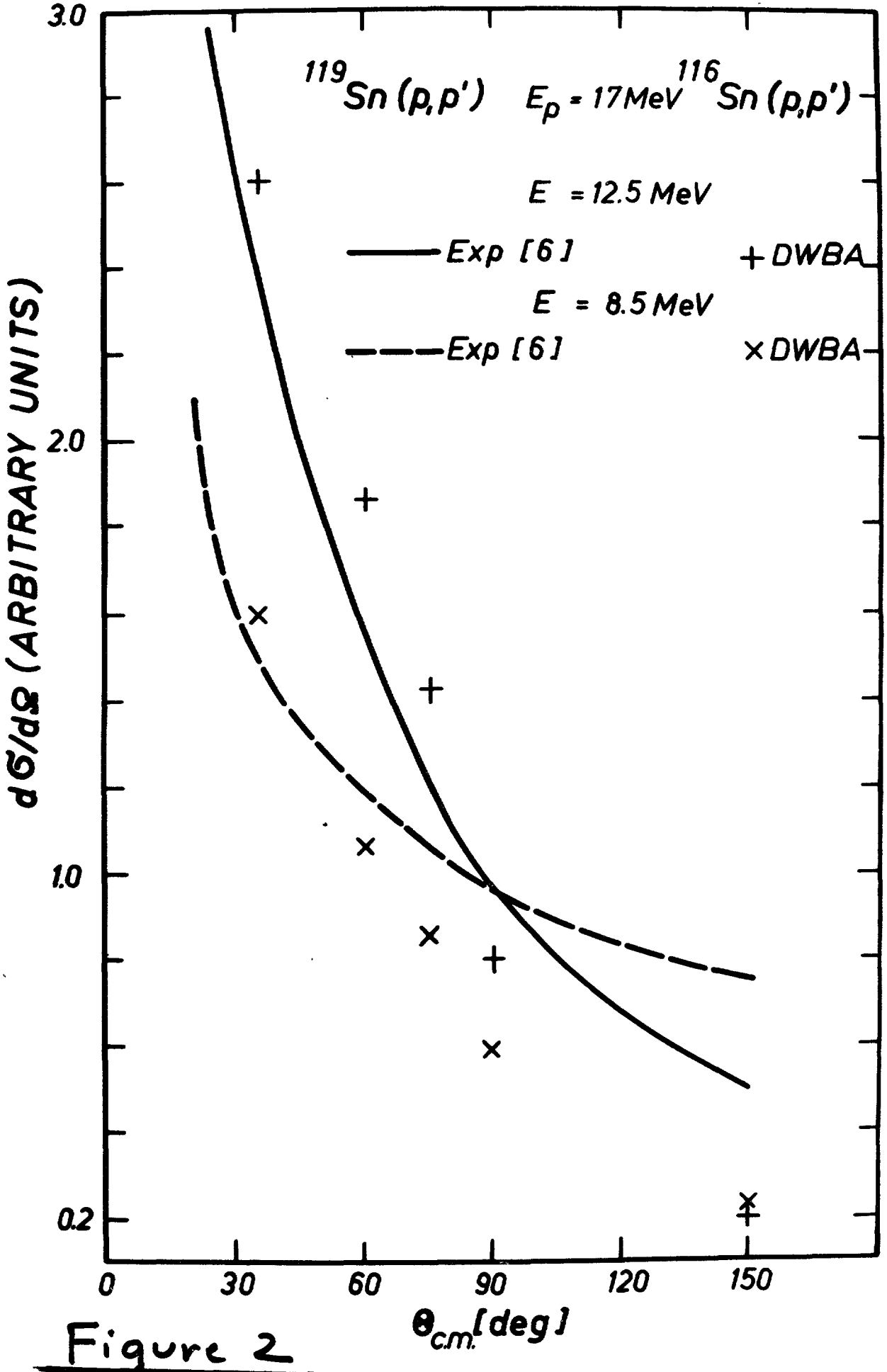

Figure 2

Next page(s) left blank

Contributed Paper No. 17

Computer calculations of neutron cross sections and γ-cascades with the statistical model with consideration of angular momentum and parity conservation.

M. Uhl

Institut für Radiumforschung und Kernphysik, Vienna.

Abstract

A computer code designed to calculate cross sections for reactions with up to six emitted particles and an arbitrary number of gamma-rays preceding or following particle emission is described. The calculations are performed within the framework of the evaporation model with consideration of angular momentum and parity conservation. For the first step of an evaporation cascade preequilibrium emission is taken into account. Some applications to neutron-induced reaction cross sections are presented and discussed.

1. Introduction

Nuclear reactions with several emitted particles and gamma-rays are most easily and often successfully treated as "evaporation cascades". In this contribution the computer code STAPRE will be described which was developed to handle such reactions essentially under the assumption that they can be represented as successive evaporations of particles and photons. Further some applications to neutron-induced reactions are presented.

In the following reactions of the type A(a,bc...zγ)Z are considered which are induced by particle a and characterized by a certain sequence (bc...z) of emitted particles; an arbitrary number of gamma decays preceeds or follows the emission of each particle (fig. 1). For such reactions the code calculates the population cross sections for levels characterized by excitation energy E, angular momentum I and parity Π or for groups of such levels. All possible "ways" of populating those levels are con-

sidered; examples of such ways which differ in the energies of the emitted particles and in the gamma-ray cascades preceeding or following the emission of particles are shown in fig. 1. Angular momentum and parity conservation are taken into account. The angular distribution of the emitted particles and gamma-rays is not calculated. By appropriate book-keeping one obtains also the spectra of the emitted particles b,c...z, the activation cross sections for the intermediate nuclei A+a, A+a-b, ... Z and the gamma-ray production spectrum for the final nucleus Z; we are just now improving the code in such a way that the energy spectrum of all gamma-rays produced by the considered reaction sequence is calculated.

The above described code can be used for the calculation of the following quantities:

1) activation cross sections
2) population of isomeric states
3) energy distribution of emitted particles and gamma-rays
4) production cross sections for gamma-rays from low excited levels.

Up to six sequentially emitted particles can be considered. The number of gamma-rays is limited only by the use of an energy grid for the calculations.

2. Models employed

The major part of the calculations is based on the statistical model. For particles emitted in the first step of the evaporation cascade a "preequilibrium decay" contribution to the cross section is included, since the statistical model alone fails to explain the hard component in the spectra of those particles observed at higher incident energies. Direct reactions which may be important for the population of low excited collective levels are not yet taken into account.

2.1. Preequilibrium model

The equilibration of the composite system formed by projectile a and target A is treated in the framework of the "exciton model" [1] - [5]. Since the method employed here differs slightly from those reported in literature a short description follows.

Starting from a simple configuration the composite system is assumed to equilibrate through a series of two-body collisions and to emit particles from all intermediate states. The states of the system are classified according to the number n of excitons or more specifically to the numbers p and h of the excited particle and hole degrees of freedom (n = p+h). No distinction is made between neutrons and protons. The application of a two-body interaction to states of a (p,h)-configuration leads to states with (p+1, h+1), (p,h) or (p-1, h-1) excited particles and holes. In competition with these internal transitions particles can be emitted from each state. For all these processes transition rates averaged over all states of a

configuration are employed.

Let $b^{(k)}(n) = b^{(k)}(p,h)$ be the population probability of the states of a (p,h) configuration resulting from k internal transitions. The corresponding quantity $b^{(k+1)}(n)$ for (k+1) internal transitions is obtained from:

$$\left.\begin{aligned} b^{(k+1)}(n) &= b^{(k)}(n+2)\,\frac{\lambda_-(n+2)}{\lambda(n+2)} + b^{(k)}(n)\,\frac{\lambda_0(n)}{\lambda(n)} + b^{(k)}(n-2)\,\frac{\lambda_+(n-2)}{\lambda(n-2)} \\ \lambda(n) &= \lambda_-(n) + \lambda_0(n) + \lambda_+(n) + \lambda^e(n);\quad \lambda^e(n) = \sum_r \int d\varepsilon_r\, \lambda_r^e(n;\varepsilon_r). \end{aligned}\right\} \quad (1)$$

In eq. (1) $\lambda_+(n)$, $\lambda_0(n)$ and $\lambda_-(n)$ are the average rates for internal transitions with a change of the exciton number by an amount of +2, 0 and -2 respectively, and $\lambda_r^e(n;\varepsilon_r)d\varepsilon_r$ is the average rate for emission of particle r with energy of relative motion ε_r. The quantity $\lambda^e(n)$ therefore represents the total rate for emission of particles. Starting from an initial population probability

$$b^{(0)}(n) = \delta_{n n_0} \quad \text{or} \quad b^{(0)}(p,h) = \delta_{pp_0}\delta_{hh_0} \quad (2)$$

successive application of eq. (1) gives the populations of the various (p,h) configurations by processes with an arbitrary number k of internal transitions. With increasing k the ratio $b^{(k-1)}(n) \,/\, b^{(k)}(n)$ becomes independent of n and k. Hence an upper limit K for the number of internal transitions to be considered for preequilibrium decay is obtained from the following condition:

$$\left.\begin{aligned} &\left|\left(b^{(k-1)}(n)/b^{(k)}(n)\right) - Q^{(k)}\right| < 0.01\, Q^{(k)} \quad \text{for all } n \text{ and } k \geq K \\ &Q^{(k)} = \left(\sum_n b^{(k-1)}(n)\right)\Big/\left(\sum_n b^{(k)}(n)\right). \end{aligned}\right\} \quad (3)$$

The preequilibrium contribution $\frac{\partial \sigma_{ab}^{pre}}{\partial \varepsilon_b} d\varepsilon_b$ to the differential cross section is given by

$$\frac{\partial \sigma_{ab}^{pre}}{\partial \varepsilon_b} d\varepsilon_b = \sigma_a^{non} \sum_{k=0}^{K} \sum_n b^{(k)}(n)\, \frac{\lambda_b^e(n,\varepsilon_b)}{\lambda(n)}\, d\varepsilon_b \quad (4)$$

where σ_a^{non} represents the optical model absorption cross section for the projectile a. The fraction q^{pre} of the initial population surviving preequilibrium emission is given by

$$q_h^{pre} = 1 - \sum_{k=0}^{K} \sum_n b^{(k)}(n)\, \frac{\lambda^e(n)}{\lambda(n)} \quad (5)$$

Although this method of treating the equilibration of the composite system employs the same assumptions as the "master equation approach to the exciton model" described by Cline and Blann [2], it is much simpler than the latter, since it does not involve the numerical solution of coupled differential equations. The results of eqns. (1) to (5) include as special cases the various approaches which neglect $\Delta n = -2$ and $\Delta n = 0$ internal transitions and (or) the depletion of the populations by particle emission.

The rates $\lambda_+(n)$, $\lambda_0(n)$ and $\lambda_-(n)$ are related by the formulae of Williams [6], corrected for the Pauli-principle by Cline[7], to the absolute square of the average effective matrix element M of residual interactions. For the dependence of this quantity on mass number A and excitation energy E of the composite system the expression

$$|M|^2 = FM\ A^{-3} E^{-1} \qquad (6)$$

proposed by Kalbach-Cline [8] is used. The rates $\lambda_\tau^e(n,\varepsilon_\tau)\,d\varepsilon_\tau$ for particle emission are calculated from detailed ballance considerations as described in ref. [2]. They depend on the inverse reaction cross sections and on the densities of particle-hole states; the latter are evaluated by means of a formula given by Williams [9].

The inverse reaction cross sections and the density g of single particle states on which all rate expressions depend are obtained from quantities used for the statistical model calculations described below: the optical model transmission coefficients and the level density parameter $a = (6/\pi^2)g$.

The characteristic parameters of the exciton model are the initial number $n_0 = p_0 + h_0$ of excitons and the value of the matrix element or of the constant FM (eq. (6)). The quantitiy n_0 depends on the projectile type. Many investigations have shown that for nucleon induced reactions the value $n_0 = 3$ $(p_0 = 2, h_0 = 1)$ is required to explain the shape of the observed particle spectra; exceptions are found near closed shells. The absolute square of the matrix element M has been estimated from analysis of experimental data by Braga-Marcazzan et al. [3] and by Kalbach-Cline [8]. Since, however, the value $|M|^2$ required to reproduce the experimental results depends sensitively on details of the employed model, as for instance the expressions for emission rates and the single particle state density g, the constant FM in eq. (6) is regarded as an adjustable parameter.

As in most models of preequilibrium emission angular momentum is not taken into account.

2.2. Statistical Model

The excited states of all nuclei relevant for a reaction of the type A(a,bc...zγ)Z are described in two different ways. At low excitation energy the quantum numbers (E_i I_i Π_i) of all known "discrete" levels are taken into account. As soon as with increasing excitation energy the experimental information about

the levels is no longer complete, a continuous level density formula $\rho(E\,I\,\Pi)$ is applied.

The equilibrium contribution to the first step of an evaporation cascade is calculated by means of the familiar Hauser-Feshbach formula [10]; if necessary the width fluctuation correction is applied [11]. In case that a particle is emitted the preequilibrium contribution is added. If the first step of an evaporation cascade populates levels $(E\ I\ \Pi)$ in an interval ΔE around excitation energy E the cross section is given by

$$\frac{\partial\sigma_1(E\,I\,\Pi)}{\partial E}\Delta E = \left\{ q^{pre}\,\frac{\partial\sigma^{HF}(E\,I\,\Pi)}{\partial E} + \frac{\partial\sigma^{pre}(E)}{\partial E}\,\frac{\frac{\partial\sigma^{HF}(E\,I\,\Pi)}{\partial E}\Delta E}{\sum_{I'\Pi'}\frac{\partial\sigma^{HF}(E\,I'\,\Pi')}{\partial E}\Delta E}\right\}\Delta E \qquad (7),$$

where $\frac{\partial\sigma^{HF}(E\,I\,\Pi)}{\partial E}$ is obtained from the Hauser-Feshbach formula and the preequilibrium contribution $\frac{\partial\sigma^{pre}(E)}{\partial E}$ from eq. (4). The quantitiy q^{pre} which is given by eq. (5) allows for the loss of initial population caused by preequilibrium emission. Since the prequilibrium model described before does not consider angular momentum and parity it is assumed in eq. (7) that the population $\frac{\partial\sigma^{pre}}{\partial E}(E)\,\Delta E$ is distributed among the levels with different spin and parity in the same way as the equilibrium contribution. For the results of the subsequent evaporation cascade calculations the application of this probably poor approximation may be of importance only in case of a dominant preequilibrium contribution. If a gamma-ray is emitted instead of a particle the second term in eq. (7) is omitted.

For all further steps of the cascade the well known formulae of the evaporation model are applied. The population of levels $(E'\,I'\,\Pi')$ by particle or photon emission from levels $(E\,I\,\Pi)$ is governed by the ratio of the average partial $\Gamma(E\,I\,\Pi\,;\,E'\,I'\,\Pi')$ to the average total decay width $\Gamma(E\,I\,\Pi)$; both quantities are obtained by appropriate sums of transmission coefficients for particles or photons. The processes provided for to compete with a particular decay mode are the emission of up to four different particles and of gamma-rays. Since fission as competing decay mode is not yet taken into account the application of the code STAPRE is limited to nuclei not susceptible to fission.

In order to obtain for a reaction of the type $A(a,bc\ldots z\gamma)Z$ the population cross section of levels $(E_f\ I_f\ \Pi_f)$ in an interval ΔE around E_f one has to add the contributions of all different ways (see fig. 1) by which these levels can be excited. If a particular way is characterized by a sequence $[s]$ of n_s emitted particles and gamma-rays and by the resulting n_s states $(E_i^s\ I_i^s\ \Pi_i^s)$, the population cross section $\frac{\partial\sigma(E_f\,I_f\,\Pi_f)}{\partial E_f}\Delta E_f$ is given by

$$\frac{\partial\sigma(E_f I_f \Pi_f)}{\partial E_f}\Delta E_f = \sum_{[s]} \Big\{ \delta_{n_s,1} \frac{\partial\sigma_1(E_f I_f \Pi_f)}{\partial E_f}\Delta E_f + (1-\delta_{n_s,1}) \sum_{I_1^s \Pi_1^s} \cdots \sum_{I_{n_s-1}^s \Pi_{n_s-1}^s} \int dE_1^s \cdots \int dE_{n_s-1}^s \frac{\partial\sigma_1(E_1^s I_1^s \Pi_1^s)}{\partial E_1^s} \times \prod_{i=1}^{n_s-1} \frac{\Gamma(E_i^s I_i^s \Pi_i^s ; E_{i+1}^s I_{i+1}^s \Pi_{i+1}^s)}{\Gamma(E_i^s I_i^s \Pi_i^s)} \rho(E_{i+1}^s I_{i+1}^s \Pi_{i+1}^s)\Delta E_f \Big\},$$

where $\frac{\partial\sigma_1(E I \Pi)}{\partial E}\Delta E$ is defined by eq. (7). The summations and integrations are restricted by the conservation of energy, angular momentum and parity. For discrete levels the level density $\rho(E I \Pi)$ has to be replaced by

$$\rho(E I \Pi) = \sum_{I_i \Pi_i} \delta_{I I_i} \delta_{\Pi \Pi_i} \delta(E - E_i).$$

A more detailed description of these calculations has been given elsewhere [12].

To perform the above described calculations additional information regarding the transmission coefficients and the level density is needed.

The transmission coefficients for particles are calculated externally by means of an optical model code. Since the channel spin coupling scheme is employed the particle transmission coefficients $T_\ell(\varepsilon)$ are assumed to depend on energy ε and angular momentum ℓ of relative motion only.

By assumption the gamma-ray transmission coefficients depend on the multipole type XL and transition energy ε. They are related to the gamma-ray strength functions $f_{XL}^s(\varepsilon)$ by $T_{XL}^s(\varepsilon) = 2\pi\varepsilon^{2L+1} f_{XL}^s(\varepsilon)$. For the energy dependence of the E1-strength function optionally the Weisskopf or the Brink-Axel model [13] can be used as well as an arbitrary combination of both models. Following the suggestion of Gardner [14] provision is also made for including a "pigmy resonance" and a "step" in order to reproduce experimental E1-strength functions. The strength functions for M1, E2 ... M3 radiation are for the present obtained from the Weisskopf model and normalized to $f_{E1}^s(\varepsilon)$. Optionally $f_{E1}^s(\varepsilon)$ can be normalized by fitting the observed average radiation width at the neutron binding energy. For gamma transitions between discrete levels, however, experimental branching ratios are used; this is of special importance for the calculation of isomeric cross sections and of production cross section for gamma-rays between low excited levels.

The level density $\rho(E I \Pi)$ is calculated within the framework of the "back-shifted" Fermi-gas-model [15]. The level density is assumed to be independent of parity. The energy and spin dependence is obtained from the expressions of Lang [16]. A simple formula for the yrast spin is employed. The parameters of the model are the level density parameter a, the effective moment of inertia Θ_{eff} and the fictive ground state position Δ.

A compilation of level density parameters for the back-shifted Fermi-gas-model has been published by Dilg et al. [17]; in this work the parameters were obtained from resonance spacing data and from the density of low excited levels.

Since a simple level density formula cannot represent adequately spins and parities of the first low excited levels it is for many applications extremely important to consider known levels as far in excitation energy as possible. As a further improvement one could apply instead of the above named model recently developed microscopic theories of level densities [18] - [20] which take into account realistic single particle states, pairing and collective states.

3. Applications

In this section some calculations for neutron induced reactions are described as typical examples to illustrate the consequences of preequilibrium decay and to emphasize the importance of the competition between particle and gamma-ray emission ("gamma-competition"). For all subsequent calculations level density parameters from ref. [17] were employed. Transmission coefficients for neutrons, protons and α-particles were calculated for global optical potentials given in refs. [21], [22] and [23]. Unless otherwise stated the E1-strength function was obtained by means of the Brink-Axel model and normalized to the average radiation width at the neutron binding energy.

Fig. 2 shows experimental data for the $^{56}Fe(n,p\gamma)^{56}Mn$ activation cross section confronted with the results of three calculations employing different assumptions about the preequilibrium contribution. The calculation without consideration of preequilibrium decay obviously fails to reproduce the data for high incident energy. Good agreement with the data is achieved by taking into account preequilibrium emission with the following values for the relevant parameters: ($p_0 = 2$, $h_0 = 1$) and FM = 750 MeV^3. The consequences of the preequilibrium emission can be seen from the following arguments. In comparison with the evaporation spectra for an equilibrated compound nucleus the energy spectra of particles emitted in the preequilibrium stage show an excess at higher energies. Therefore the influence of the Coulomb barrier on proton emission is reduced as well as the competition by (n,pnγ)-processes which is responsible for the decrease of the (n,pγ)-activation cross section at higher incident energies. Moreover the fraction of the initial population subject to preequilibrium emission increases with increasing bombarding energy. As shown in fig. 3 good agreement with experimental data for the $^{54}Fe(n,p\gamma)^{54}Mn$ activation cross section can be obtained by employing the same parameters for the preequilibrium model. The values for the square of the effective matrix element $|M|^2$ required to fit the data in these two cases are considerably larger than those reported by Kalbach-Cline [8] for proton and by Braga-Marcazzan [3] for neutron induced reactions; it has been explained, however, in section 2.1. that the values found for this quantity depend critically on the details of the model.

For (n,p)- and other reactions whose share in the total absorption cross section is small the theoretical results depend strongly on the level densities employed. In order to obtain agreement with experiment one has in most cases to adjust the level density parameters of ref.[17] within the errors quoted there. On the other hand the accuracy of predictions of such cross sections may become poor if there are only few or no experimental data at all to adjust the level densities. An improvement of the accuracy, however, can be achieved if it is possible to reproduce cross sections for the most important competing reactions.

In fig. 4 experimental data and calculations concerning the activation cross section for the reaction $^{198}Pt(n,2n\gamma)^{197}Pt$ are displayed. The calculations were performed with consideration of preequilibrium decay with parameters ($p_o = 2$, $h_o = 1$) and FM = 750 MeV^3. The E1-strength functions were derived from the Brink-Axel model and the Weisskopf model and normalized to an average radiation width of 100 meV. The difference between the results obtained with these two models for $f_{E1}^{\xi}(\epsilon)$ is very small. It has been shown by Gardner [14], however, that the gamma-ray production spectra depend sensitively on the model for the gamma-ray strength functions.

In the range of excitation energies considered here the emission of gamma-rays represents the process which for a heavy, not fissionable nucleus competes most effectively with neutron evaporation. Fig. 4 shows that the results obtained without taking into account gamma-competition deviate significantly from those including this effect whenever the competing reactions (n,n'γ) or (n,3nγ) are of importance. Therefore calculations of (n,2nγ)-activation cross sections without consideration of gamma-competition, as those described by Pearlstein [30] which formerly were frequently used for cross section evaluations, give in this mass region reliable results only for incident energies near the maximum of the excitation function. For many heavy nuclei, as for the present example, incident energies around 14 MeV for which the majority of data exists satisfy this condition.

As was already pointed out by Grover [31] the extent of gamma-competition depends strongly on angular momentum and excitation energy of the states involved. Particle emission from high spin states is hindered by the centrifugal barrier as long as due to a separation energy of several MeV only final states with much lower spins are available. Gamma-ray emission from those states, on the other hand, is not hindered to such an extent because of the higher excitation energies of the accessible final states.

Gamma-competition is more effective at the high energy portion of the $^{198}Pt(n,2n\gamma)^{197}Pt$ excitation function where the cross section is enhanced at the expense of (n,3nγ)-processes than at the low energy portion where the cross section is reduced by (n,n'γ)-processes. This behaviour can be explained by the following arguments. Due to the higher incident energies and the evaporation of two neutrons more states with high angular momentum and excitation energies near the neutron

threshold are populated for ^{197}Pt than for ^{198}Pt.

Fig. 5 shows for ^{197}Pt, besides the level schemes employed, the fraction $g_\gamma(E)$ of the population of states with excitation energy around E which by gamma-ray cascades starting from these levels contributes to the $(n,2n\gamma)$ activation cross section. The calculations were performed for an incident energy of 17.77 MeV. It can be seen that the effect of gamma-competition is strongly reduced with increasing excitation energy. The main contribution to $g_\gamma(E)$ originates from states with high angular momentum.

Recently G. Stengl [32] measured the above defined ratio $g_\gamma(E)$ for the reaction $^{56}Fe(n,n'\gamma)^{56}Fe$ by counting coincidences between neutrons leading to states of ^{56}Fe above the neutron threshold and gamma-rays from the first excited level of the same nucleus; good agreement between his results and calculations with the code described here was obtained.

From the previous considerations it is evident that the extent of gamma-competition depends critically on the spins and parities of the low excited levels accessible to neutron emission. Since for ^{196}Pt only scarce information about the levels could be found no attempt was made to improve the agreement between the calculated $^{198}Pt(n,2n\gamma)^{197}Pt$ cross section and the experimental data.

Applications of previous versions of the code STAPRE to cross section calculations for gamma-ray production by $(n,n'\gamma)$ and for isomeric state populations by $(n,p\gamma)$-reactions were described elsewhere [33], [34]. Gardner [14] reported about calculations of gamma-ray production spectra performed with a modified version of this code.

4. Conclusion

The code STAPRE is designed to calculate a variety of cross sections for processes which can be described as evaporation sequences. In particular gamma-ray cascades are treated in great detail. Therefore the code can successfully be applied to obtain cross sections for which the consideration of gamma-rays is essential. By inclusion of preequilibrium decay the code is applicable at higher bombarding energies, too.

On the other hand, important effects as fission competition and direct reaction contributions are not considered. Therefore comprehensive extensions are still required in order to increase the range of application of this code.

The results of the calculations depend on quantities - as level densities, level schemes, gamma-ray strength functions and others more - which frequently are not known very well. The influence of uncertainties in these quantities on the cross section differs from reaction to reaction. Therefore in unfavourable cases inaccurate results may be obtained even if the reaction is adequately described by the models employed. The accuracy of the result has to be investigated in each individual case. Quite generally, however, the accuracy for a particular cross section can be improved by fitting as many experimental data for competing reactions as possible with one set of values for the above mentioned quantities.

Several statistical model programs exist which perform similar calculations as the code STAPRE does. To the most frequently used belong the codes COMNUC and CASCADE developed by Dunford [35]. In contrast to STAPRE the COMNUC code calculates transmission coefficients and some related quantities internally and takes fission competition into account; besides, it can use results from direct reaction calculations as input. On the other hand these codes do not consider preequilibrium decay and do not calculate the spectra of emitted particles and gamma-rays and cross sections for gamma-ray production and isomeric state populations.

REFERENCES

[1] GRIFFIN, J.J., Phys. Lett. 17 (1966) 478.

[2] CLINE, C.K., BLANN M., Nucl. Phys. A 172 (1971) 225.

[3] BRAGA-MARCAZZAN, G.M., GADIOLI-ERBA, E., MILLAZZO-COLLI, L., SONA, P.G., Phys. Rev. C 6 (1972) 1398.

[4] MILLER, J., "Preequilibrium Processes", Proceedings of the Int. Conf. on Nuclear Physics, Munich, Sept. 1973, Vol. II, DE BOER, J., MANG, H.J., Edts., North-Holland-American Elsevier Publ. Co. (1974).

[5] KALBACH, C., Acta phys. slov. 25 (1975) 100.

[6] WILLIAMS, Jr, F.C., Phys. Lett. 31 B (1970) 184.

[7] CLINE, C.K., Nucl. Phys. A 195 (1972) 353.

[8] KALBACH-CLINE, C., Nucl. Phys. A 210 (1973) 590.

[9] WILLIAMS, Jr, F.C., Nucl. Phys. A 166 (1971) 231.

[10] HAUSER, W., FESHBACH, H., Phys. Rev. 87 (1952) 336.

[11] MOLDAUER, P.A., Revs. of Mod. Phys. 36 (1964) 1079.

[12] UHL, M., Acta Phys. Austriaca 31 (1970) 245.

[13] BARTHOLOMEW, G.A., EARLE, E.D., FERGUSON, A.J., KNOWLESS, J.W., LONE, M.A., Advances in Nuclear Physics, Vol. 7, Ch. 4, Plenum Press, New York (1973).

[14] GARDNER, D.G., Invited paper presented at the "Conference on Nuclear Cross Sections and Technology, Washington, D.C., March 3-7, 1975; and private communications.

[15] VONACH, H.K., HILLE, M., Nucl. Phys. A 127 (1969) 289.

[16] LANG, D.W., Nucl. Phys. 77 (1966) 545.

[17] DILG, W., SCHANTL, W., VONACH, H., UHL, M., Nucl. Phys. A 217 (1973) 269.

[18] MORETTO, L.G., Nucl. Phys. A 185 (1972) 145.

[19] BEHKAMI, A.N., HUIZENGA, J.R., Nucl. Phys. A 217 (1973)78.

[20] DØSSING, T., JENSSON, A.S., Nucl. Phys. A 222 (1974) 493.

[21] PEREY, F., BUCK, B., Nucl. Phys. 32 (1962) 353.

[22] MANI, G.S., MELKANOFF, M.A., IORI, I., C.E.A. Nr. 2379 (1963).

[23] HUIZENGA, J.R., IGO, G.I., ANL-6373 (1961).

[24] LISKIEN, H., PAULSEN, A., J. Nucl. Energy AB 19 (1965) 73.

[25] LISKIEN, H., PAULSEN, A., Nukleonik 8 (1966) 315.

[26] VONACH, H.K., VONACH, W.G., MÜNZER, H., SCHRAMEL, P., EANDC(E)-89 (1968) 37.

[27] SMITH, D.L., MEADOWS, J.W., ANL/NDM-10 (1975).

[28] PAULSEN, A., WIDERA, R., Conf. on Chem. Nucl. Data, Canterbury, Sept. 1971.

[29] BISSEM, H.H., BORMANN, M., MAGIERA, E., WARNEMÜNDE, R., Nucl. Phys. A 157 (1970) 481.

[30] PEARLSTEIN, S., Nucl. Data A, Vol. 3 (1967) 327.

[31] GROVER, J.R., Phys. Rev. 123 (1961) 267.

[32] STENGL, G., private communication.

[33] UHL, M., Nucl. Phys. A 184 (1972) 253.

[34] WAGNER, I., UHL, M., Acta Phys. Austriaca 37 (1973) 283.

[35] DUNFORD, C.L., "A unified model for analysis of compound nucleus reactions", AI-AEC-12931 (July, 1970).

FIGURE CAPTIONS

Fig. 1 A schematic representation of the different ways of populating final states $(E_f\ I_f\ \Pi_f)$ for a reaction A(a,bcγ)C.

Fig. 2 Experimental data and results of calculations for the $^{56}Fe(n,p\gamma)^{56}Mn$ activation cross section. Not all data from the quoted references are shown.

Fig. 3 Experimental data and results of calculations for the $^{54}Fe(n,p\gamma)^{54}Mn$ activation cross section. Not all data from the quoted references are shown.

Fig. 4 Experimental data and results of calculations for the $^{198}Pt(n,2n\gamma)^{197}Pt$ activation cross section. The data represent the sum of the cross sections for the population of ground and isomeric state.

Fig. 5 Competition between neutron and gamma-ray emission from states of ^{197}Pt populated by the $^{198}Pt(n,2n\gamma)^{197}Pt$ reaction. The quantity $g_\gamma(E)$ represents the fraction of the population of states around E which by gamma-ray cascades contribute to the (n,2nγ) activation cross section.

Fig. 1

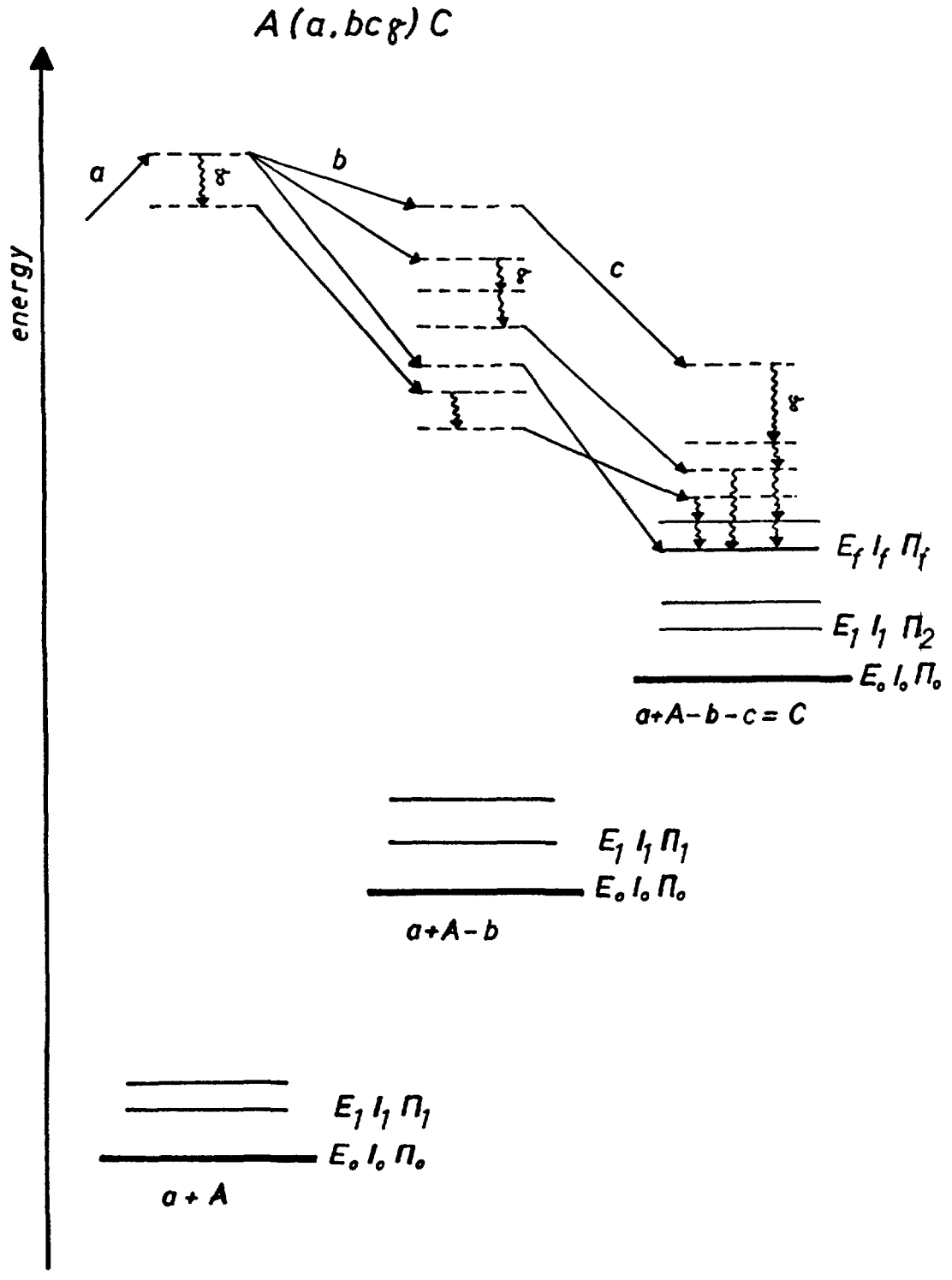
A (a, bcγ) C
energy
a
b
c
γ
$E_f\ I_f\ \Pi_f$
$E_1\ I_1\ \Pi_2$
$E_o\ I_o\ \Pi_o$
a+A-b-c = C
$E_1\ I_1\ \Pi_1$
$E_o\ I_o\ \Pi_o$
a+A-b
$E_1\ I_1\ \Pi_1$
$E_o\ I_o\ \Pi_o$
a + A

Fig. 2

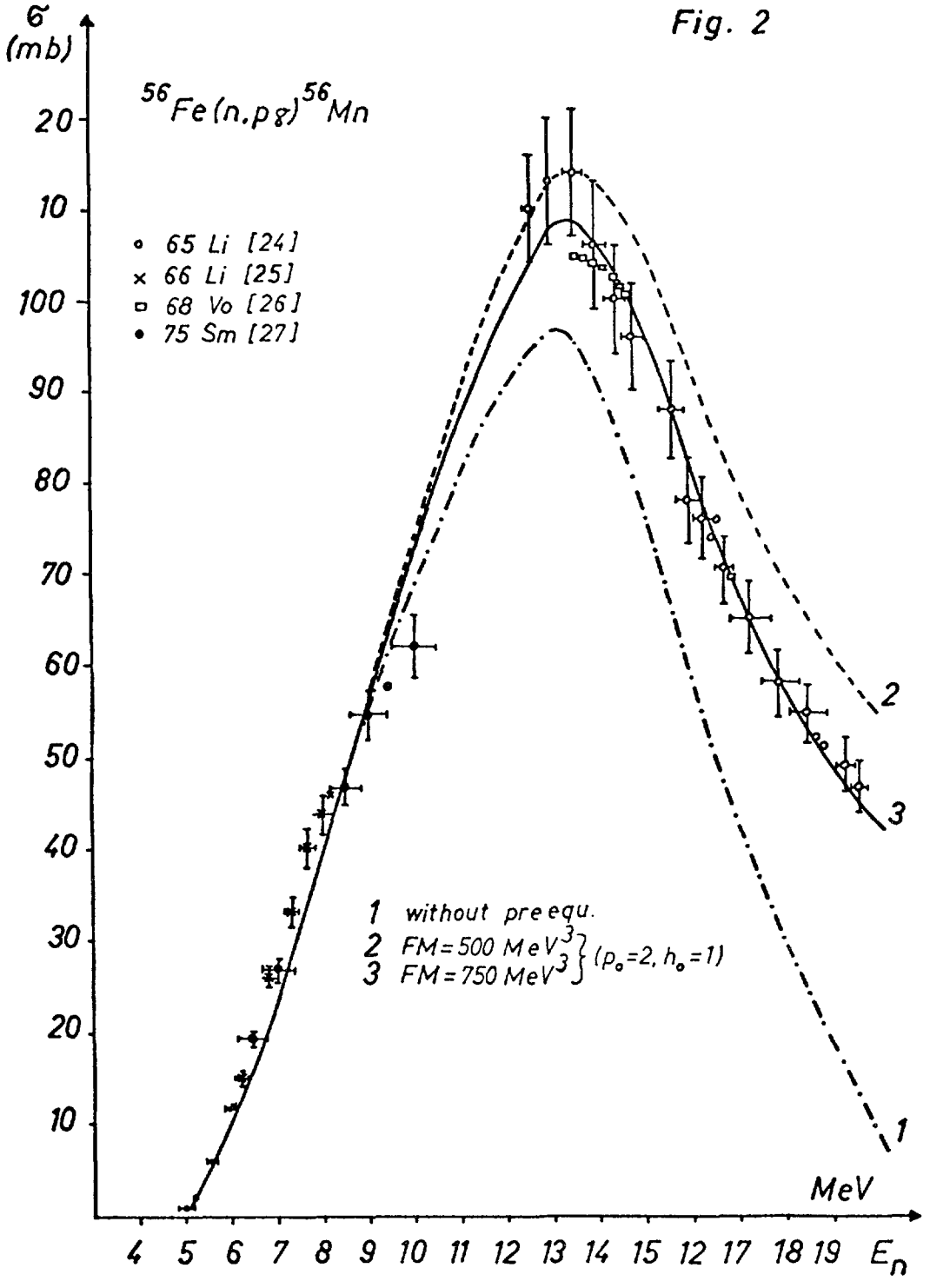
σ (mb)
$^{56}Fe(n,pg)^{56}Mn$
65 Li [24]
66 Li [25]
68 Vo [26]
75 Sm [27]
1 without pre equ.
2 FM = 500 MeV^3
3 FM = 750 MeV^3
(p_o=2, h_o=1)
MeV
E_n

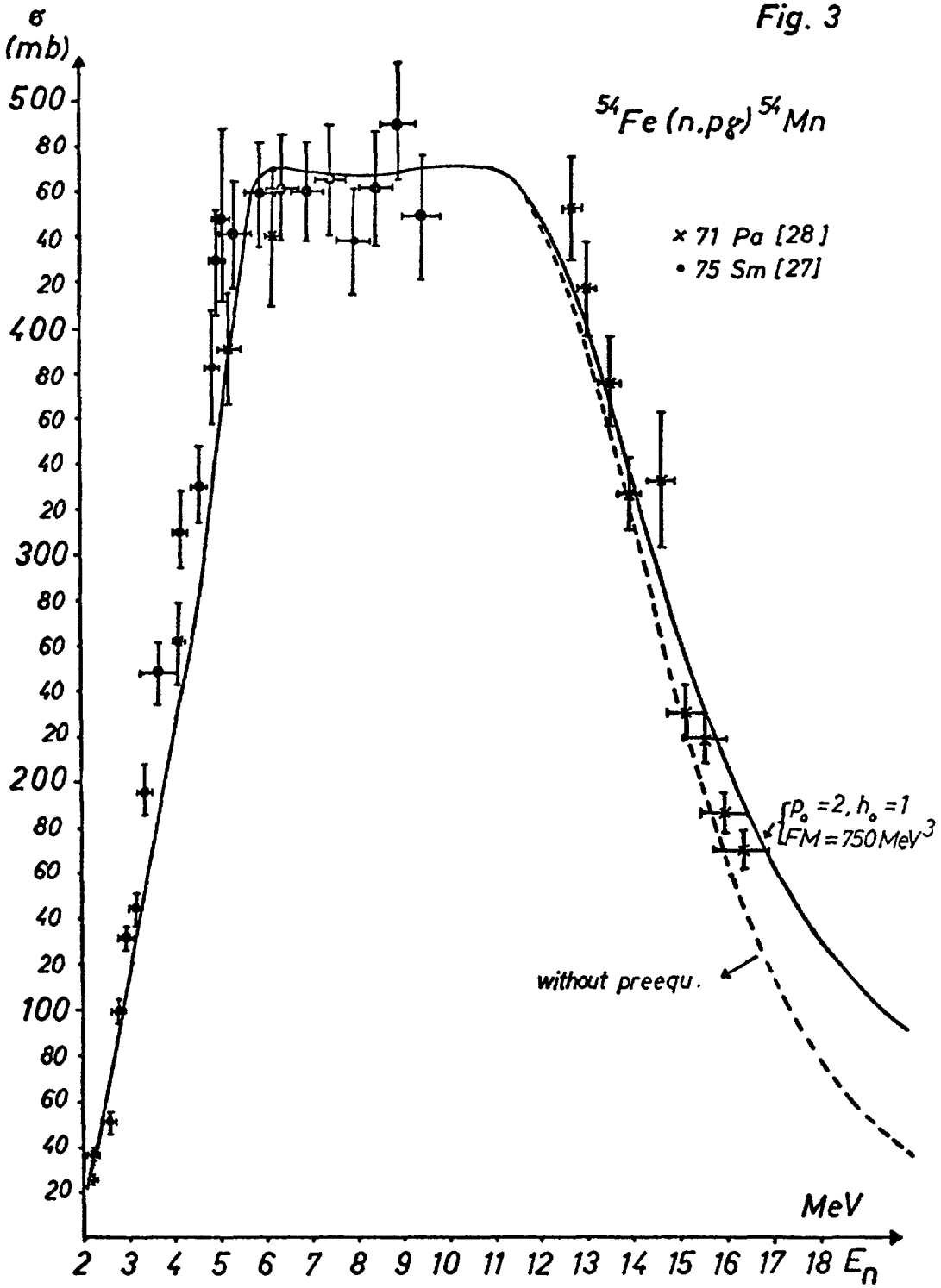
σ
(mb)
500
80
60
40
20
400
80
60
40
20
300
80
60
40
20
200
80
60
40
20
100
80
60
40
20
2 3 4 5 6 7 8 9 10 11 12 13 14 15 16 17 18 E_n
MeV
$^{54}Fe\,(n,p\gamma)\,^{54}Mn$
× 71 Pa [28]
• 75 Sm [27]
$p_o = 2, h_o = 1$
$FM = 750\,MeV^3$
without preequ.

Fig. 3

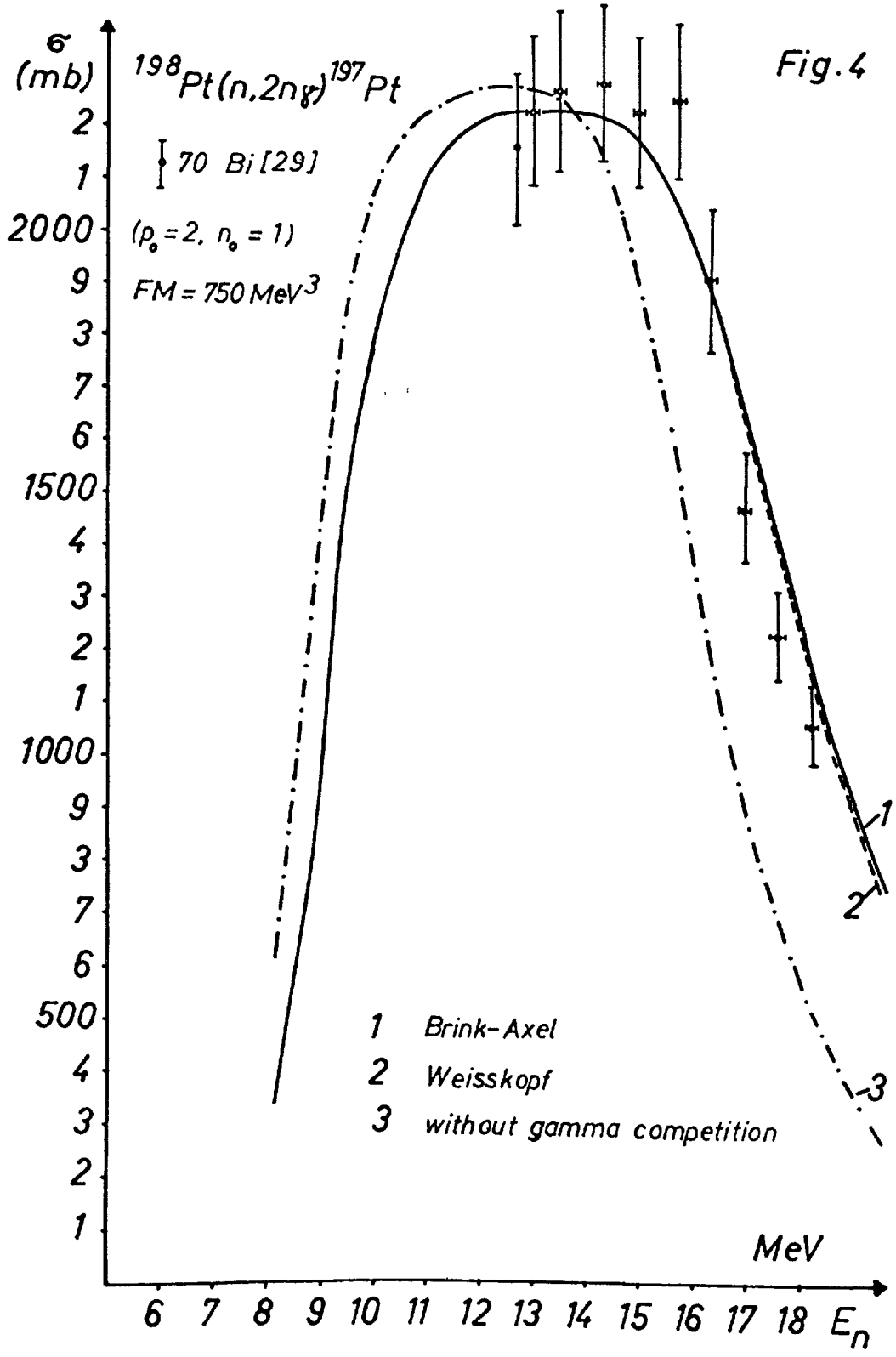
σ (mb)
198Pt(n,2nγ)197Pt
70 Bi [29]
(p0 = 2, n0 = 1)
FM = 750 MeV3
Fig.4
2000
1500
1000
500
1 Brink-Axel
2 Weisskopf
3 without gamma competition
MeV
6 7 8 9 10 11 12 13 14 15 16 17 18 En

$^{198}Pt(n,2n\gamma)^{197}Pt$
$E_n = 17{,}77\ MeV$

Fig. 5

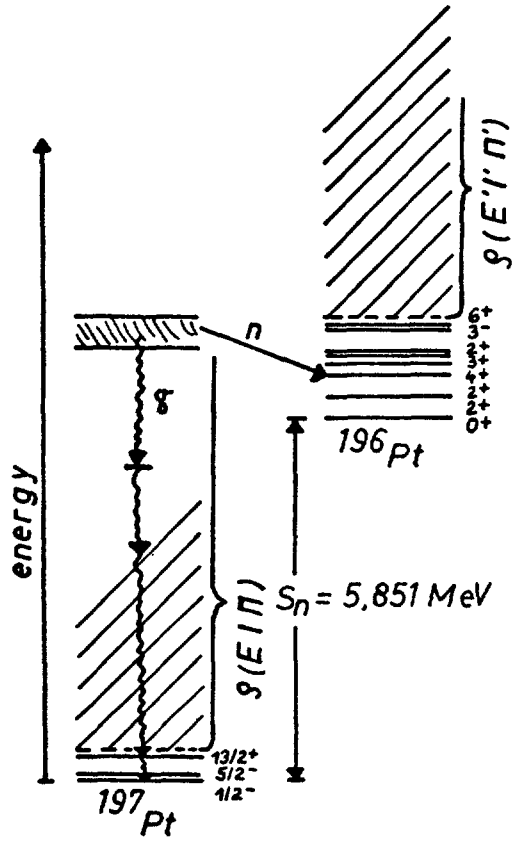

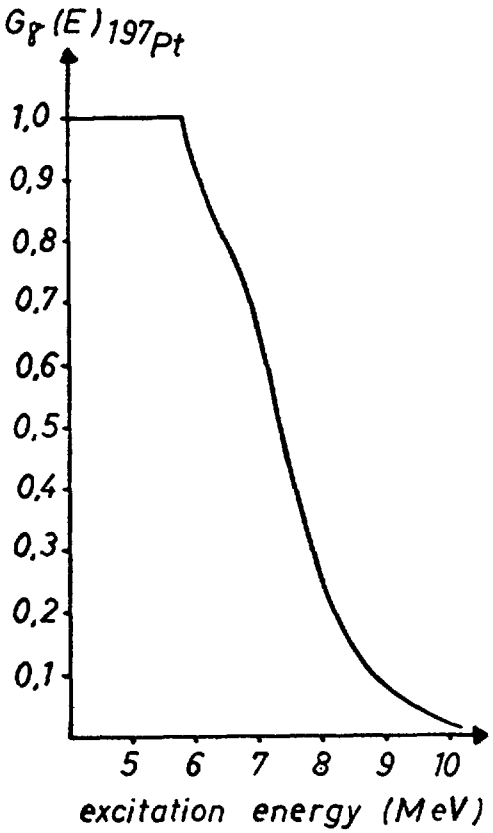

Contributed Paper No. 18

THE MODESTY-PL/1 PROGRAMME FOR THE CALCULATION OF NUCLEAR-REACTION CROSS-SECTIONS

W.MATTHES

(Euratom)

CCR - Ispra

Abstract

The Code MODESTY calculates all energetically possible reaction cross-sections and particle spectra within a nuclear decay chain initiated by a nuclear reaction.

The present version is based on the statistical nuclear model for nuclear reactions and employs the optical model for the calculation of the partial widths for particle decay and the Blatt-Weisskopf single particle model for the γ-decay. The programme is designed to simplify the evaluation of cross-section data by giving maximum output information for minimum input. All necessary nuclear data are automatically searched from an external (tape-or disc-) library of fundamental data. The programme makes extensive use of structures and external direct-access files to reduce core memory occupation which amounts to about 130K-BYTES.

Introduction

Available codes for the calculation of reaction cross-sections ask for a detailed specification of the decay chain and a tedious preparation of the input data. These are inconvenient features for the cross-section data evaluation work and for parameter studies. As a parameter change influences different reaction channels, many calculations have to be performed to balance the effect of parameter changes in cross-section fitting procedures.

To overcome this disadvantage the Code MODESTY was designed which:

a) calculates and plots all energetically possible reaction cross-sections and particle spectra within an evaporation cascade,

b) takes all nuclear data needed automatically from an external (tape-or disc-) library of fundamental data which is established once and can be used for all calculations,

c) needs a minimum of input data (e.g. type and energy of projectile, target and only a few more parameters) and, which

d) makes extensive use of structures and external direct access files to reduce the core memory occupation.

A) Description of Programme-Structure

The programme is designed to follow the population and depopulation of all nuclei within a nuclear decay chain initiated by a nuclear reaction as shown in Fig. 1. Due to this demand the main structure of the programme is already fixed and consists in the following three steps:

1) Establish a list of all nuclei appearing in the decay scheme (based on separation-energy considerations). Having this list, then

2) Populate the levels of the first compound nucleus in the list and

3) Start the decay of the first compound nucleus through particle emission (including γ -decay), populate the (second)residual nuclei and continue this process until all nuclei in the list are in their ground state (or an isomeric state).

Step 1 is obvious and consists simply in a sequence of decisions for the possibility of a particle emission from an excited nucleus. When going through the decay chain in this way we collect all the available information and put it into the list describing the cascade as shown in Fig. 2.
All nuclei in the cascade are numbered and positioned in the cascade-list according to this number.
Each nucleus is then provided with further additional information giving.

a) the "keyword" with which all fundamental nuclear data for this nucleus can be read from an external file,

b) the number of particles of different kinds (n,p,α...) by which the nucleus under investigation differs from the first compound nucleus,

c) the addresses of those nuclei in the list which can be reached by the corresponding particle emission (address-list).

Step 2 populates the first compound nucleus which is excited into the continum. This means we have to calculate the occupation density in the continum range for which we use the prescription

$$W^{(1)}(E) = \frac{\overline{\Pi}}{k^2} \frac{(2J+1)}{(2I+1)(2i+1)} \sum_{S=|I-i|}^{I+i} \sum_{L=|J-S|}^{J+S} f(L,\overline{\Pi})\, \overline{T}_L^{a}(\varepsilon)\, \delta(U - S_a - \varepsilon) \qquad (1)$$

$$f(L,\overline{\Pi}) = \frac{1}{2}\left|\overline{\Pi} + (-1)^L \overline{\Pi}_I \overline{\Pi}_a\right|$$

The formulas and symbols are taken from the paper by M. UHL(1) on which the physical part of MODESTY is mainly based.

Due to the concept of treating all nuclei and all types of particles in the cascade on the same footing,

Step 3 consists in 4 nested DO-Loops:

1) DO-Loop over all nuclei N in the Cascade-list,
2) DO-Loop over all levels $\mathcal{E}=\{U,J,\pi\}$ of each nucleus N (running from maximum excitation down to the ground state),
3) DO-Loop over all nuclei N' which can be reached by particle emission from N according to the address-list of N,
4) DO-Loop over all levels $\mathcal{E}'=\{U'J'\pi'\}$ of N'.

The physics of the procedure, as sketched in Fig. 3, is now contained in the expressions for the

a) occupation density at level $\mathcal{E}'$ of nucleus N':

$$W(N',\mathcal{E}')=\sum_{\mathcal{E}} W(N,\mathcal{E})*\frac{\Gamma'(N,\mathcal{E}\to N',\mathcal{E}')}{\Gamma'_t(N,\mathcal{E})}*\rho(N',\mathcal{E}')*DU(N,\mathcal{E}) \qquad (2)$$

b) total decay width from level $\mathcal{E}$ of nucleus N

$$\Gamma'_t(N,\mathcal{E})=\sum_{N',\mathcal{E}'}\Gamma'(N,\mathcal{E}\to N',\mathcal{E}')*\rho(N',\mathcal{E}')*DU(N',\mathcal{E}') \qquad (3)$$

where the summation over levels $\mathcal{E}$ ($\mathcal{E}'$) includes an energy-integration indicated by the integration-interval DU(N, $\mathcal{E}$) (DU(N', $\mathcal{E}'$)).

For each set $\{N, \varepsilon; N', \varepsilon'\}$ in the loops we have, therefore, simply to calculate the quantity

$$Q = \Gamma(N, \varepsilon \to N', \varepsilon') * \rho(N', \varepsilon'); \tag{4}$$

and

1) to add it to a single variable H which was initiated to "0" before Loop 3):

$$H = H + Q * DU(N', \varepsilon'); \tag{5}$$

2) to add it to an auxiliary array V(N', ε') which was initialized to "0" before Loop 4):

$$V(N', \varepsilon') = V(N', \varepsilon') + Q; \tag{6}$$

Closing Loop 3) we have the total decay width of level of nucleus N given in

$$\Gamma_t(N, \varepsilon) = H; \tag{7}$$

and, after normalizing V(N', ε') according to:

$$V(N', \varepsilon') = V(N', \varepsilon') * W(N, \varepsilon) * DU(N, \varepsilon) \Big/ \Gamma_t(N, \varepsilon) \tag{8}$$

we obtain the occupation density for all $\{N', \mathcal{E}'\}$ through:

$$W(N', \mathcal{E}') = W(N', \mathcal{E}') + V(N', \mathcal{E}') \qquad (9)$$

Finally we close loops 2) and 1).

Note that the spectra of all particles emitted from level $\mathcal{E}$ of nucleus N (in Loop 2) are now automatically given by summing the $V(N', \mathcal{E}')$ of (8) over all (J', π') of $\mathcal{E}' = \{\nu' J' \pi'\}$.

The whole procedure is sketched in Fig. 4.

To reduce main storage place we use keyed direct-access files for

a) the fundamental data of each nucleus,

b) the transmission coefficients for the different types of particles permitted as incoming and outgoing projectiles for each nucleus, and for

c) the occupation-density arrays $W(N, \mathcal{E})$ for each nucleus.

Each record on these individual files is a structure containing data of different types and is given a keyword. A whole structure can be read into the core memory from external disc or rewritten after updating on the external disc storage by simply calling the structure by the keyword (name). The core memory used by the present version of the programme is about 130K-BYTES.

The code is written in a straightforward way directly after the scheme of Fig. 4 to achieve optimal clearness and readability and is at the moment in the test-phase.

Figure Captions:

Fig. 1 - Example of a nuclear decay cascade initiated by a nuclear reaction. In this example only three particles are allowed as projectiles (n,p,α). Note that some nuclei in the cascade can be excited over more than one decay- path.
A nucleus in the cascade characterized by xyz is obtained from the first compound nucleus after the emission of x neutrons, y protons and z α's.
The cascade will be automatically extended as far as allowed by the kinetic energy of the incoming projectile.

Fig. 2 - Cascade-List

M: ranges from 1 to NC and numbers the nuclei in the cascade

NC: total number of nuclei appearing in the cascade

Keyword: Allows to read the record containing all fundamental data for the nucleus from disc into main storage

N(ν): number of particles of type ν to be removed from first compound nucleus to obtain nucleus M

AD(ν): Address of the residual nucleus in the cascade after emission of a particle of type ν from nucleus M.

Fig. 3 - The physical part of MODESTY is based on the simple expression for the total decay width and the relations between the occupation densities of the decaying nucleus and the residual nucleus as illustrated in this Figure.

$\Gamma(N,\varepsilon \to N',\varepsilon')$ is the partial decay width for the emission of a such particle as to excite nucleus N' to level ε' and is calculated from an optical model.

$\rho(N,\mathcal{E})$ is the level-density and DU($N,\mathcal{E}$) the integration-interval for the integration over the (excitation) energy.

Fig.4 -Flow diagramme of MODESTY.

$\vec{V}(N')$ indicates an auxiliary array of a length equal to the total number of levels $\mathcal{E}'=\{U'J'\pi'\}$ which can be excited: $\vec{V}(N')=\{V(N',\mathcal{E}')\}$

$\vec{W}(N') = \{W(N',\mathcal{E}')\}$ is an array of the same length as $\vec{V}(N')$ and contains the occupation density for all levels $\mathcal{E}'$ which can be excited.

Literature:

(1) M. UHL, Acta Physica Austriaca 31,245-270 (1970)

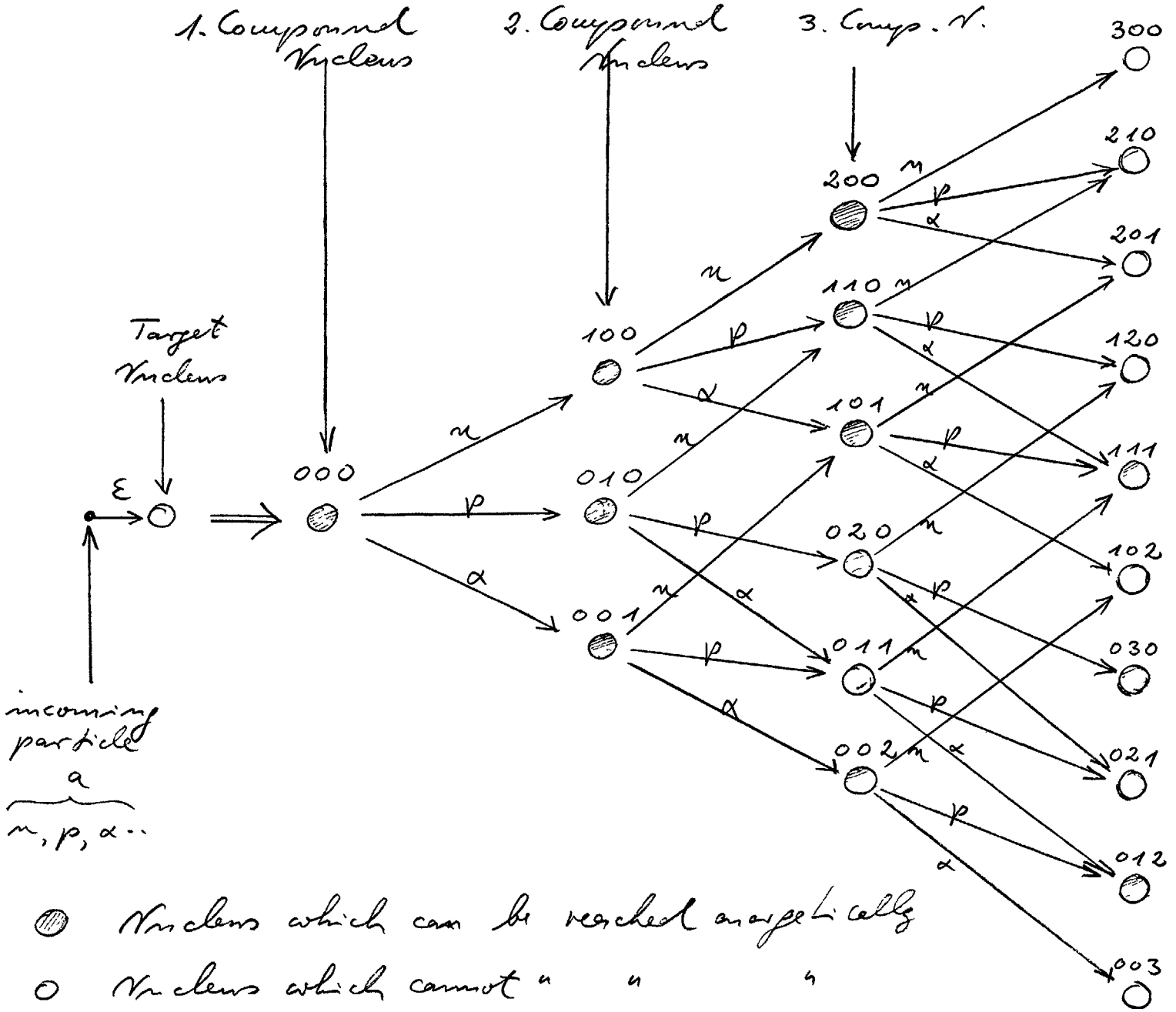

● Nucleus which can be reached energetically

○ Nucleus which cannot " " "

Fig. 1: NUCLEAR DECAY-CASCADE.

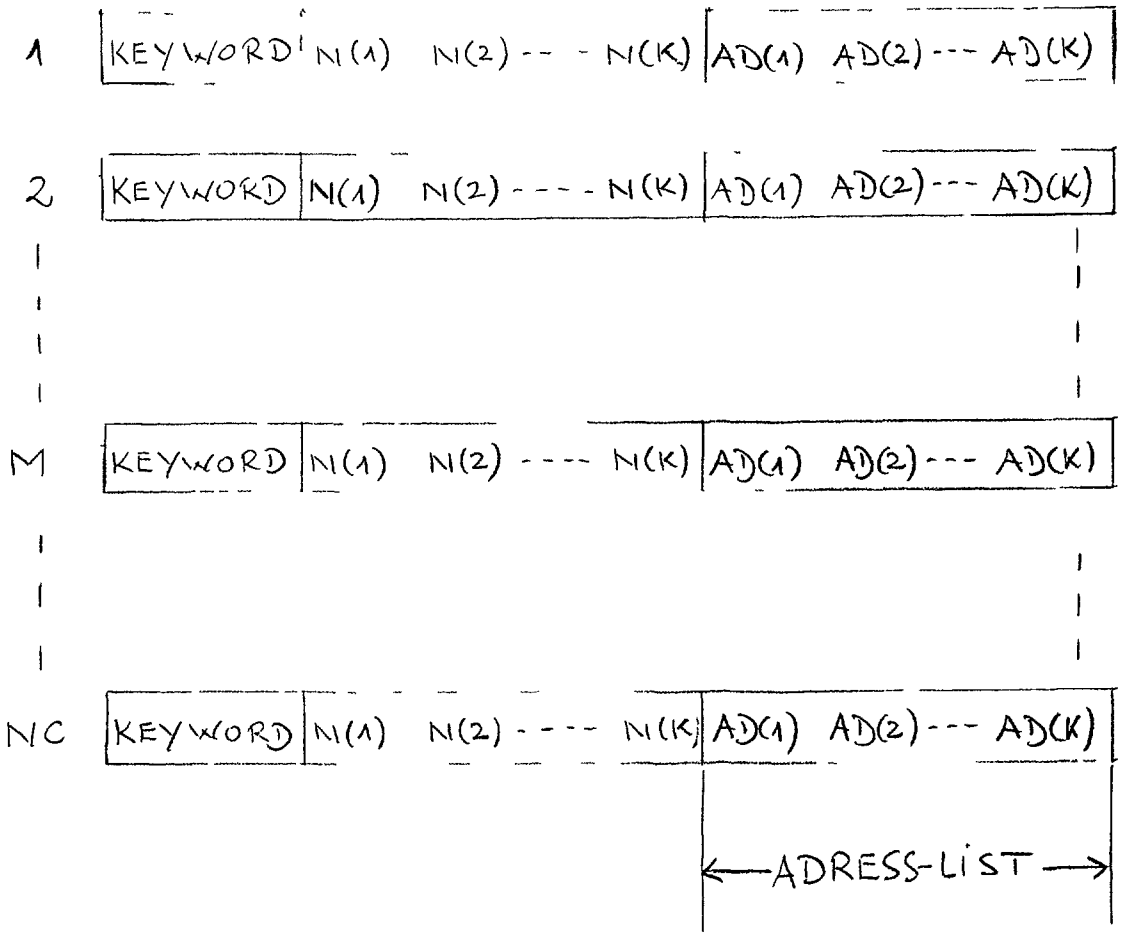

Fig. 2: CASCADE-LIST

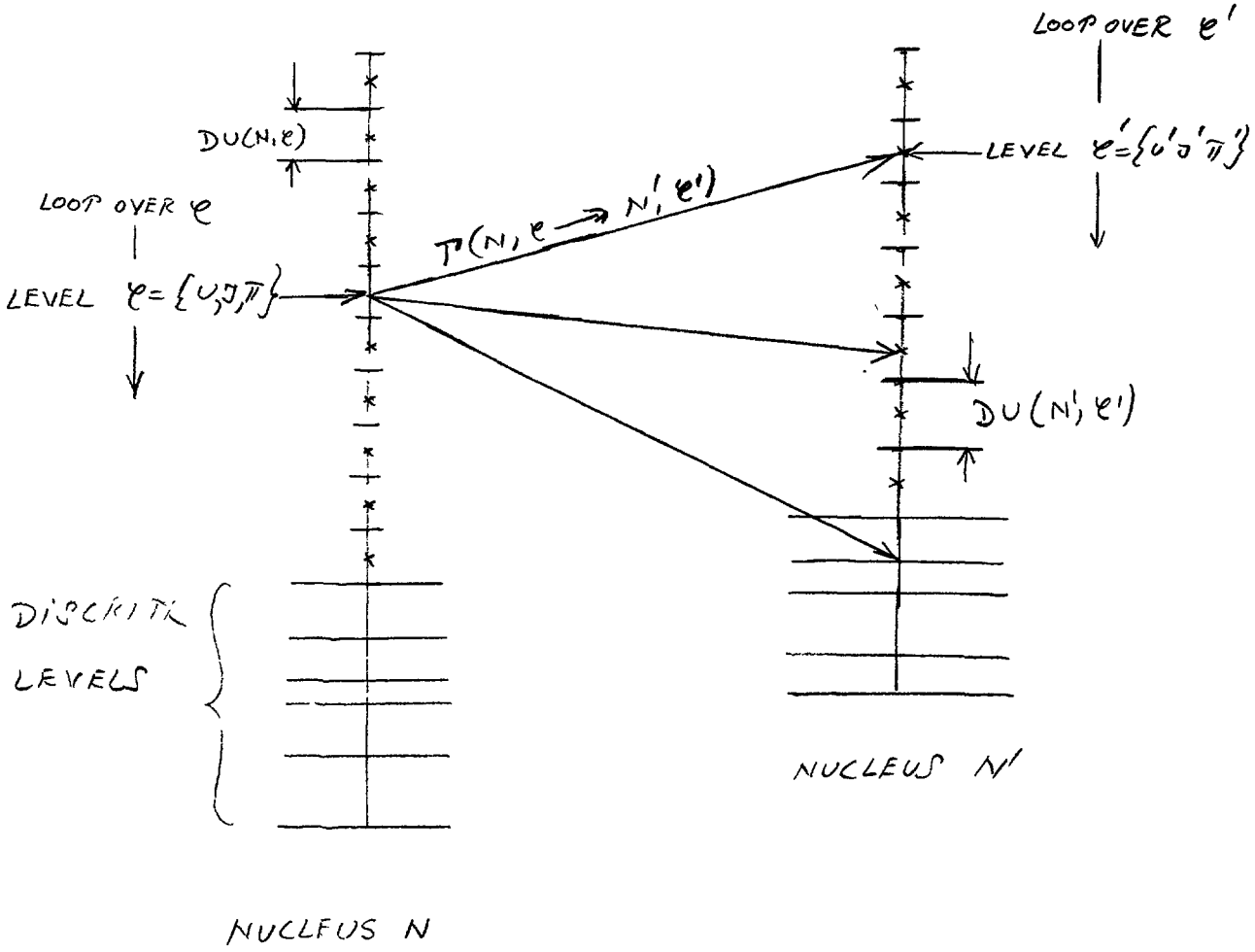

TOTAL DECAY-WIDTH OF LEVEL e OF NUCLEUS N:

$$\Gamma_t(N,e) = \sum_{N',e'} T(N,e \to N',e') * \rho(N',e') * DU(N',e')$$

OCCUPATION DENSITY OF LEVEL e' OF NUCLEUS N' THROUGH DECAY OF NUCLEUS N:

$$w(N',e') = \sum_{e} w(N,e) * \frac{T(N,e \to N',e')}{\Gamma_t(N,e)} * \rho(N',e') * DU(N,e)$$

Fig. 3: LEVEL-POPULATION EXCHANGE AS USED IN "MODESTY"

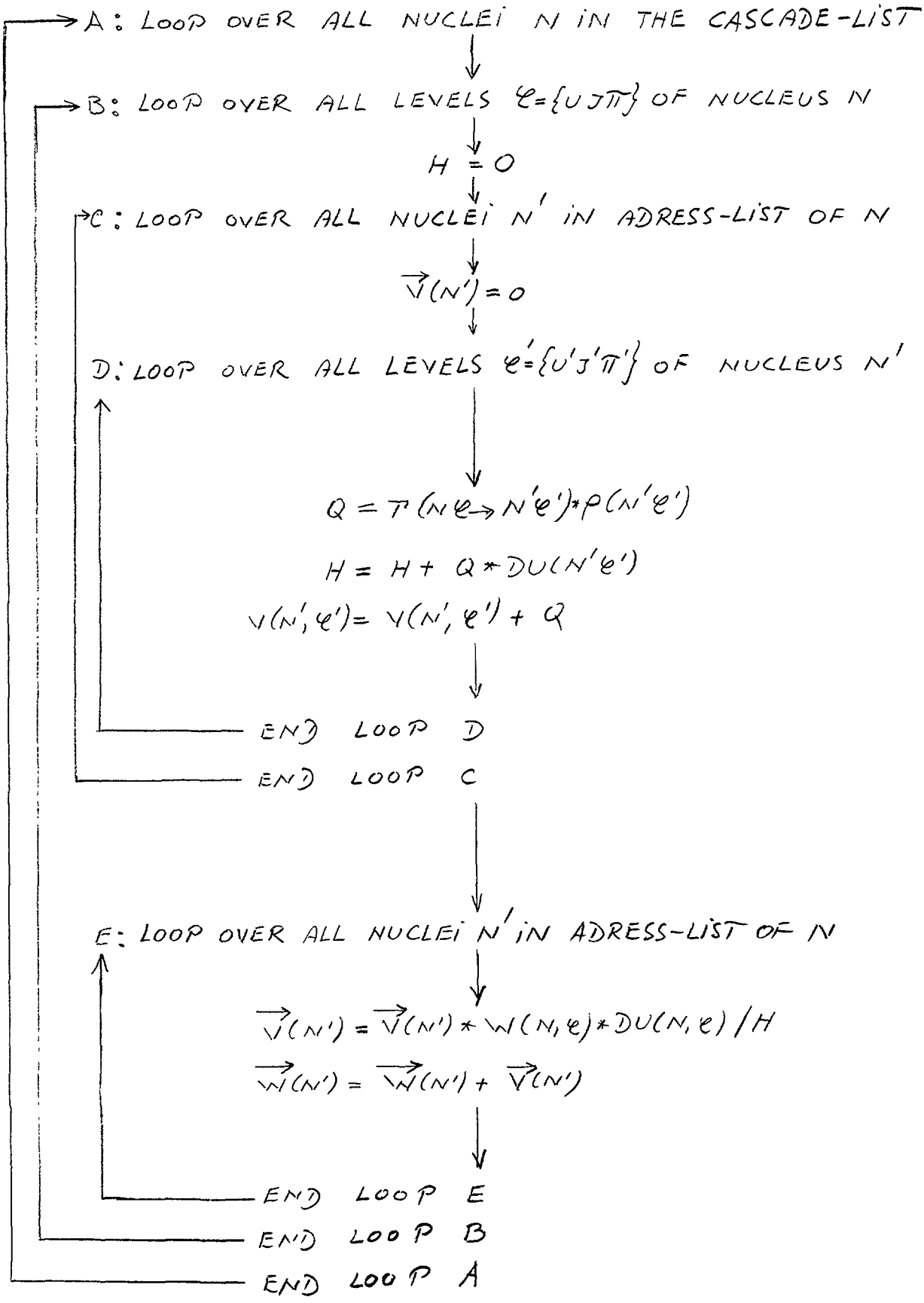

Fig. 4: FLOW-DIAGRAM OF "MODESTY"

Contributed Paper No. 19

A STATISTICAL APPROACH TO THE SCISSION MECHANISM

U. Facchini[+] and G. Sassi
Istituto di Fisica dell'Università, Milano
[+]and CISE, Segrate (Milano)

ABSTRACT

A statistical model of the scission mechanism is reported; the fission fragments are described as two spherical nuclei at given temperature and distance. The canonical formalism is introduced in order to describe the states of the system; the intrinsic freedom degrees, representing both the repartition of protons and neutrons in a given pair A_1, A_2 and the various possible configurations assumed by the excited nucleons are assumed in statistical equilibrium. The freedom degrees related to the collective motion of nucleons, which means to the fragment kinetic energies, are assumed not to be in statistical equilibrium. The partial-equilibrium model has been applied to the calculations of fragment excitation energies and to the analysis of the fragment charge distributions.

U^{235} fission induced by thermal neutrons and U^{233} fission induced by moderate energy protons have been analysed.

I. INTRODUCTION AND GENERALITIES

A number of properties of the fission process of heavy nuclei was clarified in the past years. The existence and the shape of the saddle in the potential energy of the deformed nucleus were proposed and discussed, at first by means of the liquid drop model[(1)] and lately by the introduction of the shells and the related effects[(2,3)].

The fission cross sections of actinide nuclei and other nuclei in the region of Au and Pb are now calculated with good accuracy[(4)]; in a recent work[(3)] it is shown that the asymmetric shapes are favoured by lower values of the energy saddle: this fact allows the typical asymmetries in the mass

spectrum for the low-energy fission of actinides to be understood.

The basic mechanism of fragment separation, however, is not understood yet and the properties of the nuclear system motion from the saddle point toward the scission point, have not been explained. Still lacking is an accurate description of the properties of the fission fragments such as the features of the excitation energy distributions, the values of fragment kinetic energy, the distribution of protons and neutrons in a given fragment pair.

The adiabatic model

Several different models were proposed in the past for the description of the scission process; we mention the adiabatic model first. It is based on the assumption that the separation motion of fragments is very slow and that friction processes are practically absent. During the motion the fragments have sufficient time for assuming a convenient shape, so as to keep the total potential energy of the nuclear system at minimum. The energy made available in the motion stores then into the fragments as deformation energy[5].

The total potential energy is given by

$$E_p = m_{S1}(\varepsilon_1) + m_{S2}(\varepsilon_2) + V(R, \varepsilon_1, \varepsilon_2) \qquad \text{(I. 1)}$$

where m_{S1} and m_{S2} are the masses (in MeV) of the fragments at scission point; the parameters ε_1 and ε_2 are the deformations; $V(R, \varepsilon_1, \varepsilon_2)$ is the Coulomb repulsive potential acting between the fragments. R is the distance between the fragment centres; it is given by

$$R_S = R_1 (\varepsilon_1) + R_2 (\varepsilon_2) + d \qquad \text{(I. 2)}$$

R_1 and R_2 are the radii of the deformed fragments and d is a suitable distance parameter which, in a simple way, stands for the presence of a neck connecting the two fragments up to scission point (see fig. 30 of ref.[21]). When the deformation increases, the Coulomb potential decreases, whereas the masses, after overpassing the ground state shapes, which are generally spherical or moderately deformed, increase rapidly. This causes the total potential E_p to have a minimum at a given deformation value.

It is generally supposed that scission takes place at this minimum point. Then, after the scission process, the fragments assume their final ground state shape and, owing to internal friction, the deformation energy is converted into internal excitation energy.

Accurate calculations of scission configurations and energies were reported by many authors[5,6]. It is generally shown by these authors that the calculated deformation energies do not reach the values of excitation energies, observed experimentally, which in a given region of the mass spectrum ($A \sim 115$) are particularly high.

It is noteworthy to recall that recent measurements of the number of neutrons emitted by excited fragments do not confirm the previous high figures, at least in the case of U^{235} fission induced by thermal neutrons. Consequently the whole question of high deformation energies has to be reconsidered and the fragment shape at scission and the energy stored as deformation is somehow a less critical matter. In any case, it

is necessary to assume that part of the fragment final excitation energy arises as a result of a viscous motion before the scission point is reached.

The strong viscosity model

In 1955 P. Fong[7] proposed a statistical model of the scission process, assuming that the fragment separation motion is slow and viscous, so that all the available energy is directly converted into internal excitation energy; Fong assumed than that the probability of a given scission configuration is proportional to the number of the fragment possible final excited states.

This model, like the adiabatic not viscous model, represents the extreme viewpoints. In both models scission is supposed to occur in the minimum of the potential energy ; in this region, in fact, the available energy is maximum so that the number of possible excited states of fragments is maximum as well. The total final excitation energies are obtained by adding the intrinsic excitation energies, due to the viscous motion, and the deformation energies stored into the scission shape.

The variance of the total excitation energy, the sum of $U_{1\infty}$ and $U_{2\infty} - U_{1\infty}$ and $U_{2\infty}$ being the excitation energies, respectively, at large distance of the fragments, which experimentally reaches values ranging from 7 to 12 MeV - is explained by the allowance of varying the scission point around the minimum region.

Very accurate calculations, based on this model, were made by A.V. Ignatyuk[8] and the results on energy values and charge distributions are quite reasonable; we remark that the mass spectrum, in particular the characteristic asymmetry observed in low energy fission of actinide nuclei and the

peculiar properties of fission fragment angular distributions are, at present, explained by different methods, because they are particularly related to the properties of the system at the energy saddle.

We note that two points contradict the model, at least in the formulation given by Fong and Ignatyuk. First, the discovery, due to experiments on ternary fission, that the fragments at scission point have outstanding kinetic energy: we recall that, by assuming a complete equilibrium among all freedom degrees, Fong needs that the fragments at the scission point have practically no motion and their kinetic energy is below one MeV. Second, we recall the recent interesting measurements due to C. Signarbieux et al.[9]. These authors observed that the excitation energies of the two fragments of a pair are completely uncorrelated statistically; actually, the covariance of $U_{1\infty}$ and $U_{2\infty}$ is found to be approximately zero.

This result is in contradiction with Fong's picture, where the two quantities are correlated by the fact that the sum $U_{1\infty} + U_{2\infty}$ is determined (as shown in fig. 30 of ref.[21]).

A partial equilibrium model

Starting from the consideration that, as a result of the ternary fission experiments, the fragments move at scission point with kinetic energy of the order of 10-20 MeV, one of the authors and E. Saetta-Menichella[10], in 1972, proposed a new version of the statistical model; they assumed that, owing to viscosity, the energy released in the motion from saddle point to scission point is partly converted into fragment

internal excitation energy and partly is converted into fragment kinetic energy; the internal freedom degrees are treated as in statistical equilibrium, whereas the fragment kinetic energy, which represents a collective motion of nucleons, is not in equilibrium.

When a fixed scission point and a given fragment configuration are considered, the statistical distribution of internal excitation energies and, in particular, the variance of the total excitation energy $U_{1\infty} + U_{2\infty}$ are then due to fluctuations in the partition of the total available energy between the internal excitation degrees and the collective kinetic energy. It has been shown, that, by assuming an equilibrium temperature of the order of 1 MeV, the calculated variance turns out to have the correct order of magnitude, which means 7 - 10 MeV. In the mentioned paper, hereafter referred to simply as (I), a few simplifying assumptions have been made. First, it has been assumed that the fragments at scission point have ground state shape; this assumption has been made in order to have a rapid overlook on the fragment masses. Second, it has been assumed that the fragment level densities are represented by the simple equispaced level model.

In the present analysis, the partial equilibrium model is reconsidered, but the simplifying hypotheses are dropped for more realistic ones, that is, the fragments at scission point are assumed to have particular shapes, as desired. Moreover, the level densities are treated with realistic formulae[11].

The description of the statistical system has been extended and includes all fragment configurations related to a given pair A_1, A_2, where A_1 and A_2, mass numbers of the two fragment respectively, are fixed, whereas the proton and neutron numbers can be exchanged between the fragments of the pair in any possible way.

It is then possible to predict the proton distribution of any given fragment pair.

In Sect. II, the basic properties of the model are discussed and the particular formalism, based on the introduction of the canonical partition function, is described.

In Sect. III, the basic nuclear models and parameters used in the calculations are reported.

In Sect. IV and V comparison is given between experimental and calculated results, both as to excitation energy properties and charge distributions.

The analyses are performed for U^{235} fission induced by thermal neutrons and for U^{233} fission induced by moderate energy protons.

SECTION II. BASIC FORMULAE

a) The fragments and their shapes at scission

We denote by A_1 and A_2 the mass numbers of the fragments, by Z_1 and Z_2 the proton numbers and by N_1 and N_2 the neutron numbers, respectively.

We have

$$\begin{aligned} N_1+Z_1 &= A_1 \\ N_1+Z_2 &= A_2 \end{aligned} \qquad \text{(II.1)}$$

and then

$$\begin{aligned} N_1+N_2 &= N_o \\ Z_1+Z_2 &= Z_o \\ A_1+A_2 &= A_o \end{aligned} \qquad \text{(II.2)}$$

where A_o is the mass number of the parent nucleus and N_o and Z_o its neutron and proton numbers, respectively.

We assume that at scission point - the point where the two fragments separate and any interaction, except the Coulomb repulsion, is supposed to cease - the fragments have a definite shape characterized by the deformation parameter ε_1 and ε_2.

Herein, symbols ε denote a set of deformation parameters as, for instance, those used in Nilsson's model[12].

The scission shape is assumed not necessarily equal to the final shape which the fragments assume after scission and which is generally assumed to be represented by the ground state shape of the nuclei, at least at the final stages of the process.

The deformation energy of the fragments at scission point are defined by the quantities

$$\begin{aligned} E_{D1} &= m_{S1} - m_{gs1} \\ E_{D2} &= m_{S2} - m_{gs2} \end{aligned} \qquad \text{(II.3)}$$

where m_{S1} and m_{S2} stand for the fragment mass energies (in MeV) at scission point and m_{gs1} and m_{gs2} are the relevant ground state energies. By substituing the masses by the corresponding binding energies B_s and B_{gt} we get:

$$\begin{aligned} E_{D1} &= B_{gt1} - B_{s1} \\ E_{D2} &= B_{gt2} - B_{s2} \end{aligned} \qquad \text{(II.4)}$$

As recalled in Sect. I, many authors generally assume that scission shapes are generally quite deformed and the scission point corresponds to the minimum potential energy. It is possible, in principle, to make calculations in the frame of the partial equilibrium model, by maintaining these assumptions; we try, however, to clarify a few points: first, by assuming that the separation motion is quite a sudden process, the fragments have no time to readjust their shapes, following the minimum potential lines; second, it seems that recent experimental results(°) do not confirm the particularly high fragment excitation energies, as remarked previously, and,

(°) see Sect. IV

consequently, a large deformation of fragments at scission point is not required.

We have performed most of the calculations here reported, by assuming the spherical shape as the fragment basic scission shape, that is, the most probable one. The assumption of spherical scission shape is generally made in ternary fission studies. We note that, really, the results of the present calculations do not depend strongly on the shape, whether it is spherical or with moderate deformation.

b) The scission radius

The scission radius R_S, as given by formula (1, 2) can be obtained by R_1 and R_2 values and by fixing the distance d. We get

$$R_1(\varepsilon_1) = r_o A^{1/3} (1 + f_1(\varepsilon_1))$$
$$R_2(\varepsilon_2) = r_o A^{1/3} (1 + f_2(\varepsilon_2)) \qquad (II.5)$$

In the case of spherical nuclei the deformation functions $f_1(\varepsilon_1)$ and $f_2(\varepsilon_2)$ are zero; in agreement with[16] r_o is

$$r_o = 1,2254 \text{ fermi}$$

The Coulomb potential acting between the fragments at scission point is given by

$$V(R_S) = \frac{e^2 Z_1 Z_2}{R_S} \; 1 + C(\varepsilon_1, \varepsilon_2) \qquad (II.6)$$

where e denotes the proton charge and $C(\varepsilon_1, \varepsilon_2)$ is the shape - depending correction term[13]. With spherical shapes of both fragments C is zero. Let us denote by T_S the kinetic energy of fragments at scission point and by T_∞ their kinetic energy at large distances.

With good approximation (disregarding the small Coulomb excitation between the moving fragments) we have

$$T_{\infty} = V(R_S) + T_S \qquad (II.7)$$

The average experimental values of T_{∞}, which give figures of 150-180 MeV, can be used for calculating a minimum value of R_S. In fact, by assuming $T_S = 0$, we obtain values of R_S of the order of 18 fermi and values of $d \simeq 6$-7 fermi. Taking into account that T_S has a value of 10-20 MeV, as pointed out by ternary fission experiments, we shall somewhat increase d. We assume

$$d = 8 \text{ fermi}$$

c) Energy balance

We assume that part of the final excitation energy of the fragment is built up in the saddle-scission motion, owing to viscosity, and part is due, after scission, to the readjustment of the fragment shape. We denote by U_{S1} and U_{S2} the scission excitation energies of fragments A_1 and A_2, respectively, and by U_1 and U_2 the long distance final excitation energies. We have

$$\begin{aligned} U_{\infty 1} &= U_{S1} + E_{D1} \\ U_{\infty 2} &= U_{S2} + E_{D2} \end{aligned} \qquad (II.8)$$

Considering the total energy of the system we have the conservation relation at scission point

$$E_Q = m_{S1} + m_{S2} + V(R_S) + T_S + U_{S1} + U_{S2} \qquad (II.9$$

where $E_o = m_o + U_o$ is the total initial energy, m_o is the ground state mass of the fissile nucleus and U_o is its excitation energy. As usually, we denote by Q_S the energy released at scission point and by Q_∞ the final fission energy. We have

$$Q_S = V(R_S) + T_S + U_{S1} + U_{S2} \qquad (II.10)$$

$$Q_\infty = T_\infty + U_{\infty 1} + U_{\infty 2} \qquad (II.11)$$

where the Q's are given by

$$Q_S = m_o - (m_{S1} + m_{S2}) + U_o \qquad (II.12)$$

$$Q_\infty = m_o - (m_{gs1} + m_{gs2}) + U_o \qquad (II.13)$$

d) The statistical hypothesis

Let us pay attention to all possible configurations which the fragment pair A_1, A_2 can assume at scission point, by different partition of protons and neutrons and for different excited states of the nuclei, where the top nucleons are differently located in external shell orbits. The all possible excited states correspond to different values of excitation energies U_{S1} and U_{S2} and of kinetic energy T_S.

For each given fragment pair we show then the values Z_1 and Z_2. The limiting conditions for excitation energies are as follows

$$0 \leqslant U_{S1} + U_{S2} \leq Q_S - V(R_S) \qquad (II.14)$$

and for kinetic energy are

$$0 \leqslant T_S \leqslant Q_S - V(R_S) \qquad (II.15)$$

All possible configurations of the pair A_1, A_2 are included in the given description. We assume then[10] that the intrinsic degrees representing the described configurations are in statistical equilibrium; the degrees related to the collective motion of nucleons and given by the kinetic energy T_S are not considered in equilibrium.

Saying that all possible configurations of the two fragments are statistically distributed means, as known from statistical mechanics, that, when account is taken of a large number of equivalent independent systems where all the possible states turn out to be in a given distribution $n_1, n_2, n_3, \ldots\ldots n_k$ (n_y is the number of system in a given state y), we assume that any possible set of values (n_y) is equiprobable to any other. We remark then, that the scission states correspond to fixed number of particles N_o and Z_o, but that their inner energy $E_y = E_o - T_S$, that is the energy corresponding to the freedom degrees statistically distributed, is not constant; in fact, it fluctuates around a given value $E_o - \overline{T}_S$ where $\overline{T}_S$ is the average value of T_S for a given pair A_1, A_2. The statistical ensemble of states is, therefore, a canonical one.

Under such hypothesis the quoted authors have shown that the probability of finding the system in a given state y is defined by

$$p(y) = Z_f^{-1} \cdot e^{-\beta E(y)} \qquad \text{(II.16)}$$

where

$$Z_f = \sum_{A_1, A_2 = \text{constant}} e^{-\beta E(y)} \qquad \text{(II.17)}$$

the sum being extended over all states of the system, with variations of both inner energies U_{S1}, U_{S2} and proton and neutron numbers. Z_f is the canonical partition function, $\beta = t_o^{-1}$ is a constant and t_o is the thermodynamic temperature. We shall see in Sect. IV that β is of the order of 1 MeV^{-1}.

From (II.9) we have then

$$E_y = m_{S1} + m_{S2} + V(R_S) + U_{S1} + U_{S2} \qquad (II.18)$$

e) Basic formulae

From formulae (II.16) (II.18) we have

$$p(y) = Z_f^{-1} \; e^{-\beta E_1} \; e^{-\beta E_2} \; e^{-\beta V(R_S)} \qquad (II.19)$$

where

$$\begin{aligned} E_1 &= m_{S1} + U_{S1} \\ E_2 &= m_{S2} + U_{S2} \end{aligned} \qquad (II.20)$$

The total probability of finding a pair A_1Z_1, A_2Z_2 is given by

$$p_{A_1A_2}(Z_1Z_2) = Z_f^{-1} \sum e^{-\beta E_1} \sum e^{-\beta E_2} \; e^{-\beta V(R_S)} \qquad (II.21)$$

where the sums are extended over the possible inner states of the fragments A_1Z_1 and A_2Z_2.

We denote these sums by Z_{f_1} and Z_{f_2}, respectively. These sums represent, in fact, the canonical functions of the two fragments

$$Z_{f1} = \sum e^{-\beta E_1} \quad ; \quad Z_{f2} = \sum e^{-\beta E_2} \qquad (II.22)$$

The knowledge of the fragment canonical functions is very important for both calculations of the total probabilities, given by formula (II.21), and energy distributions. In fact, the average values of E_1 and E_2 are directly related to the canonical functions.

Denoting the average values by $\overline{E_1}$ and $\overline{E_2}$, we have

$$\overline{E_1} = - \frac{d\omega_1}{d\beta}$$
$$\overline{E_2} = - \frac{d\omega_2}{d\beta} \qquad \text{(II.23)}$$

where

$$\omega_1 = \ln Z_{f1}$$
$$\omega_2 = \ln Z_{f2} \qquad \text{(II.24)}$$

The average values of fragment inner excitation energies at scission point are then given by

$$\overline{E_1} = m_{S1} + \overline{U_{S1}}$$
$$\overline{E_2} = m_{S2} + \overline{U_{S2}} \qquad \text{(II.25)}$$

The variances of the energy distributions E_1 and E_2, that

is, the variances of the U_S's distributions are given by[14]

$$\sigma^2_{u_{S1}} = \frac{d^2\omega_1}{d\beta^2}$$

$$\sigma^2_{u_{S2}} = \frac{d^2\omega_2}{d\beta^2} \qquad \text{(II.26)}$$

In order to have realistic values of ω_1 and ω_2 we introduce the relations between entropy and partition function[15]. We have in fact

$$\omega_1 = S_1 - \beta\bar{E}_1$$

$$\omega_2 = S_2 - \beta\bar{E}_2 \qquad \text{(II.27)}$$

where S_1 and S_2 denote the entropies of fragments A_1Z_1 and A_2Z_2, respectively, at the temperature t_o.

Taking into account (II.21) and (II.27), we have for the total probability $p_{AA}(Z_1Z_2)$

$$\ln p_{A_1A_2}(Z_1Z_2) = -\beta m_{S1} - \beta\bar{U}_{S1} + S_1 - \beta m_{S2} - \beta\bar{U}_{S2} + S_2 - \beta V(R_S) + \text{const.} \qquad \text{(II.28)}$$

Substituting the masses by the binding energies we have

$$\ln p_{A_1A_2}(Z_1Z_2) = \beta B_{S1} + \beta B_{S2} - \beta V(R_S) - \bar{U}_{S1} - \bar{U}_{S2} + S_1 + S_2 + \text{const.} \qquad \text{(II.29)}$$

We note what follows: in principle we can build expressions of $\omega^{(11,15)}$ which are formally correct, but not sufficiently accurate in order to represent mass, excitation energy and entropy of a given nucleus. By separation of the masses and other terms, as given in the present formalism, we can describe the masses with the most accurate mass formulae, based on the liquid drop model, as well as shell model corrections, energy and entropy of the various fragments, by making use of the single particle model, and for better accuracy, of the single particle model plus the pairing interaction. This will be shown in the next sections.

We recall finally that the average excitation energy and kinetic energy are related by

$$\overline{U}_{\infty 1} + \overline{U}_{\infty 2} + \overline{T}_{\infty} = Q_{\infty} \qquad \text{(II.30)}$$

SECTION III

a) The binding energies at scission point

In order to calculate the B_S values we have used the recent results of Seeger and Howard[16]. These authors have calculated the nuclear masses with good accuracy on the basis of the liquid drop model with the addition of shell and pairing corrections. The B expression given by these authors is

$$B(\varepsilon) = B_{LD}(\varepsilon) + \delta U(\varepsilon) + P(\varepsilon) \qquad \text{(III.1)}$$

The exact expressions of the various terms are given in Seeger's papers[16]. We only recall briefly that $B_{LD}(\varepsilon)$ denotes the liquid-drop term and contains the usual volume and surface interactions, the Coulomb interaction of protons,

the symmetry term proportional to $(N-Z)^2$ and other minor corrective addenda. Following Strutinsky 's prescriptions, the shell correction δU accounts for unevenness of shell spacing in the nucleus. We have

$$\delta U = \delta U_N + \delta U_Z \qquad \text{(III.2)}$$

where $\delta U_N, \delta U_Z$ refer to the shell correction of neutrons and protons, respectively; these quantities are generally given as functions of N and Z, respectively, but they are expressed in $\hbar\omega_N$ and $\hbar\omega_Z$ unities, given herebelow, which are proportional to $A^{-1/3}$. δU_Z and δU_N are positive for closed shell nuclei and negative for middle shell nuclei[16].

The pairing correction $P(\varepsilon)$ is given by

$$P = P_N + P_Z \qquad \text{(III.3)}$$

where P_N and P_Z are the pairing terms for neutrons and protons, respectively; they are expressed as depending on N and Z, respectively, and given in the same energy unities as δU_N and δU_Z.

P's are positive quantities, but they are practically of no account for closed-shell nuclei, whereas they affect middle-shell nuclei at the most.

Finally, we find that P_N and P_Z are about 1 MeV larger, when N or Z are even, in comparison with the nearest corresponding odd N and Z values.

The energy factor unities multiplying the various shell and pairing corrections are

$$\hbar\omega_N = V_N/A^{1/3} \quad ; \quad \hbar\omega_Z = V_Z/A^{1/3} \qquad \text{(III.4)}$$

where

$$V_N = 35.37 \text{ MeV}; \quad V_Z = 31.08 \text{ MeV}$$

All these quantities depend on the shape of the nucleus.

We are indebted to dr. Seeger for sending us the table of values $\delta U_N, \delta U_Z$ and P_N, P_Z at the various deformations.

b) The level system

In the msss analysis made by Seeger et al.[16] the shell effects and the pairing interactions are discussed by considering a definite set of neutron and proton levels. These levels are in principle described in the basic picture given by S.G. Nilsson et al.[12], but with some different choice of parameters, in order to obtain a more standardized and simplified formalism. In fact, proton and neutron energy levels are obtained by considering the nuclear average potential as given by a harmonic oscillator well; the shape of the nucleus is then introduced by means of the quadrupole deformation ε and the octupole parameter ε_4.

The level system is then expressed for all nuclei as a given sequence of values, where the energy scale depends on the particular nucleus through the usual $\hbar\omega_N$ and $\hbar\omega_Z$ as energy scale factors.

The level sequence corresponds to fig. 3 and 4 of Seeger's paper[16]. These levels, which are introduced into Seeger's works for the mass calculations, are used in the present analysis for the calculation of entropy and average energy at the given temperature t_o. The same level set is then taken into account for the introduction of the pairing interaction.

c) The pairing interaction

For discussion of the pairing interaction we refer to the general paper by Moretto and Huizenga[11].

The pairing force, acting between the two nucleons of the pair, is given by strength G_N for neutrons and strength G_Z for protons.

Following the well known B.C.S. procedure we have the relation between the energy gap and the energy levels; in the neutron case, for instance, we have

$$\frac{2}{G_N} = \sum_{\epsilon_N} \frac{1}{\epsilon'_N} \tanh \frac{1}{2} \beta \epsilon'_N \qquad \text{(III.5)}$$

where

$$\epsilon'_N = \sqrt{(\epsilon_N - \alpha_N)^2 + \Delta_N^2}$$

ϵ_N being the single particle energy and α_N the chemical potential. A similar equation holds for protons.

As discussed in ref.[11], at a given critical temperature t_c the gap Δ reduces to zero.

The value of t_c is approximately given by

$$t_c \simeq 2\,\Delta_o/3.5 \qquad \text{(III.6)}$$

where Δ_o is the ground state gap value.

At temperatures higher than t_c the pairs dissolve and the nucleus behaves like an independent particle system. The main thermodynamic functions are then well represented by the independent particle model[11]; this is true for the partition function and for entropy; the energy U_S turns out to be given by the sum of the energy $U_{i.p.}$ related

to the independent particle excitation plus the condensation energy P; this means that the curve representing U_S versus t_o is the same as in the independent particle model, but it is shifted of the P positive value. The P introduced into the excitation energy calculations is the same as that introduced into the binding energies, as discussed in the previous paragraph.

By considering the average excitation energy $\overline{U_S}$ we have then

$$\overline{U_S} = \overline{U_{i.p.}} + P \qquad \text{(III.7)}$$

$\overline{U_{i.p.}}$ being the average excitation energy as predicted by the independent particle model.

d) Calculation of entropy and average excitation energy

The independent particle model analysis directly gives the basic formulae for the calculation of entropy and average energy of the system. We recall that the analysis can be simply based on the properties of the grand canonical partition function. We give briefly

$$Z_{gc} = \overline{\sum_{N',Z',E'}} \exp\left(\alpha_N N' + \alpha_Z Z' - \beta E'\right) \qquad \text{(III.8)}$$

where the sum is made over all possible excited states and all possible numbers of particles N', Z'. Taking into account that the particles considered are fermions, $\ln Z_{gc}$ is then expressed by the following formula[11]

$$\ln Z_{gc} = \Omega = \sum_{\epsilon_N} \ln\left(1+\exp(\alpha_N - \beta\epsilon_N)\right) + \sum_{\epsilon_Z} \ln\left(1+\exp(\alpha_Z - \beta\epsilon_Z)\right) \qquad \text{(III.9)}$$

And then, with obvious meaning of notations:

$$\Omega = \Omega_N + \Omega_Z$$

Both α_N, α_Z and β are in principle independent parameters which define the ensemble properties: however, when we fix the particle numbers, either neutrons N and protons Z, we have β as an independent parameter and α_N, α_Z as quantities related to N and to Z, and depending on β.
N and Z being fixed, we have then:

$$\frac{\partial \Omega}{\partial \alpha_N} = N = \sum_{\epsilon} \frac{1}{1+\exp(\beta \epsilon_N - \alpha_N)} = \sum f_N \qquad \text{(III.10)}$$

$$\frac{\partial \Omega}{\partial \alpha_Z} = Z = \sum_{\epsilon_Z} \frac{1}{1+\exp(\beta \epsilon_Z - \alpha_Z)} = \sum f_Z$$

f_N, f_Z are the occupation numbers of the given level, ϵ_N, ϵ_Z are the level energies; the levels are considered as twofold degenerate. α_N, α_Z are called the chemical potential of the nucleus, at the temperature t_o; the α values are quite close to the Fermi energy values, that is, the energy of the last filled level in the ground state nucleus.

Under such conditions the relation between ω and Ω is given by

$$\omega = \Omega - \alpha_N \cdot N - \alpha_Z \cdot Z \qquad \text{(III.11)}$$

By considering the average total energy given by (II.23) and

taking into account formula (II.11) we have, by denoting $\overline{E}_N$ the total average energy due to neutrons :

$$\overline{E}_N = - \frac{d\omega_N}{d\beta} = - \frac{d\Omega_N}{d\beta} + \frac{d\alpha_N}{d\beta} \cdot N$$

and then (III.12)

$$\overline{E}_N = - \frac{\partial \Omega_N}{\partial \beta}$$

We obtain, then, the total average energy given by

$$\overline{E}_N = \sum \epsilon_N \cdot f_N = \sum \frac{\epsilon_n}{1 + \exp(\beta \epsilon_N - \alpha_N)} \quad \text{(III.13)}$$

and the average excitation energy given by

$$\overline{U}_{S_{N(IP)}} = \overline{E}_N - E_{oN} \quad \text{(III.14)}$$

where E_{o_N} is the ground state energy given by the independent particle model

$$E_{oN} = \sum_{\epsilon_{F_N}} \epsilon_N \quad \text{(III.15)}$$

ϵ_{F_N} being the neutron Fermi energy.

We have analogous equations for protons; finally, we have

$$\overline{U}_{S_{IP}} = \overline{U}_{S_{N(IP)}} + \overline{U}_{S_{Z(IP)}} \quad \text{(III.16)}$$

The relation between entropy S and the other thermodynamic functions is :

$$S = \Omega - \alpha_N N - \alpha_Z Z + \beta \overline{E}_N + \beta \overline{E}_Z \quad \text{(III.17)}$$

Considering Ω_N expression (III.9) we have then

$$S_N = \sum_{\epsilon_N} \ell_n (1+\exp(\alpha_N - \beta\epsilon_N)) + \beta \sum_{\epsilon_N} \frac{\epsilon_N - \alpha_N/\beta}{1 + \exp(\beta\epsilon_N - \alpha_N)} \qquad \text{(III.18)}$$

Taking neutrons and protons into account, we finally obtain the complete expression S, defined by

$$S = S_N + S_Z \qquad \text{(III.19)}$$

where the proton terms are represented in the same way as the neutron terms.

e) The excitation energy variance.

Considering formulae (II.26) and (III.11) we have directly

$$\sigma^2_{U_{fl,N}} = \frac{d^2\omega_N}{d\beta^2} = \frac{\partial^2\Omega_N}{\partial\beta^2} - \frac{\partial^2\Omega_N}{\partial\beta\partial\alpha_N} \cdot \frac{d\alpha_N}{d\beta}$$

where

$$\frac{d\alpha_N}{d\beta} = -\frac{\partial^2\Omega}{\partial\beta\partial\alpha_N} \Big/ \frac{\partial^2\Omega}{\partial\alpha^2_N}$$

we have

$$\sigma^2_{U_{fl,N}} = \frac{\partial^2\Omega_N}{\partial\beta^2} - \left(\frac{\partial^2\Omega_N}{\partial\beta\partial\alpha_N}\right)^2 \Big/ \frac{\partial^2\Omega_N}{\partial\alpha^2_N} \qquad \text{(III.20)}$$

and

$$\sigma^2_{U_{fl,p}} = \sigma^2_{U_{fl,pN}} + \sigma^2_{U_{fl,pZ}} \qquad \text{(III.21)}$$

and by considering (III,7):

$$\sigma^2_{U_{fl,p}} = \sigma^2_{U_S}$$

The expressions of Ω_N second derivatives are easily obtained from formula (III.9). They are

$$\frac{\partial^2 \Omega_N}{\partial \beta^2} = \frac{1}{4} \sum_{\epsilon_N} \epsilon_N^2 \operatorname{sech}^2 \frac{1}{2} (\beta \epsilon_N - \alpha_N) \qquad \text{(III.22)}$$

$$\frac{\partial^2 \Omega_N}{\partial \beta \partial \alpha_N} = -\frac{1}{4} \sum_{\epsilon_N} \epsilon_N \operatorname{sech}^2 \frac{1}{2} (\beta \epsilon_N - \alpha_N) \qquad \text{(III.23)}$$

$$\frac{\partial^2 \Omega_N}{\partial \alpha_N^2} = \frac{1}{4} \sum_{\epsilon_N} \operatorname{sech}^2 \frac{1}{2} (\beta \epsilon_N - \alpha_N) \qquad \text{(III.24)}$$

Similar expressions are valid for the proton level system.

f) Plan of calculations

The quantities $\overline{U}_S$, S and $\sigma^2_{u_S}$ have been calculated for all nuclei when

$$75 \leqslant A \leqslant 175$$

and for Z values ranging from plus-minus 5 unities around the so called uniform charge distribution value Z_{UCD}; Z_{UCD} is the fragment charge in the case of a uniform distribution of protons and neutrons in the two fragments of the pair.
It is

$$Z_{UCD1} = A_1 \cdot Z_o/A_o \qquad \text{(III.25)}$$

The thermodynamic functions have been calculated for a set of β values ranging from 0.8 up to 1.2 MeV^{-1}; all these values correspond to t_o values higher than the critical temperature. The shape of nuclei have been considered spherical ($\epsilon = 0$).

SECTION IV. ENERGY DISTRIBUTIONS

a) The analysis

The probability $p_{A_1A_2}(Z_1Z_2)$ has been calculated for U^{235} fission induced by thermal neutrons and for U^{233} fission induced by protons of 9.5, 14 and 20 MeV, respectively. A_1 values have been varied from 75 to $A_o/2$. Z values have been centered around Z_{UCD} in the range of $\pm$ 5 charge unities. For each fragment we have calculated the quantities B_S, S, $\overline{U}_S$ and $\overline{U}_\infty$ and the quantities V_S, Q_S and Q_∞ and the kinetic energies $\overline{T}_S$ and $\overline{T}_\infty$ for each fragment pair.

For each fragment pair A_1, A_2 we have the probability of the various possible Z_1, Z_2 values. Let us call p(Z) the relevant probability of a given Z value for the whole group of fragment pairs with given A_1, A_2 values.

We have

$$p(Z) = p_{A_1A_2}(Z_1Z_2) \Big/ \sum_Z p_{A_1A_2}(Z_1Z_2) \qquad \text{(IV.1)}$$

From p(Z) distribution, we easily obtain the average values of the most interesting quantities for the whole group of fragments with given A_1, A_2.

We have then

$$\langle \overline{U}_{\infty 1} \rangle_Z = \sum_Z \overline{U}_{\infty 1} \cdot p(Z)$$

$$\langle \overline{U}_{\infty 2} \rangle_Z = \sum_Z \overline{U}_{\infty 2} \cdot p(Z) \qquad \text{(IV.2)}$$

$$\langle Q_{\infty Z} \rangle_Z = \sum_Z Q_\infty \cdot p(Z) \qquad \text{(IV.3)}$$

$$\langle \bar{T}_{\infty} \rangle_Z = \sum_Z T_{\infty} \cdot p(Z) \qquad \text{(IV.4)}$$

$$\langle E_{def_i} \rangle_Z = \sum_Z E_{def_i} \cdot p(Z) \qquad \text{(IV.5)}$$

and so on.

These quantities can be directly compared with experimental values. We have also calculated the values of $\sigma^2_{U_{S1}}$ and of $\sigma^2_{U_{S2}}$ for each fragment pair $A_1A_2Z_1Z_2$.

Assuming that the scission point and the scission shape are well definite, U_{S1} and U_{S2} variances are also representative of the variance of the final excitation energies $U_{\infty 1}$ and $U_{\infty 2}$ at infinity. Since the final excitation energies are then completely uncorrelated the variance of the total excitation energy turns out to be given by

$$\sigma^2_{U_{\infty}} = \sigma^2_{U_{\infty 1}} + \sigma^2_{U_{\infty 2}} \qquad \text{(IV.6)}$$

and, from formula (II.11) the variance of the kinetic energy at infinity turns out to be given by

$$\sigma^2_{T_{\infty}} = \sigma^2_{U_{\infty}} \qquad \text{(IV.7)}$$

Finally, when the whole group of fragments with different Z values and given A_1A_2 is taken into account, we obtain for the variance of final kinetic energy

$$(\sigma^2_{T_{\infty}})_Z = \sum_Z \sigma^2_{T_{\infty}} \cdot p(Z) + \sum_Z T^2_{\infty} \, p(Z) - \left[\sum_Z T_{\infty} \cdot p(Z)\right]^2 \qquad \text{(IV.8)}$$

The variance $(\sigma^2_{T_{\infty}})_Z$ can be directly compared with the experimental values of the kinetic energy variance; in fact,

the experimental values generally refer to the whole group of fragments with given $A_1 A_2$ values.

b) Energy distributions in U^{235} thermal neutron induced fission

The values of $\langle \bar{U}_{\infty 1} \rangle_z \langle \bar{U}_{\infty 2} \rangle_z$ calculated in the present analysis are given in fig. 1. They can be compared with $\langle \bar{U}_{\infty 1} \rangle_z$ and $\langle \bar{U}_{\infty 2} \rangle_z$ coming out of experimental data. We have in fact[17]

$$\langle \bar{U}_{\infty 1} \rangle_z = \bar{\nu}_1 \, (\bar{S}_{N_1} + \epsilon_{Neut.}) + \bar{E}_{\gamma_1} \qquad \text{(IV.9)}$$

where $\bar{\nu}$ is the average number of emitted neutrons, $\bar{S}_{N_1}$ is the neutron binding average energy in the cascade, $\epsilon_{Neut.}$ is the neutron average kinetic energy, $\bar{E}_\gamma$ is the average energy emitted as gamma rays.

In order to calculate $\bar{U}_{\infty 1}$ from experimental data we behave as follows: $\bar{\nu}$ values have been taken from the recent results of Boldeman et al.[18]; we recall that these values differ somewhat from previous experimental values as given by Apalin et al.[19]. Apalin's data show very large $\bar{\nu}$ values for A_1 values around 110-115 and for A_2 values around 150.

As discussed in Sect. I, we recall that these large values have caused quite a difficult problem in the interpretation of scission mechanism.

We show herebelow that in the mentioned A_1 and A_2 regions Apalin's values do not correctly reproduce the total fission energy.

The $\bar{S}_N$ values are obtained from Seeger's tables: in order to have averaged values, we have considered S_N energies corresponding to the first, the second, the third and the

fourth neutron emitted and then we have averaged the four quantities: $\overline{S_N}$. The obtained values have been then averaged over the p(Z) distribution

$$\left\langle \overline{S_N} \right\rangle_Z = \sum_Z \overline{S_N} \cdot p(Z) \qquad \text{(IV.10)}$$

The ϵ_{Neut} values are taken from the results of Milton and Fraser[20]. $\overline{E_\gamma}$ is taken following the statements of Nifenecker et al.[21]

$$\overline{E_\gamma} = a + b\,\bar{\nu} \quad \text{in MeV} \qquad \text{(IV.11)}$$

with $a = 1.75$, $b = 1.10$

In fig. 1 the values $\overline{U}_{\infty 1}$ and $\overline{U}_{\infty 2}$ obtained from experimental results are compared with the theoretical $\overline{U}_\infty$'s. The calculated $\overline{U}_\infty$ values, given in formula (II.8) are the sum of two terms, the inner excitation energy at scission point and the deformation energy. The first energy term depends on the temperature, which for U^{235} low energy fission has been chosen as

$$t_o^{-1} = \beta = 1.2 \ \text{MeV}^{-1}$$

The β value is chosen by fitting the $\overline{U}_\infty$ data; in fact, the fitting has not been accurately optimized; higher values of $t_o = \beta^{-1}$ have been used with worse results.

The average deformation energy (IV.5) is reported in fig.2; it depends on the choice of scission spherical shapes.

From comparison between experimental and calculated values of U_∞ we see a general good agreement, but rough discrepancies in the region where $A \sim 100$ up to $A \sim 130$. In the region where $A \sim 100$ and $A \sim 130$ the calculated values are higher than the

experimental ones, whereas, at A values around 120, the calculated values are lower than the others.

In the double-magic nucleus region, i.e. A = 132, where both neutrons (N=82) and protons (Z=50) are in closed shells, it is quite difficult to obtain lower energy values, as predicted by experiments. In fact, for these nuclei the deformation energy is zero and the pairing condensation energy is also practically zero; the only way to assure lower excitation energy is to reduce the temperature; such a choice, however, will reduce the calculated excitation energy all over the various fragments and has the consequence of increasing the disagreement in the other mass regions.

On the other hand, it is difficult to obtain higher calculated values in the A = 110-120 region; in fact, in these regions the deformation energy, i.e. the difference between the spherical shape and the ground state shape is already large; in order to increase the deformation energy one has to assume very deformed shapes, well over the acceptable ones. It can be assumed, in principle, that the statistical hypothesis is not verified, so that the fragments in A = 132 region have lower temperature and those in region A = 110-120 have higher temperature; otherwise the average neutron energy in the fragment with $A \lesssim 132$ does not show a decrease in the temperature: we recall that the nuclear temperature and the average neutron energy are related by a proportionality law[17]. If fission at higher energy is considered, we shall see in the next paragraph that the agreement between experimental and calculated final excitation energies is quite good over all the mass values.

It is then possible to suggest that the shell effects remarked in the low energy fission are not correctly represented by Seeger's level scheme, at least not completely.

At higher energy the shell effects disappear and the calculated data agree then better with the experimental ones.

We have compared the values of $\langle Q_{\infty} \rangle_Z$ obtained (see II.10) from experimental values of $U_{\infty 1} + U_{\infty 2}$ and $\bar{T}_{\infty}$ with the $\langle Q_{\infty} \rangle_Z$ values obtained from formula (II.13) and Seeger's mass values, by taking average values over Z (as in IV.3).

The experimental $\langle \bar{T}_{\infty} \rangle_Z$ values are taken from Ribrag[22]. In fig. 3 we report the calculated and experimental $\langle Q_{\infty} \rangle_Z$ values, which showa general good agreement; in the same figure also the values of $\langle \bar{T}_{\infty} \rangle_Z$ are reported, the observed disagreement, which is not remarkable, except in the symmetric fission region, is a consequence of the discrepancies in the $\langle U_{\infty} \rangle_Z$ curve, as previously discussed. In fig. 4, as above said, we give the $\langle Q_{\infty} \rangle_Z$ values obtained from experimental values of given in ref.[19].

Finally, comparison of the calculated values of the kinetic energy variance $(\sigma^2_{T_{\infty}})_Z$ with the experimental values given in ref.[23] is shown in fig. 5.

The experimental results show $(\sigma^2_{T_{\infty}})_Z$ values higher than the calculated ones. We have to consider that in the calculated values we do not account for the energy and mass finite resolution; it is also possible that the hypothesis of a fixed scission shape is too restrictive, so that a fluctuation of the scission shape and then of deformation energy might increase the total energy variance. It is

noteworthy to say that the basic $\sigma^2_{T_{00}}$ values are of the correct order and give support to the statistical model.

We recall that the predicted absence of correlation between the excitation energies of the two fragments of the pair, as shown by the basic experiments of Signarbieux et al.[9], is in principle contained in the statistical formulae, as from (II.21) (see ref.[10]).

c) Energy distribution in U^{233} fission induced by moderate energy protons

The same analysis, as described in U^{235} thermal neutron fission, has been performed for U^{233} fission induced by protons having energy of 9.5, 14 and 20 MeV, respectively. The experimental values of the average final excitation energies $\langle \bar{U}_{00} \rangle_E$ are calculated by formula (IV.9), considering the values given by Vandenbosch et al.[24].

The values of $\bar{E}_{Neut.}$ have been taken from the same authors and E has been assumed, in a first approximation, as given by Nifenecker's formula[20].

The values S_N have been deduced from Seeger's table[16] and averaged in the same way as previously shown.

The calculation of the theoretical $\langle \bar{U}_{00} \rangle_Z$ values has been made by formulae (III.14), (III.16) and (III.7).

The values of β have been chosen as follows: in correspondence with increasing proton energies, we have

$\beta = 1$ MeV^{-1} for 9.5 MeV protons
$\beta = 0.9$ MeV^{-1} for 14 MeV protons
$\beta = 0.8$ MeV^{-1} for 20 MeV protons

The calculated values of $\langle U_{\infty 1/2} \rangle$ and $\langle U_{\infty 2/2} \rangle$ are compared with the experimental ones in fig. 6. A general agreement is found and both experimental and theoretical values show a reduction in the shell effects such as the peak in U values in the middle shell region (A = 115) and the valley in the closed shell region (A = 132).

In fig. 7 the $\langle Q_{\infty 1/2} \rangle$ values obtained from experimental values of $\langle U_{\infty 1/2} \rangle$ and $\langle T_{\infty 1/2} \rangle$, the latter defined also in ref.[24], are compared with $\langle Q_{\infty 1/2} \rangle$ values obtained from Seeger's mass tables and averaged over Z.

In fig. 8 we show the values of the variance, both calculated by formulae (III.20), (III.21), (IV.8) and obtained from experimental results. These results are taken from the experiments of Schmitt et al.[25] and refer to proton energies of 8.5 MeV and 13 MeV, respectively.

The agreement between experimental and calculated values of $\langle Q_{\infty 1/2} \rangle$, $\langle T_{\infty 1/2} \rangle$ and $\left(\sigma^2_{T_{\infty 1/2}}\right)_Z$ is reasonably good, but not completely satisfactory in the symmetric fission region.

We recall that all the calculations contain two parameters only, the value of d, which is not critical, and the temperature t_o.

SECTION V. PROTON DISTRIBUTION IN U^{235} FISSION INDUCED BY THERMAL NEUTRONS

a) The analysis

The calculation of p(Z) has been performed by formulae (IV.1), (II.29). As previously said, the β value has been

assumed of the order $1.2^{-}MeV^{-1}$.

The obtained p(Z) values are reported in table I for the various A_1 and A_2 values.

Starting from these values we have calculated the average $\overline{Z}$ and the so called proton excess in the light fragment Δ_Z:

$$\overline{Z} = \sum_{Z} Z.p(Z) \quad (V.1) \; ; \qquad \Delta_Z = \overline{Z} - Z_{UCD} \qquad (V.2)$$

where Z_{UCD} is given by (III.25).

We have then calculated the variance

$$\sigma_Z^2 = \sum_{Z} (Z - \overline{Z})^2 \; p(Z) \qquad (V.3)$$

We recall that a comparison with experimental data should take into account that the charge distributions are generally assumed for the post-neutron fragments, the so-called fission product: the distributions given in table I are referred to the scission instant, before neutron emission.

We have the well-known relation between the primary fragments, hereafter denoted by A_p, and the secondary post neutron products, hereafter denoted by A_S

$$A_S = A_p + \overline{\nu} \qquad (V.4)$$

In order to compare the data we have to refer the calculated p(Z) to the final products through a convenient averaging procedure (see further on) or to refer the experimental data to the initial primary fragments through formula (V.4).

We make the following remarks: a number of experimental data have been analysed, following a method developed by Wahl et al.[26] first, by assuming a Gaussian shape for p(Z) experimental distributions.

Under such a hypothesis the values Z_p of the most probable charge and of the Gaussian width $\sigma^2_{Z(G)}$ have been deduced from experimental values of the distribution; on the basis of the Gaussian parameters, the proton excess has been calculated. In principle, if distributions are really Gaussian, the given parameters should coincide in average $\overline{Z}$ and variance σ^2_Z, as given by formulae (V.1) and (V.3); but since the experimental distributions[26], as well as those herein calculated, are not exactly Gaussian, we have preferred to use the most direct quantities given by formulae (V.1) and (V.3), which means the actual average $\overline{Z}$ value and variance σ^2_Z, and to compare these quantities, when possible, with the experimental results directly.

b) Comparison between the predicted charge distributions and the radiochemical results

The measurement of the fission product charge probabilities has been carried on by various authors (see refs.[26-28]); there are the extensive tables of values given by [26] and [28], and lately the accurate collection of data by Amiel et al.[27], which, however, is restricted to the most probable fission products.

In order to compare p(Z) experimental values with the calculated values, shown in table I, we have calculated the corresponding average value of the primary mass A_p for each fission product A_s, by using formula (V.4) and $\overline{\nu}$ values of Boldeman et al.[18]. We have, then, simply interpolated the two p(Z) distributions corresponding to the integer values of A just above and below the A_p value.

The results of this comparison are shown in fig. 9. We have an overall general agreement between the experimental values and the calculated ones.

Starting from the experimental distributions and the interpolated theoretical ones, in table II we give the values of $\overline{Z}$ and Δ_Z.

Because of the general agreement of p(Z) distributions, we obtain, in this way, a good agreement among all quantities. It must be pointed out, however, that the calculated values of σ_Z are slightly lower than the experimental ones; owing to this fact, we shall have larger discrepancies when fission products are at the wing of the distributions, where the probabilities are quite low. The discrepancies, of the order of a factor 5-10, can be seen when the low probability fission products, given in the collections of refs.[26][28], and p(Z) values obtained by interpolation of the data of table I are considered.

c) Pairing and shell effects

The pairing terms contained in the binding energies and in the average excitation energies, when use is made of formula (II.29), disappear completely; moreover, as the other terms are dependent on the pairing forces, the statistical model predicts absence of odd-even effects in the fission probabilities.

In the experimental data, we note, in fact, the practically absolute absence of even-odd effects and this is in agreement with the theoretical predictions[26]. It is, however, possible

that small effects of thys type may survive, as reported in ref.[27] by Amiel and Felkstein, probably as a consequence of the approximation of the whole analysis.

Δ_Z values corresponding to the various pairs of A are plotted in fig. 10 versus A_p values. It is interesting to note the uniformity of the curve and the absence of marked shell effects in the double magic nucleus region ($A_2 = 132$).

In fact, when formula (II.29) is considered, the shell corrections in the binding energies are reduced by the shell effects in the excitation energies, and entropy is a less sensitive shell depending function. This is the reason why the behaviour of $p(Z)$ is mainly dependent on the liquid drop terms and particularly on the symmetry term $(N-Z)^2$.

In experimental data, as shown in table II, we note the practical absence of particular shell effects.

We recall that, in one case, a strong effect has been given for $A_S = 132$ in ref.[29] and reported in Denschlag's tables. The latest results[27], however, do not confirm the anomalous value of Δ_Z.

In fig. 10b, comparison is made between Δ_Z values calculated for the fragments (that is referred to A_p) and Δ_Z values given by Armbruster et al.[30], obtained through the β chain analysis; in fig. 10c, comparison is made between Δ_Z values obtained by Glendenin et al.[31] through the X-ray method.

Both set of data fit the theoretical predictions correctly; we make two remarks: there are no experimental data in the

symmetric fission region and in the magic nuclei region; the data of the experimental works have been given with the Gaussian fit.

CONCLUSIONS AND ACKNOWLEDGMENTS

The described analysis shows that the statistical hypothesis can explain the energy and charge distributions in the fission fragment pairs with some accuracy. The fitting requires two free parameters only, namely the scission distance and the fragment temperature. The scission distance is not a critical parameter, the temperature has been varied and increased as the initial excitation energy of the parent nucleus increases.

The values of $\beta = t_o^{-1}$ range from 1.2 (for U^{235} thermal neutron fission) to 0.8 MeV^{-1} for 20 MeV U^{233} proton-induced fission. The fitting can, in principle, be improved through a more accurate choice of temperature, by assuming, perhaps, a more sophisticated scission shape, and through a more appropriate choice of the basic level system. Choosing the simple spherical shape and the levels as given in Seeger's recent tabulation, the excitation energies of fragments turn out to be reproduced well, and better as the temperature increases. The charge distributions are also well reproduced, but not very accurately at the extreme wings of the distribution.

The authors thank dr. P.A. Seeger for sending a number of necessary data, dr. R. Vandenbosch for sending detailed results, Mr. H. Nifenecker and Mr. C. Signarbieux for kind discussions. They finally thank dr. G. Degli Antoni and dr. G. Fait of the Milan University for preparing part of the computer programme.

REFERENCES

(1) BOHR N., WHEELER J.A., Phys. Rev. 56 (1939) 426.

(2) STRUTINSKY V.M., Nucl. Phys. 95A (1967) 420.

(3) MØLLER P., NILSSON S.G., Phys. Lett. 31B (1970) 283.

(4) BACK B.B., HANSEN O., BRITT H.C., GARRETT J.D., LEROUX B., Phys. and Chem. of Fission (1973) Rochester (IAEA, Vienna).

(5) DIETRICH K., DICKMANN F., Nucl. Phys. 129A (1969) 241.

(6) SCHULTHEIS H., SCHULTHEIS R., Nucl. Phys. 215A (1973) 329.

(7) FONG P., Phys. Rev. 89 (1953) 332; 102 (1956) 434.

(8) IGNATYUK A.V., Sov. J. Nucl. Phys. 9 (1969) 208.

(9) SIGNARBIEUX C., POITOU J., RIBRAG M., MATUSSEK J., Phys. Lett. 39B (1973) 503.

(10) FACCHINI U., SAETTA-MENICHELLA E., J. Phys. A7 (1974) 975.

(11) HUIZENGA J.R., MORETTO L.G., Ann. Rev. Nucl. Sci. 22 (1972) 427.

(12) NILSSON S.G., TSANG C.F., SOBICZEWSKY A., SZYMANSKI Z., WYCECH S., GUSTAFSSON C., LAMM L., MØLLER P., NILSSON B., Nucl. Phys. 131A (1969) I.

(13) GEILIKMAN B.T., Proc. Int. Conf. Peaceful Uses Atomic Energy, A-22, P/2474 (1958) Geneva.

(14) DAVIDSON N., "Statistical Mechanics", McGraw Hill (1962), New York.

(15) ERICSON T., Adv. Phys. 9 (1960) 425.

(16) SEEGER P.A., HOWARD W.M., Nucl. Phys. 238A (1975) 491.

(17) LANG D.W., Nucl. Phys. 53 (1964) 113.

(18) DEL MUSGROVE A.R., COOK J.L., TRIMBLE G.D., Panel on fission product nuclear data IAEA (1973) Bologna.

(19) APALIN V.F., GRITSIUK Yu.N., KUTIKOV I.E., LEBEDEV V.I., MIKAELIAN L.A., Nucl. Phys. 71 (1965) 553.

(20) MILTON J.C.D., FRASER J.S., Proc. Symp. Phys. and Chem. of Fission, IAEA (1965) Salzburg.

(21) NIFENECKER H., SIGNARBIEUX C., BABINET R., POITOU J., Phys. and Chem. of Fission, (1973) Rochester (IAEA, Vienna).

(22) RIBRAG M., Rapport CEA R3309 (1967).

(23) SCHMITT H.W., NEILER J.H., WALTER F.J., Phys. Rev. 141 (1966) 1146.

(24) BISHOP C.J., VANDENBOSCH R., ALEY R., SHAW R.W., HALPERN I., Nucl. Phys. 150A (1970) 129.

(25) BURNETT S.C., FERGUSON R.L., PLASIL F., PLEASONTON F., Phys. Rev. C 7 (1973) 2510.

(26) WAHL A.C., NORRIS A.E., ROUSE R.A., WILLIAMS J.C.: IAEA Conf. on Fission (1969) Vienna.

(27) AMIEL S., FELDSTEIN H., Phys. Rev. C 11 (1975) 845.

(28) DENSCHLAG J.O., Habilitationsschrift (1971) Mainz.

(29) GUNTHER H., SIEGERT G., FERGUSON R.L., EWALD H., KONECNY E., Nucl. Phys. 196A (1972) 401.

(30) SISTEMICH K., ARMBRUSTER P., EIDENS J., ROECKL E., Nucl. Phys. 139A (1969) 289.

(31) REISDORF W., UNIK J.P., GRIFFIN H.C., GLENDENIN L.E., Nucl. Phys. 177A (1971) 337.

Figure Captions

Fig. 1 - Average excitation energies at large distance U versus the fragment mass number A. Ordinate scale in MeV.
U^{235} fission induced by thermal neutrons.

○ experimental values

▲ calculated values

Fig. 2 - Deformation energy at scission point; ordinate scale in MeV. Abscissa: mass number of fission fragments.
U^{235} fission induced by thermal neutrons.

Fig. 3 - Values of fission energy Q_∞ and fragment average kinetic energy at large distance $\overline{T}_\infty$ plotted versus the light fragment mass number A_1; ordinate scale in MeV. Q_∞ and $\overline{T}_\infty$ values are averaged over Z distribution.
U^{235} fission induced by thermal neutrons.

△ calculated values

● experimental values
(with $\overline{\nu}$ values by Boldeman et al.[18]).

Fig. 4 - Values of fission energy Q_∞ averaged over Z distribution.

△ calculated values as in fig. 3

● experimental values with $\overline{\nu}$ values by Apalin et al.[19]. The disagreement is emphasized in the regions: A ≃ 85 and A ≃ 110.

Fig. 5 - Values of kinetic energy variance $\sqrt{(\sigma^2_{T_\infty})_Z}$ plotted versus the light fragment mass number A_1.
Ordinate scale in MeV.
U^{235} fission induced by thermal neutrons.
Points (open circles) show the calculated values; full line stands for experimental results by [23].

Fig. 6 - Average excitation energy at large distance $\overline{U}_\infty$ versus the fragment mass number A. Ordinate scale in MeV.
U^{233} fission induced by moderate energy protons.

a) 9.5 MeV proton energy
b) 14 MeV proton energy
c) 20 MeV proton energy

○ experimental values
▲ calculated values

Fig. 7 - Values of fission energy and fragment average kinetic energy at large distance $\overline{T}$ plotted versus the light fragment mass number A_1; ordinate scale in MeV. The values of Q_∞ and $\overline{T}_\infty$ are averaged over Z distribution.
U^{233} fission induced by moderate energy protons.

a) 9.5 MeV proton energy
b) 14 MeV proton energy
c) 20 MeV proton energy

○ calculated values
● experimental values

Fig. 8 - Values of kinetic energy variance $\sqrt{(\sigma^2_{T_\infty})}_Z$ plotted versus the light fragment mass number A_1.
Ordinate scale in MeV.
U^{233} fission induced by moderate energy protons.
Points (open circles) stand for the calculated values; full line shows the experimental values.

a) 9.5 MeV proton energy

b) 14 MeV proton energy

Fig. 9 - p(Z) distributions for various fragment pairs.
(a,b,..,o.) p(Z) are plotted versus Z in proton charge unities.
U^{235} fission induced by thermal neutrons.
A_{S1} or A_{S2} values are reported in the figure.
▲ experimental points (ref. (27))
○ calculated values

Fig.10 - Values of Δ_Z in proton charge unities plotted versus the light fragment mass number. Calculated values: open circles.
Fig. 10a shows Δ_Z experimental values as given by radiochemical measurements and collected in table II (black points).
Fig. 10b shows Δ_Z experimental values as given in ref. (30) (black points).
Fig. 10c shows the region corresponding to the experimental results of ref. (31).

TABLE I p(Z)

A_p						A_p					
	75	Z	28	p(Z)	.003736		8I	Z	30	p(Z)	.0002I0
			29		.489563				3I		.I09I86
			30		.488794				32		.796329
			3I		.0I7893				33		.094063
			32		.0000I3				34		.0002II
	76	Z	28	p(Z)	.000283		82	Z	30	p(Z)	.000005
			29		.I66954				3I		.0I33I5
			30		.72I0II				32		.590I67
			3I		.III408				33		.392II4
			32		.000344				34		.004399
	77	Z	28	p(Z)	.0000I0				35		.00000I
			29		.02944I		83	Z	3I	p(Z)	.000749
			30		.578I42				32		.I89I52
			3I		.387342				33		.762027
			32		.005063				34		.0480I9
			33		.00000I				35		.000053
	78	Z	29	p(Z)	.002422		84	Z	3I	p(Z)	.000024
			30		.236053				32		.030565
			3I		.720473				33		.700687
			32		.04I003				34		.267085
			33		.000048				35		.00I639
	79	Z	29	p(Z)	.000090		85	Z	32	p(Z)	.002628
			30		.049647				33		.30702I
			3I		.753260				34		.665699
			32		.I9599I				35		.024637
			33		.00I0II				36		.0000I5
	80	Z	29	p(Z)	.00000I		86	Z	32	p(Z)	.000I27
			30		.0050I2				33		.069435
			3I		.42760I				34		.7683I6
			32		.55426I				35		.I6I533
			33		.0I3II8				36		.000589
			34		.000006						

TABLE I

A_p	Z	p(Z)
87	32	.000004
	33	.009076
	34	.472647
	35	.50777I
	36	.0I0498
	37	.000004
88	33	.000649
	34	.I5I364
	35	.766790
	36	.08I032
	37	.000I65
89	33	.000028
	34	.028396
	35	.64585I
	36	.322362
	37	.003362
	38	.00000I
90	33	.00000I
	34	.00300I
	35	.297070
	36	.666992
	37	.032902
	38	.000034
9I	34	.000I83
	35	.077036
	36	.754347
	37	.I67620
	38	.0008I4
92	34	.000007
	35	.0II85Z
	36	.496I08
	37	.48I483
	38	.0I0545
	39	.000005
93	35	.00I0I8
	36	.I798I6
	37	.747426
	38	.07I588
	39	.000I52
94	35	.000052
	36	.038638
	37	.679527
	38	.279I92
	39	.002590
	40	.00000I
95	35	.000002
	36	.00477I
	37	.35403I
	38	.6I66I6
	39	.024559
	40	.000022
96	36	.000330
	37	.I03956
	38	.765760
	39	.I29464
	40	.000490
97	36	.0000I3
	37	.0I8I50
	38	.568337
	39	.406959
	40	.006539
	4I	.000002
98	37	.00I738
	38	.234383
	39	.7I5097
	40	.0487I0
	4I	.000072

TABLE I

A_p 99	Z	37	p(Z)	.000094
		38		.055449
		39		.730682
		40		.2I2449
		4I		.00I325
I00	Z	37	p(Z)	.000003
		38		.007522
		39		.433047
		40		.54490I
		4I		.0I45I9
		42		.000008
I0I	Z	38	p(Z)	.000554
		39		.I39803
		40		.770444
		4I		.088990
		42		.000209
I02	Z	38	p(Z)	.000025
		39		.026585
		40		.643776
		4I		.326297
		42		.0033I7
		43		.00000I
I03	Z	38	p(Z)	.00000I
		39		.002897
		40		.299253
		4I		.66800I
		42		.02982I
		43		.000026
I04	Z	39	p(Z)	.000I90
		40		.080464
		4I		.767649
		42		.I5II22
		43		.000576

A_p I05	Z	39	p(Z)	.000008
		40		.0I3554
		4I		.53I307
		42		.447608
		43		.007520
		44		.000002
I06	Z	40	p(Z)	.00I373
		4I		.2II922
		42		.733850
		43		.052778
		44		.000077
I07	Z	40	p(Z)	.00009I
		4I		.05349I
		42		.7294I4
		43		.2I5664
		44		.00I339
I08	Z	40	p(Z)	.000004
		4I		.008729
		42		.45I992
		43		.525848
		44		.0I3420
		45		.000007
I09	Z	4I	p(Z)	.000893
		42		.I70565
		43		.752824
		44		.075545
		45		.000I72
II0	Z	4I	p(Z)	.000062
		42		.042537
		43		.69I846
		44		.263I96
		45		.002359

TABLE I

A_p III	Z	41	p(Z)	.000003	A_p II7	Z	43	p(Z)	.000002
		42		.006922			44		.005170
		43		.405663			45		.348882
		44		.568106			46		.617071
		45		.019290			47		.028841
		46		.000016			48		.000035
II2	Z	42	p(Z)	.000720	II8	Z	44	p(Z)	.000522
		43		.149768			45		.122674
		44		.754913			46		.753609
		45		.094307			47		.122674
		46		.000292			48		.000522
II3	Z	42	p(Z)	.000051					
		43		.037075					
		44		.661965					
		45		.297520					
		46		.003388					
		47		.000001					
II4	Z	42	p(Z)	.000002					
		43		.005975					
		44		.374188					
		45		.595425					
		46		.024385					
		47		.000026					
II5	Z	43	p(Z)	.000620					
		44		.135256					
		45		.754363					
		46		.109350					
		47		.000412					
II6	Z	43	p(Z)	.000043					
		44		.032868					
		45		.638477					
		46		.324284					
		47		.004326					
		48		.000001					

TABLE II

A_S	$\bar{\nu}$	A_p	$\bar{Z}_{exp.}$	$\bar{Z}_{calc.}$	$\sigma_{Z\,exp.}$	$\sigma_{Z\,calc.}$
84	.80	84.80	33.60	33.6I	.60.	.53
85	.83	85.83	34.05	34.02	.55	.49
86	.87	86.87	34.33	34.46	.60	.54
87	.93	87.93	34.73	34.89	.7I	.49
88	I.02	89.02	35.28	35.32	.63	.52
89	I.I0	90.I0	35.73	35.76	.56	.52
90	I.I7	9I.I7	36.02	36.I6	.49	.52
9I	I.22	92.22	36.40	36.57	.6I	.55
92	I.28	93.28	36.83	36.94	.65	.52
93	I.34	94.34	37.35	37.38	.64	.55
94	I.37	95.37	37.75	37.79	.60	.5I
95.	I.40	96.40	38.03	38.I7	.47	.54
I3I	.5I	I3I.5I	50.7I	50.73	.67	.54
I32	.56	I32.56	5I.23	5I.I2	.67	.52
I33	.64	I33.64	5I.66	5I.54	.54	.55
I34	.82	I34.82	52.I0	5I.93	.43	.50
I35	.97	I35.97	52.5I	52.42	.60	.54
I36	I.07	I37.07	52.99	52.86	.69	.50
I37	I.II	I38.II	53.43	53.23	.66	.52
I38	I.I5	I39.I5	53.80	53.65	.55	.54
I39	I.20	I40.20	54.I3	54.04	.62	.5I
I40	I.25	I4I.25	54.45	54.44	.65	.55
I4I	I.28	I42.28	55.06	54.8I	.67	.53
I42	I.30	I43.30	55.37	55.22	.69	.54
I43	I.36	I44.36	55.69	55.64		
I44	I.42	I45.42	56.I5	56.05		

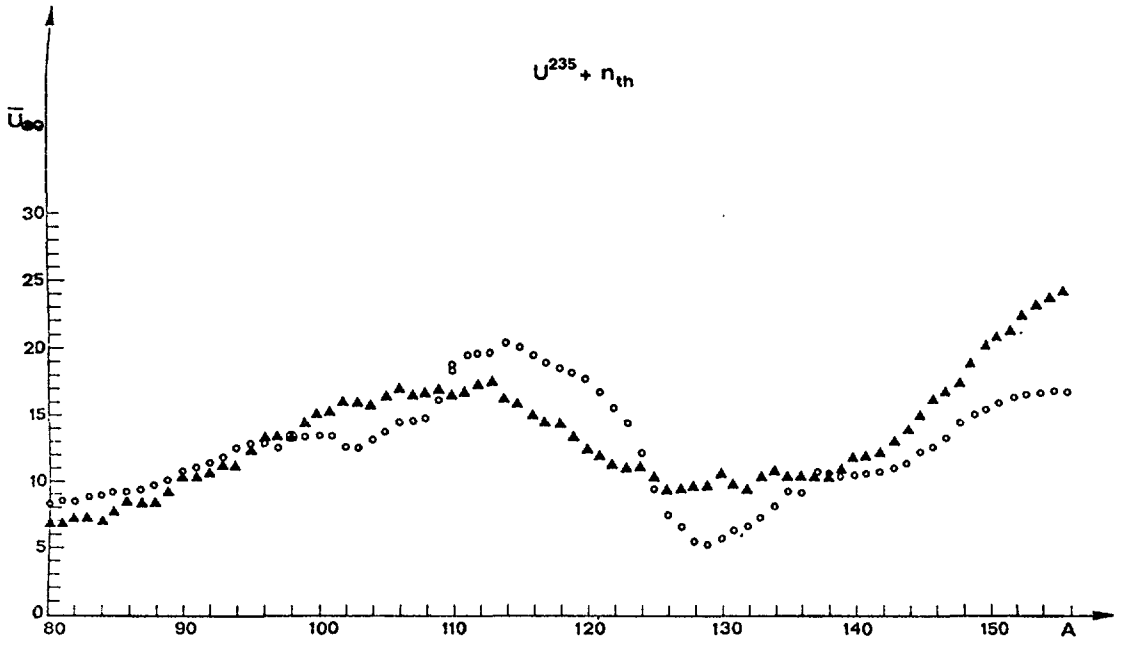
$U^{235} + n_{th}$
$\bar{U}_{sc}$
30
25
20
15
10
5
0
80
90
100
110
120
130
140
150
A

Fig. 1

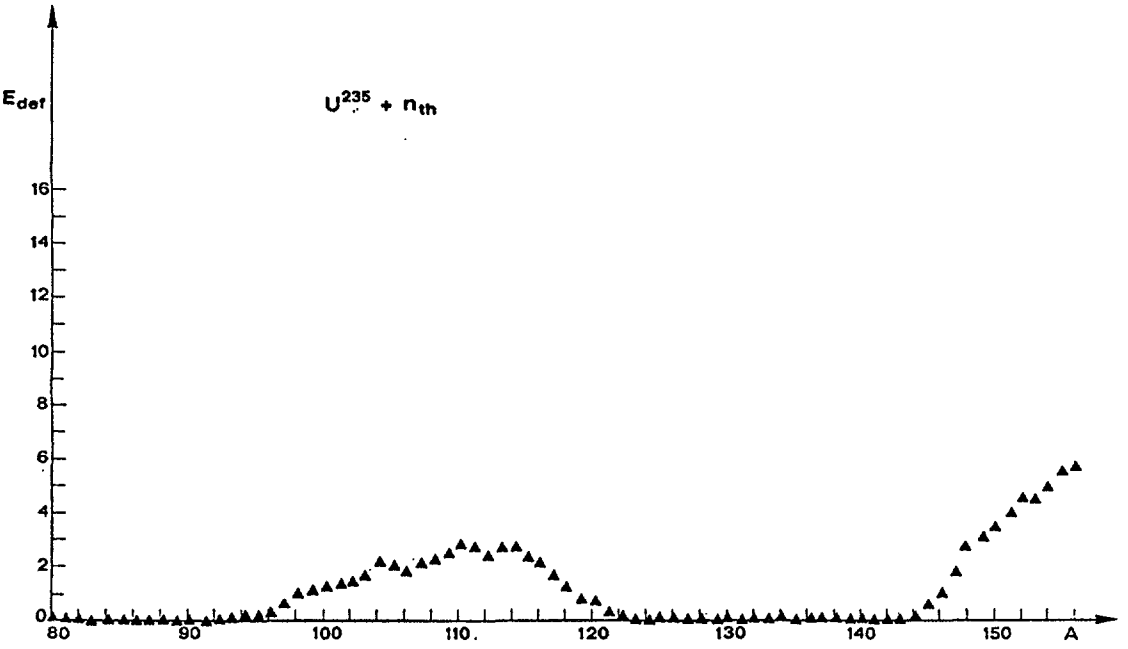
E_{def}
$U^{235} + n_{th}$
16
14
12
10
8
6
4
2
0
80
90
100
110
120
130
140
150
A

Fig. 2

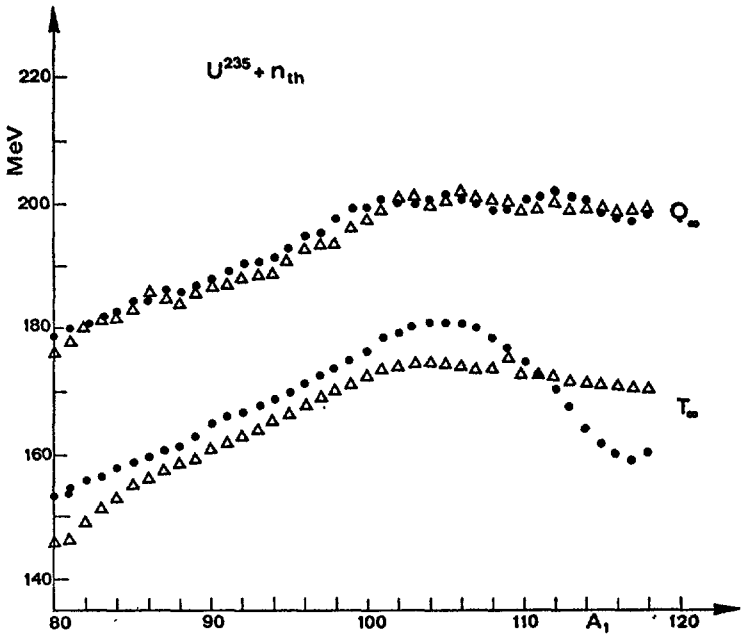
$U^{235} + n_{th}$
MeV
220
200
180
160
140
80
90
100
110
A_1
120
Q_∞
T_∞

Fig. 3

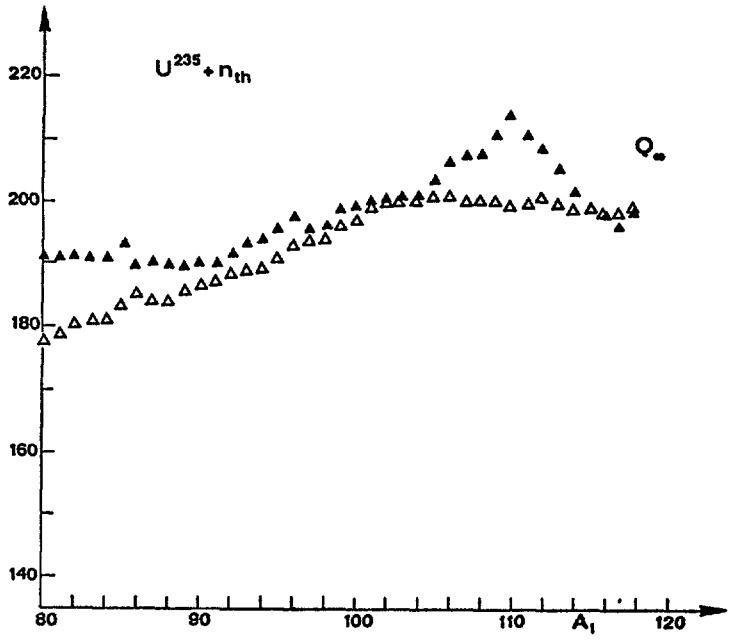
$U^{235} + n_{th}$
220
200
180
160
140
80
90
100
110
A_1
120
Q_∞

Fig. 4

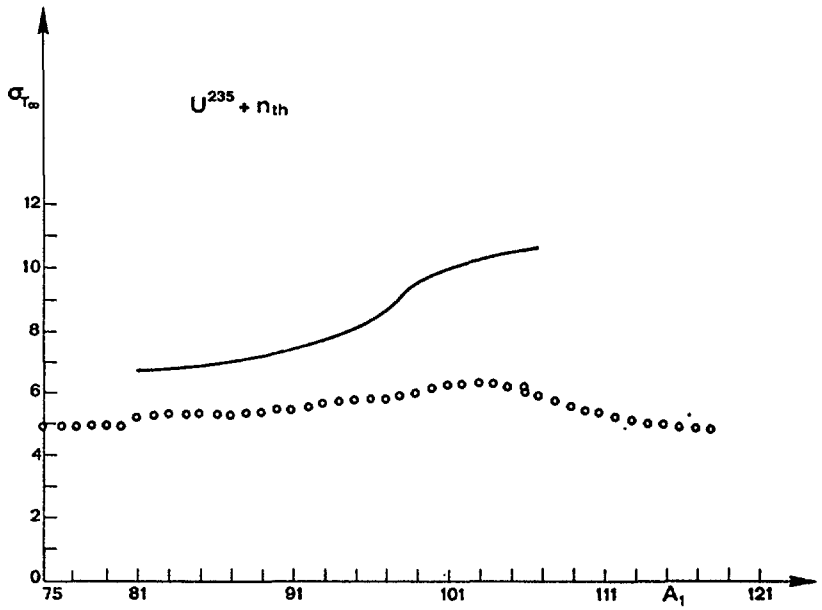
$\sigma_{\gamma\infty}$
$U^{235} + n_{th}$
12
10
8
6
4
2
0
75
81
91
101
111
A_1
121

Fig. 5

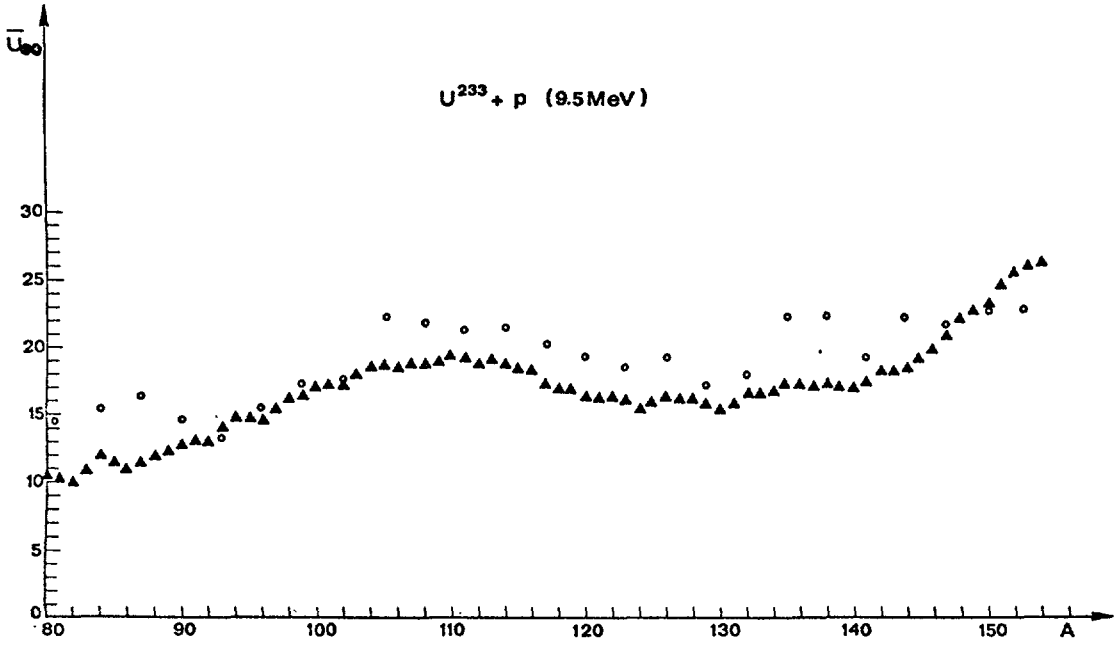
$\bar{\nu}_{\infty}$
$U^{233} + p$ (9.5MeV)
30
25
20
15
10
5
0
80
90
100
110
120
130
140
150
A

Fig. 6a

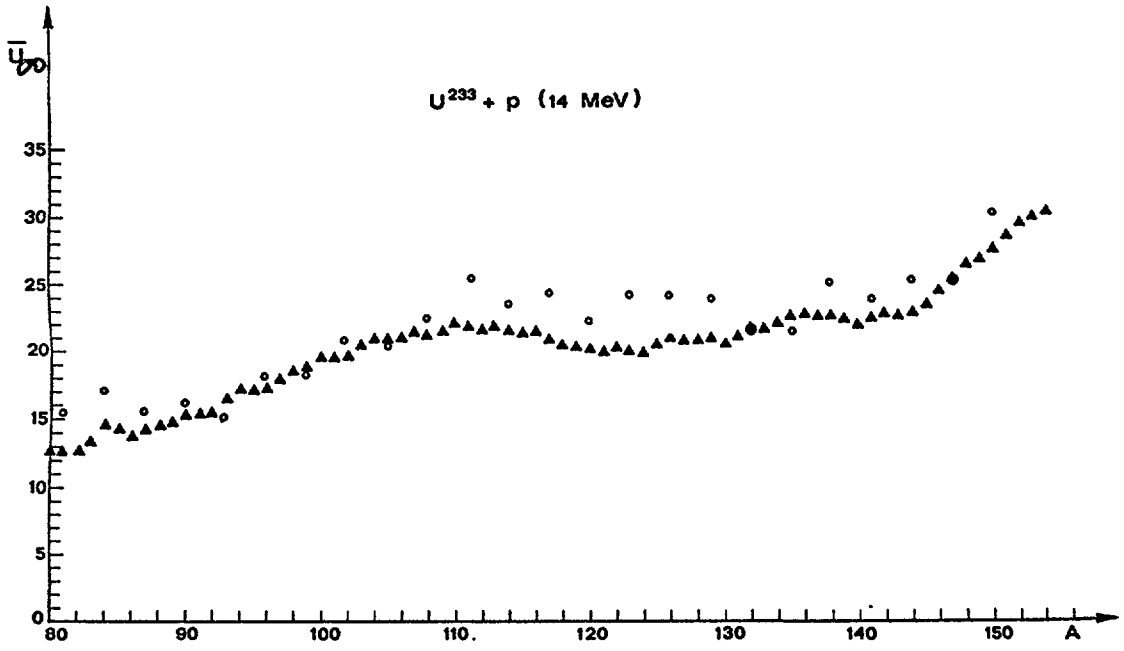
$\bar{\nu}_{00}$
$U^{233} + p$ (14 MeV)
35
30
25
20
15
10
5
0
80
90
100
110.
120
130
140
150
A

Fig. 6b

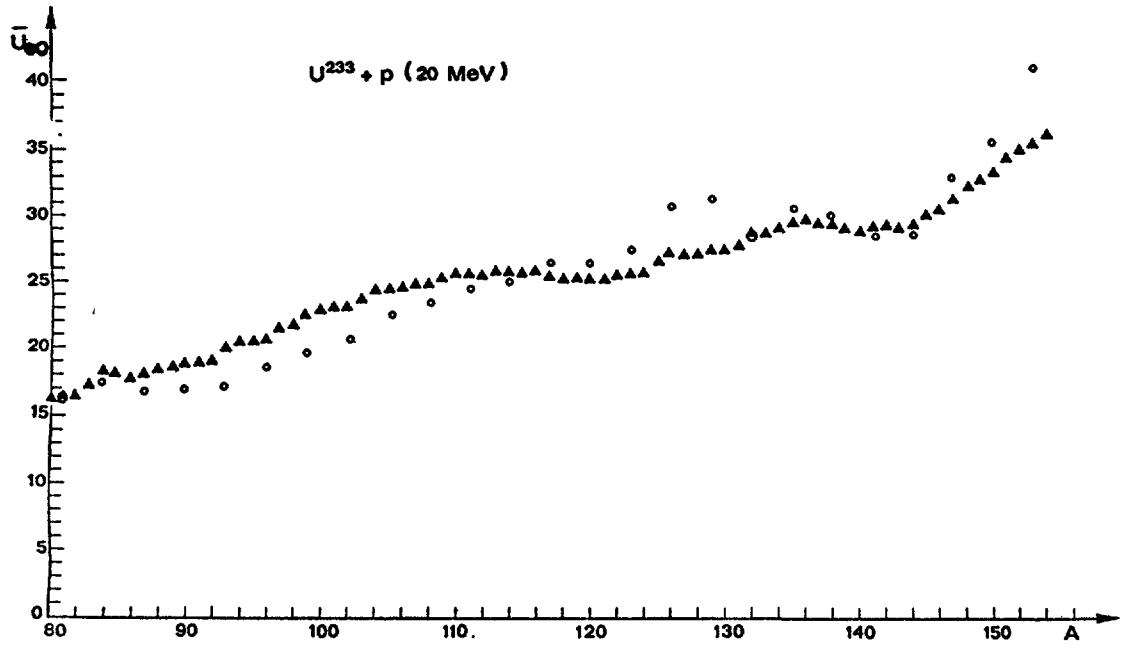
$\bar{\nu}_{00}$
$U^{233} + p$ (20 MeV)
40
35
30
25
20
15
10
5
0
80
90
100
110.
120
130
140
150
A

Fig. 6c

Fig. 7a

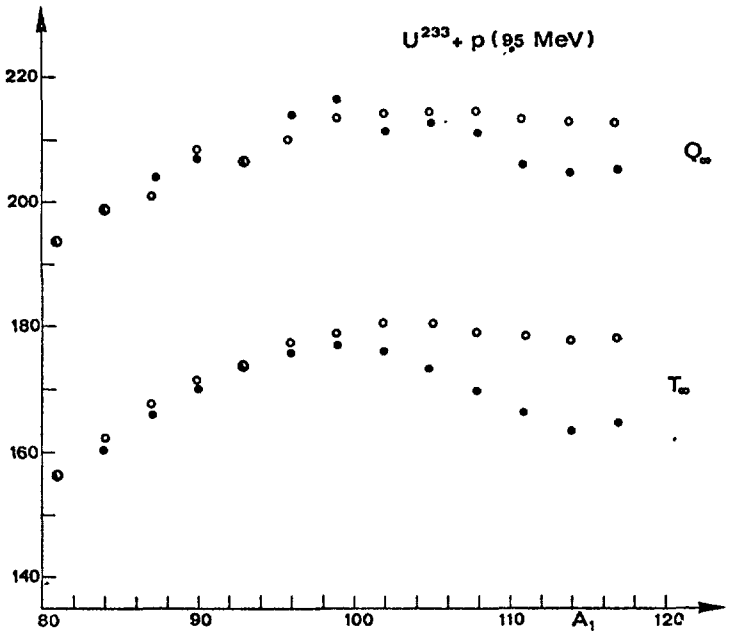

Fig. 7b

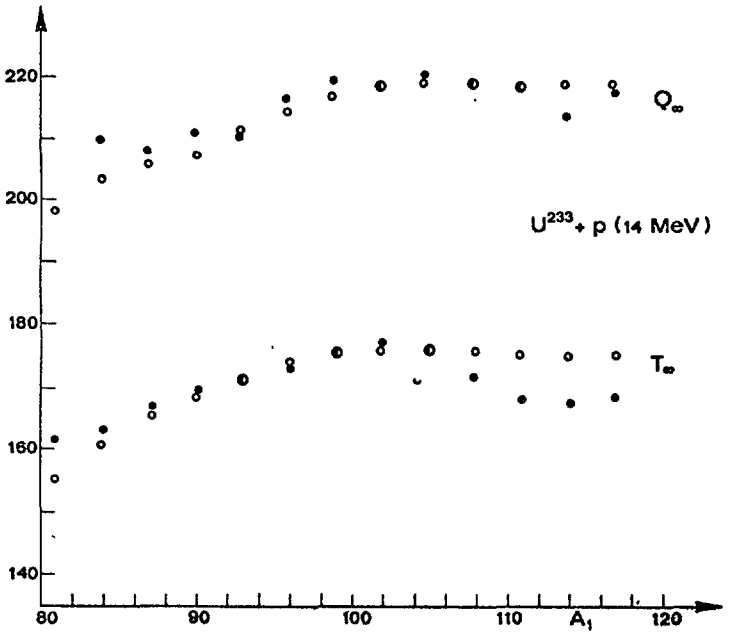

Fig. 7c

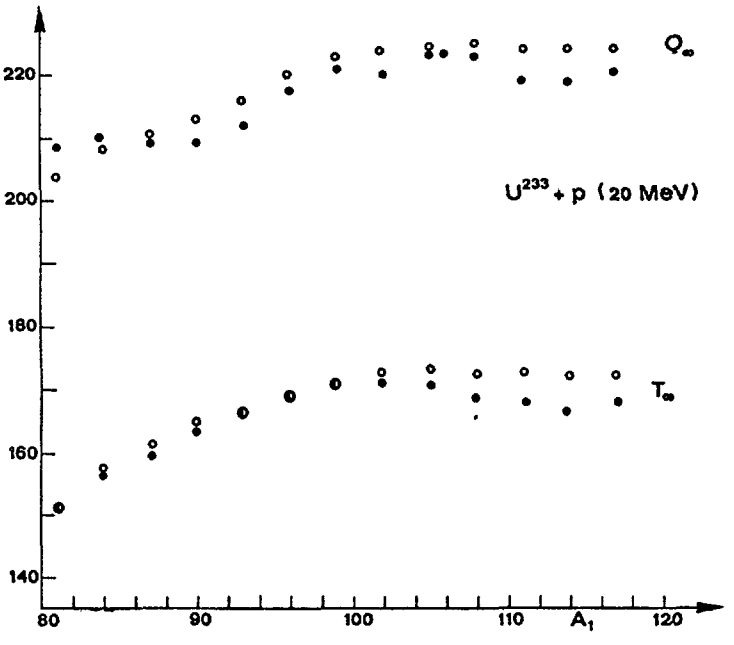

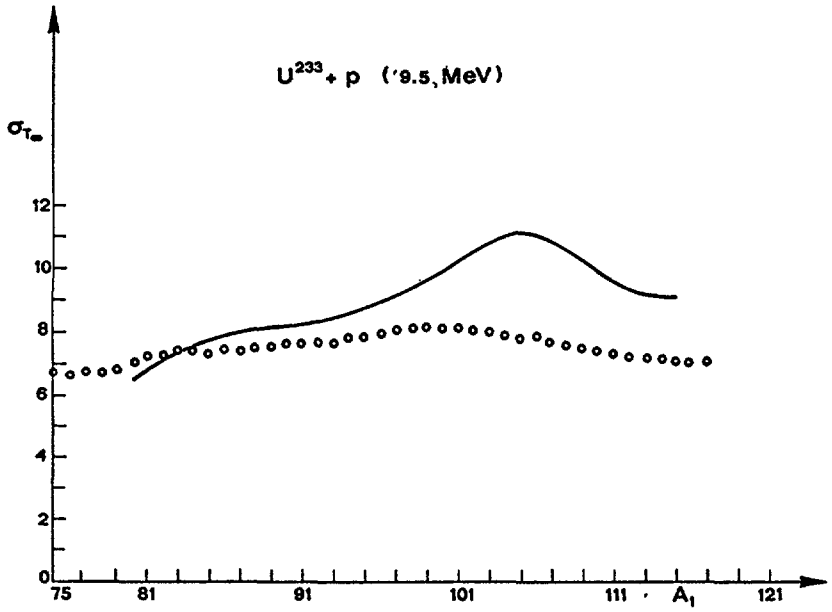
U233 + p (9.5 MeV)
σTω
12
10
8
6
4
2
0
75
81
91
101
111
A1
121

Fig. 8a

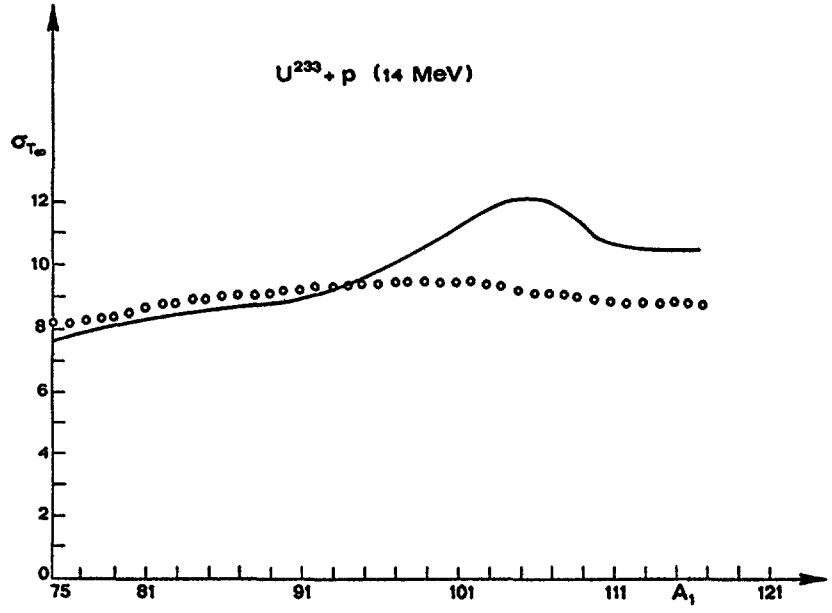
U233 + p (14 MeV)
σTω
12
10
8
6
4
2
0
75
81
91
101
111
A1
121

Fig. 8b

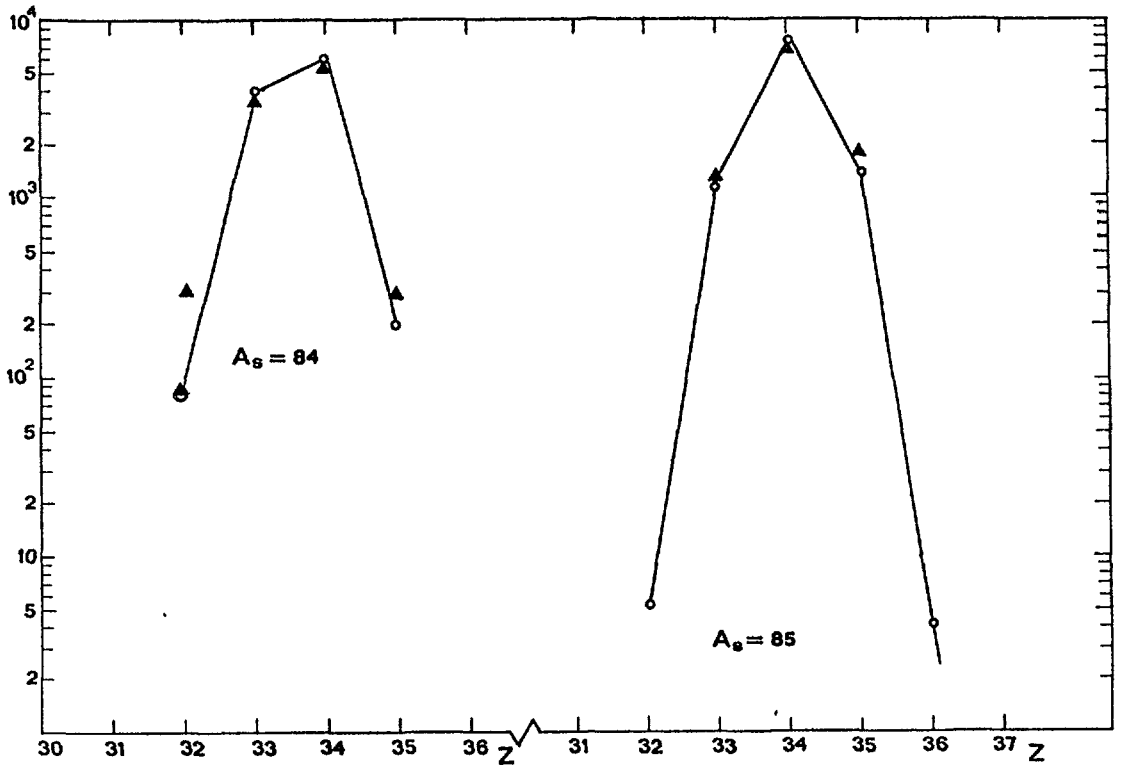

Fig. 9a

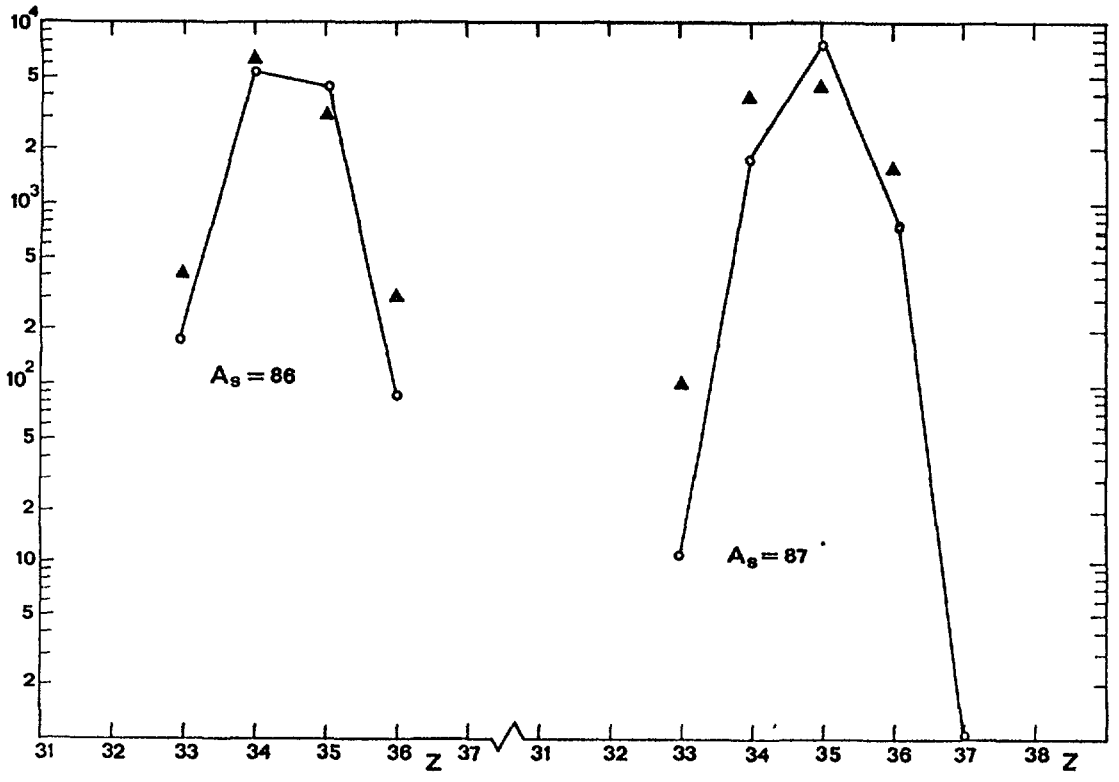

Fig. 9b

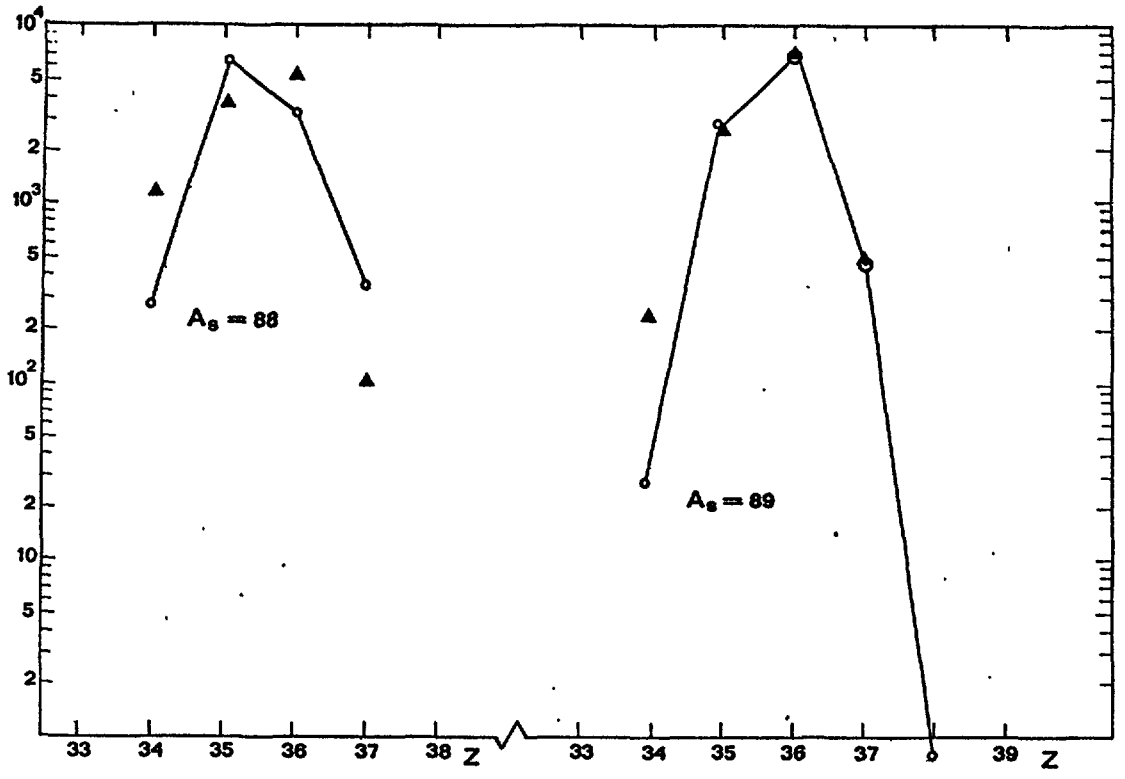

Fig. 9c

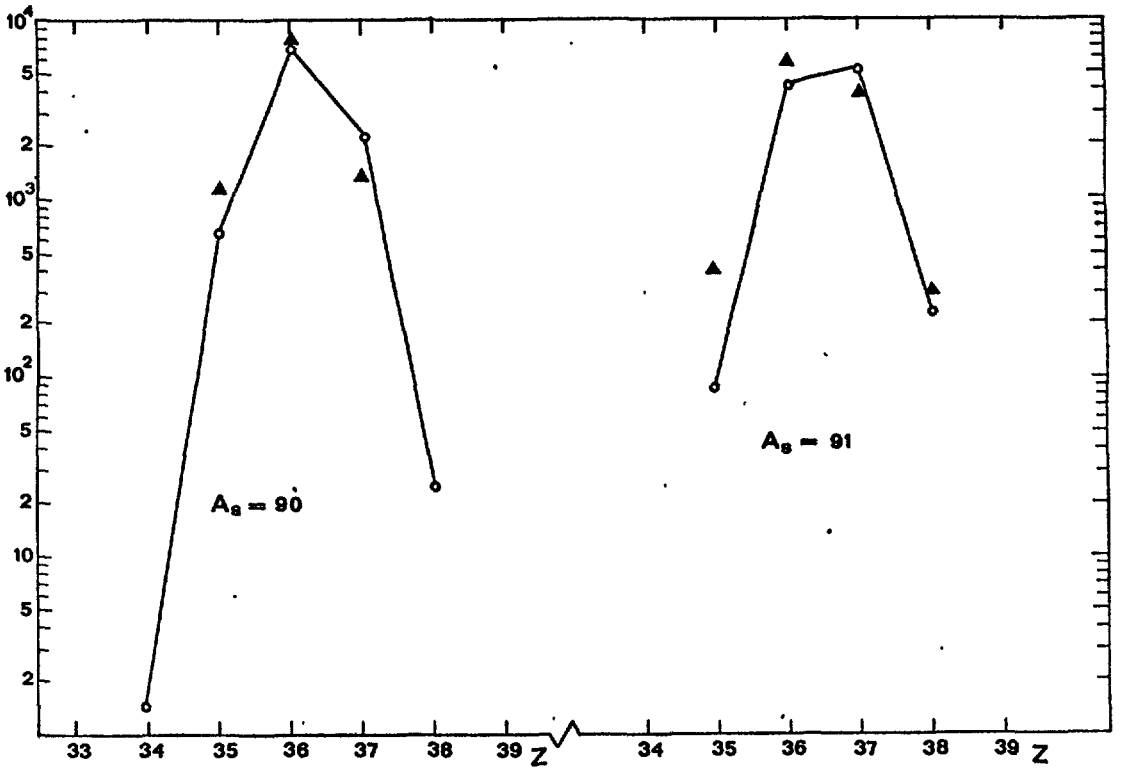

Fig. 9d

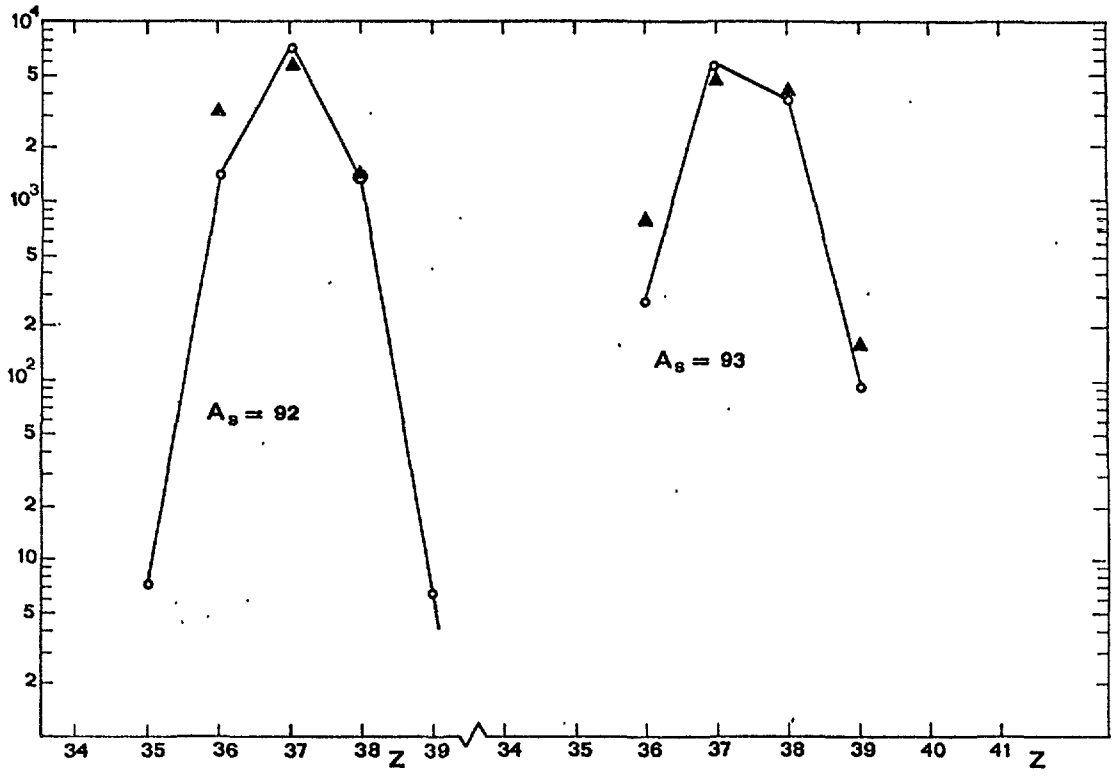

Fig. 9e

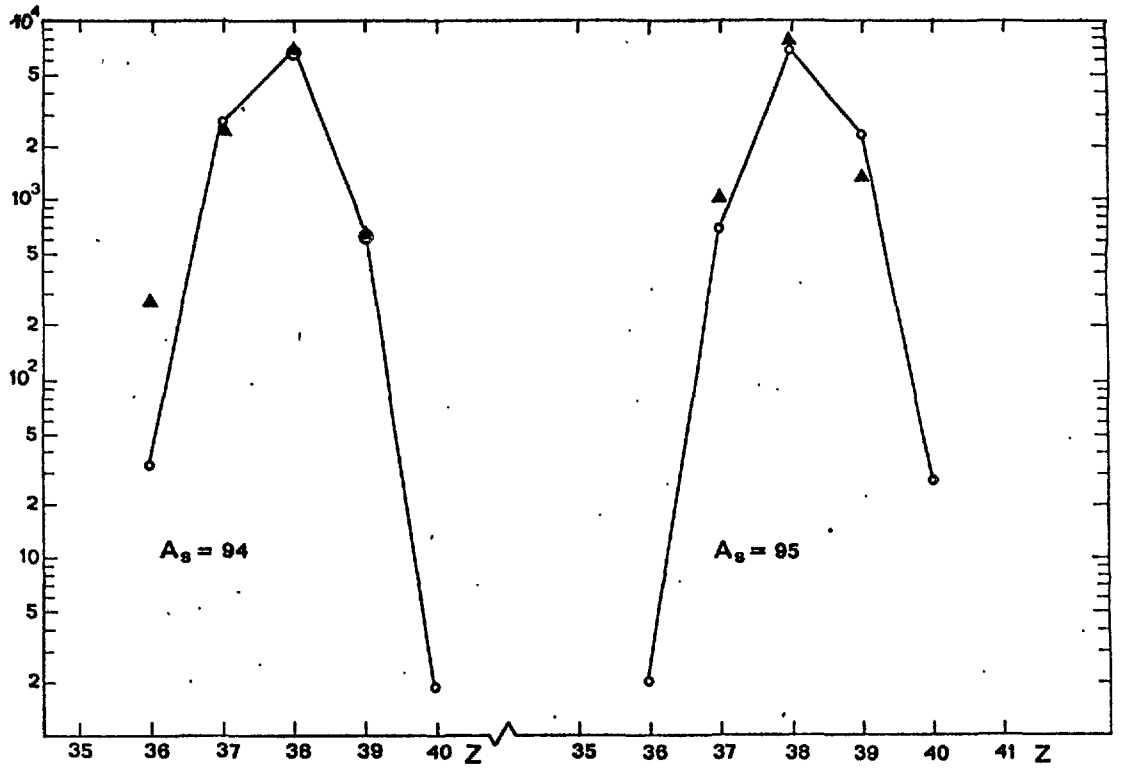

Fig. 9f

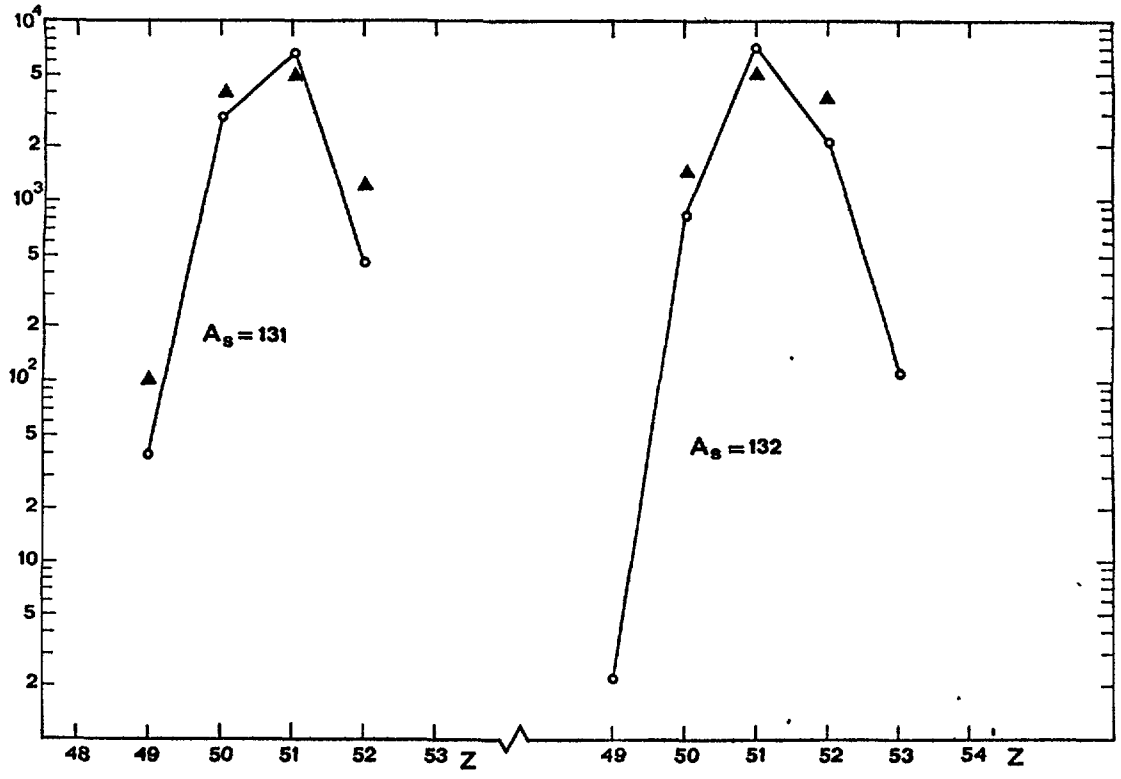

Fig. 9g

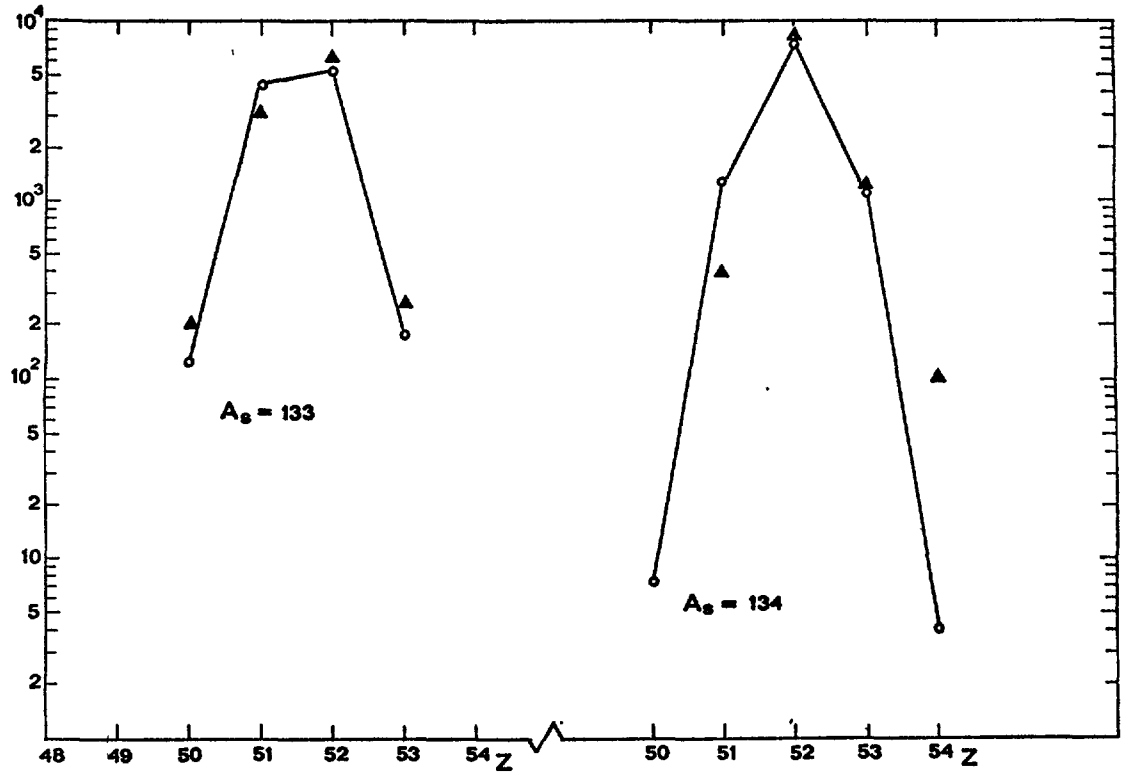

Fig. 9h

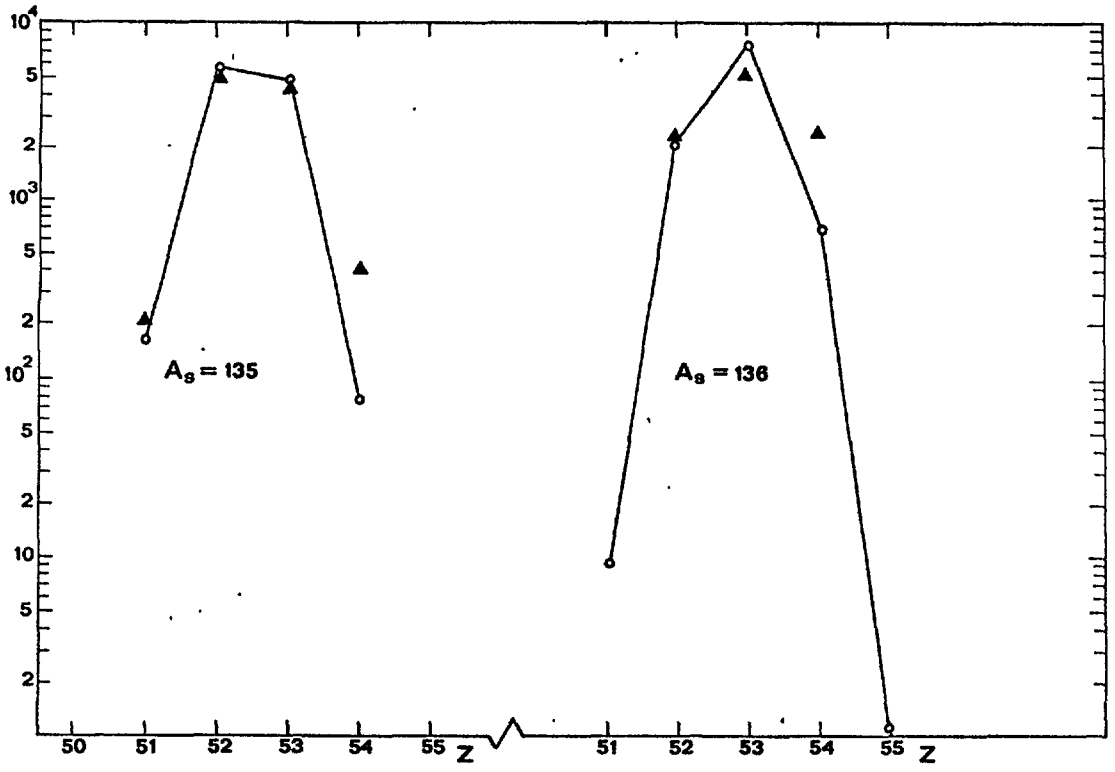

Fig. 9i

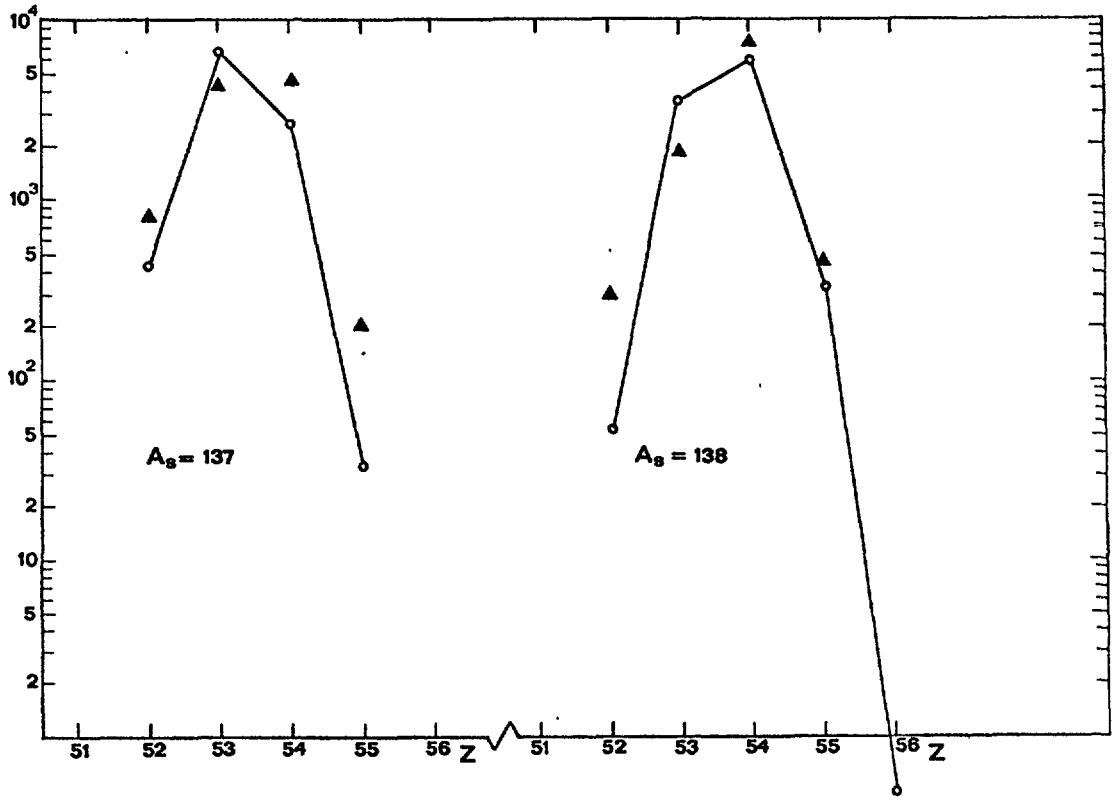

Fig. 9l

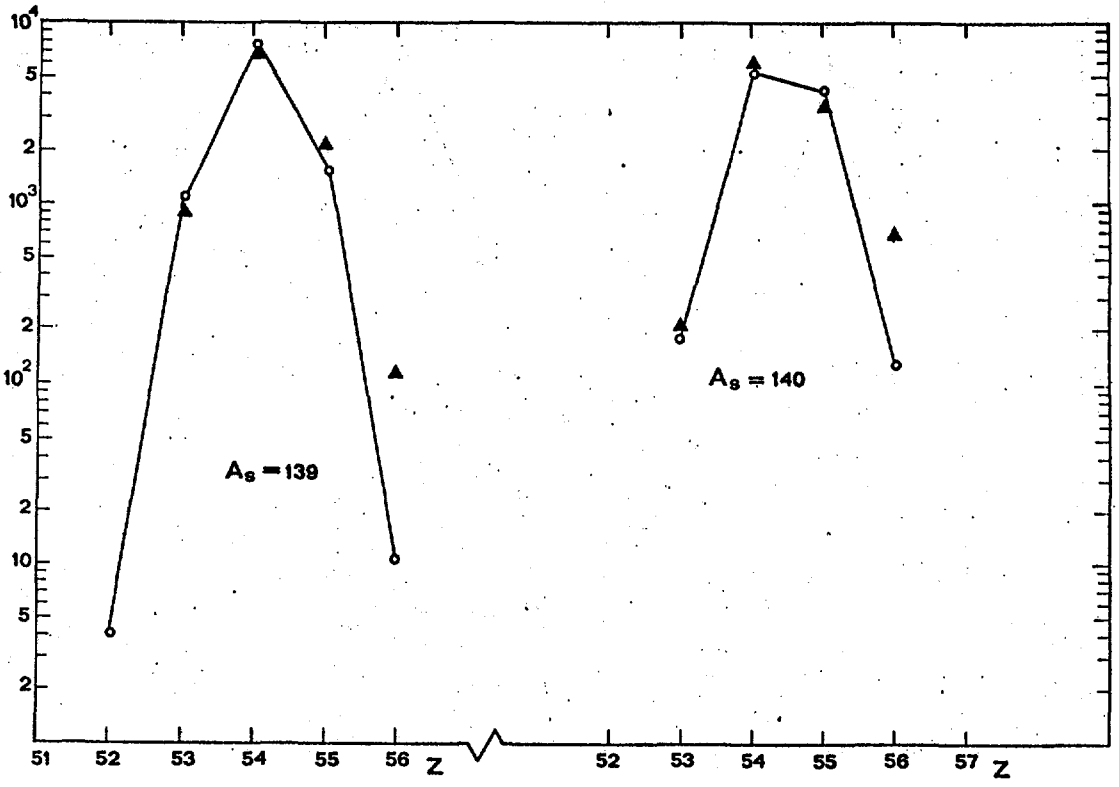

Fig. 9m

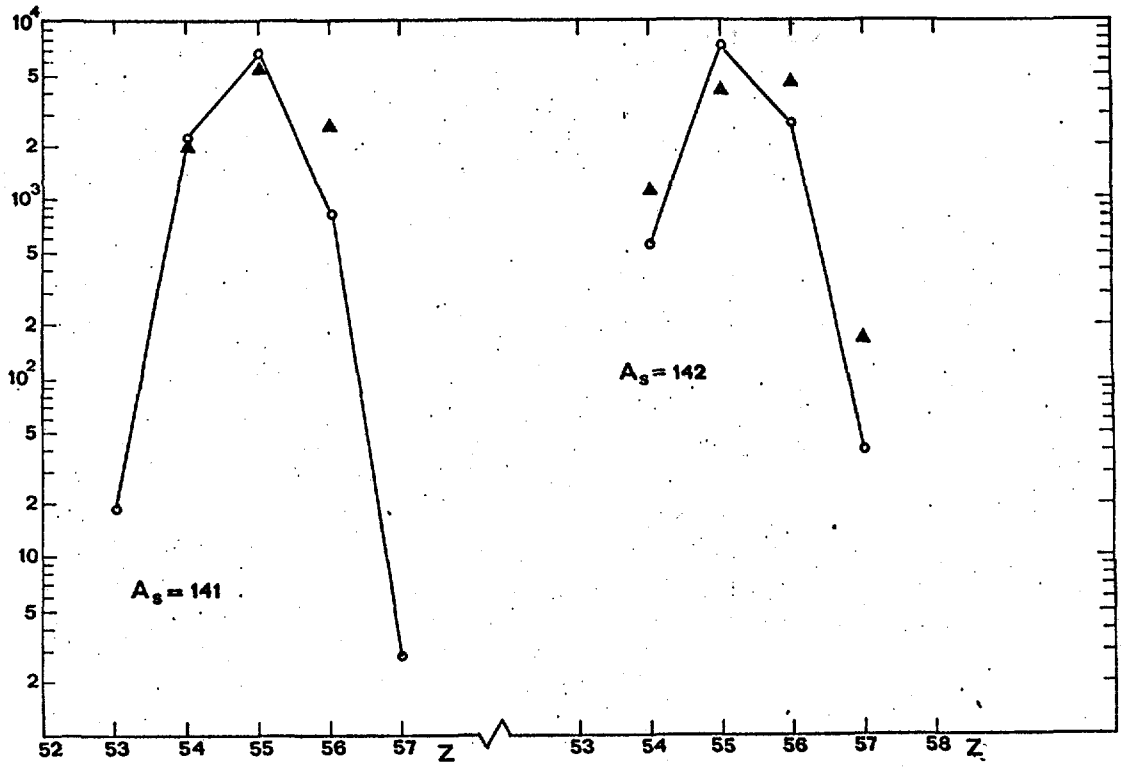

Fig. 9n

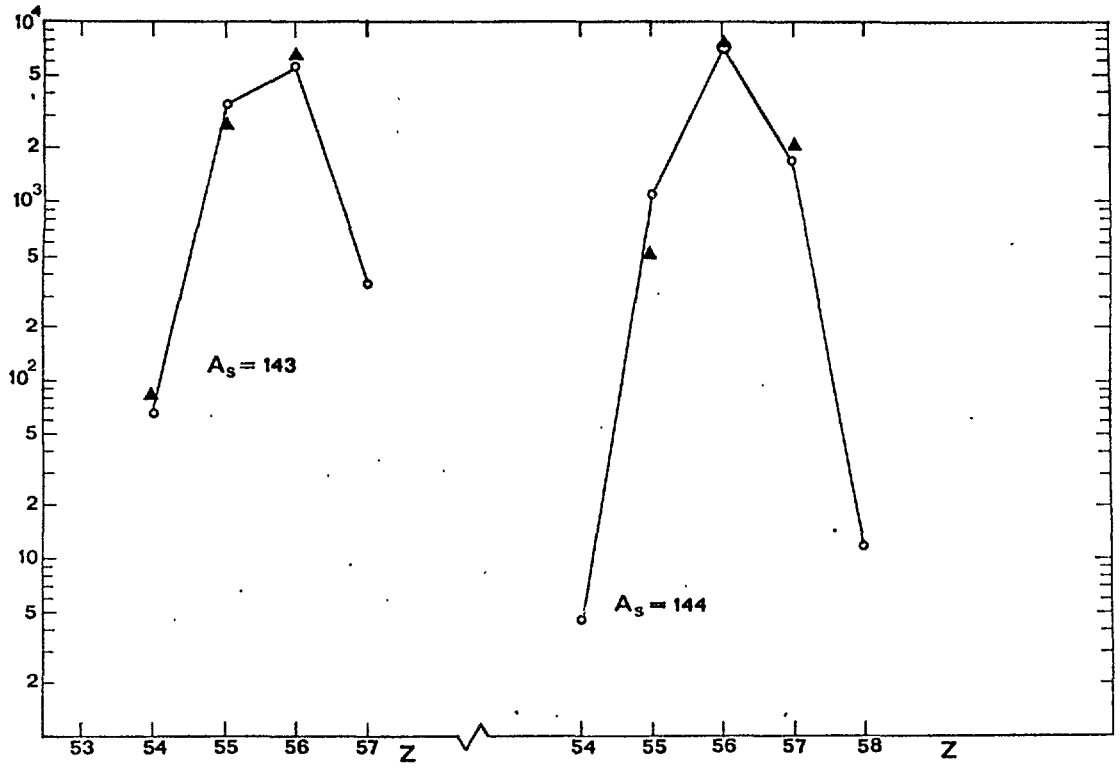
10^4
5
2
10^3
5
2
10^2
5
2
10
5
2
$A_s = 143$
$A_s = 144$
53
54
55
56
57
Z
54
55
56
57
58
Z

Fig. 9o

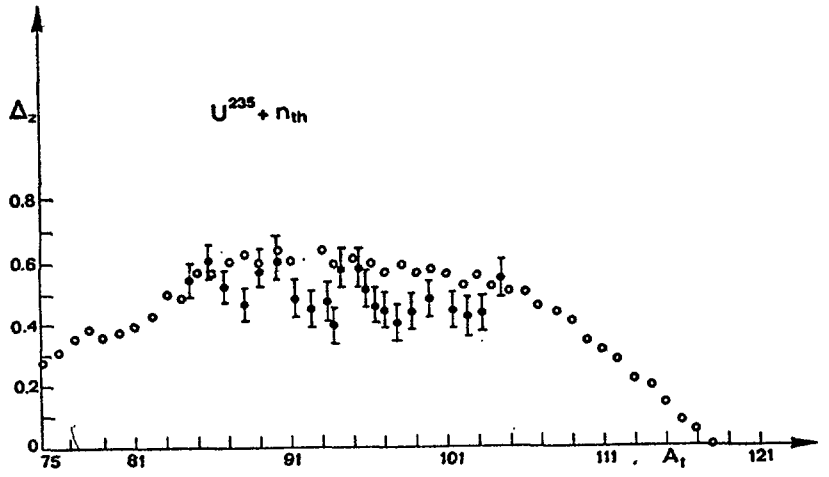

Fig. 10a

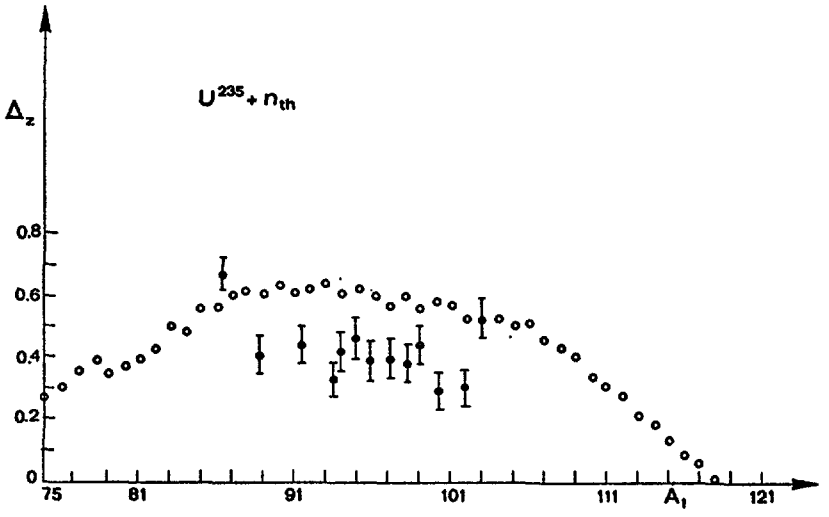

Fig. 10b

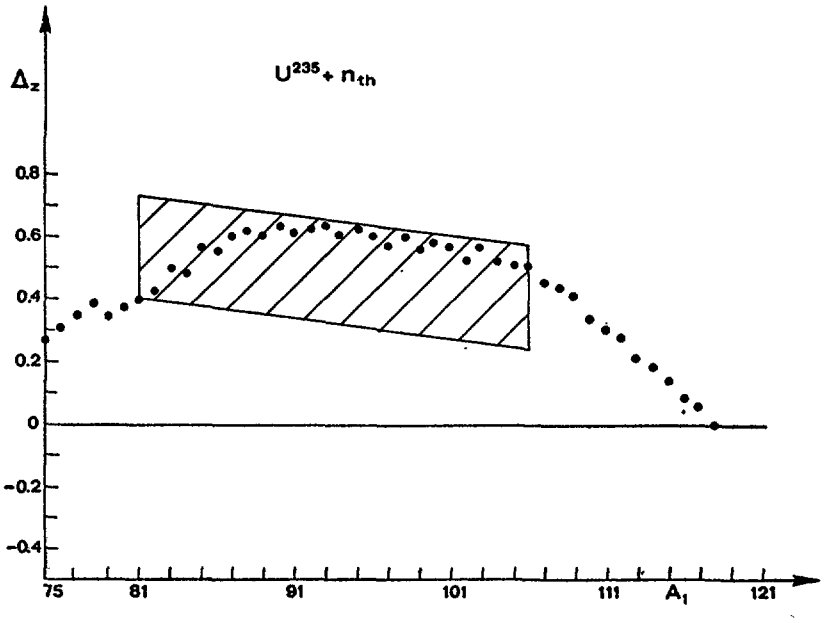

Fig. 10c

Next page(s) left blank

Contributed Paper No. 20

NOTE ON THE NEUTRON-FISSION COMPETITION IN HEAVY NUCLEI

V. BENZI

CNEN, CENTRO DI CALCOLO, BOLOGNA (ITALY)

ABSTRACT

A semiempirical approach to determination of the energy dependence of the ratio Γ_n/Γ_f for heavy nuclei is here presented. The proposed formulae are applied to the case of ^{240}Pu, for which a weak bump is found at about 4 MeV.

---

§ 1. In the last few years, a bump-like structure in the Γ_n/Γ_f ratio as a function of the excitation energy of the nucleus has been predicted by various authors [1,2], as a consequence of the variation in the single-particle spectra spacing at the minima and maxima of the fission barrier.

In particular, theoretical calculations predict a bump with a maximum at about 4-5 MeV for a large variety of heavy nuclei.

An attempt to verify this theoretical expectation was carried out by Fubini [3], on the basis of the following argument.

In the framework of the compound nucleus theory, the neutron and first-chance-fission cross sections for a target nucleus of mass number (A-1) are respectively given by

$$\sigma_n = \sigma_R \cdot (\Gamma_n / \Gamma_{tot})$$

$$\sigma'_f = \sigma_R \cdot (\Gamma_f / \Gamma_{tot})$$

σ_R being the total compound-nucleus cross section.

Thus, for an excited nucleus of mass number A, one has

$$\Gamma_n / \Gamma_f = \sigma_n / \sigma'_f = (\sigma_{n,\gamma} + \sigma_{n,n',\gamma} + \sigma_{n,2n} + \sigma_f - \sigma'_f) / \sigma'_f \qquad (1)$$

where σ_f represents the total fission cross section and the other symbols have the usual meaning.

In deriving the above equation, it is assumed that processes other than those considered, like compound elastic scattering or third-chance-fission, are negligible at the considered energies.

Equation (1) was applied by Fubini to the analysis of the ^{234}U, ^{236}U, ^{240}Pu and ^{242}Pu excited nuclei. In order to perform the calculations, the $\sigma_{n,\gamma}$, $\sigma_{n,n',\gamma}$ and $\sigma_{n,2n}$ cross sections evaluated by Langner et al. [4] were used, whereas Davey's evaluation [5] was adopted for σ_f and σ'_f. The analysis covered the energy range 1-10 MeV, but the expected bump in the ratio Γ_n / Γ_f was not found in any one of the nuclei considered.

This result might be partly due to one or more of the following reasons:

i) All the evaluated cross sections but σ_f are estimated values, because experimental data above few MeV are scarce. Thus, the adopted cross sections might be too uncertain for the purpose in hand.

ii) The evaluated $\sigma_{n,n';\gamma}$ contain a non-negligible direct component σ_{rot}, the various nuclei analysed by Fubini being rather deformed. This component was not subtracted from the adopted $\sigma_{n,n';\gamma}$ so that the numerator in the R.H.S. of Eq. (1) is overestimated.

iii) The σ'_f values above the onset of the second-chance-fission are badly underestimated and, consequently, ratio Γ_n/Γ_f is overestimated above $\sim$5.5 MeV.

In order to overcome the difficulties arising from the first two points above, it seems better to write Eq. (1) in a different form, namely

$$\Gamma_n/\Gamma_f = \left[(\sigma_T-\sigma_{se}-\sigma_{rot})/\sigma'_f\right]-1$$

$$= \left[(1-R)(\sigma_T/\sigma'_f)\right] - 1 \qquad (2)$$

where σ_T and σ_{se} represent the total and shape-elastic cross sections, respectively, and $R = \left[(\sigma_{se}+\sigma_{rot})/\sigma_T\right]$.

The ratio R can be calculated with reasonable accuracy by means of a generalized optical model adjusted to reproduce the σ_T and other experimental data like strength-functions, angular distributions, etc.... There is some degree of uncertainty about the choice of parameters on which the deformed optical potential depends. However, the calculated ratio R should not be too sensitive to the adopted parameters, because σ_T and σ_{se} have a strong positive correlation and $\sigma_{rot}/\sigma_T << \sigma_{se}/\sigma_T$. It should be noted, in

addition, that Eq. (2) takes correctly into account the contribution of the compound elastic cross section, which is neglected in Eq. (1).

For these reasons, the results obtained by means of Eq.(2), using a theoretical estimate of R together with a carefully measured σ_T, should be more reliable than those derived from Eq.(1).

As far as point iii) is concerned, it has to be noted that at high excitation energies the differential cross section for the second-chance-fission process, which occur after a neutron with energy between E' and (E'+dE') has been emitted by the parent nucleus, is given by

$$d\sigma_f''(E;E') = \sigma_{n,n'}(E)\{C(E)[\Gamma_f(E-E')/\Gamma_T(E-E')]E'e^{-E'/T}\}dE' \qquad (3)$$

with $\sigma_{n,n'}=(\sigma_T - \sigma_{se} - \sigma_{rot} - \sigma_f')$. The nuclear temperature T appearing in Eq. (3) depends on the incident neutron energy E, whereas the C(E) is a normalization factor ($\simeq 1/T^2$).

Thus, if E_f represents the threshold energy for fission of the residual nucleus (measured from the ground state), one has

$$\sigma_f''(E) = \sigma_f(E) - \sigma_f'(E) = \sigma_{n,n'}(E)\beta(E) \qquad (4)$$

with

$$\beta(E) \simeq (1/T^2)\int_0^{E-E_f} E'[\Gamma_f(E-E')/\Gamma_{tot}(E-E')]e^{-E'/T}dE' \qquad (5)$$

Equation (4) contains two unknown quantities, namely the "branching ratio" β and the first-chance-fission cross section σ_f'. The last one can be dropped if we put

$$\sigma_f'' = (\sigma_T - \sigma_{se} - \sigma_{rot} - \sigma_f + \sigma_f'')\beta$$

from which it follows that

$$\sigma_f'' = [(1-R)\sigma_T - \sigma_f)]\,[\beta/(1-\beta)] \qquad (6)$$

As far as the parameter β is concerned, an estimate can be obtained by using a relationship like Eq.(1) for the ratio Γ_f/Γ_{tot} which appears in the R.H.S. of Eq.(5); one has

$$\beta(E) \simeq (1/T^2) \int_0^{E-E_f} E' \left[\sigma_f'(E-E'-B_n)/\sigma_R(E-E'-B_n)\right] e^{-E'/T}\, dE' \qquad (7)$$

Obviously, in this case ratio (σ_f'/σ_R) refers to the fission and total reaction cross sections of the nucleus with mass number (A-2), whereas B_n is the last-neutron separation energy of the nucleus with mass (A-1).

For the nuclei considered by Fubini, the fission is a threshold reaction whose cross section can be adequately represented by a step function starting at some effective threshold energy $\bar{E}_f$.

In addition, the energy dependence of the compound nucleus reaction cross section σ_R can be reasonably well represented by means of the empirical relationship

$$\sigma_R(\varepsilon) \simeq \sigma_g(\mu + \nu/\varepsilon) \qquad (8)$$

with $\sigma_g = \pi R^2$, as suggested by Dostrovski and Fraenkel [12].

Using these approximations, the integral appearing on the R.H.S. of Eq. (7) can be very easily evaluated.

§ 2. As an application of the above considerations, the case of the ^{240}Pu excited nucleus has been considered. The R-ratio was estimated above 3 MeV using the theoretical results given by Prince et al.[6],[7],[8], whereas at lower energies the results obtained by Benzi et al.[9] were adopted, because it is felt that they are in better agreement with the most recent measurements of σ_T.

The total cross section σ_T was obtained from an empirical fit of the very accurate measurements performed by Schwarz and reported in ref. [10].

As far as the σ_f' - values of ^{239}Pu are concerned, the evaluation of σ_f carried out by Pitterle et al. [11] was adopted up to 5.5 MeV.

In order to obtain an estimate of β above this energy, the ^{238}Pu fission cross section was approximated by a step function of 2.2 barn starting at 0.4 MeV, to which a value of $\bar{E}_f \simeq 6$MeV corresponds. Such an estimate was made on the basis of the experimental values obtained by Silbert [13]

The σ_R was calculated according to formula (8). An analysis of the compound nucleus neutron cross sections, calculated for nuclei with mass $A \simeq 238$ by means of the generalized optical model, provided the following empirical values : $R=1.5A^{1/3}$ fm, $\mu=1.060$ and $\nu=0.294$ MeV. The neutron separation energy B_n of ^{239}Pu, which appears in Eq. (7), was taken from Howerton's compilation [14], which gives B_n = 5.66 MeV.

The last parameter required in order to calculate β, namely the nuclear temperature T, was estimated from the spectrum of secondary neutrons emitted by ^{239}Pu. For this purpose, the measurements carried out by Voigner et al. [15] at neutron incident energies of $\sim$14 MeV were analysed. The obtained value of $T \simeq 1$MeV was adopted as normalisation point, assuming that at high excitation energies the temperature depends on the energy of the incident neutron as $E^{1/2}$.

Inserting in Eq.(7) the values of $\sigma_f, \sigma_R, \bar{E}_f, B_n$ and T thus obtained, a value of $\beta \simeq 0.6$ was found at E=9 MeV.

With such a β - value, Eq.(6) gives $\sigma_f'' \simeq 0.66$ barn, so that $\sigma_f' \simeq 1.7$ barn. Thus, if a monotonic behaviour of σ_f' is assumed, we are led to the conclusion that σ_f' remains nearly constant above 5.5 MeV.

This result agrees with the extrapolation of σ_f' made by Schuster

and Howerton [16] in analysing the energy dependence of the average number of prompt neutrons emitted in the fission of ^{239}Pu, but strongly disagrees with Davey's estimate, as shown in Fig. 1.

In addition, the estimate of σ_f'' here obtained agrees quite well with the evaluation carried out by Hunter et al. in 1973 [17].

In Table I, the various cross sections adopted in this work are given in column under (A), together with the resulting Γ_n/Γ_f. In the same table, the cross sections appearing in Eq.(1), as adopted by Fubini, and the resulting Γ_n/Γ_f, are shown in the columns under (B).

It should be noted that use of more recent evaluations of σ_f for ^{239}Pu, e.g. ENDF/B-IV, would not in practice change the estimate of σ_f'.

For comparison's sake the two different estimates of Γ_n/Γ_f are plotted in Fig. 2. As one can see, the results obtained with the methods here adopted clearly show a bump-like behaviour, with the maximum at around 3-4MeV, as predicted by Britt et al. [1].

However, the absolute value of the bump at its maximum is much lower than predicted in Ref. [1]. In fact, from Fig. 2 one has $(\Gamma_n/\Gamma_f)_{peak} \sim 1.4(\Gamma_n/\Gamma_f)_{9MeV}$, whereas Britt et al. obtain a factor about 3.5 times larger. Such a discrepancy cannot be accounted for by any reasonable estimate of errors in the adopted cross sections.

It has to be noted that the gamma instabilities at the first saddle were not considered in the theoretical estimates of Γ_n/Γ_f given in Ref. 1. From the fact that the effect of an equilibrium gamma deformation at the taken saddle would be to decrease the shell energy and the density of single-particle states near the Fermi surface, one expects the bump-like struc

ture to be less pronounced for plutonium and heavier actinide nuclei [2] . Such an expectation is in qualitative agreement with the results here obtained for Pu-240. This seems to give some additional support to the need for more realistic models in which the equilibrium gamma deformation at the first saddle is properly taken into account.

REFERENCES

[1] BRITT,H.C.,BOLSTERLI,M.,NIX J.R. and NORTON,J.L. Phys.Rev. C, 7,801, (1973).

[2] METAG,V.,LEE,S.M.,LIUKKONEN,E., SLETTEN,G.,BJÖRNHOLM S.and JENSEN A.S., Nucl.Phys.,213A, 397, (1973).

[3] FUBINI,A. Lettere Nuovo Cimento, 9,682, (1974).

[4] LANGNER,L.,SCHMIDT,J.J.and WOLL,D. KFK-750 (1968).

[5] DAVEY,W.C. Nucl. Sc. Eng.,44,345, (1971).

[6] PRINCE,A. Proc. II. Int.Conf. on Nuclear Data for Reactors, Helsinky, vol. II, (1970).

[7] PRINCE,A. DRAKE,M.K., Proc. III Conf. on Neutron Cross Sections and Tech., Knoxville, Vol. I (1971).

[8] PRINCE,A. DRAKE,M.K. and HILAVAC,P. BNL-50388 (1973)

[9] BENZI,V. ZUFFI,L. COPPOLA,M. and KNITTER,H.N.,Proc.II Int. Conf. on Nuclear Data for Reactors, Helsinky, vol. II pag. 863 (1970).

[10] CULLEN,D.E.,HAIGHT,R.C.,HOWERTON,R.J.,McGREGOR,M.H. and PERKINS,S.T. UCRL-50400,vol. 7B (1974).

[11] PITTERLE,T.A.,PAIK,N.C. and DURSTON,C. Proc. II Conf. on Neutron Cross Sections and Techn., vol. I,(1971).

[12] DOSTROVSKI,I. and FRAENKEL,Z. Phys.Rev. 116,683 (1959).

[13] SILBERT,M.G. LA-4674-MS (1971).

[14] HOWERTON,R.J. UCRL-50400,vol.9 (1970).

[15] VOIGNIER,J.,CLAYEUX,G. and BERTRAND F. Proc. III Conf. on Neutron Cross Sections and Techn., Knoxville, vol. I, (1971).

[16] SCHUSTER,S.H. and HOWERTON,R.J. J.Nucl.Eng.A/B,18,125, (1964)

[17] HUNTER,R.E.,STEWART,L., and HIROUS T.J. LA-5172 (1973).

TABLE I

CROSS-SECTION VALUES ADOPTED FOR THE ESTIMATE OF THE ENERGY DEPENDENCE OF THE Γ_N/Γ_F RATIO IN ^{240}PU.

	(A)							(B)					
E (MeV)	σ_T(b) (eval.)	σ_T(b) (theor.)	σ_{se}(b) (theor.)	σ_{rot}(b) (theor.)	σ_f(b) (eval.)	σ'_f(b) (eval.)	Γ_n/Γ_f (calc.)	$\sigma_{n,\gamma}$(b) (eval.)	$\sigma_{n,n'\gamma}$(b) (eval.)	$\sigma_{n,2n}$(b) (eval.)	σ_f(b) (eval.)	σ'_f(b) (eval.)	Γ_n/Γ_f (calc.)
2.0	7.25	7.259	3.411	0.531	2.057	2.057	0.51	0.018	1.108	*	1.860	1.860	0.61
3.0	7.86	7.913	3.700	0.740	1.896	1.896	0.86	0.011	1.421	*	1.780	1.780	0.81
3.5	8.03	8.020	3.860	0.736	1.802	1.802	0.90	*	*	*	*	*	*
4.0	7.93	7.990	3.955	0.720	1.745	1.745	0.89	0.009	1.652	*	1.690	1.690	0.98
4.5	7.79	7.903	3.985	0.698	1.696	1.696	0.87	*	*	*	*	*	*
5.0	7.59	7.732	3.921	0.669	1.669	1.669	0.85	0.006	1.618	*	1.610	1.610	1.01
5.5	7.36	7.438	3.790	1.638	1.665	1.665	0.81	*	*	*	*	*	*
6.0	7.07	7.225	3.640	0.606	1.692	1.665	0.75	0.005	1.288	0.140	1.710	1.520	1.07
6.5	6.82	6.968	3.472	0.583	1.897	1.665	0.72	*	*	*	*	*	*
7.0	6.61	6.742	3.305	0.565	2.121	1.665	0.69	0.004	0.572	0.735	1.980	1.445	1.27
7.5	6.46	6.554	3.162	0.548	2.259	1.665	0.67	*	*	*	*	*	*
8.0	6.30	6.397	3.032	0.535	2.338	1.665	0.67	0.003	0.308	0.745	2.070	1.346	1.32
8.5	6.19	6.243	2.865	0.524	2.369	1.665	0.67	*	*	*	*	*	*
9.0	6.07	6.123	2.812	0.514	2.355	1.655	0.67	0.002	0.200	0.615	2.070	1.263	1.29

FIGURE CAPTIONS

Fig. 1 Estimated energy dependence of the first-chance-fission σ_f' in ^{239}Pu.

Fig. 2 The estimated energy dependence of Γ_n/Γ_f in the ^{240}Pu excited nucleus. The estimate by Fubini (dashed line) is shown for comparison.

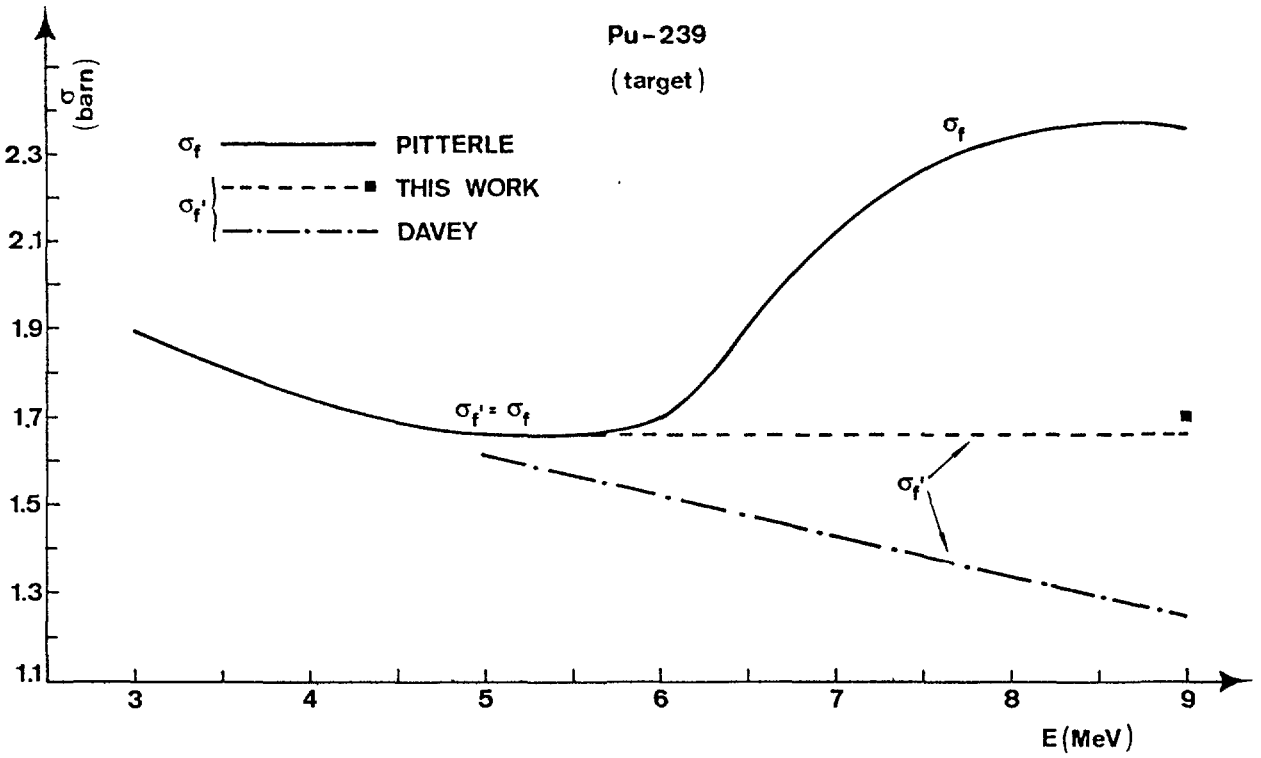
Pu-239
(target)
σ (barn)
σf PITTERLE
σf' THIS WORK
DAVEY
σf
σf' = σf
σf'
2.3
2.1
1.9
1.7
1.5
1.3
1.1
3
4
5
6
7
8
9
E(MeV)

Fig.1

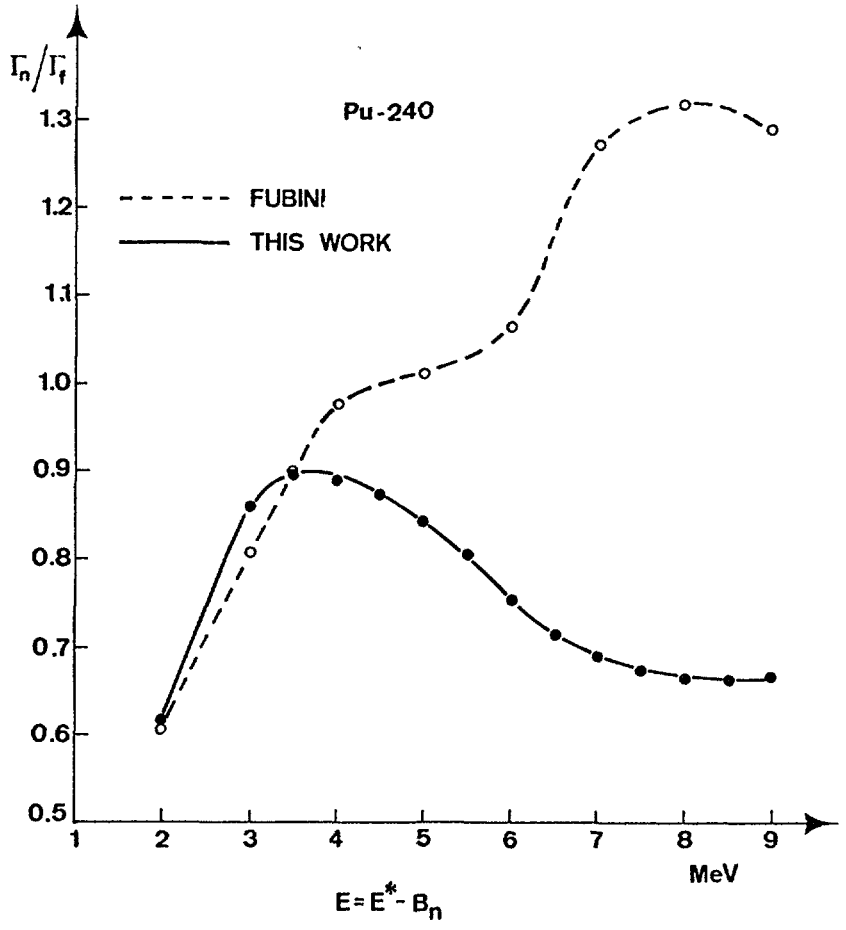
Γn/Γf
Pu-240
FUBINI
THIS WORK
1.3
1.2
1.1
1.0
0.9
0.8
0.7
0.6
0.5
1
2
3
4
5
6
7
8
9
MeV
E=E*-Bn

Fig. 2